

**Impacts of Fuel Inventory on Low Temperature Ignition Risk during
Handling and Storage of Biomass**

Yee Sing Chin

Submitted in accordance with the requirements for the degree of
Doctor of Philosophy

The University of Leeds
School of Chemical and Process Engineering

April 2017

The candidate confirms that the work submitted is her own, except where work which has formed part of jointly-authored publications has been included. The contribution of the candidate and the other authors to this work has been explicitly indicated below. The candidate confirms that appropriate credit has been given within the thesis where reference has been made to the work of others.

This copy has been supplied on the understanding that it is copyright material and that no quotation from the thesis may be published without proper acknowledgement.

The right of Yee Sing Chin to be identified as Author of this work has been asserted by her in accordance with the Copyright, Designs and Patents Act 1988.

List of Work Presented/Published

Some parts of this research had been presented or published and the details are as follows:

Part of **Chapter 4** had been presented as listed:

Y.S. Chin, A.R. Lea-Langton, L.I. Darvell, J.M.Jones, A. Williams. **An Experimental Study on Minimum Ignition Temperature**. Poster. 5th December 2014: SUPERGEN Bioenergy Hub Annual Assembly, Birmingham, UK

Y.S. Chin, L.I. Darvell, A.R. Lea-Langton, J.M.Jones, A. Williams. **Biomass Handling – Ignition Risks from Dust-Layer Ignition on Hot Surfaces**. Poster. 21st May 2015: SUPERGEN Researchers Day, Bath, UK

Y.S. Chin, L.I. Darvell, A.R. Lea-Langton, J.M.Jones, A. Williams. **Minimum Ignition Temperature and Ignition Delay Time of Dust Layers – An Experimental on Biomass Blends**. Poster. 16th-17th September 2015: International Energy Agency Clean Coal Centre – 5th Workshop on Cofiring Biomass with Coal Workshop, Selby, UK

Part of **Chapter 5** had been presented as listed:

J.M. Jones, K. Bindemann, A. Williams, M. Wang, L.I. Darvell, Y.S. Chin, A. Dyer, J. Oladipo, R. White. **Assessment of Spontaneous Combustion Risk, Including Biomass**. Poster. 6th October 2015: 64th Energy Science Lecture, London, UK

K. Bindemann, J.M. Jones, A. Williams, M. Wang, L.I. Darvell, Y.S. Chin, N.K. Brown. **Assessment of Spontaneous Combustion Risk, Including Biomass**. Poster. 20th September 2016: 65th Energy Science Lecture, Leeds, UK

Part of **Chapter 6** had been presented as listed:

Yee Sing Chin, Leilani I. Darvell, Amanda R. Lea-Langton, Jenny M. Jones, and Alan Williams. **Ignition Risks of Biomass Dust on Hot Surfaces**. Proceedings of XXII International Symposium on Combustion Processes. 22nd – 25th September 2015: XXII International Symposium on Combustion Processes, Jurassic Highland (Jura Region), Poland

Yee Sing Chin, Leilani I. Darvell, Amanda R. Lea-Langton, Jenny M. Jones, and Alan Williams. **Ignition Risks of Biomass Dust on Hot Surfaces**. Special Issue: International Symposium on Combustion Processes, Energy & Fuels 2016, 30, pp.4398–4404, DOI: 10.1021/acs.energyfuels.5b02622

Yee Sing Chin, Leilani I. Darvell, Amanda R. Lea-Langton, Jenny M. Jones, and Alan Williams. **Ignition Characteristics of Biomass Dust on Hot Surfaces**. Poster. 8th December 2015: Postgraduate Research Conference, Leeds, UK

Part of **Chapter 7** had been presented as listed:

Y.S. Chin, J.M. Jones, L.I. Darvell, A.R. Lea-Langton, A. Williams. **Biomass Handling – Dust Layer Ignition Risks**. Proceedings of IEA Bioenergy Conference. 26th – 29th October 2015: International Energy Agency Bioenergy Conference, Berlin, Germany

Part of **Chapter 8** had been presented as listed:

Y.S. Chin, A.R. Lea-Langton, J.M. Jones, A. Williams. **Emissions from Biomass on a Hot Surface**. Proceedings of International Biomass Emissions Conference. 14th – 15th September 2015: International Biomass Emissions Conference, Leeds, UK

Part of **Chapter 10** had been presented as listed:

Y.S. Chin, N.K. Brown, L.I. Darvell, K. Bindemann, J.M. Jones, A. Williams. **Biomass Self-Ignition Characteristics during Handling & Storage – Hot Storage Basket Tests on Pellets and Powder**. Poster. 22nd – 23rd March 2017: International Bioenergy Conference, Manchester, UK

Acknowledgements

First of all, a big thank you to University of Leeds for making everything possible! I am utterly grateful for the Leeds scholarship and convenience the accommodation office provided me with.

Indeed, I am thankful to have made it through this research. I owe thanks to my supervisors, Professor Jenny M Jones, Professor Alan Williams, Dr Leilani I Darvell and Dr Amanda R Lea-Langton (in University of Manchester); for their constant guidance.

Appreciation goes to my research group members, present and past – Ben Dooley, Diarmaid Clery, Douglas Phillips, Eddy Mitchell, Lee Roberts, Natalie Brown, Patrick Mason, Richard Birley, Dr. Abby Saddawi, Dr. Bijal Gudka, Dr. Farooq Atiku, Dr. Femi Akinrinola, Dr. Paula McNamee and Dr. Peinong Xing, for their valuable support and friendship. I am much indebted to Dr. Connie Ellul, Dr. Dave Waldron, Dr. Mi Wang, Mr. James Ashman and Mr. Karl Bindemann for their valuable feedback on industrial relevance from time-to-time. Also thank you to all power stations and research institutions for supplying me a variety of raw materials in this research.

I am also grateful to other university staff that had helped me along the way – Dr. Adrian Cunliffe, Ed Woodhouse, Gurdev Bhogal, Karine Thorne, Sara Dona, Simon Lloyd, Stuart Mickelthwait, Susanne Patel, David Haynes; Dr Patrick Biller and Dr Surjit Singh when they were still in Leeds. My sincere thanks go to researchers from other research groups – Aidan Smith, Amal Al-Rahbi, Andrew Dyer, Chibi Takaya, Dave Allen, Hafizah Yun, Harriet Fletcher, Hussain Al-Shamri, Hasimawaty Mat Kiah, Imran Khan, Jabbar Gardy, James Hammerton, Josh Cottom, Juniza Saad, Morgan Tachell-Evans, Sergio Solis, Yeshui Zhang, Zainab Adiya, Dr Antonio Salituro, Dr Buland Dizayi, Dr David Slatter, Dr M Anas Nahil, Dr M Azam Saeed and Dr S Zaheer Abbas for being considerate friends. Thanks is also extended to Adilah from Heriot-Watt University.

Special mention is due to Ben, Buland and Chibi who have always been encouraging and reassuring – not a day goes by that I do not think of all your kind and inspiring words that kept me going. Not forgetting my Cranfield buddies, Alastair, Catherine, Darren, Ellen; my high school besties, Sing Yee, Li Yun, Mann Yee for their endless encouragement, and their lovely kids Andrew, Benjamin, Esther and Rachel that bring me limitless joy in the UK! My other friends in Leeds, Georgios, Gioula, Kamla, Kisandra, Nassya, Rima, Shafa and Zai, thanks for your company.

Also thanks to Dr. C. Gorrard-Smith, Dr. N. Pearce, Dr. R. Chowdhury, Dr. T. Milligan, Dr. S. McCormack, Dr. A. Dworak-Kula & team, Mr. M. Philipson, Mr. I. Simmons & team and Mr. D. Mitchell for all the advice and needed support during my days in Leeds. My heartfelt thanks go to my family and loved ones who have always been thoughtful and understanding. Last but not least, my utmost thanks and sincere gratitude to my parents for their unshakeable patience, unconditional love, and for not giving up on me regardless how my condition was.

Abstract

As modernisation takes place, fossil fuel burning is one of the quickest ways to meet the ever rising energy demand. The increasing emissions of greenhouse gases, particularly carbon dioxide, as a result of excessive fossil fuel burning had been blamed for global climate change. Vegetation-based biomass is a form of bioenergy and a recognised solid renewable fuel with potential to replace coal in combating anthropogenic climate change in the power generation sector. Nevertheless, it is not a straight forward case for biomass to replace coal since biomass is an extremely reactive fuel prone to self-heating leading to self-ignition. Spontaneous biomass ignition leading to disastrous fires during biomass handling and storage could be avoided if the causes of biomass low temperature ignition are well understood.

Detailed studies on woody and herbaceous biomass fuels commonly used in UK power stations were examined according to several British Standards. On top of characterising all the biomass samples, BS EN 50281-2-1 and BS EN 15188 were adhered to specifically in investigating low temperature ignition during biomass handling and biomass storage respectively. Many power stations use a mix of different biomass in their fuel inventories which can lead to dusts of biomass mixtures. Thus the low temperature ignition characteristics of biomass blends have been studied. Other factors that may impact on ignition risks are binders (added to give strength to briquettes or pellets) and pretreatments (washing and torrefaction). Washing aims to improve ash properties towards the end of combustion process while torrefaction is used to increase the calorific value of biomass that is naturally lower than fossil fuels. The reaction kinetics of some biomass dust layers deposited on a constant temperature hot surface and corresponding ignition delay time were estimated mathematically.

Results from minimum dust layer ignition temperature determination showed that all biomass, regardless of woody or herbaceous, with or without binder, before or after pre-treatments, had critically ignited within a very small temperature range. This was consistent with the results of self-ignition propensity risk ranking that concluded that biomass possess medium-high risk of self-igniting. An exception to this is torrefied biomass which had not sustained a much higher temperature before it critically ignited as compared with the untreated counterpart; unlike many anticipations and therefore, the low temperature ignition characteristics were discussed from many other aspects, mainly on the reduced particle size or dust layer density. For biomass storage, scaling up method and Frank-Kamenetskii method derived from Thermal Explosion Theory had been applied to forecast the critical ignition temperature and ignition delay time for large-scale industrial storage from smaller laboratory scale experiments. Non-negligible error was detected when extrapolating to industrial volume especially for the ignition delay time and appropriate recommendation was made as a possible remedy.

Emissions when biomass smouldered and critically ignited that happened at 10°C apart were examined with a three-stage emission sampling and compared, with the aims of obtaining a suitable biomass self-ignition indicator. Detailed studies were required since only one organic compound was detected to be consistently different between smouldering and critically-igniting biomass dust. Within this small temperature difference, different volatile species with respective intensities had been modelled with FG-BioMass software.

Towards the end of this work, conclusions were drawn for each section and suggestion of combining both pre-treatments with binder addition were recommended for further studies. The work in the thesis provides a large data-set which will help inform power plant operators in their dust management risks. The laboratory-scale experiments give a useful risk-ranking for dust layer ignition, but uncertainties in ignition-delay times, especially for large biomass quantities, indicate that improvements are required to BS EN 15188 (biomass storage test) to enable scaling-up with more certainty.

Whatever I have tried to do in life, I have tried with all my heart to do it well; whatever I have devoted myself to, I have devoted myself completely; in great aims and in small I have always thoroughly been in earnest.

~Charles Dickens~

Table of Contents

List of Work Presented/Published.....	iii
Acknowledgements.....	v
Abstract	vi
Table of Contents	ix
List of Tables.....	xiv
List of Figures.....	xvii
List of Abbreviations.....	xxvii
List of Symbols.....	xxxii
Chapter 1 Introduction	1
1.1 Project Background	1
1.1.1 Global Emissions and Trend	2
1.1.2 Climate Change and Energy Policy – Global and the UK.....	4
1.2 Biomass and Biofuels in General	5
1.2.1 Biomass Categories.....	5
1.2.2 Biomass Components.....	6
1.3 Biomass Related Fire Accidents.....	6
1.4 Objectives and Scope of Study.....	7
1.4.1 Objectives of Study	7
1.4.2 Scope of Study	8
Chapter 2 Literature Review.....	10
2.1 Self-Heating, Self-Ignition and Smouldering Combustion of Biomass.....	11
2.1.1 Physical, Biological and Chemical Stages.....	12
2.1.2 Theory of Smouldering Combustion.....	13
2.2 Factors Affecting Self-Heating Characteristics.....	14
2.3 Handling – Biomass Dust Layer Deposition Ignition Characteristics	17
2.3.1 Ignition of Single Material Biomass	27
2.3.2 Ignition of Biomass Blended with other Materials.....	29
2.4 Reaction Kinetics Estimation and Ignition Delay Time Prediction for Dust Layer Ignition	31
2.4.1 Hot Surface Ignition Test Kinetic Parameters Estimation	32
2.4.2 Hot Surface Ignition Test Ignition Delay Time Prediction	41
2.5 Storage – Biomass Pile Ignition Characteristics	42

2.6 Pre-treatment Techniques for Biomass.....	51
2.6.1 Biomass Washing	51
2.6.2 Biomass Torrefying.....	56
2.6.2.1 The Torrefaction Process, Mass and Energy Balance.....	57
2.6.2.2 Atomic Ratio in Relation with Higher Heating Value, Torrefied Fuel Characterisation and Benefits of Torrefaction	61
2.6.2.3 Torrefied Biomass Particle Size Distribution, Surface Area and Surface Morphology Determination	68
2.6.2.4 Previous Studies on Torrefied Biomass: Addressing the Gap of Knowledge for Self-Heating and Ignition Risk	70
2.7 Emission from Biomass on a Hot Surface	72
Chapter 3 Methodology.....	76
3.1 Instruments and Procedures Applied	76
3.1.1 Sample Preparation	76
3.1.2 Proximate Analysis, Reaction Rate Kinetics and Self-Ignition Risk Ranking	80
3.1.2.1 Thermogravimetric Analysis Studies	84
3.1.3 Ultimate Analysis and Higher Heating Value Calculation.....	90
3.1.4 Biomass Dust Layer Ignition	92
3.1.5 Biomass Blends Dust Layer Ignition.....	97
3.1.6 Estimating Reaction Kinetics and Predicting Ignition Time for Biomass Dust Layer Ignition.....	101
3.1.7 Biomass Storage Ignition	105
3.2 Biomass Pre-treatment.....	111
3.2.1 Washing of Biomass.....	111
3.2.1.1 Lab Scale Biomass Water Washing Procedure.....	112
3.2.1.2 Acid Digestion of Biomass for Metals Analysis via AAS	114
3.2.1.3 Atomic Absorption Spectrophotometry on Digestate	115
3.2.1.4 Lignocellulosic Analysis	116
3.2.1.5 Ion Chromatography on Biomass Leachates	117
3.2.1.6 Total Organic Carbon Analysis on Biomass Leachates	118
3.2.2 Torrefaction of Biomass	119
3.2.2.1 Bench-Scale Torrefaction Procedure.....	119
3.2.2.2 Proximate Analysis, Reaction Rate Kinetics and Self-Ignition Risk Ranking on Torrefied Biomass	122
3.2.2.3 Ultimate Analysis, High-Heating Value Determination on Torrefied Biomass.....	123

3.2.2.4 Minimum Dust Layer Ignition Temperature (T_{LIT}) of Torrefied Biomass	123
3.2.2.5 Torrefied Biomass Particle Size Distribution	123
3.2.2.6 Torrefied Biomass Surface Area Determination	125
3.2.2.7 Torrefied Biomass Surface Morphology	127
3.3 Emissions from Biomass on a Hot Surface	129
3.3.1 Sampling.....	129
3.3.2 Extraction	134
3.3.3 Analysis	134
3.3.3.1 GC-MS Analysis of Extracts	136
3.3.3.2 TGA Analysis of Filters.....	140
3.3.4 Lower Flammability Limits	140
Chapter 4 Handling – Biomass Dust Layer Ignition Characteristics.....	142
4.1 Proximate, Ultimate Analyses and Higher Heating Values	144
4.2 Self-Ignition Propensity Risk Ranking	147
4.3 Minimum Ignition Temperature Determination, Ignition Delay Time Determination, Effects of Deposition Thickness	150
4.4 Industrial Significance.....	164
4.5 Concluding Remarks and Suggestions for Future Work	168
Chapter 5 Handling – Effects of Binders on Biomass Dust Layer Ignition Characteristics.....	171
5.1 Proximate, Ultimate Analyses and Higher Heating Values	172
5.2 Self-Ignition Propensity Risk Ranking	177
5.3 Minimum Ignition Temperature Determination and Ignition Delay Time	179
5.4 Industrial Significance.....	183
5.5 Effects of Having Different Binders.....	185
5.5.1 py-GC-MS on Binders	187
5.5.2 Pyrolysis Extent at Different Dust Layer Heights	190
5.6 Concluding Remarks and Suggestions for Future Work	196
Chapter 6 Handling – Effects of Washed Biomass Dust Layer Ignition Characteristics ..	198
6.1 Proximate, Ultimate Analyses and Higher Heating Values	199
6.2 Self-Ignition Propensity Risk Ranking and Reaction Kinetic Shift	203
6.3 Determining Dust Layer Minimum Ignition Temperature and Ignition Delay Time	206
6.3.1 Industrial Significance	212

6.4 Effects of Water Washing Biomass – Removal of Elements, Total Organic Carbon in Leachates, Changes in Lignocellulosic Composition.....	214
6.5 Concluding Remarks and Suggestions for Future Work.....	218
Chapter 7 Handling – Effects of Torrefied Biomass on Dust Layer Ignition	
Characteristics	220
7.1 Proximate, Ultimate Analyses and Higher Heating Values.....	224
7.2 Self-Ignition Propensity Risk Ranking.....	231
7.3 Minimum Ignition Temperature Determination and Ignition Delay Time	232
7.4 Particle Surface Area Determination and Morphology Analysis	239
7.5 Industrial Significance	241
7.6 Concluding Remarks and Suggestions for Future Work.....	242
Chapter 8 Comparisons of Emissions from Pre-Igniting and Igniting Biomass Dust Layers	245
8.1 Emissions from Sampler 1 – Inverted Funnel.....	246
8.2 Emissions from Sampler 2 – Filter Paper.....	251
8.3 Emissions from Sampler 3 – ORBO™ 43	255
8.4 Elemental Carbon and Organic Carbon from Biomass Emissions.....	258
8.5 Predicted Volatile Species and Intensities Modelled by FG-BioMass	260
8.6 Concluding Remarks and Suggestions for Future Work.....	263
Chapter 9 Hot Surface Ignition Test – Reaction Kinetics Estimation and Ignition Delay Time Prediction.....	265
9.1 Reaction Kinetics Estimation	265
9.2 Ignition Delay Time Prediction.....	270
9.3 Concluding Remarks and Suggestions for Future Work.....	274
Chapter 10 Storage – Hot Storage Basket Experiment	275
10.1 Fuel Characterisation and Self-Ignition Risk Ranking of White Wood Pellets (WWP).....	277
10.2 Scaling Up Method – Critical Ignition Temperature and Ignition Delay Time Comparisons between Biomass Samples in Different Forms.....	280
10.3 F-K Method – Self-Ignition Characteristics Comparison between Biomass Samples in Different Forms and Using Different Methods	294
10.4 Concluding Remarks and Suggestions for Future Work	298
Chapter 11 Overall Findings, Conclusions and Recommendations for Future Work	302
11.1 Overall Findings and Conclusions	302
11.2 Recommendations for Future Work	305

List of References	307
Appendix A Kinetic Parameters of Samples Evaluated	322
Appendix B Input and Property Values Used in Computation of Reaction Kinetics	324

List of Tables

Table 2. 1 Untreated and Torrefied Solid Fuel Properties Comparison (Jong and Ommen, 2015)	64
Table 2. 2 Transportation Costs, Hygroscopic and Biological Degradation Properties Comparison between Untreated and Treated Biomass (Jong and Ommen, 2015). 67	
Table 2. 3 Comparing Untreated Biomass with Torrefied Biomass	68
Table 2. 4 Biomass Combustion – Six Emissions Categories with Some Component Examples (Sheesley et al., 2003)	74
Table 2. 5 Pyrolysing Biomass – Some Compounds and Key Markers (D.J. Nowakowski, 2008).....	74
Table 3. 1 LFL for Major Volatile Components from Eight Biomass Samples	141
Table 4.1 Four Main Samples Used – Original Form Received and Composition	143
Table 4.2 Composition of Six Woody-Herbaceous Biomass Binary Blends.....	143
Table 4.3 Proximate Analysis of Four Parent Materials and Six Binary Blends Studied	144
Table 4.4 Ultimate Analysis of Four Main Samples and Six Binary Blends Studied Used (dry basis).....	145
Table 4.5 HHV (on Dry Basis) of Four Parent Materials Used	146
Table 4.6 Thermogravimetric T_{MWL} and E_a of Four Parent Materials and Six Binary Blends	147
Table 4.7 Range of T_{LIT} (10°C Interval) and Corresponding Ignition Delay Time for Four Parent Materials	151
Table 4.8 T_{LIT} and Corresponding Ignition Delay Time for Four Parent Materials and Six Blends Before (10°C Interval) and After Temperature Refinement (5°C Interval)	155
Table 4.9 Comparison of T_{LIT} Prediction Equations Before and After Temperature Refinement Process.....	163
Table 4.10 T_{LIT} Obtained or Estimated for Three Dust Layer Thicknesses after Temperature Refinement Procedure.....	165
Table 5. 1 Samples Used in Binder Effect Study – Original Form and Composition in Weight Percent of Ten Samples	172
Table 5. 2 Proximate Analysis of All Samples Used in Binder Effect Study	173
Table 5. 3 Ultimate Analysis of All Samples Used in Binder Effect Study	173
Table 5. 4 Ultimate Analysis of Two Binders Used in Binder Effect Study.....	174
Table 5. 5 HHV of Samples Used in Binder Effect Study	175
Table 5. 6 Binder Effect – T_{LIT} and Ignition Delay Time of Twelve Samples in Ring A....	179
Table 5. 7 MPST Calculation/Estimation Following Guideline1 and Guideline2 for 5 mm Dust Thickness	184

Table 5. 8 Ten Major Elements in Two Binders Identified by py-GC-MS	189
Table 6. 1 Samples Used in Washing Study with Respective Original Form and Washing Condition (Solvent Temperature in °C, Washing Duration in Minutes).....	198
Table 6. 2 Proximate Analysis (wt%) of all Samples Used in Biomass Washing Study ..	199
Table 6. 3 Ultimate Analysis (wt%) and Higher Heating Value (MJ/kg) of all Samples Used in Biomass Washing Study.....	202
Table 6. 4 Dust Layer Ignition Temperatures with Corresponding Ignition Delay Times and T_{LIT} Case in Bold.....	207
Table 6. 5 Concentration (mg/kg of Dry Fuel) in Untreated Fuels (AAS Analysis) and K, Ca, and Cl Removed (mg/kg of Dry Fuel) during Water Washing (IC Analysis of Leachates)	215
Table 7. 1 Samples Used in Torrefaction Studies with Respective Original Form and Torrefaction Condition (Torrefaction Temperature in °C, Residence Time in Minutes).....	221
Table 7. 2 Proximate Analysis (wt%) and Relevant Changes of all Samples Used in Torrefaction Studies	225
Table 7. 3 Ultimate Analysis, Higher Heating Value and the Relevant Changes of all Samples Used in Torrefaction Studies.....	228
Table 7. 4 Minimum Dust Layer Ignition Temperature (T_{LIT}), Ignition Delay Time and Density in Ring A of Torrefied Biomass, Untreated Biomass and Torrefied-Untreated Biomass Blend.....	234
Table 7. 5 BET Surface Area Analysis of Five Samples.....	239
Table 8. 1 Biomass Samples and Their Respective Temperatures for Emission Capture Experiment	245
Table 8. 2 Funnel – Similar Emission Components identified for all Eight Samples.....	249
Table 8. 3 Filter Paper – Similar Emission Components identified for all Eight Samples.....	254
Table 8. 4 ORBO Tube – Similar Emission Component Identified for all Eight Samples.....	257
Table 8. 5 LFL for Gases and Light Volatiles Estimated for Eight Pre-Igniting Biomass Samples.....	262
Table 8. 6 LFL for Gases and Light Volatiles Estimated for Eight Critically-Igniting Biomass Samples.....	262
Table 9. 1 Reaction Activation Energy (E) and Pre-Exponential Factor (A) Estimated with Some Dimensionless Parameters Involved.....	267
Table 9. 2 Ignition Delay Time Prediction with Four Correlations for Dust Layers Igniting on Low Temperature Hotplate.....	272
Table 10. 1 WWP Samples Used in Hot Storage Basket Test.....	276
Table 10. 2 Particle Size Distribution of Milled a.r. WWP Samples (Dooley, 2016)	276
Table 10. 3 Proximate Analysis of WWP Sample.....	277

Table 10. 4 Ultimate Analysis of WWP Sample.....	278
Table 10. 5 Higher Heating Value (HHV) Estimation of WWP Sample	278
Table 10. 6 Scaling Up Method Predicted Linear Equations for TSI and t_i Extrapolation to Larger Storage Volumes with Regression Coefficient, R^2 and Uncertainty /Error Associated.....	291
Table 10. 7 Comparison between Scaling Up Method and F-K Method.....	296

List of Figures

Figure 1. 1 Stages of Fire Triggered by Material Self-Ignition – Heating up, Self-heating, Smouldering to Glow fire [Edited from: Babrauskas et al. (2009), p.29]	2
Figure 1. 2 World Energy-Related Carbon Dioxide Emissions by Fuel Type, from 1990 to Projected 2040 [Source: U.S. Energy Information Administration (2016), p.141]... 3	3
Figure 1. 3 Total GHG Emissions and Component in the [Edited from: Office for National Statistics (2016)].....	3
Figure 1. 4 Emissions Common to Commercial Combustion and Power Generation Sector in the UK (a) Sulfur Dioxide, in million tonnes (b) Nitrogen Oxides, in million tonnes (c) Particulate Matters, in thousand tonnes [Source: DEFRA (2016), p.29]	3
Figure 1. 5 Total World Primary Energy Supply [Edited from: PBL Netherlands Environmental Assessment Agency (2016), p.48].....	4
Figure 1. 6 Biomass Composition – Hemicellulose, Cellulose, Lignin and the Chemical Structure of Each [Source: Wang et al. (2014), p. 549]	6
Figure 2. 1 Physical, Biological and Chemical Stages of the Self-Heating Process in Stored Biomass [Source: (Hogland and Marques, 2003)].....	12
Figure 2. 2 Freshly produced pellets, with pellets at elevated temperatures due to self-heating and the visible “smoke” probably is a combination of moisture and various gases [Source: (IEA Bioenergy, 2013) p.17]	13
Figure 2. 3 Understanding Fire [Source: Fire Safety Advice Centre (2016)] (a) Fire Triangle (b) Fire Tetrahedron.....	14
Figure 2. 4 Dust Layer Ignition Temperature [Source: Querol et al. (2006)] as a Function of (a) Layer Thickness (b) Layer Diameter.....	21
Figure 2. 5 Maximum Permissible Surface Temperature as a Function of Layer Depth, Depending on T_{LIT} Range (British Standard, 1999a)	24
Figure 2. 6 Minimum Dust Layer Ignition Temperature as a Function of Its Thickness – Summary from Some Studies.....	27
Figure 2. 7 Biomass Dust Layer Deposited on a Hot Plate	33
Figure 2. 8 Thermal Runaway Phenomenon (a) Heat Balance in a System Generating and Losing Heat (b) Temperature Profile within Dust Layer [Edited from: Park et al. (2009)]	35
Figure 2. 9 Correlation between δ_c , B_i , θ_a , θ_m and z_m for Asymmetrically Heated Slab [Source: Park et al. (2009)]	37
Figure 2. 10 Correlation between Q_A and E at fixed T_p [Edited from Source: Park et al. (2009)].....	39
Figure 2. 11 δ_c as a Function of α and θ_a [Edited from Source: Thomas and Bowes (1961)].....	40

Figure 2. 12 Example of Crude Estimation of E Via a Simple Correlation for Sawdust [Source: Babrauskas (2003a)]	40
Figure 2. 13 Correlation of Time to Ignition – Hot Surface Temperature for Cornflour-Wheatflour Mixture [Edited from Source: El-Sayed and Abdel-Latif (2000)].....	41
Figure 2. 14 Hot Storage Basket Experiment – Idealised Dust Temperature Versus Time Results for Dust Samples of the Same Volume [Source: British Standard (2008) p.10]	46
Figure 2. 15 Hot Storage Basket Experiment – Temperature-Time Plot of Wood Chips Subjected to Hot Storage Temperature of 213°C [Source: Saddawi et al. (2013a)]	47
Figure 2. 16 Hot Storage Basket Experiment – Superimposing TSI Results on BS 15188 Graph [Source: Saddawi et al. (2013a)]	48
Figure 2. 17 Hot Storage Basket Experiment – Superimposing t_i Results on BS 15188 Graph [Source: Saddawi et al. (2013a)].....	48
Figure 2. 18 Hot Storage Basket Experiment – TSI Results of Miscanthus at Different Harvest Period [Edited from: Everard et al. (2014)]	49
Figure 2. 19 Hot Storage Basket Experiment – TSI Results of Five Samples [Edited from: Veznikova et al. (2014)]	49
Figure 2. 20 TSI at Reduce Atmospheric Pressure [Source: Seitz et al. (2016)] of (a) Carbon Black (Norit CN 4) (b) Wheat Flour (type 405)	50
Figure 2. 21 Unique Way of Biomass DI Water Washing [Source: Deng et al. (2013)]	54
Figure 2. 22 Typical Torrefaction Products with CO ₂ and CO as Main Components [Edited from: (Dahlquist, 2013)].....	57
Figure 2. 23 Temperature-Time Profile in Biomass Torrefying Process - Five Key Stages of the Torrefaction Process [Edited from: (Bergman et al., 2005)].....	58
Figure 2. 24 Colour Variation of Woody Biomass (Top Row, Beech Wood) and Herbaceous Biomass (Bottom Row, Miscanthus) as a Function of Torrefaction Temperature (a) Untreated (b) 240°C (c) 260°C (d) 280°C (e) 300°C at a Fixed Residence Time [Edited from: (Gucho et al., 2015)].....	59
Figure 2. 25 Typical Mass (M) and Energy (E) Balance of Biomass Torrefaction Process [Source: (Bergman et al., 2005)]	60
Figure 2. 26 Example of (a) Mass Yield and (b) Energy Yield of Biomass Torrefaction [Source: (Gucho et al., 2015)]	61
Figure 2. 27 The Van-Krevelen Diagram [Source: (Basu, 2013)]	62
Figure 2. 28 Torrefied Biomass Location (in Red Box) in the Van-Krevelen Diagram [Source: (van der Stelt et al., 2011)]	63
Figure 2. 29 Transport Cost as Function of Energy and Density for Untreated and Torrefied Wood Pellets [Source: (Gårdbro, 2014)]	65
Figure 2. 30 Grindability of Torrefied Biomass (a) Particle size distribution curves for untreated and torrefied Miscanthus and four standard reference coals of HGI 32, 49, 66 and 92 [Source: (Bridgeman et al., 2010)] (b) Milling Energy Requirement for Torrefied Woodchips at Various Torrefaction Temperature and Torrefaction Time [Source: (Gårdbro, 2014)]	66

Figure 2. 31 Self-Ignition Temperatures of Wood Chips and Torrefied Wood Chips [Source: (Saddawi et al., 2013a)].....	71
Figure 2. 32 Gas Emissions Test Setup with Temperature Control and Gas Collection System [Edited from: Anez et al. (2015)].....	73
Figure 3. 1 Retsch SM300 Cutting Mill with Major Parts Labelled.....	77
Figure 3. 2 Retsch Planetary Ball Mill PM 100 used in Biomass Grinding [Source: (Retsch, 2010)].....	78
Figure 3. 3 Retsch PM100 Ball Mill (a) Counter Weight Adjusting Knob (b) Grinding Bowl and Grinding Balls (c) Grinding Bowl Clamp.....	78
Figure 3. 4 SPEX Freezer Mill for Biomass Cryomilling.....	79
Figure 3. 5 SPEX Vial, End Plugs and Metal Impactor.....	79
Figure 3. 6 Retsch Sieve Shaker AS 200.....	79
Figure 3. 7 Brown Silica Gel Desiccator to Condition the Dried Samples before Experiments.....	79
Figure 3. 8 Proximate Analysis for Moisture (a) Carbolite MFS Oven (b) Samples in Weighing Dishes and Separated Lids Entering the Oven.....	81
Figure 3. 9 Proximate Analysis for Volatile Matters (a) Carbolite AAF 1100 Furnace (b) Sample Crucibles Held by Special Stand.....	82
Figure 3. 10 Proximate Analysis for Ash Content (a) Carbolite AAF 11/18 Furnace (b) Unlidded Sample Crucibles Preparing to Enter the Furnace.	84
Figure 3. 11 Proximate Analysis Conducted via TGA Method on Empty Fruit Bunches Biomass [Source: (Slatter, 2015)].....	85
Figure 3. 12 Proximate Analysis Conducted via TGA Method on Biomass in General [Source: (Reed, 1981)].....	85
Figure 3. 13 Thermogravimetric Analysis (a)TA Q5000 Equipment (b) Loading Sample onto TGA Q5000 Platinum Pans (c) TGA Q5000 Running in Progress....	86
Figure 3. 14 Biomass TGA Decomposition Profile Subjected to Slow Combustion.....	88
Figure 3. 15 Section Selected for Kinetics Calculation.....	88
Figure 3. 16 Linear Regression of Reaction Rate Constant for one of the Biomass Samples.....	88
Figure 3. 17 Slow Combustion TGA of a Biomass– Weight Loss Curve and T_{MWL} Obtained from the Derivative Weight Loss Curve.....	89
Figure 3. 18 Self-Ignition Risk Pictorial Assessment Tool Application on (a) Twelve Materials [Source: Ramírez et al. (2010)] (b) Fourteen Materials [Source: Jones et al. (2015)].....	89
Figure 3. 19 Ultimate Analysis on Solid Fuel (a) FLASH EA1112 Elemental Analyzer (b) Dedicated Capsule Sealing Tools (c) Materials used as Standards (d) Some Materials used as Reference.....	90

Figure 3. 20 Calorific Value Determination with Bomb Calorimeter (a) Parr 6200 Isoperibol Bomb Calorimeter (b) Specac manual hydraulic press (c) Some Components of the Parr Calorimeter.....	92
Figure 3. 21 Placement of Dust Layer Ignition Rig.....	94
Figure 3. 22 Dust Layer Test Rig Manufactured by ANKO, Dust Layer TC Vertical Level Adjustment Nut.....	94
Figure 3. 23 Temperature Distribution Check (a) Actual Setup & Schematic (b) Location of Points, Top View.....	95
Figure 3. 24 Tools Used in Dust Layer Experiment – Measuring Beaker, Ring A, Ring B, Tong, Dust Collector and Leveller; Slots for Dust Layer TC.....	97
Figure 3. 25 Blending of Two Biomass Dust Species (a) Weighing Blend Constituent (b) Blending with Sieve Shaker.....	98
Figure 3. 26 py-GC-MS Analysis Components (a) All in One (b) CDS Pyroprobe 5000 Series (c) Shimadzu GC-2010 Gas Chromatograph (d) Shimadzu GCMS-QP2010 Gas Chromatograph Mass Spectrometer.....	98
Figure 3. 27 Experimented Dust in Ring A (a) Location for Dust Scooping (b) Spatula for Dust Picking.....	101
Figure 3. 28 Biomass Dust Layer Deposited on a Hot Plate – Infinite Slab of Given Thickness $2r$ Assumption.....	102
Figure 3. 29 Infrared Thermometer Used in Experiment.....	102
Figure 3. 30 A Desk Thermometer.....	102
Figure 3. 31 Biomass Thermal Conductivity [Source: Mason et al. (2016)].....	103
Figure 3. 32 Hot Storage Basket Tests (a) Experiment Setup and with Major Components (b) Oven Schematic with Inner Chamber and Parts [Edited from: British Standard (2008)] (c) Actual Inner Chamber Used.....	107
Figure 3. 33 Three Custom Made Baskets for HSBT – Basket S, Basket M & Basket L (L to R).....	108
Figure 3. 34 Three Thermocouples and Basket L Placed on Metal Structure.....	108
Figure 3. 35 Placement of Three Thermocouples.....	108
Figure 3. 36 Distilled Water Washing of Miscanthus Samples at Room Temperature and 500 rpm Stirring Speed.....	113
Figure 3. 37 Biomass Washing Pre-treatment (a) Buchner Funnel Filtration with Erlenmeyer Flask Connected to a Pump (b) Solid Residues (c) Leachate/Filtrate (Liquid) Collected.....	113
Figure 3. 38 Sample Acid Digestion in Fume Cupboard – Concentrated H_2SO_4 and Concentrated HNO_3 to be added to Biomass-Filled Conical with Tilt Measure...	114
Figure 3. 39 Agilent Varian AA240FS Fast Sequential Atomic Absorption Spectrometer	115
Figure 3. 40 IC Preparation: (a) The Dionex DX100 instrument (b) Control and Leachate Samples being Prepared in Volumetric Flasks (c) Control and Diluted Leachate Samples in Dionex DX100 Vials.....	117

Figure 3. 41 Hach Lange IL550 for Total Organic Carbon Analysis	119
Figure 3. 42 Three Zone Horizontal Furnace Used for Torrefaction	120
Figure 3. 43 Thermocouples (TC1, TC2 & TC3) Connected to Computer for Temperature Recording via a Data Logger & Hot Reactor Tube Resting on Metal Rest while Quenched by Nitrogen	120
Figure 3. 44 (a) ~100g of Cooled, Torrefied Biomass Sandwiched between Two Glass Wool Plugs Ready for Removal from Borosilicate Reactor Tube (b) Oven-Dried PineR Chips Before Torrefaction (c) After Torrefaction	121
Figure 3. 45 Torrefied biomass and Untreated Biomass (a) Contained in Measuring Cups (b) Blended Using Retsch AS 200 Sieve Shaker (c) Blend Contained in Sieve Shaker Tray.....	122
Figure 3. 46 Malvern Mastersizer 2000E with Small Volume Sample Dispersion Unit, Optical Unit and Dispersion Unit Controller	123
Figure 3. 47 The NOVA [®] 2200e Multi- station Any-gas Sorption Analyser Standard Model v10.03	126
Figure 3. 48 An Example of Adsorption/Desorption Plot, for PineC	127
Figure 3. 49 An Example of Multi-Point BET Plot, for PineC	127
Figure 3. 50 The Agar High Resolution Sputter Coater.....	128
Figure 3. 51 Hitachi TM3030 Benchtop SEM Set (a) Hitachi TM3030 SEM, Mount with Sample Holder, Computer with Appropriate Software (b) Distance Measurement between Mount Top and Sample Filled Stub before SEM (c) Sample Entering SEM Equipment for Analysis.....	129
Figure 3. 52 The Emission Samplers Clamped on a Portable Retort Stand	130
Figure 3. 53 The Schematic of the Final Experiment Set-Up	131
Figure 3. 54 An ORBO Tube with Glass Wool and Granule Spaced Alternately.....	132
Figure 3. 55 The Dedicated ORBO Tube Cutter	132
Figure 3. 56 The Universal Flowmeter Applied in Experiment	133
Figure 3. 57 The Volume Counter Used to Calibrate the Universal Flowmeter.....	133
Figure 3. 58 Set-up of Mock Runs for Flowmeter Calibration	134
Figure 3. 59 Nitrogen Blower – The Six Port Mini-Vap Evaporator/Concentrator	135
Figure 3. 60 The Perkin Elmer Clarus 560 Equipment	135
Figure 3. 61 Simplify Illustration of a Gas Chromatographer [edited from (CHROMacademy, 2016)].	136
Figure 3. 62 Sampler 1 – (a) Funnel with Yellowish /Brownish Bio-Oil Deposits (b) Funnel subjected to DCM Rinsing (c) GC-MS ready solutions and Inter Sample Injector Cleaning DCM	137
Figure 3. 63 The Dionex ASE350 equipment	138
Figure 3. 64 ASE Cell Preparation (a) Filter Paper (b) ORBO tube	138

Figure 3. 65 Sampler 2 – (a) A GF/F Filter Paper wit Emissions Captured (b) Solutions from ASE Rinsed Filter Papers (c) Nitrogen-Blower Concentration of Solutions in ASE Vial	138
Figure 3. 66 Sampler 3 – (a) A Capped ORBO Tube with Emissions Captured (b) Solutions from ASE Rinsed ORBO tube (c) A Batch of GC-MS Ready Solutions in Perkin Auto Sampler Vials	139
Figure 3. 67 Shimadzu TGA-50 Equipment	140
Figure 3. 68 Filter Paper Preparation for Shimadzu TGA-50	140
Figure 4.1 Self-Ignition Propensity Risk Ranking for Four Parent Biomass and Six Biomass Blends	149
Figure 4. 2 Result of Temperature Uniformity Check on ANKO Dust Rig	150
Figure 4. 3 T_{LIT} Determination Experiment on Wheat Straw Dust in Ring A – Temperature-Time Plot.....	152
Figure 4. 4 T_{LIT} Experiment on PM(1)5050 Dust in Ring A – Ignited at 310°C.....	153
Figure 4. 5 T_{LIT} Experiment (with Refinement Step) on PWS9010 Dust Blend in Ring A	158
Figure 4.6 log(dust thickness) vs Inverse T_{LIT} in Kelvin scale for Ten Samples (a) Before T_{LIT} Refinement for Four Parent Materials (b) After T_{LIT} Refinement (c) Before T_{LIT} Refinement for Six Blends (d) After T_{LIT} Refinement for Six Blends	162
Figure 4.7 Results of Current Work Fitted Well on the log(dust thickness) vs Inverse T_{LIT} in Absolute Temperature Scale from Some Selected Studies	162
Figure 4.8 MPST Estimation with Three Different Methods – Guideline 1 (Points), Guideline 2 (Curves, T_{LIT} from Pre-Refinement) and Power Station Practice (Constant at 150°C)	165
Figure 4.9 T_{LIT} and Guideline1 MPST Determined from Table 4.9 Equations for Ten Samples (a) Before T_{LIT} Refinement for Four Parent Materials (b) After T_{LIT} Refinement for Four Parent Materials (c) Before T_{LIT} Refinement for Six Blends (d) After T_{LIT} Refinement for Six Blends.....	168
Figure 5. 1 Chemical Structure of (a) Lignosulfonate (ChemicalRegister, 2016) (b) Corn Flour (PubChem, 2016).....	176
Figure 5. 2 Binder Effect – Self-Ignition Propensity Risk Ranking of Twelve Materials .	178
Figure 5. 3 Dust Layer Ignition Temperature Profile of Misc(2)CF980	181
Figure 5. 4 TGA Weight Loss Curves Comparison of Twelve samples – With and Without Binders.....	182
Figure 5. 5 MPST Estimations of Samples with and Without Binder with Three Different Methods – Guideline 1 (Points), Guideline 2 (Curves, T_{LIT} from Pre-Refinement) and Power Station Practice (Constant at 150°C)	185
Figure 5. 6 Slow Combustion TGA Mass Loss and Derivative Mass Loss (DTG) Profiles of (a) Ligno-Bond-DD Powder (Lignosulfonate) (b) Cornflour (i.e. Cornstarch) ...	186
Figure 5. 7 DTG Profiles Comparison of Misc(1)Lg980 and Misc(1)CF980	187
Figure 5. 8 py-GC-MS Chromatogram of (a) Ligno-Bond-DD Powder Binder (b) Cornflour Binder	188

Figure 5. 9 Colour Variation of A Biomass Dust Layer Subjected to Non-Igniting Hot Plate Temperature.....	190
Figure 5. 10 Moisture and Volatile Matters Comparisons Among Unreacted, Ignited and Pre-Ignited Dust from Eight Materials with LignoBond or Cornflour Binder for (a)Miscanthus(1) (b)Pine (c) Miscanthus(2) (d)Wheat Straw	192
Figure 5. 11 Misc(2)Lg980 (a)TGA Weight Loss Curve (b)DTG Curve.....	194
Figure 5. 12 Misc(2)Lg980 (a)TGA Weight Loss Curve (b)DTG Curve.....	195
Figure 6. 1 Palm Kernel Shell – Ash Reduction and HHV Increment Upon Water-Washing Pre-treatment [edited from: Rahman et al. (2016)]	201
Figure 6. 2 Self-Ignition Propensity Risk Comparison between Untreated and Washed Biomass.....	203
Figure 6. 3 Comparison of DTG Profiles of (a) Rice Straw (Jenkins et al., 1998a) (b) Corn Stalk (Deng et al., 2013) before and after Leaching Pre-treatment	204
Figure 6. 4 DTG Profiles Before and After Washing Pre-treatment (a) Individual Material Slow Combustion: Misc(1) and wMisc(1) (b) Blend Slow Pyrolysis: 50PineC-50Misc(1) and 50wPineC-50wMisc(1)	206
Figure 6. 5 Temperature-Time Plot of 5-mm thick PineC Dust Layer on ANKO Dust Rig	209
Figure 6. 6 Temperature-Time Plot of 5-mm thick 50wPineC-50wMisc(1) Dust Layer on ANKO Dust Rig	210
Figure 6. 7 TGA Slow Combustion Weight Loss Curves Comparison of Eight Samples – Before and After Washing	212
Figure 6. 8 MPST Estimation with Three Different Methods – Guideline 1 (Points), Guideline 2 (Curves, T_{LIT} from Pre-Refinement) and Power Station Practice (Constant at 150°C) on Untreated and Washed Biomass Samples	213
Figure 6. 9 Leachates from 1 Hour Washing Pre-treatment of (a) Miscanthus Pellets (b) Pine Chips	215
Figure 6. 10 TOC and TI Comparisons (in ppm) of Pine and Miscanthus Leachates upon 1 hour Washing Pre-treatment.....	216
Figure 6. 11 Lignocellulosic Analysis on Eight Untreated, Washed Biomass and Blends	217
Figure 7. 1 Biomass For Torrefaction (a) Untreated PineR Chips (b) Untreated Misc(1) Pellets before Torrefaction.....	221
Figure 7. 2 Torrefaction Temperature Profile of PineR Torrefied at 270°C with 30 minutes Residence Time (Stages: 1-initial heating, 2-pre-drying, 3-post-drying & intermediate heating, 4-torrfection and 5-solid cooling).	222
Figure 7. 3 Torrefaction of PineR – Yellowish tar/bio-oil Resulted at the Right Connector and Collected at the Bottom.....	223
Figure 7. 4 Biomass After Torrefaction (a) PineR Chips (b) Misc(1) Pellets	223
Figure 7. 5 The Van Krevelen Diagram of Samples Used in the Present Torrefaction Study.....	229
Figure 7. 6 Biomass, Torrefied Biomass and Coal Regions on the Van Krevelen Diagram (Medina, 2014).....	230

Figure 7. 7 Mass Yields of Torrefying Various Biomass for 30-min as a Function of Torrefaction Temperature [edited from (Gucho et al., 2015)].....	231
Figure 7. 8 Self-Ignition Risk Ranking of Torrefied, Torrefied-Untreated Blend, Torrefied-Torrefied Blend and Untreated Biomass Samples.....	232
Figure 7. 9 Samples <180µm for Dust Layer Experiment (a) Misc(1) (b) tMisc(1) (c) 50tM(1):50M(1) (d) PineR (e) tPineR.....	233
Figure 7. 10 50tM(1):50M(1) in Ring A Igniting on 290°C Hotplate	234
Figure 7. 11 Temperature-Time Plotted by ANKO Software on 50tM(1):50M(1) Blend	235
Figure 7. 12 Obtaining Sample Dust Weight using a Balance.....	236
Figure 7. 13 Particles Size Distribution of Misc(1), tMisc(1) and 50tM(1):50M(1) used in T _{LIT} Determination Experiment	236
Figure 7. 14 TGA Slow Combustion Weight Loss Curves Comparison of Five Samples – Untreated, Torrefied and Untreated-Torrefied Blend	238
Figure 7. 15 SEM Micrograph of (a) Misc(1) (b) tMisc(1) (c) 50tM(1):50M(1) (d) PineR (e) tPineR at 800x Magnification.....	241
Figure 7. 16 MPST Estimation with Three Different Methods – Guideline 1 (Points), Guideline 2 (Curves, T _{LIT} from Pre-Refinement) and Power Station Practice (Constant at 150°C) on Torrefied, Torrefied-Untreated Blend and Untreated Biomass Samples.....	242
Figure 8.1 Sampler 1 – TIC of Woody Pine Emissions	247
Figure 8.2 Sampler 1 – TIC of Blend PM(2)5050 Emissions.....	248
Figure 8. 3 Sampler 1 – Peak Area Percentages of Similar Components at Pre-ignition and Critical Ignition Stages	251
Figure 8. 4 Sampler 2 – TIC of Woody Pine Emissions.....	252
Figure 8. 5 Sampler 2 – TIC of Blend PM(2)9010 Emissions	253
Figure 8. 6 Sampler 2 – Peak Area Percentages of Similar Components at Pre-ignition and Critical Ignition Stages	255
Figure 8. 7 Sampler 3 – TIC of Herbaceous Miscanthus(2) Emissions	256
Figure 8. 8 Sampler 3 – TIC of Blend PM(2)9010 Emissions	256
Figure 8. 9 Sampler 3 – Peak Area Percentages of Similar Component at Pre-ignition and Critical Ignition Stages	258
Figure 8. 10 VM and FC of PM Retained by Filter Paper	259
Figure 8. 11 EC/OC Ratio of Filter Paper Captured PM from Biomass Samples at Critically Igniting and Pre-Igniting Temperatures	260
Figure 8. 12 Yields (dry-ash-free basis) of Volatile Species from Eight Pre-Igniting Biomass as modelled by FG-BioMass.....	261
Figure 8. 13 Yields (dry-ash-free basis) of Volatile Species from Eight Critically Igniting Biomass as modelled by FG-BioMass.....	261
Figure 9. 1 Reaction Activation Energy Estimation –Plot from Final Iteration for Miscanthus(1) Dust Layers, Detailed Method.....	266

Figure 9. 2 Reaction Activation Energy Estimation –Plot for Miscanthus(1) Dust Layers, Crude Estimation Method	269
Figure 9. 3 Reaction Activation Energy E and $\ln(\text{pre-exponential factor})$ Comparison between Two Estimation Methods.....	270
Figure 9. 4 Second Order Relation of Layer Ignition Delay Time with Layer Ignition Temperature for Four Single-Material Biomass	271
Figure 9. 5 Second Order Relation of Layer Ignition Delay Time with Layer Ignition Temperature for Six Biomass Binary Blends	271
Figure 9. 6 Linear Relation of Layer Ignition Delay Time with Dust Layer Thickness for Four Single-Material Biomass	271
Figure 9. 7 Linear Relation of Layer Ignition Delay Time with Dust Layer Thickness for Six Biomass Binary Blends	271
Figure 9. 8 Logarithm Ignition Delay Time in Seconds versus Layer Ignition Temperature in Kelvin for Four Single-Material Biomass.....	273
Figure 9. 9 Logarithm Ignition Delay Time in Seconds versus Inverse Layer Ignition Temperature in Kelvin for Four Single-Material Biomass.....	273
Figure 9. 10 Logarithm Ignition Delay Time in Seconds versus Layer Ignition Temperature in Kelvin for Six Biomass Binary Blends.....	273
Figure 9. 11 Logarithm Ignition Delay Time in Seconds versus Inverse Layer Ignition Temperature in Kelvin for Six Biomass Binary Blends.....	273
Figure 10. 1 Particle Size Distribution of WWP<180 μm	277
Figure 10. 2 T_{MWL} Determination for WWP	278
Figure 10. 3 Section Selected for WWP E_a Calculation	278
Figure 10. 4 Self-Ignition Propensity Risk Ranking of WWP and other Single-Material Biomass.....	279
Figure 10. 5 HSBT Temperature-Time Profile of WWP<180 μm in Basket S at 210°C Hot Storage Temperature	280
Figure 10. 6 TSI Definition Used by Ramírez et al. and Saddawi el al. [Source: Ramírez et al. (2010)]	282
Figure 10. 7 Superimposing HSBT Results from Baskets S, M, L onto BS 15188 TSI Graph (Pseudo-Arrhenius Plot of Self-Ignition Temperatures) [Edited from: British Standard (2008)]	283
Figure 10. 8 Superimposing HSBT Results from Baskets S, M, L onto BS 15188 t_i Graph (Dependence of Combustion Induction Times (t_i) on the Volume/Surface Ratios of Dust Heaps) [Edited from: British Standard (2008)]	283
Figure 10. 9 Comparison of TSI of WWP-Pellet and WWP<180 μm via Pseudo-Arrhenius-type self-ignition diagram, [$\lg(V/A)$ vs. $1/T$]	284
Figure 10. 10 Self-Ignition Temperature of Various Raw and Processed Biomass Samples as a Function of Storage Size [Source: Saddawi et al. (2013a)]	285
Figure 10. 11 Self-Ignition Temperature of Pine Wood as a Function of Storage Size – Chips and Sawdust Comparison [Source: Ferrero et al. (2009)]	286

Figure 10. 12 Hot Storage Basket Experiment – TSI Results of Miscanthus at Different Harvest Period [Edited from: Everard et al. (2014)]	286
Figure 10. 13 Critical Ambient Temperature that Ignited 6 mm- and 8 mm-Wood Pellets [Edited from: Pauner and Bygbjerg (2006)]	287
Figure 10. 14 Comparison of t_i for WWP-Pellet and WWP<180 μ m at the different characteristic dimensions tested, [$\lg(V/A)$ vs. $\log t_i$]	288
Figure 10. 15 t_i of Various Raw and Processed Biomass Samples as Predicted with BS 15188 Method [Source: Saddawi et al. (2013a)]	289
Figure 10. 16 t_i of Pine Samples as Predicted with BS 15188 Method [Source: Ferrero et al. (2009)]	289
Figure 10. 17 t_i of Various Fuel at Different Storage Volume [Source: García-Torrent et al. (2012)]	290
Figure 10. 18 TSI Estimations to 500,000 m ³ via Extrapolation, with error margin included	292
Figure 10. 19 t_i Estimations to 500,000 m ³ via Extrapolation, with error margin included	292
Figure 10. 20 Ignition Delay Time (t_i) from Three Different Methods [Edited from: Saddawi et al. (2013b)]	293
Figure 10. 21 TSI Estimations to 1,000 m ³ via Extrapolation (Uncertainty Margins Not Shown).....	294
Figure 10. 22 t_i Estimations to 1,000 m ³ via Extrapolation (Uncertainty Margins Not Shown).....	294
Figure 10. 23 F-K Method – Correlation between Characteristic Length of WWP Samples and Self-Ignition Temperature	296
Figure 10. 24 Autoignition Temperature – Sample Volume Relationship for Three Samples [Source: Brauer et al. (2012)].....	298
Figure 11. 1 Material Self-Ignition Propensity Risk Ranking	303
Figure 11. 2 Industrial Application: Maximum Permissible Surface Temperature Estimations with Three Methods – Guideline 1 (Points), Guideline 2 (Curves, T_{LIT} from Pre-Refinement) and Power Station Practice (Constant at 150°C)	304

List of Abbreviations

AAAS	American Association for the Advancement of Science
AAS	Atomic Absorption Spectroscopy
ADF	Acid Detergent Fibre
ADL	Acid Detergent Lignin
AES	Atomic Emission Spectroscopy
ar	As received
ARC	Accelerating Rate Calorimeter
ASE	Accelerated Solvent Extractor
ASTM	American Society for Testing and Materials
BET	Brunauer-Emmett-Teller
BFB	Bubbling fluidised bed
CAT	Critical Ambient Temperature
CCN	Cloud Condensation Nuclei
CF	Cornflour
CFB	Circulating fluidised bed
CLS	Cellulose
CTAB	Cetyl Ammonium Bromide
daf	Dry-ash-free
db	Dry basis
DCM	Dichloromethane
DI	De-ionised
DSEAR	Dangerous Substances and Explosive Atmospheres Regulations
DTG	Derivative Thermogravimetric
DUC	Dispersion Unit Controller
EC	Elemental Carbon

EFB	Empty Fruit Bunches
FC	Fixed Carbon
FGD	Flue-gas Desulfurisation
FIRCOSIM	Fire Combustion SIMulator
F-K	Frank-Kamenetskii
FRS	Fire Research Station
FTIR	Fourier Transform Infrared Spectroscopy
GC	Gas chromatographer
GC-MS	Gas Chromatography-Mass Spectroscopy
GCV	Gross calorific value
GHG	greenhouses gas
HCLS	Hemicellulose
HGI	Hardgrove Grindability Index
HHV	Higher Heating value
HPLC	High Performance Liquid Chromatography
HSBT	Hot Storage Basket Test
IC	Ion Chromatography
IEC	International Electrotechnical Commission
IMO	International Maritime Organization
IPCC	Intergovernmental Panel on Climate Change
ISO	International Standardization Organization
LEL	Lower Explosions Limit
LFL	Lower Flammability Limit
Lg	Ligno-Bond-DD powder
MIE	Minimum Ignition Energy
MPST	Maximum Permissible Surface Temperature
MS	Mass Spectrometer
NAS	National Academy of Sciences
NDF	Neutral Detergent Fibre

NFPA	National Fire Protection Association
NIST	National Institute of Standards and Technology
OC	Organic Carbon
OU	Optical Unit
PAH	Polycyclic Aromatic Hydrocarbon
PID	Proportional-Integral-Derivative
PKS	Palm Kernel Shell
PM	Particulate Matters
PTFE	Polytetrafluoroethylene
py	Pyrolyser
py-GC-MS	Pyrolysis-Gas Chromatography-Mass spectroscopy
R.O.	Renewables Obligation
rpm	Revolution per minute
RT	Retention time
RTD	Resistance Temperature Detector
SBC	Solid Bulk Cargoes
SCFA	Short-chain fatty acids
SEM	Scanning Electron Microscopy
SFPE	Society of Fire Protection Engineers
SIPS	Sample Introduction Pump System
SIT	Self-Ignition Tester
SMAFS	Smoke Movement and Flame Spread
SVDU	Small Volume Dispersion Unit
SVOCs	Semi-Volatile Organic Compounds
TC	Thermocouple
T _{charac}	Single oxidation temperature
TGA	Thermogravimetric Analysis
TI	Total Inorganic Carbon
TIC	Total Ion Chromatogram

T _{LIT}	Layer Ignition Temperature
T _{MWL}	Temperature of Maximum Weight Loss
TOC	Total Organic Carbon
U.K.	United Kingdom
UEL	Upper Explosions Limit
UFL	Upper Flammability Limit
UNFCCC	United Nations Framework Convention on Climate Change
VFA	Volatile Fatty Acid
VM	Volatile Matter
VOC	Volatile Organic Compound
WSC	Water soluble carbohydrates
WWP	White Wood Pellets
XRF	x-Ray Fluorescence

List of Symbols

t_c	cooling time to ambient temperature
t_{dry}	drying time
t_h	heating time to drying
$t_{h,int}$	intermediate heating time from drying to torrefaction
t_{tor}	reaction time at desired torrefaction temperature
$t_{tor,c}$	cooling time from the desired T_{tor} to 200°C
$t_{tor,h}$	heating time torrefaction from 200°C to desired torrefaction temperature (T_{tor})
η_M	mass yield
η_E	energy yield
T_{SI}	Self-Ignition Temperature
t_i	Ignition Induction Time
E	Reaction Activation Energy (J/mol)
T_p	Hot Plate Temperature
T_a	Ambient Temperature
λ	Dust Layer Thermal Conductivity ($W/m \cdot K$)
T	Temperature (K)
ρ	Density (kg/m^3)
Q	Heat of Reaction (J/kg)
A	Arrhenius Pre-exponential Factor ($1/s$)
R	Universal Gas Constant ($8.314 J/mol \cdot K$)
θ	Dimensionless Temperature
z	Dimensionless Distance from Hot Plate
δ	Dimensionless Heat Generation Rate
δ_c	Maximum or Critical Non-dimensional Heat Generation Term

Bi	Heat Transfer Biot Number
θ_a	Dimensionless Ambient Temperature Parameter
h_t	Total Effective Heat Transfer Coefficient ($W/m^2 \cdot K$)
h_c	Convective Heat Transfer Coefficient ($W/m^2 \cdot K$)
h_r	Radiative Heat Transfer Coefficient ($W/m^2 \cdot K$)
Ra	Heat Transfer Rayleigh number
λ_a	Thermal conductivity of air ($W/m \cdot K$)
L	Characteristic Length Equals to the Side of the Square having the Same Area of Dust Layer Surface Exposed to Ambient
ε	Biomass Dust Emissivity
σ	Stefan-Boltzmann Constant ($5.67 \times 10^{-8} W/m^2K^4$)
g	Gravitational Acceleration ($9.81 m/s^2$)
β	Inverse Film Temperature
T_s	Top Surface Temperature of Dust Layer
ν	Kinematic Viscosity (m^2/s)
α	Thermal Diffusivity (m^2/s)
θ_m	Dimensionless Maximum Layer Temperature
z_m	Dimensionless Location in Dust with Maximum Layer Temperature
T_h	Hotplate Temperature in $\ln\left(\frac{T_h^2}{d^2}\right) - 1/T_h$ Correlation
d	Dust Layer Depth in $\ln\left(\frac{T_h^2}{d^2}\right) - 1/T_h$ Correlation
t_{ign}	Ignition Delay Time
R^2	Correlation Coefficient

Organisation of the Thesis

There are all together 11 chapters in this thesis, covering some general aspects of biomass and specific concerns regarding biomass handling and storage issues in power stations.

Chapter 1 briefly introduces the global energy matters in relation to emissions, particularly anthropogenic green house gases (GHGs) that closely relate to climate change; international actions in general and UK efforts in combating the climate. Renewable energy application has been recognised as a partial solution to curb this problem and this work focused specifically on vegetation-based biomass as solid fuel. The few key research questions were clearly identified.

Chapter 2 describes some common problems faced during handling and storage of biomass, the reasons these problems occurred and some previous work in solving these concerns. Some pre-treatments aimed to remove certain undesirable features of biomass and emissions just before and after ignition were looked into.

Chapter 3 presents the instruments, experimental methods and techniques applied in this study. Operating principles of some instruments, procedures for certain experiments and some analysing process used as part of this research had been included.

Chapter 4 focuses on the basics of low temperature ignition and self- ignition of biomass dust deposition, whereby some common biomass fuels used in power stations were selected for dust layer test. The possibility of dust samples in power stations that appeared as blends of various different materials were looked into systematically via defined ratios of two different materials. In this way, the possible range of dangerous temperature that may cause a fire outbreak were identified. Nevertheless, this is indeed a rough estimation since material blends in the industry never appear in defined component ratios.

Chapter 5 concerns the effects of a common practice during biomass transportation, in which binders are included to maintain the rigidity of biomass briquettes or pellets during transportation. Subjected to the permitted maximum amount of binder allowable in biomass briquettes or pellets, whether or not these binders would increase the fire safety risk was investigated in details. The results from two common binders used were compared.

Chapter 6 investigates water-washing pre-treatment process on biomass. Impacts of water-washed biomass was the focus, though washing with other liquids is possible. The resulted leachates were taken for ion-chromatography and total organic carbon analysis. Comparisons between untreated and washed solid biomass were made; lignocellulosic analysis for detection of any hydrolysis that had taken place and mineral contents of both solids via atomic absorption spectrophotometry on diluted liquids resulted from respective acid digestion. The impacts of this pre-treatment method on fire-safety risk was explained in length.

Chapter 7 delves into a relatively new biomass pre-treatment process, the torrefaction process. The torrefaction process and impacts on calorific value and ignition had been described in details and the fire safety risk from combusting torrefied materials was high-lighted since the fire safety issues were often neglected. The improvement in material grindability, changes in particle size, particle morphology and the surface area readily available for chemical reactions were covered.

Chapters 4, 5, 6 and 7 have included industrial significance from the results obtained thus far, in which the maximum permissible surface temperature of any electrical or mechanical equipment in plant was defined.

Chapter 8 compares the emissions of biomass dust layer depositions at two temperatures just before and after ignition that were different by 10°C. The pollutants were captured experimentally and volatile species evolved in combustion modelled by software. Besides applying the experimental GC-MS method in determining the emission components, prediction of volatile species and respective intensities were predicted with FG-Biomass software.

Chapter 9 describes a mathematical method used to estimate reaction kinetics and ignition induction time for the dust layer ignition experiments. Besides applying the results from dust layer test in Chapter 4, the heat transfer concept and various dimensionless parameters had been identified to ease the calculations. The method used to empirically estimate biomass thermal conductivity was briefly mentioned.

Chapter 10 emphasises the dependence of critical self-ignition temperature and ignition induction time during storage on the form which the biomass appears, as whole pellets or as disintegrated dust. To apply the results obtained to much bigger industrial size, both the scaling-up method and Frank-Kamenetskii (F-K) method were adopted. The thermal conductivity of biomass needed in the F-K calculation was estimated with the same method as that in Chapter 9.

Chapter 11 summarises the findings that are answerable to the research questions defined earlier. Conclusions were drawn from the major findings and future work to strengthen the understanding in this area were suggested.

Chapter 1 Introduction

Over the years, as modernisation takes place, global energy demand to improve the standard of living is ever increasing. Within the last two centuries, this demand has been fulfilled mainly by non-renewable fossil fuels that deplete as time goes by, like coal and oil (BBC Ltd., 2014). Renewable energy resources, biomass being one of them, have proven to help reduce climate change caused mainly by fossil fuel burning, besides ensuring energy security by reducing dependence on non-renewable fossil fuels.

1.1 Project Background

Application of solid biomass as fuel is not without issue. The phenomenon of material self-heating that leads to self-ignition (termed spontaneous- or auto-ignition) in organic matters began to catch attention since the 19th century in the textile industry (DeHann, 1996) and studies in this area have been carried out since then, especially in relation to the power generating industry. Referring to **Figure 1. 1**, it is possible that a spontaneous smouldering reaction initiates within a solid material that self-heats at low temperatures, even as low as ambient temperature (Rein, 2016).

At relatively low temperature, chemical reaction in a material capable of self-heating is slow, taking a long period of time in heating up owing to the low reaction rate. For self-heating to happen in a material, the substance must be capable of undergoing exothermic reaction; solid materials that are porous or granular are some of the examples. As exothermic reaction takes place, in the beginning, the heat generated can be balanced by the heat losses due to cooling. More heat is generated as the exothermic reaction accelerates, the high temperature achieved at critical condition initiates a sustained smouldering. When the sustained smouldering reach the exterior surface of the substance, glow fire is observed and possibly erupt into flaming. As the material is completely burnt, the ash formed reduces the material temperature. The time scale in the figure can be at different units – hours (as in the figure), days, weeks, months or years. At any time scale, the process from material heating up to smouldering takes a much longer duration than the glow fire process, i.e. once the material catches fire, it takes a relatively shorter period of time for the temperature to reach its peak and dwindle as ash is formed.

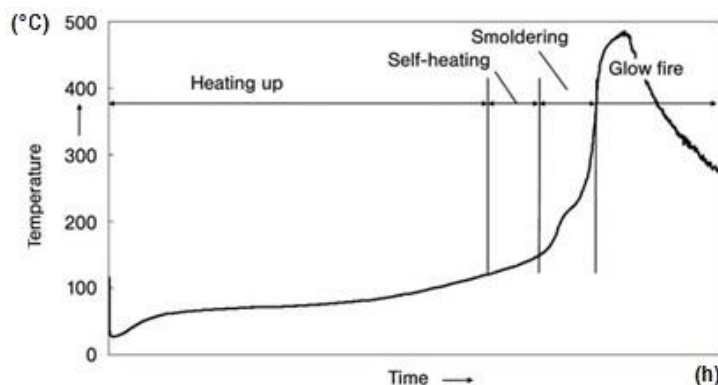


Figure 1. 1 Stages of Fire Triggered by Material Self-Ignition – Heating up, Self-heating, Smoldering to Glow fire [Edited from: Babrauskas et al. (2009), p.29]

Smoldering is mainly related to safety since many uncontrollable fires start by smoldering; it can be undetected for an extensive period of time and undergo a sudden transition to flaming combustion leading to uncontrollable fires (Martínez, 1995-2017). Be it self-ignition, spontaneous-ignition or auto-ignition; all refer to the on-set of thermal runaway reaction in which heat generation within a system exceeds heat loss leading to sustained ignition.

1.1.1 Global Emissions and Trend

Among the six greenhouses gases (GHG) as covered in Kyoto Protocol which include carbon dioxide (CO₂), methane (CH₄), nitrous oxide (N₂O), hydrofluorocarbons, perfluorocarbons and sulphur hexafluoride that absorb solar radiation and keep the Earth warm, excessive carbon dioxide emission particularly from fossil fuel combustion was recognised as the main culprit causing global warming. About 97% of climate scientists (National Aeronautics and Space Administration, 2014) from all over the world, from the American Association for the Advancement of Science (AAAS) to Intergovernmental Panel on Climate Change (IPCC), have agreed that the climate-warming trends over the past century are likely due to human activities, with the power generation sector accounts for approximately one quarter of the global CO₂ emissions.

In the UK, CO₂ is the largest of GHG emissions, amounting to 82% of the total GHGs in 2014 and according to the Climate Change Act 2008, UK has targeted to reduce its GHG emission by at least 80% from the 1990 level by 2050 (equivalent to ~160 MtCO₂e per year) (Committee on Climate Change, 2016; Office for National Statistics, 2016). Globally, CO₂ emissions from major fuel types i.e. natural gas, liquid fuels and coal rose since 1990 and the same increasing trend had been projected to 2040 (U.S. Energy Information Administration, 2016), as shown in **Figure 1. 2**. However, the UK had shown a decreasing trend in GHG emissions in general and CO₂ emission in particular (see **Figure 1. 3**) over the

period of 1990 to 2014, mainly due to the reduced use of coal in electricity generation (Department of Energy & Climate Change, 2016). According to Energy UK (2016), the UK power sector increased generation from renewable sources, managed to reduce carbon emissions by 13% between 2014 and 2015 and was the largest single contributor to UK emissions decrease.

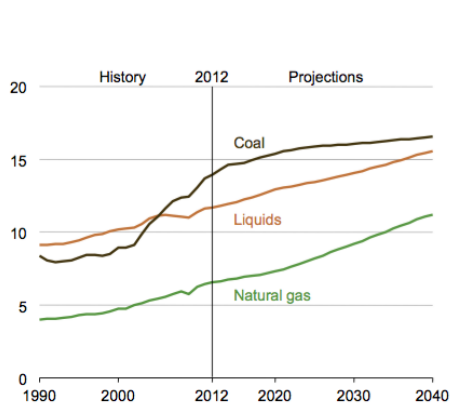


Figure 1. 2 World Energy-Related Carbon Dioxide Emissions by Fuel Type, from 1990 to Projected 2040 [Source: U.S. Energy Information Administration (2016), p.141]

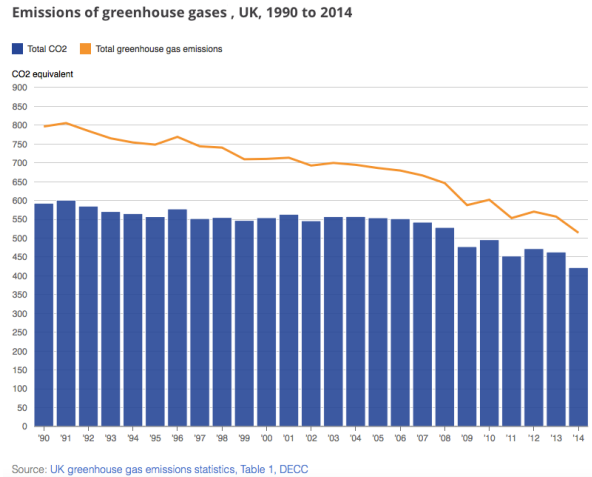


Figure 1. 3 Total GHG Emissions and Component in the [Edited from: Office for National Statistics (2016)]

Other emissions common to commercial combustion and the power generation sector in the UK, i.e. sulfur dioxide (SO_2), nitrogen oxides (NO_x) and particulate matter (PM_{10} and $PM_{2.5}$) showed decreasing trend from 1990 to 2015, as seen in **Figure 1. 4**. The decreasing trend reflected the practice in the UK that trended away from coal usage and opted for renewable energy sources (DEFRA, 2016).

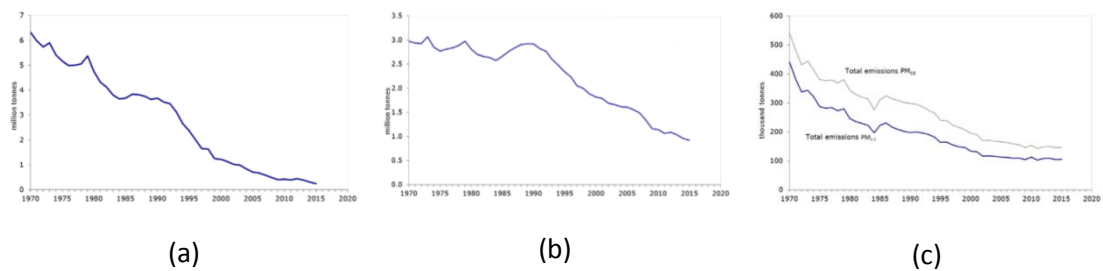


Figure 1. 4 Emissions Common to Commercial Combustion and Power Generation Sector in the UK (a) Sulfur Dioxide, in million tonnes (b) Nitrogen Oxides, in million tonnes (c) Particulate Matters, in thousand tonnes [Source: DEFRA (2016), p.29]

1.1.2 Climate Change and Energy Policy – Global and the UK

The growing world primary energy supply as shown in in **Figure 1. 5** is to fulfil the ever increasing energy demand. An increase in energy supply and demand simply means a rise in emissions. From the emission trend (especially carbon) discussed earlier, it is obvious that global climate change is closely related to the energy system adopted, and with renewable energy usage, less emissions were generated and thus less climate change.

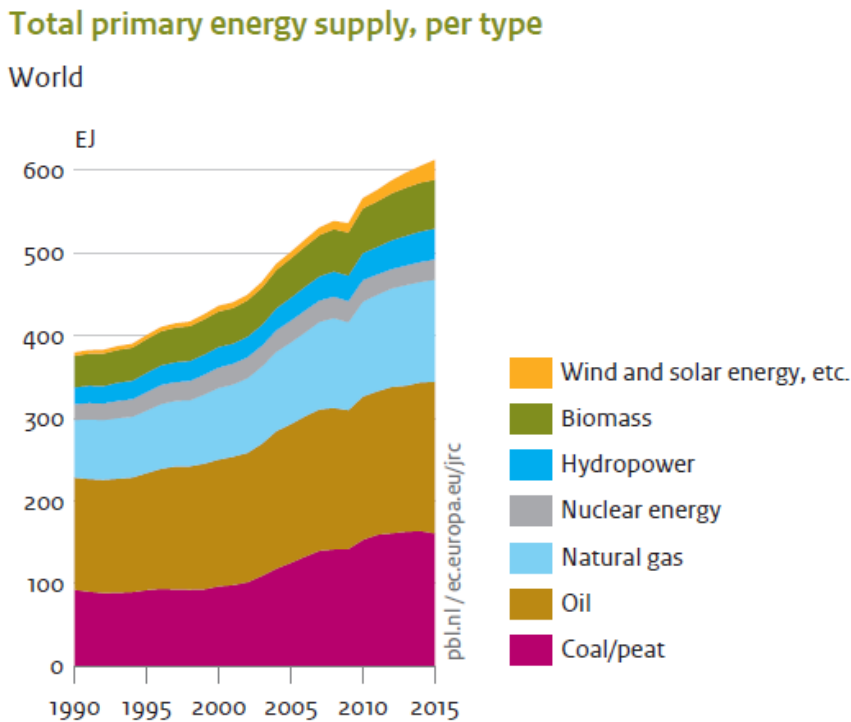


Figure 1. 5 Total World Primary Energy Supply [Edited from: PBL Netherlands Environmental Assessment Agency (2016), p.48]

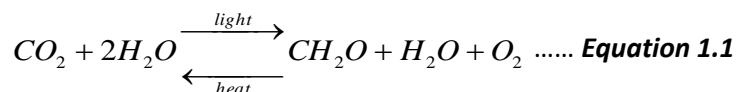
Obviously, all energy generating nations around the world are contributing to greenhouse gases emissions that cause climate change. Hence, it is a global effort towards decarbonisation. Domestically, the UK had committed to an 80% emission reduction relative to 1990 level by 2050 under the Climate Change Act 2008 and to achieve this target, the Act had established the five-yearly ‘carbon budgets’ that served as stepping stones, paving the way to achieving the final target. This Act had actually provided strong legislative depth for the UK climate change policy.

Internationally, along with hundred over other nations within the United Nations Framework Convention on Climate Change (UNFCCC), the UK was the 111th signatory (Arthur Nelsen, 2016) determined to contribute to the 2015 UN Climate Change Agreement, which is also known as the Paris Agreement (Accord de Paris). The Paris

Agreement is not just about climate change, it is an agreement about energy at its heart since it targeted at avoiding distressing climate change effects by reducing carbon emissions. This agreement sets out a common goal in tackling climate change, that aims warming limit to well below 2°C and to pursue efforts to limit to 1.5°C, which is more ambitious than previous international agreements (Committee on Climate Change, 2016). For the first time ever, all nations were brought into a common cause to undertake this ambitious effort in combating climate change, with a long term goal of achieving net zero global emissions in the second half of this century, implying phasing out fossil fuels (Arthur Nelsen, 2016).

1.2 Biomass and Biofuels in General

Vegetation-based biomass that is often referred to as lignocellulosic biomass and is recognised as an important renewable energy source, in which solar energy has been stored as chemical energy via the photosynthesis process during plant growth. Combustion of biomass can be viewed as the opposite of the photosynthesis process, in which plants produce food by themselves. The two-way relationship can be represented by the following equation (Chin and Aris, 2012):



From **Equation 1.1**, it can be seen that combustion of plant-based biomass is considered as low carbon or near carbon-neutral, where plants absorb CO_2 , convert sunlight into nutrients and energy via photosynthesis when growing and when burnt, CO_2 is released back to atmosphere. Burning of biomass can reduce by as high as 15.2 million tonnes of CO_2 compared with decomposition of the similar amount of organic matter (Biomass Power Association, 2011) due to avoidance of methane (a more potent GHG than CO_2) release during natural decomposition.

1.2.1 Biomass Categories

Biomass can generally be classified into different categories and one of the commonly used classifying consists of five categories (Biomass Energy Centre, 2011) , as follows:

- i. Agricultural residues – residues from agriculture harvesting or processing
- ii. Energy Crops – high yield crops grown specifically for energy applications

- iii. Food waste – from food and drink manufacture, preparation and processing, and post-consumer waste
- iv. Industrial waste and co-products – from manufacturing and industrial processes
- v. Virgin woods – from forestry, arboricultural activities or from wood processing.

1.2.2 Biomass Components

Lignocellulosic biomass is mainly made up of complex mixture of three polymers, namely hemicellulose, cellulose and lignin. The composition and chemical structure of lignocellulose biomass are illustrated in **Figure 1. 6**. Hemicellulose and cellulose are basically sugar polymers whereas lignin, an amorphous polymer made up of various phenolic compounds. These polymers give a plant its structural rigidity since they are the main component of cell walls.

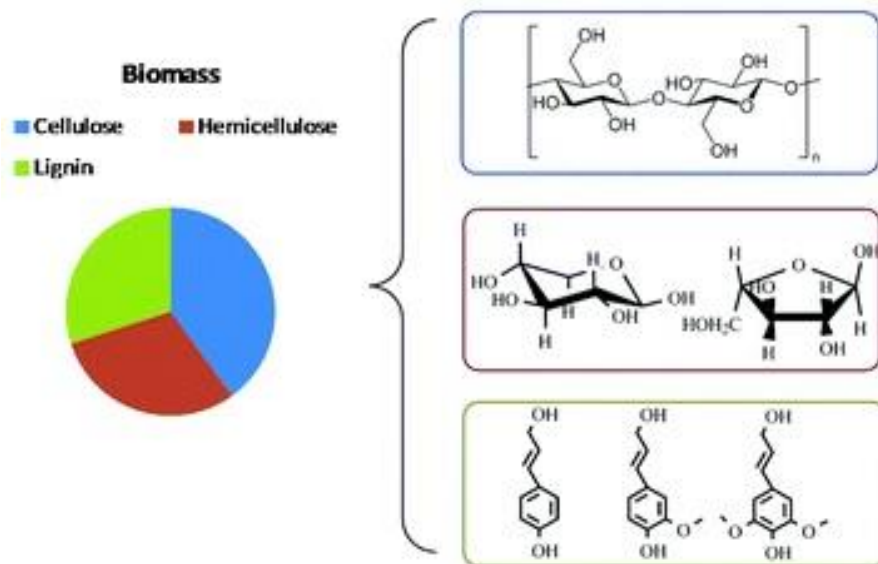


Figure 1. 6 Biomass Composition – Hemicellulose, Cellulose, Lignin and the Chemical Structure of Each [Source: Wang et al. (2014), p. 549]

1.3 Biomass Related Fire Accidents

There have been many fire accidents involving biomass around the world. In the UK, the prominent one is perhaps the RWE npower Tilbury Power Station fire in 2012. Though the fire was brought under control, for a number of days that followed, smouldering of the remaining biomass fuels in bunkers continued. Tilbury station had actually been expected to produce almost 10% of UK's renewable energy output and a reduction of around 70% GHGs emissions as compared with combusting coal by 2012 (The Green Age Ltd., 2014) but

unluckily, the mission was never achieved. Investigations had concluded that it was most likely caused by self-ignition of biomass (Guillermo Rein, 2012) that involved smouldering dust (Paul Newton, 2012).

There were other fire issues associated with wood pellets throughout North America and Europe. In April 2011, a fire in the basement and attic occurred following an explosion at Pinnacle Pellet in Armstrong, British Columbia, Canada (Postmedia Network Inc., 2012). Later in October within the same year, there was a pellet storage fire outbreak at Shur Fire Energy Norwich. Just a month after, a wood pellet silo containing 200 tonnes of wood pellets caught fire at the Port of Tyne in the UK. A year later, in March, Laurinburg Nature' Earth plant at North Carolina suffered an outbreak of fire (BBRG Biomass Pelletization Workshop, 2013), (WMBF News, 2012). In October 2013, a fire broke out at the Port of Tyne South Shields, South Tyneside, in which it involved a fire outbreak in a conveyor transfer tower storing biomass pellets (Chronicle Live Publication, 2013). A more recent fire that happened in October 2016 was the one in DONG Energy's Avedøre power station, Copenhagen, where an explosion happened on a conveyor belt feeding wood pellets from storage silo to the power station, causing wood pellets still in the silo to catch fire as the fire thrived (Luke Walsh, 2016).

This summary of recent fires related to the increasing supply and utilisation of biomass highlights a need for research in the area.

1.4 Objectives and Scope of Study

This research aimed at gaining a deeper understanding of low temperature combustion characteristics of various vegetation based biomass commonly used as solid fuels in UK power stations. These characteristics included the critical ignition temperature, ignition induction time, and emissions at and before (smouldering) critical ignition.

1.4.1 Objectives of Study

In compliance with the Dangerous Substances and Explosive Atmospheres Regulations (DSEAR) introduced in 2002, it became legal to demonstrate awareness to fire and explosion safety within an organisation, and power stations are no exclusion since ignition sources are widely present. Power stations need to identify sources of ignition (including all electrical and mechanical equipment) and assess ignition likelihood (Dodd and Lowe, 2002).

This work is to answer several key questions when biomass is applied in the power generation industry, especially during the handling and storage stages:

- i. is woody or herbaceous biomass more likely to self-ignite?
- ii. how will the self-ignition characteristics be affected when biomass are blended since power stations do not fire just a single material?
- iii. will the use of binders aimed for transportation convenience heighten self-ignition risk?
- iv. will pre-treating biomass increase or reduce the self-ignition risk?
- v. are the resulting emissions during smouldering a lot different than when the biomass ignites (flaming combustion)?
- vi. at what temperature should the biomass be stored to prevent it from catching fire?
- vii. how does pellet disintegration affect the propensity to catch fire?

The questions listed were answered through several experimental investigations.

1.4.2 Scope of Study

This work focuses on low temperature ignition characteristics of solid biomass fuel in fuel handling and storage stages. For fuel handling, the low temperature ignition characteristics were experimented following BS 50281-2-1 whereas the self-ignition characteristics during storage adhered to BS 15188. The low temperature ignition reaction kinetics of selected biomass samples during handling were looked into from the heat transfer aspect, in which mathematical iterations were involved and experimental results that adhered to BS 50281-2-1 had been applied. Prior to these, all biomass were characterised with various thermal analyses – proximate analysis, ultimate analysis, heating value determination, in accordance to BS EN 14774-3:2009, BS EN 15148:2009, BS EN 14775:2009, BS EN 14918:2009.

The samples were limited to vegetation-based biomass commonly used in UK power stations; Pine and white wood pellets (WWP) as the woody biomass, Miscanthus (energy crop) and Wheat Straw (agricultural residue) as the herbaceous resource. Subject to availability, Pine was sourced from different power stations at different times thus three different pine samples were used in this study. The WWP received was believed to consist of mixture of different parts of various woods, pine believed to be the major wood species. Besides sourcing at different times from power stations, the Miscanthus samples were obtained in different forms – pellets and untreated stems. Wheat straws, however were all received in one batch. Ignition risks of these biomass dusts and blends of their dusts were evaluated (**Chapter 4**).

In the experiment that followed BS 50281-2-1, the thicknesses of studied dust layers were 5 mm and 12.5 mm; and when woody and herbaceous biomass were blended, weight ratios of 90:10 and 50:50 were chosen. The binder amount was fixed at the

maximum allowable in the power industry (**Chapter 5**). Popular washing pre-treatment and torrefaction were carried out and the pre-treated biomass had their ignition characteristics studied (**Chapter 6 & 7**). When the reaction kinetics were estimated (**Chapter 9**), an assumption of one dimensional heat transfer was assumed with the underlying condition that the ratio of layer diameter to layer depth was >5 . As for the storage experiment with reference to BS 15188, biomass volumes of $\sim 11 \text{ cm}^3$, $\sim 67 \text{ cm}^3$ and $\sim 864 \text{ cm}^3$ were used to predict larger storage volume at industrial scale and biomass in pelleted form were compared with the same biomass in pulverised dust form (**Chapter 10**).

Chapter 2

Literature Review

Dust, according to Martinka et al. (2012), could appear in two forms – aerosol and aerogel in a work environment in an industry. The first occurred as dispersed dust whereas the latter as settled dust. Many others have defined dust from its physical dimension, ranging from $<75\ \mu\text{m}$ to $<500\ \mu\text{m}$. As defined by International Standardization Organization in ISO 4225 (DIN, 1996), dust is *small solid particles, conventionally taken as those particles below $75\ \mu\text{m}$ in diameter, which settle out under their own weight but which may remain suspended for some time*. Combustible dust is *finely divided solid particles, $500\ \mu\text{m}$ or less in nominal size, which may form an explosive mixture with air at atmospheric pressure and normal temperatures* as defined in EN 60079-10-2 (British Standard, 2015), and Ilona (2015) implied that small solids $\leq 500\ \mu\text{m}$ can accumulate due to their own weight, burn and glow in air and may form explosive mixtures in air under normal temperatures and atmospheric pressure. On the other hand, *as a very rough guide, particles below $500\ \mu\text{m}$ should be considered as particularly flammable* as reported by Chilworth Technology, part of the DEKRA organisation (Chilworth Technology Ltd., 2013). The National Fire Protection Association (NFPA) defined in NFPA 654 (National Fire Protection Association, 2006; Joshi, 2012) states that combustible dust is particles having size $<400\ \mu\text{m}$ and poses fire or explosive hazards and could be categorised into three broad classes – metal dusts (aluminium, brass etc. powders), carbonaceous dust (pulverised coal etc. in power plants) and others (food, plastic, paper, printing press by-products, pharmaceutical industry dust etc.) (Joshi, 2012).

El-Sayed and Abdel-Latif (2000), in their study about smouldering combustion of a dust layer on hot surfaces, mentioned that combustible dust when reacted with air or other gaseous oxidiser could lead to fire hazards without being noticed. Danger of smouldering combustion was emphasised since it could occur without flaming and propagate slowly in velocities of mm/hr or cm/hr that evolved into glowing, flaming combustion or erupted into explosions. Similar warning was mentioned by Martinka et al. (2012) and adding to that, it was emphasised that fire hazards were dependent on flameless combustibility of a particular dust. It was mentioned that a large amount of toxic gases was released during flameless combustion that showed no visible sign that enabled detection and would change to flame combustion at the most unexpected time. Barton (2001) in his work on dust explosion prevention and protection also highlighted the danger of combustible dust layers that could ignite and burn. Combustible dust imposes a fire hazard regardless if the fire initiated inside the industrial process plant, storage container or even layers deposited on building or plant floor. In a power station, dust accumulations

in the form of layers on any hot surfaces and during fuel storage are not to be overlooked. There are two British Standards that are related to the prevention of fire hazards caused by combustible dust layer accumulations and fuel storage – BS 50281-2-1 and BS 15188 respectively. In BS 50281-2-1 *Electrical apparatus for use in the presence of combustible dust – Part 2-1: Test methods – Methods of determining minimum ignition temperatures*; dust was defined as small solid particles that settle out under their own weight and remain suspended in air for a certain time in the atmosphere, and the recommended dust size for the proposed dust layer test should pass aperture of 200 µm (British Standard, 1999b). As for BS 15188 *Determination of the spontaneous ignition behaviour of dust accumulations*, emphasis was placed on determination of spontaneous ignition behaviour of dust accumulations and extrapolation of results to industrial scale storage is possible. In this standard, dust that passed through a 250 µm mesh aperture was the recommended dust size for the proposed hot storage basket test (British Standard, 2008).

2.1 Self-Heating, Self-Ignition and Smouldering Combustion of Biomass

Self-heating and spontaneously-heating are the two terms with similar meaning. The study of self-heating of materials started in early 1920s when Russian researchers Nikolai Semenov and David Frank-Kamenetskii developed a theory for self-heating. The theory was later called the 'F-K theory' in honour of Frank-Kamenetskii and was widely used in the 1960s after some refined studies by British researchers, Philip Thomas being one of them (Babrauskas, 2003b).

Power stations could not risk running out of fuels in their daily operations and therefore, it is a common practice for power plants to store some levels of fuel, be it coal or biomass (The Carbolea Research Group, 2014). Under different conditions, a majority of organic and some inorganic substances undergo exothermic decomposition or oxidations (Babrauskas, 2003b). Following a study on storage and spontaneous combustion of waste fuel by Hogland and Marques (2003), the self-heating process that happened in stored biomass could be categorised in a few key stages – physical, biological and chemical stages, as illustrated **Figure 2. 1**. These are discussed in the following sections.

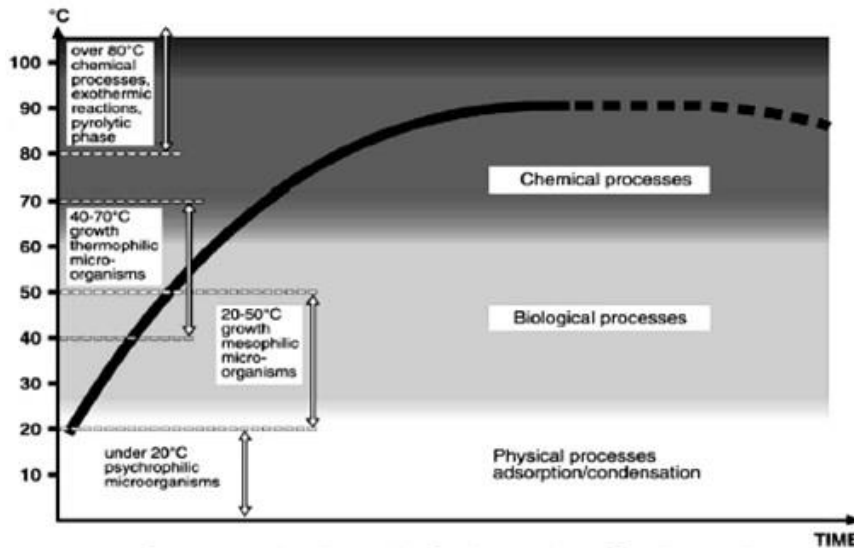


Figure 2. 1 Physical, Biological and Chemical Stages of the Self-Heating Process in Stored Biomass [Source: (Hogland and Marques, 2003)]

2.1.1 Physical, Biological and Chemical Stages

The **physical stage** of biomass self-heating often was related to the moisture content of the material. Stored biomass is often not completely dry and different moisture levels exist within biomass piles. The drier the biomass, the more hygroscopic it is. Absorbing moisture from the surroundings and condensing water vapour involve evolution of latent heat that could be adequate to cause self-heating. Even with balanced internal water movement via evaporation and condensation, some local hot spots may still appear. As time passes, moisture is gradually lost and the decline in thermal diffusivity of the drier material lessens the biomass pile stability. Provided that moisture remains in the system, liquid-phase oxidation and acid hydrolysis of hemicellulose proceeded and contributed to additional heat release (SP Swedish National Testing and Research Institute, 2003).

Related to the **biological stage**, as soon as the biomass is cut, the severed crop will naturally attempt to heal the damage by increasing its respiration. Increased respiration would result in a rise in heat production and further promote the subsequent development of microbial activity (The Carbolea Research Group, 2014). Heat produced from microorganisms is the prerequisite to achieve the temperature regime for commencement of the sequential oxidative processes (SP Swedish National Testing and Research Institute, 2003). Divided according to temperature sensitivity, there are three groups of microorganisms –psychrophilic, mesophilic and thermophilic microorganisms. The psychrophiles have growth and reproduction capability at temperatures as low as -15°C to 10°C; mesophiles’s in range of 20°C to 40°C and beyond 40°C, the reproduction capability

of mesophiles becomes very limited whereas for thermophiles, they are competent to surviving up to roughly 70°C (IEA Bioenergy, 2013).

Mesophilic lactic acid bacteria contribute to the most important initial microbial activity, where they ferment water soluble carbohydrates (WSC) to volatile fatty acids (VFA) that are also known as short-chain fatty acids (SCFA). The process liberates heat (exothermic) and decreases the pH. Studies had found that lactic acid bacteria increase rapidly after crop harvest and the exothermic fermentation process causes an increase in the biomass pile temperature. As these biological reactions proceed, temperature increases and the biomass pile gets hotter to an extent that is intolerable for the microorganisms. From then on, abiotic chemical processes will take place (The Carbolea Research Group, 2014).

The **chemical stage** focused on abiotic heat generation that had been recorded as low as 27°C to 65°C, concurrently with microbial activity (The Carbolea Research Group, 2014). As microbial activity proceeds, the temperature will keep rising until the lethal limit for bacteria that is around 80°C. Thenceforth, biomass degradation will be dominated by abiotic chemical processes. An illustration of biomass self-heating in a storage site is shown in **Figure 2. 2**.



Figure 2. 2 Freshly produced pellets, with pellets at elevated temperatures due to self-heating and the visible “smoke” probably is a combination of moisture and various gases [Source: (IEA Bioenergy, 2013) p.17]

2.1.2 Theory of Smouldering Combustion

Smouldering combustion is a term frequently associated with self-combustion that was initiated by the self-heating process in materials. By definition, smouldering combustion is a slow, flameless form of combustion and happens at relatively lower temperatures. Heat is evolved when oxygen directly attacks surfaces of a condensed-phase fuel and this heat would sustain the smouldering combustion. According to the Society of Fire Protection

Engineers (2002), from various aspects, smouldering in the science of solid fuel combustion is quite distinct from flaming but could be equivalently complex and diverse. Smouldering, though slow with no flame seen, is hazardous for two major reasons; first, it yields a substantial amount of conversion from fuel to toxic compounds than does flaming and second, it could lead to flaming, from heat sources that were too weak to directly produce flames.

Besides the physical factors that favour smouldering like the quantity of fuel material available in the fire triangle or fire tetrahedron (see **Figure 2. 3**, chemical factors (fourth component added to fire triangle) play a major role as well in supporting smouldering. Apart from having greater surface area per unit mass, chars formed from fuel could be defined as materials having higher carbon content than the original fuel. A common characteristic of char is its susceptibility to rapid oxygen attack at moderate temperatures of around 397°C or higher. When thermally degraded, all cellulosic materials, for example biomass, will form chars. According to Jones et al. (2015) in a study about low temperature ignition of biomass, ignition delay depends on the pyrolysis duration of each biomass. During this charring process as pyrolysis proceeds, evolving volatiles prevented oxygen diffusion to the freshly formed char, but once pyrolysis is about to end, commencement of oxygen diffusion accelerated oxidation rate and the high temperature resulted in char eventually lead to a flaming combustion.

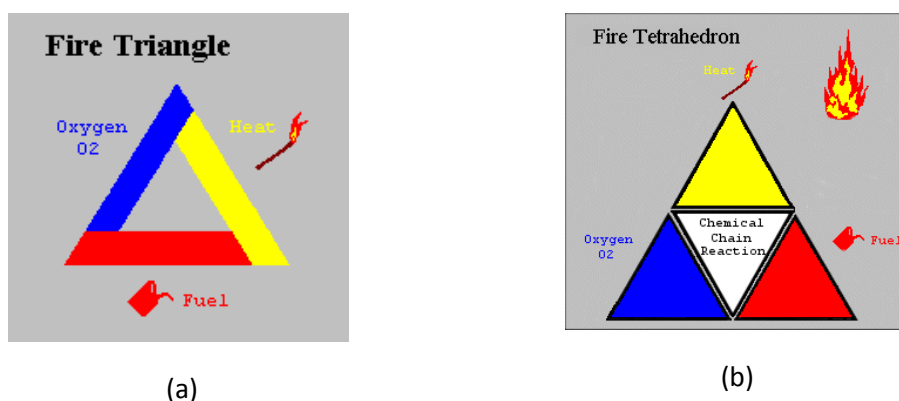


Figure 2. 3 Understanding Fire [Source: Fire Safety Advice Centre (2016)] (a) Fire Triangle
(b) Fire Tetrahedron

2.2 Factors Affecting Self-Heating Characteristics

There are actually many aspects that affect the self-heating characteristics of a biomass pile in storage. Mainly, they are two groups – **biomass type** and **biomass pile properties**. The first group is due to properties of the biomass itself and the second is due to the

properties of the storage pile like the physical dimensions and level of aeration. All in all, the most important factor is the temperature that dictates the biomass degradation process, whether it is a biological or a chemical process and the extent of that particular process (The Carbolea Research Group, 2014). Similar mechanisms actually apply to biomass dust sedimentation on various surfaces.

Biomass type simply implies the characteristics of the material – the biomass material would need to be sufficiently porous and reactive (SP Swedish National Testing and Research Institute, 2003) for self-ignition to take place after the self-heating process. The type of biomass prescribes the compositions of cellulose, hemicellulose and lignin contents of a particular biomass. For woody biomass, lower sapwood content with higher level of lignification would promote stability in storage. Other factors like having low water soluble carbohydrates (WSC) portion, lower nitrogen and lower hemicellulose contents would most likely promote the stability of the biomass pile, concluded in a comprehensive study by The Carbolea Research Group (2014).

Particle size of the stored biomass matters since particle size is relevant to heat production and convection. Small particles have surface area to volume ratios higher than that of large particles, indicating that small particles have greater heat fluxes per unit mass for heat radiation. For biotic or abiotic oxidations that take place on the particles surface, the reactions rates and thus temperature rise are faster for smaller particles since they have more surface areas per unit mass than the large particles. The biomass pile with smaller particles tends to be denser since more particles can fit into the same pile volume, giving the pile a compaction effect (The Carbolea Research Group, 2014). The study of Pastier et al. (2013) on the minimum ignition temperature of wood dust layers concluded that the dust particles size effect is less significant than the dust layer depth effect on the ignition temperature. Conversely, it was found that dust particle size had an effect when coal and oil shale dusts were experimented in the study of Miron and Lazzara (1988). It has also been discovered in the study of Pastier et al. (2013) that the packing density effect on minimum dust layer ignition temperature is more important for thin layers than thick ones.

The physical dimensions of a **biomass pile** or heap affect the pile temperature and the rate of heat dissipation from the pile. Radiative area is where heat transfer can happen. In practice, the common biomass stack shape built is usually of triangular cross section, in which the radiative area to volume ratio will be decreasing towards to pile top. For such storage piles, higher temperatures appear in the centre of the pile. As for biomass dust, when dust is accumulated in different areas, the sedimentation geometry will greatly affect the ignition onset location within the dust layer. From the study of Joshi (2012) that compared locations of dust ignition onset on three different wedge-shaped hot surface geometries, it was found that the ignition location moved towards the apex as the wedge angle increased.

It is important to ensure that the biomass pile is free from metal contamination. The presence of iron for instance, could serve as a catalyst that amplifies the rate of self-heating (Hogland and Marques, 2003). This could be difficult to achieve in actual power plant where many different operations take place simultaneously, causing the composition of dust formation to be beyond a plant personnel's control.

Perhaps, the interaction among biomass particle sizes, pile compaction and the level of pile aeration is the most crucial factor that dictates the self-heating characteristics of a biomass pile. To save transportation cost, biomass to be utilised and stored is usually of reduced size and conveyed pneumatically onto the storage pile. This process tends to pack the small particles more tightly, increase the pile compactness, decrease the free air space and thus reduce the degree of pile aeration. Poor biomass pile thermal conductivity encourages the heat development and temperature increment within the pile. Also, dust is generated along the conveying process and could accumulate on any hot surface in a power station.

Materials self-heating if left undetected, could lead to catastrophic outbreak of fire due to self-ignition. If the principles behind are well understood, preventive steps could be taken during biomass storage and transportation, to prevent biomass self-heating and therefore disastrous fire could be avoided. There were various different approaches to determine the critical temperature at which a particular biomass self-ignites when subjected to different conditions and also the ignition delay time. Different thermal analysis methods were employed to gain deeper understanding of the characteristics of a particular biomass material before it self-ignites. For example, thermogravimetric analysis (TGA)-differential thermogravimetric (DTG), Differential Scanning Calorimetry (DSC) methods had been widely applied in many studies (Fei and Liang, 2011; IEA Bioenergy, 2013; Ramírez et al., 2010); thermogravimetry-differential thermal analysis (TG-DTA) technique had been applied by Li et al. (2006) in a study on thermal characteristics of waste wood chips related to self-heating and spontaneous ignition.

Knowing the danger of possible fires caused by self-ignition of self-heating materials, Ramírez et al. (2010) had proposed a method of assessing self-ignition propensity (see **Chapter 3**) of different materials based on the apparent reaction activation energy and oxidation characteristic temperature (see **Figure 3. 18(a)**). Jones et al. (2015) had later modified this pictorial self-ignition risk assessment (see **Figure 3. 18(b)**), whereby the maximum weight loss temperature (T_{MWL}) obtained from thermogravimetric analysis (TGA) replaces the oxidation characteristic temperature of the former.

2.3 Handling – Biomass Dust Layer Deposition Ignition Characteristics

In relation to materials smouldering on hot surfaces and transforming into flaming combustion, Hagen (2013) mentioned that uniform heating at all surfaces of a sample as assumed by many researches was hardly a reality. According to Hagen (2013), one side of a sample was heated while the others cooled is a more common situation and dust layer being heated on a hot surface is among the best examples.

In almost all industrial plant, for instance a power station, virtually all the processes within the plant generate combustible dust that can deposit and accumulate on any exposed heated surfaces. As mentioned by Querol et al. (2006), hot surfaces can be produced electrically and mechanically or even a combination of both mechanisms. Dust deposits in layers on surfaces of motor housing, conveyer belt idlers, bearings etc., when the surface gets sufficiently hot, self-heating of dust layer happens and ignition may occur eventually, causing fire and as air dispersed the dust, an explosion may occur (Reddy et al., 1998). A fire initiated from combustible dust accumulation on hot surfaces could lead to explosions and secondary explosions and since the minimum ignition temperature of a dust layer is lower than its corresponding dust cloud (Wilén et al., 2013; Barton, 2001; Polka et al., 2012), hot surfaces are capable of igniting dust clouds (Kasalová and Balog, 2011), i.e. an igniting dust layer serves as the ignition source for sequential dust explosion. Amyotte (2013) clarified the misunderstanding that lots of dust is needed for a work place dust explosion to occur. In reality, combustible dust clouds could be generated from dust layers having thickness on the scale of millimetres or even less deposited on workplace surfaces.

In the beginning when no standard procedures for determining minimum ignition temperature of dust layer have been defined, there were many different methods conducted by a pool of different researchers. Apparatus wise, there was a variety of ways to fabricate the test rig with different kinds of hot plate temperature control.

The hot surface used by Bowes and Townshend (1962) was a 0.65 cm thick horizontal plane circular aluminium alloy plate with 19 cm diameter, electrically heated on the underside and having accuracy within 1°C. Tyler and Henderson (1987) had used dust layer of 75 mm diameter whereas Miron and Lazzara (1988) used 100 mm in diameter.

The time as of when to load the sample dust onto the hot surface differed among researchers; in the study of Palmer and Tonkin (1957), dust was loaded at the very beginning as the hot plate was heated but in the study of Bowes and Townshend (1962), the sample dust was loaded onto a pre-heated plate. These two different ways severely impacted the determination of ignition induction period or more commonly known as time to ignition, defined as the time between initial heating and onset of glowing (Barton, 2001).

A hot plate test for determination of minimum hot-surface ignition temperature of dust layers was recommended by the National Academy of Sciences (NAS) Committee on Evaluation of Industrial Hazards and a similar test had been proposed by the International Electrotechnical Commission (IEC). In the context of ignition, there are various different definition of ignition termed by different research bodies or individual. The NAS defined ignition as the initiation of combustion whereby ignition was considered to have occurred if one of these happen – red glow or flame seen in sample; slope of the temperature-time curve for the thermocouple in the middle of dust layer continues to increase; a dust temperature rise of 50°C or more as compared with the hot plate temperature or the dust melts. It had also been mentioned that char formation and /or smoke evolution without entailment of a minimum temperature rise in dust layer were insufficient. IEC defined ignition the same as NAS except that a dust temperature rise of 20°C instead of 50°C was considered as one of the ignition indicators (Miron and Lazzara, 1988). Also, ignition as defined by Bowes (Bowes and Establishment, 1984) was a bit different from that defined in BS EN 50281-2-1 (British Standard, 1999b); the former considered melting of dust layer and a temperature rise of more than 50°C of the hot surface temperature as ignition but the latter considered dust ignition when dust reached 450°C and a rise of 250°C above the heated plate, though both took visible glowing or flaming of dust as ignition.

The IEC 61241-2-1 (IEC, 1994) replaced by ISO/IEC 80079-20-2:2016 (ISO/IEC, 2016), the ASTM 2021-15 (ASTM, 2015; Park, 2006) and the BS 50281-2-1:1999 (British Standard, 1999b) standards have always been considered on par with each other since all are looking into hot surface ignition temperature of dust layers but they do exhibit some differences. The most obvious difference among the three is that ASTM used 12.7 mm dust thickness whereas both IEC and BS used 5 mm as standard. The particles size requirement differs too, in which ASTM required at least 90% sample to be <75 µm but 100% <200 µm (CCPS-AIChE, 2005) for the other two. Anyway, all the three standards used 10 cm diameter disk-shaped dust layer sample placed on a 20 cm diameter heated plate.

The question of whether a constant heat flux or a constant temperature to be the heat source for the hot plate test was studied and debated before a practical guideline was finally decided. In the 1960s, Shirliffe and Orr (1967) had compared two different modes of operation for guarded hot plate apparatus in their study that emphasised transient characteristics. The existence of an optimum heat flux boundary condition was compared for the guarded hot plate apparatus operating on constant heat flux and constant temperature modes. These two modes of hot plate control were chosen because they were the commonly used ones. At that time when technology had not advanced to the electrical and electronics advancement of today, constant heat flux at plate surface supplied by constant power was the simplest therefore most widely used for hot plates. The constant temperature mode was less popular since an extra temperature controller

was required to make the temperature constant. It was known that this mode was capable of speeding up tests but not used much because of the extra equipment therefore extra cost incurred and lack of knowledge in this field as compared with the constant heat flux mode. Thus, the constant temperature mode was forgone at that time. Later, as electrical and electronics knowledge advanced, both the modes had been applied in hot plate tests to obtain the minimum ignition temperature of dust layer. Besides the impractical length of time needed for a test, the difficulty to get extremely stable environment such that stable temperature could be achieved had caused the constant power constant heat flux mode to be rejected (Querol et al., 2006).

After many feedbacks and improvements, there are several standards widely accepted and applied nowadays for dust layer minimum ignition temperature determination. The BS 50281-2-1:1999 *Electrical apparatus for use in the presence of combustible dust – Part 2-1: Test methods of determining minimum ignition temperatures* is among one of them (British Standard, 1999b). It should be noted that this standard is applied in selection of suitable electrical apparatus for use in an atmosphere where combustible dust is present and the method outlined in this standard is not meant for use on substances having explosive properties. The Method A in this standard is mainly about dust layer on heated surface at a constant temperature, whereby the preparation of dust samples, test apparatus, procedures applied and test acceptance criteria are described in detail. This method determines the minimum temperature of a prescribed hot surface that would cause dust layer ignition when a specified dust thickness was deposited on the hot surface. The results are particularly relevant to industry equipment with which combustible dusts present on hot surfaces and are exposed to the atmosphere.

First of all, it is important that the dust sample can pass through an aperture size of 200 μm . As for the test rig i.e. heated plate, it was made of a metal plate of at least 20 cm diameter and 2 cm thick. This plate is to be electrically heated with its temperature controlling device i.e. the thermocouple (the sensing element) mounted in the plate near the plate centre, which the junction of this control thermocouple lies within 1 ± 0.5 mm of the upper surface and is in good thermal contact with the plate. Another thermocouple of the same kind positioned near the control thermocouple is connected to a temperature recorder for surface temperature recording during the experiment. The hot plate is designed to achieve a maximum temperature of 400°C without a dust layer and its temperature remains constant within $5 \pm \text{K}$ throughout the experiment period. The heated plate temperature is measured and uniformity could only be confirmed when the steady state temperature was within 5 K. Also, it is important that all thermocouples are calibrated and inaccuracy limit is 3 K at most. A metal ring with internal diameter of nominally 100 mm with slots at opposite ends to fit the dust layer thermocouple is used and left in place during while sample dust is tested. Upon filling the ring cavity, levelling

the sample layer to the top of ring is carried out. Dust thickness of 5.0 ± 0.1 mm is the recommended starting dust height and other heights like 12.5 ± 0.1 mm or $15.0 \text{ mm} \pm 0.1$ mm is useful too. These sizes were recommended such that the assumption of one dimensional heat transfer is valid based on works of many researchers.

In the study of Querol et al. (2006), besides varying the dust thickness (see **Figure 2. 4(a)**), the dust layer diameter (ring diameters of 100, 140, 180, 200 and 260 mm were used) was varied too by using metal rings with different diameters (see **Figure 2. 4(b)**). It was found that the impact of dust thickness was more significant than that of diameter on T_{LIT} of a particular dust. Similar conclusion was drawn from the study of Henderson and Tyler (1988), which had stated that the minimum ignition temperature of thin, natural or synthetic organic as well as inorganic material powder relied on a number of factors and layer depth was particularly important. In the ignition handbook of Babrauskas (2003a), the conclusion that dust layer depth significantly affected the dust layer ignition temperature were drawn upon obtaining results from 5-, 10-, 20-mm thick Beech sawdust, coal, cork and lycopodium dust experiments. The results showed that the layer ignition temperature decreased as the layer depth increased. Realising the impact of layer thickness to T_{LIT} of a particular material, Barton (2001) came up with a rule of thumb that says ignition temperature drops 5°C for every 1 mm increase in layer thickness, implying a linear relationship between T_{LIT} and layer thickness. This is consistent with the finding of Jespen (2016) that claims layer ignition temperature often decrease nearly linearly as thickness increases.

Owski et al. (2010) referred to the procedure in EN 50281-2-1 when examining the influence of dust layer thickness on ignition temperature of five exotic wood dusts, namely jatoba (*Hymenaea courbaril* Linn.), lapacho (*Tabebuia* sp.), teak (*Tectona grandis* L.), eucalyptus (*Eucalyptus grandis* W. Hill.) and European oak (*Quercus robur* L.). Wood samples of $<500 \mu\text{m}$ were used and among the three thicknesses explored (5, 10, 15 mm), the five wood species showed slight difference of dust layer ignition temperature among themselves though teak wood dust was the most resistant to ignition. The dust layer thickness has a more significant impact on the ignition temperature, whereby the thinnest (5 mm) showed layer ignition temperature that ranged from $310\text{-}340^{\circ}\text{C}$ whereas the thickest (15 mm) showed temperature range reduced to $270\text{-}280^{\circ}\text{C}$.

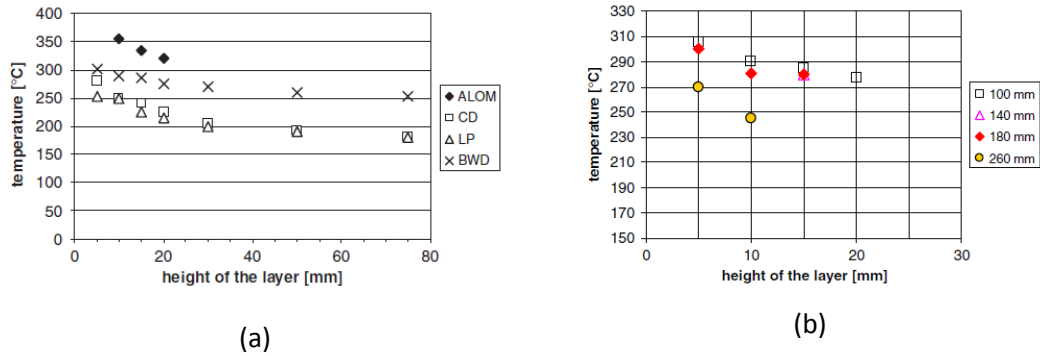


Figure 2. 4 Dust Layer Ignition Temperature [Source: Querol et al. (2006)] as a Function of (a) Layer Thickness (b) Layer Diameter

Joshi (2012) in a study of factors governing spontaneous ignition of combustible dusts had mentioned that the ratio of dust layer diameter (D) to its thickness (d), D/d , is preferably greater than 5 since heat transfer in the radial direction becomes increasingly important as the dust thickness increases i.e. D/d ratio decreases towards less than 5. This recommendation was consistent with findings from studies of Bowes and Establishment (1984), Anthony and Field (1975), Hensel et al. (1994), Dyduch and Majcher (2006) on self-heating characteristics of dust layer leading to ignition under various conditions.

Miron and Lazzara (1988) examined the dust layer ignition temperature of a few different dust species – brass powder, corn starch, grain, Lycopodium, Pittsburgh coal and oil shale, in which the samples were categorised into two particle size ranges, 22-61 μm for fine and 207-450 μm for coarse. It was found that particle size had impacted the oxidation rate and affected the minimum ignition temperature of dust layer, and caused the dust layer ignition temperature to increase as the particle size increased.

Bowes and Townshend (1962) studied Beechwood dust layers, where they had looked into the effects of three factors; layer depth, particle size and packing density on dust layer ignition temperature. They had used particles size in the range of <124 μm to 853 μm which led them to the conclusion that layer depth was the most significant factor affecting dust layer ignition whereas particle size impact was mild within the range studied and packing density was less significant and only thin layers were affected.

Palmer and Tonkin (1957) had used cork dust and mixed wood sawdust with particle size ranged from 65 μm to 3800 μm and layer depth that ranged from 2.5 cm to 5.0 cm to examine whether dust particles size and layer depth affected the dust layer ignition temperature. Besides concluding dust layer ignition temperature fell as the layer depth increased, they also concluded that dust layer ignited at lower temperature as the dust particles got finer.

From the various researches conducted, it can be seen that the effect of particle size on dust layer ignition temperature depends on the range of particle size studied. A bigger difference in size had shown the effects more significantly than when the size range was limited. A crude conclusion from these studies was that dust layer made up of fine dust ignited at lower temperature than the corresponding layer consisting of coarser dust particles. It should be born in mind that in the torrefaction process, where dust fines were easily formed, coupled with the dryness of the torrefied samples, particle size did become a significant factor for self ignition which then leads to explosions. This will be discussed in greater length in **Section 2.7** later.

Applying the procedures in BS 50281-2-1, Polka et al. (2012) examined the minimum ignition temperature of dust layers with the aim to identify threats from industrial equipment when operating these apparatus with constant temperature hot surfaces in environment that creates combustible dust layers. The seventeen materials used were barley, beech, buckwheat, cornflakes, corn starch, dried carrot, flour, hop, lemon balm, malt, nettle, oatmeal, rice flakes, semolina, senna fruit, sunflower husk and valerian. Polka et al. had fixed the dust diameter to 10 μm on a hot plate and desired set point and had used dust thickness of 5 mm and 12.5 mm. Sweis (1998) had confirmed that layer depth and particle size were the important factors that affected the ignition temperature in a study of oil shale and tar sand in hot environments.

The minimum layer ignition temperature (T_{LIT}) of a dust material actually depends on a set of conditions during the test, whereby no absolute ignition temperature exists for a dust layer consisting of a particular material (Janès and Carson, 2013a) & (Reddy et al., 1998) and ignition happens when the right combination of factors happens. This situation is analogous to the water boiling point that shows 100°C at atmospheric pressure but less than 100 at lower atmospheric pressure at higher altitudes and higher than 100 at higher atmospheric pressure at altitudes below sea level.

Nichols (2013) did mention that hot surface ignition is rather probabilistic in nature, in the sense that no single temperature can be defined as the minimum hot surface ignition temperature of a particular material. The ignition temperature was affected by many factors that fall into four main categories; surface properties, environmental factors, physical properties and others. Surface properties are like size, geometry and surface roughness and nature of that material; environment factors are like surrounding air temperature, air flow rate and humidity; physical properties are like the chemical composition, volatility and flash point of that material whereas other factors could be the period of time a material is exposed to a certain environment. Also, differences in determination approach leading to widely differed experimental values had been recognised by Henderson and Tyler (1988).

In agreement with the ignition temperature being dependent on many factors, Querol et al. (2006) mentioned that there are two reference standards that complimented each other under similar operating conditions, the BS 50281-2-1 (British Standard, 1999b) as described earlier and the BS 50281-1-2 (British Standard, 1999a) that applied the T_{LIT} results obtained from the former to an industrial context. Besides BS 50281-2-1, BS 50281-1-2 in many instances is used in combination with the BS EN ISO/IEC 80079-202:2016 standard as well. It should be noted that there are actually two main guidelines that are slightly different when applying the obtained T_{LIT} in defining the maximum permissible surface temperature (MPST) of an electrical apparatus operating in dusty industrial environment.

In one of the sets of guidelines that had been widely practised in Germany (Hensel et al., 1994; Reddy et al., 1998) following the German standard DIN 57165/VDE 0165, the MPST was defined as the temperature that caused glowing of a dust layer diminished by a safety margin of 75 K; this guideline is termed Guideline1 hereafter. The glow temperature was the temperature on a controllable hot plate that caused glowing in a layer of 5 mm-thick dust deposited on the hot plate. It was found that a 75 K reduction across the board was especially insufficient for layer thicknesses exceeding 5 mm. Thus, for layers thicker than 5 mm, the respective MPST was determined by deducting 75 K from the glow temperature found for that particular layer thickness instead. The safety margin of 75 K (or 75°C) was the value commonly used as the maximum allowable temperature for any electrical equipment applied in dusty environments (Barton, 2001; BRE, 2016).

Jaskółowski et al. (2014) in a study on minimum ignition temperatures of dust layer and dust cloud of oak, eucalyptus and lapacho dusts had mentioned that it is good to ensure the temperature of hot surfaces are less than 2/3 of the minimum dust cloud ignition temperature or 75 K below the 5 mm thick minimum dust layer ignition temperature.

In a study on determination of minimum ignition temperature of seventeen different species (barley, beech, buckwheat, cornflakes, corn starch, dried carrot, flour, hop, lemon balm, malt, nettle, oatmeal, rice flakes, semolina, senna fruit, sunflower husk and valerian) dust layers, Polka et al. (2012) recommended that surface temperature of power electronics devices installed in environments where flammable dust is present is to be at least 75 K lower than the ignition temperature of 5 mm thick dust layer, as a means to oblige to the legal regulations set out by the Polish State Fire Service .

In another work of examining minimum dust layer ignition temperature of wood sawdust originated from alder, ash, poplar, spruce trees cutting and the particle and fibre board industry, Pastier et al. (2013) recommended that the surface temperature of electric power equipment applied in dusty environment should be at least 75 K lower than the minimum layer ignition temperature of the 5 mm dust.

Another set of guidelines for MPST, denoted as Guideline2 is from the BS 50281-1-2 (British Standard, 1999a), which complimented the BS 50281-2-1 (British Standard, 1999b) that had been widely used in this study when determining the minimum T_{LIT} of different samples. Depending on the 5 mm T_{LIT} value obtained from BS 50281-2-1 procedure, the MPST varied (with sizeable safety margin, not consistently 75 K throughout like Guideline1) following three different curves (see **Figure 2. 5**). The three curves are based on the temperature range of 5 mm T_{LIT} ; bottom most curve is applied when the 5 mm T_{LIT} lies within this range of $250\text{ }^{\circ}\text{C} \leq T_5 < 320\text{ }^{\circ}\text{C}$, medium curve when it is this range $320\text{ }^{\circ}\text{C} \leq T_5 < 400\text{ }^{\circ}\text{C}$ and finally the top curve applies to 5 mm T_{LIT} of $\leq 400\text{ }^{\circ}\text{C}$. As seen from the figure, MPST depends on the deposition thickness and not in a linear fashion, in which the allowable temperature dropped tremendously in a non-linear way as the dust depth increase linearly. With results obtained from lab scale dust layer test, estimation of MPST for industrial machineries in a bigger picture is made possible where precaution could be taken to avoid running any apparatus exceeding this safe surface temperature range.

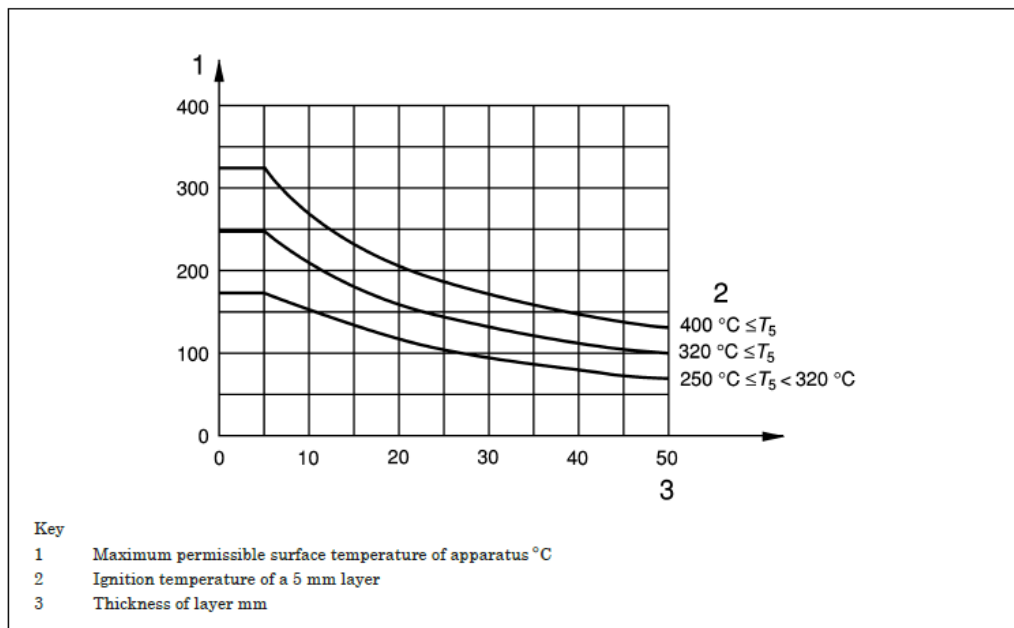


Figure 2. 5 Maximum Permissible Surface Temperature as a Function of Layer Depth, Depending on T_{LIT} Range (British Standard, 1999a)

Application of this BS 50281-1-2 MPST method had been proposed by Querol et al. (2006) in the study of dust layer ignition temperature of four dust samples, i.e. beechwood dust, lycopodium, coal dust and calcined alumina. After obtaining the dust layer ignition temperature as functions of dust layer diameter (see **Figure 2. 4(b)**) and layer thickness (see **Figure 2. 4(a)**), it had been suggested that the maximum permissible surface

temperature of an electrical device to be estimated with the graph shown in **Figure 2. 5**, the graphical method described in BS EN 50281-1-2:1999 (British Standard, 1999a).

In application of BS 50281-1-2 for estimation of MPST for one of the materials, which had its 5 mm T_{LIT} as 305°C, Querol et al. (2006) used the bottom curve (see **Figure 2. 5**) to estimate the MPST when the dust deposition was 30 mm, which had led to a value of ~95°C. The 30 mm T_{LIT} as determined from experiment was 270°C. Computed with the first practice in which a reduction of 75 K was required, 230°C was the MPST for the 5 mm thickness but reading from the BS 50281-1-2 chart, following the bottom curve, led to ~175°C. The difference between two guidelines was 55°C, with BS 50281-1-2 being more conservative. Setting the MPST of 150°C regardless of dust deposition thickness is another practice in a U.K. power station (Engineer, 2016). Taking the same example from Querol et al., at 5 or 30 mm thickness, both MPST would be 150°C. For MPST of the thinner 5 mm thickness, the fixed 150°C was 80°C and 25°C lower than estimated with Guidelines 1 and 2 respectively, indicating that this practice in power stations was the most conservative. As for the 30 mm thickness MPST, 150°C was 45°C lower but 55°C higher than estimated with Guideline1 and Guideline2 respectively. For this thickness, the U.K. power station practice was moderately conservative. In both MPST estimations, Guideline1 gave the most lenient estimate and as the dust layer gets thicker, the estimation from BS 50281-1-2 was even more conservative than the practice in a U.K. power station.

There are other practices within the European continent. For instance, Cemp, established as early as 1954, is one of the first companies in Italy that manufactures flameproof motors. This company defined the safe temperature of motor operation as the lowest between T_{S1} and T_{S2} , in which T_{S1} is defined as 2/3 of ignition temperature of the dust cloud and T_{S2} is the ignition temperature of a 5 mm layer of dust deducted by 75 K. T_{S2} is similar to the practice in Guideline1. When talking about the effectiveness of ignition, Rogala (2015) mentioned briefly that the maximum temperature was calculated by deducting 75°C from the 5 mm layer self- ignition temperature. This is somewhat similar to the practice in Guideline1. The Dangerous Substances and Explosive Atmospheres Regulations 2002 (DSEAR), on the other hand, recommend 220°C as the limit of safe surface temperature of an industry equipment.

In the other continent, the National Fire Protection Association (NFPA), a trade association in the United States that creates copyrighted standards adopted by the local government, had its own guideline about MPST. It was mentioned in NFPA 499 standard that the ignition temperature of an organic dust layer (biomass dust in this study is an example), could decrease as time elapses since the dust dehydrates. For this kind of material, the NFPA 70 states that the surface temperature of the heat producing equipment should not exceed the surface ignition temperature or 165°C, whichever is lower (NFPA, 2013).

It has been stated clearly in BS 50281-2-1 (British Standard, 1999b) that the ignition of combustible dust layers strongly depends upon the conditions local to a particular industry like the temperature distribution in that specific environment and that no single method suits every scenario in the wide range of industry processes. Thus, it is necessary that industry personnel adopt an appropriate method that goes well with that specific industry situation. In this case, researches and experiments are of ultimate importance.

It has been mentioned in BS 50281-2-1, that it is possible to estimate the minimum ignition temperature on heated surfaces of dust layers having intermediate or greater thicknesses than suggested in the standard, provided these results had been obtained following the procedures outlined in the standard. The ignition temperature of the new thickness could be estimated from linear interpolation or extrapolation of results from experiments performed, by plotting logarithm of the known layer thicknesses against the reciprocal of their corresponding absolute layer ignition temperatures in Kelvins (British Standard, 1999b). This estimation method is true for some materials and actual testing with the required thickness was preferred. Querol et al. (2006) had mentioned about estimating unknown T_{LIT} of desired layer thicknesses that had not been tested by plotting logarithm of layer thickness with corresponding known reciprocal of absolute T_{LIT} values.

In the biomass industry, be it in the processing plant (pellet- or briquette- making plant) or power station using the biomass as fuel, from the point of sourcing to the point of using, dust generation and accumulation are unavoidable along the whole process. Dust layer deposited on hot surfaces is a fire hazard and this danger can be eliminated if the self-heating characteristics leading to ignition is well understood. Since the operating conditions differ from one plant to another, each plant might adopt a set of practice that suits one's plant with appropriate reference to published guidelines.

The relationship of minimum dust layer ignition temperature (T_{LIT}) with its thickness from some studies reviewed here are summarised in **Figure 2. 6**. In essence, all work converge to one point – T_{LIT} decreases as layer thickness increases.

Holding the heat dissipation cross-sectional area constant, the reason for inverse relationship between T_{LIT} and dust layer thickness can reasonably be explained from the heat transfer perspective. A thicker dust layer causes the temperature gradient for heat transfer to lessen which results in an overall reduction in heat conduction rate. This is inline with the Fourier's Law of heat conduction, $q'' = -\lambda \nabla T$, which stated a phenomenological linear relationship between heat flux (q'') and temperature gradient (∇T) when heat transfers through a medium with constant thermal conductivity, λ . Consequently, local temperature increase within the dust layer accelerated the exothermic reaction, causing the dust layer to ignite at a lower hot plate temperature. Furthermore, the upper portion of thick dust layer insulates the centre portion. As a result, it is harder

for heat generated due to exothermic reaction at the layer centre to dissipate to the surroundings. Contrariwise, with the same heat loss cross-sectional area, the thinner dust layer of the same material experiences a relatively larger heat loss and thus, the layer can be heated to a higher T_{LIT} to reach ignition.

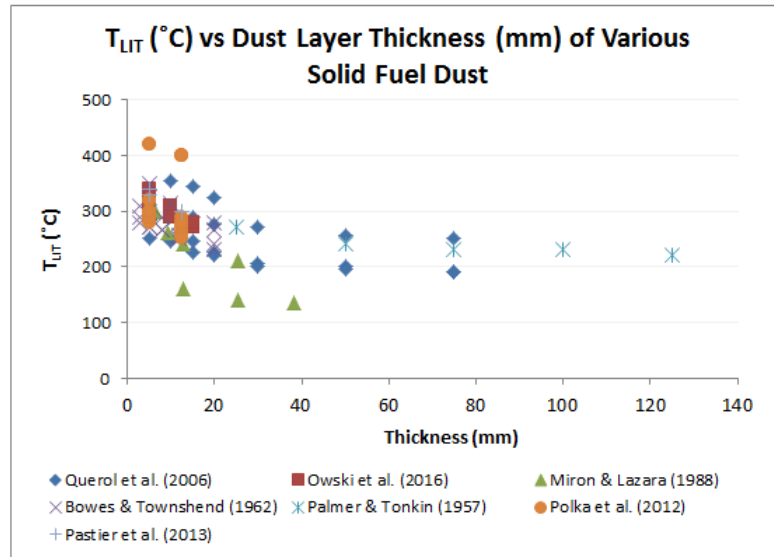


Figure 2. 6 Minimum Dust Layer Ignition Temperature as a Function of Its Thickness – Summary from Some Studies

2.3.1 Ignition of Single Material Biomass

There had been a few studies on dust layer ignition applying different methods on many different kinds of materials.

Jones et al. (2015) had used the BS 50281-2-1 to assess the minimum dust layer ignition temperature of seven biomass samples, namely mesquite, miscanthus, olive cake, plane, pine heartwood, red-berry juniper and sunflower husks. From the dust layer test, the ignition temperature of all these samples ranged from 290 to 320°C, with olive cake showing the lowest ignition temperature whereas pine heartwood showed the highest. Since flaming combustion had never been observed in dust layer tests for all samples but only smouldering combustion, it was concluded that the heated surface temperatures were insufficient to auto-ignite the volatiles. When natural log of ignition delay time was plotted against the inverse of hot plate temperature that ignited the dust in absolute temperature scale, a linear relationship was found. This implied that a high hot plate temperature would reduce the ignition delay time of a sample in the dust layer experiment.

El-Sayed and Khass (2013) investigated the smouldering characteristics of rice husk dusts on a hot surface. The effects of particle size and dust layer thickness on minimum temperature that caused the dust layer to ignite and the ignition times were considered. This study employed the method regarding evaluation of industrial hazards by using a hot plate as suggested by National Academy of Sciences (NAS). A circular aluminium plate of 20 cm diameter, 2 cm thick and powered by 750 W disc heater had been used in the risk husk study. The ignition temperature was determined from the onset of inflection or change in slope of the sample temperature-time profile. The minimum hot plate temperature that resulted in ignition and the ignition times of rice husk in three different sizes – 75-106 μm , 106-120 μm and 120-150 μm were compared. It was concluded that the delay time of the samples in ranges of 75-106 μm and 106-120 μm were quite similar, which was longer than that of 120-150 μm .

Querol et al. (2006) had used the BS 50281-2-1 procedure in determining the minimum dust layer ignition temperature of several dust samples, namely Beechwood dust, lycopodium dust, coal dust and dust blend comprising of 1/3 aluminium powder and the rest calcined alumina. The study had also mentioned briefly that the maximum permissible surface temperature (MPST) of those dust deposited in layers on electrical and mechanical apparatus could be estimated using the method described in BS 50281-1-2. A 5 K temperature interval was used in the dust layer test, with the effects of dust contained in variable ring diameters (100 to 260 mm) and layer thickness (5 to ~80 mm) studied. Besides the constant temperature method, the constant heat flux method was applied too but it was concluded that the constant power method was rather time consuming to be practical.

Upon realising that many powders regardless of being natural, synthetic, organic or inorganic would actually ignite even when present in a shallow layer when deposited on a hot surface, Henderson and Tyler (1988) had used sodium dithionite ($\text{Na}_2\text{S}_2\text{O}_4$) in a study about dual ignition temperatures for dust layers. Dual ignition temperature of dust layer were noticed when a material decomposes in a multistage process. The study had applied a 75 mm diameter ring to contain sodium dithionite particles that had been sieved through 60-80 mesh. The sample layer was fixed at 5 mm thick and its temperature was measured with a thermocouple located at half distance i.e. 2.5 mm from the hot plate. The plate temperature for the dust layer test was bracketed within a span of 5 or 10°C and ignition was considered when dust thermocouple showed at least 50°C above the plate temperature.

Polka et al. (2012) applied both Method A and Method B in BS 50281-2-1 to examine the minimum ignition temperature for dust layer and dust cloud respectively and later estimated the maximum permissible surface temperature of an apparatus. For the dust layer test, the effect of layer thickness of seventeen dust samples i.e. barley, beech,

buckwheat, cornflakes, corn starch, dried carrot, flour, hop, lemon balm, malt, nettle, oatmeal, rice flakes, semolina, senna fruit, sunflower husk and valerian were examined. It had been concluded from this wide range of samples used that dust from sunflower husk and medicinal herbs posed the greatest fire and explosion risk due to the combination effect of low bulk density and high heat of combustion of these materials.

Applying BS 50281-2-1, Pastier et al. (2013) had investigated the minimum dust layer ignition temperature of various wood dust – dust from particle board and fibreboard industry and dust that came from alder, ash, poplar and spruce tree cutting. Wet and dried samples had been used in that study and it was concluded from the temperature-time plot of these samples that the ignition temperature was affected insignificantly but a longer time was needed for a glow (indication of ignition) to be observed.

In a study on determining dust layers smouldering temperature based on adiabatic tests, Engel et al. (2016a) had used DIN EN 50281-2-1 (Method A) and simulations based on the famous theory of Frank-Kamenetski and Thomas to obtain the minimum ignition temperature of dust layers. The dust samples used were cellulose, wheat flour, cocoa powder and charcoal powder and the smouldering temperature of a material was defined as the minimum ignition temperature of its dust layer. The effects of having two different dust thicknesses on smouldering temperature were considered using both methods and comparison between the experimental value and that obtained from simulation showed a difference of <8%. It was also suggested that a safety margin of 75 K (75 K lower than the material smouldering temperature) to be used to set the maximum permitted surface temperature of pumps, pipings and other equipment in a plant.

2.3.2 Ignition of Biomass Blended with other Materials

In the power generation sector, co-firing a renewable fuel source like biomass with fossil fuel coal is increasingly popular as utilising biomass as green energy is deemed to defer climate change caused by global warming. It is therefore not uncommon that the dust accumulated and deposited on the floor, beams, machinery surfaces etc. was made up of blends of coal dust and biomass dust. Also, a power station fires a variety of solid biomass fuels in its daily operation and thus, the dust deposits on hot surfaces within a power station or any industrial plant could consist of mixture of several combustible dust materials. This forms a large part of this thesis and there have been little work published in this area.

Reddy et al. (1998) investigated the effects of having either of the two inert materials i.e. dolomite or limestone added to two coal samples, Prince coal and Pittsburgh coal on their dust layer ignition temperature and ignition induction time. The hot plate used resembled the design and setup of Miron and Lazzara, in which a 2.4 kW domestic

stove heating element was utilised to heat the 20 mm thick stainless steel plate of 200 mm diameter. Similar to others' works, the dust material to be tested was contained within a metal ring of 100 mm diameter and heights of 5, 10, 15, 20, 25 mm were used. The dust layer thermocouple was fixed at the level where its junction lay 3 mm above the hot plate. The dust layer experiments with inerts added were only conducted with the Ring of 10 mm height. Prince coal was blended with dolomite in 0, 40, 50, 60 and 70 wt% dolomite and it was found that as the amount of dolomite increased, the ignition temperature increased (250°C to >400°C) and induction time decreased. The blend with 70 wt% dolomite showed a complete loss of ignition. Pittsburgh coal blended with limestone or dolomite showed the same trend as Prince coal that was blended with dolomite in different ratios.

Adding binders to powdery or loosely-bounded solid fuel to reduce the bulkiness and hence eases fuel transportation is one of the many reasons of binder addition to solid fuel. The usage of binders had started as early as before 1900s for which at that time binders application focused on improving the then popular solid fuel – coal. Not all binder are of the same nature (Yohe, 1964) and mainly, they were categorised into two main groups; inorganic and organic binders. When briquetting or pelleting are concerned, clay, lime, magnesia and various cements are examples of inorganic binders used whereas tar from various wood, sugar factory residues, different kinds of starches, natural asphalts and some petroleum products are examples of organic binders. It is well known that using inorganic binders often decreases the heating value of the fuel since this increases the ash content (Mills, 1908).

It is a common practice in the power industry to receive solid fuels in briquetted or pelleted form and binder addition in briquettes or pellets is a recognised economical means of reducing bulkiness of biomass fuel. Biomass briquettes or pellets with binder hold the solid fuel in shape along the lengthy transportation journey from one place to the other, for instance shipping from the North American to the United Kingdom. Having binders reduces the chances of biomass solid fuel briquettes/pellets from generating dusts, and remaining intact upon reaching the final shipping destination. In the U.K., there is legislation that prohibits pellet producers from using any form of artificial binder; applying pressure and producing frictional heating that softens the cell wall's lignin content and thus forming a kind of natural binding mechanism is preferred, but other ways of binding is practised too because this method is not always strong enough to hold the briquette or pellet in place as it starts to degrade the moment binding is formed (Atkinson, 2016).

Having binders in biomass fuel briquettes or pellets had been proven to make the solid fuel stronger, more sustainable to mechanical compression and more impact resistant, as shown in various studies about fuel briquettes (Chin and Aris, 2012; Demirbas, 1999; Yaman et al., 2000; Chin et al., 2013). Having good mechanical properties implies less material loss along the transportation process from source point to application point.

According to Mills (1908), one of the desired qualities of a binder material is its properties that hold strongly the raw material and produce a sufficiently hard but not too brittle briquette. Knowing this fact, it is important for a briquette producer to formulate the just-enough binder material to be added to the raw material. In another study by Chin and Aris (2013) that compared using waste paper binder and starch binder on fuel briquettes made of oil palm mill residues, it was found that briquettes with either binder exhibited mechanical properties superior to the briquettes without any binder.

Tarasov et al. (2013) investigated the effects of having additives in wood pellets and found that the presence of additives altered the physical and thermal characteristics of the wood pellets. A major positive impact was that the mechanical durability which is important in biomass pellets transportation and storage did improve – the pellets with additives have become more abrasion and impact resistant and that maize starch (corn starch or cornflour) and lignosulphonate were found to be better additives for power consumption per unit of wood pellet output as compared to the other additives.

Ugwu (2013) evaluated the properties of fuel briquettes made of empty fruit bunches when either of the two binders – asphalt or cassava flour starch were added. Briquettes properties like physical appearance, calorific value, moisture content, ignition time, power output, burning rate, smoke and odour were compared between the briquette with asphalt binder to the one with starch binder. The study concluded that the briquette with starch binder had better desirable performances and could be a candidate for use in industrial heating or industrial boilers.

According to Holm-Nielsen (2016) and Ehimen (2016), binders may be used in the biomass pelletisation process and during the binder addition process, pressure and heat were applied. Raw material of the pellets i.e. biomass dust could be deposited on various surfaces of the pellets making machine. It may be worth checking the dust layer minimum ignition temperature of a particular raw material for pellet-making and taking precautions to ensure that the surface temperature of pelletising machine is kept below the maximum permissible surface temperature (MPST) estimated.

2.4 Reaction Kinetics Estimation and Ignition Delay Time Prediction for Dust Layer Ignition

A definite and straight forward method to determine the reaction activation energy, E , for a dust layer that ignited upon heating on a hot surface has yet to be achieved but researches are on going to improve the current techniques. As mentioned by Babrauskas (2003a), despite knowing the hot plate temperature, T_p , and ambient temperature, T_a , from hot plate experiments, the value of E for a particular dust layer tested on a hot

surface experimental setup is generally not known a priori. At present, most methods involve laborious iterations.

2.4.1 Hot Surface Ignition Test Kinetic Parameters Estimation

Thermal runaway happens in a material when heat generated by a chemical reaction taking place within the body fails to dissipate sufficiently rapidly to its surroundings (Beever, 1986). Thermal runaway or supercritical self-heating can be termed more simply as spontaneous ignition and has been recognised as a serious hazard. Dust layer ignition due to thermal runaway are among the most frequent causes of fires in industry, followed by dust explosions (Dyduch and Majcher, 2006). Thermal runaway caused by thermal imbalance between heat generation and heat loss rates results in a sudden temperature increase. Pioneers in this study proposed theories on thermal runaway; Semenov's thermal runaway theory assumes constant temperature distribution throughout a reaction zone with heat loss at the boundary whereas Frank-Kamenetskii assumed temperature distribution in the reaction zone but without heat transfer at the boundary (Park et al., 2009). Thomas and Bowes (1961) overcame the limitations in each with consideration of both temperature distribution in the reaction zone and heat loss on the boundaries. According to Hagen (2013), the situation where one side of a sample being heated and the other surfaces being cooled is a more common situation encountered, as compared with uniform heating at all surfaces of a sample. Examples like dust deposited on hot surfaces of an electrical equipment (Hagen, 2013), dust layer accumulated on flat surfaces such as above false ceiling, ducts and floors in industry handling fine powders (Joshi, 2012) are common.

The heat transfer involving heat generation and heat loss happening in a biomass dust layer deposited on a hot surface could be modelled following the theory of thermal ignition (Thomas and Bowes, 1961) developed by Thomas and Bowes (Joshi, 2012). In that study, Thomas and Bowes (1961) developed the theory focusing on thermal ignition of a slab of reactive material held at a constant high temperature on one face and Newtonian cooling at the other. In the current study, the biomass dust layer deposited on a hot surface (see **Figure 2. 7**) resembled the slab of reactive material, the dust layer bottom was the face held at constant temperature whereas the dust layer top exposed to the surroundings was the face subjected to Newtonian cooling.

Based on the conservation of energy principle, transfers of energy in and out of a differential control volume of a system (slab in this case) exclusively by conduction can be represented by three terms illustrated as follows:

$$\left[\begin{array}{c} \text{Net Thermal Energy Transfer} \\ \text{into the Control Volume} \end{array} \right] + \left[\begin{array}{c} \text{Thermal} \\ \text{Energy} \\ \text{Generation} \end{array} \right] = \left[\begin{array}{c} \text{Change in} \\ \text{Thermal} \\ \text{Energy Storage} \end{array} \right]$$

From the energy conservation, the differential equation of heat conduction that provides the temperature distribution in a system (slab in this case) can then be written mathematically in Cartesian coordinates as:

$$\left[\frac{\partial}{\partial x} \left(\lambda \frac{\partial T}{\partial x} \right) + \frac{\partial}{\partial y} \left(\lambda \frac{\partial T}{\partial y} \right) + \frac{\partial}{\partial z} \left(\lambda \frac{\partial T}{\partial z} \right) \right] + [\dot{q}] = \left[\rho c_p \frac{\partial T}{\partial t} \right]$$

In this layer of heated dust, heat conducted from the heated plate through the layer increased the dust layer temperature, leading to greater heat generation rate within the layer and this heat generation was actually competing with the heat loss via convection and radiation at its top surface. This slab analogy had been adopted by many other researchers in this field; El-Sayed and Mostafa (2016) in the study of sugarcane bagasse and cotton stalks dust layer on hot surface ignition tests , Joshi (2012) in a study on factors affecting spontaneous ignition of combustible dust, among others.

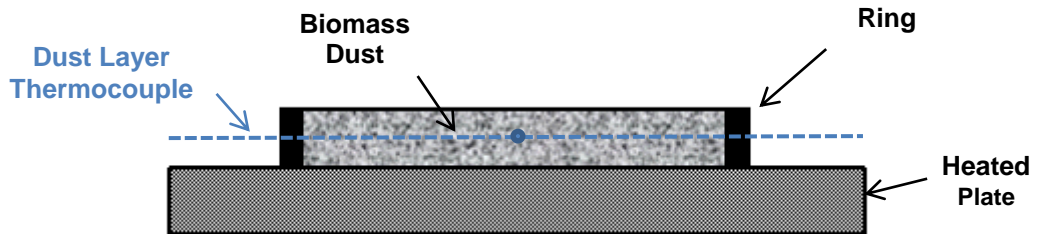


Figure 2. 7 Biomass Dust Layer Deposited on a Hot Plate

Considering the dust deposited on a hot plate in **Figure 2. 7** as a case of infinite slab of a given thickness being heated (Drysdale, 2011; Park et al., 2009; El-Sayed and Mostafa, 2016), the heat generation rate (\dot{q}) follows the zeroth order (the heat generation reaction involves no depletion or consumption of reactant) Arrhenius equation (Joshi, 2012) as an exponential function of temperature ($Ae^{-E/RT}$) and thus the one dimensional (either x-, y- or z- direction only) steady state (independent of time, negligible $\partial T/\partial t$) heat conduction (Park et al., 2009) was written as follows:

$$\lambda \frac{\partial^2 T}{\partial x^2} = -\rho Q A e^{-E/RT} \dots \text{Equation 2.1}$$

where

- λ is thermal conductivity of dust layer ($W/m \cdot K$)
- T is temperature in (K)
- x is distance parameter (vertical in this case) for heat transfer in (m)
- ρ is density (kg/m^3)
- Q is heat of reaction (J/kg)
- A is Arrhenius pre-exponential factor ($1/s$)
- E is reaction activation energy (J/mol)
- R is universal gas constant ($= 8.314 J/mol \cdot K$)

The parameters used in **Equation 2.1** are described further in the later part of this section and **Section 3.1.6**.

Heat generation rate follows the Arrhenius equation and thus presented as an exponential function of temperature whereas heat loss is represented as a linear function of temperature and the thermal runaway phenomenon experienced by a heated dust layer is illustrated in **Figure 2. 8** and can be described as follows (Park et al., 2009):

If the hot plate is set at temperature T_{p2} , in the beginning, the heat generation rate exceeds the heat loss rate and causes increase in dust layer temperature until thermal balance is achieved at point A. Thermal balance point C is deemed unstable since heat loss is greater than heat generation below point C and any small perturbation that caused layer temperature to reach beyond point A will be directed back to thermal balance point A. The dust layer temperature remains in steady state when the hot plate is fixed at T_{p3} since heat generation rate in dust layer equals to the heat loss rate. Any increase in hot plate temperature from T_{p2} to T_{p3} will cause point C to decrease towards point A, resulting in point B. However, if the hot plate temperature is increased slightly to T_{p4} , heat generation rate begins to exceed heat loss rate, resulting the dust layer temperature to continuously increase and reach thermal runaway.

Dust layer with assumed thickness of $2r$ is asymmetrically heated with heated plate at position $x = 0$, the slope of temperature distribution is determined by heat loss at the top boundary ($x = 2r$) and thermal conductivity (λ) of the dust material. Lines 2 and 3 (correspond to T_{p2} and T_{p3}) show steady state with Line 3 the maximum possible steady

state condition to occur in the dust layer. At T_{p4} which is slightly hotter than T_{p3} , transient temperature profile (Line 4) signifying thermal runaway appears within the heated dust layer.

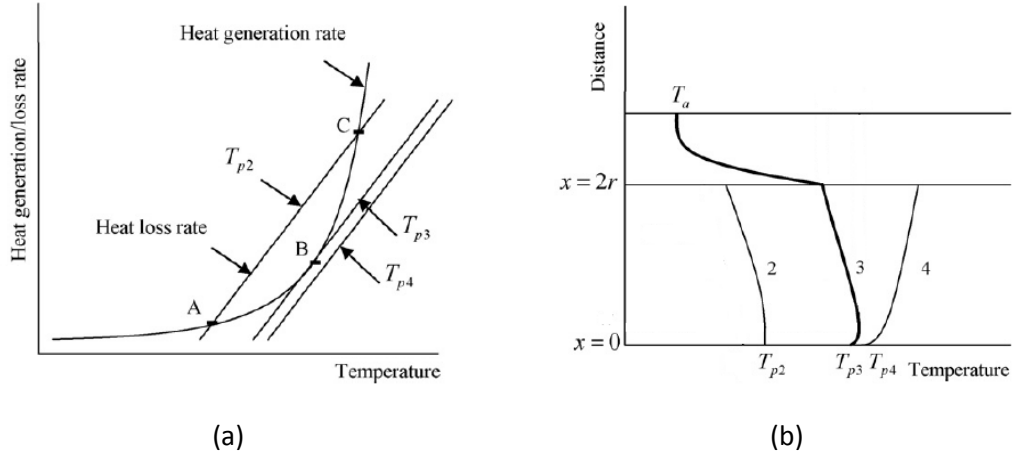


Figure 2. 8 Thermal Runaway Phenomenon (a) Heat Balance in a System Generating and Losing Heat (b) Temperature Profile within Dust Layer [Edited from: Park et al. (2009)]

To simplify **Equation 2.1**, the non-dimensional equation (**Equation 2.2**) for this steady state (Park et al., 2009) was obtained as:

$$\frac{\partial^2 \theta}{\partial z^2} = -\delta e^\theta \dots\dots \text{Equation 2.2}$$

where dimensionless terms for temperature (θ), distance from hot plate (z) and heat generation rate (δ) were defined as:

$$\theta = \frac{E}{RT_p^2} (T - T_p) \dots\dots \text{Equation 2.3}$$

$$z = x/r \dots\dots \text{Equation 2.4}$$

$$\delta = \frac{E}{RT_p^2} \frac{r^2 \rho Q A}{\lambda} e^{(-E/RT_p)} \dots\dots \text{Equation 2.5}$$

with r equals to half the dust layer thickness and T_p signifies the hotplate temperature.

The maximum non-dimensional heat generation term, δ_c , at steady state condition for this an asymmetrically heated biomass dust layer could be approximated with the following correlation:

$$\delta_c \approx \frac{1}{2} \left(\frac{Bi}{1+2Bi} \right)^2 (1.4 - \theta_a)^2 \dots\dots \text{Equation 2.6}$$

where Bi is the Biot number and θ_a is the dimensionless parameter for ambient temperature, defined respectively as:

$$Bi = h_t r / \lambda \dots\dots \text{Equation 2.7}$$

$$\text{with } h_t = h_c + h_r \dots\dots \text{Equation 2.8}$$

$$\text{and } \theta_a = \frac{E}{RT_p^2} (T_a - T_p) \dots\dots \text{Equation 2.9}$$

where h_t is the total effective heat transfer coefficient, h_c the convective heat transfer coefficient and h_r the radiative heat transfer coefficient with all in $(W/m^2 \cdot K)$ and T_a is the ambient temperature.

The convective heat transfer coefficient, h_c , and h_r the radiative heat transfer coefficient were calculated as such:

$$h_c = \frac{0.54 Ra^{0.25} \lambda_a}{L}, \text{ for } 10^5 \approx < Ra \approx < 10^7 \dots\dots \text{Equation 2.10}$$

$$h_r = \varepsilon \sigma (T_s^2 + T_a^2) (T_s + T_a) \dots\dots \text{Equation 2.11}$$

with Ra the Rayleigh number, λ_a the thermal conductivity of air, L the characteristic length equals to the side of the square having the same area of dust layer surface exposed to ambient and ε the biomass dust emissivity, σ the Stefan-Boltzmann constant ($5.67 \times 10^{-8} W/m^2 K^4$), T_s the top surface temperature of dust layer

The Rayleigh number was calculated with the following correlation:

$$Ra = \frac{g \beta (T_s - T_a) L^3}{\nu \alpha} \dots\dots \text{Equation 2.12}$$

with g the gravitational acceleration ($9.81 m/s^2$), β the inverse film temperature whereby film temperature is the average of top surface temperature, T_s , and the ambient temperature, T_a , ν the kinematic viscosity of air and α the thermal diffusivity of air, both ν and α evaluated at film temperature and having m^2/s as the unit.

An equation relating the logarithm of dimensionless heat generation rate, δ_c , and the critical layer ignition temperature, T_p , could be plotted as:

$$\ln \left(\frac{\delta_c T_p^2}{r^2} \right) = -\frac{E}{RT_p} + \ln \left(\frac{E}{R} \frac{\rho Q A}{\lambda} \right) \dots\dots \text{Equation 2.13}$$

in which the reaction activation energy is then calculated from the slope of equation.

The critical heat generation rate, δ_c , for this asymmetrically heated biomass dust layer that had been approximated to an infinite slab could also be estimated from **Figure 2.9** besides calculating from **Equation 2.6**. This biomass dust layer heating case was considered a scenario of asymmetrically heated layer since the layer maximum temperature did not happen in the centre of the slab (Tamburello, 2011). As suggested by the word critical, the heat generation rate had just surpassed the heat loss rate and ignition was initiated at this condition.

Figure 2.9 shows the relation between a few dimensionless parameters, δ_c , Bi , θ_a , θ_m and z_m , for an asymmetrically heated slab. In the biomass dust layer context, the two parameters, θ_m and z_m that signify the maximum layer temperature and the location in dust where it happens, respectively, can be disregarded when the maximum temperature in the dust is assumed to happen exactly at the hot surface, i.e. dust layer was in perfect thermal contact with the hot surface, although in reality it happens slightly above the bottom most location. This assumption had actually led to another boundary condition, $\frac{d\theta}{dz} = 0$ at $z = 0$; which implies δ_c can be approximated without the z_m and θ_m terms (Park et al., 2009).

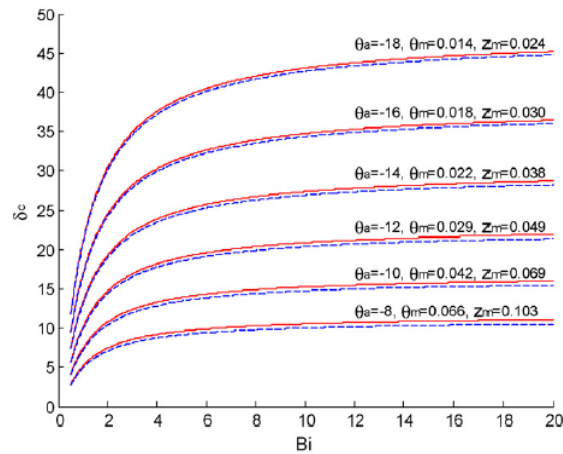


Figure 2.9 Correlation between δ_c , Bi , θ_a , θ_m and z_m for Asymmetrically Heated Slab [Source: Park et al. (2009)]

Almost all the above correlations and equations have been applied by many researchers in determining reaction activation energy, E , of various dust samples subjected to hot surface ignition test. Park et al. (2009) estimated the kinetic parameters, i.e. activation energy, E and coupled term QA of heat of reaction and Arrhenius pre-exponential factor on Pittsburgh seam coal. E and coupled term QA for sugarcane bagasse and cotton stalk were investigated the same way by El-Sayed and Mostafa (2016). Wu et al. (2014) investigated the E for South African coal, Sebuku coal and Pittsburgh coal when the

dust layers were subjected to hotplate tests under normal air atmosphere and different oxy-fuel combustion atmospheres. The heat of reaction term, Q , was taken to be equal to the gross calorific value of the sample.

The hot surface ignition experiments on various different dust samples in the work of Park et al. (2009) and El-Sayed and Mostafa (2016) had adopted the test guidelines in *ASTM E2021 Standard Test Method for Hot-Surface Ignition of Dust Layers*, which was slightly different as compared with the *BS EN 50281-2-1 Electrical apparatus for use in the presence of combustible dust. Test methods. Methods of determining minimum ignition temperatures* that had been applied by Wu et al. (2014). These studies used iterative methods to some extent to reach E and coupled term QA values of respective dust materials.

Park et al. (2009) applied numerical and experimental methods in combination in the study of estimating thermal and kinetic parameters of coal dust layer experimented in hot surface ignition test.

Looking at **Equation 2.1**, it was recognised that having unknown parameters E and QA (coupled term QA was treated as one unknown) caused the equation rather complicated to solve even with numerical method. Therefore, an approach to correlate E and QA was attempted such that two unknowns were reduced to one, achieved by re-expressing **Equation 2.5** in a logarithm format which showed correlation between E and QA , as in **Equation 2.14**.

$$\ln(QA) = \frac{1}{RT_p} E + \ln\left(\frac{\delta_c RT_p^2 \lambda}{Er^2 \rho}\right) \dots\dots \text{Equation 2.14}$$

To obtain a correlation between QA and E , plotting $\ln(QA)$ with respect to E was the way used. The initial value of E was obtained from other published literature whereas the T_p value used was obtained from experiment. Holding constant the T_p value, a range of $\ln(QA)$ could be plotted with the range of E values in published literature (see **Figure 2. 10**). The δ_c term that appeared as in the y-intercept was determined from **Equation 2.6**, and the required Bi and θ_a values were solved with **Equation 2.7** and **Equation 2.9** respectively. Since the thermal properties in the study by Park et al. (2009) were estimated with assumption of inert dust layer, the Bi and λ was respectively simplified to $Bi = \frac{h_t r}{\lambda} = \frac{T_p - T_s}{2(T_s - T_a)}$ and $\lambda = -h_t(T_s - T_a) \frac{dx}{dT} = \frac{-h_t(T_s - T_a) dx}{(T_s - T_p)}$. The T_s value was determined from the steady state temperature profile of the dust layer that was obtained experimentally. The E value that was required in the equations was fixed within the range published in literatures. With the correlation between QA and E obtained, two unknowns were now reduced to only one unknown.

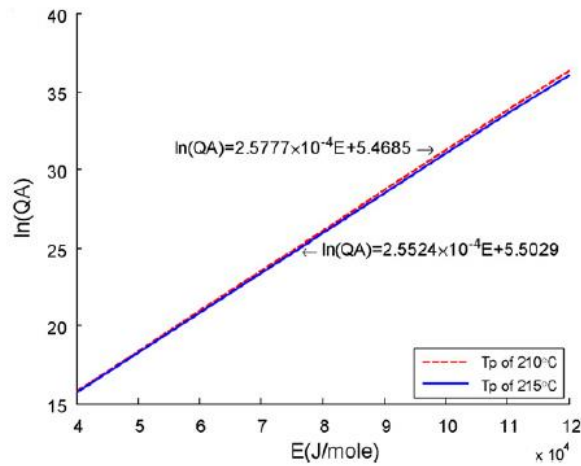


Figure 2. 10 Correlation between QA and E at fixed T_p [Edited from Source: Park et al. (2009)]

A similar approach as Park et al. (2009) was applied by El-Sayed and Mostafa (2016) where different θ_a values were calculated to obtain the corresponding δ_c values for T_p values that varied within the critically igniting and non-igniting temperatures.

Wu et al. (2014) on the other hand, calculated the E by assuming δ_c a function of dust sample geometry only. δ_c of 0.88 was given to all dust layer samples since these dust layers were assumed to take the shape of infinite slab. In these three respective hot surface studies, the experimental T_s values were obtained from an extra thermocouple located 1-2.7 mm below the top dust layer surface.

According to Beever and Thorne (1981) in a study about isothermal methods for assessing combustible powders, E/R value was first assumed to estimate a θ_a value. This θ_a value, coupled with the corresponding Biot number of that particular dust layer would then lead to a δ_c value by applying the graph (see **Figure 2. 11**) given by Thomas and Bowes (1961). With different δ_c values obtained for each different dust layer thickness, a straight line with $\ln\left(\delta_c \frac{T_p^2}{r^2}\right)$ versus $1/T_p$ was then plotted. The slope of the line was E/R and the new found E enabled a more accurate prediction of θ_a . Plotting of $\ln\left(\delta_c \frac{T_p^2}{r^2}\right)$ versus $1/T_p$ line using the new set of δ_c values for each dust layer thickness was possible with the updated θ_a . This process was repeated until value of E/R converged.

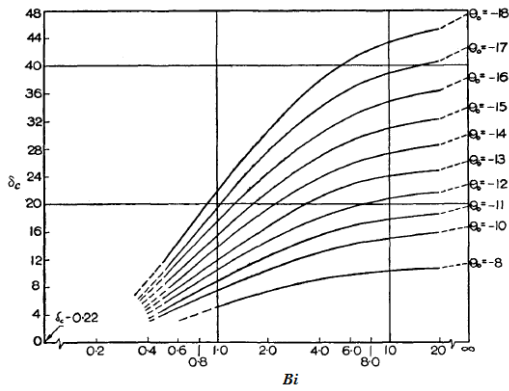


Figure 2. 11 δ_c as a Function of α and θ_α
 [Edited from Source: Thomas and Bowes (1961)]

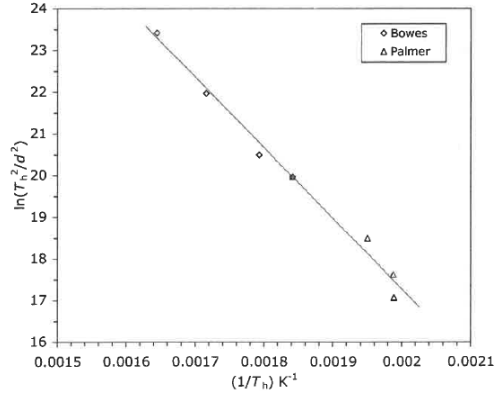


Figure 2. 12 Example of Crude Estimation of E Via a Simple Correlation for Sawdust [Source: Babrauskas (2003a)]

A quick but crude estimation of the reaction E had been proposed by Babrauskas (2003a) since theory-based calculations were quite onerous. This quick method involved plotting $\ln\left(\frac{T_h^2}{d^2}\right)$ as a function of $1/T_h$ where T_h is the hotplate temperature (K) and d is the dust layer depth (m). The slope of this straight line is E/R and E was easily calculated with the known gas constant value of R . An example of applying this quick method is illustrated in **Figure 2. 12**, with sawdust data from Bowes and Palmer and a reasonably straight line was obtained. However, it should be noted that the accuracy of this method was valid within 5 to 75 mm since massive deviation was discovered when the dust depth exceeded 75 mm.

Many researchers predicted the dust layer thermal conductivity with the assumption of the dust being an inert material (El-Sayed and Mostafa, 2016; Wu et al., 2014; Park et al., 2009; Beever and Thorne, 1981). By assuming an inert dust layer, i.e. thermal conductivity a constant not varying with temperature, the complicated Arrhenius heat generation term in **Equation 2.1** was neglected and linear temperature profile was obtained throughout the dust layer. With the ambient, hot plate, and top surface temperatures T_a , T_p and T_s and dust layer depth known, the thermal conductivity, k , was easily determined by simply applying one dimensional Fourier’s Law of heat conduction within the layer and equating it to the convective and radiative heat loss (Beever and Thorne, 1981). Following a solid biomass thermal conductivity study by Mason et al. (2016), it had been found that thermal conductivity and density of woody biomass showed a linear relationship. As for the emissivity value for radiative heat transfer, most work took the value of $\varepsilon = 0.9$ for biomass. This value is consistent with published values; 0.82-0.92 (Cengel and Boles, 2008) and 0.895 (Maloney, 2007).

2.4.2 Hot Surface Ignition Test Ignition Delay Time Prediction

There have been a few studies that delved into the ignition delay time correlation for the hot surface ignition test. In the study by El-Sayed and Mostafa (2016) on sugarcane bagasse and cotton stalk dust layer ignition on hot surface for four dust thicknesses, holding the particle size constant, the empirical correlation between ignition delay time t_{ign} and dust thickness (d) had been found as $t_{ign} = 2d - 7.11$ with correlation coefficient $R^2 = 0.956603$ for sugarcane bagasse and $t_{ign} = 3d - 16.15$ with $R^2 = 0.958688$ for cotton stalks. In another hot surface ignition study by El-Sayed and Khass (2013) on Egyptian rice husk dusts, a correlation of $\tau = 23.851h + 19.569$ (τ is ignition delay time in minute, h is dust thickness in cm) had been found for dust particles of 106-120 μm contained in 5 cm diameter ring with four varying ring heights. El-Sayed and Abdel-Latif (2000) had investigated the relationship between time to ignition t_{ign} and hot surface temperature T_p for cornflour and mixture of 80% wheatflour with 20% cornflour and the correlation of $t_{ign} = 0.028 (T_p)^2 - 18.1T_p + 2936$ was found within accuracy of 4% (see **Figure 2. 13**). One important thing to note is that all the experiments conducted by El-Sayed and Mostafa (2016), El-Sayed and Khass (2013) and El-Sayed and Abdel-Latif (2000) were conducted in accordance to ASTM E2021 and the ignition had been defined as 50°C above T_p .

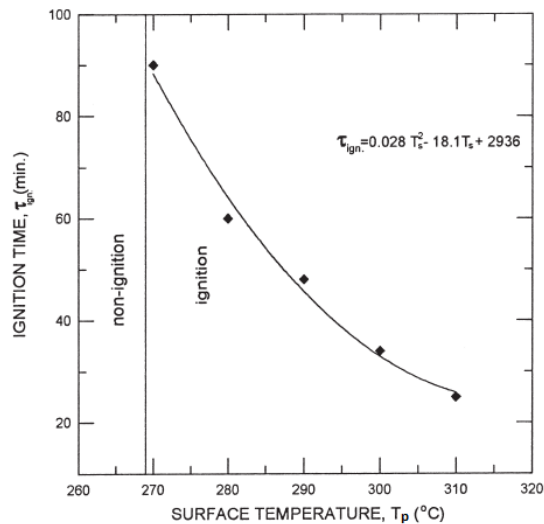


Figure 2. 13 Correlation of Time to Ignition – Hot Surface Temperature for Cornflour-Wheatflour Mixture [Edited from Source: El-Sayed and Abdel-Latif (2000)]

As mentioned by Beever and Thorne (1981), prediction of times to ignition is frequently poor. Therefore, it is not surprising that it is difficult to get a robust standard that enables empirical correlation to compare with. In any event, all empirical correlations from various studies show a similar trend – for the same material, the ignition delay time

increases as the dust gets thicker and that ignition delay time decreases as the hotplate temperature get higher.

2.5 Storage – Biomass Pile Ignition Characteristics

In studying the low temperature or self-ignition risk of biomass during storage, many different methods had been adopted. These approaches were generally divided into computer simulations and experimental measurements. Finite element method applying the software COMSOL Multiphysics had been used by Ferrero et al. (2009) in a self-ignition study during pine woodchip and pine sawdust storage. Blanchard (2007) on the other hand used a computation fluid dynamics (CFD) method in the study of wood pellets self-ignition, applying the Smoke Movement and Flame Spread (SMAFS) and Fire Combustion SIMulator (FIRCOSIM) softwares.

There are numerous experimental approaches in exploring material self-ignition characteristics, mainly the adiabatic method or the more common isothermal method. Back in the 19th century (DeHann, 1996), the problem of materials' self-heating was apparent from fire occurrences during the cotton and linen treatment process when different oils were applied. As a consequence, the Mackey test to determine the characteristics of oil type suitable for the treatment process emerged, and was first documented in 1895. The test was quite straightforward, in which a sample of oiled-fabric was exposed to a 100°C, constant temperature steam bath (representing the ambient temperature) for two hours and if the oiled-fabric reached 200°C in two hours, the materials was deemed unsuitable. The original version of the Mackey test indicated a good beginning for self-heating characterisation.

At present, the experimental way of assessing self-heating that leads to self-ignition characteristics are divided into two main types – the adiabatic approach and the isothermal approach. The common adiabatic experiments are the ones using adiabatic calorimetry, that are the Self-Ignition Tester (SIT) and Accelerating Rate Calorimeter (ARC). On the other hand, the conventional isothermal tests often applied are Oven Basket Test/ Wire Mesh Cube Test, United Nations Test N.4 and the Hot Storage Basket Test.

As the word adiabatic suggests, the SIT operates with an adiabatic furnace where heat losses to the surroundings have been minimised as far as possible. The adiabatic SIT is deemed more advanced than conventional isothermal tests according to Li et al. (2006) because the slight heat contributed by microorganism respiration and fermentation liberated at the initial stage of self-heating could be traced. This equipment has proven useful in studies of the transition from self-heating to spontaneous ignition of a material according to Li et al. (2006) in a study of spontaneous ignition of wood chips. Furthermore,

SIT produced reliable results and required a lot less material as compared with conventional isothermal tests. In another study by Li et al. (2008) on thermal behaviour of sewage sludge, comparison of results from SIT with that from wire mesh cube test showed that the latter had failed to capture weak heat source due to significant heat loss experienced in the isothermal wire mesh cube. Moreover, it was found that the wire mesh cube test did not retain the moisture needed for biological activities of the sample material and thus the wire mesh cube test cannot consider all possible heat sources that trigger-self ignition. Conversely, the SIT operated on adiabatic retains moisture required for biological activities thus considers all contributing heat sources in self-ignition assessment. The accelerating rate calorimeter (ARC) was mainly applied to examine a runaway reaction, which is the transition from self-heating to the self-ignition phase. Applying the Heat-Wait-Search (H-W-S) mode, exothermic reactions like thermal decomposition is detected and the first temperature at which heat accumulation starts is obtained (Fei and Liang, 2011). With the ARC, the onset or critical ignition temperature of materials that possess self-heating characteristics (Exponent Engineering and Scientific Consulting Inc., 2010) could be determined.

The isothermal Oven Basket Test or known as Wire Mesh Cube Test in some literatures, the United Nations Test N.4 and the Hot Storage Basket Test adhering to BS EN 15188 share some similar features. All these tests involve an oven set at a constant temperature represents the hot environment which a sample is subjected to and the sample temperature is monitored for a certain period of time.

The oven basket test was initiated at the U.K. Fire Research Station (FRS) by Philip Bowes and colleagues and the tests were refined over the decades. Beever (2013), a researcher in the fire dynamics field, has summarised this test method and included it in a Society of Fire Protection Engineers (SFPE) Handbook (IEA Bioenergy, 2013). Employing the FRS test method, the sample to be investigated is placed inside a wire mesh cube and the cube is placed inside a fixed temperature oven. Over time, the oven temperature and sample temperature measured at the centre of the sample are recorded. From the self-ignition experiments conducted on a few wood flour, Beever (1986) observed the sample temperature distribution at different distances measured from the centre of the test basket with a total of 15 thermocouples. At a storage temperature that critically ignited a sample, the maximum temperature of as high as $>1000^{\circ}\text{C}$ was recorded at the centre of the basket after the sample ignited.

The United Nations (UN) and the United States Department of Transportation (DOT) have developed an appropriate classification procedure with relevant tests to categorise goods to be transported (Chilworth Technology Inc., 2012), (United Nations, 2009). In Part III of the UN manual, under Class 4 Division 4.2, there is a section detailing the test procedures of substances liable to spontaneous combustion. The Test N.4: Test

method for self-heating substances includes assessments to classify these substances (United Nations, 2009). The UN Test N.4 involves an isothermal storage experiment, aimed to examine the ability of a substance undergoing oxidative self-heating in a volume by exposing it to air at constant environment temperatures of 100°C, 120°C and 140°C (Li et al., 2006). The test involves a hot-air circulating type oven that has an inner volume of at least 9 litres and is capable of achieving internal temperature of 100°C, 120°C and 140°C with precision of $\pm 2^\circ\text{C}$. There are two cubic sample containers, one with 25 mm and the other with 100 mm for each of their respective three sides. Both sample containers are made of 0.05 mm mesh opening stainless steel net and have their top surface open. While filling the container with sample in powder or granular-form, it is tapped several times to ensure the container is filled to the brim. Two temperatures are measured with two separate 0.3 mm diameter Chromel-Alumel (k-type) thermocouples; one placed in the centre of the test sample and the other between the sample container and the oven wall. Throughout the test, both the sample temperature and oven temperature are to be recorded continuously. At first, the test is usually conducted with the 100 mm cube at 140°C. A positive result means either spontaneous ignition is seen or the sample temperature exceeds the oven temperature by 60°C within the 24 hour test duration. When negative results are obtained, there will not be any further tests; but if a positive result is achieved, a second test with the 25 mm cube at 140°C will then be conducted. If a positive result is obtained for the 25 mm cube at 140°C, the material would be categorised under Packing Group II or else, the test would be repeated with the 100 mm cube at 120°C followed by 100 mm cube at 100°C if the previous test yields a negative result. All these results would be used together with the UN Recommendations that provide appropriate guide for marking, labelling, packaging, segregating and documentation of that particular item (New Zealand Ministry of Transport, 2008) and the safest mode of transport could then be decided. However, according to Li et al. (2006) this UN Test N.4 neglects heat contributions from low temperature faint reaction during material self heating.

The other commonly used isothermal test for material self-ignition characteristics is the hot storage basket test BS EN 15188:2007 – *Determination of spontaneous ignition behaviour of dust accumulations*. Besides determining the self-ignition temperatures, the induction times to achieve materials ignition could be obtained from the hot storage test. The BS 15188 specifies analysis and evaluation procedures involved in determining self-ignition temperatures (T_{SI}) of sample materials (in dust or granular form) as a function of volume via hot storage experiments in ovens. T_{SI} is defined as the highest temperature at which the dust does not ignite for a given dust volume. The mesh wire baskets to contain the samples could either take the cube shape or a cylinder that has height to diameter ratio of one. Compared to UN Test N.4; similarities are that the basket is tapped several times throughout the filling process to loosely fill but not compress the dust, sample temperature and oven temperature are recorded throughout the test but differences are

that a minimum of three different volume baskets and ~120 litres of useful oven volume are required in the hot storage test. This BS 15188 Hot Storage Basket test method had been applied in this study and the details of experiment setup is described in **Chapter 3**.

The sequential analysis is performed following recommendations from BS 15188. The temperature-time plot of each experiment is useful in determining the critical ignition temperature or self-ignition temperature (T_{SI}) of a sample and the idealised temperature-time plot is illustrated in **Figure 2. 14**. ϑ_A , ϑ_B and ϑ_C represent three different, constant hot storage temperatures used in the hot storage experiment. Curve A that corresponds to hot storage temperature of ϑ_A indicates a test temperature that is lower than T_{SI} . At a higher temperature of ϑ_B , the sample temperature exceeds the hot storage temperature for a certain time and it is believed that oxygen is reacting more vigorously with the sample dust than at ϑ_A , denoting the beginning of the self-heating process before self-ignition occurs. Curve C represents the scenario of hot storage temperature at ϑ_C that is higher than T_{SI} . At this temperature, the sample heat production has greatly surpassed the heat losses, and the material will self-ignite after an induction time, t_i . For each sample volume, sufficient tests are conducted to determine the highest oven temperature that shows no ignition (indicating scenario B) and the lowest oven temperature that shows ignition (showing scenario C). It is important to use fresh samples for every replication for results as accurate as possible. Following BS 15188, the hot storage experiment can stop when scenarios B (corresponds to hot storage temperature at ϑ_B) and C (corresponds to hot storage temperature at ϑ_C) have been achieved since the sample dust T_{SI} is actually between ϑ_B and ϑ_C . Self-ignition of dust material is described by either of the two situations according to this standard:

- i. dust sample temperature reaches at least 60 K above the hot storage temperature
- ii. dust sample temperature shows an inflection point occurring above the oven temperature

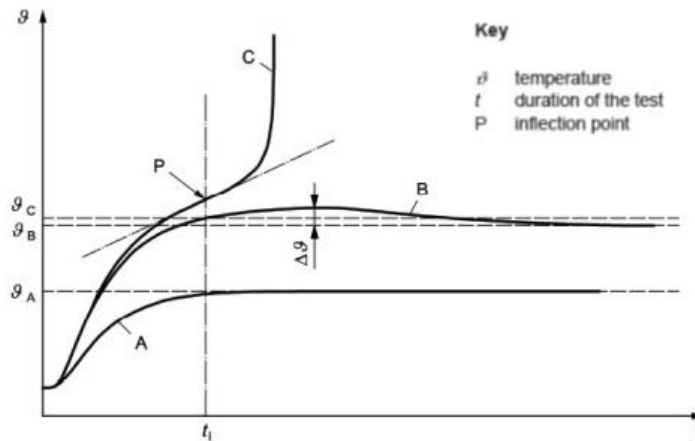


Figure 2. 14 Hot Storage Basket Experiment – Idealised Dust Temperature Versus Time
Results for Dust Samples of the Same Volume [Source: British Standard (2008) p.10]

With a minimum of three different-volume baskets used, a meaningful graph of logarithms of different volume/surface ratios ($\lg [V/A]$) (representing dust deposits of various sizes) versus the reciprocal of the corresponding self-ignition temperatures ($1/T_{SI}$) can be plotted and a straight line is expected. Other useful information that can be obtained from this test is the ignition induction time (t_i) required to produce critical ignition in cases with different test volumes. The t_i is defined as the interval of time between the sample dust reaching the hot storage temperature and ignition; and is usually expressed in hours. To obtain this involves plotting ($\lg [V/A]$) versus ($\lg t_i$) and from the plot, the time required for a certain amount of sample material to self-ignite during storage can be estimated.

Following the guidelines in BS 15188, Saddawi et al. (2013a) employed this method to study the thermal stability of five solid fuels – wood chip, torrefied wood chip, torrefied pellets, sunflower shell pellets and Kellingley coal. Different baskets with different dust heap sizes were studied with the aim to extrapolate the fuel behaviour to larger volumes thus represented industrial silos. The self-ignition temperature was calculated as the mean of the highest temperature at which ignition does not happen and the lowest temperature that self-ignition occurred. As for the induction time, it was taken as the duration for a sample temperature to exceed that of the isothermal oven by 60°C and each material was investigated using three mesh wire baskets with volumes of ~ 11 , ~ 67 and $\sim 864 \text{ cm}^3$. A typical temperature-time plot for wood chips that had ignited in a 213°C oven is shown in **Figure 2. 15**.

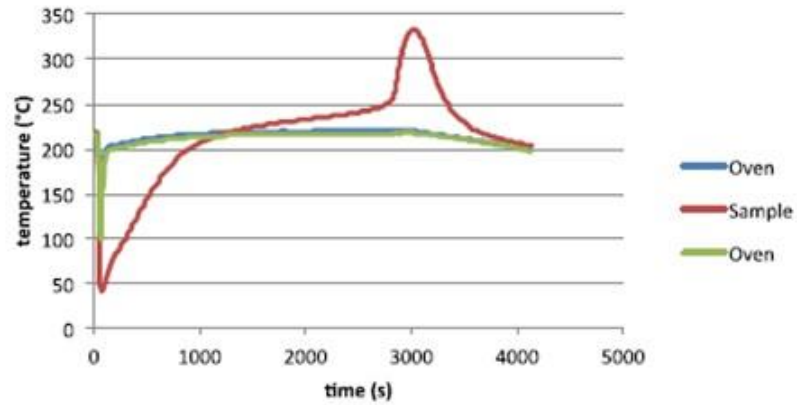


Figure 2.15 Hot Storage Basket Experiment – Temperature-Time Plot of Wood Chips Subjected to Hot Storage Temperature of 213°C [Source: Saddawi et al. (2013a)]

Saddawi et al. (2013a) utilised the scaling method in BS 15188 to predict material thermal behaviour when stored in large piles. The critical ignition temperatures and combustion induction time were superimposed on the Pseudo-Arrhenius self-ignition temperature and induction time plots on graphs available in BS 15188, as shown in **Figure 2.16** and **Figure 2.17** respectively. The straight line passing through the T_{SI} values (hollow circles in **Figure 2.16**) separates the graph into steady and unsteady behaviour regions of dust volumes. Self-ignition would occur in the region above that line for that particular sample. As seen in **Figure 2.16**, Kellingley coal result (indicated by black circle) was very close to the data line provided in the standard and at the same characteristic dimension (V/A), the T_{SI} of all biomass (represented by green, yellow and blue circles) was higher than that of the coal sample. Similarly, for combustion induction time, t_i , result from Kellingley coal was very near the data line provided in the standard and shorter t_i for biomass as compared with coal was observed in **Figure 2.17** at the same characteristic dimension.

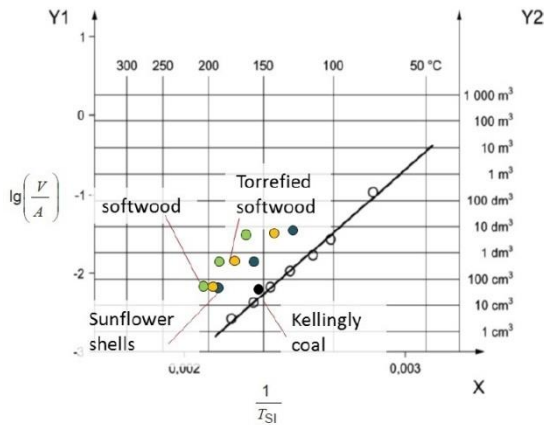


Figure 2. 16 Hot Storage Basket Experiment – Superimposing T_{SI} Results on BS 15188 Graph [Source: Saddawi et al. (2013a)]

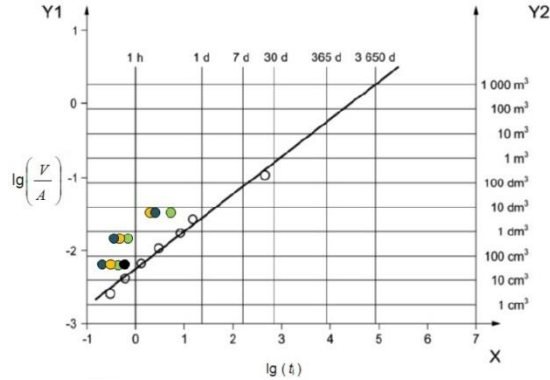


Figure 2. 17 Hot Storage Basket Experiment – Superimposing t_i Results on BS 15188 Graph [Source: Saddawi et al. (2013a)]

The EN15188 isothermal basket test helps determine the critical ignition temperature of materials that undergo self-heating and is useful in helping the plant operation in industry to predict material behaviour during material storage (BRE, 2016). With the assessment from this test, the result enables classification of a materials for packaging, transportation and carriage, in line with the UN Test N.4.

Tests comparable to the wire mesh cube test and hot storage experiments in determining the T_{SI} had been carried out by many different researchers on many dust species ranging from coal to various biomass dust. Realising heaps or piles of flammable dust deposits could undergo chemical reaction leading to self-heating and eventually self-ignition of that material, Leuschke (1981) looked into T_{SI} determination via the wire mesh cube test. The experiments were carried out at Bundesanstalt für Materialprüfung (BAM) on various dust species like coal, tobacco, starch, lycopodium and cork with wire mesh baskets.

Everard et al. (2014) compared the T_{SI} of chipped Miscanthus of ~ 18 mm and ground Miscanthus six times finer of around ~ 3 mm and also examined the effect of Miscanthus harvest period on T_{SI} . From the comparison between February and March harvested Miscanthus, no significant T_{SI} difference had been discovered for compatible storage piles (see **Figure 2. 18**). Veznikova et al. (2014) had applied the method in EN 15188 in evaluating the safe storage of some solid fuels with regard to their tendency to spontaneous combustion. Five samples – three coal samples (two bituminous coals and a brown coal) and two biomass samples (wood pellets and spruce sawdust) were ground to <2 mm before filling mesh wire baskets, and then subjected to the hot storage test. As seen in **Figure 2. 19**, the two bituminous coal samples showed straight lines with smaller

gradients than those of wood pellet or sawdust, indicating that changes in T_{SI} of biomass samples are more significant than bituminous coal when the storage volume changes. Ferrero et al. (2009) applied DIN EN 15188 in an examination of T_{SI} of two biomass fuel storage piles, one of pine chips the other pine sawdust. Besides comparing the hot storage experimental results of pine chips and pine sawdust, it was also concluded from their mathematical modelling results that this hot storage method had overlooked the heat contribution from microbial activity in the initial stage since hot storage test usually start at $>100^{\circ}\text{C}$.

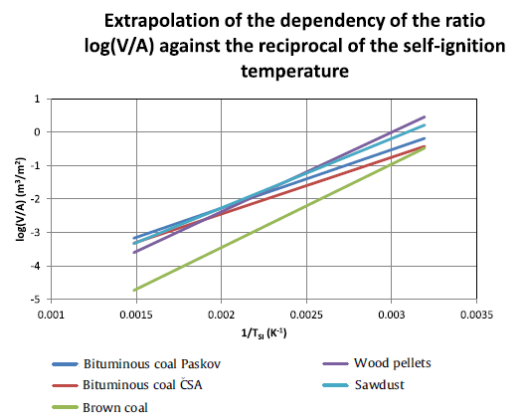
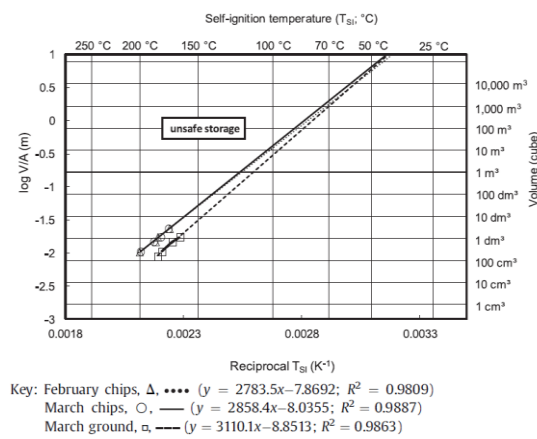


Figure 2.18 Hot Storage Basket Experiment – T_{SI} Results of Miscanthus at Different Harvest Period [Edited from: Everard et al. (2014)]

Figure 2.19 Hot Storage Basket Experiment – T_{SI} Results of Five Samples [Edited from: Veznikova et al. (2014)]

Pauner and Bygbjerg (2007) investigated the spontaneous ignition characteristics of wood pellets and protein powders using the wire mesh cube test. Like in BS 15188 hot storage basket test, five cubic steel mesh baskets with side lengths of 50, 100, 150, 200 and 300 mm were fabricated, though not all baskets were used for all samples test. However, critical ambient temperature (CAT) had been used in place of T_{SI} and was determined to a finer accuracy of ± 1 K.

There is another set of test procedure that resembles the setup of BS 15188 but is quasi-isothermal, called the Nordtest NT FIRE 045. The nordtest method (1992) involves rising slowly the oven temperature with a steady temperature ramp rate, i.e. linearly, until spontaneous ignition occurs. By doing this, spontaneous ignition always will occur in the first test (Pauner et al., 2004) but unfortunately, there is lack of information as of what temperature the self-ignition occurs. Also, this test specifies that the maximum temperature ramp rate is $\leq 0.0017^{\circ}\text{C/s}$ or $\sim 6^{\circ}\text{C/hour}$, which neglects the possibility that different temperature ramp rates could result in different results (Pauner et al., 2004).

Engel et al. (2016b) used another kind of heat storage test that was not fully isothermal and was termed adiabatic storage test. In the test, a wire basket filled with sample was kept in a hot air convection oven at storage temperature of 90°C for about 24 hour as a start. If the sample temperature increased during this storage period due to the self-heating process, then the oven temperature was set to track the sample temperature and this actually generated a quasi-adiabatic environment. If the opposite happened i.e. no self-heating was observed during the isothermal storage period, then the oven temperature was ramped up at a rate of 1 K/h to the point where self-heating was observed and the same way was applied to track the sample temperature.

There was also another interesting study that used both the UN Test N.4 and DIN EN 15188 hot storage test methods in determining the self-ignition behaviour of two bulk materials contained in cubic wire baskets. In this study by Seitz et al. (2016) on two samples – Carbon Black (Norit CN 4) and wheat flour (type 405), the effects of having lower than atmospheric pressure was looked into, with the aim to see the possibility of increasing drying temperature in a vacuum dryer but not at the expense of process safety.

Pressure reduction reduces oxygen volume concentration. With less oxygen concentration, the reactivity and therefore heat production in a sample material decreases, leading to higher T_{SI} . Furthermore, a reduction in atmospheric pressure lessens the thermal conductivity of a sample which in turn increases the T_{SI} . It was found that the T_{SI} change was not uniform with pressure change and the results of Carbon Black and Wheat flour are shown in **Figure 2. 20**. The T_{SI} was found to have decreased with reduced atmospheric pressure and a longer time was required to complete burning off a sample, believed to be the result of low oxygen concentration.

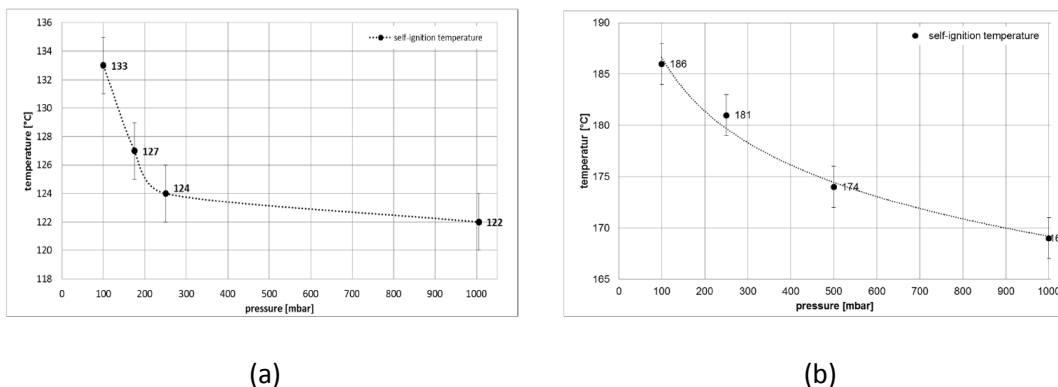


Figure 2. 20 T_{SI} at Reduce Atmospheric Pressure [Source: Seitz et al. (2016)] of (a) Carbon Black (Norit CN 4) (b) Wheat Flour (type 405)

2.6 Pre-treatment Techniques for Biomass

Biomass is a natural composite made up of three major biopolymers: hemicellulose, cellulose and lignin (Huang and Rein, 2016). Owing to the characteristics and properties of biomass, there are many issues associated with putting them into energy use, making raw biomass an inferior fuel as compared with fossil hydrocarbons. Nonetheless, biomass as the world fourth largest energy resource after oil, coal and gas (Drax, 2012) and being one of the most economical renewable technologies to construct as compared with solar, tidal or wind power generations (Ibrahim, 2013), massive effort has been implemented into many pre-treatment techniques to improve biomass properties prior to using as solid fuel. Energy densification methods, such as briquetting and pelletising are now commercial. Two techniques which change the chemistry of the biomass, namely washing and torrefying methods, which are at the research and development/ demonstration stage, were studied in detail for their effect on biomass self-heating/ self-ignition.

2.6.1 Biomass Washing

Using biomass as a sustainable renewable energy source is not without problems but after recognising the issues associated with utilising biomass as solid fuel, many pre-treatment methods have been developed and some are developing to remedy the undesired biomass properties. Among them, biomass washing had been identified as the only pre-treatment option (Maciejewska et al., 2000) that mitigates problems like bed agglomeration, deposit formation (be it slagging or fouling) on boiler tubes and thermal conversion equipment, corrosion, hazardous emissions, aerosol formation and so on.

There are various minerals critical for the growth of plants that remain in the plant even after harvest. Examples of major elements that exist in vegetation biomass are aluminium (Al), calcium (Ca), iron (Fe), magnesium (Mg), phosphorous (P), potassium (K), silicon (Si) and sodium (Na), whereas chromium (Cr), cobalt (Co), copper (Cu), manganese (Mn), nickel (Ni), sulfur (S), zinc (Zn) exist in smaller quantities (Raveendran et al., 1995). Chlorine, is also a micronutrient essential to plant growth. Potassium, calcium, chlorine and sulfur elements are harmful to the operation of an industrial biomass-fired boiler (Deng et al., 2013). Depositions build-up and cause fouling, slagging and agglomeration problems; when this happens on heating surfaces of a boiler, heat transfer reduction happens and as the deposition worsens on the convective heat transfer surfaces, unplanned boiler shutdown for manual removal of deposits causes unexpected loss to a plant due to the unforeseen plant downtime.

High temperature corrosion is prone to happen when there are depositions on super heater tubes surfaces in straw-fired boilers. It has been proven that these deposits contain high amount of potassium, calcium, chlorine and modest amount of sulfur. To

improve the boiler efficiency, the temperature of superheated steam could be raised and this causes the corrosion problem to worsen. Alkali metals particularly potassium is extremely volatile and when encounters hot surfaces in boilers, potassium will combine with chlorine and sulphur and acidic gases. Apart from causing negative impacts to the environment, unavoidable corrosion on boiler components costs a plant a lot for repairs. Under a heated environment and upon transformation into sulphates, severe fouling happens at the heat convective boiler regions as potassium tend to reduce the ash fusion temperature. As concluded in many studies, the undesired troublesome elements are effectively removed via washing pre-treatment before the biomass fuels are burnt in a boiler furnace (Deng et al., 2013).

Washing pre-treatment can be done naturally at the biomass harvesting site by rainwater or in a controlled manner where water flowrate, flow duration and washing agent temperature are known. Aiming at elimination of undesired elements, many researchers worldwide had applied various washing methods, using different washing agents in combination with different pre-treatment duration and temperature in search of the optimum pre-treatment condition best suited for commonly used solid fuel biomass. As expected, any biomass pre-treatment creates additional cost, but the benefits one gained towards the end e.g. to improve operating efficiency and reduce plant maintenance cost (Kasparbauer, 2009) or environment cost which could make made pre-treatments justifiable, particularly for low-grade biomass. Tumuluru et al. (2012) found biomass washing or leaching was a good way to make problematic biomass fuel more suitable for co-firing with fossil fuel coal through reduction of potential problems like ash deposition, slag formation, corrosion, sintering and agglomeration.

Simple water washing or quick rinsing applied by many researchers has been recognised as an efficient method that removes large amounts of unwanted biomass surface minerals (Davidsson et al., 2002) coming from soil contact during harvesting or transporting. At a minimum, contaminants like dirt get washed out, besides some water soluble minerals particularly potassium and sodium salts and chloride. Some of these biomass minerals that have negative impacts on combustion operation are actually nutrients critical for plants growth, and therefore it could be a good practice to send the leachates back to field for nutrient recycling, and in this way, wastage is minimised.

In the study on effects of biomass pre-treatments, Kasparbauer (2009) had washed loblolly pine for 45 minutes in tap water and deionised water. In that study, water analysis was performed for water soluble fractions, and X-Ray fluorescence (XRF) for biomass mineral content analysis. It was found that even though tap water-washing eliminated some undesired minerals, calcium was deposited onto biomass rather than being washed away.

Saddawi et al. (2012) used three washing agents to wash four biomass fuel samples – water, ammonium acetate and hydrochloric acid to wash short rotation coppiced willow, eucalyptus, miscanthus and wheat straw in either chipped or chopped form. A chemical fractionation procedure was conducted progressively to remove metal content in each biomass fuel. First, was deionised water washing, followed by 1 M ammonium acetate solution washing and finally 1 M hydrochloric acid washing. It was found that simple ionic salts like alkali chlorides were easily dissolved in deionised water. Ammonium acetate, served as an ion exchanger medium and allowed inorganic elements bonded to the organic structure with an ionic bond in the biomass sample to exchange ions with the solution. Finally HCl removed alkali earth carbonates, sulphates and sulphides. It was concluded that water washing removed high amount of alkali metal ions, potassium ion (K^+) in particular and chloride (Cl^-), especially from herbaceous biomass sample. It was also found that washed samples had become less reactive to thermal degradation and the cause was believed to be removal of catalytic metal species, K in particular. Water washing pre-treatment was found to be the most beneficial pre-treatment when ash fusion was concerned.

In a study of the effects of water washing on fuel properties of six biomass i.e. wheat straw, rice straw, corn stalk, cotton stalk, candlenut wood and rice hull, Deng et al. (2013) soaked the samples in deionised (DI) water at three different temperatures (303 K, 333 K and 363 K) and washing efficiency at different temperatures were compared. For all samples, the biomass:water ratio remained constant at 12 g biomass submerged in 1L of DI water and a unique way of lab-scale water washing was applied (see **Figure 2. 21**). In this method, biomass was filled in nylon sieve cloth wrapped stainless steel cuboid frames, and water soaking lasted for 3 hours. The frames were submerged in beakers in a water bath, and the water temperature was controlled and regulated by electric power. It was found that water washing was effective in removing potassium, sulfur and chlorine that are harmful to boiler operation from biomass and ash removal efficiency increased with water temperature. Also, higher heating value (HHV) was slightly increased and volatiles were released at a higher temperature for the water-washed samples.

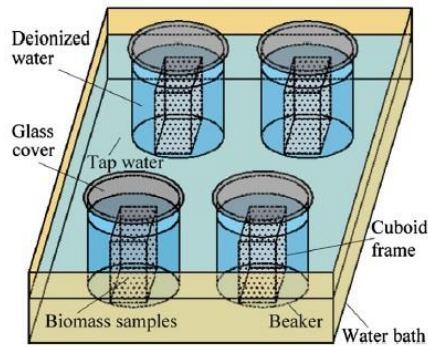


Figure 2. 21 Unique Way of Biomass DI Water Washing [Source: Deng et al. (2013)]

There are other washing pre-treatment studies on many types of biomass. using various washing agents under different washing conditions. Abdullah and Sulaiman (2013) had used water to leach empty fruit bunches (EFB) in order to examine the properties of leached EFB. In that study, EFB was soaked in tap water of 25-28°C for a pre-treatment residence time that varied from 5 to 40 minutes and 24 hours, using ratio of 3 L water to 100 g EFB. The focus was on reducing EFB ash content via tap water washing and it was concluded that the most effective ash removal means was by soaking EFB for 24-hour. The findings were consistent with another study by Abdullah and Gerhauser (2008) where fast pyrolysis characteristics of untreated and washed EFB were compared. In that study, EFB feedstock of 250-355 µm was soaked in distilled water for 24 hours and the ash removal in both studies were comparable.

There have been a few studies on leaching different straws – wheat straw, rice straw and corn straw. Jenkins et al. (1996), in a study about properties of washed straws, used a variety of washing methods to pre-treat wheat and rice straws. The methods included spraying the surface of a 30 mm thick, 100 g bed of straws with water for around 1 minute; submerging or soaking 100 g straws in 7 L water of 20-25°C for 24 hours; flushing or pouring 20 L water through 100 g straws in a controlled manner at 1 L increment, and leaving straws in field for natural rain water leaching. It was found that soaking was most effective on wheat straw, and significant reductions in chlorine, sodium, potassium and ash contents were shown. In the investigation of untreated and water washed Danish wheat straw, Blasi et al. (2000) concluded that soaking 1 g straw in 100 ml distilled water for 7200 s was effective in reducing ash. In another study in which corn straw was leached with water at 60°C and 0.5% nitric acid, Yang et al. washed corn straw by soaking and stirring every 1 g sample with 100 ml of either washing agent for 12 hours (Abdullah and Sulaiman, 2013). It was concluded that acid washing was more effective than water washing when ash removal was concerned. Potassium with >95% removal was shown by both washing agent, indicating water-leach or acid leach was equally efficient in potassium

removal from corn straw potassium removal, however, calcium removal was better when acid was used in leaching corn straw.

In a study on the effect of lignin and inorganic species in biomass on pyrolysis oil yields, quality and stability by Fahmi et al. (2008), *Festuca* grass and switchgrass were washed in 25°C deionised water for 2 hours as a means to reduce metal contents. Four metals, namely calcium, potassium, magnesium and sodium were removed with potassium and sodium removals significantly high from both samples.

Das et al. (2004) had the ultimate objective of removing ash from bagasse and both water leaching and acid leaching were conducted. The leaching agent used in acid leaching were hydrochloric acid and hydrofluoric acid solutions, where 12.5 g bagasse corresponded to 150 ml leachate for all the three leaching agents. It was found that HCl-leached sample showed an increase in ash, attributed by relatively much higher removal of other components such as hemicellulose in bagasse. Water-leached bagasse showed a moderate effect on ash removal.

Several methods were used to detect the amount of metals that exist in biomass. Tan and Wang (2009) in an experimental study of acid washing effects on biomass pyrolysis applied atomic absorption spectroscopy (AAS) to quantify the concentration of metal ions in white pine and rice husk biomass, namely calcium (Ca^{2+}), magnesium (Mg^{2+}), potassium (K^+), iron (Fe^{2+}) and sodium (Na^+) in untreated and acid washed biomass. Three acids were used in the leaching of both biomass – hydrochloric acid, Sulfuric acid and Phosphoric acid and all the metal removal efficiencies were compared. It was found that HCl was the most efficient in removing potassium from both biomass.

In the study of Abdullah and Sulaiman (2013), atomic emission spectroscopy (AES) was applied to determine the alkali and alkaline earth metals in EFB. AES is a chemical analysis that uses light intensity emitted from a flame at a particular wavelength. The amount of a specific element is determined by the intensity of light emitted, since it is proportional to the number of atoms of that particular element contained in a biomass.

In detecting the amount of metals dissolved in a leachate, electrical conductivity analysis were carried out. In the study of Abdullah and Sulaiman (2013) concerning EFB pre-treating.

Kasparbauer (2009), in a study about effects of biomass pre-treatment on fast pyrolysis product, used the XRF method to measure the concentrations of minerals present in loblolly pine. Concentrations of potassium, phosphorous and sodium in both treated and untreated pine were quantified to evaluate the efficiency of water washing pre-treatment adopted.

Gudka et al. (2016) had done a comprehensive summary of leaching various inorganic elements from 25 types of biomass fuels. Included are the particle size of the

fuels, the leaching conditions (leaching solvent, temperature and duration) and the inorganic removal amounts at the particular condition.

In summary, water-washing can be very effective in removing varying quantities of K, Na, Cl, Ca, Mg and Fe. One consequence of removing the catalytic metal species (particularly K and Na) is that the biomass becomes less reactive and the yields of volatiles vs char change. This could be significant for the ignition risk of the biomass, i.e. it could be reduced, and hence investigating this is one of the aims of this work; something that has not been studied previously.

2.6.2 Biomass Torrefying

The torrefaction process is a thermochemical treatment aimed at upgrading the physicochemical properties of biomass that gained attention recently. The term 'torrefaction' originated from the French verb 'torréfier' which means roasting (Jong and Ommen, 2015). This low temperature, mild and slow pyrolysis process was the backbone of the industrial revolution, whereby the concept was applied in metal ore reduction processes. However, technical development of the torrefaction process only started in late 1900s for coffee production and quite a few patents were actually granted within the 1897-1952 period (Dahlquist, 2013). There was actually research ongoing in the 1930s and according to records (Bergman et al., 2005), the concerned woody biomass torrefaction and the production of gasifier fuels was researched by groups in France.

The torrefaction process gained attention again when it was recognised that torrefied wood could be used as a reducing agent in metallurgic applications. This led to a demonstration plant erection in late 1980s by the company Pechiney (Dahlquist, 2013), which operated for some years but was dismantled in early 1990s for economic reasons. There is various open literature research about biomass torrefaction and to sum up, the two recent torrefaction rediscovery periods are dominated by French from 1984 and Dutch since 2002, within which scientists and engineers gathered experimental data to see how biomass benefit from the torrefaction process. It is worth mentioning that besides the efforts from the French and Dutch, there were other researchers involved and contributed in torrefaction studies, e.g. Pentanunt, Felfli et al., Pach et al., Arcate, Alen et al. and Lipinsky et al. as mentioned by Dahlquist (2013) and Bridgeman et al. (2008) in many aspects of biomass torrefaction.

The torrefaction process has been considered as a clean and convenient way of increasing the energy density of biomass as solid fuel. Torrefying biomass simply means roasting biomass in an oxygen -starved or -deficient, inert environment, altering the chemical structure of biomass hydrocarbon (Basu, 2013). In short, with this pre-treatment process, many undesirable and challenging properties when using raw biomass as fuel are

altered and biomass becomes a better quality fuel. It is achieved through the mild pyrolysis process of torrefaction that partly decomposes and devolatilises the basic biomass polymeric constituent. The hemicellulose, cellulose and lignin depolymerise at different temperature ranges, typically 225-300°C for hemicellulose, 305-375°C for cellulose and 250-500°C for lignin. Each polymer is believed to react independently to heat with no synergetic effect (Basu, 2013). Typical torrefaction temperatures are <300°C. Various volatiles are given off, leaving a dry, darkened, hardened, solid that is called torrefied biomass or sometimes referred to as biocoal. The torrefaction products are illustrated in **Figure 2. 22** and regarding the mass and energy distributions of the products depend on both the biomass species and the torrefaction severity (Dahlquist, 2013).

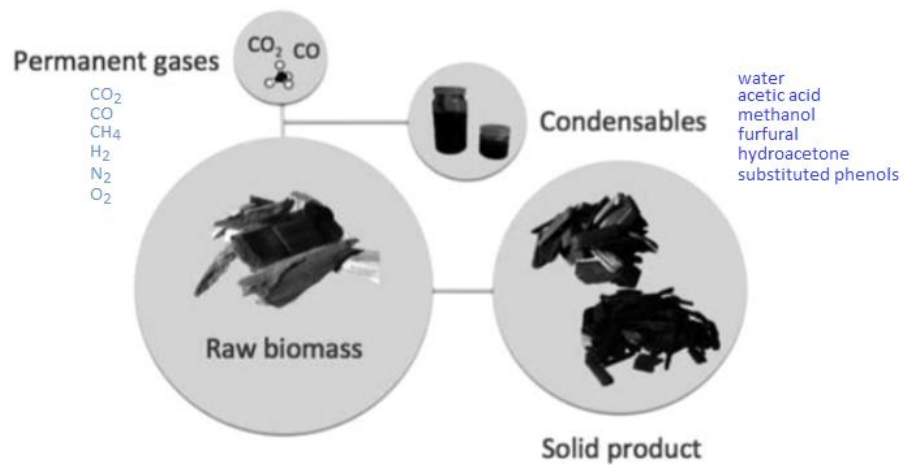
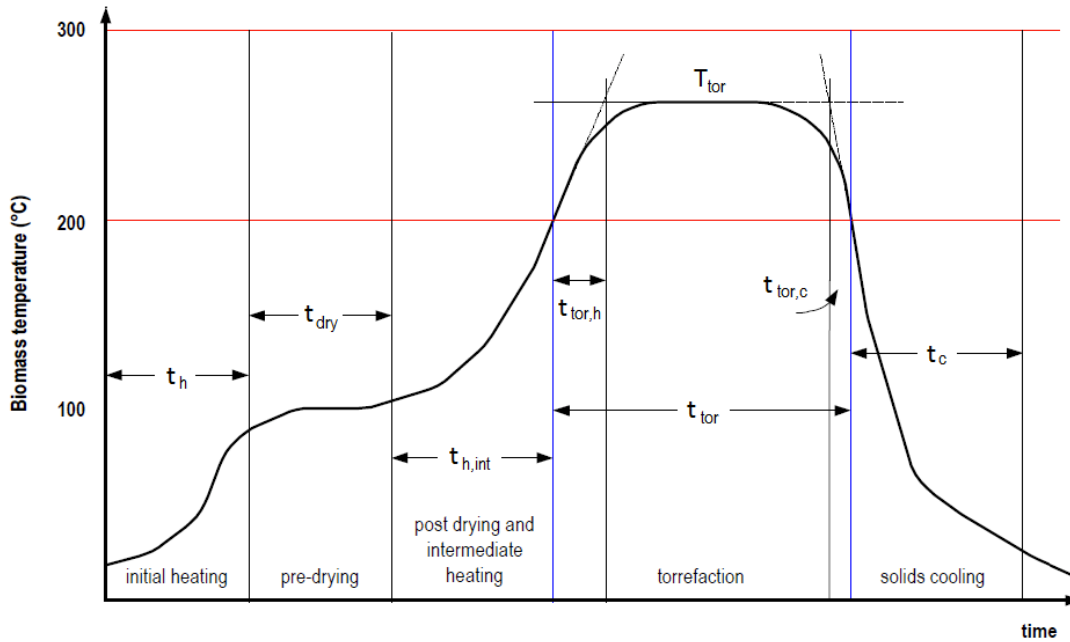


Figure 2. 22 Typical Torrefaction Products with CO₂ and CO as Main Components [Edited from: (Dahlquist, 2013)]

2.6.2.1 The Torrefaction Process, Mass and Energy Balance

Studies on torrefaction have generally concluded that there are five primary stages involved in the process. Different researchers have used slightly different terms for each stage but they basically refer to similar reactions that takes place within the torrefaction reactor. The five key stages that biomass experiences in the torrefaction process are initial heating, pre-drying, post drying & intermediate heating, torrefaction and solid cooling, as illustrated the idealised temperature-time graph in **Figure 2. 23** below.



t_h – heating time to drying; t_{dry} – drying time; $t_{h,int}$ – intermediate heating time from drying to torrefaction; t_{tor} – reaction time at desired torrefaction temperature; $t_{tor,h}$ – heating time torrefaction from 200°C to desired torrefaction temperature (T_{tor}); $t_{tor,c}$ – cooling time from the desired T_{tor} to 200°C; t_c – cooling time to ambient temperature

Figure 2. 23 Temperature-Time Profile in Biomass Torrefying Process - Five Key Stages of the Torrefaction Process [Edited from: (Bergman et al., 2005)]

The major changes that happen to biomass in each of the five primary stages of torrefaction (Bergman et al., 2005; Basu, 2013) are described as follows:

At the initial heating stage, biomass is heated up from room temperature to a point where moisture evaporation takes place. As soon as biomass temperature hits above 100°C, free water evaporates at a constant rate, indicating the pre-drying stage in which the biomass temperature remains quite constant. After all the surface moisture or free water is driven off, the biomass temperature starts to increase gradually to 200°C, signifying the post-drying & intermediate heating stage. In this stage, intramolecular drying takes place and pores start to open up, resulting in the release of traces of trapped gases (Dahlquist, 2013). Some mass loss is expected when physically bound moisture and some light volatile organic compounds like terpenes, extractives and oils start to escape. Once the biomass temperature exceeds 200°C, the torrefaction stage starts as devolatilisation commences and continues. From >200°C to the desired torrefaction temperature (usually less than 300°C), the bulk of the biomass depolymerisation takes place, mainly degradation of the most reactive biopolymer, hemicellulose and some minor decomposition from lignin

and cellulose. The severity of torrefaction is defined by the degree of biomass depolymerisation, determined by the torrefaction temperature and the biomass residence time.

From various studies, it has been found that torrefaction temperature is more influential than residence time on the torrefaction products (Bridgeman et al., 2008; Bridgeman et al., 2010), whereby mass loss become quite insignificant after about an hour of residence time (van der Stelt et al., 2011; Toscano et al., 2015). Within the temperature range of 250°C to 300°C, the biomass cell structure is completely destroyed and this makes the torrefied biomass non-fibrous and brittle. The torrefied biomass changes colour from light brown, darker brown to almost black as the degree of torrefaction increases. **Figure 2. 24** shows example of colour variation in woody and herbaceous biomass as the torrefaction intensity increases as a function of torrefaction temperature (from 240°C to 300°C) while residence time was fixed at 30 min (Gucho et al., 2015). The solid cooling stage starts when biomass leaves the torrefier at torrefaction temperature, i.e. the highest temperature in the system. The hot torrefied biomass is cooled to less than 200°C or sufficiently below its ignition temperature to prevent the hot torrefied biomass catching fire upon exposure to air.



Figure 2. 24 Colour Variation of Woody Biomass (Top Row, Beech Wood) and Herbaceous Biomass (Bottom Row, Miscanthus) as a Function of Torrefaction Temperature (a) Untreated (b) 240°C (c) 260°C (d) 280°C (e) 300°C at a Fixed Residence Time [Edited from: (Gucho et al., 2015)]

A typical mass (M) and energy (E) balance of the torrefaction process is illustrated in **Figure 2. 25**. As illustrated, 30% of the mass (0.3M) that carries 10% of the biomass original energy (0.1E) has been converted into torrefaction gas. As a consequence of biomass thermal disintegration and losing torrefaction gas, the torrefied biomass

experience a reduction in mass (0.7M) and energy (0.9E) but an increase in energy density by a factor of around 1.3 (ratio of 0.9/0.7).

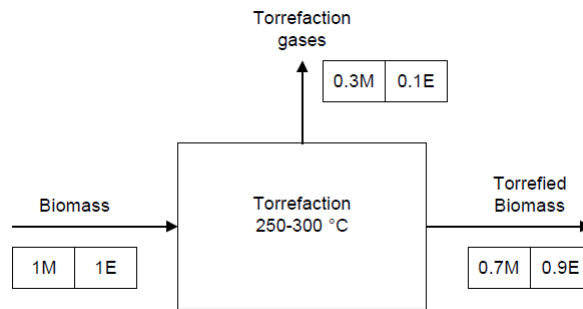


Figure 2. 25 Typical Mass (M) and Energy (E) Balance of Biomass Torrefaction Process
[Source: (Bergman et al., 2005)]

Mass and energy losses increase according to the severity of torrefaction. These lead to two parameters that characterise the torrefied products – mass yield (η_M) and energy yield (η_E). Mass yields of 70-90% with corresponding energy yields of 70-95% are usual numbers of torrefaction processes (Akinrinola, 2014). The two yields are defined as follows (McNamee et al., 2016):

$$\eta_M = \frac{mass_{treated,dry}}{mass_{untreated,dry}} \times 100 \dots\dots \text{Equation 2.15}$$

$$\eta_E = \eta_M \frac{HHV_{treated,dry}}{HHV_{untreated,dry}} \times 100 \dots\dots \text{Equation 2.16}$$

Experimental investigations by Gucho et al. (2015) had proven that both the mass and energy yields reduced as torrefaction temperature or residence time was increased, as shown in **Figure 2. 26** (a) & (b) for mass yield and energy yield respectively.

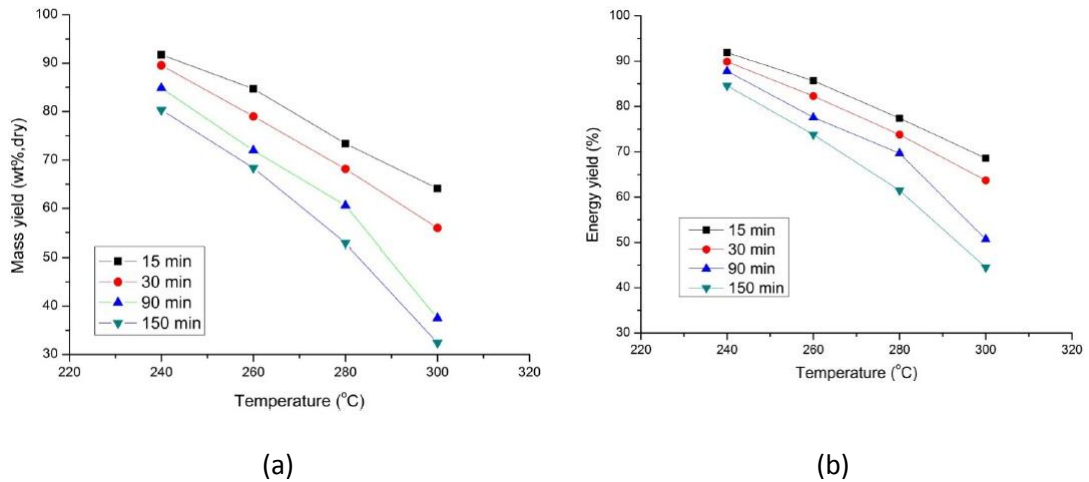


Figure 2. 26 Example of (a) Mass Yield and (b) Energy Yield of Biomass Torrefaction [Source: (Gucho et al., 2015)]

2.6.2.2 Atomic Ratio in Relation with Higher Heating Value, Torrefied Fuel Characterisation and Benefits of Torrefaction

On a dry-ash-free basis, two atomic ratios – hydrogen-to-carbon (H/C) and oxygen-to-carbon (O/C) are plotted on the well-known Van Krevelen diagram (see **Figure 2. 27**). These atomic ratios are based on the hydrogen, oxygen, and carbon content of the fuel of interest. Heating value is one of the useful pieces of information retrievable from solid fuel atomic ratio classification. Comparing the extreme of high HHV of carbon-rich anthracite fossil fuel that appears at the bottom-left of Van Krevelen diagram with the other extreme of low HHV carbon-deficient biomass at the top-right of Van Krevelen diagram, it seems that HHV is increased as the H/C and O/C ratios reduce. Biomass has the highest oxygen content among all hydrocarbon fuels but unfortunately this does not increase the heating value and results in high volatile yields (Basu, 2013). Torrefaction is one of the processes that produce carbon-rich solid fuels from biomass, therefore positioning torrefied biomass closer to high HHV carbon-rich fossil fuel. Among all the torrefied biomass data compiled, it was found that torrefied biomass showed HHV increase ranged from 1- 58% as compared with their respective untreated counterpart (Dahlquist, 2013).

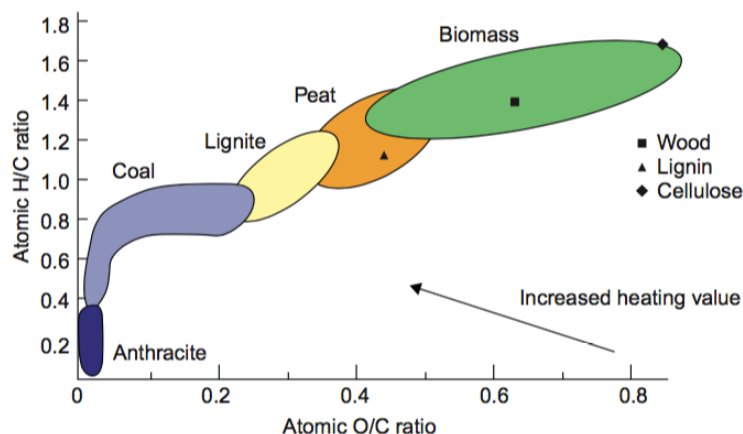


Figure 2. 27 The Van-Krevelen Diagram [Source: (Basu, 2013)]

From the available torrefaction studies, torrefied biomass was found to place itself closer to the lowest rank coals, i.e. peat and lignite, with reduction in both H/C and O/C ratios. According to van der Stelt et al. (2011), torrefaction involves oxygen removal from the original biomass which in turn influences the properties of torrefied biomass (the solid product). As seen in **Figure 2. 28**, after losing hydrogen and oxygen, the properties change in the direction of carbon that makes the solid product denser in energy and moves towards coal i.e. it becomes more coal-like (van der Stelt et al., 2011). Depolymerisation results in the relative increase of carbon content while reducing oxygen content such that in torrefaction increases the HHV of biomass. Torrefaction is not just removing the moisture/water from biomass but also O- and H- rich gas species, giving a total elemental dehydration effect. It approaches the coal-like composition as torrefaction severity increases, since it goes through an increasingly severe elemental dehydration process (Dahlquist, 2013). Oxygen is lost at a higher rate than carbon owing to the rapid decomposition of the reactive hemicellulose component. In this anaerobic thermal conversion process of torrefaction on biomass, the rate of massloss (typically ~30%) is more than energy loss (typically ~10%) thus making the remaining torrefied residue display a higher energy content than the untreated counterpart (Dahlquist, 2013).

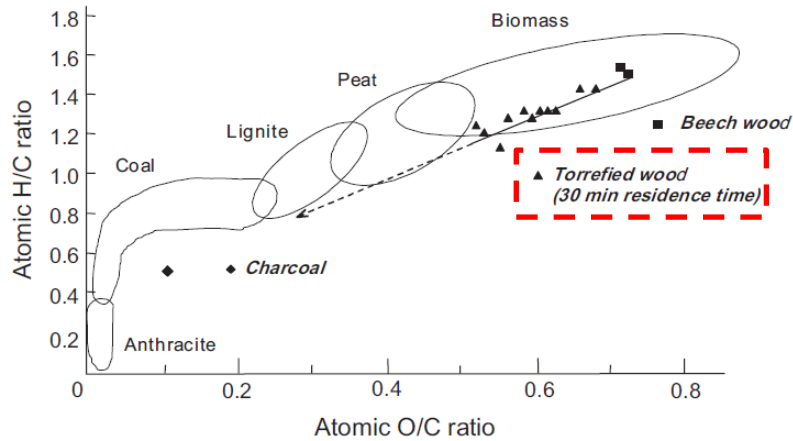


Figure 2. 28 Torrefied Biomass Location (in Red Box) in the Van-Krevelen Diagram [Source: (van der Stelt et al., 2011)]

A typical example of proximate analysis comparisons from wood pellet and torrefied wood pellets is shown in **Table 2. 1**. Moisture content is reduced from 7-10% to just 1-5%; volatile matter reduces from 75-85% to 55-80% whereas fixed carbon increases from 16-25% to 20-40% (Jong and Ommen, 2015). McNamee et al. (2016) studied torrefaction of North American pine at four different torrefaction severities (250°C for 30 min, 270°C for 30 min, 270°C for 60 min and 290°C for 30 min), and the same trend was observed. Moisture (on as-received basis), that was 7.08% in the untreated pine decreased to 1.13-2.43% after torrefaction; volatile matters (on dry-basis) decreased from 83.78% of the untreated biomass to 72.78-81.66%; fixed carbon (on dry-ash-free basis) increased from 15.89% of the untreated pine to 17.89-26.66% whereas ash (on dry basis) increased from 0.34% of untreated pine to 0.35-0.55%. Original volatile matter, that ranged from 80-88%, was reduced by 1.5 to 35% of the original values for various wood species (Dahlquist, 2013). The reduction in moisture is explained by biomass moisture or water content removal during the initial heating and drying stages, while the elimination of various volatiles from biopolymers decomposition causes an overall volatile matter reduction in the solid product (Hornung, 2014).

Ash is defined as the inorganic solid residue that remains after a fuel has completed the combustion process. In the study of McNamee et al. (2016) on North American pine, the ash content (on dry basis) of all four torrefied samples showed an increase compared to the untreated pine. Similarly, under nine different torrefaction conditions (250-300°C with residence time of 1 hour), all five vegetation samples (rice husk, sawdust, peanut husks, bagasse and water hyacinth) showed ash increasing during the thermal process. Ash of rice husk rose from 16.94% to 21.56-34.29%; sawdust from 1.48% to 1.69-3.83%; peanut husks from 18.31% to 24.48-33.77%; bagasse from 1.53% to 2.69-5.32% and water hyacinth from 15.68% to 50.16-65.43% (Pimchuai et al., 2010) The

rise in ash composition can be explained by significant loss of organic matter during torrefaction (Phanphanich and Mani, 2011). When moisture and volatile matter reduce upon torrefaction, fixed carbon and inorganic ash components have thus become relatively higher.

Table 2. 1 Untreated and Torrefied Solid Fuel Properties Comparison (Jong and Ommen, 2015)

Content (Basis)	Wood Pellets ,wt%	Torrefied Wood Pellets, wt%
Moisture (wet basis)	7-10	1-5
Volatile Matter (dry basis)	75-85	55-80
Fixed Carbon (dry basis)	16-25	20-40

As for ultimate or elemental analysis, many studies have found that there is an increase in the carbon content and a decrease in the oxygen content during torrefaction as illustrated in **Figure 2. 28**. In the same study of McNamee et al. (2016) on North American pine, it was found that the carbon content (on dry-ash-free basis) increased from 49.68% to 51.88-54.95% depending on the degree of torrefaction, whereas the oxygen content (that was calculated by difference) decreased from 44.46% to 39.37-41.89%. During all torrefaction conditions, when the biopolymers decomposes, some oxygen-rich fraction volatilises to form incondensable and condensable gas products (see **Figure 2. 22**) and thus reduces the oxygen content in the solid product. The higher loss of oxygen content compared to carbon has thus yielded a relatively higher overall carbon content in the solid product (Dahlquist, 2013).

There are many recognised advantages of using torrefied biomass compared to raw biomass, from the product characteristics perspective and system application viewpoint (Dahlquist, 2013). Increase in heating value of torrefied biomass is one of the most significant benefits of torrefying biomass (Jong and Ommen, 2015). In the torrefaction process, significant amount of chemically bound water and some gases that do not contribute to energy content are lost (e.g. CO₂), resulting in higher energy content in the solid matter left behind. Torrefied biomass thus has a higher energy density as compared with the raw untreated counterpart particularly when pelleted and this reduces solid fuel transportation cost due to its relative lower weight to volume ratio (Hornung, 2014). With higher energy density than untreated biomass, larger transportation distances can be considered economically (Bergman et al., 2005). Torrefaction led to 10% higher energy density on mass basis in a study of combustion characteristics comparison between

untreated and torrefied willow (Fisher et al., 2011). Following the study of Gårdbro (2014), **Figure 2. 29** compares the transportation costs of untreated and torrefied white wood pellets as function of energy and bulk density. Torrefied biomass with higher energy density is obviously more beneficial in transportation costs compared to dealing with traditional pellets. It is clear that as torrefaction increases the biomass energy density, so it incurs less cost per unit energy. If combined with pelletising or briquetting technology, this compacted energy-densified solid fuel has the advantage of easy long distance transportation in an economical way and having a heating value possibly up to 25 MJ/kg (which is in the same range with that of low rank coal) (Dahlquist, 2013) makes the torrefied fuel attractive. The transportation cost comparison for untreated and heat-treated biomass pellets are shown in **Table 2. 2**.

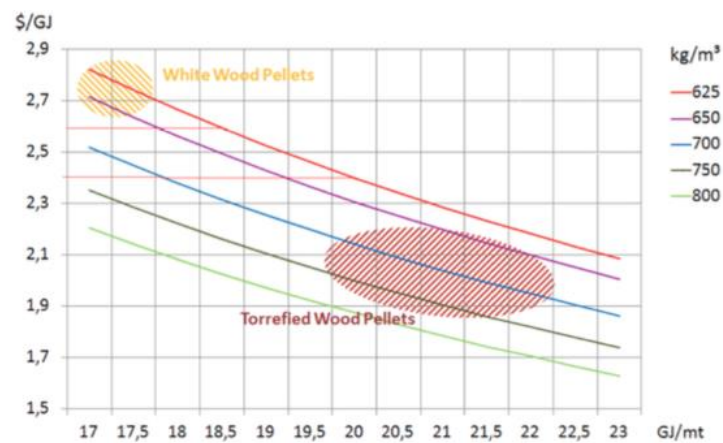


Figure 2. 29 Transport Cost as Function of Energy and Density for Untreated and Torrefied Wood Pellets [Source: (Gårdbro, 2014)]

Improved grindability is another improved feature of torrefied biomass (Bridgeman et al., 2010) which addresses a key disadvantage of biomass, i.e. the expensive cost of fine milling of biomass (Dahlquist, 2013). Solid fuels need to be pulverised to a certain size before supplying to pulverised fuel boilers or entrained flow gasifiers, and the fibrous, tenacious characteristics of raw biomass demand significant amount of grinding energy. The torrefaction process, that causes cellulose decomposition, shortens the fibre length, and hemicellulose depolymerisation ruins the interconnections between biopolymers. Grinding thus requires less energy, resulting in particles with higher sphericity and better particles size distribution (see **Figure 2. 30(a)** for Hardgrove Grindability Index (HGI) for various fuels). Since torrefaction weakens biomass cell wall, the end product become more brittle and reduces the grinding energy consumption (Gårdbro, 2014). The higher the degree of torrefaction/depolymerisation, the less milling energy is required before applying in industrial burners (Gårdbro, 2014). **Figure 2. 30(b)** shows the milling energy of

torrefied wood chips by three different torrefaction temperatures and different torrefaction times. Fisher et al. (2011) in their study of combustion characteristics comparison between raw willow and torrefied willow, suggested that the improved grinding characteristics of torrefied biomass enabled co-grinding with coal.

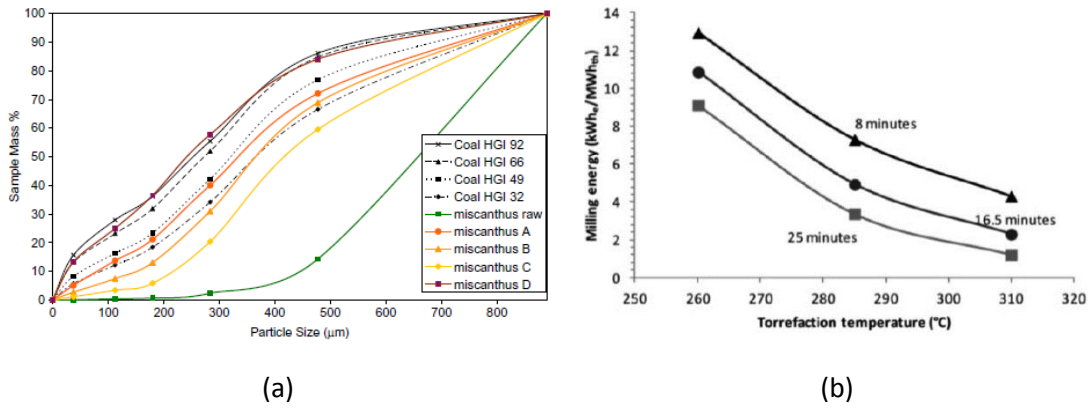


Figure 2.30 Grindability of Torrefied Biomass (a) Particle size distribution curves for untreated and torrefied Miscanthus and four standard reference coals of HGI 32, 49, 66 and 92 [Source: (Bridgeman et al., 2010)] (b) Milling Energy Requirement for Torrefied Woodchips at Various Torrefaction Temperature and Torrefaction Time [Source: (Gårdbro, 2014)]

Hydrophobicity is another improvement upon torrefaction (Jong and Ommen, 2015). Hemicellulose, that is the most hydrophilic polymer in the biomass structure is predominantly decomposed during torrefaction; losing of free hydroxyl groups that serve as hydrogen bonding sites thus increases the hydrophobicity. The removal of monosaccharides and the destruction of the hemicellulose component during the torrefaction process leads to feedstock sterilisation. With much reduced moisture, these factors lessen the ease of fungi and mould generation which is especially useful when it comes to feedstock storage. To a certain extent, torrefaction helps reduce the biochemically induced self-heating in biomass storage piles, and when combined with the hydrophobic characteristics, the torrefied feedstock can be stored outdoors in open space for longer periods of time without taking up water (Hornung, 2014). Thus, it can use infrastructures similar to those used by coal, leading to reduced cost requirements for indoor storage infrastructure. The durability against fungi increases following the improvement in hydrophobicity (Dahlquist, 2013). Fungi growth (*Postia placenta*, *Coniophora puteana*, *Trametes versicolor*, *Gloeophyllum trabeum*) was compared via an accelerated fungal durability test for raw spruce and torrefied spruce showed that thermally-treated spruce was more durable when exposed to those fungi, but it was suggested that more studies were needed concerning biological activity in torrefied

material. The hygroscopic and biological degradation properties among wood pellets, torrefied wood pellets, charcoal and coal are compared in **Table 2. 2**.

Studies have shown that torrefaction increases the uniformity in the final product quality. Upon torrefaction, different woods for instance woodcuttings, demolition wood, waste wood have quite similar chemical and physical properties despite vast variation prior torrefaction (Bergman et al., 2005). To quite a considerable extent, feedstock seasonal influences on these properties are expunged. In the long run, this is a useful solution to curb the problem of variability in biomass supply.

Cofiring biomass with coal in power stations, especially the direct cofiring method in which biomass is fed directly into the coal pulverising mill, has been widely practised as a means to reduce GHG emissions. Due to similarity between coal and torrefied wood, the operation problem potential is much reduced and a greater amount of biomass can be cofired with coal if torrefied biomass is used instead of untreated ones (Basu, 2013). To facilitate a large percentage of biomass being co-fired with coal in power stations in existing coal boilers, the behaviour and properties of biomass combustion are desired to be compatible with coal as far as possible, and torrefying biomass is one of the potential methods (Li et al., 2016). In pelleted or briquetted form, the torrefied biomass can be milled in normal coal mills without having to modify the coal grinding equipment (Dahlquist, 2013).

Table 2. 2 Transportation Costs, Hygroscopic and Biological Degradation Properties Comparison between Untreated and Treated Biomass (Jong and Ommen, 2015)

Property	Wood Pellets	Torrefied Wood Pellets	Charcoal	Coal
Transportation Costs	Medium	Low	Medium	Low
Hygroscopic	Hydrophilic	Moderately Hydrophobic	Hydrophobic	Hydrophobic
Biological Degradation	Moderate	Slow	None	None

All in all, torrefied biomass shows potential to overcome a lot of the disadvantages of utilising untreated biomass as solid fuel. **Table 2. 3** summarises and compares the

features of untreated biomass with torrefied biomass, thus highlighting the benefits of torrefaction.

Table 2. 3 Comparing Untreated Biomass with Torrefied Biomass

Untreated Biomass	Torrefied Biomass
low heating value	higher heating value (Jong and Ommen, 2015; Bridgeman et al., 2008)
low energy density	higher energy density (Hornung, 2014; Fisher et al., 2011; Bridgeman et al., 2008)
Higher fuel transportation cost	lower fuel transportation cost (Gårdbro, 2014; Hornung, 2014)
hydrophilic	hydrophobic (Jong and Ommen, 2015; Ibrahim et al., 2013)
non-negligible biological activity	reduced biological degradation (Dahlquist, 2013)
impossible outdoor storage	longer outdoor storage period (Hornung, 2014)
fibrous and tenacious	brittle, friable, higher grindability (Jong and Ommen, 2015; Gårdbro, 2014; Bridgeman et al., 2010)
irregular fuel quality and shape	increased fuel quality and shape homogeneity (Dahlquist, 2013)
limited amount to be co-fired with fossil fuel coal	increased amount that can be co-fired with fossil fuel coal (Li et al., 2016; Basu, 2013)

2.6.2.3 Torrefied Biomass Particle Size Distribution, Surface Area and Surface Morphology Determination

Medina (2014), in the study on explosion safety of biomass and torrefied biomass powders, had used laser diffraction analysis for the particle size distribution of both her untreated and torrefied biomass samples. In the study of explosibility of biomass powders, Slatter (2015) applied the same technique to analyse the size distribution of the powdered biomass samples. Their method of obtaining particle size distribution of untreated and

torrefied biomass powder using the Malvern Mastersizer equipment was adopted on all biomass dust in this study, for untreated, torrefied and untreated-torrefied blend.

Ibrahim (2013) in a study on the fundamentals of torrefaction of biomass and its environmental impacts had used the Brunauer, Emmett and Teller (BET) theory to determine the particle surface area of untreated and torrefied solid biomass. Surface areas of the untreated and torrefied willow and eucalyptus samples fall within the range of 1.1-3.8 m^2g^{-1} . In the study of explosion safety of biomass and torrefied biomass powders, Medina (2014) also applied BET theory to determine the surface area of samples since it is known that surface area is a property of solids that typically affects combustion. The variety of biomass samples studied ranged from untreated wood and untreated wood pellets to torrefied species of different woods that had been sieved to different sizes; the BET surface area analysis showed values within 0.65-2.10 m^2g^{-1} . In comparison, the surface areas of coal samples were consistently much higher than that of biomass sample, ranging from 3.69-15.8 m^2g^{-1} (Medina, 2014) and biomass surface area increases after devolatilisation (McNamee et al., 2015). Untreated willow and eucalyptus had surface area that ranged within 1.1-3.8 m^2g^{-1} whereas surface area of untreated and torrefied willow and eucalyptus chars were 10-94 m^2g^{-1} .

Ibrahim (2013) applied Scanning Electron Microscopy (SEM) to examine the surface morphology changes experienced by solid biomass when subjected to torrefaction. The SEM images of raw and torrefied willow and eucalyptus (thermally treated for 30 min residence time at 270°C and 290°C) were compared, and it was observed that biomass lost its fibrous structure upon torrefaction. Medina (2014) compared SEM images of her wide range of biomass species and particle sizes. The smaller <63 μm samples consisted needle-shaped particles that varied in length whereas the bigger <500 μm sample were made up of bigger brick-like shaped particles. Blends of coal-biomass and coal-torrefied biomass samples showed mixture of particle shapes – spherical particles from coal, flock-type particles from biomass and mixture of spheres and flock-type particles from the blends. Torrefied samples appeared to be more homogeneous when compared to untreated samples. In the study of explosibility of biomass powders, Slatter (2015) compared morphologies of powdered oak, pine and wood before and after explosion, with particle size as the varying parameter i.e. <63 μm , 63-150 μm , 150-300 μm and <500 μm . Oak sample of <63 μm had the most spherical particles observed among all samples. Oak particles in size range of 63-150 μm were almost identical to those in the 150-300 μm range but slightly thinner and more elongated. The 150-300 μm oak particles showed cylindrical particles with fibrous protrusions. Oak particles of <500 μm consisted of a mixture of observations of other ranges with large particles seen to occupy a large volume fraction. Pine with particle size 300-500 μm showed images identical to that observed from oak of 150-300 μm range. The as-received wood particles, were crushed from pellets, and smooth edges were

seen as evidence that the particles had been compressed before. A porous structure was observed on all pre-combustion particles (Slatter, 2015). Several willow and eucalyptus SEM images (100x magnification) of untreated, torrefied (under two torrefaction conditions) and their respective chars were captured and analysed by McNamee et al. (2015). Apparent changes in surface morphology were observed via SEM upon torrefaction and formation of char. Both untreated fuels appear more compact with bulky xylem tissues more obvious compared to their respective torrefied counterparts (McNamee et al., 2015).

2.6.2.4 Previous Studies on Torrefied Biomass: Addressing the Gap of Knowledge for Self-Heating and Ignition Risk

Biomass is more reactive than fossil fuel coal due to its higher volatile matter content and more porous particle structure than that of coal (Basu, 2013). From the Van Krevelen diagram, torrefied biomass has become more coal-like with increases in heating value and reduction in volatile matter, resulting in lower reactivity (Basu, 2013). Akinrinola (2014) in his studies on torrefaction and combustion properties of some Nigerian biomass speculated that torrefied fuel would have lower propensity for self-heating due to its hydrophobicity.

Wilén et al. (2013) conducted thermal stability analysis on untreated and torrefied biomass dust. Interestingly, the Minimum Ignition Energy (MIE) of a dust cloud measured for torrefied wood dust was 160 mJ, which is of the same magnitude as that of other biomass dusts. In accordance to BS EN 50281-2-1:1999 where minimum ignition temperature for dust layers were determined using a hot plate, the flammability temperature determined for torrefied wood dust layers was lower than that of untreated wood dust. They concluded that the torrefied wood dust was more sensitive to ignition than other untreated dust.

Saddawi et al. (2013a) investigated the self-ignition temperatures of untreated and torrefied biomass fuels. Employing the hot storage basket test method outlined in BS:EN 15188:2007 Standard, self-ignition temperatures of wood chip and torrefied wood chip were examined for materials contained in three different volumes (red, blue and green dashed-lined-box for small (~11 cm³), medium (~67 cm³), large volumes (~864 cm³) respectively in **Figure 2. 31**. For all the three volumes investigated, it was found that the self-ignition temperatures of raw, untreated wood chips were always higher than that of the torrefied wood chips.

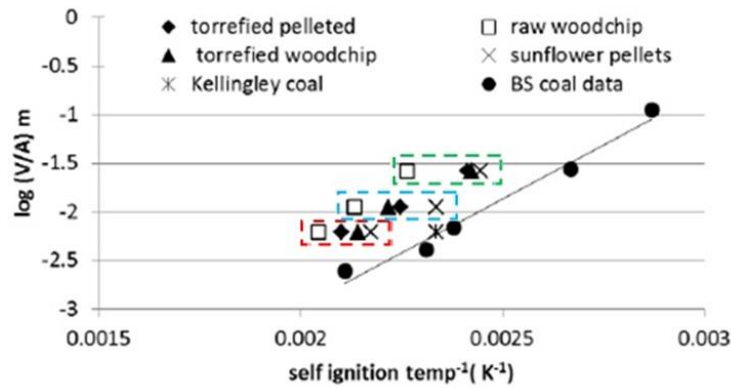


Figure 2. 31 Self-Ignition Temperatures of Wood Chips and Torrefied Wood Chips [Source: (Saddawi et al., 2013a)]

It is known that lignin degrades gradually over a temperature range of 250-500°C, and it actually starts softening in range of 80-90°C (Basu, 2013). During the torrefaction process, some lignin components that serve as natural binders in fuel pellets or briquettes are degraded, and thus the torrefied biomass becomes brittle. Tumbling or any frictional, heat generating movement involving torrefied biomass results in the formation a large quantities of fines (Jong and Ommen, 2015). Brittleness that makes torrefied biomass easier to mill actually imposes a safety hazard with respect to dust explosion or fire in the fuel handling and conveying stage. According to Basu (2013), when dealing with fine dusts generated from the torrefaction process, dust explosion is susceptible to happen. Besides explosion risk, torrefied biomass carries fire potential with it due to its low ignition temperature and unfortunately, some biomass plants had already experienced this. Owing to the fact that torrefied biomass dust is low in moisture content, it is thermally more reactive and can potentially ignite easily. This implies an increased explosion and fire risk (due to its lower ignition temperature) within mills or conveying pipes. Since fire issues have happened in some power plants, further investigation to compare the self-ignition propensity of untreated and torrefied biomass dust is needed before practising torrefaction on a large commercial scale because there could be other factors that affect the reactivity of a solid fuel (Basu, 2013).

In summary, many advantages in utilising torrefied biomass have been proven, with speculation of reduced self-ignition risk. On the other hand, there is evidence to show increased explosion and fire risk when torrefied biomass is used. This implies that the self-heating and self-ignition characteristics of torrefied biomass has not been well-addressed yet and these are studied in this thesis.

2.7 Emission from Biomass on a Hot Surface

In the quest to combat global climate change, the use of bioenergy is gaining popularity everyday. In UK power stations, using biofuels instead of fossil fuel coal is very much encouraged or rather an obligation with the implementation of Renewables Obligation (RO) that requires U.K. electricity suppliers to source an increasing proportion of electricity from renewable source. Renewable biomass is deemed a greener energy than coal but burning biomass, like any combustion process, does generate smoke and emit aerosols, particulate matters (PMs), polycyclic aromatic hydrocarbons (PAHs), semi-volatile organic compounds (SVOCs) and volatile organic compounds (VOCs). Some of these emissions are carcinogenic, some impose short or long term negative effects on human health, like headache, asthma, acute respiratory infections or even chronic obstructive pulmonary disease, blindness (Bari et al., 2011).

A study by the Partnership for Policy Integrity (Partnership for Policy Integrity, 2011) in the U.S. claimed that biomass is a heavily polluting technology after analysing data from air permit applications and real smoke stack tests. Following a study by Yee et al., biomass burning has been identified as a major source of atmospheric organic aerosol (Yee et al., 2013), with contributions from anthropogenic sources as well as natural wildfires. Globally, aerosol from biomass burning was about 90% of all primary organic carbon emitted from combustion sources, much of this is from forest fires and much from biomass combustion in rudimentary cook stoves and stoves. As defined by Jenkins et al., particulate matter (PM) includes soot, ash, condensed fumes (tars/oils) and sorbed materials include VOC and PAH (Jenkins et al., 1998b).

There have been many studies to analyse the emissions from pyrolysing or burning biomass, which provide insight into the experiments undertaken here, where emissions from pre-igniting and critically igniting biomass dust layer were captured for later analysis. Oros and Simoneit in their study on identification and emission factors determination of molecular tracers in organic aerosols from biomass burning (Oros and Simoneit, 2001) had sampled their smoke particulate matter from trees undergoing controlled burning (smouldering or flaming) with quartz fibre filter. The filtered particles were then extracted with dichloromethane, followed by analysis with gas chromatography-mass spectroscopy (GC-MS) equipment. They found that the concentration of organic compounds in smoke aerosols were dependent on combustion temperature. The GC-MS analysis approach had been widely adopted by researchers in a variety of biomass emission studies. As mentioned by Ikan, the quantities of recognisable organic compounds emitted from biomass burning are large and GC-MS is a powerful tool for analysis of these compounds (Ikan, 2008).

There was effort trying to detect initiation of self-ignition via gas emission analysis, conducted by Anez et al. (2015). Equipment for gas emission test was placed in an isothermal oven and coupled with Tedlar gas sampling bags for gas collecting followed by analysis (see **Figure 2. 32**). This examination was conducted on various biomass samples and two emitted gases, CO and CO_2 were measured during the heating process that was fixed between 20 to 200°C, with measurement taken every 20°C. Besides concluding gas emissions strongly depend on sample temperature, the study found that this gas emission test was able to detect biomass self-ignition earlier than other conventional method e.g. TG-DSC analyses, particularly with CO measurements.

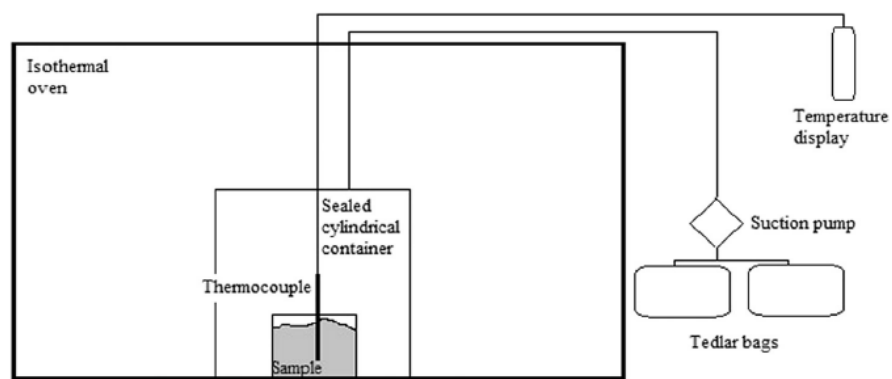


Figure 2. 32 Gas Emissions Test Setup with Temperature Control and Gas Collection System [Edited from: Anez et al. (2015)]

Besides detecting permanent gases like CO and CO_2 , Sheesley et al. (2003) had characterised organic emissions from biomass combustion in details and found that the emissions could basically be grouped into six categories for reaction within 180 to 220°C. The six organic compound emission groups with some commonly detected components are summarized in **Table 2. 4**. In another study, Yee et al. (2013) had looked into organic aerosol formation from biomass burning, focusing on oxidation of three components; phenol, guaiacol (2-methoxyphenol) and syringol (2,6-dimethoxyphenol). It was found that phenols are produced from pyrolysis of lignin that comprises the secondary cell wall of plants. Guaiacol emission was found from both soft and hard wood combustions whereas syringol primarily from soft wood burning.

Table 2. 4 Biomass Combustion – Six Emissions Categories with Some Component Examples (Sheesley et al., 2003)

No.	Organic Compounds Group	Examples
1	Aromatic Hydrocarbons	2-Phenyl-naphthalene, Fluoranthene, Acephenanthrylene, Pyrene
2	Sugar Anhydrides	Levoglucosan, Galactosan, Mannosan
3	Substituted Phenols	Catechol, Methylbenzenediols, Hydroxybenzaldehydes, Methyl 3-(4-hydroxyphenyl)-2-propenoate
4	Guaiacyl Compounds	Guaiacol, Eugenol, Vanillin, Coniferyl aldehyde
5	Syringyl Compounds	Syringol, Ethylsyringol, 4-Propenylsyringol, Syringaldehyde,
6	Sterols and Stanols	Coprostanol, Stigmastan-3,5-diene, Stigmasterol, Stigmasta-3,5-dien-7-one

There have been various studies that characterised the compounds evolved from biomass pyrolysis or combustion. A study from Gudka et al. (2012) that pyrolysed wheat-based Dried Distillers Grains and Solubles (DDGS) at 250°C found mainly three markers for compounds evolved; cellulose (furfural as an example), oil (Linoleic acid as an example) and amino acid (4H-Pyran-4-one, 2,3-dihydro-3,5-dihydroxy-6-methyl- as example). In another study that pyrolysed biomass cell-wall constituents at 600°C, Nowakowski and Jones (2008) found many compounds evolved and some are shortlisted in **Table 2. 5**. Some similar compounds as tabled in **Table 2. 1** were found when short rotation coppice willow was pyrolysed at 600°C, as reported in the study by Nowakowski et al. (2007).

Table 2. 5 Pyrolysing Biomass – Some Compounds and Key Markers (Nowakowski, 2008)

No.	Compound/Chemical Formula	Key Marker
1	4-Hydroxy-3,5-dimethoxybenzaldehyde (C ₉ H ₁₀ O ₄)	Syringol lignin
2	2,6-Dimethoxyphenol (C ₈ H ₁₀ O ₃)	Syringol lignin

No.	Compound/Chemical Formula	Key Marker
3	4-Hydroxy-3-methoxy-benzaldehyde (vanillin) (C ₈ H ₈ O ₃)	Guaiacol lignin
4	2-Hydroxy-3-propenyl-2-cyclopenten-1-one (C ₈ H ₁₀ O ₂)	Cellulose
5	1-(3,4-Dimethoxyphenyl)ethanone (C ₁₀ H ₁₂ O ₃)	Lignin

Gas phase combustion of biomass involved burning of volatile matters during pyrolysis as the biomass is heated and burning of these volatiles is as rapid as the volatiles are released. Homogeneous volatiles burning is then followed by a relatively slower heterogeneous char oxidation (Jenkins et al., 1998b). Among these volatile matters released are some undesired organic emissions, the pollutants to the environment, i.e. PAH, SVOCs, VOCs.

It has been found experimentally that when a fuel gas is mixed with air, flame propagation cannot occur if the fuel gas concentration is too small or too great (Babrauskas, 2003a). The limiting concentration lies within the lower flammability limit (LFL) and upper flammability limit (UFL) in which were termed lower explosion limit (LEL) and upper explosion limit (UEL) in older literature. In short, UFL and LFL refer to the lowest and highest fuel concentration by volume for which a mixture is flammable (Babrauskas, 2003a).

Lower flammability limit (LFL) or sometimes called lean flammability limit, is defined as the lowest concentration of a gas vapour that will just support the propagation of flame away from a pilot ignition source (Babrauskas, 2003a). More precisely, the LFL is the value half-way between the lowest concentration at which flame propagation occurred and the highest concentration at which it did not (Babrauskas, 2003a). It is usually measured in volume percent and depends on the atmosphere – its composition, pressure and temperature (Babrauskas, 2003a). The LFL in air and in pure oxygen are usually identical. Generally, a lower flammability limit signifies a greater volatile ignition risk. McNamee et al. (2016) had modelled the composition and yields of volatile stream species with FG-BioMass from AFR Inc. where she had obtained ten major volatile species from four different biomass samples. The ten species identified from the model were reaction water, phenol, acetone, methanol, formaldehyde, formic acid, acetic acid, acetaldehyde, carbon dioxide and carbon monoxide.

Chapter 3

Methodology

Throughout this study on low temperature ignition and self-ignition characteristics of biomass, two situations where biomass is likely to self-heat and self-ignite were looked into – during biomass handling and biomass storage stages. Some modelling of the experimental work was carried out too. All samples for the planned experiments were prepared with suitable equipment and later analysed following appropriate standards. For biomass handling, biomass dust deposition on hot surfaces were investigated, this included dust originating from different biomass species, dust blended among themselves at different weight ratios or with different binders and dust that was pre-treated with different pre-treatment technologies. For biomass storage, the self-ignition characteristics of biomass subjected to isothermal conditions was investigated. Emissions from biomass dust during smouldering and flaming combustions were investigated too.

3.1 Instruments and Procedures Applied

Several different laboratory equipment were applied for materials preparation and suitable techniques and procedures were followed for findings analysis.

3.1.1 Sample Preparation

Prior to any analysis or experiment, biomass samples were prepared using different equipment following suitable operating procedure of that equipment. First of all, all the as-received biomass materials were oven dried to constant weight. Biomass samples to be dried were loaded into heat resistant Nalgene tubs, after which the biomass filled containers were transferred into the oven. The dried biomass were then sized appropriately, relevant to requirements of respective analysis standards. Three different grinding or milling equipment were used for biomass size reduction – Retsch SM300 cutting mill Retsch planetary ball mill PM100 and SPEX 6770 freezer mill.

The Retsch SM300 cutting mill (see **Figure 3. 1**) was the first attrition equipment used to size down all biomass samples. To avoid cross contamination among samples, different biomass species were milled on different days and the equipment was cleaned with alcohol before and after cutting each time.

The samples to be milled were loaded onto a clean container (Nalgene tub in this study) and readied to be poured into the cutting mill via the feed hopper safety guard. The

machine was switched on and the cutting speed was adjusted to 1500 rpm at the control panel. Biomass was scooped into the feed hopper gradually and the grinding progressed as biomass passed the bladed parallel section rotor. Sample biomass was comminuted by the cutting and shearing forces that took place between the blades and stationary double acting cutting bars inserted at the housing. Passing through the rotor, the ground biomass were collected at the collecting receiver after being screened by the specific size bottom sieve (only 1 mm-hole screen available for this study). After repeating the feeding process a few times, the milled biomass in the collecting receiver was emptied to another clean container, ready for the next size reduction process.

Since the required particle size of all analyses in this study was less than the 1 mm resulted from SM300, further grinding in Retsch PM100 and SPEX 6770 freezer mill was necessary.

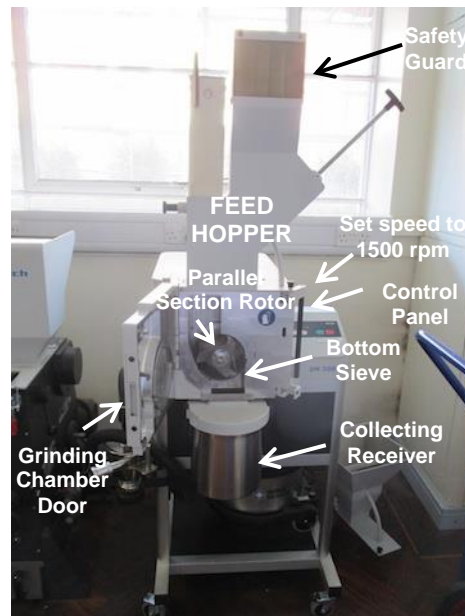


Figure 3. 1 Retsch SM300 Cutting Mill with Major Parts Labelled

The Retsch Planetary Ball Mill PM 100 (see **Figure 3. 2**) was used to grind the biomass samples further and the essential parts of the mill are shown in **Figure 3. 3**. For each grinding cycle, ~25 g of biomass was loaded into the grinding bowl, clamped in and after balancing with a counter weight of the ball mill, the biomass sample was milled for ~5 minutes at a speed of 500 rpm with the aid of 10-15 grinding balls. The weight of material actually depended on the filling level of the grinding bowl since a level too high or too low would increase the wear and tear of the ball mill leading to damage eventually. The balancing weight, depending on weights of sample and grinding balls clamped in the grinding bowl, was adjusted using the knob. The grinding speed and number of balls were

chosen so as the noise level was in accordance with DIN 45635-31-01-KL3 (Retsch, 2010). Owing to the limitation of jar capacity, this process took a considerable period of time to obtain sufficient material for experiments that followed.



Figure 3. 2 Retsch Planetary Ball Mill PM 100 used in Biomass Grinding [Source: (Retsch, 2010)]



Figure 3. 3 Retsch PM100 Ball Mill (a) Counter Weight Adjusting Knob (b) Grinding Bowl and Grinding Balls (c) Grinding Bowl Clamp

The freezer mill (see **Figure 3. 4**) is a cryogenic laboratory mill operating with liquid nitrogen that has a boiling point as low as -196°C as the coolant. Cryogenic milling was chosen since fibrous biomass was made brittle at such a low temperature and thus grinding to small particle size was possible. Containing a stainless steel metal impactor, biomass sample was filled to around one third full of a SPEX 6770 freezer mill transparent vial (see **Figure 3. 5**) and was sealed with two metal plugs at both ends of the vial. Liquid nitrogen was transferred from a large volume storage dewar to a smaller flask and later, the required amount was poured to fill up to the level required by SPEX 6770. With the appropriate minimum amount of liquid nitrogen coolant, the freezer mill that had been programmed was started to cryo-mill each sample for 5 minutes. Sealed between the two end plugs and immersed in liquid nitrogen within the grinding cycle, the integrity of the sample was well preserved. Applying the electromagnetic principle, the steel impactor were driven back and forth by dual electromagnets (SPEX, 2010) and operating at high frequency, fibrous biomass that had been made brittle was able to mill to fine particles.

The cryo-milled particles were then sieved to $\leq 90 \mu\text{m}$ for material characterisation via thermogravimetric analysis (TGA) and ultimate analysis. This size was chosen for optimum heat transfer based on a study on kinetics of pyrolysis or devolatilisation of various fuels by Hayhurst (2013).



Figure 3. 4 SPEX Freezer Mill for Biomass Cryomilling



Figure 3. 5 SPEX Vial, End Plugs and Metal Impactor

The milled biomass samples were then sieved with Retsch AS 200 sieve shaker (see **Figure 3. 6**) where sieves of appropriate mesh size had been chosen. For TGA experiments, the particle size followed recommendation from studies of Hayhurst (2013) whereas the self-ignition dust layer test followed procedures from BS EN 50281-2-1:1999 (British Standard, 1999b) that mentioned the dust particles should pass through $200 \mu\text{m}$ aperture. Due to availability, a sieve of $180 \mu\text{m}$ was chosen. The appropriate sieves ($90\mu\text{m}$ and $180\mu\text{m}$) were filled half full or less with milled biomass for each sieving cycle. The sieve was placed on top of a collector tray, covered with lid of the right size, securely tighten to the sieve shaker and the sieving process started. Normally, each sieving cycle was fixed at ~ 20 minutes and shaking frequency of $\sim 60\text{-}80\text{Hz}$. The bigger particles that retained above the mesh were take for regrinding, following the process done previously.

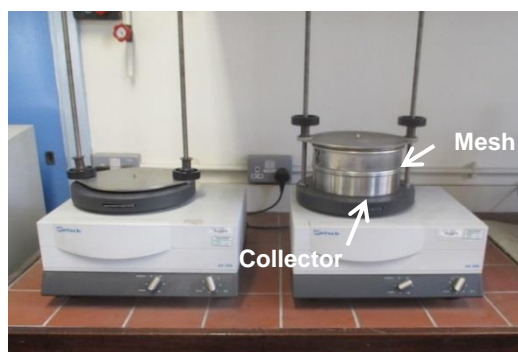


Figure 3. 6 Retsch Sieve Shaker AS 200



Figure 3. 7 Brown Silica Gel Desiccator to Condition the Dried Samples before Experiments

Before any analysis, the oven-dried, pulverised and sieved materials were kept in a brown silica gel desiccator (see **Figure 3. 7**) for around a day. The non-toxic brown silica gel was used instead of the desiccant with cobalt chloride indicator (blue for dry, pink for exhausted) that was deemed toxic (GeeJay, 2016). The microporous structure of amorphous silicon dioxide manufactured in the form of granular beads possesses high surface area that traps moisture. Based on the colour of silica gel desiccant, as the desiccant turned from dark orangey brown to pale yellowish brown, the desiccant were taken for regeneration by heating at 150°C in an oven. After an appropriate cooling process in the desiccator, the desiccant was reused and the regeneration process was repeated as the desiccants were exhausted again.

3.1.2 Proximate Analysis, Reaction Rate Kinetics and Self-Ignition Risk Ranking

Proximate and ultimate analyses are the two most common fuel characterisation techniques (Ibrahim, 2013) used before designing any biomass combustion system, be it a gasifier, bubbling fluidised bed (BFB) combustor or circulating bed combustor (CFB) (BioEnergyConsult, 2016). Proximate analysis is a more typical way of categorising organic composition of a biomass into moisture, volatiles, fixed carbon or char, and ash (bioenarea, 2016). The ultimate analysis, also known as elemental analysis or sometimes termed CHNS analysis, presents the components in the organic part of the material rather than based on chemical structure or combustion behaviour. Carbon, hydrogen and oxygen are usually the main elements identified whereas nitrogen, sulfur and chlorine are the secondary elements (bioenarea, 2016).

Proximate analysis is a technique widely used to determine physiochemical properties like moisture, volatile matter, fixed carbon and ash contents of a solid fuel of interest, e.g. biomass. In this study, proximate analysis on all the samples used was conducted following several British Standards – BS EN 14774-3:2009 *Solid biofuels-Determination of moisture content-Oven dry method Part 3: Moisture in general analysis sample, for moisture amount determination*; BS EN 15148:2009 *Solid biofuel-Determination of the content of volatile matter, for volatile matters amount determination* and BS EN 14775:2009 *Solid biofuels-Determination of ash content, for ash amount determination*. These determinations were carried out at least in duplicate.

Following the BS EN 14774-3:2009, before determining the moisture amount in a sample (British Standard, 2009a), an empty weighing dish and its lid were dried to constant mass at $(105 \pm 2)^\circ\text{C}$, after which they were left to cool to room temperature in a desiccator. Nitrogen gas was piped in to the moisture oven, i.e. Carbolite MFS oven (see

Figure 3. 8(a)) and the float of the nitrogen rotameter was ensured to be around the 100-200 cc/min level.



(a)



(b)

Figure 3. 8 Proximate Analysis for Moisture (a) Carbolite MFS Oven (b) Samples in Weighing Dishes and Separated Lids Entering the Oven

When the weighing dish and lid were cooled, a minimum of 1 g sample was added into the weighing dish in an even layer. With the lid on, the weighing dish and lid with the ~1 g sample were weighed to the nearest 0.1 mg. The uncovered weighing dish with sample and the separated lid were placed into the Carbolite MFS oven (see **Figure 3. 8(b)**). After a drying duration of 3 hours, the hot uncovered dish with sample and the separated lid were all transferred into a desiccator and allowed to cool to room temperature. The cooled, dried weighing dish set and sample were weighed rapidly upon removal from desiccator since small particle-sized dried biomass were quite hygroscopic. The moisture content, M_{ad} , as analysed, expressed as a percentage of mass was calculated using the following formula:

$$M_{ad} = \frac{(m_2 - m_3)}{(m_2 - m_1)} \times 100 \dots\dots \textbf{Equation 3.1}$$

where

- m_1 is the mass of the empty dish plus lid, in g
- m_2 is the mass of the dish plus lid plus sample before drying, in g
- m_3 is the mass of the dish plus lid plus sample after drying, in g

Adhering to BS EN 15148:2009, cylindrical crucibles with well-fitting lid both made of fused silica were used in determination of biomass volatile matters (British Standard, 2009c). The determination was conducted using the Carbolite AAF 1100 furnace (see **Figure 3. 9(a)**). Weights of cool empty crucible and lid was taken and (1 ± 0.1) g of samples

was weighed to the nearest 0.1 mg. With lid on, the sample filled crucible was tapped several times on clean hard surface to form an even thickness layer of biomass. After weighing, four lidded crucibles were placed in a special-designed steel crucible stand (see **Figure 3. 9(b)**). With face shield and thermal gloves on, the crucible stand designed to hold four crucibles was transferred into the oven that had been heated to $(900 \pm 10)^\circ\text{C}$ and was left in the oven for 7 minutes \pm 5 seconds. After the 7-minute duration, the extremely hot crucible stand holding four glowing hot volatile crucibles was removed to a thick thermo-resistant plate and left to cool to 30-50°C above room temperature and later the partially cooled crucibles were allowed to cool to room temperature in a desiccator. The cooled crucibles were then weighed to the nearest 0.1 mg. The volatile matter contents, V_d , expressed as a percentage by mass on dry basis, was determined using the following equation:

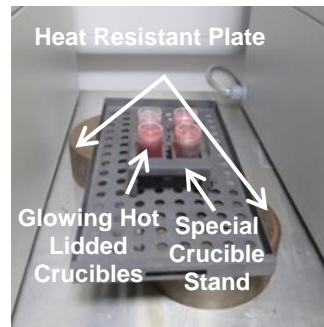
$$V_d = \left[\frac{100(m_2 - m_3)}{m_2 - m_1} - M_{ad} \right] \times \left(\frac{100}{100 - M_{ad}} \right) \dots\dots \text{Equation 3.2}$$

where

- m_1 is the mass of the empty crucible and lid, in g
- m_2 is the mass of the crucible with sample and lid before heating, in g
- m_3 is the mass of the crucible with sample and lid after heating, in g
- M_{ad} is the percentage moisture determined by BS EN 14774-3:2009



(a)



(b)

Figure 3. 9 Proximate Analysis for Volatile Matters (a) Carbolite AAF 1100 Furnace (b) Sample Crucibles Held by Special Stand

The BS EN 14775:2009 was followed closely for ash determination (British Standard, 2009b), where ash content was calculated from residual mass that remained after a sample was heated by controlled air condition. In this study, the Carbolite AAF 11/18 Furnace (see **Figure 3. 10(a)**) was applied, in which the required temperature at different times and ventilation rate specified in that standard were achieved. As required by the standard, the inert crucible to contain sample was ensured that sample loading did not exceed 0.1 g/cm² of its bottom area.

Prior to filling up samples into the inert material crucible, the clean empty crucible was heated for at least 60 minutes in the furnace that had been set to (550 ± 10)°C. The crucible was left to cool for 5-10 minutes on a clean heat resistant plate after being removed from the furnace and later transferred to a desiccant-free desiccator for further cooling to ambient temperature. Weighing to the nearest 0.1 mg was started only after the crucible was cooled. Like before, a minimum of 1 g sample was weighed and spread in an even layer over the crucible (see **Figure 3. 10(b)**).

The sample filled crucible then entered the oven that had been programmed to increase its temperature evenly from initial cooled condition to 250°C at 5°C/min within 30-50 minutes and remained at 250°C for 60 minutes to ensure volatiles left the sample before ignition. After the 1-hour duration, the furnace temperature was raised evenly to (550 ± 10)°C within 30 minutes at a rate of 10°C/min. The furnace was to remain at this temperature for at least 120 minutes. The hot crucible was then allowed to cool on a heat resistant plate for 5-10 minutes after removal from the furnace, after which it was moved to the desiccant-free desiccator where it cooled to ambient temperature. The crucible and its content were weighed to the nearest 0.1 mg and the mass recorded as soon as ambient temperature was achieved. The ash content, A_d , expressed as a percentage by mass on dry basis was calculated with the following equation:

$$A_d = \frac{(m_3 - m_1)}{(m_2 - m_1)} \times 100 \times \frac{100}{100 - M_{ad}} \dots\dots \text{Equation 3.3}$$

where

- m_1 is the mass of the empty crucible, in g
- m_2 is the mass of the crucible plus sample, in g
- m_3 is the mass of the crucible plus ash, in g
- M_{ad} is the % moisture content of the sample used

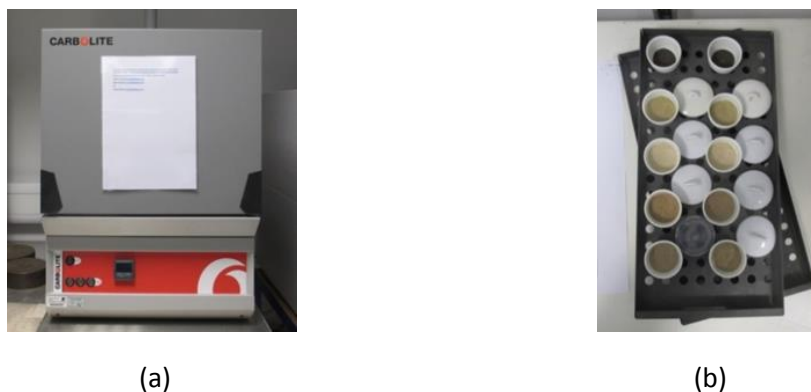


Figure 3. 10 Proximate Analysis for Ash Content (a) Carbolite AAF 11/18 Furnace (b) Unlidded Sample Crucibles Preparing to Enter the Furnace.

The proximate analysis is also possible to be estimated using a thermogravimetric analyser. Estimation via TGA is widely practised in the industry since it uses less material and is less time extensive. Some commonly practised procedure is outlined as follows.

After weighing 4-6 mg of sample material of $<500\mu\text{m}$ into an alumina crucible (other suitable crucibles may be used), at a heating rate of $10^{\circ}\text{C}/\text{min}$, the sample was heated under nitrogen from room temperature to 110°C and was held for 10 minutes. This is in association to obtaining the sample moisture content. The furnace temperature was then ramped to 910°C at a heating rate of $25^{\circ}\text{C}/\text{min}$. It was held for 10 minutes at 910°C and the weight loss during this step signified volatile matter content. After increasing the furnace temperature slightly to 920°C , flowing gas was switched to air to burn off the fixed carbon in the sample. Both nitrogen and air flow rates were fixed at 50 ml/min. Weight of inert ash contained within the sample was obtained from the remaining weight after oxidation had completed. An example of TGA-proximate analysis following this method is shown in **Figure 3. 11**.

3.1.2.1 Thermogravimetric Analysis Studies

Some researchers have used lower temperature, in order to prevent possible volatilisation of alkali metals in biomass. Biller and Ross (2014) in a study on novel analysis techniques to determine the biochemical composition of microalgae, used an air flow rate of 50 ml/min and moisture of microalgae was determined by heating the TGA furnace from room temperature to 105°C and holding for 15 minutes. Ash, on the other hand was determined by ramping the temperature to 550°C and was held for 80 minutes.

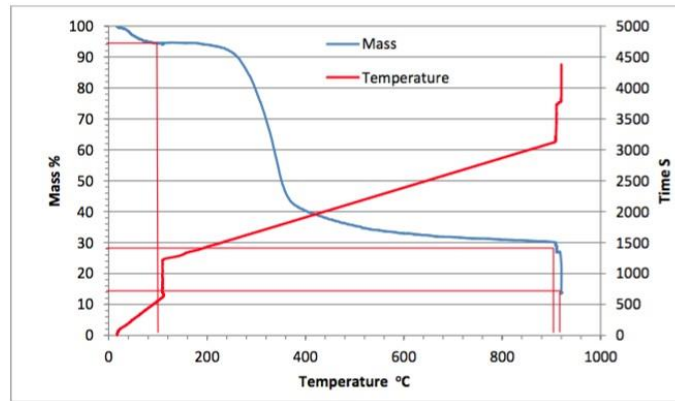


Figure 3. 11 Proximate Analysis Conducted via TGA Method on Empty Fruit Bunches Biomass [Source: (Slatter, 2015)]

Reed (1981); Akinrinola (2014) also used TGA to conduct proximate analysis with TGA method. Sample materials of $<53\mu\text{m}$ was heated from room temperature to 900°C at a heating rate of $10^{\circ}\text{C}/\text{min}$ was held at the final temperature for 10 minutes. Nitrogen gas was used during this step, after which, gas was changed to air to obtain ash content of the sample. The TGA-proximate analysis procedure for biomass in general is illustrated in **Figure 3. 12**.

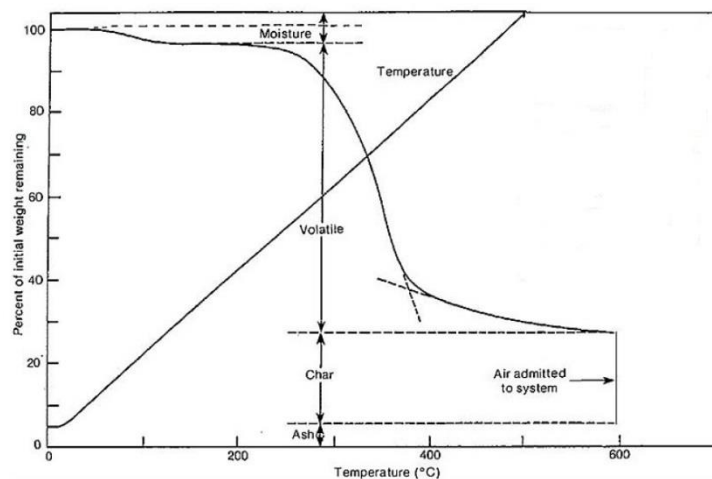


Figure 3. 12 Proximate Analysis Conducted via TGA Method on Biomass in General [Source: (Reed, 1981)]

Thermogravimetric analysis (TGA) is a branch in thermal science that identifies mass or weight changes of a material of interest as a function of temperature or time. The biomass self-heating reaction kinetics in this study was simulated in the TGA with a slow combustion process utilising the TGA Q5000 laboratory equipment (see **Figure 3. 13(a)**). Before running any analysis with this equipment, around 4-6 mg of $<90\ \mu\text{m}$ pulverised

biomass samples were weighed with a microbalance and loaded onto platinum pans (see **Figure 3. 13(b)**). A slow combustion procedure was programmed in the equipment software, in which the process started with purging nitrogen gas at 100 ml/min to ensure no air exist before the actual upcoming slow combustion process. The furnace was held at the initial ambient temperature for 5 minutes, after which nitrogen purging was lowered to a stable rate of 20 ml/min. Data recording and storage was started at a frequency as high as 0.5 second per data point. It was then followed by switching of nitrogen gas to air and was held isothermal for another 5 minutes before ramping up to 105°C at a heating rate of 5°C/min. The furnace remained at 105°C for 10 minutes before heating up to 800°C at a heating rate as slow as 5°C/min. The sample was then held isothermal at 800°C for the subsequent 10 minutes before the slow combustion process ended. For each sample, the same TGA procedure was carried out in duplicate or triplicate. The glowing red section in **Figure 3. 13(c)** shows a sample being run with other samples pending on the TGA tray.

A similar TGA process for slow pyrolysis were conducted on selected of the materials. The slow pyrolysis procedures programmed were quite similar to that of the slow combustion process, with the same heating rate, terminal temperatures and isothermal duration for each heating stage. The difference was that nitrogen was used most of the time instead of air; gas was changed to air only after holding the temperature at 800°C towards the end. Air was introduced for 15 minutes to burn off pyrolysis residues left on the TGA pans.

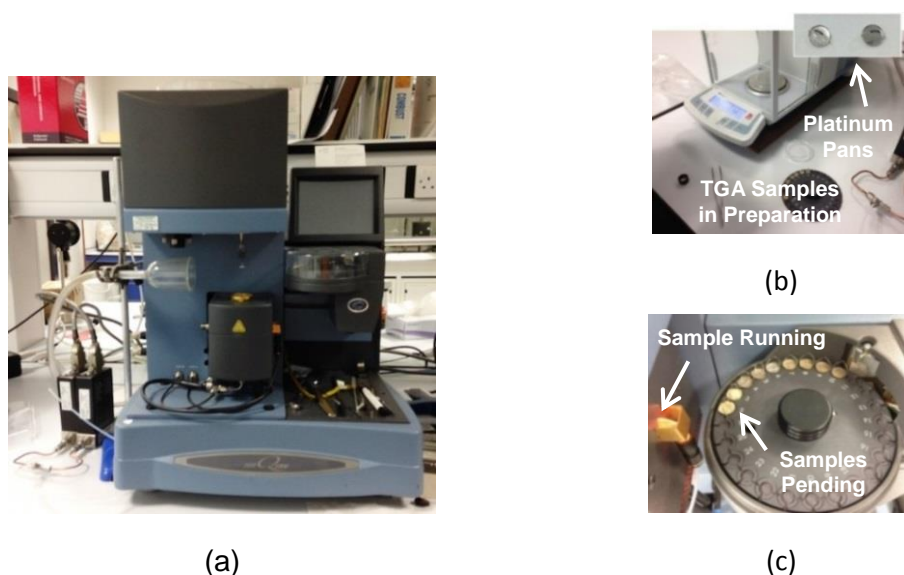


Figure 3. 13 Thermogravimetric Analysis (a)TA Q5000 Equipment (b) Loading Sample onto TGA Q5000 Platinum Pans (c) TGA Q5000 Running in Progress

The apparent activation energy, E_a , was calculated from the TGA weight loss curve with application of the reaction rate kinetics. Following the reaction rate kinetics

calculation recommended and done by Ramírez et al. (2010) and Saddawi et al. (2010), the widely-used first order reaction rate constant mathematical method was applied to derive the pre-exponential factor (A) and activation energy (E_a) from the TGA experiments. It was assumed that the reactions followed the Arrhenius function:

$$k = A \exp \left(-\frac{E_a}{RT} \right) \dots\dots \text{Equation 3.4}$$

where k is reaction rate constant in s^{-1} , A is pre-exponential factor in s^{-1} , E_a is activation energy in J/mol , R is gas constant of $8.314 J/mol \cdot K$ and T is temperature in K .

Assuming the weight loss with time curve is the result of one or more first order reactions, each reaction may be described as follows:

$$k_t = -\frac{1}{(m-m_\infty)} \frac{dm}{dt} \dots\dots \text{Equation 3.5}$$

where m is the mass and m_∞ is the terminal mass.

For biomass combustion, two combustion sections involving volatiles and chars respectively were identified from the derivative thermogravimetric (DTG) curve, the section with the first tall peak signified volatiles combustion whereas section with second lower peak indicated combustion of char (see **Figure 3. 14**). The DTG curve is the first derivative curve obtained from differentiating mass changes within a certain period of time, signifying the mass change rate.

Linear regression of the reaction rate constant curve was performed after moisture loss (indicated after $\sim 105^\circ C$ on the TGA weight loss curve) to before onset of char combustion of the TGA weight loss curve (see **Figure 3. 15** for TGA section selected for reaction rate kinetics calculation). This section was selected since biomass combustion was dominated by combustion of its volatile matters. For each TGA run of biomass sample, the values of A and E_a were determined from the intercept and gradient of the $\ln k$ versus $1/T$ plot following the linearised Arrhenius equation:

$$\ln k = \ln A - \frac{E_a}{R} \left(\frac{1}{T} \right) \dots\dots \text{Equation 3.6}$$

Figure 3. 16 illustrates a typical linearised Arrhenius plot for the selected TGA section of a biomass sample, i.e. after moisture loss to before onset of char combustion. From the gradient and intercept of the resulted linear equation and, in this example, the E_a and $\ln A$ values were found to be 75.40 kJ/mol and 11.038 respectively.

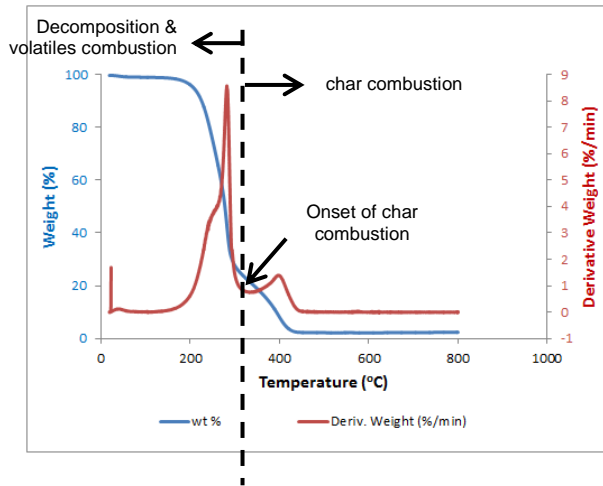


Figure 3. 14 Biomass TGA Decomposition Profile Subjected to Slow Combustion

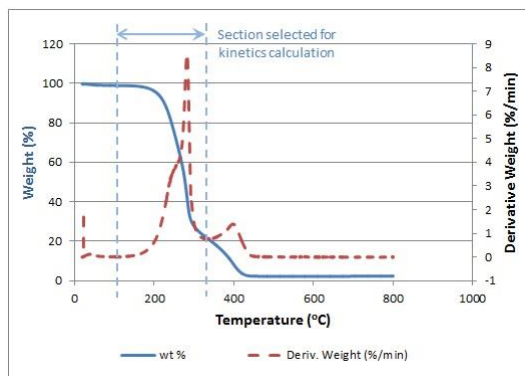


Figure 3. 15 Section Selected for Kinetics Calculation

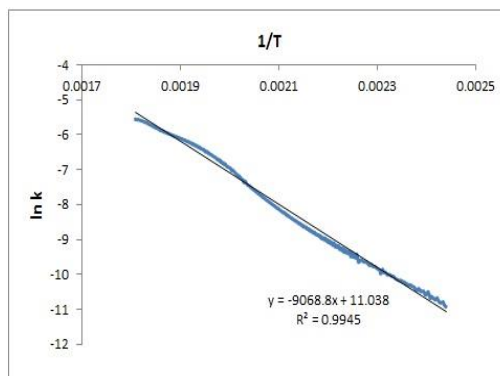


Figure 3. 16 Linear Regression of Reaction Rate Constant for one of the Biomass Samples

With reference to the solid fuel self-ignition graphical risk ranking method of Ramírez et al. (2010), slight modifications were made in this study following the alteration done by Jones et al. (2015). The single oxidation temperature (T_{charac}) plotted on the vertical axis by Ramirez et al. was replaced by the maximum weight loss temperature for the solid fuel pyrolysis in the air stream (T_{MWL}) in the studies of Jones et al. Consistent with findings of Jones et al., a single peak temperature of T_{charac} found by Ramírez et al. was hardly found in the oxygen stream combustion. Since the air stream T_{MWL} corresponded to the highest peak in the first derivative TGA mass/weight loss curve, i.e. the derivative

thermogravimetric (DTG) curve, the T_{charac} of Ramírez et al. was replaced by T_{MWL} in this study **Figure 3. 17** shows a typical TGA weight loss curve and its DTG curve for one of the biomass samples used in this study, where the highest peak of the DTG curve corresponded to T_{MWL} of that material.

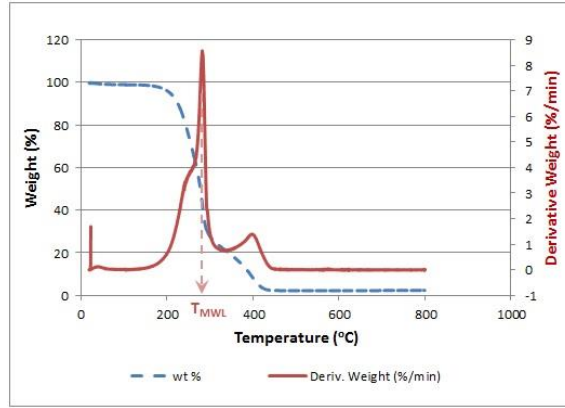


Figure 3. 17 Slow Combustion TGA of a Biomass– Weight Loss Curve and T_{MWL} Obtained from the Derivative Weight Loss Curve

With the information of E_a and T_{MWL} for each sample obtained from the methods outlined above, the self-ignition risk were ranked graphically into four categories – low risk, medium risk, high risk and very high risk. Since the range of E_a and T_{MWL} (T_{charac}) was 60-100 kJ/mol and 220-400°C respectively; in cases where the E_a fell outside this range, extrapolation was made. Sample plots from the studies of Ramírez et al. and Jones et al. are shown in **Figure 3. 18** respectively. Kinetic data for the samples in this study is shown in **Appendix A**.

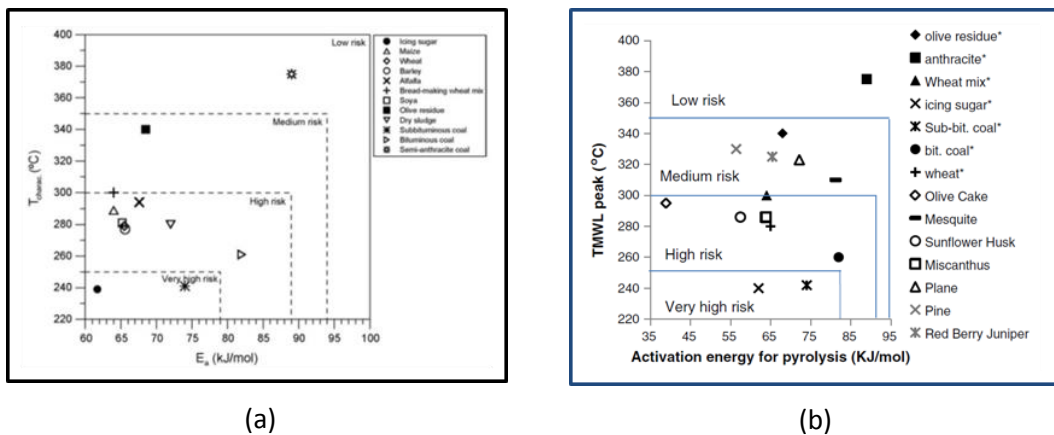


Figure 3. 18 Self-Ignition Risk Pictorial Assessment Tool Application on (a) Twelve Materials [Source: Ramírez et al. (2010)] (b) Fourteen Materials [Source: Jones et al. (2015)]

3.1.3 Ultimate Analysis and Higher Heating Value Calculation

Ultimate analysis or elemental analysis is another common characterisation technique conducted on solid fuels where the composition of a material is given as the weight percentage of carbon (C), hydrogen (H), nitrogen (N), sulfur (S), and oxygen (O) by difference. In this study, the ultimate analysis was performed using the FLASH EA1112 Elemental Analyzer (see **Figure 3. 19(a)**). Around 2-4 mg of each pulverised sample was weighed with microbalance and filled into tin capsules with dedicated set of spatula and tweezer as capsule sealing tools (see **Figure 3. 19(b)**). The tin capsules were then sealed properly and carefully to remove as much air as possible.

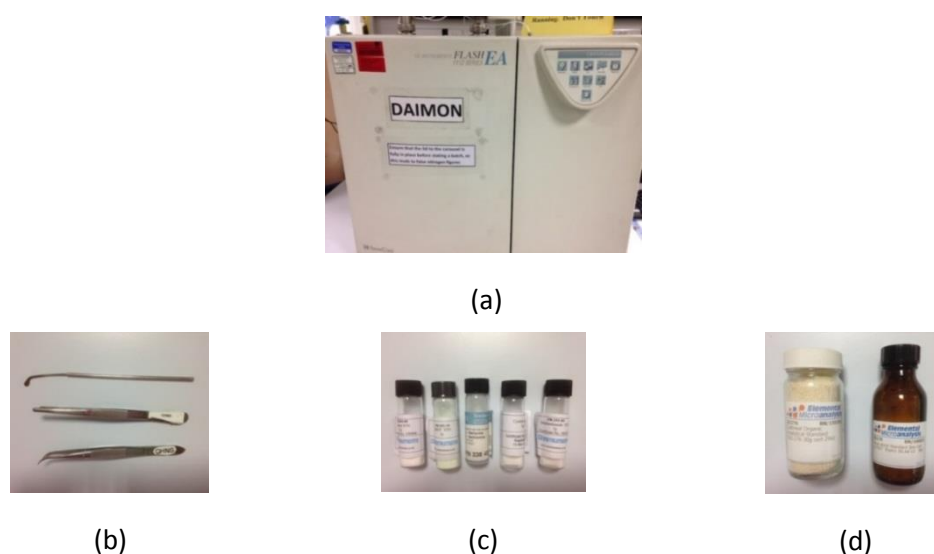


Figure 3. 19 Ultimate Analysis on Solid Fuel (a) FLASH EA1112 Elemental Analyzer (b) Dedicated Capsule Sealing Tools (c) Materials used as Standards (d) Some Materials used as Reference

After loading the tin capsules into the carousel, the equipment was programmed to drop a capsule into the combustion chamber. Here, the sample capsule was combusted, producing carbon dioxide, water vapour and nitrogen that were separated in a chromatography column. A thermal conductivity detector was used to detect the quantity of each, and later compared with standards to determine the percentages of C, H, N. The standards used in this study were atropine, 2, 5 – (Bis (5-tert-butyl-2-benzo-oxazol-2-yl) thiophene (BBOT), dl-Methionine, L-Cystine and Sulphanilamide (see **Figure 3. 19(c)**). After running every 10 samples, reference material e.g. olive stone (for high carbon), oatmeal (for high nitrogen), soil (for no sulphur) or coal (for high carbon) with know elemental compositions was included (see **Figure 3. 19(d)**). The reference material within the same category as sample was selected and results were later compared to correct any drift that might happened during the analysis. For difficult combusting materials, a tiny amount of

<0.5 mg of Vanadium pentoxide (that is moderately toxic) was added as catalyst to help the sample to combust. For each sample, the analysis was done in duplicate or triplicate and the mean value was reported.

With the moisture content information obtained from proximate analysis, the dry basis C, H and N weight percentages were determined following the BS EN 15104:2011 standard. The conversions from as received biomass C, N and H weight percentages to the dry basis weight percentages following the standard (British Standard, 2011) are as follows:

$$C_d = C_{ad} \times \frac{100}{100 - M_{ad}} \dots\dots \text{Equation 3.7}$$

$$N_d = N_{ad} \times \frac{100}{100 - M_{ad}} \dots\dots \text{Equation 3.8}$$

$$H_d = \left(H_{ad} - \frac{M_{ad}}{8.937} \right) \times \frac{100}{100 - M_{ad}} \dots\dots \text{Equation 3.9}$$

where d is dry basis, ad is as determined and M_{ad} is the moisture content of the general analysis sample when analysed.

Soon after obtaining the dry basis C, H, N and O contents from the FLASH EA 1112 Analyser, the higher heating value (HHV) or gross calorific value (GVC) of each biomass was calculated by employing an empirical correlation from Friedl et al. (2005), as follows:

$$HHV = 3.55C^2 - 232C - 2230H + 51.2C \times H + 131N + 20600 \dots\dots \text{Equation 3.10}$$

in which HHV is in the unit of kJ/kg on dry mass basis; C, H and N are the mass percentages of carbon, hydrogen and nitrogen on dry mass basis as well. HHV is based on complete combustion of a sample biomass to carbon dioxide and liquid water (PlanetPower, 2016), therefore HHV includes the latent heat from water vapour.

The Friedl correlation had been validated by previous studies and was revalidated in this study using a bomb calorimeter, following the procedure outlined in BS EN 14918: 2009 (British Standard, 2009). The correlation estimated HHV was checked with experimental run using a bomb calorimeter, the Parr 6200 Isoperibol Bomb Calorimeter in this study (see **Figure 3. 20(a)**). Owing to the characteristics of the biomass powder in use, pulverised biomass samples were pelletised (SPECAC, 2013) using an Specac manual hydraulic press (see **Figure 3. 20(b)**) before placing in the metal sample holder held in a thick-walled vessel (more commonly known as the bomb). Fuse wire of a known length was measured and wrapped through the designated structure on top of the sample holder with the wire close to but never touching the sample. After tightening the sample holder

with wire in the bomb, the bomb was transferred to a bucket filled with known amount of deionised water. The calorimeter was started after pressuring the bomb and with a current flowing through the wire from electrodes, combustion was initiated. Some of the major parts of the bomb calorimeter are shown in **Figure 3. 20(c)**. Heat of combustion produced from sample was absorbed by the medium i.e. deionised water in this case and could then be calculated by multiplying the temperature rise in the calorimeter by the heat capacity of deionised water. For materials where combustion is difficult to start, combustion heat produced by spiking material or combustion aid added to the sample was deducted from the total energy released (Parr®, 2007).

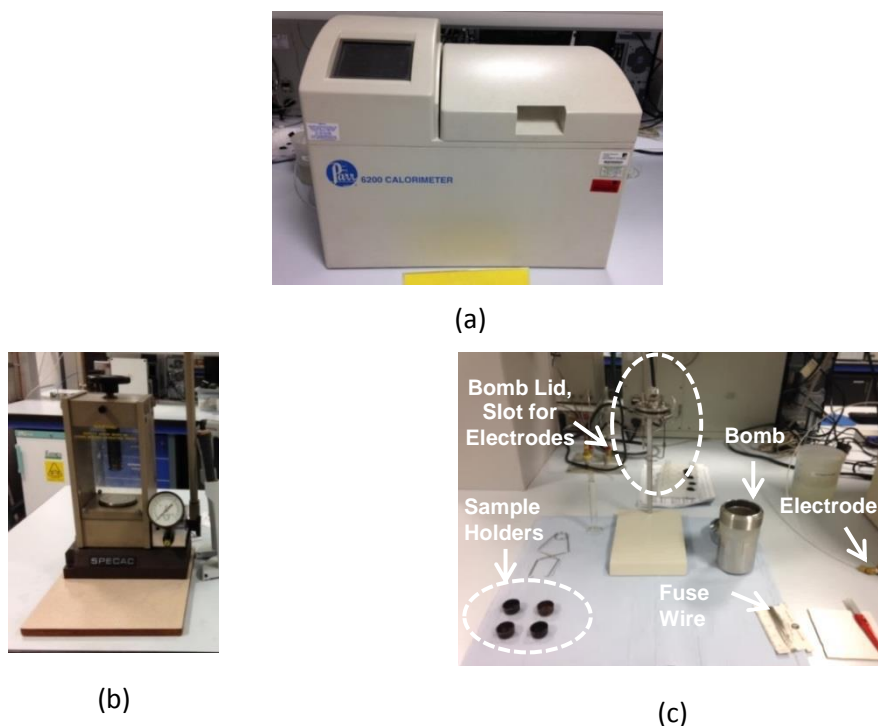


Figure 3. 20 Calorific Value Determination with Bomb Calorimeter (a) Parr 6200 Isoperibol Bomb Calorimeter (b) Specac manual hydraulic press (c) Some Components of the Parr Calorimeter

3.1.4 Biomass Dust Layer Ignition

The minimum ignition temperature (T_{LIT}) of a sample dust layer was determined with the dust layer rig manufactured by ANKO-lab. This equipment, termed 'ANKO dust rig' hereafter, had been designed to fulfil the requirements in the following standards: i. BS EN 50281-2-1 *Methods for determining the minimum ignition temperatures of dust, Method A: Dust layer on a heated surface at a constant temperature*; ii. ASTM E2021 *Standard test method for hot-surface ignition temperature of dust layers*; iii. ISO/IEC 80079-20-2:2016 (replaced IEC 61241-2) *Electrical apparatus for use in the presence of combustible dust*,

Test methods: Methods for determining the minimum ignition temperatures of dust; iv. ISO/IEC 80079-20-2:2016 Explosive atmospheres. Material characteristics. Combustible dusts test methods

In this study, the BS EN50281-2-1 standard was followed closely. To meet this requirement of *'The apparatus shall be set up in a position free from draughts, and preferably under a hood capable of extracting smoke and fumes'* stated in the standard, the ANKO rig was placed under a fume hood (see **Figure 3. 21**) that managed to remove the sample pyrolysis or combustion products but not in a fume cupboard where unwanted gas was drawn at a much higher speed. From the study of Park about the effects of dust layer ignition temperature on hot surfaces with and without combustible additives, it had been proven that the strong air flow above the test bench drawn by fume hood changed the oxygen concentration inside a dust layer and subsequently altered the dust layer ignition temperature (Park, 2006). It is also important to note that the ANKO dust rig was designed for a maximum hot plate temperature of 400°C and that it was impossible to set a hot plate temperature above 400°C with considerable accuracy.

There were three major components working together in the ANKO rig T_{LIT} experiment – the laptop, the heating plate unit and the control & data acquisition block. The laptop was installed with the ANKO ReqTemp® software for recording temperature-time data; the heating plate laid on top of a stainless steel body with thermal protection was made of anodised aluminium with corrosion protection and electrical heater present below the plate (see **Figure 3. 22**) and finally the control & data acquisition block which a user controls input commands to the rig e.g. setting the hot plate temperature. There were three thermocouples (TCs), two Inconel shielded for sensing the heating plate temperature and one for detecting the dust layer temperature, all are of type-K which is best suited for application within -200-1250°C temperature range (OMEGA, 2016). There were two nuts (on opposite sides) for vertical level adjustment for the dust layer thermocouple, as shown in **Figure 3. 22**. This ANKO dust rig package came with some tools required by this dust layer T_{LIT} experiment; they are the dust layer thermocouples, metal rings, leveller, paintbrush, glass rod, 650 g stainless steel weight, stainless steel stand and a glass rod with type K thermocouple installed at one end. The dust layer thermocouples had a welded junction to be embedded in the centre of the dust layer during experiment and each and every dust layer thermocouple came with a calibration certificate, indicating the values to alter when a dust layer thermocouple was changed. There were three rings that came with the package with the following dimensions: 10 mm internal diameter with 5 mm height, 100 mm internal diameter with 12.5 mm height and 102 mm internal diameter with 12.5 mm height.

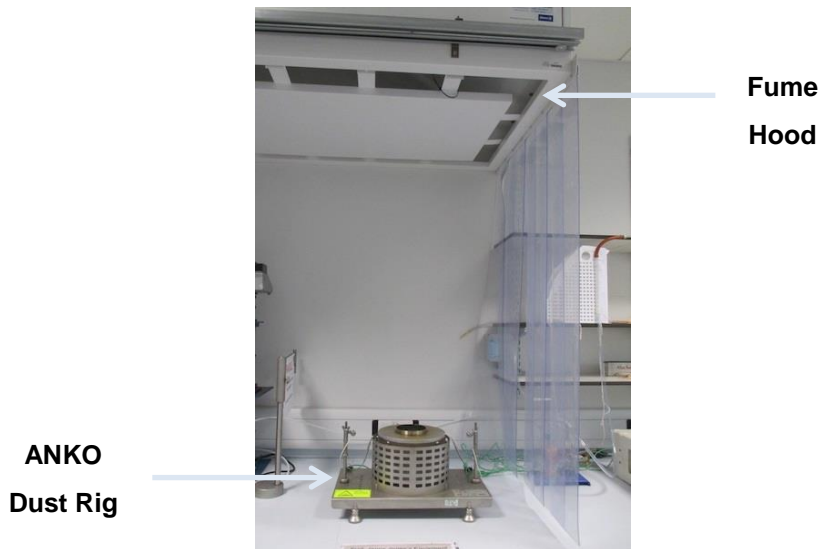


Figure 3.21 Placement of Dust Layer Ignition Rig

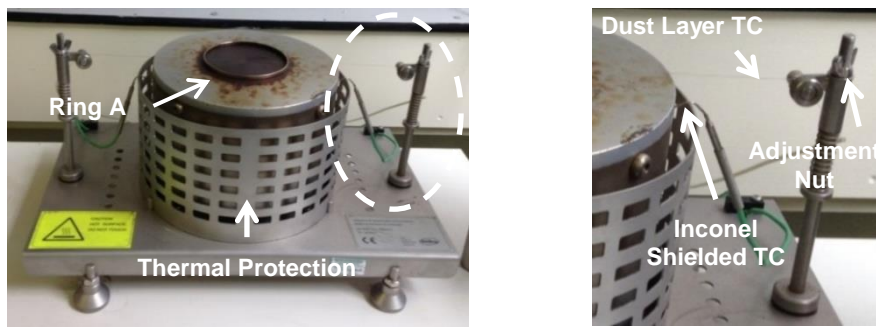


Figure 3.22 Dust Layer Test Rig Manufactured by ANKO, Dust Layer TC Vertical Level Adjustment Nut

Prior to starting any experiment, the temperature distribution of the heated plate was checked, since it had been stated in BS EN 50281-2-1:1999 that the maximum deviation from the set point temperature is 8 K. This was to ensure that no hot spot that would trigger an ignition at a particular area exist on the hot plate. For temperature distribution checking purpose, the setup recommended in the standard (see **Figure 3.23(a)**) was followed. One of the hot plate thermocouples was replaced with a fine thermocouple having its junction flattened and brazed to a disc of brass or copper foil. It was then placed at a specific point where the temperature was to be checked. A vertical glass rod with one end connected to a metal weight and the other to a thermocouple was placed within a guide tube. With the metal weight, constant contact pressure occurred between the thermocouple and the particular hot plate point which the temperature was to be measured. In this study, before determining the T_{LIT} for sample dust, 16 points on the hot plate was defined, as illustrated in **Figure 3.23(b)**. These 16 points selected included

locations where dust would and would not be deposited later. These temperatures were then compared with the temperature set at the hot plate. If temperatures from these 16 points deviated more than 8°C (i.e. 8 K) from the desired set point temperature, the dust layer thermocouple calibration was rechecked.

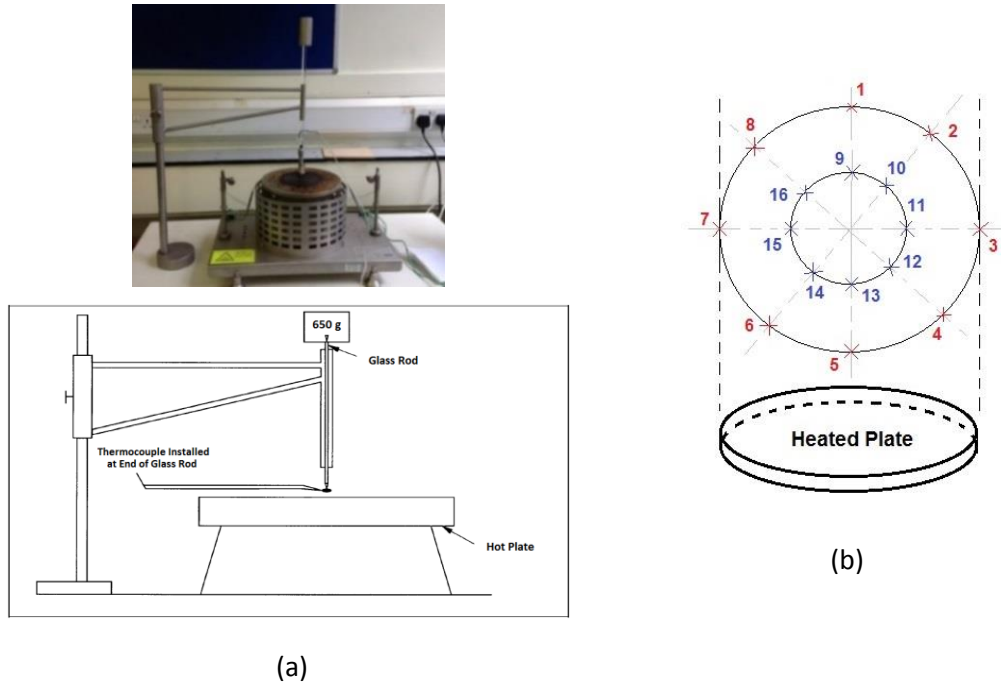


Figure 3.23 Temperature Distribution Check (a) Actual Setup & Schematic (b) Location of Points, Top View

The determination of T_{LIT} started with connecting the ANKO rig to the laptop and heating up the hot plate to the desired temperature; from ambient temperature of around 25°C , it usually took at least 30 minutes to heat the hot plate to $\sim 300^{\circ}\text{C}$ and longer time required for hot plate temperatures like 350°C or 370°C . The standard test proposed using the 100 mm internal diameter ring with 5 mm height as a start. As suggested by the standard, the dust layer thermocouple was slit through the two grooves (see **Figure 3.24**) drilled radially and opposite each other on the ring without touching the ring. By adjusting the nuts holding the thermocouple, the height of the dust layer thermocouple was fixed at $\sim 2\text{-}3$ mm above the hot plate, parallel to the hot surface but not touching the hot plate at all. The Ring with 10 mm internal diameter, 5 mm height and 12.5 mm height were called Ring A and Ring B respectively in this study. It is important to note that the layer diameter (D) to layer thickness (d) ratio, D/d was more than 5 (Joshi, 2012) in this study and thus the assumption of 1-Dimensional heat transfer (only in the direction of thickness i.e. axial direction) was valid. The D/d was 20 and 8 for Ring A and Ring B respectively and

therefore heat transfer was safely assumed to happen in the direction of dust thickness only and not radially across the dust layer diameter.

With the needed gadgets (see **Figure 3. 24**), after the hot plate temperature stabilised for 10 minutes at the desired set point temperature, pre-measured dust in the beaker was poured into the ring cavity. The amount of dust needed to fill the ring was estimated and was transferred to the beaker for ease of pouring into the ring on hotplate later. All events to take place within 2 minutes – the ring cavity filled with sample dust to the brim, dust layer levelled off with the metal leveller, excess dust outside the ring boundary removed, stop watch for timing started and software record button clicked start. To fulfil the requirements of BS 50281-2-1, during the placement of dust samples, the dust layer thermocouple was checked to ensure that the temperature change was less than $\pm 5K$ and within 5 minutes of dust placement, the original set point temperature was restored with an accuracy of $\pm 2K$. The ignition delay time was defined as the time once sample dust was loaded and levelled to the time when the first glow was observed, consistent with the method used by Dooley (2013).

Three temperatures from three different thermocouples were recorded, two for the hot plate and one for the dust sample. From now on, the changes on the dust layer, colour of smoke emitted etc. were observed. As stated in the standard, ignition is considered to have occurred if one of the three events happen:

- i) glowing or flaming seen in the material
- ii) the dust showed temperature of $450^{\circ}C$ or higher and
- iii) dust temperature rise $250^{\circ}C$ or more with respect to the hotplate temperature.

As recommended by the standard, the hotplate temperature was set in intervals of $10^{\circ}C$. When the dust ignited within 30 minutes, the next hot plate temperature was set $10^{\circ}C$ lower and the same ignition rule applied for a 30- minute observation. The same was repeated until a set point temperature that failed to show any sign of ignition. At that temperature, two confirmation tests were carried out to ensure that the dust was definitely not igniting at the lower temperature. Whenever the dust layer did not ignite at the particular hot plate set point temperature, the sample was left for a minimum 30 minutes on the heated plate as specified in the standard. Dust at this non-igniting temperature could be left for a much longer duration (around 2-3 hours) as a means to comply with BS 50281-2-1 that requires a long enough duration to check that the dust layer temperature has decreased to a steady value lower than the temperature of the heated surface (British Standard, 1999b). As a safety measure, a bucket filled with water

was on standby next to the rig to extinguish the dust on fire should ignition happen or to quench the hot but non-igniting dust if ignition did not happen. It should be noted that fresh biomass dust was used for every test, regardless of whether ignition happened or not.



Figure 3. 24 Tools Used in Dust Layer Experiment – Measuring Beaker, Ring A, Ring B, Tong, Dust Collector and Leveller; Slots for Dust Layer TC

It is possible to estimate the T_{LIT} of other dust thicknesses from a set of T_{LIT} results experimented on known thicknesses of a particular species. This is achieved by plotting the logarithm of the dust thickness as a function of inverse T_{LIT} in absolute temperature scale (British Standard, 1999b) and assuming a linear relationship between the two parameters, linear interpolation or extrapolation could be used to determine the desired, unknown T_{LIT} . Anyway, the standard recommends to conduct tests with the required thickness for better accuracy.

3.1.5 Biomass Blends Dust Layer Ignition

In this study, the effect of having different biomass within a layer was considered as well. This was inline with the industrial situation where the dust accumulation at various places in the power station for instance may consist of blends of several materials. As a start, only binary blends were considered, in two different weight percent ratios, 90:10 woody:herbaceous and 50:50 woody:herbaceous biomass dusts. To get the blends as well-mixed or homogeneous as possible, equal weights of each blend constituent was weighed **Figure 3. 25(a)**, poured to and mixed manually in a sieve shaker collector, after which the pre-mixed blend was subjected to high frequency shaking by the sieve shaker (see **Figure 3. 25(b)**) operating at 60-70 Hz for a duration for ~30 minutes.

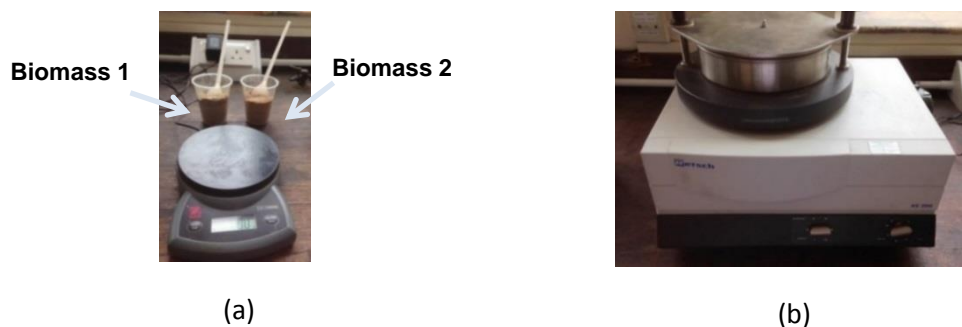


Figure 3. 25 Blending of Two Biomass Dust Species (a) Weighing Blend Constituent
(b) Blending with Sieve Shaker

This blending method was applied too when a binding material was added to the parent materials. Following suggestion from the industry where a maximum of 2wt% binder were allowed in a biomass briquette or pellet; every 100 g of final biomass dust contained 2g organic binder (either lingo-bond-DD powder or cornflour) at most. Therefore, 2 wt% binder were added and stirred manually to a parent biomass material held by the sieve shaker collector and later the blend was shaken by the Retsch AS 200 sieve shaker at high frequency and a 30-minute duration, aiming for efficient mixing that resulted in blends as homogeneous as possible.

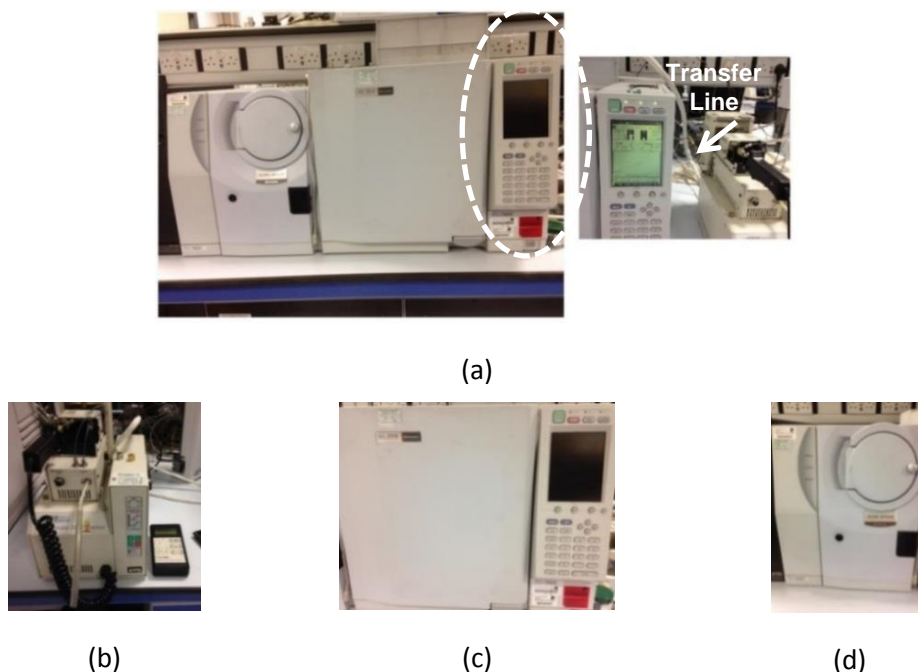


Figure 3. 26 py-GC-MS Analysis Components (a) All in One (b) CDS Pyroprobe 5000 Series (c) Shimadzu GC-2010 Gas Chromatograph (d) Shimadzu GCMS-QP2010 Gas Chromatograph Mass Spectrometer

Besides examining if this little bit of binder material added to a parent biomass would affect the overall dust T_{LIT} , the components that made up both binders were analysed via Pyrolysis-Gas Chromatography-Mass Spectroscopy (py-GC-MS).

As the name suggests, the py-GC-MS consists of three major parts – pyrolyser (py), gas chromatographer (GC) and mass spectrometer (MS) and in this study, specifically they were CDS Pyroprobe 5000 Series, Shimadzu GC-2010 Gas Chromatograph and Shimadzu GCMS-QP2010 Gas Chromatograph Mass Spectrometer (see **Figure 3. 26**). To identify the components in a material, the sample was first pyrolysed in the pyrolyser, then the products injected to and separated on the GC column and finally species abundance in the smaller broken molecule fragments was measured and detected by the mass spectrometer from signal intensities and matching the time each species eluted from GC to a standard database.

Binder samples were prepared carefully prior entering CDS pyroprobe. Small pieces of rolled quartz wool, CDS fire-polished quartz tube of 25 mm length and 2 mm internal diameter (id) and tweezers were all heated with a Bunsen burner as a means to remove any pre-analysis contaminants. The first piece of rolled quartz wool was inserted towards one end of the CDS tube and the weight of them (CDS tube + quartz wool1) was noted. A small amount of sample ~2mg was then carefully scooped into the CDS tube and their weight (CDS tube + quartz wool1 + sample) was taken. Another rolled quartz wool was then plugged into the other end of the tube, having the sample in the middle of the tube, sandwiched by two quartz wool plugs. This weight of four components – CDS tube, quartz wool 1, sample and quartz wool2 was recorded as pre-pyGCMS weight. The prepared and weighed CDS tubes were stored in a desiccator to prevent any contamination before analysis and was held by a CDS sample tube holder soon before entering the pyroprobe.

The pyroprobe served to thermally degrade a sample (two different binder materials in this study) with relatively large, complex molecules into smaller fragments or components. In the CDS Pyroprobe 5000 series, it comes with a platinum filament configured as a coil and was designed to hold samples in reusable quartz tubes (CDS, 2011) that were applied in this study. This advanced pyroprobe had programmable pyrolysis time that ranged from as short as 0.01 second to as long as 999.99 minutes and 4 minutes in total were used in this study. Prior to pyrolysing a sample, CSI 6000 Solid State Flowmeter was used to check that carrier gas helium was purged at ~20 ml/min to remove any oxygen from the sample and CDS pyroprobe method was programmed to heat a sample from an initial temperature to a desired pyrolysis temperature at heating rate of 20°C/ms and held at the desired temperature for a certain duration (4 min). The pyrolysis temperature was fixed at 500-600°C for the two binders in this study, as this temperature range was commonly used for py-GC-MS analysis of biomass (Biller and Ross, 2014; Atiku, 2015; Atiku

et al., 2016). With the CDS pyrolyser operating in adsorbent mode, the sample portion that had been pyrolysed at the set temperature were trapped on Tenax® TA adsorbent trap after which it was desorbed onto a the GC column via heated transfer line connecting the py to the GC. With the unique interfacing design of CDS Pyroprobe (CDS, 2011), pyrolysates were directed to be immediately picked up by the GC inlet for further processing.

In this study, a minute before pyrolysis ended, Shimadzu GC-2010 was made to start running for 67 minutes, in which the GC was set to adopt the temperature programme of 40°C with holding time of 2 minutes then ramping to 280°C at a rate of 6°C/minute with static time of 25 minutes; the column head pressure was 2 bar at 40°C. The pyrolysates were separated on 60 m Rtx 1701 capillary column with 0.25 mm id and 0.25 µm film thickness, for which this fused-silica capillary column was designed for high-sensitivity microanalysis with minimal bleeding (SHIMADZU, 2008). The tube was removed from pyroprobe 5 minutes after completion of GC run and was weighed. The weight of the experimented CDS tube, quartz wool1, sample and quartz wool2 was recorded as post-pyGCMS weight and to obtain the amount of sample pyrolysed, the post-pyGCMS weight was deducted from pre-pyGCMS weight.

Mass spectrometer with ion source set to 230°C with scanning frequency of once per second resulted in molecular ion separation which created a spectrum for qualitative and quantitative analysis. Components of a pyrolysate were identified following the method used by Atiku (2015); (Biller and Ross, 2014; Fitzpatrick et al., 2009), in which chromatogram with retention time (RT) on the x-axis and intensity on the y-axis was plotted and the peaks identified based on the NIST Mass Spectral Library database and from previous literature.

Contained within Ring A, the pyrolysed extent of the 5-mm thick biomass dust with binder that had undergone the dust layer experiment were examined. The pyrolysed extent was judged by comparing the moisture and volatile matter contents of the picked dust determined via TGA slow pyrolysis simulation in the TA Q5000 equipment. The experimented dust samples were chosen from two experimental runs, listed as follows:

- i. ignited dust when hot plate was at T_{LIT}
- ii. 10°C below the T_{LIT}

Since 5 mm was quite thin a layer, for dust experimented at hot plate temperatures below the T_{LIT} (case (ii) on the list above), only dust from two locations representing two extremes were picked for this pyrolysed extent study – the dust at layer

surface most exposed to ambient air and the dust closest to the hot plate (see **Figure 3. 27(a)**). The dusts scooped from the two locations were termed 'Top Dust' (for the most exposed to ambient air) and 'Bottom Dust' (for the closest to hot plate) respectively hereafter. From the TGA slow pyrolysis profile, the moisture content was determined from sample weight loss when it was heated to 105°C whereas the volatile matters content were taken after 105°C to 550°C.

For the case when hot plate temperature was at T_{LIT} (case (i)), experimented dust was scooped from the ignited region and nearby area once a glow on the dust layer was observed and the ignition delay time had been noted. Picking of dust from the hot plate at temperatures lower than T_{LIT} (case (ii)) was done carefully without disturbing much the original dust placement within the ring. A micro spatula with a spoon end and a flat end (see **Figure 3. 27(b)**) was used – spoon end for Top Dust and flat end for Bottom Dust.

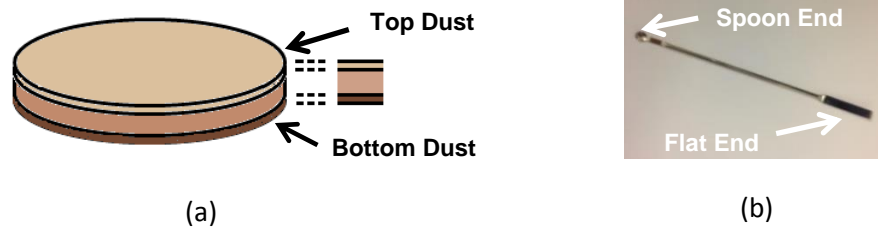


Figure 3. 27 Experimented Dust in Ring A (a) Location for Dust Scooping (b) Spatula for Dust Picking

3.1.6 Estimating Reaction Kinetics and Predicting Ignition Time for Biomass Dust Layer Ignition

The reaction kinetics for four single-material biomass samples and six of their biomass blends at two different weight ratios were considered in this section. The ten samples considered are Miscanthus(1), Miscanthus(2), Pine, Wheat straw, PM(1)9010, PM(1)5050, PM(2)9010, PM(2)5050, PWS9010 and PWS5050. To estimate the kinetic parameters of various biomass dust layers that were experimented on the ANKO hotplate, the following approach was formulated.

As described in **Chapter 2**, three temperatures, T_p , T_s and T_a were required from each experiment to enable one dimensional heat transfer calculation of a biomass dust layer (see **Figure 3. 28**). T_p was the hot plate temperature set at the ANKO dust rig when determining the minimum dust layer ignition temperature (T_{LIT}) of each biomass sample with different thicknesses, $2r$, in which r was the characteristic length of dust layer (Drysdale, 2011; Park et al., 2009; Joshi, 2012; El-Sayed and Mostafa, 2016). The r values for Ring A (5 mm thick) and Ring B (12.5 mm thick) were 0.0025 m and 0.00625m

respectively. T_s was the dust layer top surface temperature for each biomass at different T_p values and was measured with a portable infrared thermometer (see **Figure 3. 29**). The ambient temperature, T_a , was measured with a commercial office desk thermometer (see **Figure 3. 30**), where the portable desk thermometer was brought into the lab and the readings were noted around every half-hourly and the average was used in heat transfer calculation. **Figure 3. 28** shows the biomass dust layer and the appropriate boundary conditions in the heat transfer calculation follows.

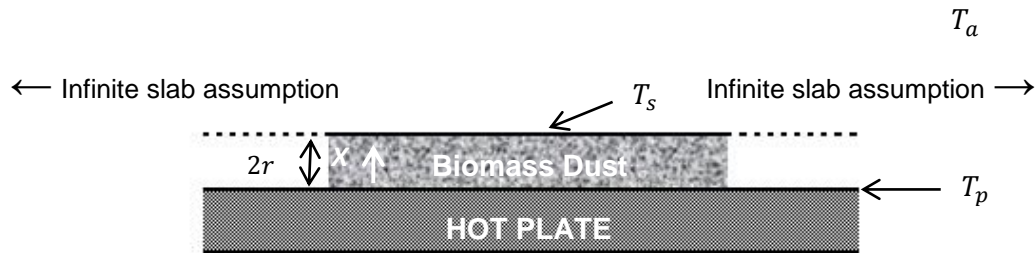


Figure 3. 28 Biomass Dust Layer Deposited on a Hot Plate – Infinite Slab of Given Thickness ($2r$) Assumption



Figure 3. 29 Infrared Thermometer Used in Experiment

Figure 3. 30 A Desk Thermometer

The Boundary conditions:

$$T = T_p \quad \text{at} \quad x = 0$$

$$-\lambda \frac{dT}{dx} = h_t (T_s - T_a) \quad \text{at} \quad x = 2r$$

For the heat transfer properties needed in the 1D steady-state heat transfer calculation of each biomass dust layer, thermal properties of air were well established and easily obtained. Since the experiment procedure adhered closely to BS 50281-2-1 which required placement of the ANKO hotplate in an environment free from draughts, the quiescent environment with air velocity of ~ 0.01 m/s had thus led to natural convection. The rising of less dense warm air near from biomass dust layer closest to the hot plate was replaced by denser cool ambient air and this buoyancy-driven air flow that drives the free

convection enabled calculation of Rayleigh number (Ra) in determining the convective heat transfer coefficient, h_c . The ν , α , λ_a required in Ra calculation were easily obtained from published literatures or handbooks. As for radiative heat transfer, it is well known that any object >0 K emits radiation and this much hotter than ambient biomass dust layer is no exemption. The emissivity, ε , of biomass was taken to be 0.9 after considering various data published for several vegetation and biomass and noting the fact that dependence of ε value on temperature could be ignored in most practical application (Cengel and Boles, 2008). The value for various important inputs and properties of each biomass dust sample used in computation are summarised in **Appendix B**.

The effective biomass thermal conductivity value, λ , used in heat transfer calculation in this study was obtained from a rig assembled by fellow research and the results have been validated and published (Mason et al., 2016). It is important to note that these biomass thermal conductivities are assumed to be dependent on respective biomass density but not its temperature in this study. The density, ρ , of each different biomass sample experimented in different rings were calculated by dividing the weight of biomass dust needed to fill the ring by the volume of the ring that resembled a cylinder. Calculation of biomass dust density in different rings fell within the range of ~ 164 - 241 kg/m^3 . Based on this density range, the chart (see **Figure 3. 31**) showing density between 0- 1500 kg/m^3 was selected for developing correlation for different biomass species. For Miscanthus(1) and Miscanthus(2) samples in this study, a correlation between density and miscanthus thermal conductivity data points (the hollow triangles in **Figure 3. 31**) was found to be $\lambda_{miscanthus} = 0.00009\rho_{miscanthus} + 0.042$. The same was performed on wheat straw using the straw data points (solid triangles in **Figure 3. 31**) and the correlation of $\lambda_{wheatstraw} = 0.0001\rho_{wheatstraw} + 0.0241$ was achieved. Thermal conductivity of pine and the six blends used the correlation developed for wood i.e. $\lambda_{wood} = 0.00013\rho_{wood} + 0.037$ (Mason et al., 2016) since pine is a kind of wood and the blends have at least half their compositions as pine.

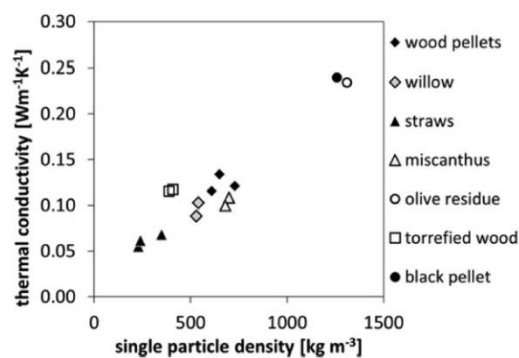


Figure 3. 31 Biomass Thermal Conductivity [Source: Mason et al. (2016)]

With all these needed thermal properties, three modes of heat transfer – heat conduction, convection and radiation were evaluated for the biomass dust layer heated on a hot surface.

Upon obtaining all ambient conditions which the experiments were conducted and all required thermal properties of surroundings and test samples, the reaction kinetics of each was then estimated systematically.

Prior to plotting the logarithmic relationship as shown in **Equation 2.13** for determining the reaction activation energy (E) from the slope of equation $\left(\frac{E}{R}\right)$, the critical heat generation rate, δ_c , was determined from **Equation 2.6**. Calculation of total effective heat transfer coefficient, h_t (which consisted of convective heat transfer coefficient, h_c , and radiative heat transfer coefficient, h_r) was required to compute a Bi value for a particular biomass ignition case. Ignition happened at different T_p values for different samples and varied when layer thickness varied; all these resulted in a range of T_s values and therefore, dissimilar heat transfer interaction between ambient air and the heated biomass were expected for each different biomass with different thicknesses. With this, δ_c was expected to be different for each biomass case, consistent with the claim by Babrauskas (2003a) that a different δ_c would be obtained for each experimental point at different hot plate temperature (T_p) of the hotplate ignition test.

Taking the example of 5 mm-thick Miscanthus(1) that ignited at $T_p = 305^\circ\text{C}$ (578 K) when contained in Ring A with $2r$ of 0.005 m, the average ambient temperature (T_a) was found to be 20°C (~ 293 K) and the measured top surface temperature (T_s) was 225C (~ 498 K). The Rayleigh number (Ra) was found with **Equation 2.12** to be 3.638×10^6 with kinematic viscosity, ν , and thermal diffusivity, α , of air evaluated at film temperature of 122.5°C (395.5 K) and characteristic length, L , of 0.0886 m. Convective heat transfer coefficient, h_c , was found to be $\sim 8.903 \text{ W/m}^2 \cdot \text{K}$ using **Equation 2.10** whereas the radiative heat transfer coefficient, h_r , was $\sim 13.476 \text{ W/m}^2 \cdot \text{K}$ as calculated with **Equation 2.11**. Biot number, Bi , was calculated as ~ 0.932 with **Equation 2.7** with thermal conductivity, λ , of Miscanthus(1) estimated to be $0.06 \text{ W/m} \cdot \text{K}$. The dimensionless ambient temperature, θ_a , was fixed within these boundary values of -8 and -18 following the studies of Thomas and Bowes (1961) and Bowes and Townshend (1962). With both Bi and θ_a known, the corresponding δ_c value was calculated using **Equation 2.6**. From the found Bi and δ_c combination, a data point (x, y) of $\left(\left(1/T_p\right), \ln\left(\frac{\delta_c T_p^2}{r^2}\right)\right)$ for **Equation 2.13** was obtained. The same procedure was repeated for Ring B that had thickness $2r$ of 0.0125.

A straight line was then plotted with the data points resulted from Ring A and Ring B and its gradient allowed the activation energy, E , to be obtained easily since gas constant R was a known value. With the values of T_a and T_p remain, the just found E value

was then substituted to **Equation 2.9** and an updated θ_a value was found. Coupled with the Bi found earlier, a new updated δ_c was calculated with **Equation 2.6**. The data point $\left((1/T_p), \ln\left(\frac{\delta_c T_p^2}{r^2}\right) \right)$ had now become different from the previous one since δ_c had changed and a new and updated **Equation 2.13** was plotted with new δ_c values found for each layer thickness involved. From the updated **Equation 2.13**, a new value for activation energy was then calculated. Iterations in this way was performed until convergence was achieved, that was when δ_c values from the final two iterations were found differ not more than 1% from each other.

The activation energy found with plotting points that involved the last δ_c value was assumed to be the final estimate of the reaction activation energy. The activation energy values estimated in this study were applicable to the ten biomass materials, dust thicknesses used in the specific surroundings where experimental data were obtained from. Should the experimental environment alter, different set of values would be obtained when the same estimation procedures were applied.

As for the ignition delay time estimation, it was rather challenging to model a delay time that suits practical applications since ignition was contributed by external factors e.g. environment apart from inherent internal properties of a biomass. The ignition delay time for biomass dust layers heated on hot surfaces depends on many factors, e.g. sample particle size, chemical properties of sample, temperature of surroundings, ambient air velocity; thus the ignition delay time predicted in this work was valid for the biomass species, experimental condition which the samples were tested and following the ignition criterion as defined in BS 50281-2-1 (British Standard, 1999b). As in some previous works by El-Sayed and Khass (2013) and El-Sayed and Abdel-Latif (2000) where a first order relation of time-to-ignition with dust thickness and a second order polynomial correlating the time-to-ignition and hot surface temperature were reported, the same were performed in this study on four single-material biomass samples i.e. Miscanthus(1), Miscanthus(2), Pine and Wheat Straw and six of their binary blends, i.e. PM(1)9010, PM(1)5050, PM(2)9010, PM(2)5050, PWS9010 and PWS5050.

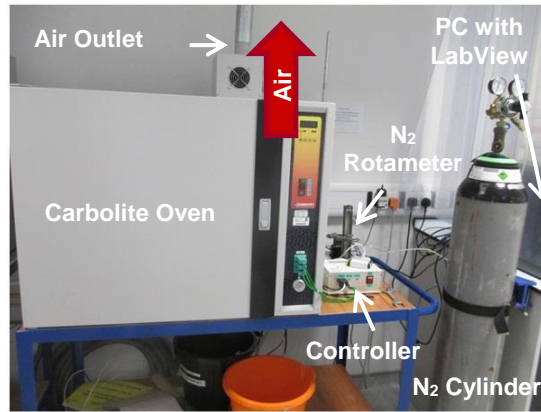
3.1.7 Biomass Storage Ignition

Besides looking at fire risk due to biomass dust accumulated at various locations during the fuel handling stage, another potential fire risk originates from biomass heaps or piles during storage. Since it is of interest to compare the self-ignition or critical ignition temperatures of biomass pellet and the dust disintegrated from the compacted pellets, biomass pellets commonly stored and used as fuel in a U.K. power station were chosen – white wood pellets. White wood pellets (denoted as WWP hereafter) used in this study had been pelleted and shipped from North America. The few kilograms of WWP received

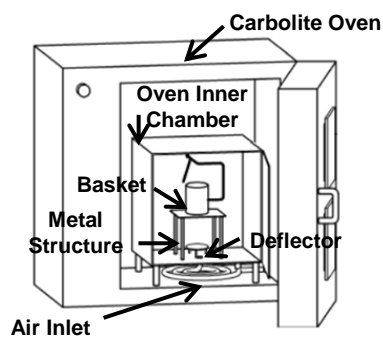
consisted of some foreign, non WWP materials and therefore, sieving was done before using the WWP in self-ignition analysis. After some obvious non-WWP, materials were manually removed, the rest of the as-received WWP was sieved with a 2.8 mm sieve. The <2.8 mm portion was mostly disintegrated pellets and this was disregarded whereas the >2.8 mm was the portion to be used in this study.

The hot storage basket test (HSBT) that was conducted here focused on biomass self-ignition characteristics during storage and adhered to the BS 15188 (British Standard, 2008). Mainly, the techniques revolves around obtaining the self-ignition temperature (T_{SI}), and ignition delay time (t_i) of differently-sized bulk volumes of samples in isoperibol (approximately isothermal) hot storage and the main procedures are summarised as follows. The portion of WWP sample > 2.8 mm were further segregated into two portions of equal weights, one portion was retained as pellets and the other subjected to milling and sieving, as described in **Section 3.1.1**. The dust size in <180 μm range was chosen for consistency purpose since this was the size used in dust layer test

Following the guidelines in BS 15188 (British Standard, 2008), a commercial oven (Carbolite) that fulfilled the requirements was chosen. This had a controllable temperature range of 35 to 300°C and was stabilise to within $\pm 1\%$ as air flows through it. The oven has an air inlet opening of ~ 8 mm diameter in the lower section and an air outlet opening of ~ 10 mm diameter in the upper section that allowed a prescribed fresh air flow through the chamber and leaves the oven with all gaseous combustion products in the event of a combustion reaction. An important assumption here was that the dimensionless parameter, Biot number (hL/k) where h is convective heat transfer coefficient, L is characteristic length and k is thermal conductivity (Incropera and DeWitt, 2002) in each HSBT experiment was sufficiently high such that the sample surface temperature was deemed equal to the hot storage temperature that the sample was subjected to. Within this oven that has useful volume of ~ 120 litres as recommended by BS 15188, a custom made inner chamber that housed thermocouples had been installed. The overall experimental setup with the main parts used in this hot storage study are shown in **Figure 3. 32**. The setup was connected to a computer with a LabView programme that had been coded to record all temperature data, turn the oven on/off and trigger nitrogen purge for cooling in cases when temperature of the ignited sample exceeds the acceptable hot storage-sample temperature difference. Ignition was defined in BS 15188 as when the temperature at the centre of the sample exceeds at least 60 K i.e. 60°C above the hot storage temperature (British Standard, 2008).



(a)



(b)



(c)

Figure 3. 32 Hot Storage Basket Tests (a) Experiment Setup and with Major Components (b) Oven Schematic with Inner Chamber and Parts [Edited from: British Standard (2008)] (c) Actual Inner Chamber Used

Prior to any tests, samples in either pellet and or powder forms were dried to constant weight at 50°C in a drying chamber before the hot storage basket test was conducted on these samples, as required by BS 15188 (British Standard, 2008). For the baskets, three cylindrical baskets with height to diameter ratio of 1 were custom made instead of cubic baskets.

Three baskets were fabricated to fulfil the suggestion in the standard which specified that at least three different-volume mesh wire baskets were to be used to allow assessment of self-ignition behaviour of dust accumulations of sizes larger than laboratory-scale. These three baskets were open-top, closed-bottom and the narrow-meshed wire net that wrapped around the sides were carefully selected such that the wire mesh prevented samples from falling through but not hindered oxygen in the oven air from diffusing into the dust sample. Following recommendations in the standard which state that the smallest volume should be in order of 10 cm³ and the basket that followed within the series should exceed the previous by at least a factor of 2, the three baskets used here had volumes of

~11 cm³, ~67 cm³ and ~864 cm³ and were denoted as Basket S, Basket M and Basket L indicating smallest, medium and largest basket respectively (see **Figure 3. 33**). Basket L sitting on the metal structure with three thermocouples within the oven inner chamber are shown in **Figure 3. 34**.

Three thermocouples were used in this experiment, two of them were used to measure the hot storage temperature and one for sample temperature. All were sheathed and have external diameter of 1 mm, as recommended in BS 15188 (British Standard, 2008). The two hot storage thermocouples (termed TC1 and TC2 henceforth) were freely installed in the air space within the oven inner chamber, horizontally, adjusted to half the distance between the chamber wall and dust sample surface; whereas the sample thermocouple (denoted as TCsp hereafter) was adjusted inside the sample basket, such that it measures the temperature right at the centre of the basket filled with sample material later, i.e. TCsp hot junction positioned in the centre of a dust sample. In this study, as far as possible, the vertical distance of the three thermocouples were adjusted to the same level in every experiment (indicated by dashed line in **Figure 3. 35**, which shows the distance measured from the metal structure to the thermocouple tip) to reduce inaccuracies or temperature discrepancies due to differences in elevation. The vertical distance however, depended on the basket size; Basket S had elevation of three TCs closest to the metal structure, Basket M slightly higher whereas Basket L a lot higher due to its height that showed a centre position higher than the other two.



Figure 3. 33 Three Custom Made Baskets for HSBT – Basket S, Basket M & Basket L (L to R)



Figure 3. 34 Three Thermocouples and Basket L Placed on Metal Structure

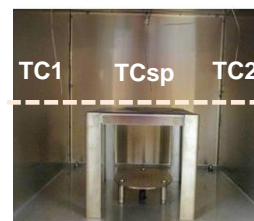


Figure 3. 35 Placement of Three Thermocouples

For every HSBT experiment using any sample, prior to heating up the oven to a desired test temperature, the positions of all three thermocouples were adjusted such that TCsp would be in the middle of the basket (which would be filled to the brim with sample later) and TC1 & TC2 halfway between the inner chamber wall and the basket outer boundary. The lengths of these thermocouples were also adjusted (by bending if

necessary) such that all were at the same elevation. It should be noted that there were some discrepancies between the temperature set on Carbolite oven and the temperatures detected by TC1 and TC2. The average of TC1 and TC2 readings were taken as the hot storage temperature since they were located in the same oven inner chamber as the sample and, i.e. this average temperature resembled more to the hot environment which biomass fuel was subjected to. The Carbolite oven temperature was adjusted such that the hot storage temperature as read by TC1 and TC2 achieved the desired test temperature.

The temperatures sensed by all three thermocouples were shown in the LabView programme and both temperatures from TC1 and TC2 were monitored closely to help decide when to click-start the experiment. While waiting for TC1 and TC2 to reach the desired set point, wire-mesh baskets were filled up with sample that had been conditioned according to BS 15188. Be it pelleted or pulverised, while filling, the basket was tapped a few times and any surplus was removed from the upper margin. The weight of sample was taken just before entering the hot oven that had reached the desired temperature set point. It is important to note that only fresh sample was used in every experiment and weight taking was essential because any subsequent repeats aimed to achieve a similar weight. This was to ensure that the sample density contained in each of Basket S, Basket M and Basket L could be as close as possible to each other. Sample-filled Basket S was always used as the starting point of the HSBT experiments since it consumed the least material among the three baskets. Always, the first estimated oven temperature and hot storage temperature were set purely by guessing based on previous data.

When the temperatures of TC1 and TC2 had reached the desired hot storage set point, the deviation between the two was checked to ensure the difference was small and that the condition remained stable for at least 10 minutes. After these checks, the temperature recording function of the computer controlled LabView programme was initiated. The weighed, sample-filled basket was then rapidly transferred into the hot oven inner chamber and the pre-adjusted sample thermocouple was inserted into the centre of the sample contained in the basket (this process took <1 minute). After closing the inner chamber and oven doors as quickly as possible, the temperature readings displayed on LabView programme were monitored to ensure that the sample was really heating up. All the three temperatures were recorded throughout the experiment.

In this study, taking into consideration the uncertainties due to the accuracy of the thermocouples, ignition was taken at 65°C above the average of TC1 and TC2 temperatures instead of the 60 K (i.e. 60°C) recommended by BS 15188 (British Standard, 2008). Once TCsp reached a minimum of 65°C above average of TC1 and TC2, the sample temperature increased exponentially and at this instant, to prevent undesired fire outbreak, nitrogen started purging for a certain duration to cool the ignited sample and quench the reactions following the LabView codes. In another extreme when ignition did not happen, the

sample was left overnight in the oven at the prescribed hot storage temperature and monitored remotely. It was important to monitor for a longer period of time since ignition could happen later if the material possesses great heat capacity and showed a much longer ignition delay time, t_i .

According to BS 15188 (British Standard, 2008), in deciding the final critical self-igniting temperature, T_{SI} , of a sample, there were two options – 5 K or 2 K between the temperature that just caused material ignition (ϑ_c in **Chapter 2**) and the temperature that just failed to (ϑ_B in **Chapter 2**). In either option, the T_{SI} obtained was rounded down to the nearest degree and the latter option was used when extrapolation was intended to predict results of much larger storage volume. With a margin of 2 K, the T_{SI} estimation was deemed to be more accurate when scaled-up to massive storage.

Towards the end of each test, whether ignition happened or did not, the storage temperature as sensed by TC1 and TC2 was ensured to be $<40^\circ\text{C}$ before removing the tested sample from the oven inner chamber. This was a safety measure to ensure re-ignition would not happen on the sample. Also, weight of the experimented sample that had cooled to $<40^\circ\text{C}$ in the oven was taken. The three temperatures recorded were later plotted and analyses were conducted on the temperature-time profiles. The laboratory scale results were later extrapolated to industrial size where the storage volume was much larger.

The ignition delay time, t_i , were defined by two important points of time. First, the time when TCsp broke even with the average of TC1 and TC2, i.e. when sample temperature reached the hot storage temperature. Second, the time when TCsp exceeded the average of TC1 and TC2 by 65°C , i.e. when ignition occurred as defined in this study. A stop watch was clicked start at the instant when TCsp was seen reaching the hot storage temperature (average of TC1 and TC2) and set running and finally clicked stop when the TCsp exceeded the hot storage temperature by 65°C (indicated by the start of nitrogen purging). This was a rough estimate by visualising the temperature readings displayed on the LabView screen and served as a reference when the actual t_i was later determined from the temperature recorded as a function of time. The temperature recorded by LabView had been programmed to have a frequency of one temperature record in every five seconds. From these temperature-time record, the exact time when TCsp reached the same as hot storage temperature (average of TC1 and TC2) to the time exactly when TCsp surpassed the hot storage temperature by 65°C were taken as ignition delay time. This t_i was counter checked with the rough estimate obtained from the stop watch.

Upon obtaining critical ignition temperature (T_{SI}) and ignition delay time (t_i) required to describe self-ignition characteristics of the samples, two analysis method recommended in BS 15188 were followed. The first method of scaling up from experimental data was more straightforward than the second method that applied the

thermal explosion theory. The slightly more sophisticated method used thermal explosion theory developed by Frank-Kamenetzki. These two methods were known as 'Scaling Up method' and 'F-K method' henceforth.

In the Scaling Up method, the T_{SI} and t_i values from HSBTs of the three baskets experimented were plotted on log(characteristic length) vs inverse of absolute self-ignition temperature (in unit of Kelvin) and log(characteristic length) vs log(ignition delay time, in unit of hour) graphs respectively. The T_{SI} and t_i for other storage volumes involved interpolation or mostly extrapolation of the correlations obtained from the HSBTs of the three baskets.

As for the F-K method, lengthier calculations were involved since knowledge of bulk density, calorific value and heat conductivity value of the sample were required besides deciding on a suitable critical F-K parameter to be used. Since the sample basket used in this study was fabricated with diameter to height ratio of one, the critical F-K parameter (δ_{cr}) recommended by BS 15188 (British Standard, 2008) was 2.76. The self-ignition properties could then be estimated from the correlation obtained by plotting natural logarithm of $\left(\delta_{cr} \frac{T_{SI}^2}{r^2}\right)$ vs inverse absolute self-ignition temperature $\left(\frac{1}{T_{SI}}\right)$.

The bulk density of each sample were determined by dividing the net sample weight contained in each basket by corresponding cylinder volume. The gross calorific value were obtained the same way as other biomass samples in this research, i.e. calculated from a correlation by Friedl et al. (2005) that had been validated with bomb calorimetry results in this research. The thermal conductivity (λ) on the other hand, was determined the same way as described in **Section 3.1.6**, which the λ of each sample depended on its density. Application of the 'Scaling Up method' and 'F-K method' were described further in **Chapter 10** with the two WWP samples used in this study.

Besides this hot storage basket test, just like other biomass samples, WWP used in this HSBT study underwent material characterisation and self-ignition risk ranking. Preparation for these analyses followed the methods outlined previously.

3.2 Biomass Pre-treatment

3.2.1 Washing of Biomass

In the many studies of biomass washing, most have used deionised water, distilled water or even tap water as the washing agent. Simple water washing with distilled water at room temperature was selected in this study such that possible biomass composition changes due to elevated temperatures were minimised. Furthermore, it was proven by Jenkins et al. (1998a) that simple water washing leached alkali metals and chlorine from biomass and

improved dramatically the ash fusion temperature. In this study, distilled water washing was conducted on biomass samples from two categories – herbaceous miscanthus pellets and woody pine chips. It should be noted that the miscanthus pellets were from a different supply batch from those reported in **Chapter 4**, whereas the pine chips originated from a different batch as those used in **Chapter 7**.

In this study distilled water washing of biomass, the proximate analysis, reaction rate kinetics, self-ignition risk ranking, ultimate analysis, higher heating value, dust layer minimum ignition temperature (T_{LIT}) and ignition delay time determinations of untreated and pre-treated (by washing) are similar to the procedures described in **Section 3.1**. The apparent first-order reaction rate kinetics were calculated from derivative thermogravimetric analysis (DTG) profile to obtain the activation energy (E_a) and the temperature of maximum weight loss (T_{MWL}). This enabled the ranking of self-ignition risk following the method modified by Jones et al. (2015). Like before, the ignition delay time and dust layer minimum ignition temperature (T_{LIT}) were determined following BS EN 50281-2-1:1999 (British Standard, 1999b) and the T_{LIT} was used to obtain the maximum permissible surface temperature (British Standard, 1999a) of a plant. The details of biomass washing and the analyses after washing are described in the following sections.

3.2.1.1 Lab Scale Biomass Water Washing Procedure

In this study, both biomass samples were washed with distilled water at room temperature. The solvent agitation method was used where the three-hotplate Stuart SB162-3 Electrical stirrer was used. A comparison study on leachate characteristics of water-leached biomass by batch and semi-continuous operations had used the magnetic stirring method (Liaw and Wu, 2013).

Without turning the heater on, beakers of 600-800 ml were placed on each of the hotplate. The amount of distilled water depended on the weight of biomass contained in each beaker, in which the biomass to distilled water ratio was fixed at 1:5, i.e. every 1 g biomass was washed by 5 ml of distilled water. Magnetic stirring bars were then added into the beakers with distilled water and biomass and as agitation (at 500 rpm) started in each beaker, the timer was started too. Since the washing duration was fixed at 60 minutes, the electrical power was switched off immediately when the 60-minute was up. The setup of this simple washing is illustrated in **Figure 3. 36** where miscanthus was washed in three separate beakers. The same procedures applied to pine washing.



Figure 3. 36 Distilled Water Washing of Miscanthus Samples at Room Temperature and 500 rpm Stirring Speed

After the 60-minute wash, the wet biomass in each beaker was drained with a strainer, and the solid washed biomass and liquid leachate were separated. The filtering process was conducted with a Buchner funnel and 150 mm diameter Fisherbrand QT260 filter paper were used for fast flow rate as shown in **Figure 3. 37**. The wet solid biomass were then dried as described in **Section 3.1** and the liquid leachate was collected in a 250 ml bottle and stored in the fridge (see **Figure 3. 37**). Both the solids of untreated and washed biomass were oven-dried at 80°C to constant weight and later taken for further analysis after appropriate pre-processing following the procedures described in **Section 3.1**. Material characterisations included proximate analysis, ultimate analysis, higher heating value determination, reaction rate kinetics calculation via thermogravimetric analysis, dust layer ignition delay time and minimum layer ignition temperature (T_{LIT}) determination; acid digestion and lignocellulosic analysis were also conducted on the biomass solids. As for the liquid collected, ion chromatography (IC) and total organic carbon (TOC) analysis were carried out on the leachates.

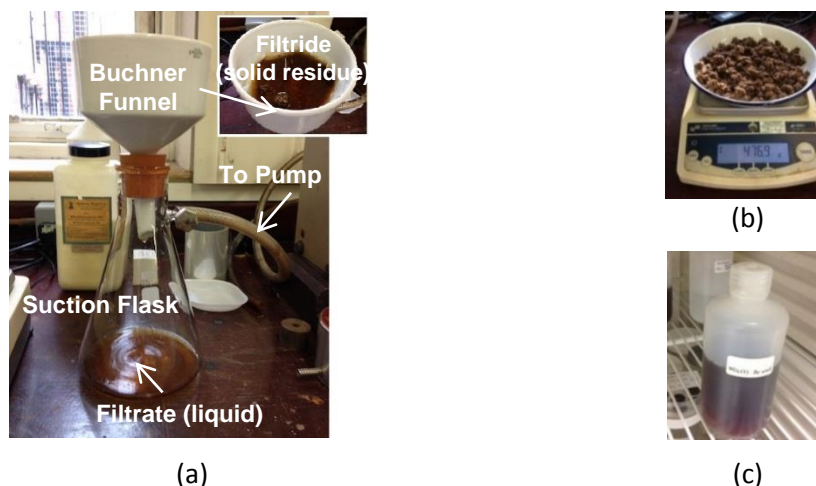


Figure 3. 37 Biomass Washing Pre-treatment (a) Buchner Funnel Filtration with Erlenmeyer Flask Connected to a Pump (b) Solid Residues (c) Leachate/Filtrate (Liquid) Collected

3.2.1.2 Acid Digestion of Biomass for Metals Analysis via AAS

The acid digestion technique was applied on the untreated biomass in this study. An acid digestion or commonly known as sample digestion is a method to completely dissolve a sample into a solution containing all its constituent elements by reaction with acids and heat (HARIBO Scientific, 2016). In this study, the acid digestion method was coupled with the Atomic Absorption Spectroscopy (AAS) to determine the concentration of its constituent elements.

Prior to AAS analysis, herbaceous miscanthus and woody pine were acid digested, where dried samples were milled and sieved to $\leq 100 \mu\text{m}$ and around 1 g of each sample were weighed and transferred to a small conical flask. Wearing corrosive resistant gloves and face shield, 5 ml of concentrated sulphuric acid were added to the conical flask, followed by 10 ml of concentrated nitric acid, where volume measurement of both acids were done with the tilt measure in a fume cupboard (see **Figure 3. 38**). Containing biomass and two acids, the conical flasks were moved onto a sand bath that had been pre-heated at 200°C . For each of the conical flask located on the 200°C sand bath, a small glass funnel was attached on top for acid reflux (see **Figure 3. 38**). For the 30-minute duration on the hot sand bath, the conical flasks were observed closely to prevent acid-overflow and were shaken gently on and off to clear precipitates sticking on the conical flask walls. Whenever the liquid in the conical flask started to bubble, the conical flask was moved to a cooler sand bath (at ambient temperature) to prevent overflowing of acid. After the 30 minutes, the hot sand bath temperature was raised to 250°C . Once the hot sand bath reached 250°C , all small funnels were removed from the conical flasks and the flasks were left on the 250°C hot sand bath for 30 minutes. After this, all heated conical flasks were moved to the cool sand bath for a 10-minute cooling. Approximately 20 ml of distilled water were added to each of the cooled conical flasks. Moving out from the fume cupboard, the contents in the conical flasks were diluted to 100 ml in a volumetric flask. The solutions were then ready to undergo elemental analysis with AAS (see **Figure 3. 38**).



Figure 3. 38 Sample Acid Digestion in Fume Cupboard – Concentrated H_2SO_4 and Concentrated HNO_3 to be added to Biomass-Filled Conical with Tilt Measure

3.2.1.3 Atomic Absorption Spectrophotometry on Digestate

The acid digested biomass solutions were taken for element analysis using the atomic absorption/emission spectroscopy (AAS) technique. The fast sequential Agilent Varian AA240FS Atomic Absorption Spectrophotometer was used in conjunction with its Windows-based worksheet software (SpectrAA). The instrument placed under a suction hood with major components labelled is shown in **Figure 3. 39**.

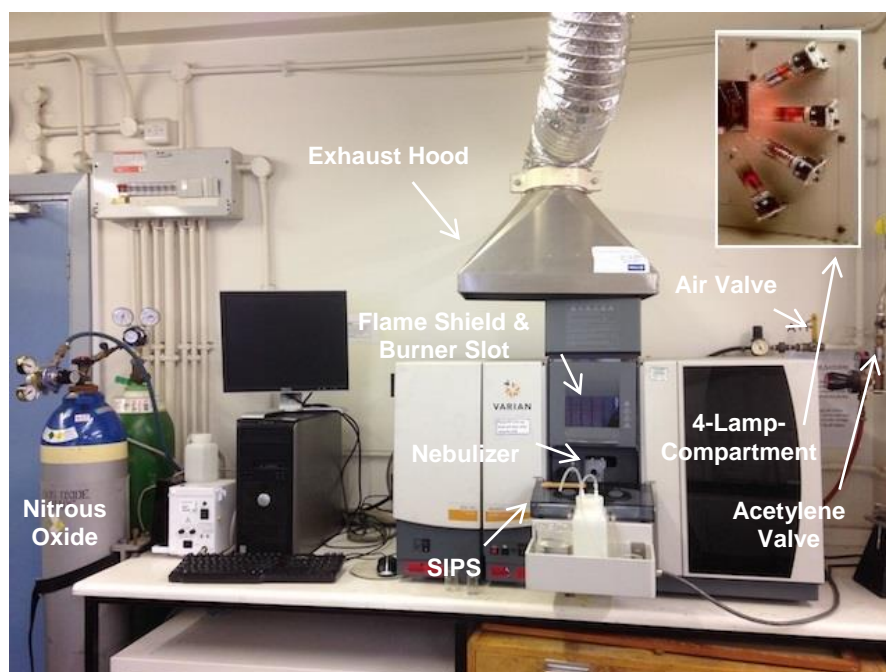


Figure 3. 39 Agilent Varian AA240FS Fast Sequential Atomic Absorption Spectrometer

Atomic absorption spectrophotometry provides quantitative analysis on metal elemental concentration contained in a liquid sample (digestate in this study). The quantification is based on the intensity of light transmitted by the digestate solution. As shown in **Figure 3. 39**, the 4-Lamp-Compartment holds four different hollow cathode lamps on a turret that matches the elements of interest, and in this case the Potassium (K)-Lamp and Calcium (Ca)-Lamp were among the four. The hollow cathode lamps were the light source that produced lights of different wavelengths depending on the specific element under investigation.

The solution was nebulised into a burner (see **Figure 3. 39**) in the atomizer section to disperse atoms in the flame. A flame atomiser was used in this study as the heat provider for dissociation of molecules to free atoms. An oxidant-fuel pair was needed to sustain the flame and acetylene was the fuel used in this study, paired with either air or

nitrous oxide (N₂O) as the oxidant. The air-acetylene pair reached a temperature as high as 2300 K with a high burning velocity whereas the N₂O-acetylene pair reached 2900 K with a lower burn rate (San Diego Miramar College, 2016). The suitable oxidant-fuel pair was selected based on recommendation in the Manual (Agilent Technologies Inc., 2015) that came with the instrument, and appropriate amounts of each were premixed before reaching the nebuliser. The burner used was based on the oxidant-fuel pair selected and was aligned properly in the burner slot so as not to miss the incoming light. The air-acetylene pair was chosen for K detection whereas N₂O-acetylene pair for Ca following the guidelines in the manual.

As the light of specific wavelength passed through the atomic cloud, the sample absorption was captured by a detector which recorded the intensity and later had the signals analysed by the appropriate software. For each different element of interest in a sample, at least five standards with known concentrations were prepared for instrument calibration; Potassium (K) was calibrated with 80, 160, 240, 320 and 480 ppm standard solutions whereas Calcium (Ca) with 80, 160, 240, 320 and 400 ppm standards. These calibration ppm values were important to match the wavelength and slit width suggested in the Manual for optimised results. While running the experiments, the Sample Introduction Pump System (SIPS) was used to draw samples into the system for atomisation. The system draws a known amount of deionised (DI) water to dilute the sample if the concentration is outside the calibrated range and the executed dilution is reported in the software display later. For this instrument, the metal concentration was reported in ppm. Besides selecting the analysis method and entering sample information to the SpectrAA software, flame optimisation was done for each sample as well to ensure the element concentrations in the samples were recorded as accurately as possible.

3.2.1.4 Lignocellulosic Analysis

Lignocellulosic biomass is made up of three polymeric component, namely hemicellulose, cellulose and lignin. The fraction of each component for all the eight samples in this biomass washing study were taken for lignocellulosic analysis at IBERS Analytical Chemistry Laboratory at the University of Aberystwyth, UK. This lignocellulosic examination used modified methods developed by Van Soest using the Gerhardt fibre cap system (Allison et al., 2012) and involves gravimetric analysis on three measurements – Neutral Detergent Fibre (NDF), Acid Detergent Fibre (ADF) and Acid Detergent Lignin (ADL).

In this analysis, NDF is the measurement of the total cell wall, that shows the amount of ash-corrected residue remaining after an hour of refluxing in a neutral buffered detergent solution. ADF is a measurement of cellulose and lignin, that shows the ash-corrected residue left after refluxing the sample in a solution of Cetyl Ammonium Bromide

(CTAB) in 2 M sulphuric acid. ADL is to obtain the crude lignin, which the amount is obtained after treating ADF with 72% sulphuric acid to solubilise the cellulose. Ash in samples is obtained after heating at 600°C in a muffle furnace for a minimum of 4 hours (Allison et al., 2011). The concentrations of hemicellulose (HCLS) and cellulose (CLS) were calculated following the equations (Akinrinola, 2014) as follows:

$$\% HCLS = \% NDF - \% ADF \dots\dots \text{Equation 3.11}$$

$$\% CLS = \% ADF - \% ADL \dots\dots \text{Equation 3.12}$$

3.2.1.5 Ion Chromatography on Biomass Leachates

The filtered leachates/filtrate in the 250 ml sample bottles were removed from the fridge ~30 minutes before conducting any analysis on the leachates. This was to ensure that the particulate matter-free leachates entering the ion chromatographer (IC) had its measured volume as close as possible to the desired volume.

The biomass leachates were taken for ion chromatography in the Dionex DX100 Ion Chromatograph instrument, which is a variant of high performance liquid chromatography (HPLC), having the ability to separate and identify ionic species in aqueous solutions and it is ideal for parts per million (ppm, equivalent to mg/L) level analysis. In this study, detection of cations (potassium, K^+ and Calcium, Ca^{2+} and anion (chloride, Cl^-) leached from biomass was conducted in two separate but identical ICs. It is important to note that appropriate dilutions with deionised water were made to fit the instrument calibrated detection range (~0.5 to ~40 ppm) (Energy Research Institute, 2016) and later appropriate corrections were made on the instrument reported results. The Dionex DX100 instrument, IC preparation and leachate dilution to 10 ml procedures are briefly illustrated in **Figure 3. 40**.

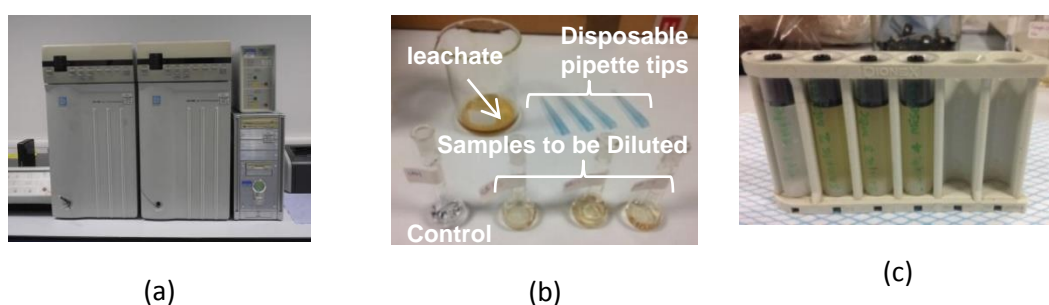


Figure 3. 40 IC Preparation: (a) The Dionex DX100 instrument (b) Control and Leachate Samples being Prepared in Volumetric Flasks (c) Control and Diluted Leachate Samples in Dionex DX100 Vials

The principle of operation is as follows (Earth Institute, 2011): the sample solution is injected into the eluent i.e. the carrier fluid and the sample solution-eluent mixture passes through a column containing stationary adsorbent material. Compounds in the analyte are then separated between mobile eluent-analyte and stationary adsorbent entity. Each dissolved component adheres to the adsorbent with different forces and those strongly adhered ones move through the adsorbent slowly as mobile eluent flows pass. As eluent flows through the column, different components in the analyte will move down the column, each with different speed and therefore the components are separated. Towards the end of the column lies a conductivity detector that generates a measurable signal that shows results in a form of chromatogram. With the help of a suppressor unit, the background noises are eliminated whereas the conductance of sample ions enhanced. The chromatogram plots the electrical conductivity signal against the corresponding retention time of each component in the sample, and since each retention time on the chromatogram is unique to a particular ion, specific ions in a sample can be identified. The IC equipment in this study uses the conductivity detection method and thus relies on retention time to identify analytes; cations like lithium, sodium, ammonium, potassium, calcium, magnesium and anions like fluoride, chloride, nitrite, bromide, nitrate, phosphate and sulphate are within its detection (Energy Research Institute, 2016).

3.2.1.6 Total Organic Carbon Analysis on Biomass Leachates

The Total Organic Carbon (TOC) analysis was conducted with the equipment from Hach Lange IL550 as shown in **Figure 3. 41**. For this instrument, the calibrated range is 10-1000 ppm and therefore, samples were diluted with deionised water following the same procedure practised in IC sample dilution, and the results reported by the software were corrected in the same manner as the IC samples correction. The aqueous solution samples made up of filtered biomass leachates were analysed for the organic carbon content. The total carbon (TC) includes both the organic and inorganic constituents and total organic carbon (TOC) and total inorganic carbon (TI) can be related to TC as follows (Bernard et al., 2016):

$$TI(\%) = TC(\%) - TOC(\%).....\textbf{Equation 3.13}$$



Figure 3. 41 Hach Lange IL550 for Total Organic Carbon Analysis

3.2.2 Torrefaction of Biomass

Torrefaction is a well-known thermochemical pre-treatment process that upgrades biomass properties to a solid fuel that closely resemble fossil fuel coal. It is of interest to find out how this thermal treatment on biomass affects the self-ignition characteristics of its dust. To answer the question of whether torrefied biomass dust reduces the self-ignition risk of biomass, relevant procedures were carried out.

Woody pine chips and herbaceous miscanthus pellets were sourced from two different U.K. power stations and were termed PineR and Misc(1) hereafter. In this study, the raw materials were air-dried to constant weight upon receipt and were then divided into two groups – untreated and torrefied. Both sets of material were subjected to similar preparation procedures prior to any analytical experiment. Owing to the limited raw materials, only one torrefaction condition was selected for further studies on self-ignition characteristics of torrefied biomass dust.

3.2.2.1 Bench-Scale Torrefaction Procedure

At bench scale, torrefaction was performed using a small Three Zone Horizontal Furnace manufactured by Elite Thermal System Limited, the TMH 12/75/750, 2416 CG:2x2216E model to be exact, as shown in **Figure 3. 42**. This furnace comes with a 75 mm inner diameter tube and heated zone length of 750 mm, capable of reaching 1200°C when operating at maximum power of 2.7 kW. It has been designed with three heated zones such that temperature uniformity along the tube can be achieved. This tube houses a 60 mm internal diameter, 800 mm length borosilicate reactor tube where biomass to be torrefied is placed. As shown in **Figure 3. 43**, within the reactor tube, there were three thermocouples (thermocouples 1, 2 and 3 denoted as TC1, TC2 & TC3 respectively) spaced roughly 20 cm apart to track three temperatures within the reactor tube during biomass torrefaction process. Going through a data logger, all the temperatures were recorded and saved by a software for later temperature profile plotting and interpretation. As illustrated

in **Figure 3. 42**, nitrogen supply was controlled by a valve-flowmeter, ensuring a continuous inert environment throughout the whole torrefaction process.

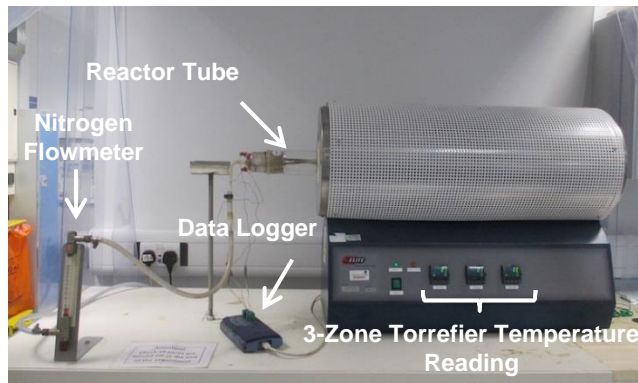


Figure 3. 42 Three Zone Horizontal Furnace Used for Torrefaction

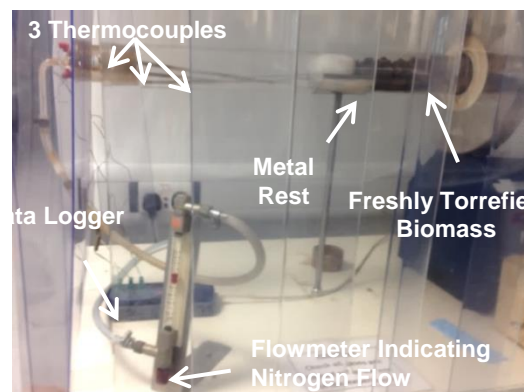


Figure 3. 43 Thermocouples (TC1, TC2 & TC3) Connected to Computer for Temperature Recording via a Data Logger & Hot Reactor Tube Resting on Metal Rest while Quenched by Nitrogen

Owing to the size of the torrefier available, the biomass samples were torrefied in batches of ~100g/batch. Prior to entering the furnace, around 100g of biomass was placed in the borosilicate reactor tube, trapped between two thermally stable glass wool plugs. The left end of the reactor tube was connected to the inert nitrogen gas supply and three thermocouples positioned at desired locations: Once the biomass-filled reactor tube was slid into the furnace from the left, the right end of the reactor tube was connected to a 90-degree glass connector with a collection system placed beneath its outlet, capable of collect the bio-oils or tars resulting from the torrefaction process although this was not an aim of the current work.

With inert nitrogen flow at 1.2 l/min, the biomass was heated at a rate of 10°C/min from room temperature to 150°C and held for 60 minutes to remove inherent moisture. After drying the biomass, at the same heating rate, the temperature was further raised to the final, desired torrefaction temperature, which was 270°C in this study. This temperature was held for a certain duration (the torrefaction residence time). In this study, residence time was defined as the period of time that biomass was treated at maximum reaction temperature i.e. the torrefaction temperature which in this case, was consistently 30-minute for every batch of both samples. During the process, temperatures detected by all the three thermocouples were recorded through a data logger to the computer and were recorded for later use. After the desired residence time, and after removing the 90-degree glass connector on the right, the reactor tube was quickly pulled out of the furnace to the metal tube-rest on the right (see **Figure 3. 43**). Nitrogen gas remained flowing to quench the hot, torrefied biomass and to maintain the inert environment thus prevented further reaction. The reactor tube with torrefied biomass after nitrogen cooling and still sandwiched between the two glass wool plugs is shown in **Figure 3. 44** and comparison of biomass appearance before and after torrefaction is shown. Torrefying biomass had made the colour darker and this observation was consistent with work from other researchers. During the torrefaction process, it had also been observed that the thermocouple readings exceeded the desired torrefaction temperature by <20°C, (which usually started halfway of the torrefaction process). This outcome suggested that torrefaction is an exothermic process and such a finding was consistent with studies by (Ibrahim, 2013; Akinrinola, 2014; McNamee et al., 2016). After the torrefaction process, the tube was weighed and the torrefied material removed, then reactor tube was soaked overnight in NaOH 10% w/v solution and warm water was used for rinsing the next day.

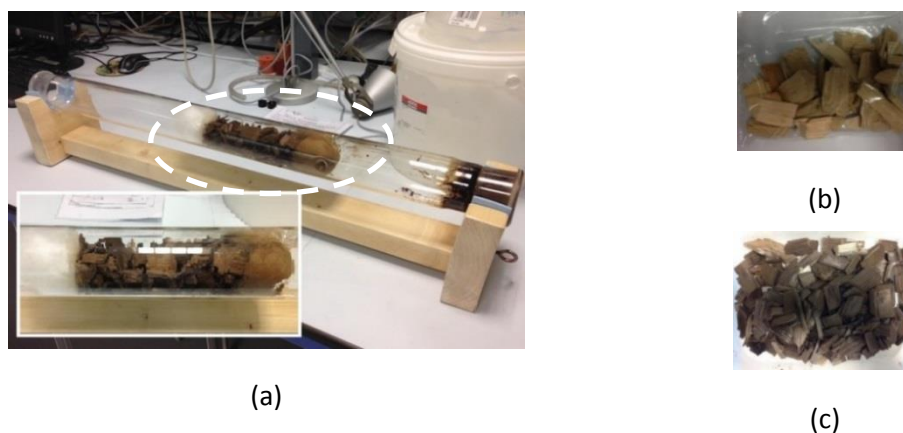


Figure 3. 44 (a) ~100g of Cooled, Torrefied Biomass Sandwiched between Two Glass Wool Plugs Ready for Removal from Borosilicate Reactor Tube (b) Oven-Dried PineR Chips Before Torrefaction (c) After Torrefaction

It was of interest to know how the self-ignition characteristics changes when untreated and torrefied materials appeared together. Therefore, a blend with half its composition (by weight%) made up of milled untreated biomass and the rest of torrefied biomass was created. **Figure 3. 45**(a)-(c) show the blending procedures involved; where in (a), same weights of torrefied miscanthus and untreated miscanthus were contained in two separate measuring cups and were then poured into a sieve shaker tray and subjected to a 20 minutes shake by AS 2200 sieve shaker shown in (b) after being manually mixed and the final outcome is displayed in (c). The milling procedure is described in **Section 3.1.1**.



Figure 3. 45 Torrefied biomass and Untreated Biomass (a) Contained in Measuring Cups (b) Blended Using Retsch AS 200 Sieve Shaker (c) Blend Contained in Sieve Shaker Tray

3.2.2.2 Proximate Analysis, Reaction Rate Kinetics and Self-Ignition Risk Ranking on Torrefied Biomass

Similar to the procedures applied on the single-material biomass dust (refer to **Section 3.1**), proximate analysis, reaction rate kinetics and self-ignition risk ranking on torrefied biomass was conducted, with proximate analysis following British Standards BS EN 14774-3:2009 for moisture, BS EN 15148:2009 for volatile matter, BS EN 14775:2009 for ash and fixed carbon by difference. Reaction rate kinetics were computed from the linearised Arrhenius equation for apparent first order release of volatiles during temperature programmed combustion via thermogravimetric analysis. The self-ignition risk was ranked following the method of Jones et al. (2015) in the study of biomass low temperature ignition characteristics that had been modified from the method developed by Ramírez et al. (2010) in their study about several materials commonly stored in silos. The results of untreated biomass and torrefied biomass was later compared.

3.2.2.3 Ultimate Analysis, High-Heating Value Determination on Torrefied Biomass

Identical to the method used on single-material biomass (refer to **Section 3.1**), ultimate analysis followed by high-heating value (HHV) determination was carried out. The HHV was determined using the correlation developed by Friedl et al. (2005) upon obtaining elemental analysis results on dry basis with reference to BS EN 15104:2011 (British Standard, 2011)]. Comparisons between untreated and torrefied biomass were made later.

3.2.2.4 Minimum Dust Layer Ignition Temperature (T_{LIT}) of Torrefied Biomass

The sample preparation and experimental procedures followed closely to British Standard BS EN 50281-2-1:1999. The minimum ignition temperature of torrefied biomass dust layer (T_{LIT}) was carried out following the steps applied on the single-material biomass and the duration taken to reach the dust layer ignition point at the corresponding T_{LIT} was recorded as the ignition delay time, t_i , as detailed in **Section 3.1**.

3.2.2.5 Torrefied Biomass Particle Size Distribution

Torrefaction increases the brittleness and thus grindability of a biomass therefore the fines fraction is expected to increase. To meet the objective of obtaining the minimum ignition temperature of dust layer (T_{LIT}) in accordance to BS EN 50281-2-1:1999 and subjected to the facilities available, the torrefied dust was milled and sieved down to $<180\mu\text{m}$. After the milling and sieving the biomass dust, the particle size distribution of all the five samples (untreated, torrefied and blended) involved in this study were analysed using Malvern Mastersizer 2000E (see **Figure 3. 46**) that had been connected to a computer with an appropriate software installed.

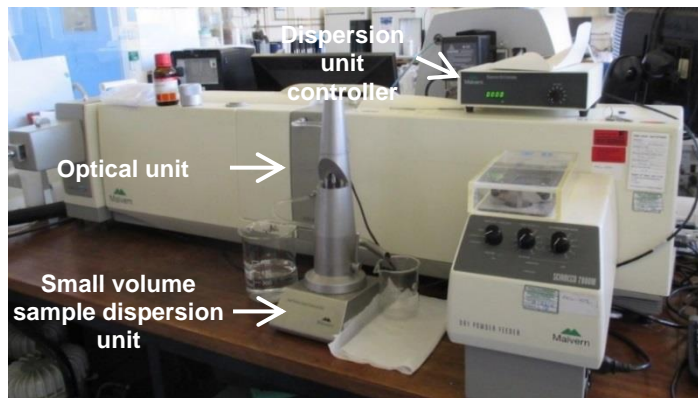


Figure 3. 46 Malvern Mastersizer 2000E with Small Volume Sample Dispersion Unit, Optical Unit and Dispersion Unit Controller

Malvern Mastersizer 2000E applies the laser diffraction technique which assumes the shape of particle as spherical in its particle size measurements. Prior to entering this equipment for particle size analysis, samples can be prepared in emulsions, suspensions or even dry powders and this equipment is capable of measuring particle size that ranged from 0.1-1000 μm without the need of lens change. This instrument measures the intensity of light scattered as the laser beam passed through the sample dispersed in a medium, in this study, deionised water.

With a few drops of deionised water added, a few milligrams of each sample were manually stirred with clean disposable universal spatula in a small plastic beaker such that they mixed well with deionised water and became a slurry, in paste form. Deionised water was then filled into the small volume dispersion unit (SVDU) and upon setting the dispersion unit controller (DUC) to a certain rotational speed, water was pumped into the optical unit (OU) housing the analysis cell and recirculating within the SVDU and OU. The DUC-controlled SVDU electrical stirrer was adjusted such that the agitation was not too rough to cause deionised water loss. Without any sample, water was recirculated then drained to a waste beaker at least twice for the purpose of cleaning the optical unit analysis cell. The sample paste was then transferred into the SVDU that had been filled with fresh deionised water and sample particles were left to suspend in the water recirculating between the SVDU and OU. In this study, it was found that a DUC speed of around 2000 rpm stirred the sample particles well enough for particles dispersion without loss of deionised water and without sample particles depositing at the bottom of SVDU.

As the sample paste was added into the deionised water-filled SVDU, agitation from the stirrer helped to disperse the sample in deionised water that was flowing through the lens of the OU. In the analysis cell, a focused laser beam scatters the light at an angle which is inversely proportional to the sample particle size i.e. large particles scatter light at small angles whereas small particles scatter light at large angles relative to the laser beam. The intensity of the scattered light is then measured by a series of photosensitive detectors.

The Mastersizer software employs the Mie theory of light scattering in calculation of particle size distribution, assuming an equivalent sphere volume for all particles. The intensity of light scattered is a function of wavelength scattering angle, particles size and relative refraction index of material and medium. With known refraction index, Mie theory is able to compute the particle size. The relation between scattering intensity and angle is used to calculate the particle size and refraction index of material is important to ensure a calculation as accurate as possible. In this analysis, refraction index of the sample material was matched with a similar material within the database stored in the computer. For the untreated and torrefied biomass samples, 1.386 and 1.680 were used as respective refraction index following the values used by Medina (2014) in the study of Explosion

safety of biomass and torrefied biomass powders. The Mastersizer used was calibrated monthly with calibration samples supplied by equipment manufacturer to ensure its accuracy and precision.

The sample size distribution reported by the equipment software was an average of 10 measurements and in each measurement, it was ensured that there was no agglomeration of particles in the suspension. The results were then reported in volume percentage versus particle size (in logarithm scale), signifying the quantity of particles of a certain size and generally showing a bell-shaped distribution.

It is important to note that since torrefied biomass is hydrophobic a chemical was added to the <180µm dust to reduce its surface tension such that the slurry paste could be formed. The chemical added was a non-ionic liquid, IGEPAL® CA-630 (by Sigma-Aldrich) of molecular biology grade, that helped the samples to be wetted and mixed well with deionised water without altering the nature of the sample.

3.2.2.6 Torrefied Biomass Surface Area Determination

Typically, surface area is one of the properties that affects the combustion rate of solid fuels. Like many other researchers, this study applied the well known Brunauer-Emmett-Teller (BET) method to determine the surface area of all samples – untreated, torrefied and untreated-torrefied blend of solid fuels as this method is cheap, fast and reliable in determining the surface area.

The NOVA® 2200e Multi- station Any-gas Sorption Analyser Standard Model v10.03 by Quantachrome Instruments (see **Figure 3. 47**) was used in this study. All the air-dried and pulverised samples that had been sieved to <180 µm were filled into pre-weighed, acetone-cleaned sample tubes, after that the net sample weight was obtained. After unplugging the tube blockers, the biomass-filled sample tubes were screwed into each of the ports at the vacuum degassing station (see **Figure 3. 47**). Degassing is the surface cleaning process before determining the surface area, either by evacuation or inert gas (e.g. nitrogen) flowing and in this study, evacuation means was used. The degassing temperature was set at 105°C for 4 hours (Medina, 2014) to avoid structural damage to the sample since it was observed by TGA that volatiles release started after 105°C (see **Figure 3. 47**) and escape of volatiles could alter the surface structure. For each sample, ~0.2 g was filled into each sample tube and the weights before and after degassing were recorded to obtain the clean sample weight.

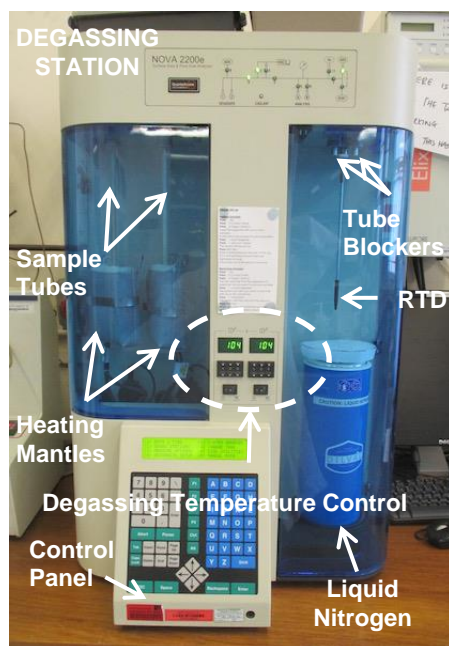


Figure 3. 47 The NOVA[®] 2200e Multi- station Any-gas Sorption Analyser Standard Model v10.03

When the 4-hour degassing process finished, the two heated sample tubes were unscrewed and with rubber bungs placed at the tube outlets, were left to cool to room temperature. While cooling, liquid nitrogen was poured into the dewar (see **Figure 3. 47**) located at the other station and the cooled sample tube was reweighed. Before screwing the sample tubes to the analyser ports next to the resistance temperature detector (RTD), filler rods were incorporated to sample tubes such that the analysis would not consider the tube section without samples.

Subjected to the low temperature of liquid nitrogen, At -196°C , the amount of gas which the sample adsorbed for different gas partial pressures was plotted against the ratio of actual pressure of adsorbed gas to the gas saturation pressure, thus creating the adsorption isotherm. Conversely, desorption isotherms were plotted when pressure was reduced as gas was removed. As a result, full adsorption/desorption isotherms (see **Figure 3. 48**) were plotted for each sample and using the BET calculation method, BET surface area in unit of m^2/g was obtained from the multi-point BET plot (see **Figure 3. 49**) at relative pressure range of ~ 0.05 to ~ 0.3 in this study, consistent with the range of McNamee et al. (2015). Since each sample took ~ 6 hours to analyse, samples were left to run overnight. Analysed samples were removed from the dual-sample analyser the next day, the tubes cleaned thoroughly with acetone, and then oven-dried in preparation for the next set of samples on the next experiment day.

In the BET method, surface area of a sample was determined by calculating the amount of adsorbate gas physically adsorbed by the solid surface since adsorption results

from the weak Van der Waals forces between adsorbate gas molecules and the adsorbent surface area (Industry, 2016). Among all gases commonly used as an adsorption gas like nitrogen, argon or krypton, nitrogen has the smallest cross-sectional area of an adsorbed molecule of 0.162 nm² compared to 0.155 nm² and 0.210 nm² of argon and krypton respectively. From this point of view, using nitrogen gas in this study should yield high accuracy (Trunschke, 2007).

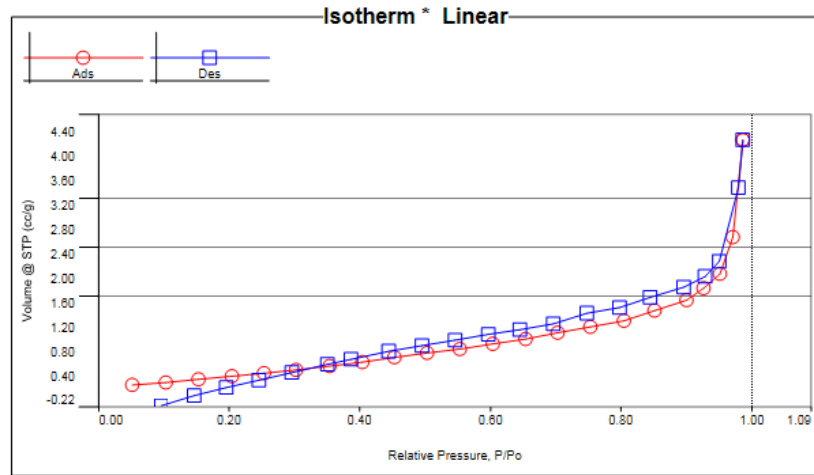


Figure 3. 48 An Example of Adsorption/Desorption Plot, for PineC

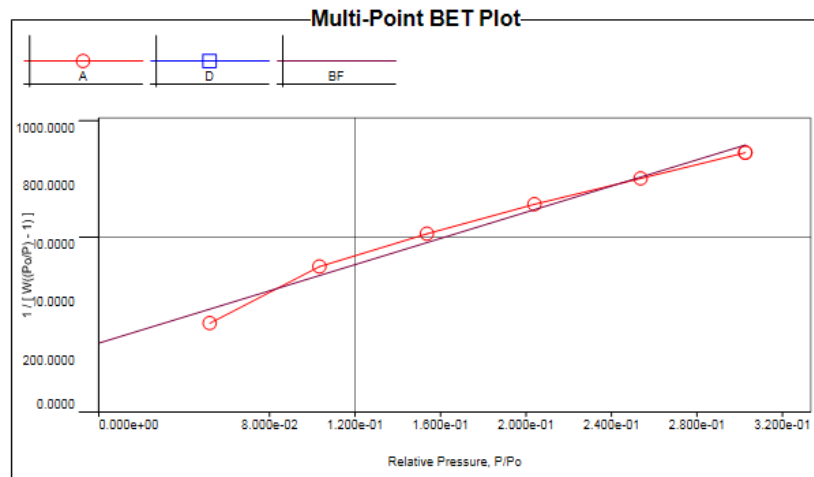


Figure 3. 49 An Example of Multi-Point BET Plot, for PineC

3.2.2.7 Torrefied Biomass Surface Morphology

To compare the changes in particle structure upon thermal treatment by torrefaction, surface morphologies of untreated, torrefied and untreated biomass blended with torrefied biomass particles were compared using the scanning electron microscopy (SEM)

method. Some pulverised sample of each of the five samples of interest were spread on a standard double-sided conductive carbon tape adhered to an aluminium stub of ~15 mm diameter. An air duster was applied to remove any loose particles surrounding the adhesive carbon tape after spreading a thin layer of dust on the tape and to prevent contamination of the delicate microscope. Since all the five biomass samples were non-conductive, each of the samples was coated with 20 nm thick layer of iridium using the Agar high resolution sputter coater (see **Figure 3. 50**) to prevent charging of the sample material. As a precaution to avoid mixing up of samples, each sample was carefully labelled before iridium coating since all looked alike after the sputter coating process.



Figure 3. 50 The Agar High Resolution Sputter Coater

Figure 3. 51 shows the Hitachi TM3030 Bench Top SEM Microscope package used in this study of particle morphology, with the mount (black structure) positioned in between the microscope and the computer with appropriate software. The sample-filled stub was screwed to the top of the sample holder and the distance between the stub to the top of the mount was fixed between 1-10 mm measured from the top of mount for image accuracy, in which the closer the stub was to the top, the higher the image resolution. The sample chamber drawer was then pulled out and the sample was transferred to sample holding slot which the centre position was aligned to the guiding notch. Upon closing the drawer and evacuating the chamber, the sample was ready for analysis. An electron beam was directed towards the sample where interaction intensities between the beam and sample were measured and data stored by the software. The electron beam focusing on the sample area was partially absorbed by the sample and depending on the conductivity of the sample, the beam was partially reflected as backscattered electrons. The software created SEM images depending on the brightness variations and magnification magnitude set and here, 15 kV incident electron beam bundled with different degrees of magnification (300x, 500x, 800x and 2500x) were set.

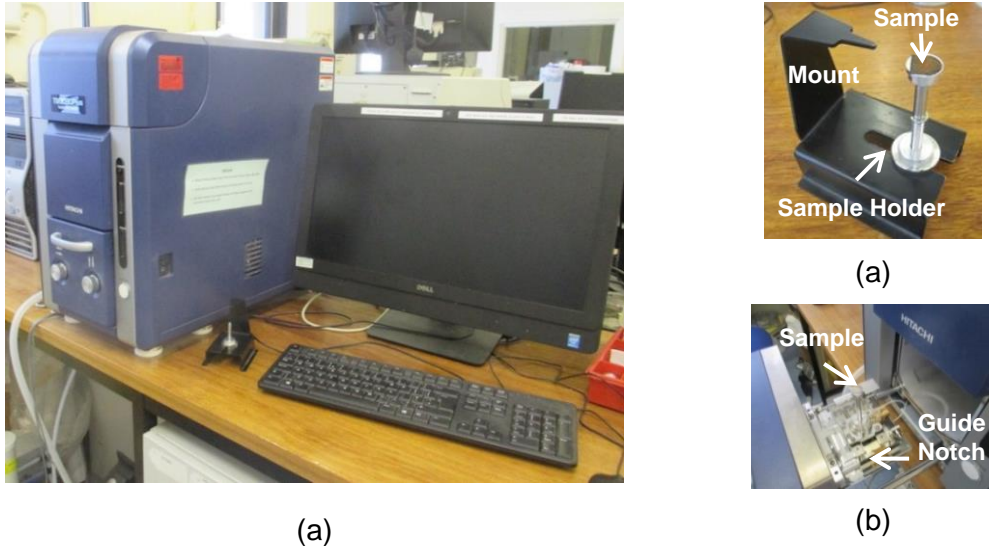


Figure 3. 51 Hitachi TM3030 Benchtop SEM Set (a) Hitachi TM3030 SEM, Mount with Sample Holder, Computer with Appropriate Software (b) Distance Measurement between Mount Top and Sample Filled Stub before SEM (c) Sample Entering SEM Equipment for Analysis

3.3 Emissions from Biomass on a Hot Surface

The setup of this experiment for capturing emissions from critically igniting and pre-igniting biomass dust layers was inspired by the study of Yokelson et al. (1997). The current experiment had amended their setup where they used open-path Fourier Transform Infrared Spectroscopy (FTIR) to measure the emissions from smouldering combustion of biomass. In essence, the experiment applied the buoyancy concept where lower density hot gas rose and denser cool air from the sides were drawn to replace the vacancy formed by the rising hot gas and thus creating a natural draft.

3.3.1 Sampling

Biomass dust deposited on a hot surface could ignite or pyrolyse as stated in in previous section. It is of interest to understand the emission under conditions where thermal runaway (ignition) does and does not take place, since it could provide useful information with respect to monitoring. Different from the published method that measured CO and CO_2 emissions, this work applied novel equipment setup to capture $VOCs$ and $PAHs$ and endeavour to obtain insights of self-ignition initiation from amount of organic volatiles instead of permanent gases. In order to capture and later analyse the chemical constituents emitted from biomass burning or pyrolysing, a few laboratory components were connected and integrated to the existing hot plate which the critical or minimum

layer ignition temperature (T_{LIT}) of a biomass dust layer had been determined earlier. The three major emission capture components were:

- i) inverted funnel,
- ii) filter paper and
- iii) ORBO™ 43 Supelpak™ 20 tube (termed 'ORBO tube' henceforth).

This set of three components along the emission sampling line are termed 'Sampler 1 , Sampler 2 and Sampler 3' hereafter. These emission samplers were held in place using three clamps on a moveable retort stand (see **Figure 3. 52**) and are labelled in the schematic in **Figure 3. 53**. Their respective positions were adjusted in the beginning and remained unchanged throughout experiments on all samples, implying that the varying parameter of emission capture distance was not studied here. As shown in **Figure 3. 52**, the bottom jaw was for holding the inverted funnel (Sampler 1), middle jaw for the filter paper holder (Sampler 2) and the top rubbery jaw was to provide extra grip when holding the fragile ORBO tube (Sampler 3). These samplers were then connected to a Dreschel bottle, then to a flowmeter and a pump after going through a screw valve. All the components were connected by non-reactive, polytetrafluoroethylene (PTFE) tubing, sized accordingly. The schematic of the final set-up is illustrated in **Figure 3. 53**. For every pre-igniting (at $T_{LIT}-10^{\circ}\text{C}$) and critically igniting (at T_{LIT}) experiment, the sampling time was fixed to 30 minutes.

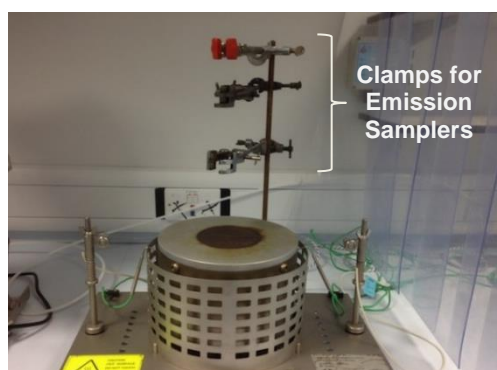


Figure 3. 52 The Emission Samplers Clamped on a Portable Retort Stand

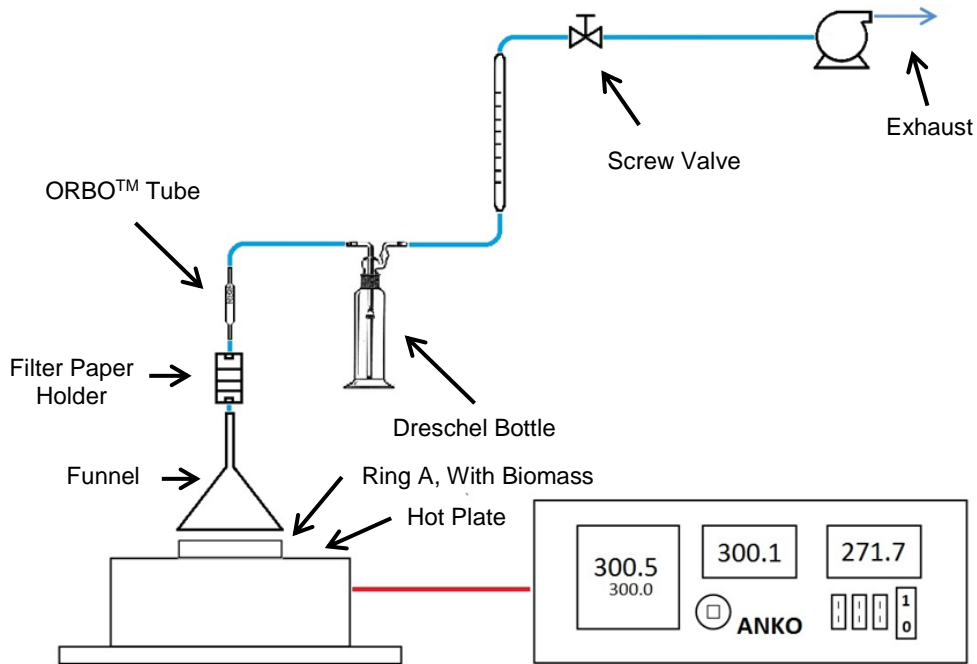


Figure 3. 53 The Schematic of the Final Experiment Set-Up

The function of all main components applied in this experiment is briefed as follows, and pre-weighed when they were emissions-free, i.e. before the sampling time:

i) Sampler 1 – Inverted Funnel

A relatively inert borosilicate glass funnel manufactured by Pyrex was placed 1.0 cm above Ring A. Its orientation was inverted with its stem facing up to converge the emission flow into the adjoining PTFE tubing. The filter paper holder was the next component joined by the PTFE tubing.

ii) Sampler 2 – Filter Paper Holder

To fit nicely in the filter paper holder available, a 37 mm diameter filter paper was used. Whatman GF/F grade binder free borosilicate glass fibre microfiber filter paper was chosen and the filter papers were dried in a silica gel filled desiccator for 24-hour before any experiment. After the filter paper component was the ORBO tube, joined by PTFE tubing. Prior to any sampling, the clean filter paper was stored in a Petri dish PetriSlides.

iii) Sampler 3 – ORBO™ 43 Supelpak™ -20 Tube

The delicate and fragile glass tube was 8 mm in diameter and 100 mm in length, and packed with two materials – glass wool and granule slotted alternately (see **Figure 3. 54**). Prior to using, the two ends of the sterile ORBO was broken with a dedicated ORBO tube cutter, as shown in **Figure 3. 55**. The two red caps (see **Figure 3. 54**) were fixed to the ends

immediately after the ORBO ends were cut to avoid possible contamination before running any experiment.



Figure 3. 54 An ORBO Tube with Glass Wool and Granule Spaced Alternately **Figure 3. 55** The Dedicated ORBO Tube Cutter

Once the sampling system was in place, the dust layer test was began and immediately after the 30-minute sampling time, the portable retort stand holding the emission samplers was moved away from the hot plate.

iv) Dreschel Bottle

A 250 ml Dreschel bottle filled with silica gel was placed immediately after the emission samplers as a pump protecting step, i.e to avoid moisture (water vapour is a combustion product) from entering the pump as moist could possibly damage the pump.

v) Pump & Screw Valve

The main purpose of the pump which was to control emission flow at a fixed rate throughout the experiment sampling time was achieved in presence of a control screw valve.

vi) Flowmeter

A universal flowmeter (see **Figure 3. 56**) was used to gauge the emission flow rate in this experiment. Assuming air density variation within the temperature range in this experiment was negligible and not differing much from that of gaseous products from biomass pyrolysing/combusting; the flowmeter was calibrated with air heated by 300°C hot plate. With a stopwatch used for timing and a standard volume counter (see **Figure 3. 57**), the flowmeter was calibrated with mock runs (see **Figure 3. 58**) with all the experimental components present but without sample biomass pyrolysed/ ignited on the hot plate. The volume counter used has capability to calculate flowrates ranged from 0.016 m³/h (~4.4 ml/s) to 2.5 m³/h (~694.4 ml/s), which was sufficient in this application. During calibration, a tubular spirit level was used to ensure no horizontal and vertical plane deviations had occurred. Several flowrates were made by adjusting the screw valve and

the relevant marking scales were marked by the side of the flow meter. The flowmeter calibration steps are summarised as follows:

Flowmeter Calibration Steps:

1. Pump (operating at single stage) was connected to the volume counter and started.
2. The screw valve was turned on and the flowmeter float level was marked.
3. As the value on of volume counter hit a new number (volume 1), the timer was started (time 1); both the volume counter value and stopwatch time were recorded.
4. When the volume counter read another new number (volume 2), stopwatch was stopped (time 2); both the volume counter and stopwatch values were recorded.
5. The flowrate at that particular float indicator level was calculated as $(\text{volume 2} - \text{volume 1}) / (\text{time 2} - \text{time 1})$.
6. Step 1 to 5 were repeated for other screw valve openings.



Figure 3. 56 The Universal Flowmeter Applied in Experiment



Figure 3. 57 The Volume Counter Used to Calibrate the Universal Flowmeter

Flow rates obtained ranged from ~ 8.50 ml/s to ~ 22.90 ml/s and 13.05 ml/s was used for the experiments.

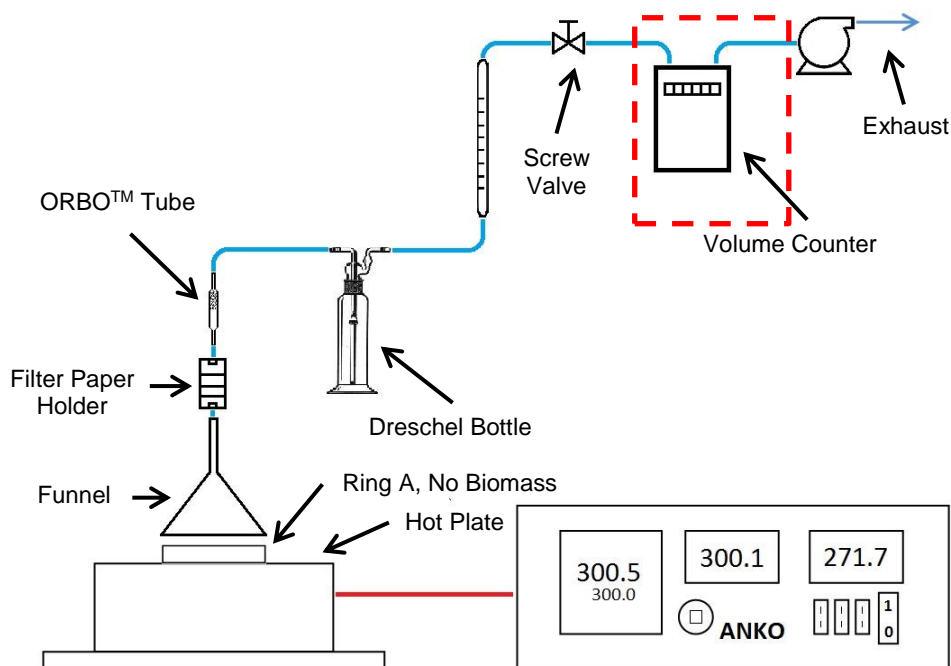


Figure 3. 58 Set-up of Mock Runs for Flowmeter Calibration

3.3.2 Extraction

Each of the three components was separated with care when they had cooled considerably. The funnel was then held by the jaw of a another retort stand clamp with its stem facing down and a 14 ml glass collector vial placed at the bottom. The deposits on the glass funnel were then rinsed out by analytical reagent grade Dichloromethane (DCM) solvent. After removal from the filter paper holder, the emission-filled filter paper was well kept in a PetriSlides. whereas the two red caps were fixed back to the ORBO ends to avoid contamination by non-experimental emission. Containing emission from experiments, the 14ml glass vial, PetriSlides, and capped ORBO tubes were temporary refrigerated before performing further analyses.

3.3.3 Analysis

Several analyses were then performed on emissions that had been collected from the three emission samplers and were stored temporarily in the fridge. Before getting the sample solutions for emission chemical components analysis via Gas Chromatography-Mass Spectroscopy (GC-MS), the solutions collected were subjected to evaporation or concentration with a portable nitrogen blower – the Six Port Mini-Vap Evaporator/Concentrator (see **Figure 3. 59**). All were then re-dissolved in 1 ml DCM and placed 1 minute in ultrasonic bath to maximise emission components recovery. As soon as

ultrasonic bath was completed, the solutions were transferred to smaller, 2 ml GC-MS vials (Perkin auto sampler vials) ready for analysis in Perkin Elmer Clarus 560 machine (see **Figure 3. 60**).

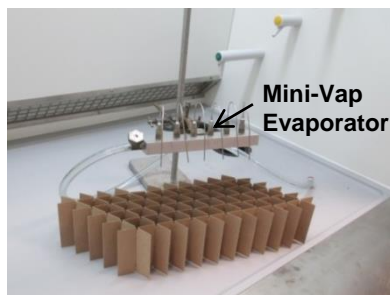


Figure 3. 59 Nitrogen Blower – The Six Port Mini-Vap Evaporator/Concentrator



Figure 3. 60 The Perkin Elmer Clarus 560 Equipment

The GC-MS is an instrument that has combined the gas chromatographic separating power with the mass spectrometry ability of identification, and emerged as one of the most accurate tools for analysing environmental samples (Center for Public Environmental Oversight, 2016). It is a superb analytical method that is capable of separating very complex mixture of volatile analytes (Martin and Synge, 1941) and is well suited for this experiment where emissions from igniting and pre-igniting biomass dust was concerned. As the sample solution was injected into the GC, upon volatilising, was transported through the column containing the stationary phase by mobile phase inert carrier gas, helium or nitrogen. The carrier gas used in this study was Helium.

The separation process takes place in a heated environment to prevent condensation of analyte (CHROMacademy, 2016). Within a solution made up of different chemical constituents, each has different affinity for the stationary phase in the column and thus each chemical component is separated as they travel throughout the length of the column. Each analyte remains and elutes from the column at different times (i.e. the retention time), then enters the mass spectrometer where it gets ionised and identified based on the retention time and mass-to-charge (m/z) ratio. The speed at which molecules travel through GC column depends on their chemical and physical characteristics whereby lower mass molecules travel swiftly (Bombay, 2016), indicating shorter retention times for lighter components. Later, the identity of each component is matched to a library of known spectra consisting of several thousand compounds stored on a computer (Center for Public Environmental Oversight, 2016). A simplified illustration of a GC is shown in **Figure 3. 61**.

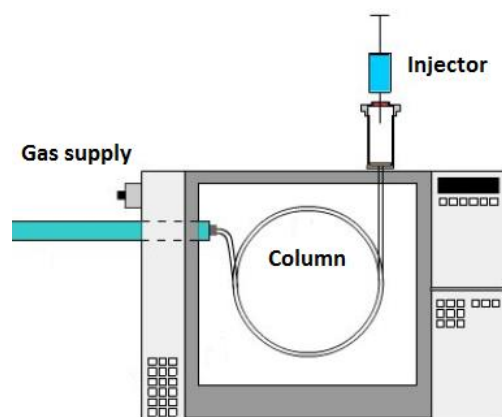


Figure 3. 61 Simplify Illustration of a Gas Chromatographer [edited from (CHROMacademy, 2016)].

From a GC-MS, the simplest data output from MS is the total ion chromatogram (McMaster, 2008) or TIC in short. A TIC simply plots the signal intensity on the y-axis against retention time on the x-axis and percentage intensity scale is commonly used (Hübschmann, 2015). For a chemical mixture, each constituent component is eluted at different times (represented by retention time on the x-axis) and ionisation of different components yield different ion currents. The computer adds up all the ion peaks in each mass spectrum and give a total ion current for a mass spectrum (Elmer, 2016). The TIC sums up intensities of all mass spectral peaks (all signals representing all different ions seen in the mass spectrum (Kenkel, 2014) from the same scan (Shimadzu, 2016). Once a TIC is obtained, different peaks that correspond to different retention time enables matching to a series of elements in the built in database and the constituents of a mixture can thus be identified.

3.3.3.1 GC-MS Analysis of Extracts

Bio-oil deposited on inverted funnel (see **Figure 3. 62**) was rinsed with DCM, as shown. Besides transferring the GC-MS ready solutions into small 2 ml Perkin auto sampler vials, extra DCM solutions for GC inter-sample injector rinsing were prepared in bigger vials, ready to be placed at designated auto sampler turret positions.

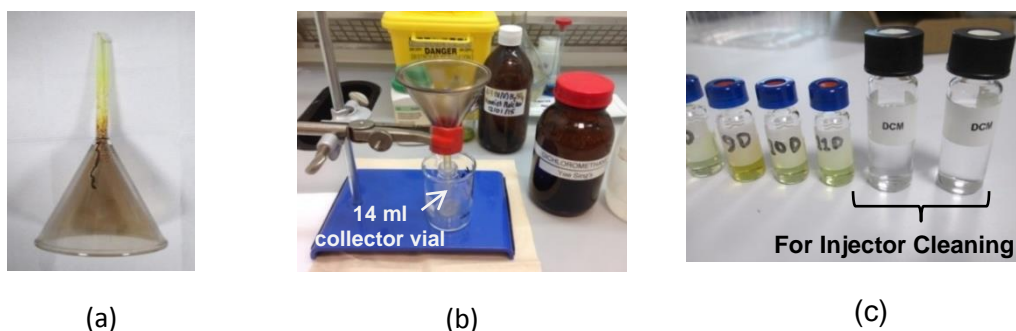


Figure 3. 62 Sampler 1 – (a) Funnel with Yellowish /Brownish Bio-Oil Deposits (b) Funnel subjected to DCM Rinsing (c) GC-MS ready solutions and Inter Sample Injector Cleaning DCM

The next sampler after inverted funnel along the emission sampling line was the filter paper holder housing a 37 mm filter paper. In general, most combustion generated particles are less than 1 μm in size (Jenkins et al., 1998b). Therefore, for the purpose of capturing particulate matters (PM) and some particulate polycyclic aromatic hydrocarbon (PAHs), the high loading capacity GF/F binder free borosilicate glass fiber microfibre filter paper of 420 μm thickness, capable of retaining fine particles down to 0.7 μm and having rapid flow rate was selected.

Unlike the emissions on inverted funnel that was extracted by simple DCM rinsing, the emissions captured by filter paper and ORBO tube were extracted using a pressurised fluid extractor. Dionex ASE350 (see **Figure 3. 63**) was applied to dissolve the emissions captured by GF/F filter paper and ORBO tubes, reason being the ASE extraction happened at elevated temperature and pressure, thus extraction was faster, more efficient and less solvent intensive than other technology like traditional Soxhlet extraction (ThermoFisherScientific, 2016). Accelerated extraction kinetics resulted by high operating temperatures and solvent that remained as liquid above its boiling point due to operation at elevated pressures are desirable features for optimised extraction. Acetone:hexane (1:1, v/v) was the solvent used in ASE here and **Figure 3. 64(a)&(b)** showed preparation of filter paper (with emissions folded in) and ORBO tube (emptying the granule and wool via a small funnel) respectively before entering the ASE cell.

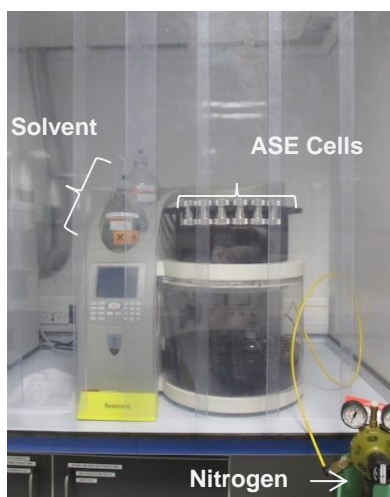
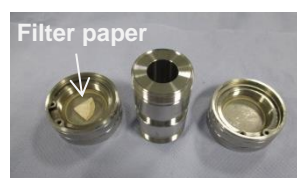


Figure 3.63 The Dionex ASE350 equipment



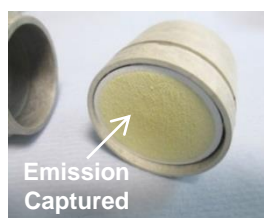
(a)



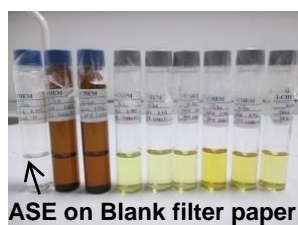
(b)

Figure 3.64 ASE Cell Preparation (a) Filter Paper (b) ORBO tube

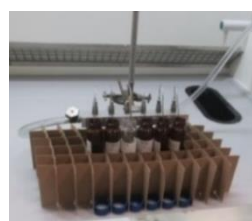
A filter paper sample with emissions captured is shown in **Figure 3.65**. After applying ASE procedures on emission-filled filter papers, the solutions were taken for nitrogen blower concentration, re-dissolving in 1 ml DCM, followed by transferring the GC-MS ready solution into Perkin auto sampler vials. Analysis were then performed on TICs obtained.



(a)



(b)



(c)

Figure 3.65 Sampler 2 – (a) A GF/F Filter Paper with Emissions Captured (b) Solutions from ASE Rinsed Filter Papers (c) Nitrogen-Blower Concentration of Solutions in ASE Vial

The last sampler on the emission sampling line was the ORBO tube. The ORBO tube was aimed to collect gas-phase constituents. All emission that did not condense and deposit on the funnel wall, managed to bypass the GF/F filter were retained by the ORBO tube. The absorbent matrix used in ORBO tube is specially treated AMBERLITE® XAD-2 resin manufactured by Supelco. In traditional Soxhlet extraction, acetone/hexane (1:1) had been used for resin elution. Since Dionex ASE350 had proved eluting with acetone:hexane (1:1 v/v) the XAD-2 resin spiked with polycyclic aromatic hydrocarbon (PAH) efficiently without

damaging the hard, spherical opaque resin beads (ThermoScientific, 2016), thus this solvent was used in both the ASE processes involved in this experiment – filter paper and ORBO tube emissions extraction. The pale yellowish emissions captured in ORBO tubes (see **Figure 3. 66** for an emission-filled ORBO tube) was subjected to ASE process for emissions extraction, after which the Perkin auto sampler vials preparation followed and finally TICs were obtained for analysis.

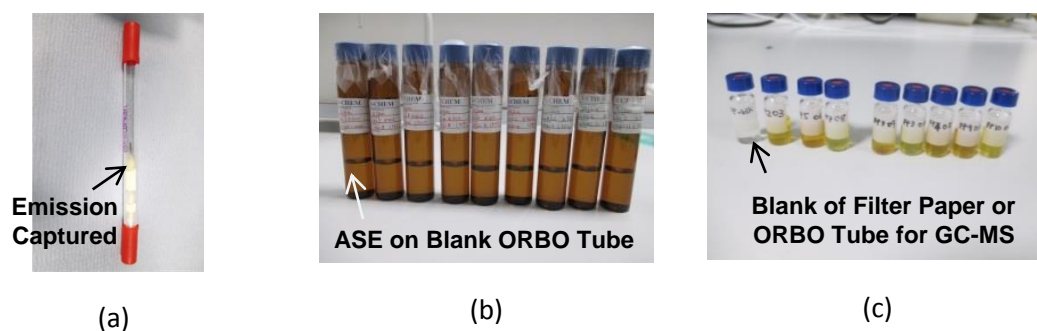


Figure 3. 66 Sampler 3 – (a) A Capped ORBO Tube with Emissions Captured (b) Solutions from ASE Rinsed ORBO tube (c) A Batch of GC-MS Ready Solutions in Perkin Auto Sampler Vials

Similar to that of inverted funnel, solutions collected from filter paper and ORBO tube rinsing were subjected to GC-MS analysis for chemical components and prior entering the Perkin Elmer Clarus 560 GC-MS equipment, the nitrogen-blowing, 1ml DCM re-dissolving, ultrasonic bathing and finally transferring to Perkin auto sampler vials steps were carried out the same like for inverted funnel.

The splitless sample injection mode was used in the GC-MS experiment where the split vent was closed during the injection, implying the sample was forced to proceed to the column for chemical components separation and not to be vented (Trajan Scientific Australia, 2015). This led to much higher detection limits and deemed suitable here since all samples were limited and presumably having quite low analytes concentration for each biomass contained in Ring A that was less than 10 g.

The oven of GC component of Perkin Elmer Clarus 560 was heated from room temperature to 40°C and held constant at this temperature for 10 minutes. The temperature was then ramped at 5°C/min to 300°C, after which it was held constant for 15 minutes. The vapourised analytes were then transferred to the MS component and mass spectral detection was set within the range of 50 to 500 Dalton, where Dalton is a commonly used non SI mass unit in mass spectrometry, equivalent to 1/12 of the mass of carbon isotope ^{12}C . Identifies of components were estimated from the NIST2008 Library and by consultation with the literature.

3.3.3.2 TGA Analysis of Filters

As for the filter papers, thermogravimetric analysis (TGA) was also performed using the Shimadzu TGA-50 equipment (see **Figure 3. 67**). The preparation for filter paper TGA analysis was different from that of combustion kinetics determination with TGA Q5000 equipment. Here, filter paper with emissions folded in (see **Figure 3. 68**) was wound by a platinum wire instead of using platinum pans before hooking to the equipment hang down.

Upon obtaining the consistent weight of emissions filled filter paper, the TGA temperature programme was started by ramping at 20°C/min from room temperature to 105°C. It was held constant for 5 minutes before ramping to 550°C at the 20°C/min in nitrogen atmosphere. At the temperature ramping step, volatile matters (VM) from the emission was obtained. The TGA was then changed to air atmosphere and the temperature was held constant at 550°C for 10 minutes. This enabled determination of fixed carbon (FC) from filter paper. The TGA programme ended with holding the temperature at 560°C for 10 minutes. It should be noted that the same TGA programme was conducted on emission-free, new filter paper and the net volatile matter (VM) and fixed carbon (FC) from the emission-filled filter paper was obtained by the difference. This thermogravimetric analysis on filter paper was to predict the ratio of black carbon or elemental carbon (EC) and organic carbon (OC) contained in PM retained by the 37 mm GF/F filter paper.



Figure 3. 67 Shimadzu TGA-50 Equipment

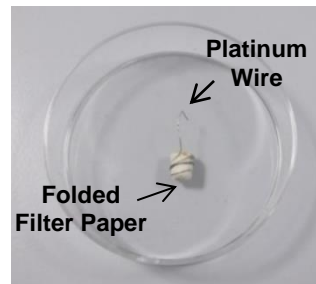


Figure 3. 68 Filter Paper Preparation for Shimadzu TGA-50

3.3.4 Lower Flammability Limits

As mentioned in **Section 2.7**, an LFL gives indication of volatiles ignition risk, greater risk when LFL is low. In a study about low temperature ignition of biomass by Jones et al., the FG-BioMass model had been applied to estimate biomass pyrolysis volatile mixture concentration (Jones et al., 2015) and enable the calculation of lower flammability limits

(LFLs) of each volatile mixture by using the Le Chatelier's principle. The equation for calculation using the Le Chatelier's principle is as follows:

$$LFL_{mix} = \frac{1}{\sum_{i=1}^n \frac{y^i}{LFL_i}}$$

where y^i = mole fraction of the i^{th} species and LFL_i = Lower flammability limit of the i^{th} species.

The LFL values for each major volatile components (LFL_i) are shown in **Table 3. 1** With these values, the LFL (% in air) for all the eight samples were calculated.

Table 3. 1 LFL for Major Volatile Components from Eight Biomass Samples

Volatile Component	Chemical Formula	LFL (vol% in air)
Acetaldehyde	C ₂ H ₄ O	310
Acetic Acid	C ₂ H ₄ O ₂	5.4
Acetone	C ₃ H ₆ O	2.6
Ammonia	NH ₃	15
Carbon Monoxide	CO	12.5
Ethylene	C ₂ H ₄	2.7
Formaldehyde	CH ₂ O	7
Formic Acid	CH ₂ O ₂	18
Hydrogen Cyanide	CHN	5.6
Methane	CH ₄	5
Methanol	CH ₄ O	6.7
Phenol	C ₆ H ₆ O	1.7

Chapter 4

Handling – Biomass Dust Layer Ignition Characteristics

In almost all industrial environment, formation of combustible dust is unavoidable and there are various definitions of on combustible dust, as described in **Chapter 2**. In industrial factories, hot surfaces come from lighting and machines but for a power station, the fire risk from dust deposition on hot surfaces could be even higher because of the combination of using a dusty fuel and since there are many hot machineries handling solid fuels to be combusted in high temperature furnaces later. Often, this risk leads to a far more dangerous explosion risk in the plant as the ignition from hot surfaces serves as the source that triggers massive explosions. In line with applying green technology in power generation, using alternative fuels, for instance biomass solid fuels in power generation are practised in many power stations since this deemed to be a means that will defer the global warming effect. Co-firing biomass with coal had been practised for quite some time and now fully firing biomass had been tried and is practised by some power stations around the world, e.g. Drax, Ironbridge and Lynemouth in U.K., Gardanne in France, Hasselby CHP in Sweden, Atikokan in Canada, Yeong Dong in Korea (Doosan, 2014). In the U.K., firing 100% biomass is very much encouraged from the attractive prices and increasing tariffs provided under the Renewable Obligation (RO) scheme introduced since April 2002 that resulted in the dramatic increase in biomass firing percentage in 2002-2005 period (Livingston et al., 2016).

The solid biomass fuel commonly used in U.K. power stations had been identified as softwood (especially pine), miscanthus and wheat straw, from two major groups of vegetation – woody and herbaceous, with pine in the woody group and the rest in herbaceous. In this study, all biomass samples were received from different power stations and it is worth noting that miscanthus had been received in different batches, in two different forms and from two different places; the one in pellet form was named Miscanthus(1) and the other in powder form called Miscanthus(2) to distinguish them in this study.

Besides materials characterisation via proximate and ultimate analyses, the calorific values, ranking of ignition risk and determining the minimum dust layer ignition temperature (termed T_{LIT} henceforth) of these solid biomass fuel regularly used in U.K. power stations were investigated. The original form of biomass samples received and their respective compositions are tabulated in **Table 4.1**. Adhering to the requirements stated in different standards, all the four single-material (termed parent materials hereafter) samples were prepared according to the procedures outlined in **Chapter 3** – drying, milling and sieving.

Table 4.1 Four Main Samples Used – Original Form Received and Composition

Sample Name	Original Form Received	Composition (wt%)
Miscanthus(1)	Pellet	100% miscanthus pellets
Pine	Powder	100% pine
Miscanthus(2)	Powder	100% miscanthus stem
Wheat Straw	Powder	100% wheat straw

Depending on the biomass fuel supply, it is possible that a power station fires more than just a single kind of biomass throughout its operation. It is therefore not surprising that dust accumulations in various locations in a power station are made up of blends of different biomasses since biomass supply relies on availability. Since biomass is the focus of this study, impacts of having biomass dust blends in different weight ratios depositing on hot surfaces were looked into as well.

As a start, binary blends of woody-herbaceous biomass dust at two different woody to herbaceous weight ratios (90wt% to 10wt% and 50wt% to 50wt%) were examined. There were six binary woody-herbaceous blends being investigated here and the names of the blends with their respective compositions are tabulated in **Table 4.2**. The nomenclature of PM(1)9010 simply means woody pine and herbaceous miscanthus(1) blend with 90 wt% of pine and 10 wt% of miscanthus(1), with the last four digits representing the weight percentages. The other blends followed the same naming pattern. In preparation for experiments, the six blends were formed by mixing the right proportion of pulverised dust that had been sieved following the procedures described in **Chapter 3**.

Table 4.2 Composition of Six Woody-Herbaceous Biomass Binary Blends

Biomass Sample	Composition (wt%)
PM(1)9010	90% Pine & 10% Miscanthus(1)
PM(1)5050	50% Pine & 50% Miscanthus(1)
PM(2)9010	90% Pine & 10% Miscanthus(2)
PM(2)5050	50% Pine & 50% Miscanthus(2)
PWS9010	90% Pine & 10% Wheat straw
PWS5050	50% Pine & 50% Wheat straw

4.1 Proximate, Ultimate Analyses and Higher Heating Values

Following the methodology described in **Chapter 3**, sample characterisation that involved proximate and ultimate analyses were conducted following the appropriate standards and using the suitable equipment. The results of proximate analysis are shown in

Table 4.3. As seen from the results, the moisture and ash contents varied between ~1 to ~3 wt% and ~2 to ~5 wt% respectively on an as-received basis whereas the volatile matters (VM) and fixed carbon (FC) ranged from ~82 to ~87 wt% and ~13 to ~18 wt% respectively on dry-ash-free (daf) basis. Among the four single-material parent samples experimented, VM (daf basis) of the three herbaceous biomass were slightly higher than that of the sole woody biomass sample in this study. The woody biomass (i.e. pine), on the other hand, showed relatively higher FC content on daf basis than the three other herbaceous biomass samples, (i.e. miscanthus in either form and wheat straw). The results were consistent with a biomass overview mentioned by bioenarea (2016), in which it had been generalised that herbaceous biomass have volatile matters in 70-85% range whereas woody 60-80% on daf basis.

Considering the possibility that several species of solid fuel dust occurred altogether in various places in an industrial environment, the proximate analysis results of the binary blends of six woody-herbaceous mixture are included in

Table 4.3. On dry-ash-free basis, the blends showed VM and FC contents that ranged from ~82 to 88 wt% and ~13 to ~18 wt% respectively. Comparing the VM and FC of two blends, VM of the 5050 ratio was marginally higher than the 9010 counterpart that had slightly more woody biomass in its composition whereas the FC showed an opposite trend in which the 9010 ratio showed somewhat a higher value than shown in the 5050 counterpart. Differences are small, however, and the VM and FC composition values found in this study varied in a very narrow range.

Table 4.3 Proximate Analysis of Four Parent Materials and Six Binary Blends Studied

Biomass Sample	Moisture (ar) (wt%)	Volatile Matter (daf) (wt%)	Fixed Carbon^d (daf) (wt%)	Ash (ar) (wt%)
Miscanthus(1)	3.27 ± 0.51	83.76 ± 0.65	16.24 ± 0.86	5.54 ± 0.37
Pine	2.80 ± 0.30	81.85 ± 0.52	18.15 ± 0.61	4.17 ± 0.08
Miscanthus(2)	1.13 ± 0.65	87.31 ± 0.23	12.69 ± 0.66	2.39 ± 0.26
Wheat Straw	1.90 ± 0.31	86.10 ± 0.23	13.90 ± 0.60	5.36 ± 0.50

Biomass Sample	Moisture (ar) (wt%)	Volatile Matter (daf) (wt%)	Fixed Carbon^d (daf) (wt%)	Ash (ar) (wt%)
PM(1)9010	3.56 ± 0.72	83.99 ± 0.44	16.01 ± 0.75	3.58 ± 0.63
PM(1)5050	2.11 ± 0.89	84.98 ± 0.51	15.02 ± 0.52	2.98 ± 0.72
PM(2)9010	2.61 ± 0.85	85.47 ± 0.54	14.53 ± 0.56	2.10 ± 0.55
PM(2)5050	2.59 ± 0.79	87.62 ± 0.61	12.38 ± 0.72	3.11 ± 0.31
PWS9010	2.72 ± 0.42	85.03 ± 0.51	14.97 ± 0.68	3.59 ± 0.34
PWS5050	1.65 ± 0.61	85.41 ± 0.68	14.59 ± 0.38	4.51 ± 0.37

^d by difference

The elemental analysis results are shown in **Table 4.4**. The sulfur content was not detected in all parent and blended samples, it could be either the samples did not contain any sulfur or the sulfur content was too low beyond the detection capability of the equipment. After expressing the contents of each element on dry basis (db) following the conversion formulated in BS EN 15104 standard (British Standard, 2011), the higher heating values (HHV) from these materials were predicted using a correlation from Friedl et al. (2005) as described by **Equation 3.10** in **Chapter 3**. The calorific values of the four parent materials varied in a small range of ~17.5 to ~18.6 MJ/kg, with the highest for pine and lowest for wheat straw. After blending, the 90woody:10herbaceous showed a slight HHV surplus as compared with respective 50woody:50herbaceous counterparts. The estimated HHVs for the six blends fell within a small range of ~17.9 to ~18.3 MJ/kg. The difference was rather minor among the six woody-herbaceous biomass blends. Considering all the parent materials and their blends, the calorific values varied within a small range that was not more than 1.5 MJ/kg.

Table 4.4 Ultimate Analysis of Four Main Samples and Six Binary Blends Studied Used (dry basis)

Biomass Sample	C (wt%)	H (wt%)	N (wt%)	O (wt%)	HHV^x (MJ/kg)
Miscanthus(1)	48.57 ± 0.09	6.6 ± 0.1	0.691 ± 0.006	44.140 ± 0.006	18.22
Pine	48.9 ± 0.8	6.50 ± 0.04	1.05 ± 0.02	43.6 ± 0.9	18.67

Biomass Sample	C (wt%)	H (wt%)	N (wt%)	O (wt%)	HHV^x (MJ/kg)
Miscanthus(2)	46.6 ± 0.7	6.26 ± 0.04	0.252 ± 0.004	46.9 ± 0.6	18.03
Wheat Straw	46.7 ± 0.6	6.58 ± 0.03	0.618 ± 0.003	46.1 ± 0.6	17.53
PM(1)9010	47.71 ± 0.03	6.5 ± 0.2	0.968 ± 0.009	44.8 ± 0.2	18.32
PM(1)5050	47.19 ± 0.3	6.4 ± 0.1	0.842 ± 0.005	45.6 ± 0.2	18.22
PM(2)9010	46.9 ± 0.5	6.38 ± 0.04	0.944 ± 0.006	45.8 ± 0.5	18.30
PM(2)5050	47.23 ± 0.5	6.60 ± 0.04	0.640 ± 0.002	45.5 ± 0.5	18.20
PWS9010	47.4 ± 0.7	6.8 ± 0.1	0.893 ± 0.01	44.9 ± 0.8	18.21
PWS5050	47.3 ± 0.4	6.57 ± 0.06	0.65 ± 0.05	45.5 ± 0.4	17.94

^x Correlation estimated

The calorific values for the four parent materials were later validated with bomb calorimeter experiments and HHV results from both methods are shown in **Table 4.5**. The difference between the correlation estimated and bomb calorimeter determined HHV varied less than ± 0.3 MJ/kg, thus the correlation estimated HHV approach was applied in this study hereafter.

Table 4.5 HHV (on Dry Basis) of Four Parent Materials Used

Sample Name	HHV^x (MJ/kg)	HHV^y (MJ/kg)	Difference (MJ/kg)
Miscanthus(1)	18.22	18.10	0.12
Pine	18.67	18.50	0.17
Miscanthus(2)	18.03	18.30	0.27

Sample Name	HHV ^x (MJ/kg)	HHV ^y (MJ/kg)	Difference (MJ/kg)
Wheat Straw	17.53	17.70	0.17

^x Correlation estimated ^y Bomb Calorimetry determined

4.2 Self-Ignition Propensity Risk Ranking

Biomass self-ignition propensity had been illustrated graphically (see **Figure 3. 18(a) &(b)**) by Ramírez et al. (2010) and later modified by Jones et al. (2015) in a study on low temperature ignition of various biomass samples. Both plotted a temperature when maximum thermogravimetric mass loss rate occurred in respective thermogravimetric runs (T_{charac} for the former and T_{MWL} for the latter) on the y-axis and assuming an Arrhenius function, the first order reaction rate kinetics was applied to calculate the apparent reaction activation energy E_a (to be plotted on the x-axis) for the combustion reaction simulated in the TGA. Looking at the x-axis of both ignition risk ranking plots, as the reaction activation energy increases, the safer the material is from being easily ignited as more energy is required to start the reaction; as for the y-axis, as the maximum mass loss rate temperature increases, implying higher temperature is required to provide the energy needed such that a material could gain enough kinetic energy to initiate an ignition reaction and therefore the material is relatively safer than those showing lower TGA maximum mass loss rate temperature.

In this study, the latter method from Jones et al. had been adopted, with reaction T_{MWL} obtained from TGA experiment plotted on y-axis and activation energy E_a on the x-axis. The E_a was calculated from the gradient of linearised Arrhenius equation (plot of $\ln k$ versus $1/T$ of a particular reaction) as detailed in **Chapter 3** and the results are tabulated in **Table 4.6**. With these values, each data point was defined and plotted on the risk ranking chart, as shown in **Figure 4.1**.

Table 4.6 Thermogravimetric T_{MWL} and E_a of Four Parent Materials and Six Binary Blends

Biomass Sample	T_{MWL} (°C)	E_a (kJ/mol)
Miscanthus(1)	268	84.87
Pine	280	69.62
Miscanthus(2)	283	85.40

Biomass Sample	T_{MWL} (°C)	E_a (kJ/mol)
Wheat Straw	249	75.40
PM(1)9010	280	74.03
PM(1)5050	274	81.03
PM(2)9010	281	60.07
PM(2)5050	281	78.64
PWS9010	282	85.96
PWS5050	280	84.76

As seen from the risk ranking chart, unfortunately none of the ten biomass samples fall into the low risk, not even the medium risk category; they all fall in the high risk category. Both risk ranking charts (by Ramírez et al. and Jones et al.) indicated that a material would be categorised in low self-ignition risk group when the temperature showed >350°C on the y-axis in combination with activation energy >94 kJ/mol on the x-axis.

According to a study on thermal behaviour and kinetics of solid fuels, Gil et al. (2010) found that the temperature at which maximum mass loss rate occurred on the TGA is actually inversely proportional to the reactivity and combustibility of a material. It implied that a lower T_{charc} or T_{MWL} signified an increased reactivity of the material. Applying the Arrhenius's concept of activation energy, if the combustion reaction of a particular material requires a lower activation energy than other materials, many molecules of this material could easily obtain enough kinetic energy upon heating to overcome the energy barrier (activation energy required) to transform from reaction reactants to products.

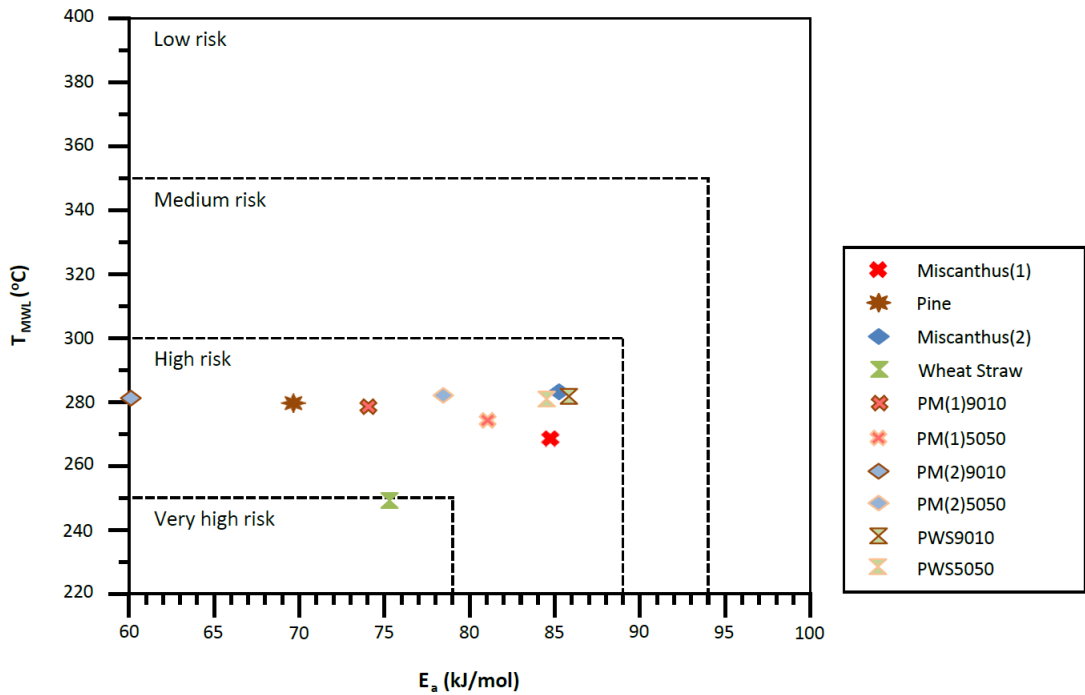


Figure 4.1 Self-Ignition Propensity Risk Ranking for Four Parent Biomass and Six Biomass Blends

The E_a calculated for the four parent samples ranged from ~ 70 kJ/mol to ~ 85 kJ/mol and the T_{MWL} obtained fell in a range of $\sim 248^\circ\text{C}$ $\sim 283^\circ\text{C}$. Wheat straw was the only sample that showed higher risk than three other parent samples in high risk category since it had the lowest T_{MWL} ($\sim 248^\circ\text{C}$) among all four parent materials.

Even for the six binary blends in two different weight ratios, their T_{MWL} and E_a ranged from ~ 274 to $\sim 282^\circ\text{C}$ and ~ 60 to ~ 86 kJ/mol respectively. This had led the blends to be grouped in the high risk self-ignition category. Blending the parent materials had not shifted the self-ignition risk tremendously, not making them safer or more dangerous – all were still high risk in self igniting. Though the border line wheat straw case had its self-ignition risk shifted from very high risk to high risk upon blending, there is not a great difference for wheat straw compared to its pine-wheat straw blends. From the results of all the ten biomass samples studied here, all their T_{MWL} and E_a was $< 300^\circ\text{C}$ and < 89 kJ/mol respectively, the biomass self-ignition risk was narrowly confined within a narrow risk group – high risk.

4.3 Minimum Ignition Temperature Determination, Ignition Delay Time Determination, Effects of Deposition Thickness

Although there are various different standards and practices in determining the minimum ignition temperature of a specific dust layer (termed T_{LIT} henceforth), the British Standard BS 50281-2-1 was followed closely in this study. Details about T_{LIT} and ignition delay time determinations in relation to this standard had been described in length in **Chapter 3**.

Prior to starting the dust layer, the temperature uniformity of the hot plate was checked following the process described in **Chapter 3**. The sixteen locations on the hot plate as described in **Chapter 3** had their temperatures consistency checked against the temperature set on the control and data acquisition block. **Figure 4. 2** illustrates an example of temperature plot at the sixteen locations when the hot plate was set at 295°C. As seen from the temperature plot, the temperature distribution was uniform with a calculated standard deviation of <1.7°C and thus, experiments to determine T_{LIT} of various biomass dust were initiated.

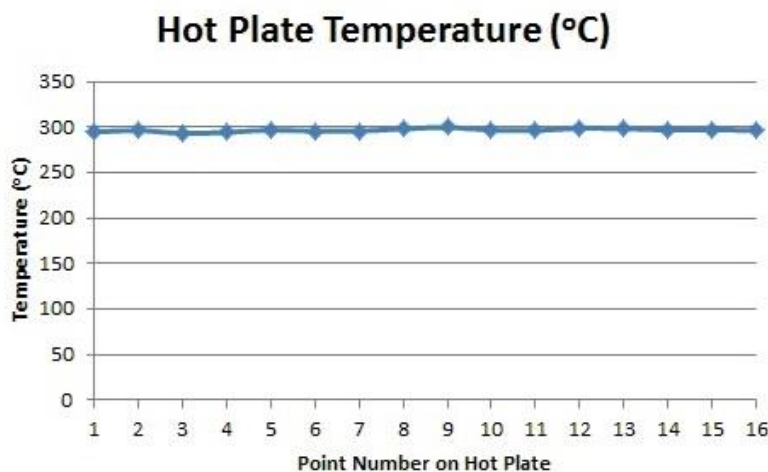


Figure 4. 2 Result of Temperature Uniformity Check on ANKO Dust Rig

Since the layer diameter (D) to layer depth (d) ratio was >5 in both Ring A (5 mm) and Ring B (12.5 mm) used in this study, one dimensional heat transfer in the axial direction could be safely assumed here, as done by Joshi (2012), Bowes and Establishment (1984), Anthony and Field (1975), Hensel et al. (1994), Dyduch and Majcher (2006). Considering major heat transfer happened in one direction (dominant in axial direction and a lesser extent in radial direction), when a dust layer was deposited on the hot surface, heat transfer occurred from the hot plate surface set at a certain high temperature to the dust layer surface that was exposed to atmosphere through the layer of dust material. The temperature of the dust layer increased as a result of heat flux passing through it and this

initiated chemical reactions within the dust layer. Heat was dissipated to the surroundings but at a particular hot surface temperature, the chemical reaction rate increased to an level that the heat transfer to the surroundings happened too slowly to compensate for the heat generated from the increasing chemical reaction within the layer. At this critical point, ignition of the dust layer happened.

The T_{LIT} obtained when materials were tested in shorter Ring A (5 mm height) and taller Ring B (12.5 mm height) and corresponding ignition delay times for the four parent materials are tabulated in **Table 4.7**. The reason for using a range of T_{LIT} was because a dust layer might ignite at any temperature within this 10°C range though ignition and non-ignition were confirmed at the upper limit and the lower limit respectively in this reported range. The values in bold are the upper limits that ignition was confirmed and the reported ignition delay time applied to that particular temperature.

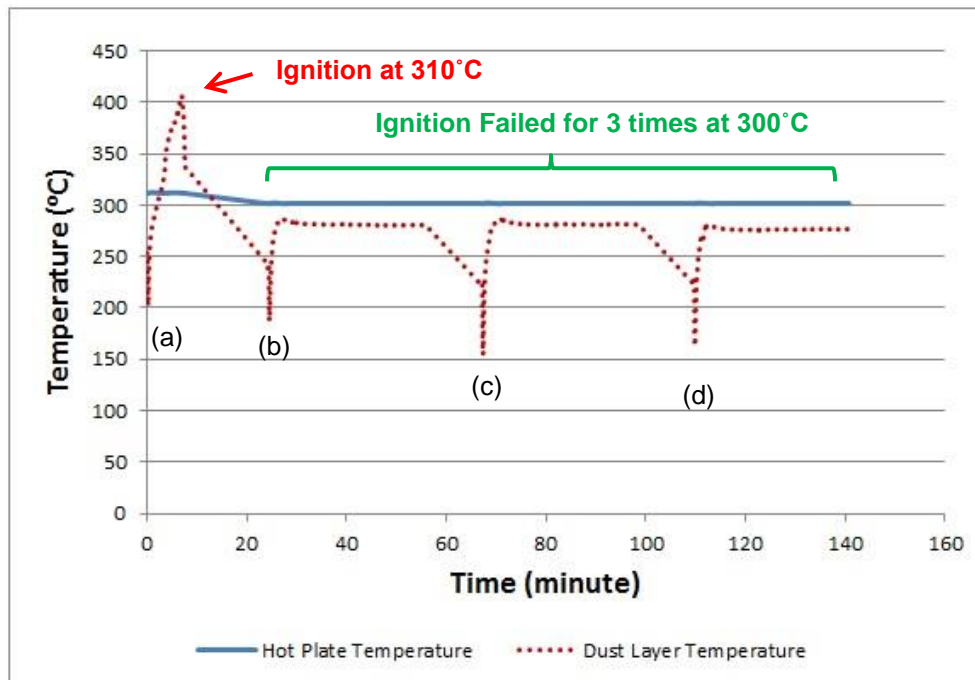
Table 4.7 Range of T_{LIT} (10°C Interval) and Corresponding Ignition Delay Time for Four Parent Materials

Biomass Sample	Minimum Dust Layer Ignition Temperature, T_{LIT} (°C) Range		Ignition Delay Time (min)	
	Ring A	Ring B	Ring A	Ring B
Miscanthus(1)	300- 310	270- 280	2.40	14.42
Pine	300- 310	270- 280	8.20	16.07
Miscanthus(2)	340- 350	290- 300	3.10	20.33
Wheat Straw	300- 310	270- 280	3.50	14.20

From the temperature range results with confirmed ignition at the upper limit, T_{LIT} of biomass was found to be confined in a very narrow ignition range of 310-350°C for the 5 mm Ring A. Three out of the four parent materials showed the same T_{LIT} value (310°C and 280°C for Miscanthus(1), Pine and Wheat straw) when contained in Ring A and Ring B respectively, though the ignition delay time differed.

An example of the temperature-time plot for wheat straw dust from the T_{LIT} determination experiment is displayed in **Figure 4. 3**. The red-dotted spike in the figure shows an increase in dust layer temperature relative to the hot plate temperature when it was set at 310°C (hot plate temperature was represented by the blue line). Besides noting higher dust layer temperature than the hot plate on the plot, a red visible glow on the dust was observed too and the time taken when the first glow appeared was taken as the

ignition delay time (see **Chapter 3** for details). Applying the 10°C interval as suggested in the standard, when wheat straw ignited at 310°C hot plate temperature, the next hot plate temperature was reduced by 10°C, i.e. 300°C. When the fresh dust failed to ignite at 300°C after a minimum duration of 30 minutes, the same experiment was repeated for two other times at 300°C for non-ignition confirmation. It should be noted that fresh sample was used in each experiment, whether ignition occurred or had not.



- (a) Wheat Straw Dust Sample 1 – Hot plate temperature set at 310°C, ignition happened
- (b) Wheat Straw Dust Sample 2 – Hot plate temperature set at 300°C, 1st time no ignition
- (c) Wheat Straw Dust Sample 3 – Hot plate temperature set at 300°C, 2nd time no ignition
- (d) Wheat Straw Dust Sample 4 – Hot plate temperature set at 300°C, 3rd time no ignition

Figure 4.3 T_{LIT} Determination Experiment on Wheat Straw Dust in Ring A – Temperature-Time Plot

Following the standard, the dust that failed to ignite was left on the heated plate for a prolonged period of more than 30 minutes. In this study, dust that failed to ignite was left on the hot plate fixed at the first non-igniting temperature for >120 minutes duration. Miscanthus(1) dust contained in Ring B (with $T_{LIT, pre-refinement}$ of 280°C and $T_{LIT, post-refinement}$ of 275°C) was left on the hot plate set at the first non-igniting temperature i.e. 270°C. It was clearly seen that the dust layer temperature never exceeded the hot plate temperature. It was therefore concluded that Miscanthus(1) dust was not able to ignite at the first non-

igniting hot plate temperature even when the test duration was extended beyond 30 minutes, 180 minutes (3 hours) for this particular sample.

Since three out of the four parent materials showed the same T_{LIT} when contained in Ring A or Ring B, to distinguish material reactivity from the T_{LIT} view point, a refinement test was proposed and executed on the dust layers. Taking the example of 310°C as the T_{LIT} for three parent materials experimented in Ring A, since ignition failed for all at 300°C but glowed at 310°C , applying the bi-sectioning concept in mathematics, the midway temperature of 305°C was used to distinguish the reactivity among them and at the same time, the corresponding midway temperature ignition delay time was recorded as well.

The smaller temperature interval used that was halved from the suggested interval was based on a few reasons. This temperature refinement span was inspired by the works of Henderson and Tyler (1988) that studied on dual ignition temperatures for dust layer in which T_{LIT} was determined by bracketing within intervals of 5 or 10°C of the hot surface; Bowes and Townshend (1962) applied hot surface temperatures that differed by intervals of 5°C whilst investigating the characteristics of combustible dust igniting on hot surfaces. Furthermore, BS 50281-2-1 requires that the heated surface temperature to be constant within 5 K i.e. 5°C throughout the test period (British Standard, 1999b). The test rig used in this experiment had been manufactured according to the requirements in BS 50281-2-1. Therefore, it was sensible that the refined temperature span was not any smaller than the accuracy range which the equipment was designed for.

Similar T_{LIT} determination experimental procedures were carried out on biomass blends after the blending process described in **Chapter 3**. A sample of biomass blend, PM(1)5050 that ignited when contained in Ring A, is illustrated in **Figure 4. 4**. The T_{LIT} and ignition delay time results for four parent samples and six biomass blends before and after T_{LIT} refinement test are tabulated in **Table 4.8**.

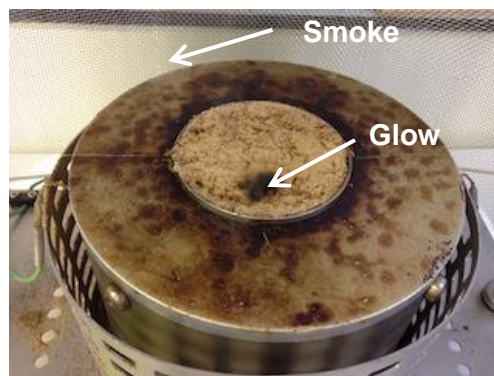


Figure 4. 4 T_{LIT} Experiment on PM(1)5050 Dust in Ring A – Ignited at 310°C

For all the ten samples (four parent materials and six binary blends), whether contained in short Ring A or taller Ring B, whether ignition occurred or failed, smoke of different colours were observed. In igniting cases, some yellowish-grey smoke was seen as compared with a lesser extent of whitish-grey smoke emitted in non-igniting cases, in the beginning of the dust layer experiments.

Table 4.8 T_{LIT} and Corresponding Ignition Delay Time for Four Parent Materials and Six Blends Before (10°C Interval) and After Temperature Refinement (5°C Interval)

Biomass Sample	Before Refinement				After Refinement			
	Minimum Ignition Temperature, T_{LIT} (°C)		Ignition Delay Time (min)		Minimum Ignition Temperature, T_{LIT} (°C)		Ignition Delay Time (min)	
	Ring A	Ring B	Ring A	Ring B	Ring A	Ring B	Ring A	Ring B
Miscanthus(1)	310	280	2.40	14.42	305	275	6.42	22.53
Pine	310	280	8.20	16.07	310	280	8.20	16.07
Miscanthus(2)	350	300	3.10	20.33	345	300	7.97	20.33
Wheat Straw	310	280	3.50	14.20	310	275	3.50	17.07
PM(1)9010	310	280	7.32	19.30	305	280	12.10	19.30
PM(1)5050	310	280	3.98	13.08	305	280	7.25	13.08
PM(2)9010	320	290	4.87	12.45	315	285	4.87	19.72
PM(2)5050	340	300	3.12	10.08	335	295	4.85	13.43
PWS9010	310	280	3.43	21.73	305	280	10.50	21.73
PWS5050	310	280	4.12	18.98	305	280	6.12	18.98

Ring B used in this study was actually representing thicker dust layer accumulation in an industrial environment. Two obvious observations when compared with shorter Ring A that represented thin layer of dust deposition were that thicker dust layer reduced the minimum layer ignition temperature and lengthened the ignition delay time. These two observations were the same as seen by El-Sayed and Khass (2013) in a study on smouldering combustion of rice husk dusts on hot surfaces, where ignition time increased and ignition temperature decreased with increasing dust layer depth

The temperature observation is consistent with the heat transfer mechanism – as the dust layer thickness increases, there is more material therefore more obstruction for heat to dissipate to the surroundings. Due to difficulty in releasing heat to the environment, more heat is trapped easily within the layer, promoting heat generating exothermic chemical reaction and thus resulting in ignition at a lower temperature.

Dust layer thickness plays an important role in defining the T_{LIT} (Querol et al., 2006), (Henderson and Tyler, 1988) and (Babrauskas, 2003a). The Ring A and Ring B results obtained here show that as the dust thickness increases from Ring A thickness (5 mm) to Ring B thickness (12.5 mm), the corresponding T_{LIT} decreases, as expected. As for the ignition delay time, as the dust thickness increases from Ring A to Ring B, there is a longer ignition delay time, in line with findings from Jones et al. (2015) about an inverse relationship between sample ignition temperature and ignition delay time.

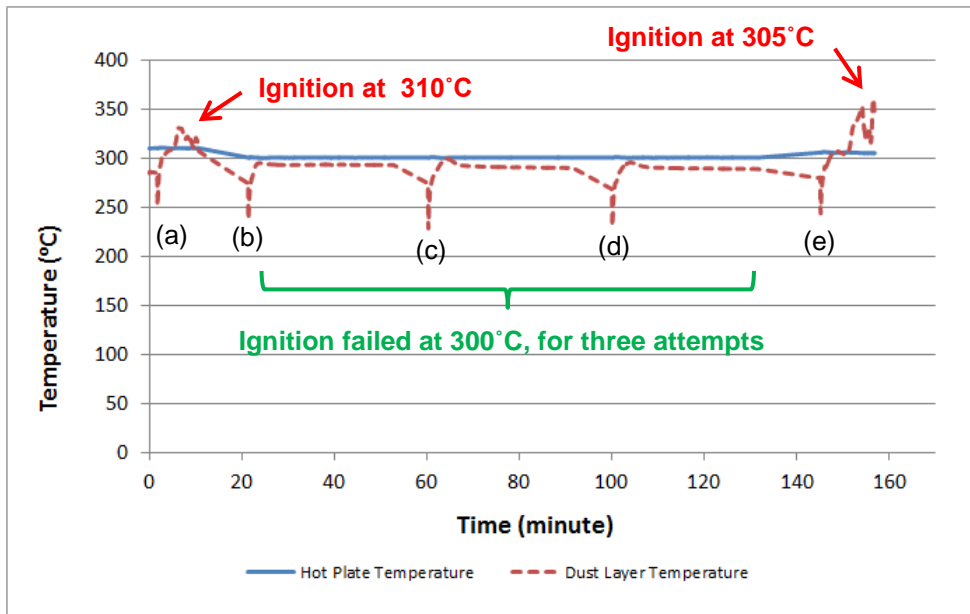
Besides the longer ignition delay time seen for ignition in Ring B as compared with Ring A, evident in **Table 4.8**, the ignition delay time is longer if a material ignited at the midway refinement temperature, as compared to that before the refinement. Though not all biomasses ignited at the midway temperatures, for those that ignited, the ignition delay time was lengthier than the ignition temperature before refinement. Because of this 5°C reduction in temperature less energy is supplied to the sample, so chemical reactions happen at a slower rate within the dust layer and the material requires a longer period of time to gain enough energy for its exothermic combustion reaction and to start to glow i.e. ignite.

There was no particular defined pattern of increment observed for these ten materials in Ring A and Ring B before and after refinement. The three parent materials in Ring A showed the same T_{LIT} of 310°C before the refinement method was applied, Miscanthus(1) had the shortest ignition delay time whereas pine the longest. But when refinement test was performed at 305°C, miscanthus(1) showed a longer ignition delay time than when it was subjected to 310°C hot plate; this slightly lower temperature slowed down the chemical reaction and thus a longer duration was required to finally reach ignition. For this thin layer, pine and wheat straw remained unignited at 305°C.

Among the three parent materials studied in Ring B all but Miscanthus(2) showed the same T_{LIT} before temperature refinement. Miscanthus(1) and wheat straw were the most reactive since they ignited 5°C lower for Ring B. Pine was the only material that remained unignited during both Ring A and Ring B refinement test at the 5°C interval. Judging from the refinement test results, the reactivity of the three parent materials that showed T_{LIT} of 310°C for 5 mm layer was distinguished – Miscanthus(1) most reactive, followed by wheat straw and finally pine was the least reactive. This was consistent with findings before the refinement tests. The ignition delay time differentiates the reactivity of parent materials with the same 5 mm T_{LIT} – for example, miscanthus had the shortest ignition delay time whereas pine the longest, inspite of both having T_{LIT} of 300°C. This gives the reactivity ranking found previously , i.e, Miscanthus(1) > Wheat straw > Pine.

Considering material blends in Ring A before refinement tests, PM(1)9010, PM(1)5050, PWS9010 and PWS5050 had all ignited at 310°C, the same as the T_{LIT} of their parent materials. For the blend in which the T_{LIT} of each parent material differed, the minimum ignition temperature inclined towards that of the more reactive material which had ignited at a lower temperature. Using PM(2)9010 as an example, T_{LIT} was 310°C and 350°C for Pine and Miscanthus(2) respectively but was 320°C for PM(2)9010 blend, i.e. the temperature is much closer to the lower of the T_{LIT} of the Pine and Miscanthus(2). It is important and worth noting that the more reactive material would ignite the less reactive material, and this synergetic effect changes the overall fuel reactivity. This outcome was consistent with the work of Mortari et al. (2010) in a study about combustion of biomass-coal blends in which the more reactive biomass enhanced the reactivity of the less reactive material. The ignition temperature of both 50-50 and 25-75 bagasse-coal blends was 275°C, a temperature far from 427°C of coal alone but closer to 256°C of neat bagasse.

Figure 4. 5 shows a sample T_{LIT} determination experiment result of PWS9010 dust blend tested in Ring A. Both pine and wheat straw had shown the same Ring A T_{LIT} of 310°C before refinement application. The temperature-time plot is showing the scenario when the midway refinement procedure was applied. The PWS9010 dust in Ring A ignited when the hot plate was set at 310°C but failed all the three subsequent attempts at 300°C. Following the midway temperature refinement method, the hot plate temperature was then increased by 5°C from the non-igniting temperature to 305°C, which was in between the igniting and non-igniting temperatures. It was evident that PWS9010 ignited at 305°C from the temperature-time plot showing the red dotted line (representing the dust layer temperature) which exceeded the blue line (indicating constant 305°C hot plate temperature) and with glowing red spots observed on the dust layer surface.



- (a) PWS9010 Dust Sample 1 – Hot plate temperature set at 310°C, ignition happened
- (b) PWS9010 Dust Sample 2 – Hot plate temperature set at 300°C, 1st time no ignition
- (c) PWS9010 Dust Sample 3 – Hot plate temperature set at 300°C, 2nd time no ignition
- (d) PWS9010 Dust Sample 4 – Hot plate temperature set at 300°C, 3rd time no ignition
- (e) PWS9010 Dust Sample 5 – Hot plate temperature set at 305°C, ignition happened

Figure 4. 5 T_{LIT} Experiment (with Refinement Step) on PWS9010 Dust Blend in Ring A

Taking another material blend example, in which the parent materials had the greatest T_{LIT} difference, i.e. pine-miscanthus(2) blend, the effect of parent T_{LIT} and blending ratio was observed. When contained in Ring B, PM(2)9010 had T_{LIT} at 290°C. This PM(2)9010 blend had a lower T_{LIT} than that of miscanthus(2) alone (T_{LIT} of 300°C) but higher than 280°C of pine alone. This showed that the lower T_{LIT} constituent ignited the higher T_{LIT} constituent in a material blend. On the other hand, the PM(2)5050 which had equal proportion of pine and miscanthus(2) ignited at 300°C, at the same T_{LIT} as miscanthus(2) alone. This implies that T_{LIT} of a blend is not linearly proportional to the T_{LIT} of its constituent materials or the amount of its constituents. It is worth noting that there was a drastic difference (~two times) between the ignition delay times of pure miscanthus(2) and PM(2)5050 blend, 20.33 and 10.08 minutes respectively, even though both samples showed the same 12.5 mm T_{LIT} of 300°C when 10°C interval method was applied. However, in the 5°C interval refinement tests, the 50:50 blend showed T_{LIT} reduced to 295°C. Since 295°C is 5°C lower than 300°C, it was not surprising that the ignition delay time was 13.43 min, i.e. 3.35 min longer than when T_{LIT} was at 300°C. The reduced T_{LIT} at the refined stage made it clear that the pine parent had had caused the

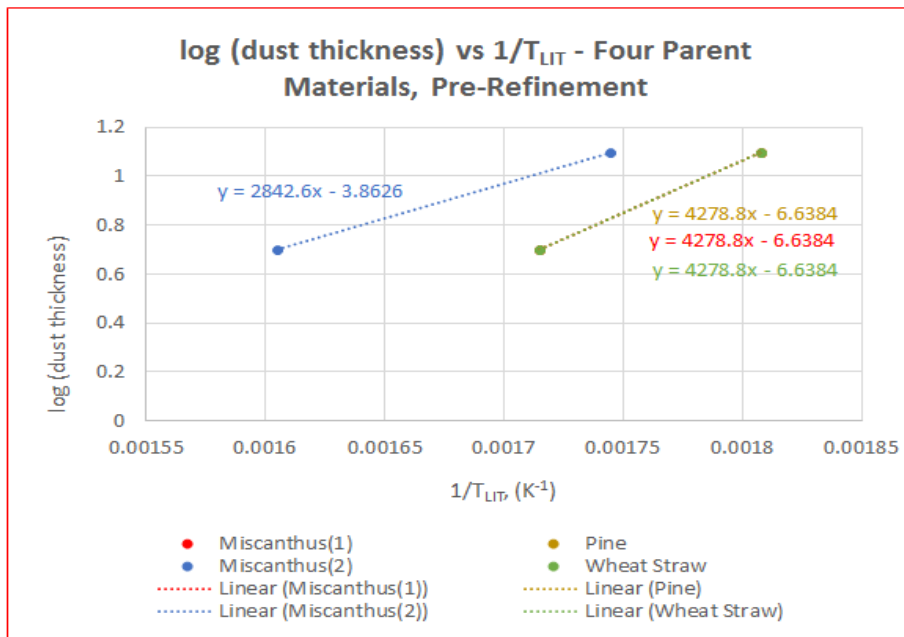
overall 50:50 blend to ignite at a lower temperature. By applying the refinement technique in the dust layer test, it was obvious that biomass dust reactivity assessment from the minimum layer ignition temperature could be achieved.

The finding that T_{LIT} decreases as dust layer thickness increases was consistent with results from a study of Polka et al. (2012) on seventeen dust samples, namely barley, beech, buckwheat, cornflakes, corn starch, dried carrot, flour, hop, lemon balm, malt, nettle, oatmeal, rice flakes, semolina, senna fruit, sunflower husk and valerian. These authors that used dust that had been sieved to below 200 μm mesh and followed closely the procedures outlined in BS 50281-2-1. According to that study, the 5 mm T_{LIT} of all the samples experimented ranged from 290 to $>400^\circ\text{C}$ but dropped to 250 to $>400^\circ\text{C}$ when the dust thickness was increased to 12.5 mm, with the temperature reduction varied for each sample. Reddy et al. (1998) in a study of solid fuel dust layer ignition, concluded that the minimum layer ignition temperature decreased as the dust layer increased in thickness. Also, it was observed that the induction time (analogous to ignition delay time in this study) increased as the solid fuel dust layer thickness increased. Engel et al. (2016a) had applied EN 50281-2-1 (Method A) to determine the minimum ignition temperature of dust layer contained in same-diameter ring but two different heights (5 mm and 12.5 mm). Four different sample dust – cellulose, wheat flour, cocoa powder and charcoal powder had been used. The 5 mm thick dust showed minimum ignition temperatures within 250 to $>400^\circ\text{C}$ but when the thickness increased to 12.5 mm, the ignition temperature dropped to 210 to 360°C . Pastier et al. (2013) examined the minimum dust layer ignition temperature of various wood dust (from particleboard and fibreboard industry, and sawdust resulted from poplar, spruce, alder and ash trees cutting) of 5 mm and 12.5 mm thick but of the same diameter, following EN 50281-2-1 procedures. The 5 mm T_{LIT} showed a very narrow range of $330\text{--}340^\circ\text{C}$ and dropped to a constant 12 mm T_{LIT} of 300°C .

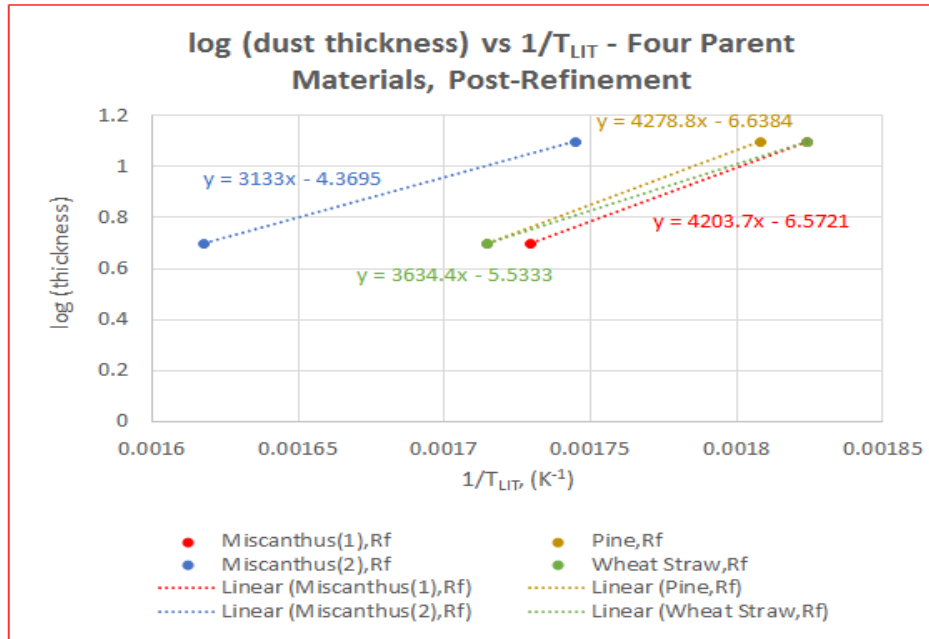
Querol et al. (2006) studied varying ring diameter from 10, 14, 18 to 26 cm for constant height and found that the T_{LIT} maximum change was $<40^\circ\text{C}$ for ~ 2 times increase in ring diameter. However, when the ring diameter was fixed, ~ 2 times increase in layer depth had caused the T_{LIT} to change $>40^\circ\text{C}$. Querol et al. concluded that the effect from increasing dust layer diameter was not as significant as increasing the dust layer thickness and also a very long test duration was required for large diameter and thick dust layers. Referring to the results of Querol et al. and coupled with findings from Henderson and Tyler (1988) and Babrauskas (2003a), the effects of altering the dust ring diameter on T_{LIT} and ignition delay time had not been considered in the present study.

According to BS 50281-2-1, T_{LIT} of unknown dust thicknesses can be estimated from the known T_{LIT} s obtained from experiments conducted, via a plot of logarithm of each dust layer thickness against the reciprocal of respective T_{LIT} in absolute temperature scale. An equation for $\log(\text{thickness})$ vs inverse T_{LIT} in Kelvin scale was generated for each of the

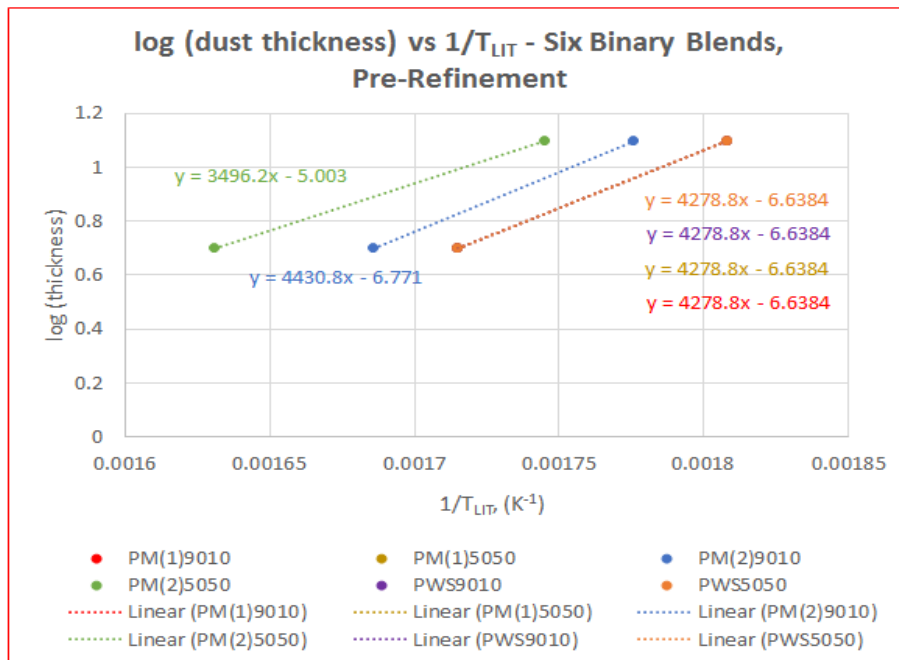
ten samples. With the linear equation found, the T_{LIT} of other untested dust layer thicknesses could be predicted by interpolation or extrapolation for a specific sample. The results of $\log(\text{dust thickness})$ vs $1/T$ (K^{-1}) for four single-material parent biomass and six binary biomass blends are shown in **Figure 4.6** after obtaining the T_{LIT} s from thin layer Ring A (5 mm) and thicker layer Ring B (12.5 mm) experiments, for both pre-refinement ($10^\circ C$ interval) and post refinement ($5^\circ C$ interval). The results of minimum dust layer ignition temperature as a function of its thickness obtained from some studies reviewed here are summarised in **Figure 4.7**. A linear relationship was consistently obtained from these studies when logarithm of dust layer thickness versus the inverse of minimum layer ignition temperature (T_{LIT}) in Kelvin scale was plotted. The results from this study fit well within the values obtained from these studies, as boxed in red in **Figure 4.7**. The linear equations predicted with both methods in this study were summarised in **Table 4.9**.



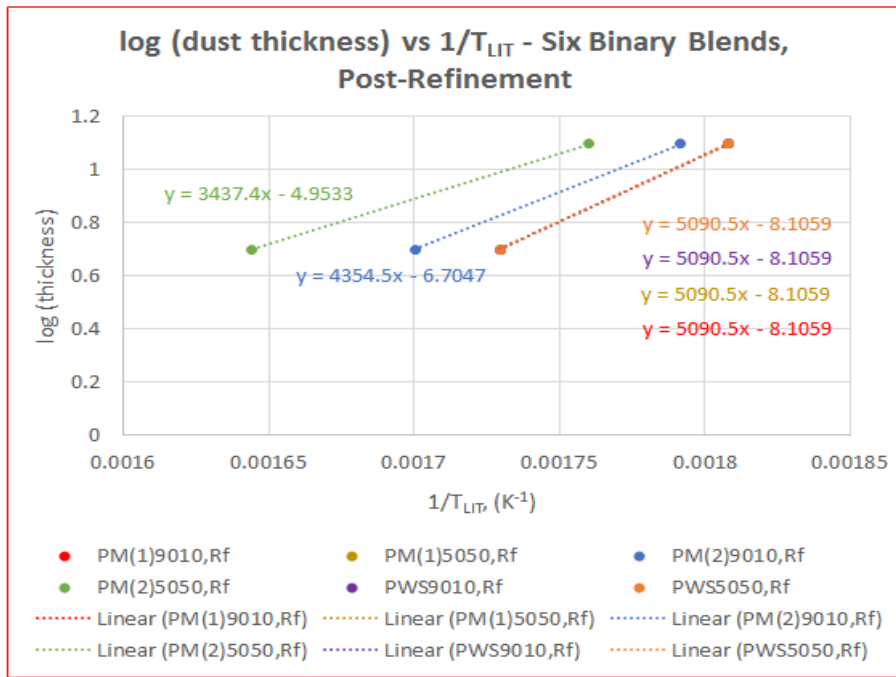
(a)



(b)



(c)



(d)

Figure 4.6 log(dust thickness) vs Inverse T_{LIT} in Kelvin scale for Ten Samples (a) Before T_{LIT} Refinement for Four Parent Materials (b) After T_{LIT} Refinement (c) Before T_{LIT} Refinement for Six Blends (d) After T_{LIT} Refinement for Six Blends

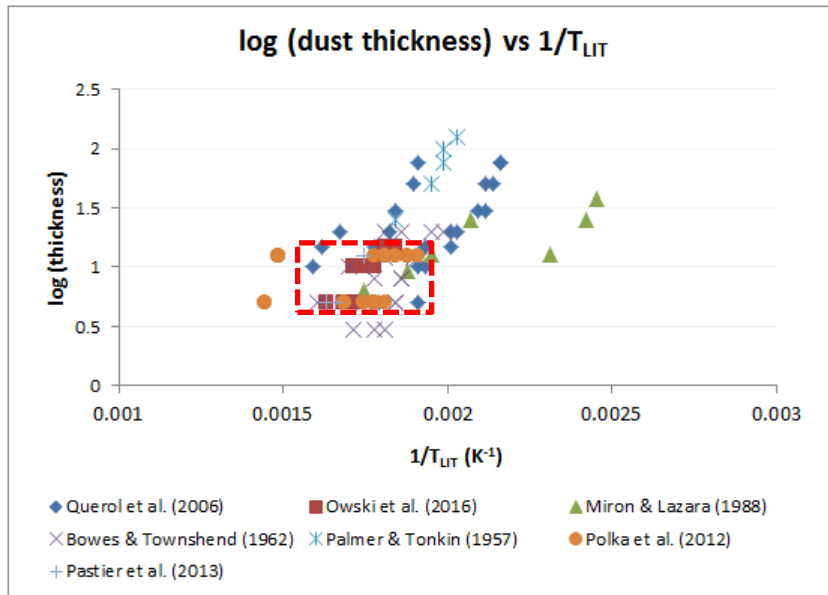


Figure 4.7 Results of Current Work Fitted Well on the log(dust thickness) vs Inverse T_{LIT} in Absolute Temperature Scale from Some Selected Studies

Table 4.9 Comparison of T_{LIT} Prediction Equations Before and After Temperature Refinement Process

Biomass Sample	Estimated Linear Equation for T_{LIT} Prediction of Other Dust Layer Thicknesses	
	Before Refinement Step	After Refinement Step
Miscanthus(1)	$y = 4278.8x - 6.6384$	$y = 4203.7x - 6.5721$
Pine	$y = 4278.8x - 6.6384$	$y = 4278.8x - 6.6384$
Miscanthus(2)	$y = 2841.6x - 3.8626$	$y = 3133.0x - 4.3695$
Wheat Straw	$y = 4278.8x - 6.6384$	$y = 3634.4x - 5.5333$
PM(1)9010	$y = 4278.8x - 6.6384$	$y = 5090.5x - 8.1059$
PM(1)5050	$y = 4278.8x - 6.6384$	$y = 5090.5x - 8.1059$
PM(2)9010	$y = 4430.8x - 6.6771$	$y = 4354.5x - 6.7047$
PM(2)5050	$y = 3496.2x - 5.0030$	$y = 3437.4x - 4.9533$
PWS9010	$y = 4278.8x - 6.6384$	$y = 5090.5x - 8.1059$
PWS5050	$y = 4278.8x - 6.6384$	$y = 5090.5x - 8.1059$

where y is $\log(\text{dust thickness})$, in mm; x is $1/T_{LIT}$, in K^{-1}

In general, these equations expressed the effect of dust thicknesses on the corresponding T_{LIT} . The equations predicted showed difference before and after refinement method whenever there was difference between the pre-refinement and post-refinement T_{LIT} obtained from experiments. Pine was the only material whose T_{LIT} remained constant before or after the refinement method (310°C and 280°C) thus it was the only material that had the equations unchanged, i.e. $y = 4278.8x - 6.6384$. As for the blends, since PM(1)9010, PM(2)5050, PWS9010 and PWS5050 had the same T_{LIT} s of 310°C and 280°C before refinement, therefore they shared the same equation – $y = 4278.8x - 6.6384$. Even after refinement, all the four had their T_{LIT} s changed to 305°C and 280°C, thus resulting in the same equation for the four of them, i.e. $y = 5090.5x - 8.1059$. These equations are applied to thicker dust layers in **Section 4.4**.

Querol et al. (2006) did recommend this method in predicting T_{LIT} for untested dust thickness from known results but as mentioned in BS 50281-2-1, the T_{LIT} for different dust layer thickness is preferred to be obtained from experiments though interpolation or extrapolation are possible ways.

4.4 Industrial Significance

With reference to the results shown in **Table 4.8**, for all the ten samples, T_{LIT} reduced by 30-50°C for Ring B when compared with values from Ring A. For instance T_{LIT} of Pine reduced from 310 to 280°C (30°C difference) when changed from Ring A to Ring B whereas Miscanthus(2) varied from 350 to 300°C (50°C difference) when altered from Ring A to Ring B. Using the 10°C interval, the T_{LIT} for the four parent materials and six blends ranged from 310 to 350°C (40°C range) when contained in Ring A but this T_{LIT} range was halved when these ten dust species were confined in taller Ring B, from 280 to 300°C (20°C range). When the refinement method with 5°C interval was applied, the range in T_{LIT} for the ten materials in Ring A remained at a 40°C (305 to 345°C) whereas that for Ring B had become 25°C, (275 to 300°C), i.e. the T_{LIT} range for these ten samples had become narrower as the dust thickness increased. The narrower range of T_{LIT} of different materials igniting in Ring B implies that as the dust layer gets thicker, the ignition temperature becomes less sensitive towards the material type and would ignite at lower temperatures regardless of the material. This trend is consistent with the MPST plot (see **Figure 2.5**) in BS 50281-1-2 – as the layer thickness increases towards 50 mm, the three curves showed a converging trend approaching an MPST that is not too varied. Therefore, routine cleaning of various power station locations is very much encouraged to avoid building-up of thick dust layers.

The maximum permissible surface temperature (MPST) was estimated using three different methods as described in **Chapter 2** i.e. Guideline1, Guideline2 and a practice in a U.K. power station. The pre-refinement 5 mm T_{LIT} was used (results displayed in **Table 4.8**) when applying Guidelines1 and 2. The MPST results are illustrated in **Figure 4.8**, with the three curves from Guideline2 as the illustration basis, Guideline1 points are superimposed onto the chart whereas the practice in a power station was represented with a dotted red line since the practice was a constant temperature maximum.

In this study, since the 5 mm T_{LIT} of all the ten samples ranged from 310 to 350°C, only the middle and bottom curves were applied when using Guideline2. If a 5 mm dust layer was deposited on an apparatus, for a sample showing 5 mm T_{LIT} of 310°C, the MPST calculated using Guideline1 was 235°C. When applying Guideline2, the bottom curve was used and the MPST was estimated to be ~175°C. The most conservative estimation still came from the power station that set at a constant MPST value of 150°C. If the maximum of the range i.e. 5 mm T_{LIT} at 350°C was considered, 275°C was the MPST calculated using Guideline1, ~200°C was estimated using the middle curve following Guideline2 and the power station estimate was still the most conservative. As observed in the figure, the 150°C limit set by the power station was most conservative when thin dust layers are deposited on hot surfaces, but became the most lenient when the dust deposit became thicker.

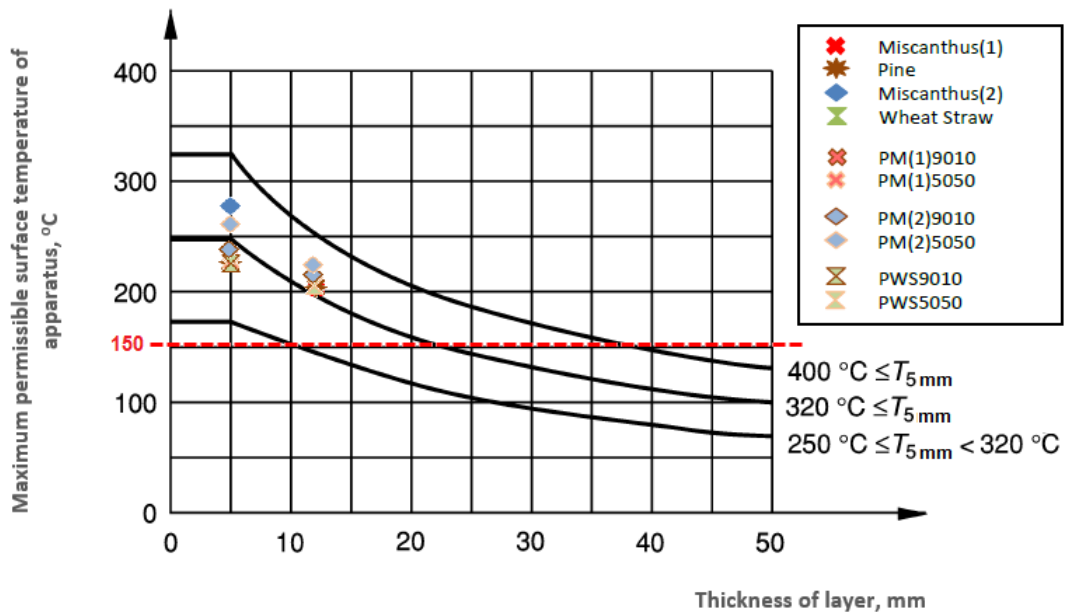


Figure 4.8 MPST Estimation with Three Different Methods – Guideline 1 (Points), Guideline 2 (Curves, T_{LIT} from Pre-Refinement) and Power Station Practice (Constant at 150°C)

Assuming the 5°C interval method was more accurate in predicting T_{LIT} of biomass, T_{LIT} predictions for 25 mm- and 50 mm-thick dust layers were made by applying appropriate equations summarised in **Table 4.9**. All 12.5 mm T_{LIT} s obtained from Ring B experiments and the predicted 25 mm and 50 mm T_{LIT} s were displayed in **Table 4.10**. The three thicknesses were selected since they are multiples of each other and 50 mm was the limit shown in the BS 50281-1-2 graph (British Standard, 1999a).

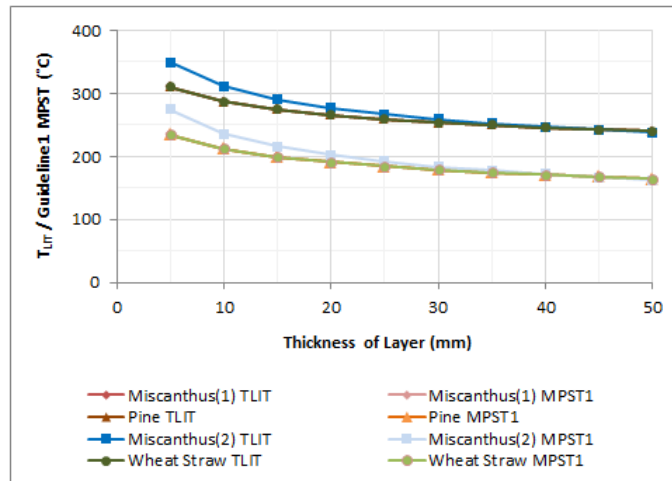
Table 4.10 T_{LIT} Obtained or Estimated for Three Dust Layer Thicknesses after Temperature Refinement Procedure

Biomass Sample	Experimented/Estimated T_{LIT} Using Predicted Equations (°C)		
	12.5 mm	25 mm	50 mm
Miscanthus(1)	275	254	235
Pine	280	259	240
Miscanthus(2)	300	270	243
Wheat Straw	275	251	229
PM(1)9010	280	262	246

Biomass Sample	Experimented/Estimated T_{LIT} Using Predicted Equations ($^{\circ}C$)		
	12.5 mm	25 mm	50 mm
PM(1)5050	280	262	246
PM(2)9010	285	264	245
PM(2)5050	295	268	244
PWS9010	280	262	246
PWS5050	280	262	246

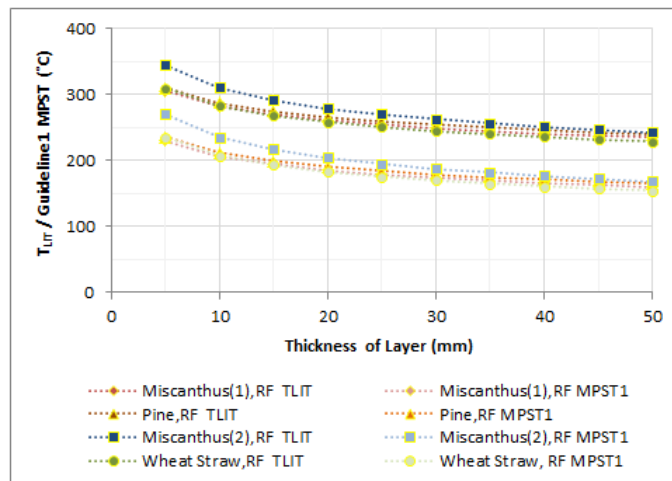
The results showed a trend that the T_{LIT} decreased when the layer thickness increased, as proven by the Ring A and Ring B results in this study and findings of layer thickness effect from other literatures (Querol et al., 2006), (Henderson and Tyler, 1988) and (Babrauskas, 2003a). For all these ten materials, among the three dust layer thicknesses chosen for comparison, as the thickness doubled, the T_{LIT} range became narrower. For 12.5 mm thick dust of all the ten materials, the lowest T_{LIT} was $275^{\circ}C$ where as the highest was $300^{\circ}C$, giving a range of $25^{\circ}C$. As the dust thickness doubled to 25 mm, the corresponding range reduced to $19^{\circ}C$ ($251^{\circ}C$ minimum and $270^{\circ}C$ maximum) and when the layer increased to 50 mm (two times of 25 mm thickness), the range decreased even further to $17^{\circ}C$ ($229^{\circ}C$ minimum and $246^{\circ}C$ maximum). It showed that when the dust thickness approached a certain threshold value, the T_{LIT} converge to a certain value regardless the biomass species. This is consistent with three converging curves in the BS 50281-1-2 graph for MPST estimation (British Standard, 1999a). Mathematically, the prediction performed here could have higher accuracy if more T_{LIT} points were plotted i.e. more layer thicknesses were experimented. As recommended in BS 50281-2-1 (British Standard, 1999b), if extensive prediction was intended, it would be good to determine ignition temperatures for more than two layer thicknesses, with emphasis on thicker layers.

Applying the equations tabulated in **Table 4.9**, T_{LIT} prediction for other thicker dust layers (up to 50 mm to be consistent with the thickness range in **Figure 4.8**) is plotted and illustrated in **Figure 4.9**. With reference to Guideline1 in MPST determination, the MPST values corresponded to every estimated T_{LIT} was shown in the same plot. As before, T_{LIT} decreases as layer gets thicker and both T_{LIT} and MPST values seem to converge to a certain temperature regardless the biomass species or blending effect. The results before of after temperature refinement procedure do not defer much.



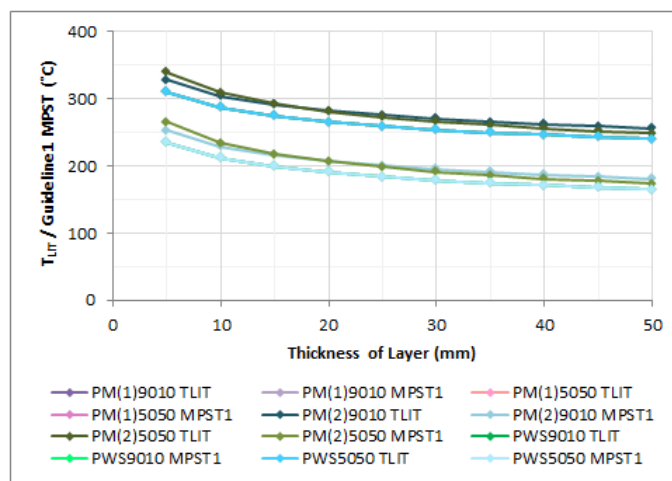
} T_{LIT}
} MPST,1

(a)



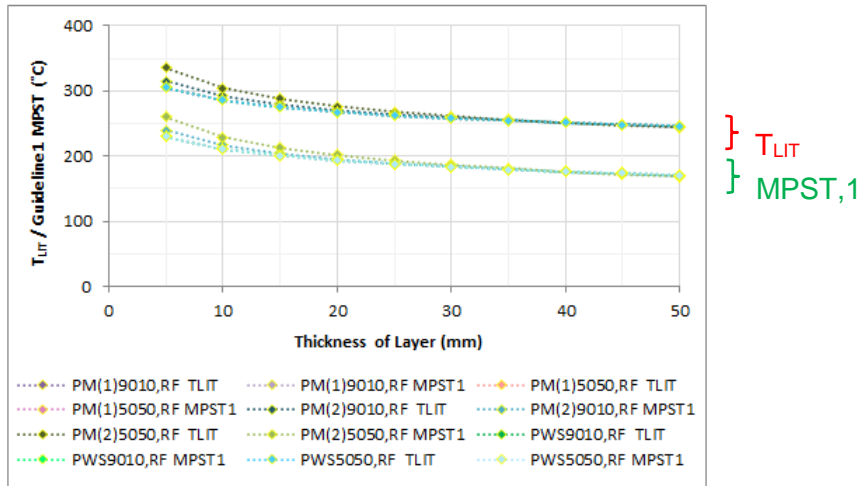
} T_{LIT}
} MPST,1

(b)



} T_{LIT}
} MPST,1

(c)



(d)

Figure 4.9 T_{LIT} and Guideline1 MPST Determined from **Table 4.9** Equations for Ten Samples (a) Before T_{LIT} Refinement for Four Parent Materials (b) After T_{LIT} Refinement for Four Parent Materials (c) Before T_{LIT} Refinement for Six Blends (d) After T_{LIT} Refinement for Six Blends

4.5 Concluding Remarks and Suggestions for Future Work

In general, it has been found that as the biomass dust layer thickness increased, the T_{LIT} reduced but the ignition delay time lengthened, in line with the work of other researchers. From the T_{LIT} and ignition delay time results of the six blends used here, it is evidenced that dust layers made up of a biomass mixture can be more reactive than dust layers that consist of individual constituent biomass. A more reactive blend component causes the overall blend to ignite at a temperature lower than when it appears alone, PM(2)9010 and PM(2)5050 were the best examples. It was possible to estimate T_{LIT} of certain dust thicknesses from known T_{LIT} values, but experimental determination was still preferred if the thickness variation was large.

From the various methods applied to determine Maximum Permissible Surface Temperature (MPST) of a plant equipment, the MPST was found to be less sensitive to material species as the dust layer thickness increased when the British Standard was used. Different methods had actually resulted in different level of conservativeness during MPST estimation and there is no hard and fast rule as to which method is the best – suitability depends on the application situation since a wide range of industry conditions exist.

Since the T_{LIT} lowered with increasing dust thickness and since there is an inverse relationship between the ignition temperature and ignition delay time, the small difference in ignition behaviour reported for these ten samples would be increasingly

significant for thicker dust layers. Provided the biomass dust layers deposited on hot surfaces were thin, no major changes on current plant management in terms of housekeeping operations or dust management need to be imposed since the T_{LIT} s obtained in this study were confined within a very narrow range.

There are some recommendations for future work that help understand potential fire risk originated from dust layer ignition. There are many possibilities to improve this current test in quest of dust T_{LIT} and the corresponding ignition delay time. Some alterations could be made on the current experiment setup that had been based on BS 50281-2-1, as follows:

Besides the recommended ambient temperature within 15 to 35°C stated in the standard, slightly warmer environment e.g. ~40°C could be used. This is consistent with hotter environment e.g. near boiler house in an industry. If possible, the effect of environment humidity might be assessed as well. In short, the dust layer test could be carried out in different controlled environments of varied ambient temperature-humidity combinations.

Other than using a metal ring, to contain the dust sample, this could be changed to insulating material like ceramic and changes to the T_{LIT} noted. With a low thermal conductivity ring, there may be effects on T_{LIT} and ignition delay time. Using a non metal ring to hold sample materials on the hot plate is similar to the work by Joshi (2012). Using solid metal rings of different wall thicknesses while retaining the internal diameter could be applied to hold sample dust and the temperature distribution could be counter checked with the help of an infrared camera. With this, the best experimental setup could be determined with a suitable ring wall thickness justified. Alternatively, a perforated ring that gives a ventilation effect could be used. This can be a method to check if atmospheric air drawn from the sides, entering via the tiny holes of the perforated ring would alter the T_{LIT} and ignition delay time of sample dust layer and if so, to what extent.

BS 50281-2-1 suggested dust particles that past through 200 μm to be used in the hot plate experiment. It is known from various literatures that particle size impacts T_{LIT} and ignition delay time, consequently it is worth segregating the dust of <200 μm further to different size categories. It could happen that the <50 μm dust ignites at a lower temperature because the dust density increases.

Besides using a flat hot plate as suggested in the standard, hot surfaces of other orientations e.g. wedge shape, ridged surface etc. could be used. This is to simulate all possible situations in the industry whereby hot surface may not be flat at all times. The resulted T_{LIT} can then be compared with that obtained from using the commonly used flat hotplate and a correlation might be derived.

Apart from using a hot plate to simulate a hot environment, localised hot spot introduced into a pool of dust could be applied too. This represents a possibility of fire outbreak whereby hot objects accidentally drop into combustible dust and initiate a fire. For instance a mechanical failure in which a faulty hot bearing drops onto a pool of raw materials awaiting further process . At lab scale, this scenario could be done by heating a piece of metal with known weight to a desired temperature, which was then dropped into a pool of sample dust. The critical metal temperature that caused an ignition e.g. instant flaring-up could be noted and, the smouldering degree of dust sample could be tracked by noting the amount/area of darkened particles.

Chapter 5

Handling – Effects of Binders on Biomass Dust Layer Ignition Characteristics

Binder material is sometimes added to a parent biomass during pellet production. Legislation prohibits pellet producers from using artificial binder in any form and natural binding results from frictional heating caused by pressure application (Atkinson, 2016), nevertheless additional binders may be added to improve pellet durability. A small amount of organic binder has been added to the parent materials in this study. The two binders of interest in this study were Ligno-Bond-DD powder and cornflour. It had been mentioned in the study of Tarasov et al. (2013) about additives effect on wood pellets that lignosulphonate, dolomite, starches, potato flour and peel, some motor and vegetable oils are common binders used in wood pellet production. The Ligno-Bond-DD powder used here consisted fully of lignosulphonate and was made up of soluble fibre from plant origin (Borregaard, 2016). Lignosulfonates, also known as sulfonated lignin are water-soluble anionic polyelectrolyte polymers and are usually found as byproducts of sulphite pulping production of wood pulp (Wikipedia, 2016), (Tarasov et al., 2013). The cornflour used here was just commercial cornflour or sometimes known as corn starch or maize starch. Tarasov et al. (2013) in a review on additives effect on wood pellets mentioned that usually 1-3% of lignosulphonate are used to effectively bind wood pellets. As practised in the industry, the amount of binder has never exceeded 2 wt% of the final biomass briquette or pellet weight (Engineer, 2015) and this amount was well within the range suggested by Tarasov et al. Here, the effect of having binders in biomass dust was studied to check if this would affect dust layer self ignition.

In this study, two different organic binders i.e. Ligno-Bond-DD powder and commercial cornflour added to four parent materials (miscanthus(1), pine, miscanthus(2), wheat straw) had been carried out. The samples were abbreviated as such: Misc for Miscanthus, WS for wheat straw, Lg for Ligno-Bond-DD powder, CF for cornflour and value 980 indicated that a material consisted of only 98% parent material. All the samples examined in this study are listed in **Table 5. 1** and had undergone the necessary preparation process as detailed in **Chapter 3**.

Table 5. 1 Samples Used in Binder Effect Study – Original Form and Composition in Weight Percent of Ten Samples

Sample Name	Original Form	Composition (wt%)
Miscanthus(1)	Pellet	100% miscanthus(1) <180 µm
Misc(1)Lg980	Powder	98% miscanthus(1) <180 µm + 2% Ligno-Bond –DD Powder
Misc(1)CF980	Powder	98% miscanthus(1) <180 µm + 2% Cornflour
Pine	Powder	100% Pine <180 µm
PineLg980	Powder	98% pine <180 µm + 2% Ligno-Bond-DD Powder
PineCF980	Powder	98% pine <180 µm + 2% Cornflour
Miscanthus(2)	Powder	100% miscanthus(2) <180 µm
Misc(2)Lg980	Powder	98% miscanthus(2) <180 µm + 2% Ligno-Bond-DD Powder
Misc(2)CF980	Powder	98% miscanthus(2) <180 µm + 2% Cornflour
Wheat Straw	Powder	100% wheat straw <180 µm
WSLg980	Powder	98% wheat straw <180 µm + 2% Ligno-Bond-DD Powder
WSCF980	Powder	98% wheat straw <180 µm + 2% Cornflour

5.1 Proximate, Ultimate Analyses and Higher Heating Values

Fuel characterisations for all samples were conducted following procedures in **Chapter 3**. These results are reported in the following **Table 5. 2**, **Table 5. 3**, **Table 5. 4** and **Table 5. 5** for proximate analysis results, ultimate analysis (all sample materials and binders only) and the estimated HHV results respectively.

Table 5. 2 Proximate Analysis of All Samples Used in Binder Effect Study

Biomass Sample	Moisture^a (wt%)	Volatile Matter^c (wt%)	Fixed Carbon^d (wt%)	Ash^a (wt%)
Miscanthus(1)	3.27	83.76	16.24	5.54
Misc(1)Lg980	2.40	83.59	16.41	7.34
Misc(1)CF980	1.71	84.83	15.17	6.67
Pine	2.80	81.85	18.15	4.17
PineLg980	3.94	81.28	18.72	6.73
PineCF980	3.54	81.04	18.96	6.64
Miscanthus(2)	1.13	87.31	12.69	2.39
Misc(2)Lg980	1.12	85.77	14.23	2.76
Misc(2)CF980	1.47	84.90	15.10	2.34
Wheat Straw	1.90	86.10	13.90	5.36
WSLg980	6.28	87.95	12.05	7.28
WSCF980	5.82	88.02	11.98	6.65

^a as received (ar) ^c dry-ash-free basis (daf) ^d by difference

Table 5. 3 Ultimate Analysis of All Samples Used in Binder Effect Study

Biomass Sample	C^c (wt%)	H^c (wt%)	N^c (wt%)	S^c (wt%)	O^d (wt%)
Miscanthus(1)	48.57 ± 0.09	6.6 ± 0.1	0.691 ± 0.006	N.D.	44.140 ± 0.006
Misc(1)Lg980	47.4 ± 0.3	6.37 ± 0.05	0.68 ± 0.01	0.12 ± 0.06	45.4 ± 0.4
Misc(1)CF980	47.00 ± 0.09	6.2 ± 0.8	0.655 ± 0.009	0.05 ± 0.07	46.08 ± 0.09
Pine	48.9 ± 0.8	6.50 ± 0.04	1.05 ± 0.02	N.D.	43.6 ± 0.9
PineLg980	48.60 ± 0.04	6.3 ± 0.3	1.4038 ± 0.0005	0.14 ± 0.04	43.6 ± 0.2

Biomass Sample	C^c (wt%)	H^c (wt%)	N^c (wt%)	S^c (wt%)	O^d (wt%)
PineCF980	47.8 ± 0.6	6.26 ± 0.07	1.402 ± 0.001	0.04 ± 0.05	44.5 ± 0.7
Miscanthus(2)	46.6 ± 0.7	6.26 ± 0.04	0.252 ± 0.004	N.D.	46.9 ± 0.6
Misc(2)Lg980	48.3 ± 0.5	6.31 ± 0.09	0.188 ± 0.001	0.104 ± 0.002	45.1 ± 0.6
Misc(2)CF980	47.7 ± 0.5	6.31 ± 0.01	0.198 ± 0.002	N.D.	45.8 ± 0.5
Wheat Straw	46.7 ± 0.6	6.58 ± 0.03	0.618 ± 0.003	N.D.	46.1 ± 0.6
WSLg980	47.6 ± 0.5	6.81 ± 0.06	0.96 ± 0.01	0.12 ± 0.04	44.6 ± 0.5
WSCF980	47.7 ± 0.3	6.773 ± 0.003	0.95 ± 0.02	N.D.	44.6 ± 0.3

^c dry-ash-free basis (daf) ^d by difference N.D. – not detected

Table 5. 4 Ultimate Analysis of Two Binders Used in Binder Effect Study

Binder	C^c (wt%)	H^c (wt%)	N^c (wt%)	S^c (wt%)	O^d (wt%)	Moisture^a (wt%)	Ash^a (wt%)
Ligno-Bond-DD	54.0 ± 0.4	6.64 ± 0.05	0.191 ± 0.001	7.0 ± 0.4	32.143 ± 0.003	5.90 ± 0.07	18.0 ± 0.4
Cornflour	42.2 ± 0.7	7.01 ± 0.04	0.04 ± 0.06	0.2 ± 0.6	50.6 ± 0.1	4.2 ± 0.2	0.3 ± 0.1

^a as received (ar) ^c dry-ash-free basis (daf) ^d by difference

Table 5. 5 HHV of Samples Used in Binder Effect Study

Sample Name	HHV (MJ/kg)	Change (%)
Miscanthus(1)	18.22	n.a.
Misc(1)Lg980	17.42	-4.4
Misc(1)CF980	17.4	-4.5
Pine	18.67	n.a.
PineLg980	18.03	-3.4
PineCF980	17.75	-4.9
Miscanthus(2)	18.03	n.a.
Misc(2)Lg980	18.63	3.3
Misc(2)CF980	18.45	2.3
Wheat Straw	17.53	n.a.
WSLg980	17.47	-0.3
WSCF980	17.64	0.6

^b dry basis (db) n.a. – not applicable

For proximate analysis, reported on dry-ash-free basis, the volatile matters and fixed carbon contents (see **Table 5. 2**) from samples with addition of either binder did not differ much from those of their respective parent sample. However, ash content was found to have increased with the addition of binder. Comparing samples from the same parent material but with either Ligno-Bond-DD (made up of lignosulphonate in this study) binder or cornflour binder, the one with Ligno-Bond-DD always showed ash increment more than the one with cornflour. This was related to the ash content of Ligno-Bond-DD binder alone that was much higher than that of cornflour alone, as seen in **Table 5. 4**. Ash increase with binder addition was actually not desirable. According to Mills (1908), one of the qualities desired in binder was that it did not increase the percentage of ash as this in return would increase unwanted clinker in boilers.

With binder material as little as 2 wt% added to the parent materials, the most significant change on elemental composition was sulfur content. From **Table 5. 3**, it can be seen that sulfur contents in all four parent materials were below or close to the detection limit. However, with only 2 wt% of either binder materials added to the parent biomass, the sulfur content of the blend became significant enough to be detected.

From the results of ultimate analysis, both binders showed sulfur content with Ligno-Bond-DD containing much higher sulfur when compared with cornflour binder. On dry-ash-free basis, Ligno-Bond-DD powder showed sulfur content of ~7 wt%, which was > 35 times higher than that contained in commercial cornflour that showed only ~0.2 wt%. Binding with Ligno-Bond-DD increased the overall sulfur contents to 0.10-0.14 wt% daf, whilst those with cornflour binder showed sulfur content of ≤ 0.05 wt% in two out of the four biomass materials studied. With the molecular formula of $C_{20}H_{26}O_{10}S_2$ (CAS Registry Number of 8062-15-5), it was not surprising that sulfur was detected in the elemental analysis of pure Ligno-Bond-DD binder. As for the commercial cornflour, the little bit of sulfur content most probably originated from the preservative additives (sulfur dioxide and sulphites) in the cornflour added to prevent microbial growth so that the cornflour does not degrade so soon. The chemical structure of both binders are illustrated in **Figure 5. 1**.

Based on these results from the elemental analysis of the two binders, it was therefore anticipated that sulfur dioxide emission would be higher from biomass dust with Ligno-Bond-DD binder compared to the respective counterparts with cornflour binder. This prediction was in line with findings in the study of Tarasov et al. (2013) about the effect of additives on physical and thermal characteristics of wood pellets. Here, in which wood pellets with lignosulphonate additives showed a significant increase in sulfur content and had therefore increased detection of SO_x emission. Ház et al. (2013) in a study on determination of temperature regions in thermal degradation of lignin had highlighted the popularity of commercial lignosulphonates in fuel materials processing. From the results of eight different lignosulphonate samples studied, the conclusion drawn emphasised the importance not to release any toxic emissions due to the sulfur content in lignosulphonate.

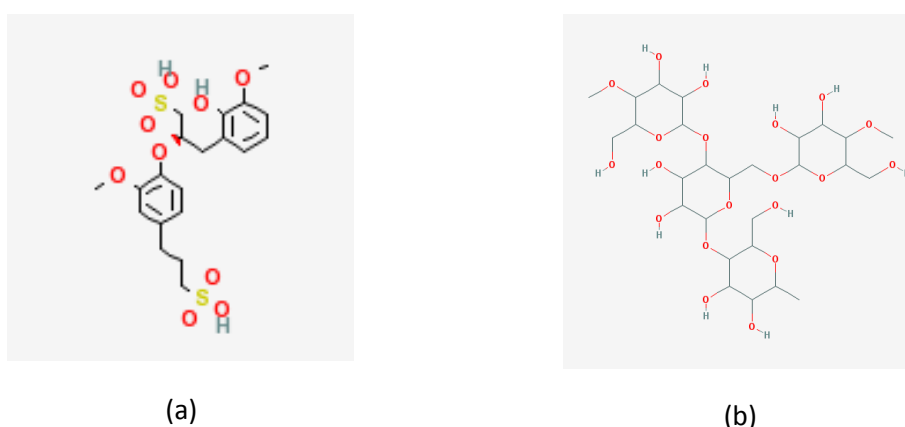


Figure 5. 1 Chemical Structure of (a) Lignosulfonate (ChemicalRegister, 2016) (b) Corn Flour (PubChem, 2016)

The higher heating value (HHV) for all the twelve materials were estimated using the correlation developed by Friedl et al. (2005) and the results are shown in **Table 5. 5**. The addition of binders did not significantly alter the elemental compositions of the fuels, therefore the HHVs calculated did not change much ($<\pm 5\%$). This finding was consistent with the trend found by Tarasov et al. (2013) in a study on additives and physical and thermal characteristics of wood pellets, in which it was found that additives like lignosulphonate, potato flour or potato peel residues did not significantly impact the calorific values of wood pellet though, there was a general trend of reduction. In this study, most of the samples with binder showed reduction in the predicted HHV; only three samples with binder i.e. Misc(2)Lg980, Misc(2)CF980, WSCF980 showed slightly higher HHV amounting to 3.3%, 2.3% and 0.6% respectively when compared with the binderless parent material. It should be noted that a small prediction error could have occurred since the effect from sulfur content had not been captured in the Friedl's HHV correlation.

According to Mills (1908), it is desirable that the heating value increases with binder addition such that the heat units obtainable from a certain weight of fuel were not reduced. The HHV results from samples with binder here showed very little change when compared with respective parent material and this had a minor effect on the heat units contributed by the same weight of fuel of parent sample or the sample with binder.

5.2 Self-Ignition Propensity Risk Ranking

The material self-ignition propensity risk was ranked following the method developed by Ramírez et al. (2010) and modified by Jones et al. (2015) and the pictorial risk ranking for twelve samples, four parent materials and eight materials with two different binders is shown in **Figure 5. 2**. As mentioned before, this modified version has the T_{MWL} from TGA combustion in air (instead of T_{charac} obtained from reaction in oxygen) and E_a for slow combustion plotted on the y-axis and x-axis respectively. T_{MWL} and E_a had been determined from the apparent first order reaction rate kinetics calculated using the method described in **Chapter 3**.

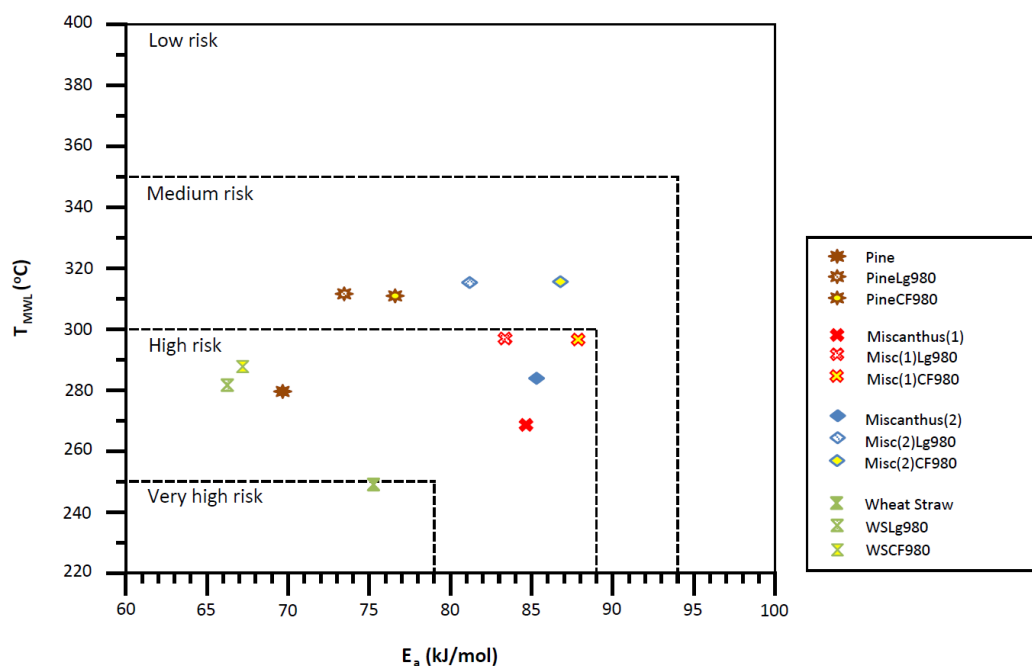


Figure 5. 2 Binder Effect – Self-Ignition Propensity Risk Ranking of Twelve Materials

As seen from the graphical self-ignition risk ranking plot illustrating binder effect, with a small amount (2 wt%) of binder in the samples, be it Ligno-Bond-DD powder or cornflour, the self-ignition risk of the sample with binder had reduced a little as compared with respective binderless parent material. For instance, wheat straw was the only sample found to exhibit very high risk in predicting the self-ignition risk, but with either binder added to wheat straw, the predicted self-ignition risk had reduced from ‘very high risk’ to ‘high risk’. Comparing between the effects of both binders, the T_{MWL} was found to be less than $\sim 10^\circ\text{C}$ difference and the E_a of each was quite close to each other. Pine and Miscanthus(2) without binder showed ‘high risk’ but for both the self-ignition risk improved to slightly safer ‘medium risk’ with the addition of binder. It should be noted that the T_{MWL} increased $\sim 20^\circ\text{C}$ when binder was added to pine and the E_a calculated for pine with Ligno-Bond-DD powder binder or cornflour binder showed a difference of ~ 7 kJ/mol between the them. Similar trend was observed in Miscanthus(2) with either binder – T_{MWL} of Misc(2)Lg980 and Misc(2)CF980 increased $\sim 20^\circ\text{C}$ whereas E_a with binders differed from that without binder by < 5 kJ/mol. The only material that had the self-ignition propensity risk predicted without much changes was Miscanthus(1), where the risk remained in ‘high risk’ category even with binder added into the sample. However, the two samples with binder showed their self-ignition risk much closer to the border of lower ‘medium risk’ category. It is good to note that addition of any of the two binders had only modest impact on their respective ignition risk and not increased the risk since all samples with binder were still in either ‘high risk’ or ‘medium risk’. It seems to show that the binders have imposed an inerting effect by lowering the reactivity of a biomass fuel.

5.3 Minimum Ignition Temperature Determination and Ignition Delay Time

Like the single-material biomass dust, the dust samples with either binder were subjected to dust layer ignition experiment using the ANKO rig applying the procedures outlined in **Chapter 3**. The determination of minimum temperature for dust layer ignition (T_{LIT}) of each sample contained in Ring A (5 mm thickness) and the corresponding ignition delay time were conducted and the result are displayed in **Table 5. 6**. Comparisons between the sample with and without binder and between samples with the same parent material but having different binders were carried out.

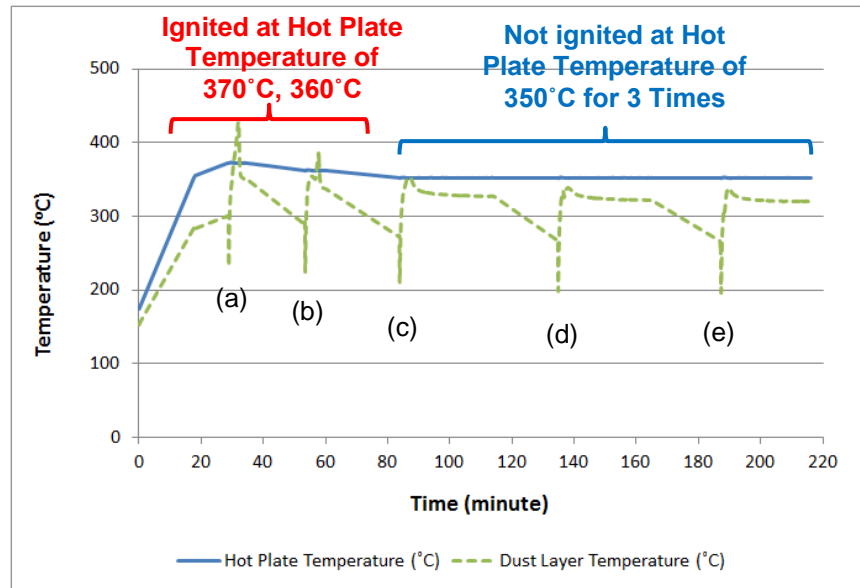
Table 5. 6 Binder Effect – T_{LIT} and Ignition Delay Time of Twelve Samples in Ring A

Biomass Sample	T_{LIT} (°C)	Change-T_{LIT} (% °C)	Ignition Delay Time (min)	Change- Ignition Delay Time (% min)
Miscanthus(1)	310	n.a.	2.4	n.a.
Misc(1)Lg980	310	0	8.7	263
Misc(1)CF980	310	0	6.4	167
Pine	310	n.a.	8.2	n.a.
PineLg980	330	6	5.3	-35
PineCF980	330	6	4.5	-45
Miscanthus(2)	350	n.a.	3.1	n.a.
Misc(2)Lg980	360	3	5.8	87
Misc(2)CF980	360	3	5.0	61
Wheat Straw	310	n.a.	3.5	n.a.
WSLg980	320	3	5.1	46
WSCF980	320	3	4.5	29

n.a. – not applicable

From **Table 5. 6**, two obvious observations were seen – most samples with binder had the T_{LIT} increased as compared with those of their respective parent material and if the T_{LIT} remained the same as the parent material, the ignition delay time was lengthened. Misc(1)Lg980 and Misc(1)CF980 had the same T_{LIT} as compared with their parent material (Miscanthus(1)) but the ignition delay time of both increased tremendously. When mid-way refinement test (5°C interval) was conducted on Misc(1)Lg980 and Misc(1)CF980, the former failed to ignite but not the latter. Misc(1)CF980 ignited at 305°C with a delay time of 7.7minutes, taking slightly longer than when it was subjected to 310°C. This showed that the sample with cornflour binder was a bit more reactive than the sample with Ligno-Bond binder (for Miscanthus(1)). Misc(2)Lg980, Misc(2)CF980, WSLg980 and WSCF980 showed 10°C increase in the T_{LIT} as compared with those of their respective parent material. From the results of T_{LIT} , woody biomass (pine) seemed to be more sensitive to binder addition, as seen from the 20°C (6% change) in T_{LIT} in PineLg980 and PineCF980 samples as compared with only 10°C (3% change) T_{LIT} change in the four herbaceous samples i.e. Misc(2)Lg980, Misc(2)CF980, WSLg980 and WSCF980.

The dust layer ignition profile of Misc(2)CF980 is shown in **Figure 5. 3**. The T_{LIT} of both Ligno-Bond-DD powder and cornflour binders had not been conducted in this study. Values from various literatures (Lignotech, 2002; Kasalová and Balog, 2011; Martinka et al., 2012) showed that dust layers consisting of either binder ignited at ~400°C or greater; with 400°C as autoignition temperature of Ligno-Bond-DD powder dust (Lignotech, 2002); 445-590°C (Kasalová and Balog, 2011) and >400°C (Martinka et al., 2012) for cornflour dust settled in thin layers of ~5mm. A constraint existed in this situation, whereby the equipment available in this study (ANKO-lab rig) was only accurate to 400°C. A more confirmed conclusion regarding woody or herbaceous biomass dust layer ignition sensitivity as a result of binder addition could only be drawn after sampling studying more woody and herbaceous biomass species.



- (a) Misc(2)CF980 Dust Sample 1 – Hot plate temperature set at 370°C, ignition happened
- (b) Misc(2)CF980 Dust Sample 2 – Hot plate temperature set at 360°C, ignition happened
- (c) Misc(2)CF980 Dust Sample 3 – Hot plate temperature set at 350°C, 1st time no ignition
- (d) Misc(2)CF980 Dust Sample 4 – Hot plate temperature set at 350°C, 2nd time no ignition
- (e) Misc(2)CF980 Dust Sample 5 – Hot plate temperature set at 350°C, 3rd time no ignition

Figure 5. 3 Dust Layer Ignition Temperature Profile of Misc(2)CF980

When the ignition delay time of all twelve samples were compared, apart from PineLg980 and PineCF980, all the other six herbaceous biomass samples with binder i.e. Misc(1)Lg980, Misc(1)CF980, Misc(2)Lg980, Misc(2)CF980, WSLg980 and WSCF980 showed increased ignition delay time when compared with those of their respective parent sample. From the results **Table 5. 6**, high increases were seen for Misc(1)Lg980 and Misc(1)CF980, (263% and 167% increase) as compared with parent Miscanthus(1). The four other samples, i.e. Misc(2)Lg980, Misc(2)CF980, WSLg980 and WSCF980 showed delay time increases of 87%, 61%, 46% and 29% respectively, compared with respective parents. One interesting point to note was that the delay time from the samples with Lingo-Bond-DD powder binder were always greater than the respective counterparts with cornflour binder: i.e. the same biomass with cornflour binder tended to ignite earlier than its counterpart with Lingo-Bond binder when subjected to the same hot temperature. PineLg980 and PineCF980 were the two samples that showed a reduction in ignition delay time when compared with parent Pine. There appeared to be compensation effect between T_{LIT} and ignition delay time. As seen in previous chapter, the general trend was that higher T_{LIT} reduced the ignition delay time and this trend applied to PineLg980 and

PineCF980 that had shown 20°C increase in their T_{LIT} when compared with Pine without binder.

These T_{LIT} results were actually consistent with material self-ignition risk predicted using the pictorial risk ranking method. WSLg980, WSCF980, PineLg980, PineCF980, Misc(2)Lg980 and Misc(2)CF980 showed increases in T_{LIT} as compared with respective parent material and this was reflected as a self-ignition risk reduction from the risk ranking curve **Figure 5. 2**. On the other hand, the T_{LIT} s of Misc(1)Lg980 and Misc(1)CF980 that were found to be the same as the parent material Miscanthus(1) and these had their self-ignition risk predicted in the same category as their parent material. Thus, **Figure 5. 2** could be applied with success in this study.

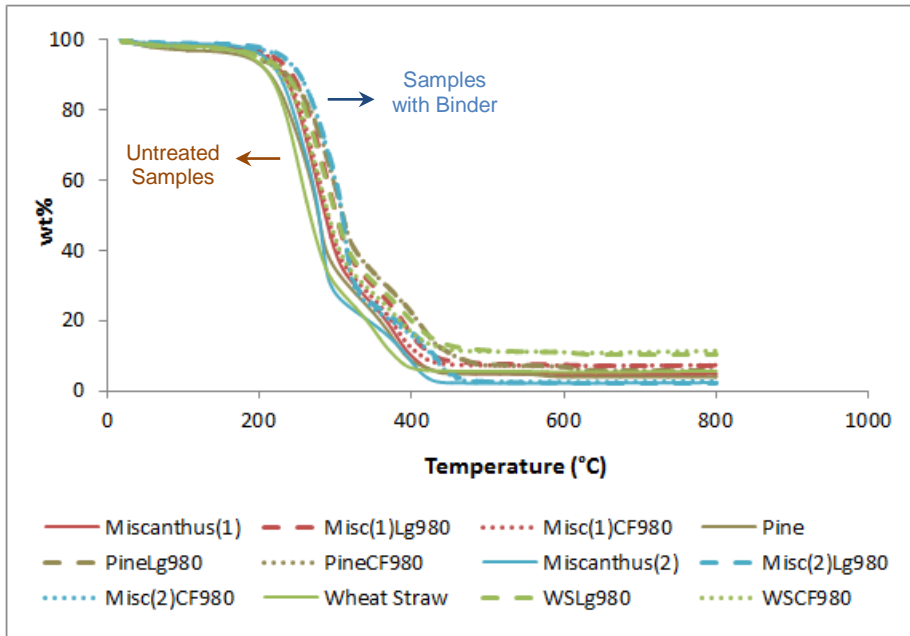


Figure 5. 4 TGA Weight Loss Curves Comparison of Twelve samples – With and Without Binders

The weight loss curves (see **Figure 5. 4**) as determined by TGA shows slowest weight loss for biomass with Ligno-Bond-DD powder binder (curves towards the right), fastest for the biomass without any binder (curves towards the left) whereas those with cornflour binder lay in the middle. This is consistent with the biomass reactivity from the T_{LIT} view point in which biomass with any two binders showed higher T_{LIT} or longer ignition delay time. Comparing the same biomass with different binders, the one with cornflour had always ignited with shorter delay time than its Ligno-Bond-DD powder counterpart, in line with the faster weight loss depicted in the TGA curves. Referring to the kinetics data in **Appendix A**, the pre-exponential factor (frequency factor), A , of the biomass without

binder is always greater than counterparts with either binder. This implies an inerting effect with binder addition that was proven higher T_{LIT} or longer ignition delay time.

5.4 Industrial Significance

Determination of the maximum permissible surface temperature (MPST) of an electrical apparatus operating in dusty environment was performed by referring to Guideline1, Guideline2 as described in **Chapter 2** and a power station practice. The values obtained from Guideline1 and Guideline2 are shown in **Table 5. 7** for the eight samples with binder used in this study. As in the previous chapter, the numerical values calculated using Guideline1 were superimposed onto the three-curve chart of Guideline2 (see **Figure 5. 5**). The other method of a fixed MPST value at 150°C as applied by a U.K. power station is shown as a dotted red line in the same figure.

When following Guideline1, the values were simply a deduction of 75°C (75 K safety margin) from each 5 mm T_{LIT} and the values are illustrated as different points on the Guideline2 chart with three curves for three different temperature ranges. On the other hand, when Guideline2 was followed, depending on the range of respective 5 mm T_{LIT} , the MPST of each sample was read off from the appropriate curve. It should be noted that since the 5 mm T_{LIT} of eight samples fell within range of 310-360°C, only the bottom and middle curves were used.

Taking WSCF980 as example, its 5 mm T_{LIT} was 320°C and, when Guideline1 was adopted, the resultant point (245°C) was plotted onto Guideline2 chart (shown as a yellow-filled green hour-glass symbol in **Figure 5. 5**). When Guideline2 was followed, since its 5 mm T_{LIT} was exactly 320°C and less than 400°C, the middle curve was referred to and, the resultant reading was ~250°C for a 5 mm dust layer. The values obtained from both the guidelines were far higher than the fixed 150°C MPST method applied in the U.K. power station. For this thin layer case, the power station method was the most conservative. Due to insufficient biomass, the dust rig experiment had not been conducted to determine the T_{LIT} of 12.5 mm thickness (using Ring B) but it was estimated to be 30°C lower than its 5 mm counterpart, leading to 290°C. Like before, when Guideline1 was followed, the point of 215°C (290-75°C) was plotted onto the chart of Guideline2 with x-axis at 12.5 mm chart. Following Guideline2, reading off the middle curve, ~200°C was the MPST found. Again, the fixed MPST of 150°C was the most conservative value among the three practices. Looking at the dotted red line in **Figure 5. 5**, the 150°C fixed MPST got closer to values computed from two other methods as the layer thickness increases and eventually, the BS 50281-1-2 method i.e. Guideline2 would be the most conservative of all.

Looking at the bottommost curve which is valid for those samples whose 5 mm T_{LIT} range from -250 to 320°C (a range of <70°C), , all samples within this <70°C range would have the same predicted MPST, e.g. ~175°C for 5 mm thick layer. This implied the safety margin is smaller for the lower end and the safety margin increases as T_{LIT} approaches the higher end of <320°C (safety margin would be <145°C, i.e. <320-175°C). The same applies to the middle and top curves.

Moving towards the boundary of the x-axis when dust layer thickness approaches 50 mm, as seen from the bottom curve, both lower and higher values of 5 mm T_{LIT} (250°C and <320°C respectively) predict MPST of <75°C, which was just half the value practised in the U.K. power station referred here. This shows that MPST estimation with Guideline2 could be too conservative for thick layers. The negative impact could be a plant operates an apparatus at a temperature too low to achieve the desired equipment efficiency but the plant is definitely safe from fire risk originating from the combustible dust ignition on hot surfaces. This conservativeness was seen in an actual example of a 30 mm thick layer in the study of Querol et al. (2006). For one of the materials examined, 305°C was tested to be the 5 mm T_{LIT} and 270°C the 30 mm T_{LIT} . With these, 195°C would be the MPST following the method in Guideline1. If Guideline2 was followed, reading from the bottom curve led to an MPST value as low as 95°C. The MPST predicted with these two guidelines differed by 100°C. If taking the third method that fixed MPST at 150°C into consideration, Guideline2 from BS 50281-1-2 was the most conservative prediction of all.

Table 5. 7 MPST Calculation/Estimation Following Guideline1 and Guideline2 for 5 mm Dust Thickness

Sample Name	5-mm T_{LIT} (°C)	MPST _{Calculated,} Guideline1 (°C)	MPST _{Estimated,} Guideline2 (°C)
Misc(1)Lg980	310	235	~175
Misc(1)CF980	310	235	~175
PineLg980	330	255	~250
PineCF980	330	255	~250
Misc(2)Lg980	360	285	~250
Misc(2)CF980	360	285	~250
WSLg980	320	245	~250
WSCF980	320	245	~250

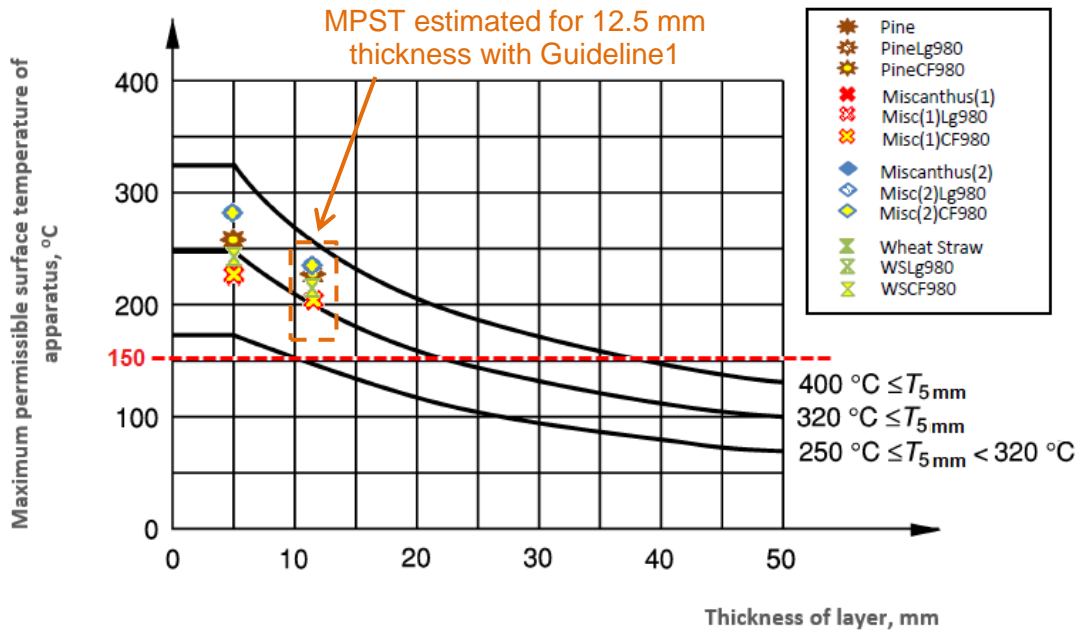


Figure 5.5 MPST Estimations of Samples with and Without Binder with Three Different Methods – Guideline 1 (Points), Guideline 2 (Curves, T_{LIT} from Pre-Refinement) and Power Station Practice (Constant at 150°C)

5.5 Effects of Having Different Binders

The two binders used in this study, Lignosulphonate and cornflour (or corn starch) are two among the few common binders used in biomass briquettes or pellets (DeVallance, 2013; Tarasov et al., 2013; Rajaseenivasan et al., 2016; Kuokkanen et al., 2011). The results of dust layer test conducted on eight samples from four parent material with either binder showed those with cornflour binder was slightly more reactive than those with Ligno-Bond-DD powder (lignosulphonate) binder, although for both binders there appeared to be a slight inerting effect.

This was investigated further by examining the TGA slow combustion weight loss and first derivative weight loss (DTG) profiles of both binders. There was an obvious difference between them: The DTG profile of cornflour showed higher mass loss rate (in unit of %mass loss/time) than Ligno-Bond-DD powder (see **Figure 5.6**). As mentioned by Barlin et al. (2016) in an analysis on thermal evolution profile of coal and wood, peak height of the DTG profile is one characteristic of the reactivity of a sample. The more reactive biomass wood samples showed DTG peaks ~5 times higher than shown by coal in that study. Consistent with the observation of Barlin et al. (2016), the taller DTG peak in cornflour samples here implied that this binder was more reactive than Ligno-Bond-DD powder. As seen from the DTG profile (see **Figure 5.6**) of Ligno-Bond-DD powder and

cornflour, the peaks fluctuated around <2%/min for the lignosulphonate binder but a peak of >15%/min was observed for the cornflour binder.

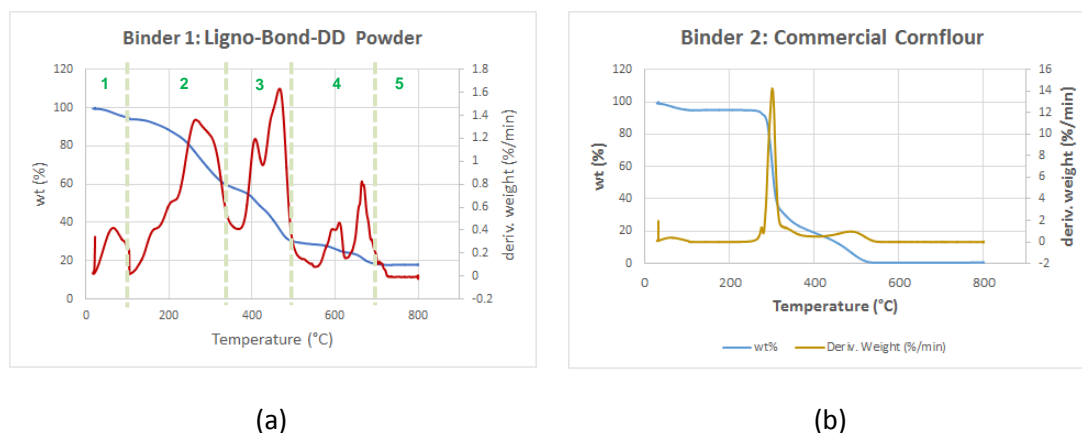


Figure 5. 6 Slow Combustion TGA Mass Loss and Derivative Mass Loss (DTG) Profiles of (a) Ligno-Bond-DD Powder (Lignosulfonate) (b) Cornflour (i.e. Cornstarch)

The numerous peaks in Ligno-Bond-DD powder DTG profile was caused by the multi- step thermal degradation of lignosulphonate in TGA runs. Ház et al. (2013) investigated the eight lignosulphonate samples via TGA and the TGA mass loss profile showed the samples degraded in five steps within five temperature regions – 0 to ~100°C; ~100 to ~200°C; ~200 to ~470°C; ~470 to ~650°C and ~650 to 800°C and all DTG profiles showed multiple peaks. Since different heating rates and holding times were used in this study, the TGA mass loss profile for Ligno-Bond-DD powder showed five thermal degradation regions similar to that discovered in the work of Ház et al. but the numerical values were a bit different. The five temperature regions in this study were ~25 (ambient) to ~100°C; ~100 to ~350°C; ~350 to 500°C; 500 to 700°C and ~700 to 800°C.

Recall that binder is only present as 2wt% in the biomass with binder. The effect of higher reactivity of cornflour was reflected in the TGA profiles of materials with binder but is not too obvious. Taking the example of Misc(1)Lg980 and its counterpart Misc(1)CF980 (that showed 5°C difference in 5 mm dust layer T_{lit}), the derivative mass loss values for the first and second peaks (signifying volatile combustion and char combustion regions) were ~4.1%/min and ~1.6%/min respectively for Misc(1)Lg980 whereas the values were ~4.6%/min and ~1.7%/min respectively for Misc(1)CF980. This comparison is illustrated in **Figure 5. 7** and it is worthwhile to note that peak temperature for Misc(1)CF980 is less than that of Misc(1)Lg980.

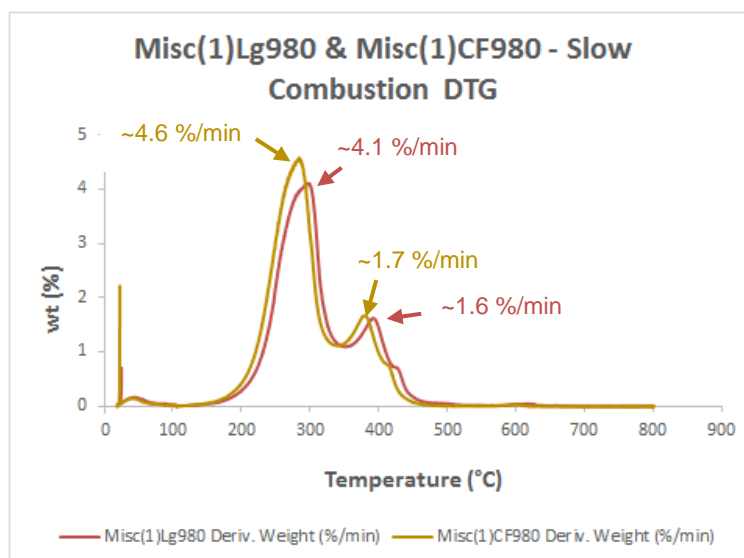
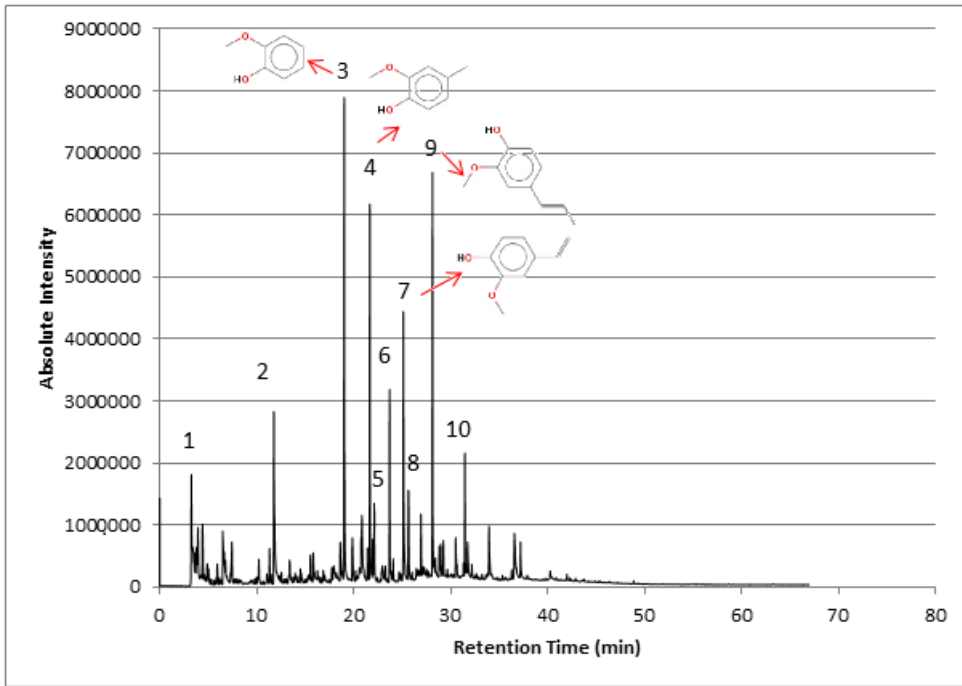


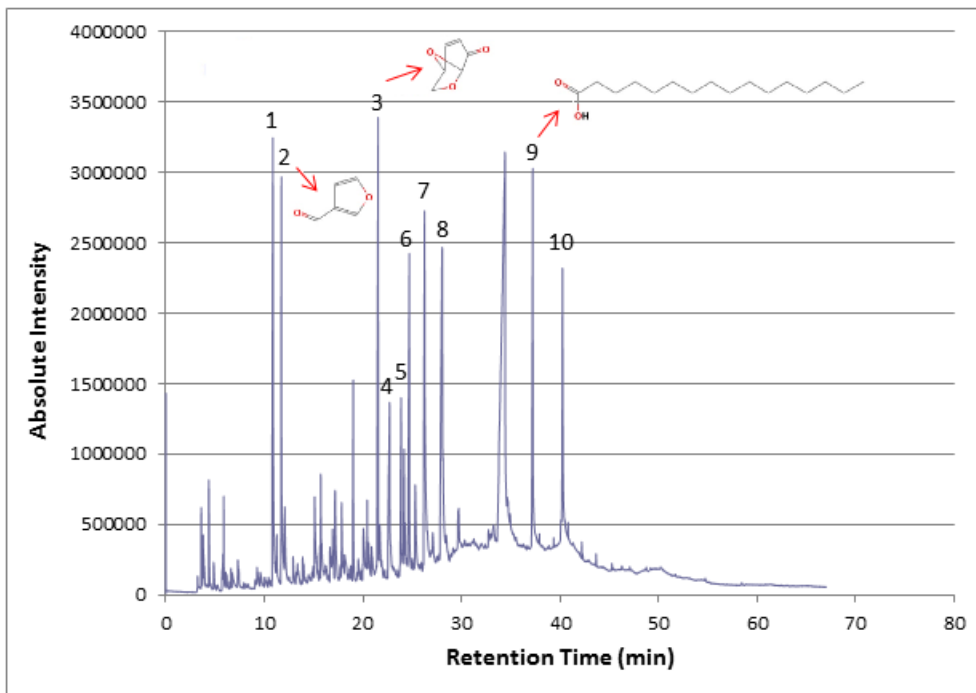
Figure 5. 7 DTG Profiles Comparison of Misc(1)Lg980 and Misc(1)CF980

5.5.1 py-GC-MS on Binders

The chemical composition of both the binders used here were analysed with the py-GCMS method, as described in **Chapter 3**. The relatively complex structure of the binders were decomposed into smaller molecules, separated by the gas chromatographer, detected by the mass spectrometer and later matched to the element-library before any results were reported. The chromatographs and major elements in Ligno-Bond-DD powder and commercial cornflour identified using this method are shown in **Figure 5. 8** and **Table 5. 8** respectively. The chemical structures of the four most abundant elements are shown as well. The py-GC-MS results showed Ligno-Bond-DD powder were broken down into 2-methoxyphenol; 2-methoxy-4-(1-propenyl)phenol; 2-methoxy-4-methyl Phenol and 2-Methoxy-4-vinylphenol as the top most abundant elements whereas Levoglucosenone; Furanone compound; n-Hexadecanoic acid and 3-Furaldehyde were the top most available components in cornflour.



(a)



(b)

Figure 5. 8 py-GC-MS Chromatogram of (a) Ligno-Bond-DD Powder Binder (b) Cornflour Binder

Table 5. 8 Ten Major Elements in Two Binders Identified by py-GC-MS

(a) Ligno-Bond-DD Powder (Lignosulphonate)

Peak Number	Retention Time	Element
1	3.262	Unknown
2	11.774	Furfural
3	19.03	Phenol, 2-methoxy-
4	21.673	Phenol, 2-methoxy-4-methyl-
5	22.125	Benzene, 1,2-dimethoxy-4-methyl-
6	23.712	Phenol, 4-ethyl-2-methoxy-
7	25.124	2-Methoxy-4-vinylphenol
8	25.647	Phenol, 2-methoxy-4-(2-propenyl)-, acetate
9	28.134	Phenol, 2-methoxy-4-(1-propenyl)-
10	31.472	2-Propanone, 1-(4-hydroxy-3-methoxyphenyl)-

(b) Commercial Cornflour (Corn Starch)

Peak Number	Retention Time	Element
1	10.868	Furanone compound
2	11.731	3-Furaldehyde
3	21.54	Levoglucosenone
4	22.705	4H-Pyran-4-one, 3,5-dihydroxy-2-methyl-
5	23.877	Cyclohexanol, 4-methyl-, cis-
6	24.708	4,5-Octanediol, 2,7-dimethyl-
7	26.248	2-Furancarboxaldehyde, 5-(hydroxymethyl)-
8	28.038	3-cis-Methoxy-5-cis-methyl-1R-cyclohexanol
9	37.225	n-Hexadecanoic acid
10	40.243	Octadecanoic acid

5.5.2 Pyrolysis Extent at Different Dust Layer Heights

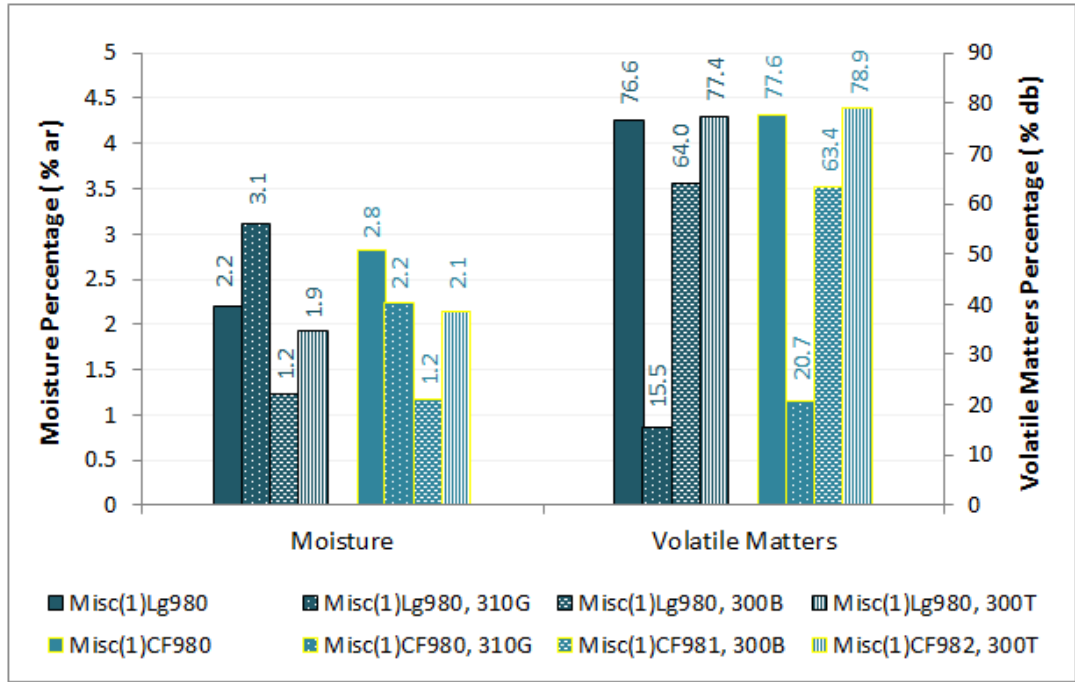
Park (2006) examined temperatures at two different dust layer depths, ~quarter thickness and ~half thickness distances measured from the hot plate within the dust layer. At a hot plate temperature that did not cause ignition in dust layer, It was found that the temperature at ~quarter thickness distance from the hot plate was higher than that at ~half thickness distance, by ~20°C. This indicated that the dust closer to the hot plate could have under gone a greater extent of pyrolysis as compared with the dust located farther from the hot plate. Inspired by this work the dust layer was studied further to examine colour variation throughout the dust layer tested on a hot plate (see **Figure 5. 9**). Also, the pyrolysis extent was examined based on the moisture and volatile matter contents found using the steps briefed in **Chapter 3**.

The moisture content was determined on the samples as experimented and therefore denoted as as-received (ar) basis whereas the volatile matters reported disregarded this moisture content and thus was in dry basis. The pyrolysis extent investigation was carried out on three categories of each sample – unreacted, just-ignited and pre-ignited samples representing the original dust before undergoing the dust layer test, the dust that ignited at the minimum dust layer ignition temperature (T_{LIT}), and 10°C below the minimum dust layer ignition temperature respectively. The method of collecting the samples for the two latter cases was described in **Chapter 3**.

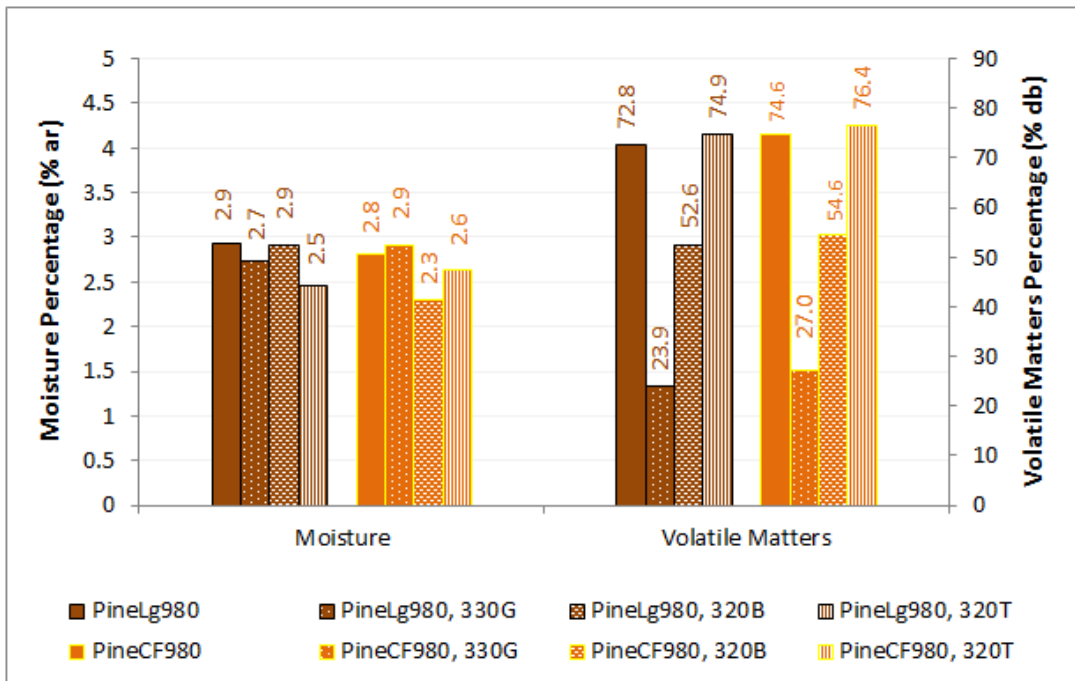


Figure 5. 9 Colour Variation of A Biomass Dust Layer Subjected to Non-Igniting Hot Plate Temperature

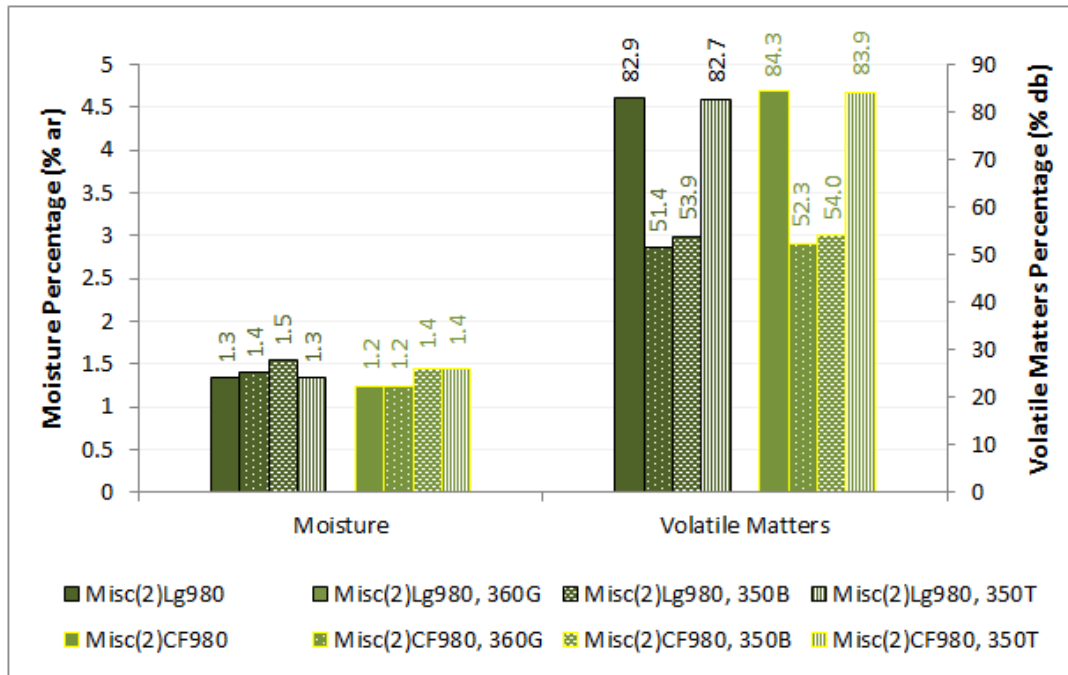
Adhering to the method described in **Chapter 3**, TGA slow pyrolysis runs were conducted on the Top Dust and Bottom Dust collected from the samples with two different binders. The moisture and volatile matters contents of all eight samples with binder in the three categories are displayed in **Figure 5. 10**. When comparing, for consistency purpose, it should be noted that all dust samples used had been sieved to <180 μm to match the dust size used in dust layer ignition test.



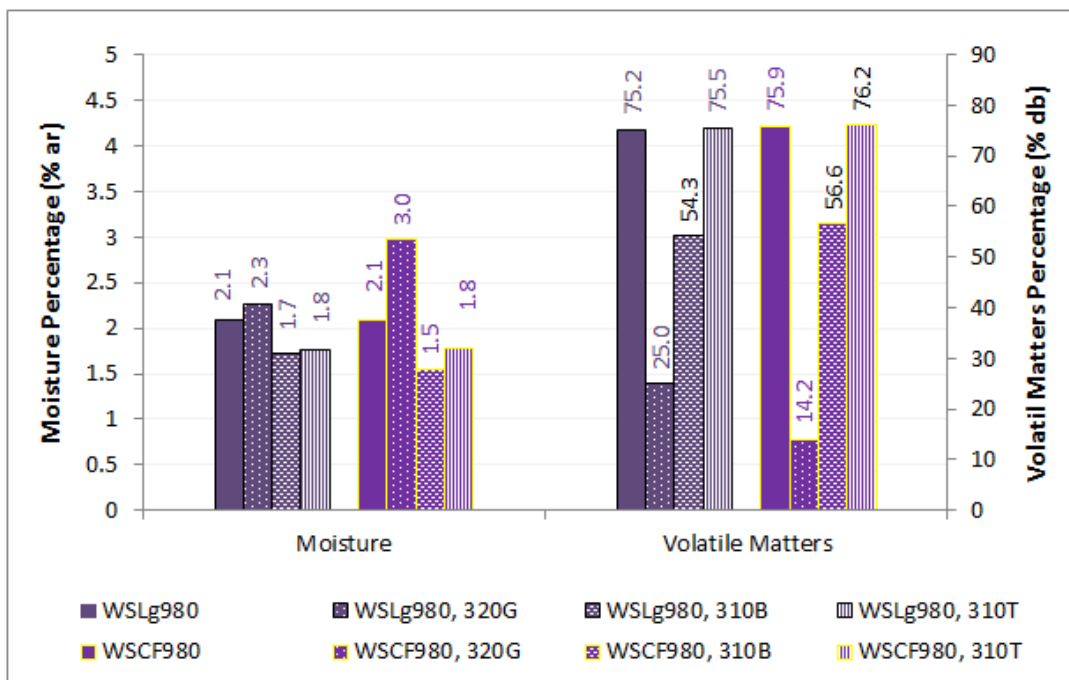
(a)



(b)



(c)



(d)

Figure 5. 10 Moisture and Volatile Matters Comparisons Among Unreacted, Ignited and Pre-Ignited Dust from Eight Materials with LignoBond or Cornflour Binder for (a)Miscanthus(1) (b)Pine (c) Miscanthus(2) (d)Wheat Straw

The composition of the samples shown in **Figure 5. 10** was as listed in **Table 5. 8** in the beginning of this chapter. Referring to the legend of the bar charts, besides the sample names, the legend had also included the hot plate temperature (in °C) and the condition of the dust tested; 'G' signified glow and meant the just-ignited dust; 'B' and 'T' indicated the Bottom and Top Dust respectively when the hot plate was fixed at the pre-igniting temperature of respective samples.

As seen from the bar charts, comparing the just- and pre-ignited dust collected from the dust layer test or unreacted dust prior dust layer test, all the just-ignited dust showed the least volatile matters as compared with those of the pre-igniting dust from either location or the unreacted dust. All just-ignited dust showed volatile matters reductions of >60% relative to the unreacted dust, except the two samples from miscanthus(2) parent that exhibited <40% reduction relative to respective unreacted dust. For just-ignited dust, Misc(2)Lg980 and Misc(2)CF980 showed volatile matters of ~50% but all other samples showed ~14 to ~28% on dry basis. The amount in all samples showed ~50 to ~60% of volatile matters on dry basis for pre-igniting bottom dust.

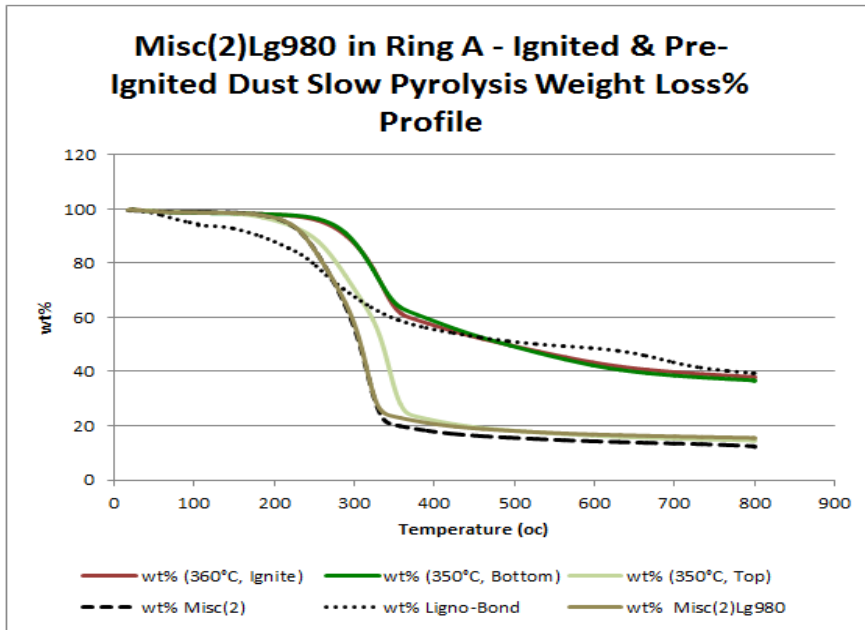
There was an interesting observation in this experiment, where maximum volatile matters was shown on samples picked from the top location of pre-igniting dust were slightly more than those of the respective unreacted counterparts (not more than 3%). The volatile matter of top pre-igniting dust of Misc(1)Lg980 and Misc(1)CF980 increased by <2%, PineLg980 and PineCF980 by <3% and WSLG980 and WSCF980 by <0.5% when compared with respective unreacted counterparts. This observation was valid for all samples except Misc(2)Lg980 and Misc(2)CF980 samples, where volatile matter from pre-igniting top location decreased slightly when compared with respective unreacted dust

The phenomenon that the top pre-igniting dust showed more volatiles than the unreacted counterpart could be explained this way: as the material gained energy, the volatile matter trying to liberate themselves to the atmosphere were migrating upwards to the top. Most likely, the volatile matter was trapped at the cooler top layer since they had yet to gain enough energy to liberate to the atmosphere, therefore they were accumulating at the top surface. As the temperature was increased (say by 10°C towards the ignition temperature), indicating heightened reactions, more volatiles migrated to the top surface and escaped.

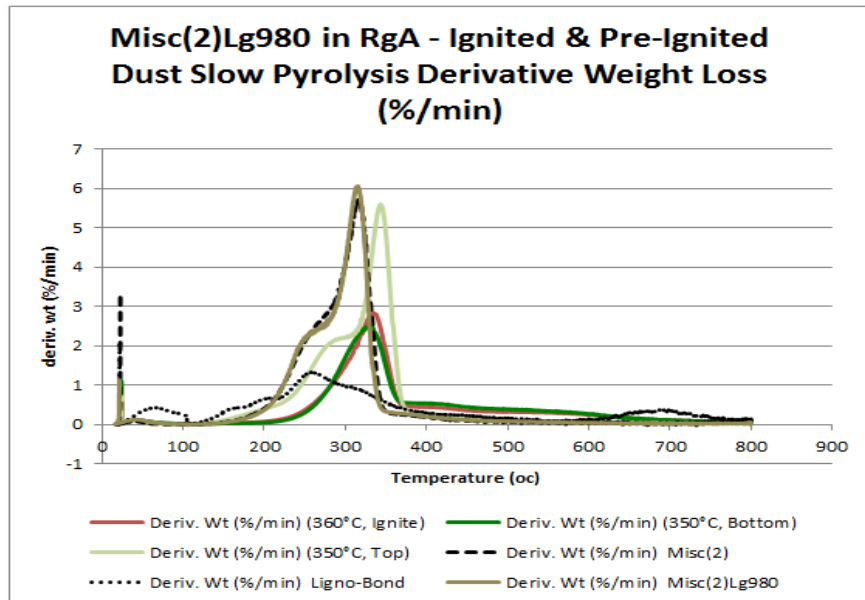
The exception to this observation (Misc(2)Lg980 and Misc(2)CF980) was probably due to the nature of both untreated samples. The volatile matters in both untreated samples were >80% and therefore it was not surprising that even after ignition, the volatile matters remained quite high, giving values of >50%. Therefore, for the top layer of pre-igniting samples, unlike the six other samples, the volatile matter of Misc(2)Lg980 and Misc(2)CF980 that were migrating to the top surface had yet to reach the level that it exceeds the original content in respective unreacted counterparts. Anyway, it should be

noted that the volatile matter content in the top layer of pre-igniting dust of all eight samples was just marginally more or less of those of the unreacted dust.

The TGA weight loss and DTG plots for Misc(2)Lg980 and Misc(2)CF980 are shown in **Figure 5. 11** and **Figure 5. 12** respectively. The corresponding TGA weight loss and DTG profiles for other samples were very similar.

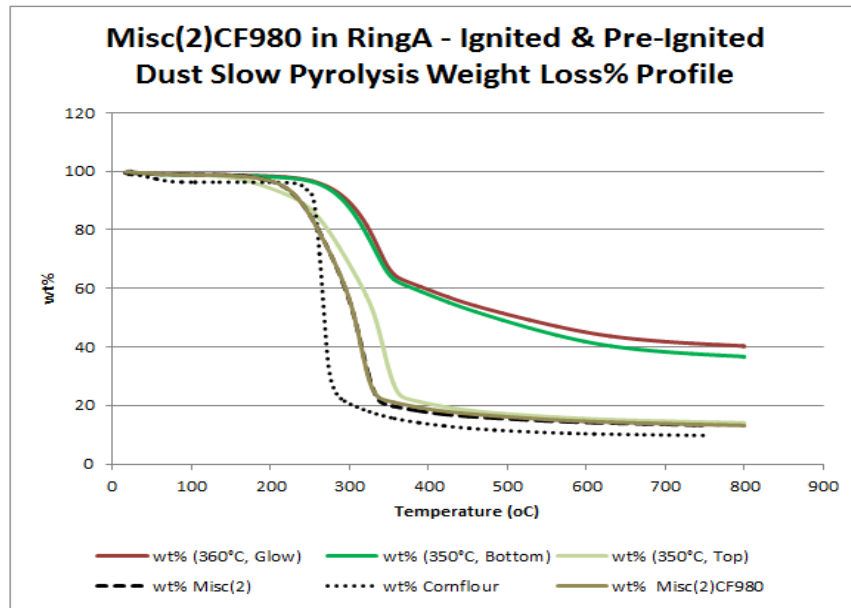


(a)

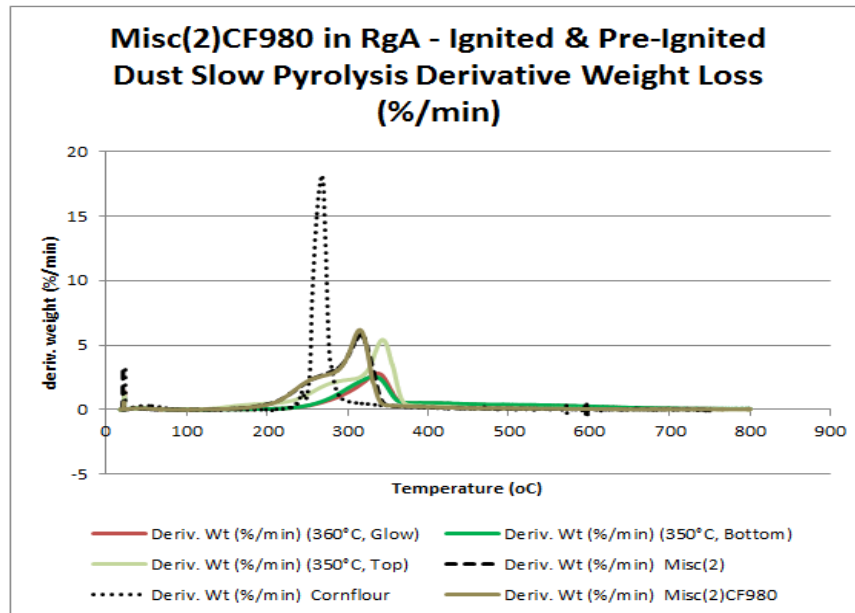


(b)

Figure 5. 11 Misc(2)Lg980 (a)TGA Weight Loss Curve (b)DTG Curve



(a)



(b)

Figure 5. 12 Misc(2)Lg980 (a)TGA Weight Loss Curve (b)DTG Curve

It was observed that the degradation profile of the pre-igniting bottom layer of dust followed closely the profile of the ignited dust whereas the pre-igniting top layer of dust had its degradation profile similar to the unreacted dust. As seen from all TGA weight loss curves, the curves showed a right-shift from unreacted dust blend to pre-igniting top dust, and then to pre-igniting bottom dust and finally the ignited dust. The shift indicated a transition of pyrolysed degree, from least pyrolysed to most pyrolysed (i.e burnt).

5.6 Concluding Remarks and Suggestions for Future Work

From this section about the effect of binder on dust layers ignition, some general conclusions were drawn from examinations conducted on having two different binders in four commonly used solid biomass fuel.

Consistent with the maximum amount of binder allowable in solid fuels, it seems that both of the two binders used here exhibit an inerting effect on the parent biomass, in either of these two ways – increase in T_{LIT} or lengthened ignition delay time when the T_{LIT} remained unchanged. The resultant T_{LIT} increase from either binder did not vary much from the binderless parent material, and 20°C was the maximum increase observed. With the inverse relationship between T_{LIT} and ignition delay time, the higher the resultant T_{LIT} , the shorter the delay time.

As for concerns on fire risk, from the MPST prediction using three different methods, it was found that as long as the dust layers were thin, the changes in T_{LIT} was not significant enough to change the dust management policy in current practice. Even when the other MPST guideline from the National Fire Protection Association (NFPA) was referred to, no housekeeping management changes were necessary in terms of combustible dust management. This was because the MPST in the NFPA 499 standard had already been considered in the three methods described in length here. This was further justified from the biomass self-ignition risk ranking that was based on the T_{MWL} and E_a calculated from TGA slow combustion reaction for each sample (with and without binder) that had shown none of them fall into the low risk group despite slight increases in T_{LIT} . This investigation had at least proven that addition of binders would not increase the ignition risk when thin dust layers of ~5 mm were exposed to < ~360°C (the maximum T_{LIT} found from the biomass samples used in this binder effect study) for a considerable period of time.

Comparing the two binders used here, Ligno-Bond-DD powder as a by product from paper pulping process, showed much higher amount of sulphur as compared with that from cornflour. The impact of sulphur content would be important if air pollution regulation is a concern.

There are a few things that could improve this investigation of binder effects on dust layer ignition characteristics and help understanding the matter further.

To get a better picture of binder effects on material T_{LIT} , more woody and herbaceous biomass samples could be used. Other common woody biomass used as fuel like eucalyptus, willow, spruce and herbaceous biomass like switchgrass, corn stover are potential parent materials to have binder added to them and have their respective T_{LIT} s studied. With a bigger sample size, the effect on binder particularly on woody and herbaceous biomass could be recognised.

For the analysis on pyrolysis extent, dust experimented on many more hot plate temperatures for a single sample could be collected for TGA analysis. With the moisture and volatile matter results from dust tested at say at least five different temperatures, the pyrolysis process of that particular dust could be monitored in a better sequence from before ignition to the point the dust finally ignited.

Besides Ligno-Bond-DD powder and cornflour, other organic binders easily obtainable like asphalt, cassava flour, tapioca starch, molasses could be used. With the T_{LIT} and ignition delay time information experimented on various parent materials bound by these different binders, the fire risk and cost incurred could be evaluated. This would then lead to and the safest and most economical production of renewable biomass solid fuel.

Since the sulfur content seemed to be much more in the samples with Ligno-Bond binder than respective counterpart with corn flour binder, it may be of interest to examine and compare the emissions from both samples. With that, whether or not burning these fuels would significantly impact the air quality and to what extent could be justified. The experiment setup and analysis for this emission comparison purpose could adopt that method outlined in **Section 3.3** with analysis described in **Chapter 8** later.

Chapter 6

Handling – Effects of Washed Biomass Dust Layer Ignition Characteristics

There has been much research centred on impacts of eliminating alkali metals, alkaline earth metals, chlorine, sulphur on corrosion and deposition problems. Some of these components are known to catalyse the pyrolysis of biomass (Nowakowski, 2008; Nowakowski and Jones, 2008; Nowakowski et al., 2007) and therefore it was of interest to study the effect of washing on biomass ignition properties. Very little research has been done regarding the effects of elimination of these problematic elements on biomass self-ignition propensity. Thus, the effects on self-ignition of washed biomass dust layers on heated surfaces are the focus of this chapter. In this study, biomass dust layer ignition characteristics were compared between the untreated biomass and the washed biomass.

Dusts from two biomass species – woody pine and herbaceous miscanthus and their blends in different weight ratios were studied in depth by comparing the characteristics before and after washing pre-treatment. Biomass blends represent the power station scenario where a number of biomass are fired under daily operation. The pre-treatment involved washing biomass fuel with distilled water as described in **Section 3.2.1**. There were eight biomass samples chosen in this washing pre-treatment study, single-material and blends. It should be noted that not all samples had undergone each and every experiment due to constraint on material amount, only important experiments were prioritised for some of the samples. The complete list of samples with their respective original forms, compositions and the sole pre-treatment condition are tabulated in **Table 6.1**.

Table 6.1 Samples Used in Washing Study with Respective Original Form and Washing Condition (Solvent Temperature in °C, Washing Duration in Minutes)

Sample Name	Original Form	Composition (wt%)	Washing Condition (°C, minutes)
Misc(1)	Pellet	100% miscanthus	n.a.
wMisc(1)	Disintegrated Pellet	100% miscanthus	Room temperature, 60 minutes
PineC	Chip	100% pine	n.a.
wPineC	Chip	100% pine	Room temperature, 60 minutes

Sample Name	Original Form	Composition (wt%)	Washing Condition (°C, minutes)
90PineC-10Misc(1)	Powder, <180 µm	90% pine + 10% miscanthus	n.a.
90wPineC-10wMisc(1)	Powder, <180 µm	90% pine + 10% miscanthus	Room temperature, 60 minutes
50PineC-50Misc(1)	Powder, <180 µm	50% pine + 50% miscanthus	n.a.
50wPineC-50wMisc(1)	Powder, <180 µm	50% pine + 50% miscanthus	Room temperature, 60 minutes

n.a. – not applicable

6.1 Proximate, Ultimate Analyses and Higher Heating Values

One of the major objectives of biomass washing pre-treatment is to reduce the ash content therefore lessening ash-related operational issues especially in furnaces and boilers within power stations. Proximate analysis was conducted on all eight biomass samples shortlisted for this study in accordance to British Standards BE EN 14774-3:2009, BS EN 15148:2009 and BS EN 14775:2009 for moisture, volatile matter and ash respectively (see **Chapter 3** for details). The proximate analysis results that showed washing pre-treatment impacts on biomass composition are tabulated in **Table 6. 2**.

Table 6. 2 Proximate Analysis (wt%) of all Samples Used in Biomass Washing Study

Sample Name	Moisture ^a (wt%)	Volatile Matters ^b (wt%)	Fixed Carbon ^d (wt%)	Ash ^b (wt%)
PineC	6.98 ± 0.30	84.92 ± 0.15	14.75 ± 0.18	0.329 ± 0.034
Misc(1)	5.84 ± 0.46	76.94 ± 0.25	17.63 ± 0.35	5.426 ± 0.095
90PineC-10Misc(1)	6.99 ± 0.27	83.83 ± 0.60	15.28 ± 0.69	0.894 ± 0.087

Sample Name	Moisture ^a (wt%)	Volatile Matters ^b (wt%)	Fixed Carbon ^d (wt%)	Ash ^b (wt%)
50PineC-50Misc(1)	5.92 ± 0.29	81.001 ± 0.27	16.70 ± 0.34	2.292 ± 0.022
wPineC	6.48 ± 0.35	85.247 ± 0.61	14.45 ± 0.79	0.306 ± 0.017
wMisc(1)	5.17 ± 0.22	78.72 ± 0.35	17.42 ± 0.38	3.856 ± 0.027
90wPineC- 10wMisc(1)	6.51 ± 0.73	84.82 ± 0.28	14.68 ± 0.25	0.501 ± 0.032
50wPineC- 50wMisc(1)	5.49 ± 0.64	83.52 ± 0.34	15.21 ± 0.62	1.27 ± 0.028

^a as received (ar) ^b dry basis (db) ^d by difference

In general, after washing all fuels showed a slight increase in volatile matters with a small decrease in the fixed carbon content and a significant decrease in ash amount. On dry basis, for volatile matters, untreated miscanthus showed ~77% and was increased a little to ~78% and the increment was even less for pine. The blend with higher miscanthus composition i.e. 50PineC-50Misc(1) showed a greater increase than the other blend with less miscanthus content. As for fixed carbon, the content decreased a little upon washing pre-treatment. This finding was consistent with results of Kasparbauer (2009) in a study on effects of biomass pretreatments on products of fast pyrolysis and mild leaching of herbaceous Napier grass with water. The later found volatiles to increase from ~82% to ~84% at the expense of reducing fixed carbon from ~16% to ~14%. A study of Nowakowski et al. (2007) on short rotation willow coppice in which the water-washed pre-treated willow showed increased volatiles and decreased char with respect to the untreated material. The increased char formation from a demineralized sample impregnated with potassium led to the conclusion that potassium has a crucial effect on char formation by catalysing the pyrolysis stage. It is believed that the presence of catalytic potassium promotes char formation at the expense of volatiles, and thus, removal of this metal decreases fixed carbon formation. Similarly, in a study on combustion characteristics of water-leached straw, Jenkins et al. (1998a) had concluded that metals in biomass did have impact on reaction rates and believed that it was catalytic to pyrolysis process.

Comparing a sample with its leached counterpart, it was found that the ash composition had decreased after undergoing an hour of distilled water washing. The impact was most obvious for herbaceous miscanthus in which the ash reduced from ~5.4% to ~3.8% in dry basis but not so much for woody pine that reduced only a little. The effect from miscanthus was apparent in the fuel blends of two different weight ratios; 50PineC-50Misc(1) having miscanthus as half its composition showed a greater impact in ash reduction upon washing, from ~2.3% to ~1.3%. According to Kasparbauer (2009), as a minimum, water washing pre-treatment is expected to decrease the ash in a biomass, and the slight increase in volatiles with a minor decrease in fixed carbon was caused by the reduction in ash content. In a study using different ways to leach rice straws by Jenkins et al. (1996), from 19.6% ash of the untreated rice straw; 1-minute-water-spraying reduced the ash content by 0.5%, flushing tap water and distilled water were found to be more effective with both resulting ~18% ash after leaching, submerging 24-hour in distilled water reduced the ash to 17.6% whereas the naturally rain washed sample showed an 8% ash reduction after a 65 mm of rainfall. It is well-proven that biomass leaching can effectively reduce the ash content. Ash reduction upon water-washing pre-treatment (see **Figure 6. 1**) was also proven in the study by Rahman et al. (2016) about influence of washing medium on palm kernel shell (PKS) characteristics. The study by Mohammed et al. (2016) showed ash reduction as well upon water washing in the experiments conducted on leached herbaceous Napier grass.

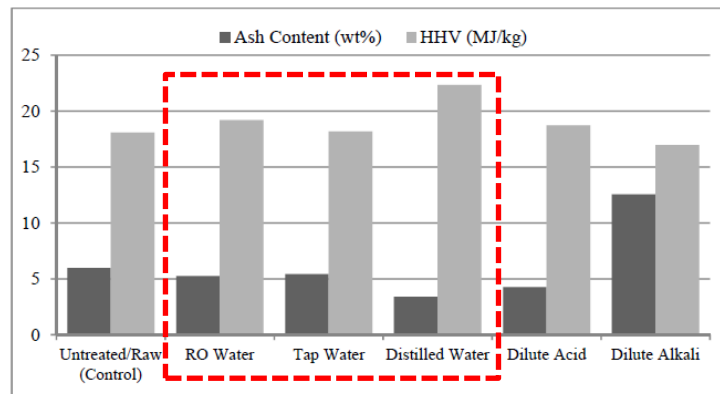


Figure 6. 1 Palm Kernel Shell – Ash Reduction and HHV Increment Upon Water-Washing Pre-treatment [edited from: Rahman et al. (2016)]

The ultimate analysis results with the corresponding HHV values are shown in **Table 6. 3** applying the experimental procedures described in **Section 3.1**.

Table 6. 3 Ultimate Analysis (wt%) and Higher Heating Value (MJ/kg) of all Samples Used in Biomass Washing Study

Sample Name	C (%) ^c	H (%) ^c	N (%) ^c	HHV (MJ/kg) ^b
PineC	48.52 ± 0.39	6.34 ± 0.16	0.172 ± 0.017	19.26
Misc(1)	48.20 ± 0.69	6.46 ± 0.10	0.70 ± 0.17	18.05
90PineC-10Misc(1)	51.68 ± 0.93	6.80 ± 0.17	0.176 ± 0.027	20.67
50PineC-50Misc(1)	50.42 ± 0.32	6.63 ± 0.20	0.354 ± 0.024	19.69
wPineC	49.42 ± 0.81	6.38 ± 0.55	0.135 ± 0.028	19.66
wMisc(1)	48.37 ± 0.72	6.43 ± 0.10	0.666 ± 0.020	18.46
90wPineC-10wMisc(1)	51.72 ± 0.14	6.76 ± 0.76	0.146 ± 0.091	20.79
50wPineC-50wMisc(1)	50.80 ± 0.33	6.59 ± 0.17	0.305 ± 0.055	20.12

^b dry basis (db) ^c dry-ash-free basis (daf)

The ultimate analysis results showed small elemental changes after washing pre-treatment. There was no general trend observed for the change of each element common to all biomass samples, which was consistent with findings of many other researchers (Deng et al., 2013; Saddawi et al., 2012) in their biomass washing pre-treatment works. The elemental change trend for distilled-water-washed pine in this study showed a similar trend found in the work of Kasparbauer (2009). The water-washed loblolly pine in that study reported slight carbon and hydrogen increases from 47.8% to 47.9% and 6.23% to 6.31% for carbon and hydrogen respectively. On the other hand, the elemental composition change for washing miscanthus was in line with the trend observed in mild water leaching of another herbaceous biomass, Napier grass (Mohammed et al., 2016), in which slight increase was detected for carbon content and minor reduction was found for hydrogen and nitrogen contents. However, these trends are within experimental error, so not statistically significant.

In this study, the HHV of woody pine and herbaceous miscanthus after distilled water wash was found to increase a little and this increase was consistent with findings from works of other researchers. In the work of Rahman et al. on PKS leaching, HHV increased upon water-washing (see **Figure 6. 1**); mild water-leaching of Napier grass increased the HHV from 18.11 to 18.22 MJ/kg in the study of Mohammed et al. (2016); HHV of water-washed rice straw increased as compared with untreated counterpart was found in a study of Jenkins et al. (1996) and the same observation of rising HHV after water leaching was noticed in the study of Deng et al. (2013) on several biomass samples.

6.2 Self-Ignition Propensity Risk Ranking and Reaction Kinetic Shift

Applying the biomass self-ignition risk ranking method developed by Ramírez et al. (2010) and later modified by Jones et al. (2015), the reaction rate kinetics for slow combustion simulated in the TA Q5000 TGA equipment were calculated for all the eight samples used in this washing pre-treatment study following the procedure as described in **Chapter 3**. The pictorial representation of the risk using temperature of maximum weight loss (T_{MwL}) and reaction activation energy (E_a) information from slow combustion kinetics calculation was plotted and is shown in **Figure 6. 2**.

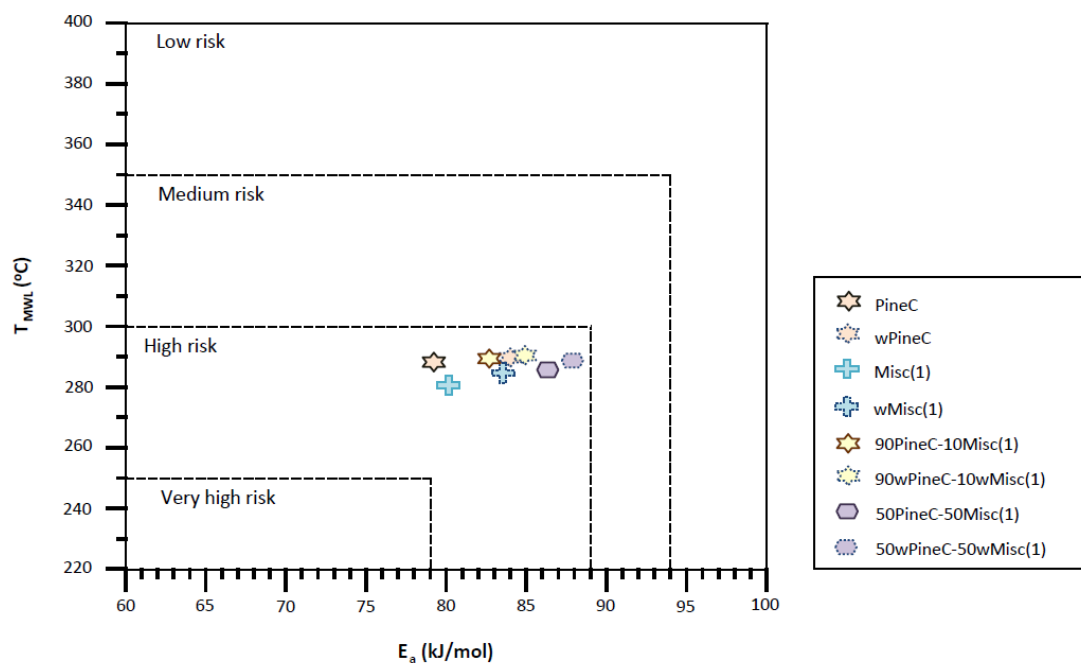


Figure 6. 2 Self-Ignition Propensity Risk Comparison between Untreated and Washed Biomass

As seen in **Figure 6. 2**, all samples used in this washing pre-treatment study showed high risk, regardless before or after washing pre-treatment. Similar to results in the studies of Saddawi et al. (2012) and Fahmi et al. (2007), the T_{MWL} of washed samples did shift to the right i.e. the temperature at maximum weight loss rate happened at a higher temperature. It was believed that this decrease of reactivity in washed biomass was due to catalytic potassium and calcium elements being washed out of the biomass. It was noticed that the T_{MWL} range for all sample was small and limited to within 280 to 300°C. The E_a fell within a small range also of 79 to 89 kJ/mol such that the self-ignition risk for all samples was confined within the 'high risk' zone. These results are consistent with the conclusion made in the study by Demirbas (2004) on many different kinds of biomass, even though the structural, proximate and ultimate analyses values differed, the ignition temperatures change was in a narrow interval.

The derivative thermogravimetric (DTG) profiles of the slow combustion procedure and slow pyrolysis processes were examined. For both profiles, it was apparent that a shift in reaction rates did exist for washed biomass relative to their untreated counterparts, consistent with findings from Jenkins et al. (1998a) and Deng et al. (2013) in studies on combustion properties of biomass and effect of water washing on biomass fuel properties respectively (see **Figure 6. 3** (a)&(b) respectively).

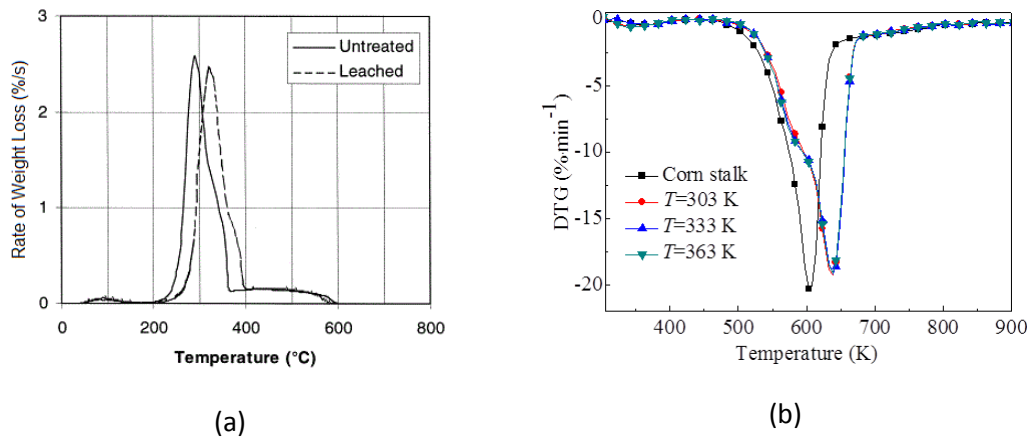
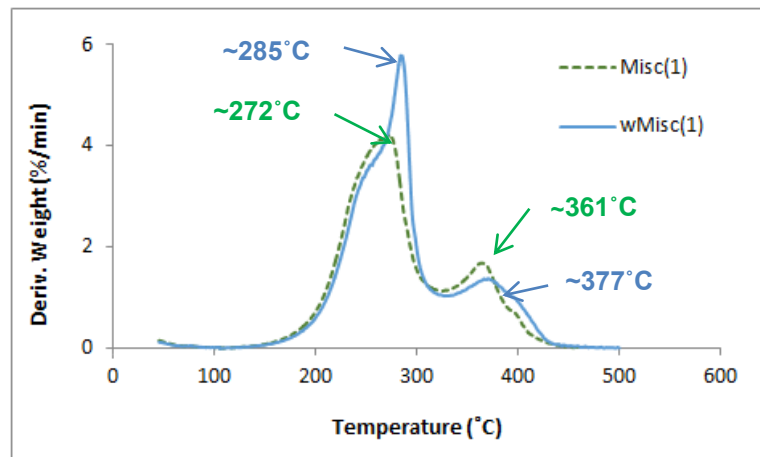


Figure 6. 3 Comparison of DTG Profiles of (a) Rice Straw (Jenkins et al., 1998a) (b) Corn Stalk (Deng et al., 2013) before and after Leaching Pre-treatment

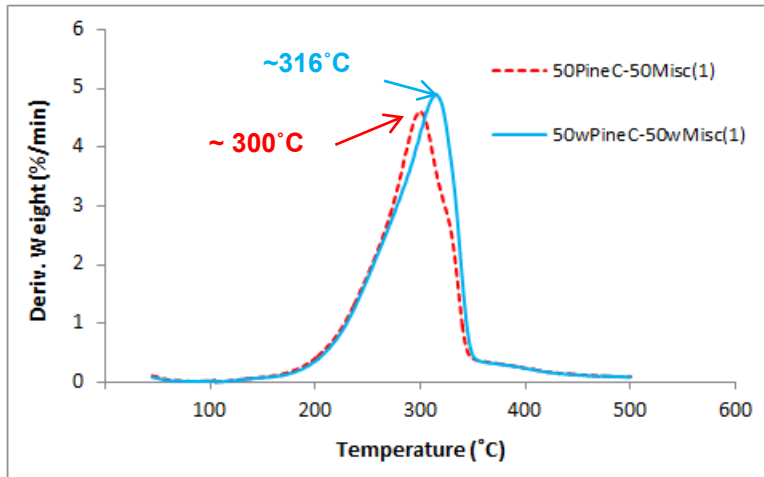
In this study, the slow combustion DTG profiles of all biomass and their blends showed both the T_{MWL} (maximum weight loss was the peak at volatiles combustion section, before ~300°C) and T_{char} (the peak at char combustion section >350°C) were moved to slightly higher temperatures. However, this kinetic shift was more obvious in herbaceous miscanthus than woody pine used in this study. The DTG profiles for slow combustion of Misc(1) and slow pyrolysis of 50PineC-50Misc(1) and those of their

respective washed counterparts are shown in **Figure 6. 4**. As seen in **Figure 6. 4(a)**, the T_{MWL} and T_{char} of wMisc(1) were respectively $\sim 13^{\circ}\text{C}$ and $\sim 16^{\circ}\text{C}$ higher than those of Misc(1). Biomass blends exhibited a similar temperature shift effect after washing pre-treatment. As seen in **Figure 6. 4(b)**, slow pyrolysis DTG profile of 50PineC-50Misc(1) showed $\sim 16^{\circ}\text{C}$ of T_{MWL} increase after being washed. The shift on the 90PineC-10Misc(1) upon washing was less than 5°C , revealing characteristics that resembled more of pure pine. Since woody biomass contained less ash and alkali components (Tumuluru et al., 2012) hence less problematic elements to be removed, it was not surprising that water washing was seen to be more effective when applied on herbaceous biomass that had higher alkali and ash contents.

The change in T_{MWL} observed in this study was consistent with findings from Deng et al. (2013). For the six biomass samples used in that study, it had been concluded that the derivative thermogravimetric profile showed devolatilisation began at a higher temperature during both combustion and pyrolysis processes and a typical result for herbaceous corn stalk is shown in **Figure 6. 3(b)**. In another study on properties of washed oil palm empty fruit bunches (EFB) by Abdullah and Sulaiman (2013) it had been concluded that reduction in alkali metal and inorganics upon EFB water washing was the reason for the shift in the DTG profiles.



(a)



(b)

Figure 6. 4 DTG Profiles Before and After Washing Pre-treatment (a) Individual Material Slow Combustion: Misc(1) and wMisc(1) (b) Blend Slow Pyrolysis: 50PineC-50Misc(1) and 50wPineC-50wMisc(1)

6.3 Determining Dust Layer Minimum Ignition Temperature and Ignition Delay Time

The minimum ignition temperature of biomass dust layer (T_{LIT}) were conducted following the procedure outlined in BS EN 50281-2-1. As described in **Chapter 3**, the ignition delay time of the dust layer was noted and later the maximum surface temperature permissible on any equipment was calculated according to BS EN 50281-1-2 and later plotted. Owing to the limited materials available for biomass washing, all pulverised biomass that had been sieved to $< 180 \mu\text{m}$ were tested only in Ring A that had thickness of 5 mm. It had been assumed that the results trend for Ring B to be the same as found earlier, i.e. lower T_{LIT} as dust layer thickness increased from Ring A 5 mm to Ring B 12.5 mm. The T_{LIT} and corresponding ignition delay time for all the eight biomass samples and some hot plate temperatures higher than T_{LIT} with their respective ignition delay times were all tabulated in **Table 6. 4**. As seen from the table, consistent with observation by Jones et al. (2015) in a study on low temperature ignition of biomass, there was an inverse relationship between dust layer ignition temperature and its ignition delay time.

Table 6. 4 Dust Layer Ignition Temperatures with Corresponding Ignition Delay Times and T_{LIT} Case in Bold

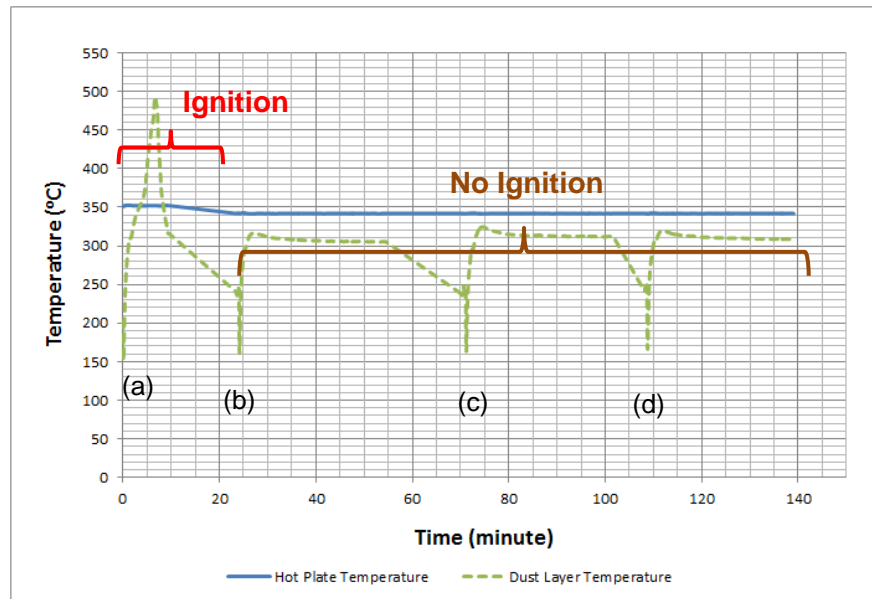
Sample Name	Layer Ignition Temperature (°C)	Ignition Delay Time (min)
PineC	350	7.40
Misc(1)	310	4.65
90PineC-10Misc(1)	350	5.47
50PineC-50Misc(1)	340	3.57
	330	5.90
wPineC	370	4.10
wMisc(1)	350	2.50
	340	2.72
	330	4.18
90wPineC-10wMisc(1)	370	2.82
	360	3.92
50wPineC-50wMisc(1)	350	3.60
	340	6.43

As described in **Chapter 3**, the biomass dust layer was poured into Ring A of 5 mm thickness and placed on a hot plate with pre-set temperature and whether or not ignition occur was noted. If no ignition was found within 30 minutes, the process was repeated with fresh dust layer and new hot plate temperature that was 10°C higher. Heat was transferred within the dust layer from hot plate to atmosphere and with heat increasing within the dust layer, exothermic chemical reactions accelerated causing increasing temperature within the dust layer. As long as heat was dissipated at a higher rate than it was produced, i.e. the hot plate temperature was below a critical value of the dust layer, no ignition was seen. At the particular critical point when the heat absorbed by dust layer failed to liberate to atmosphere at a fast enough rate, ignition occurred. Here, ignition was recognised when the first glow was seen.

In line with the trend observed for T_{MWL} obtained from DTG of each sample, washed biomass showed a higher T_{LIT} than its untreated counterpart; 370°C for washed pine, 350°C for untreated pine (20°C difference) and 330°C for washed miscanthus, 310°C for untreated miscanthus (20°C difference). Untreated woody pine that showed a higher T_{MWL} than Miscanthus was proven to be less reactive when its dust layer ignited at 350°C,

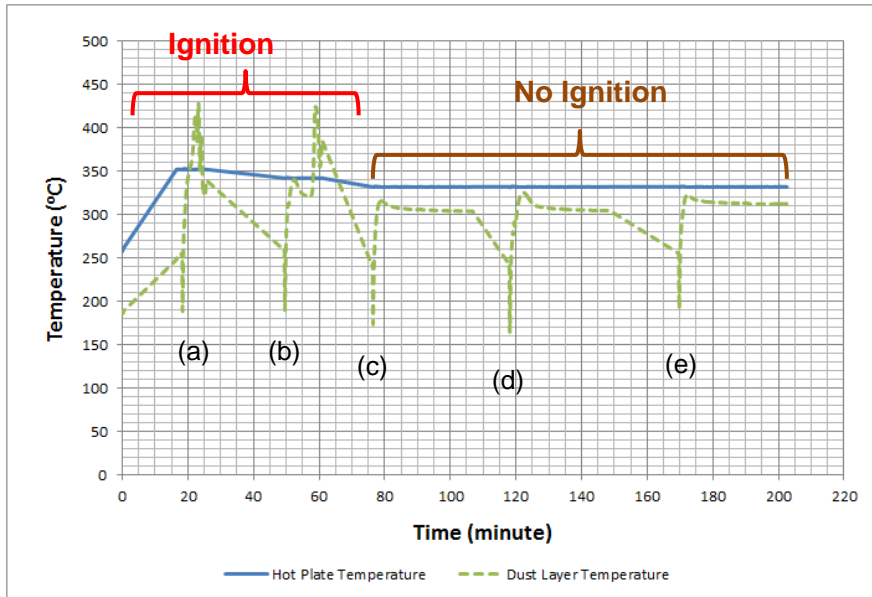
which was 40°C higher than that of miscanthus. Woody pine was less reactive than herbaceous miscanthus regardless washing pre-treatment. For the blends, 90wPineC-10wMisc(1) showed T_{LIT} of 360°C, only 10°C higher than its untreated counterpart. The same temperature difference was found for the other blend with T_{LIT} of 50wPineC-50wMisc(1) that showed 340°C compared with 330°C of 50PineC-50Misc(1). Removal of catalytic potassium metal was believed to be the cause of higher T_{LIT} of washed biomass. Potassium is the dominant source of biomass alkali metal and is known to catalyse the pyrolysis process. From the T_{LIT} results of eight samples in this biomass-washing study, the effect of washing pre-treatment was seen to be more marked on pure biomass than on their blends. The T_{LIT} of washed pine and washed miscanthus increased by 20°C as compared with their respective untreated counterparts but only a 10°C increment was observed for both the 90-10 and 50-50 blends when washed.

Typical temperature-time plots of the T_{LIT} experiment are displayed in **Figure 6. 5** and **Figure 6. 6**). 5-mm PineC dust layer ignited at 350°C but did not ignite for three attempts at 340°C, whereas 50wPineC-50wMisc(1) ignited at 350°C and 340°C but failed to ignite for three trials at a hot plate of 330°C. As seen in these two figures, ignition was marked by a rapid increase of dust layer temperature which exceeded that of the hot plate. On the other hand, when the dust failed to ignite, dust layer temperature showed a small exotherm close to the hotplate temperature in the beginning which then dropped and stabilised to a temperature lower than that of the hot plate and maintained this within the test duration. Similar procedures were repeated for two times with fresh dust every time to confirm that ignition did not happen at that particular hot plate temperature.



- (a) PineC Dust Sample 1 – Hot plate temperature set at 350°C, ignition happened
- (b) PineC Dust Sample 2 – Hot plate temperature set at 340°C, 1st time no ignition
- (c) PineC Dust Sample 3 – Hot plate temperature set at 340°C, 2nd time no ignition
- (d) PineC Dust Sample 4 – Hot plate temperature set at 340°C, 3rd time no ignition

Figure 6. 5 Temperature-Time Plot of 5-mm thick PineC Dust Layer on ANKO Dust Rig



- (a) 50wPineC-50wMisc(1) Dust Sample 1 – Hot plate temperature set at 350°C, ignition happened
- (b) 50wPineC-50wMisc(1) Dust Sample 2 – Hot plate temperature set at 340°C, ignition happened
- (c) 50wPineC-50wMisc(1) Dust Sample 3 – Hot plate temperature set at 330°C, 1st time no ignition
- (d) 50wPineC-50wMisc(1) Dust Sample 4 – Hot plate temperature set at 330°C, 2nd time no ignition
- (e) 50wPineC-50wMisc(1) Dust Sample 5 – Hot plate temperature set at 330°C, 3rd time no ignition

Figure 6. 6 Temperature-Time Plot of 5-mm thick 50wPineC-50wMisc(1) Dust Layer on ANKO Dust Rig

The T_{LIT} of 90wPineC-10wMisc(1) was 360°C, a temperature closer to that of its main component, wPineC that showed 370°C. However, the 50:50 blend was more reactive than washed miscanthus, T_{LIT} of 50wPineC-50wMisc(1) dropped to 340°C, a T_{LIT} value closer to that of pure wMisc(1). This simply shows that the reactivity of a blend is dominated by its more reactive component. For the untreated blends, the low temperature ignition characteristics of 90PineC-10Misc(1) blend seemed the same as pure PineC, where both showed T_{LIT} of 350°C. This indicates that the behaviour of blend is dominated by pine that is present in a much greater amount. When both pure pine and 90PineC-10Misc(1) dust layers showed minimum T_{LIT} at 350°C, refinement analysis (which

was half the 10°C interval) was conducted and the blend was deemed riskier since it ignited at 345°C but pure pine did not. Thus, the presence of just 10% of miscanthus lowers the ignition temperature and makes the blend more reactive from the minimum T_{LIT} viewpoint. This result, where the more reactive component increased the overall reactivity of a blend was consistent with observations reported in **Chapter 4** regarding the ignition characteristics of various untreated biomass blends.

The ignition delay time reported in **Table 6. 4** was not suitable as an indicator of ignition risk because of the inverse relationship between minimum ignition temperature and ignition delay time as mentioned earlier. Nonetheless, comparing at equal T_{LIT} of different materials, for instance at 350°C, it was seen that pure pine had the lowest ignition risk since it took the longest time to ignite. Upon blending with 10% of (more reactive) miscanthus, the T_{LIT} at 350°C, the ignition delay time was shortened by ~2 min, indicating a slight risk increase. Washed miscanthus that ignited at 350°C showed the shortest ignition delay time and this was considered riskier than pure untreated pine. On the other hand, when the blend consisted of equal amount of washed materials from both species, the fuel was slightly safer since its delay time at 350°C was slightly longer than that of washed miscanthus.

Comparing the slow combustion weight loss curves as determined by TGA (see **Figure 6. 7**), the washed samples had their curves shifted slightly towards the left as compared with respective unwashed counterpart. From the dust layer test results, the weight loss trend by TGA is consistent with T_{LIT} results, indicating washed biomass has become less reactive since washed biomass sustained a higher ignition temperature. Kinetics data in **Appendix A** showed higher activation energy and pre-exponential factor for the slow combustion reaction. Eliminating minerals like potassium did reduce the biomass reactivity, showing higher TLIT for every biomass and blend studied here.

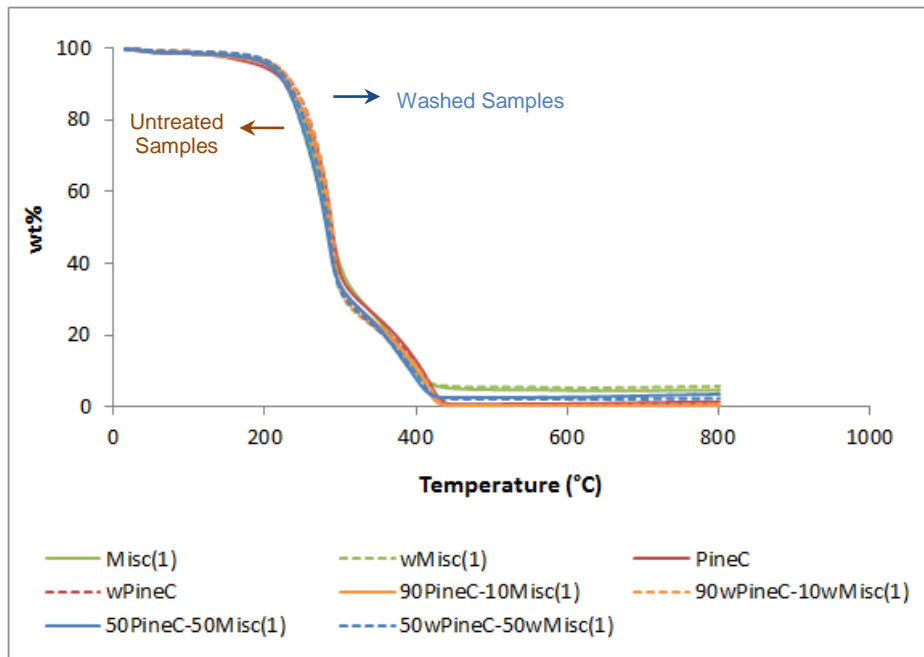


Figure 6. 7 TGA Slow Combustion Weight Loss Curves Comparison of Eight Samples – Before and After Washing

6.3.1 Industrial Significance

As discussed in **Section 2.3**, there are three maximum permissible apparatus temperatures (MPST) determination methods commonly used and the results are illustrated in **Figure 6. 8**. The values that were estimated for 12.5-mm thick dust layer when Guideline1 was used is boxed in the figure. The results trend was consistent with T_{LIT} values obtained experimentally from the ANKO hot plate, in which the maximum apparatus permissible temperature decreased as the dust layer got thicker. It is reasonable because the thicker the dust layer gets, more mass is available to retain heat generated from the constant temperature hot plate but the surface area to dissipate heat remains unchanged; this accelerates the exothermic reaction and causes the dust layer to ignite at a lower temperature.

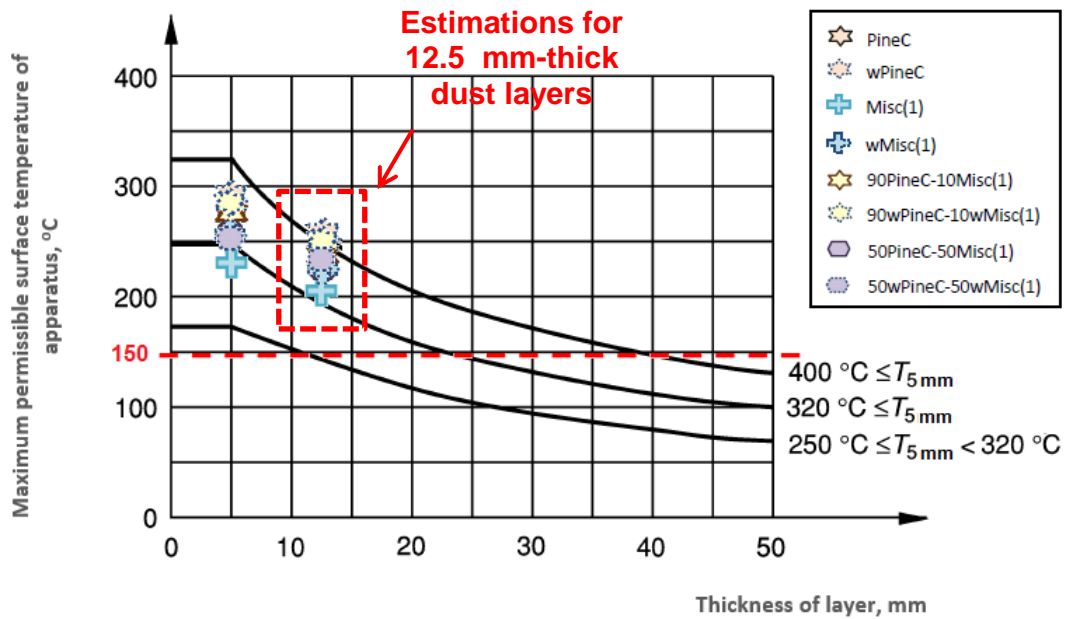


Figure 6. 8 MPST Estimation with Three Different Methods – Guideline 1 (Points), Guideline 2 (Curves, T_{LIT} from Pre-Refinement) and Power Station Practice (Constant at 150°C) on Untreated and Washed Biomass Samples

Adopting Guideline2, MPST for PineC dust layer follows the middle curve whereas Misc(1) the bottom curve. If the power station practice that fixed MPST at 150°C is applied, the maximum allowable dust accumulation would extrapolate to ~22.5 mm and ~10 mm for PineC and Misc(1) respectively if Guideline2 is followed.

From the constant temperature hot plate T_{LIT} determination experiment, the general conclusion was that washing pre-treatment, that resulted in removal of catalytic elements like potassium from biomass, makes its dust layer less reactive. However, like previous observations on untreated biomass, even with presence of a minor 10 wt% of more reactive material in a biomass blend, the overall reactivity was heightened. The T_{LIT} of eight samples in this study was within the range of 310-370°C but with the inverse relationship between ignition temperature and its delay time, the small difference reported here will be increasingly important as dust layers get thicker. As concluded previously, provided the dust layers formed is thin, the minor changes in T_{LIT} is not significant enough to affect plant management in terms of housekeeping and dust management.

It is well known that washed biomass increases the ash fusion temperature (proven by many studies), lessens ash formation and reduces boiler tube corrosion. Thus using washed biomass has potential for improving the durability of biomass-fired power boilers and furnaces that operate at high temperatures in a power station. Hence, the major reason to apply washing pre-treatment to biomass fuel would be for better operation of

major thermal conversion equipment in a power station. Even so, the slightly reduced low temperature dust layer ignition risk is another plus point to help justify applying washing pre-treatment on biomass fuels. Any additional costs incurred for pre-treatments can be compensated by better operability of the boiler and combustion process (Maciejewska et al., 2000).

6.4 Effects of Water Washing Biomass – Removal of Elements, Total Organic Carbon in Leachates, Changes in Lignocellulosic Composition

The herbaceous miscanthus and woody pine digestates produced from reaction with H_2SO_4 and HNO_3 were analysed with Atomic Absorption Spectroscopy (AAS), in which the concentrations of two major problematic metal elements, potassium (K) and calcium (Ca) that occurred naturally in biomass were the focus on. Alkali metals, particularly potassium, are very volatile and enter their vapour phase as alkali chlorides or hydroxides during combustion. After transforming into sulphates, fouling at heat convective boiler regions occurs because of the lower ash fusion temperature. Potassium combines with chlorine and sulphur resulting troublesome deposits of potassium chloride and potassium sulphate (Runge et al., 2013) when steam reaches high temperature in excess of $450^\circ C$. Since chlorine facilitates mobility of inorganic compounds particularly potassium (Jenkins et al., 1998a), the well-known corrosion mechanism of potassium with chlorine (Tumuluru et al., 2011b) causes detrimental effects on pendant tubes and other heat transfer surfaces e.g. heat exchangers or super-heaters in thermal conversion systems and in the long run, excessive potassium chloride deposits could rupture these tubes and cause a power station down time and increase maintenance cost. Calcium in the presence of chlorine shows effects similar to that of potassium, and results in corrosion and lower ash fusion temperature Tumuluru et al. (2012). Also, chlorine is related to hydrochloric acid emission in flue gases and using biomass that has its chlorine washed away is beneficial to the environment.

Taking into account the digested biomass mass (~1g) and its digestate dilution, the concentration results were finalised to the mass of metal element detected over the mass of original biomass being digested, in mg/kg unit. The leachates containing all elements dissolvable in distilled water were bottled for ion chromatography (IC) analysis. From visual observation, the leachates from Miscanthus pellets washing were brownish whereas those from Pine chips were just pale yellow (see **Figure 6. 9**). In the IC, apart from K and Ca, the other problematic element, chlorine, was investigated as well. Cation analysis were conducted to obtain the concentrations of K^+ and Ca^{2+} whereas anion analysis was performed for Cl^- . There were definitely losses of some amount of dissolved elements

during the experiment e.g. transferring sample from one container to the other, but it had been assumed that the amount was not significant to impact on the overall results.



Figure 6. 9 Leachates from 1 Hour Washing Pre-treatment of (a) Miscanthus Pellets (b) Pine Chips

The concentrations reported by the IC were converted from ppm to mg of undesired ion detected per unit mass of biomass i.e. mg/kg unit. The effectiveness of washing pre-treatment in terms of percentage removal of undesired elements was then calculated and the results are tabulated in **Table 6. 5**.

Table 6. 5 Concentration (mg/kg of Dry Fuel) in Untreated Fuels (AAS Analysis) and K, Ca, and Cl Removed (mg/kg of Dry Fuel) during Water Washing (IC Analysis of Leachates)

	In Fuel		Removal				
	K	Ca	K ⁺	% K	Ca ²⁺	% Ca	Cl ⁻
PineC	342	584	130	88	19	3	31
Misc(1)	2998	5409	2709	90	1017	18	2781

It was found that a large fraction of potassium ion (K⁺) and chloride ion (Cl⁻) was removed from miscanthus (90% K and 2781 mg Cl/kg miscanthus) and smaller but significant amounts were washed out from pine. The removal of K and Ca was in keeping with that obtained by Saddawi et al. (2012) where various biomass fuels e.g. short-rotation coppice (SRC) willow, eucalyptus, miscanthus and wheat straw were washed. The washing of miscanthus chips showed 62 and 19% of K and Ca removal respectively, and 80% for Cl. From the study of Abdullah and Sulaiman (2013) about properties of washed oil palm

empty fruit bunches, it was found that ash reduction was not proportional to alkali metals removal though alkali and alkali earth metals dominate the overall ash content reduction. As it has been shown that potassium is a major alkali metal source that catalyses the biomass pyrolysis process (Nowakowski et al., 2007), removal of potassium in this study is expected to show that washed fuel becomes slightly safer (with a higher dust layer ignition temperature) – this is presented in **Section 6.3**.

The total organic carbon (TOC) and total inorganic carbon (TI) were determined from the total carbon in conjunction with calculation using **Equation 3.13** and the results shown in **Figure 6. 10**. Under the same pre-treatment condition of 1 g biomass washed by 5 ml of distilled water, it was obvious that miscanthus leachate had much higher TOC concentration of ~1127 ppm (equivalent to ~5635 mg/kg Miscanthus) than that contained in pine leachate which showed ~195 ppm (equivalent to ~975 mg/kg Pine). The TI concentrations from both leachates were quite low, not reaching even 20 ppm; ~16 ppm for Miscanthus (equivalent to ~80 mg/kg Miscanthus) and ~18 ppm for pine (equivalent to ~90 mg/kg pine). This simply showed that not much inorganic carbon was washed out as compared with the organic counterpart in this experiment context of 1 hour distilled water washing. Considering the herbaceous miscanthus and woody pine used here were analogous to leaf and mallee wood respectively, the results were consistent with the findings from Liaw and Wu (2013) in which the TOC amount from leaf leachates were more than that from mallee wood for both the batch and semi-continuous leaching process in their study.

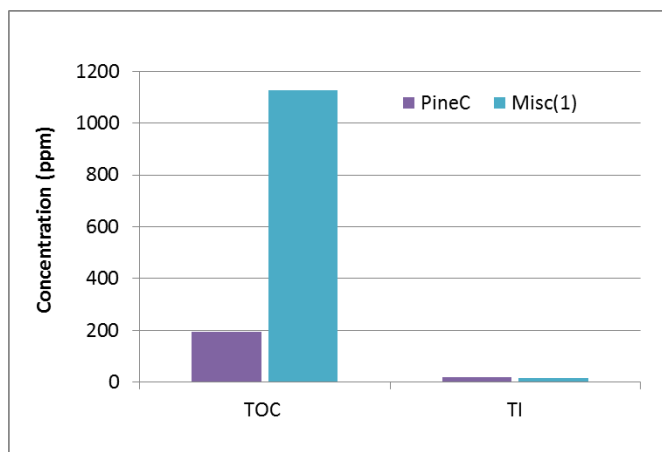


Figure 6. 10 TOC and TI Comparisons (in ppm) of Pine and Miscanthus Leachates upon 1 hour Washing Pre-treatment

Two different methods for lignin determination were conducted for this study following the way adopted by Akinrinola (2014).

Following the lignocellulosic analysis conducted by IBERS, Aberystwyth, the biomass composition in terms of %hemicellulose (HCLS), %cellulose (CLS) and lignin (both %Acid Detergent Lignin (ADL) and %Klason Lignin) is shown in **Figure 6. 11**. The Klason lignin content was found to be always higher than the corresponding ADL content whereas the HCLS and CLS were calculated according to **Equation 3.11** & **Equation 3.12**. Regardless which way the lignin was determined, the lignocellulosic composition of any fuel did not sum up to 100%. The difference accounted for the intrinsic moisture of the cell wall, some hydroxycinnamates (aromatic acids with simple C6-C3 chemical backbone) (Teixeira et al., 2013), ash, proteins and other components of the cell wall (Akinrinola, 2014). As seen in **Figure 6. 11**, washing pre-treatment did not alter too much the contents of HCLS, CLS and Lignin of both herbaceous miscanthus (Misc(1) vs wMisc(1) bars), woody pine (PineC vs wPineC bars) and their blends in two different weight ratios. The reason for using room temperature water in washing was to avoid biomass compositional changes due to reaction at higher temperature and results show this was the case. It was believed that biomass lignocellulosic composition was not the major reason that caused T_{LIT} increment of washed biomass.

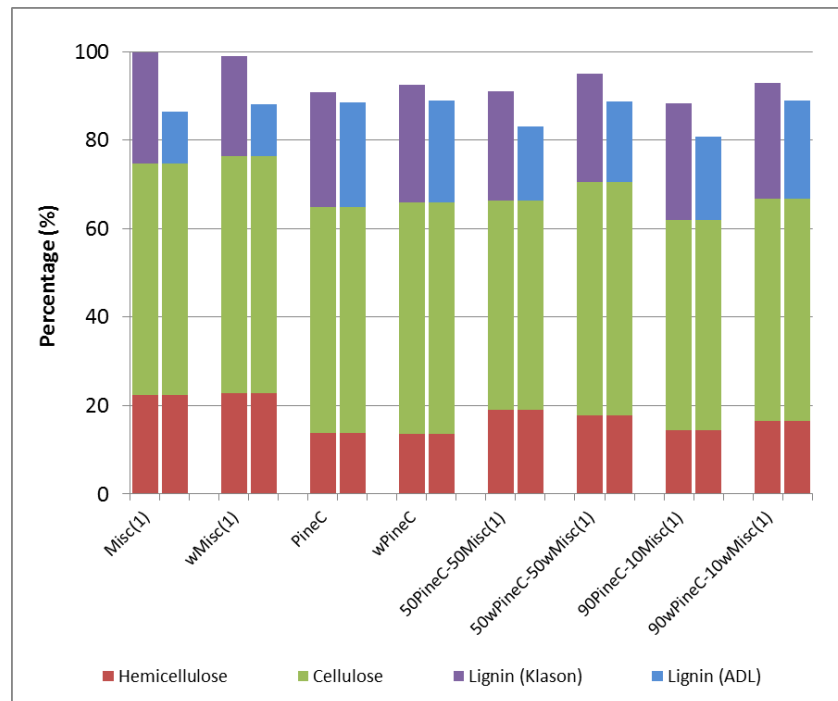


Figure 6. 11 Lignocellulosic Analysis on Eight Untreated, Washed Biomass and Blends

6.5 Concluding Remarks and Suggestions for Future Work

The results from this study show that simple water washing of biomass removes undesired elements/minerals e.g. potassium, calcium and chlorine that are harmful to boiler operation, especially from herbaceous biomass, which was miscanthus in this study. The T_{LIT} of washed single-material-biomass dust layer, be it woody or herbaceous, showed a slight increase in T_{LIT} when compared with their untreated counterpart. The T_{LIT} increase was halved for the washed woody and herbaceous blend dust layers of two different weight ratios. The DTG profiles of slow combustion and slow pyrolysis reactions of all the eight samples did show kinetic shift to slightly higher temperature. From the T_{LIT} determination experiment and self ignition risk ranking of all the samples before and after washing pre-treatment, it is concluded that washed biomass and their blends were slightly safer than untreated counterparts, but that small change is not significant enough to cause drastic changes to the normal plant dust management and operation. Nevertheless, it does change the estimated safe working dust layer thickness.

In order to make this study more comprehensive, more species of woody and herbaceous biomass could be used. The effects of using such pre-treated biomass on its self-ignition or low temperature ignition characteristics could be examined. Apart from conducting similar studies on a greater variety of woody and herbaceous biomass, washing method and washing parameters like washing agent type, washing agent temperature, biomass to washing agent ratio, washing speed and washing duration could be varied.

Besides stirring biomass in washing agent, there are other washing methods that could be applied, among some - field leaching (Jenkins et al., 1996), soaking in stagnant washing agent, spraying with washing agent, water flushing (Deng et al., 2013). If the biomass is leached in field, or better known as natural leaching, it is a good way for nutrient recycling (Springer Science+Business Media B.V., 1997) since plant site leaching would incur extra cost to recycle the nutrients back to the biomass field. Other than using neutral (or close to neutral) washing agents like distilled water, deionised water or tap water, slightly acidic, mild alkaline agent, ammonia or ammonium acetate could be used. Dilute acids like mild hydrochloric acid is suggested since it was known that acid leaching was more thorough and effective in reducing alkali emissions from waste wood and wheat straw than using water (Davidsson et al., 2002). Ionic liquids are candidates of washing agent since recent studies reported that ionic liquid solvents are effective in reducing biomass recalcitrance (Tumuluru et al., 2012). It is worth checking the impacts on the T_{LIT} of biomass dust layer that had been washed by different methods or solvent agents.

It is worthwhile to see the effects of using washing agent at different temperatures. The study of Deng et al. (2013) had proven that undesirable elements were removed more effectively at elevated temperatures. Further study can be carried out in

search of the optimum washing temperature when a particular solvent is used on washing a certain biomass. The usage of elevated temperature solvent is practically achievable because the effluent from power station has much higher temperature than normal room temperature and the process heat generated is not wasted if used to pre-treat biomass. It is worth checking the impacts on self-ignition temperatures of the various biomass dust layers washed at different temperatures.

Apart from that, the effect of varying biomass:washing agent ratio is another parameter recommended for further studies. The more the washing agent (the solvent) used, the more the undesired elements are washed out but saturation point would be reached at a certain extent. The sensitivity of biomass T_{LIT} change with respect to percentage removal of undesirable elements are worth noting. On the other hand, the agitation speed in biomass washing could be more effective as the speed increases but again, there could be a threshold point in which the biomass T_{LIT} will not alter when the stirring speed changes. The washing duration is another parameter that affects the amount of desirable elements removal. The longer the biomass is treated, the more the undesirable minerals are removed. Like stated in the washing effect study on EFB by Abdullah and Sulaiman (2013), washing residence time would be expected to impact the efficiency.

Chapter 7

Handling – Effects of Torrefied Biomass on Dust Layer Ignition Characteristics

There has been speculation that torrefied fuel would have lower self-heating propensity due to its hydrophobicity (Akinrinola, 2014) and lower reactivity. However, Basu (2013) stated that apart from explosion potential, there is fire risk associated with torrefied biomass because of its low ignition temperature that this had been experienced by some biomass plants. Referring to some previous work, it seems that torrefied dust is easily ignited as compared with the untreated counterpart. Thus, it is of interest to investigate this matter further. In the study of Wilén et al. (2013) on utilisation prospects of torrefied wood via pilot tests, they found that torrefied wood dust layer had actually ignited at 330°C that was 10°C lower than the untreated counterpart that ignited only at 340°C. There have been no other investigations on this topic, and hence this work compares raw and torrefied biomass and their blends

Two biomass samples (from the two major biomass groups – woody and herbaceous) and a blend between 50wt% torrefied and 50wt% untreated biomass were the focus of the study. The woody pine used here was originally in chips form from a different power station (not the same pulverised pine studied in **Chapter 4**) and therefore it was denoted as PineR whereas the miscanthus (denoted as Misc(1) here) was pelleted miscanthus but different from that in **Chapter 4**. The corresponding torrefied biomass were denoted with a small letter 't' before their original material name.

The five samples were used in this study and their respective original form and compositions are tabulated in **Table 7. 1**. **Figure 7. 1(a)&(b)** show woody pine and herbaceous miscanthus in their original chips and pellets form respectively. As mentioned before, subjected to limited material constrain, only one torrefaction condition was chosen. Gucho et al. (2015) in their experimental study on dry torrefaction of beech wood and miscanthus had found that effects of residence time on mass and energy yields became obvious when torrefaction temperature exceeded 280°C. It was also found that the optimum residence time for miscanthus torrefaction was 30 min within the 15-150 min range investigated. Studies from Wilén et al. (2013) estimated that optimum torrefaction temperature range for woods was 250-260°C and Basu (2013) concluded that torrefaction process is slightly exothermic over temperature range of 250-300°C (Basu, 2013). Nonetheless, higher temperature could be applied on pine chips that were less exothermal (Wilén et al., 2013) among the wood studied. Considering findings from these studies and to ensure mass and energy yields were only moderately compromised, a torrefaction temperature of 270°C and residence time of 30 min were selected for Misc(1) and PineR in

this study. 50tM(1):50M(1) was blended from pulverised sample, in which the particle size was selected to suit the requirement of the specific experiment.

Table 7. 1 Samples Used in Torrefaction Studies with Respective Original Form and Torrefaction Condition (Torrefaction Temperature in °C, Residence Time in Minutes)

Sample Name	Original Form	Composition (wt%)	Torrefaction Condition (°C, minutes)
Misc(1)	Pellet	100% miscanthus	n.a.
PineR	Chip	100% pine	n.a.
tMisc(1)	Pellet	100% torrefied miscanthus	270°C, 30 minutes
tPineR	Chip	100% torrefied pine	270°C; 30 minutes
50tM(1):50M(1)	Powder, <180 µm	50% torrefied miscanthus + 50% miscanthus	n.a.

n.a. – not applicable



(a)



(b)

Figure 7. 1 Biomass For Torrefaction (a) Untreated PineR Chips (b) Untreated Misc(1) Pellets before Torrefaction

Following the torrefaction procedure described in **Section 3.2.2.1**, the temperature profiles for both biomass samples were tracked by the three separate thermocouples (denoted by TC1, TC2 and TC3), transmitted through data logger and recorded by a software. The PineR torrefaction temperature profile is shown in **Figure 7. 2**, with each torrefaction stage labelled (1-initial heating, 2-pre-drying, 3-post-drying & intermediate heating, 4-torrefaction and 5-solid cooling).

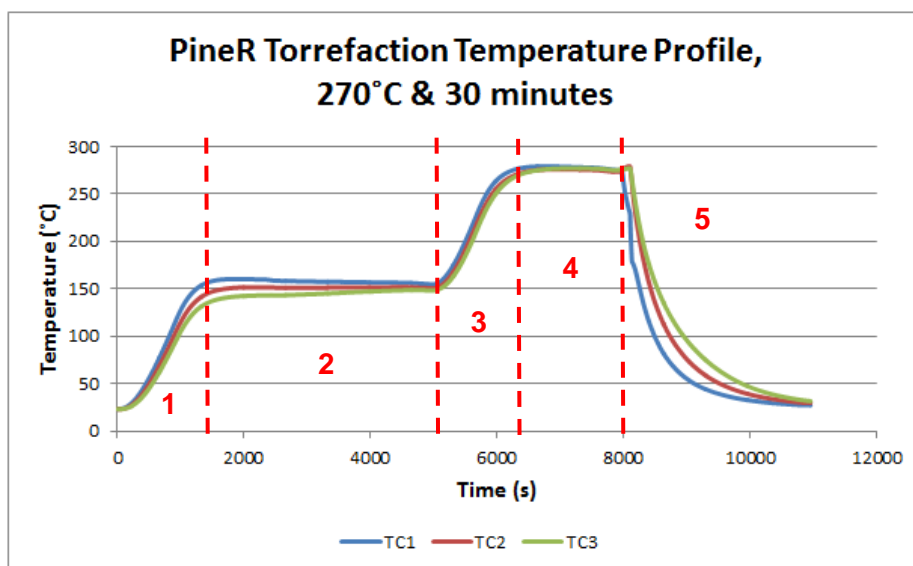


Figure 7. 2 Torrefaction Temperature Profile of PineR Torrefied at 270°C with 30 minutes Residence Time (Stages: 1-initial heating, 2-pre-drying, 3-post-drying & intermediate heating, 4-torrefaction and 5-solid cooling).

Consistent with the stages of torrefaction process described in **Section 2.6.2.1**, the first section with temperature rise from ~25°C to 150°C indicated the initial heating stage, after which the temperature was held constant for 60 minutes for the pre-drying stage. Along this process, pale yellowish gases were seen liberated from the 90-degree glass connector outlet on the right. At the end of this period holding temperature constant at 150°C, the sample went through the post-drying & intermediate heating stage in which sample temperature increased and proceeded to the torrefaction stage, where the sample temperature was held constant at the desired torrefaction temperature of 270°C with a residence time of 30 minutes. The collection beaker that aimed to collect tars and other liquids like bio-oil during the torrefaction process started to fill up. Comparing the tar/bio-oil colour from Misc(1) and PineR (see **Figure 7. 3**), Misc(1) yielded an oil slightly darker in colour (brownish) than from PineR (yellowish). This was probably because Misc(1) had advanced to further reactions releasing more components with higher molecular weight along the torrefaction stage, since miscanthus is a more reactive biomass fuel than pine. This liquid was not analysed further, since for this work, only the solid product is of interest.

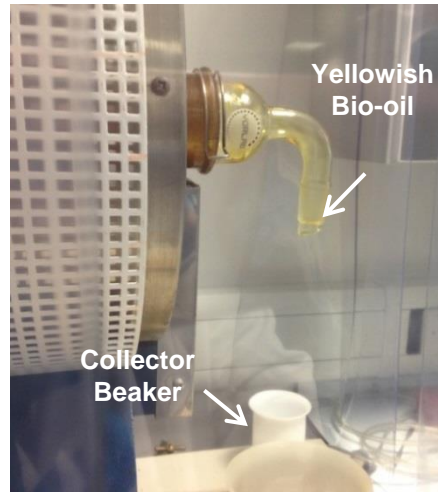


Figure 7.3 Torrefaction of PineR – Yellowish tar/bio-oil Resulted at the Right Connector and Collected at the Bottom

After the 30-minute residence time, the torrefaction reactor tube was removed from the furnace and the torrefied sample entered the solid cooling stage where inert nitrogen purged for another ~60 minutes to prevent further reaction. The torrefied samples – tPineR and tMisc(1) are illustrated in **Figure 7.4** (a) & (b) respectively. For both materials, the colour had become darker upon torrefaction and this observation was consistent with findings from various torrefaction studies (Gucho et al., 2015; Bridgeman et al., 2008; Tumuluru et al., 2011a; Tumuluru, 2016; Dahlquist, 2013) that had concluded that the colour of solid darkens as torrefaction severity increases.



(a)



(b)

Figure 7.4 Biomass After Torrefaction (a) PineR Chips (b) Misc(1) Pellets

7.1 Proximate, Ultimate Analyses and Higher Heating Values

The two common fuel characterisation methods – proximate and ultimate analyses were carried out in accordance to appropriate British Standard as described in **Chapter 3**. For all the five untreated, torrefied and untreated-torrefied blend biomass samples, the analysis were done in duplicate or triplicate and their averages, standard deviations were reported. Proximate analysis can also be performed using the thermogravimetric analysis (TGA) method, which is preferred in industry because it is quicker. In this study as far analyses on other samples, TGA was mainly used to obtain self-ignition process kinetic parameters, hence a slow combustion process was programmed in the TGA equipment to simulate the self-heating process leading to self combustion. Ultimate analysis, when determined on a dry-ash-free (daf) basis enabled plotting of the Van Krevelen diagram that provided further insights of a fuel. Applying the correlation developed by Friedl et al., the higher heating values (HHVs) of all biomass fuel involved were estimated with high accuracy (Friedl et al., 2005) by eliminating the moisture content determined from proximate analysis, i.e. in dry basis (db). This equation has had some prior validation for torrefied biomass (Bridgeman et al., 2008).

7.1.1 Proximate Analysis and Reaction Rate Kinetics

Proximate analysis in accordance to British Standards as detailed in **Chapter 3**. For proximate analysis, the average values were used in further calculation. For the reaction rate kinetic parameters as determined for the torrefied fuels, the activation energy, E_a for volatiles combustion was determined from the linearised Arrhenius equation (from $\ln k$ vs $1/T$ graph) and results showed that their respective correlation coefficient, R^2 (Gil et al., 2010) value was quite close to 1, ranging from 0.9891 to 0.9978, suggesting a good and strong relationship. The E_a and temperature of maximum weight loss (T_{MWL} , obtained from DTG profile) values were later used in the pictorial self-ignition propensity risk ranking later, as detailed in **Section 4.1** earlier. The proximate analysis results are tabulated in **Table 7.2**.

Table 7. 2 Proximate Analysis (wt%) and Relevant Changes of all Samples Used in Torrefaction Studies

Sample Name	Moisture ^a (wt%)	Volatile Matters ^b (wt%)	Fixed Carbon ^d (wt%)	Ash ^b (wt%)	Change % Moisture ^a	Change % Volatile Matters ^b	Change % Fixed Carbon ^d	Change % Ash ^b
Misc(1)	5.84 ± 0.46	76.94 ± 0.25	17.63 ± 0.35	5.426 ± 0.095	n.a.	n.a.	n.a.	n.a.
PineR	1.80 ± 0.54	80.55 ± 0.012	18.43 ± 0.022	1.018 ± 0.034	n.a.	n.a.	n.a.	n.a.
tMisc(1)	2.21 ± 0.87	70.459 ± 0.0915	23.53 ± 0.82	6.0099 ± 0.0510	-62.08	-8.42	33.44	10.77
tPineR	1.301 ± 0.298	76.885 ± 0.0952	22.075 ± 0.429	1.040 ± 0.0363	-27.22	-4.55	19.77	2.12
50tM(1):50M(1)	3.99 ± 0.26	73.16 ± 0.084	21.16 ± 0.22	5.671 ± 0.0457	n.a.	n.a.	n.a.	n.a.

^a as received (ar) ^b dry basis (db) ^d by difference n.a. – not applicable

It was apparent that torrefaction thermal pre-treatment had reduced the equilibrium moisture content of biomass significantly. The equilibrium moisture content of herbaceous Misc(1) decreased by more than half, and that in woody PineR reduced by just over a quarter. For the 50tM(1):50M(1) blend, its equilibrium moisture content was around the average of tMisc(1) and Misc(1). The first two steps in torrefaction that included initial heating and pre-drying stages drives off most of the biomass moisture and then the solid equilibrates with ambient humidity. The equilibrium moisture content then depends on the hydrophobicity of the solid. This is related to the extent of dehydration and decarboxylation during torrefaction. tMisc(1) torrefied more than tPine because it is more hydrophobic. For volatile matters, both tMisc(1) and tPineR showed reduction from those contained in Misc(1) and PineR respectively whereas 50tM(1):50M(1) showed volatile matters somewhere between that contained in tMisc(1) and Misc(1). Misc(1) has torrefied to a greater extent than PineR and this is reflected in the larger decrease in VM. Reduction in both moisture and volatiles contents had increased the fixed carbon content. Both Misc(1) and PineR that fixed carbon around 17-18 wt%, and this increased to more than 20 wt% upon torrefaction. It was observed that the torrefaction process was slightly exothermal and it is speculated that when heat was released, volatiles that consisted of many hydrogenated and oxygenated compounds (Gucho et al., 2015), escaped the solid at a higher rate. The cleaving of H-C and O-C bonds (dehydration between organic constituents) increased the carbon content at the expense of hydrogen and oxygen, leaving behind the solid torrefied product with higher fixed carbon concentration (Ferro et al., 2004). The higher the fixed carbon content, the darker the colour of the torrefied solid product (Gucho et al., 2015). A consequence of torrefaction is concentration of ash. Both tMisc(1) and tPineR show higher ash contents than Misc(1) and PineR respectively and 50tM(1):50M(1) blend has an ash content somewhere in between that of tMisc(1) and Misc(1). Since ash is the non-combustible component of a biomass, its absolute amount remains because almost none was driven away during the torrefaction process (Nhuchhen et al., 2014). With the reduction of moisture and volatiles, ash content therefore has become more concentrated and the concentration increases as the torrefaction condition gets more severe (Phanphanich and Mani, 2011; Medina, 2014). As the torrefaction severity increases, the fuel becomes more coal-like and coal contains higher ash than biomass (Ciolkosz, 2010).

In summary, the reducing trend of moisture and volatiles contents and the increasing trend of fixed carbon and ash were consistent with findings from previous studies. Decomposition and devolatilisation during torrefaction removes from biomass a number of oxygen-rich volatile matter and gases and in essence concentrates the fixed carbon and ash contents (Lasode et al., 2014).

7.1.2 Ultimate Analysis, Higher Heating Value and the Van Krevelen Diagram

The elemental analysis on the five samples in this torrefaction study was conducted, in duplicate or triplicate and the average value with standard deviation was reported. Like the biomass samples reported earlier, these samples had low sulfur content, below the detection limit of the equipment. The correlation developed by Friedl et al., that had been validated by bomb calorimeter results, was applied to calculate the high heating values (HHV) (Friedl et al., 2005) of all samples here. Besides calculating the caloric values, the atomic ratios of H/C and O/C were calculated too. The nitrogen analysis results are interesting since they imply a loss of nitrogen from both fuels from both fuels during torrefaction. There has been mixed findings for the behaviour of fuel-N during torrefaction. Nitrogen analysis on North American pine chips torrefied at different temperatures and residence times conducted by McNamee et al. (2016) showed minor decreases at various torrefaction conditions. In the work of Akinrinola (2014) on some Nigerian biomass, Gmelina torrefied at 270°C for 30 and 60 minutes showed reduction in nitrogen but other samples like Terminalia, Lophira and Nauclea showed the opposite upon torrefaction. Often the N-calculated in biomass is close to the detection limit, so it is difficult to make confident judgement. However, the N-contents of the Misc(1) and tMisc(1) in particular, suggest some loss of N during torrefaction. This is important when considering torrefied biomass for combustion application, because of the relationship between fuel-N and NO_x emission. The ultimate analysis and calculated HHV of the five samples are shown in **Table 7. 3**. The changes the torrefaction process brought to carbon, hydrogen, oxygen elements (daf basis) and the HHV (db) are tabulated in the same table. It is seen that the change in carbon content was positive whereas negative changes were observed for both hydrogen and oxygen contents. The HHV changes were mostly influenced by the carbon content changes – an increase in carbon content of ~15% increased the HHV by ~15% for miscanthus and ~11% for pine. Miscanthus was more sensitive than pine to this particular torrefaction condition when HHV was concerned.

Table 7. 3 Ultimate Analysis, Higher Heating Value and the Relevant Changes of all Samples Used in Torrefaction Studies

	C (%)^c	H (%)^c	N (%)^c	S (%)^c	O (%)^d	C (change %)^b	H (change %)^b	O (change %)^c	HHV (kJ/g)^b	HHV (change%)^b
Misc(1)	48.20 ± 0.69	6.46 ± 0.10	0.70 ± 0.17	N.D.	44.64	n.a.	n.a.	n.a.	18.05	n.a.
PineR	46.25 ± 0.48	6.16 ± 0.18	0.15 ± 0.11	N.D.	47.44	n.a.	n.a.	n.a.	18.13	n.a.
tMisc(1)	55.57 ± 0.82	6.236 ± 0.082	0.58± 0.35	N.D.	37.63	15.29	-3.497	-15.75	20.80	15.24
tPineR	51.52 ± 0.60	5.890 ± 0.016	0.089± 0.016	N.D.	42.501	11.38	-4.456	-10.385	20.22	11.54
50tM(1):50M(1)	51.95 ± 0.11	6.39 ± 0.027	0.61 ± 0.49	N.D.	41.05	n.a.	n.a.	n.a.	19.46	n.a.

^b dry basis (db) ^c dry-ash-free basis (daf) ^d by difference N.D. – not detected n.a. – not applicable

From the elemental composition, calculated on daf basis, the atomic ratios H/C and O/C were determined and plotted onto a Van Krevelan diagram as shown in **Figure 7. 5**.

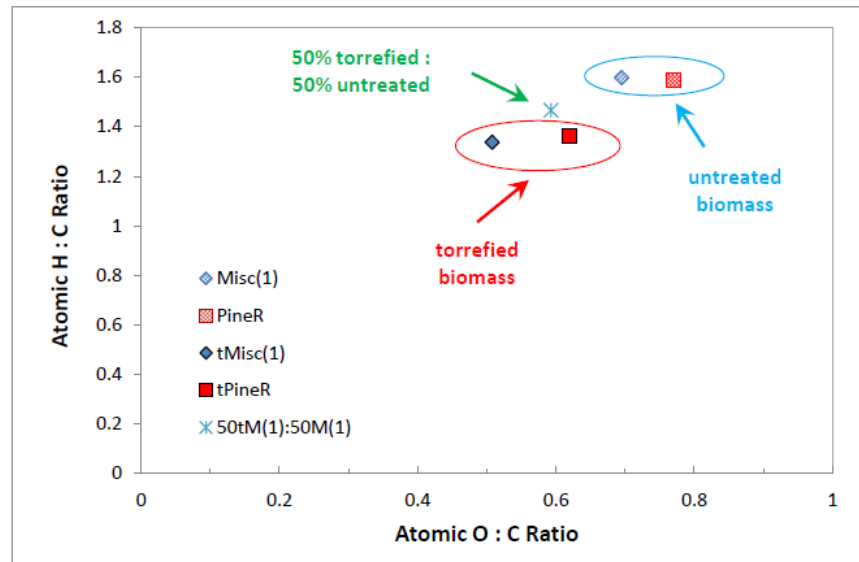


Figure 7. 5 The Van Krevelan Diagram of Samples Used in the Present Torrefaction Study

Torrefaction caused reduction of both H/C and O/C ratios of woody pine and herbaceous miscanthus. As both the ratios decreased, the fuel characteristics move towards fossil fuel coal located at the bottom left of a Van Krevelan diagram. The H/C for untreated PineR and Misc(1) was ~1.6 had reduced to ~1.3 after torrefaction whereas the O/C for both untreated biomass was ~ 0.7-0.8 which changed to ~0.5-0.6 after the thermal treatment. Reaction during torrefaction include dehydration, which decreases hydrogen and oxygen elements The main products from torrefaction are H₂O, CO, CO₂ and CH₄ with small concentration of oxygenated volatile organics. Thus, another key reaction is decarboxylation, which decreases the O/C ratio.

A consequence of the reductions in H/C and O/C ratios is the increase in HHVs: the carbon content had become higher and oxygen does not contribute to HHV (Basu, 2013). The atomic H:C and O:C ratios found in the present study were consistent with the findings of a previous study (see **Figure 7. 6**) that showed the torrefied samples having atomic H:C ratio <1.3 and O:C ratio around 0.5.

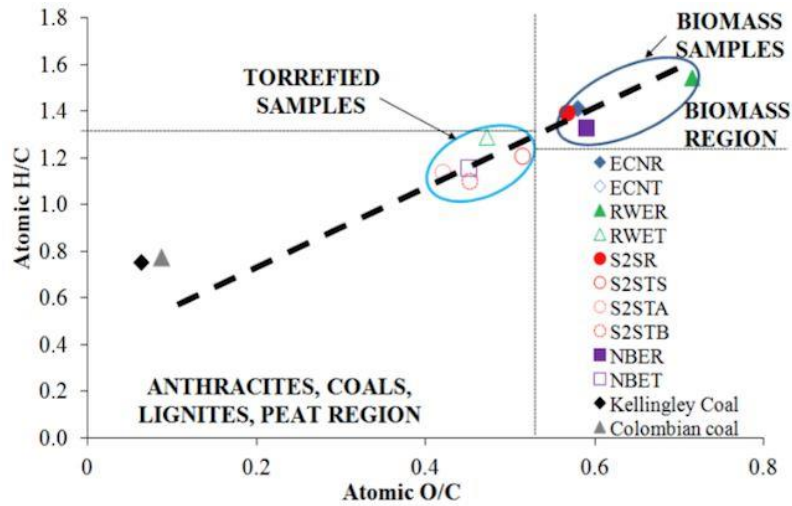


Figure 7. 6 Biomass, Torrefied Biomass and Coal Regions on the Van Krevelen Diagram (Medina, 2014)

The two parameters important to characterise torrefied fuel, i.e. mass yield (η_M) and energy yield (η_E) were calculated using **Equation 2.15** & **Equation 2.16** respectively. Mass yields for tMisc(1) and tPineR were 73.5% and 77.2% respectively whereas energy yields were 84.7% for tMisc(1) and 86.1% for tPineR. These numbers fall within the torrefaction process commonly operated on biomass – 70-90% for mass yield and 70-95% for energy yield. **Figure 7. 7** shows mass yields of torrefying various biomass for 30-min residence time which suggested that torrefaction at 270°C resulted in a mass yield of ~75% (Gucho et al., 2015) and calculations from this study tally with the findings. Comparing the mass yield and energy yield of Misc(1) and PineR, woody pine retained slightly more mass than miscanthus and while the higher heating value increased upon torrefaction, this increase was less than that of herbaceous miscanthus pre-treated under the same condition.

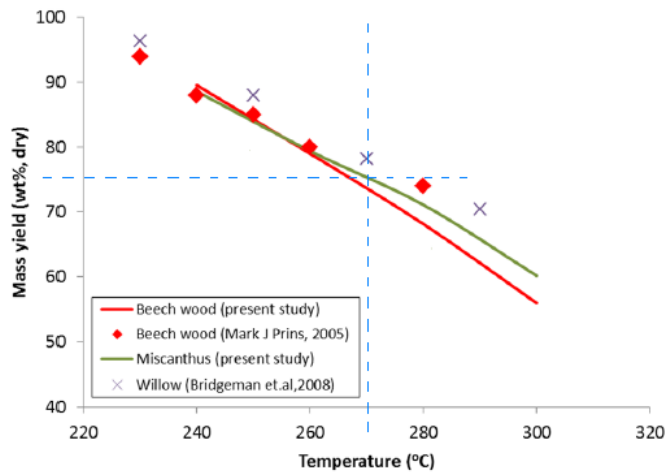


Figure 7.7 Mass Yields of Torrefying Various Biomass for 30-min as a Function of Torrefaction Temperature [edited from (Gucho et al., 2015)]

7.2 Self-Ignition Propensity Risk Ranking

Using the reaction rate kinetics as detailed in **Section 3.1.1**, the self-ignition propensity of torrefied biomass and torrefied-untreated biomass blend was ranked and compared with their corresponding untreated counterparts. The self-ignition risk ranking results are shown in **Figure 7.8**. As shown in the figure, all the torrefied samples had self-ignition risk rank reduced from 'high risk' to 'low risk'; the apparent activation energy E_a values increased from ~ 79 kJ/mol of PineR and ~ 80 kJ/mol of Misc(1) to ~ 96 kJ/mol and ~ 99 kJ/mol respectively whereas T_{MWL} increased from $\sim 287^\circ\text{C}$ of PineR and $\sim 281^\circ\text{C}$ of Misc(1) to $\sim 313^\circ\text{C}$ and $\sim 289^\circ\text{C}$ respectively. As suggested by this risk ranking method, the self-ignition risk reduced as E_a and T_{MWL} increased, signifying that thermal treated torrefied biomass samples were generally safer than the untreated counterparts when self-ignition is concerned. As for the torrefied-untreated blend of miscanthus (50tM(1):50M(1)), its risk closely resembled that of the untreated material, implying the self-ignition risk was dominated by the untreated ingredient.

TGA slow combustion runs require a lot less materials than dust-layer experiments and so the study could be expanded to three other blends, namely 90tM(1):10M(1), 50tPineR:50tM(1) and 90tPineR:10tM(1) that represent blends of 90 wt% torrefied miscanthus to 10 wt% untreated miscanthus, 50 wt% torrefied pine to 50 wt% torrefied miscanthus and 90 wt% torrefied pine and 10 wt% torrefied miscanthus respectively. From **Figure 7.8**, it is seen that 90tM(1):10M(1) had low self-ignition risk comparable to that of tMisc(1), i.e. 100% torrefied miscanthus. If the blend consisted of both torrefied materials (the 50tPineR:50tM(1) and 90tPineR:10tM(1) blends), self-ignition risk was reduced tremendously with E_a a lot higher than those of the untreated biomass. The interesting

finding was that the T_{MWL} of both torrefied-torrefied blends did not vary too much from that of individual torrefied material. The higher E_a values of torrefied material compared to that of the respective untreated material was most probably due to loss of reactive volatile matter during the torrefaction process.

The results obtained this way suggest that torrefied fuels were inherently safer than the untreated ones when self-ignition was concerned. Since there were studies that showed the opposite – torrefied dust was more sensitive than untreated dust to ignition (Medina, 2014), additional experiments of another kind were conducted.

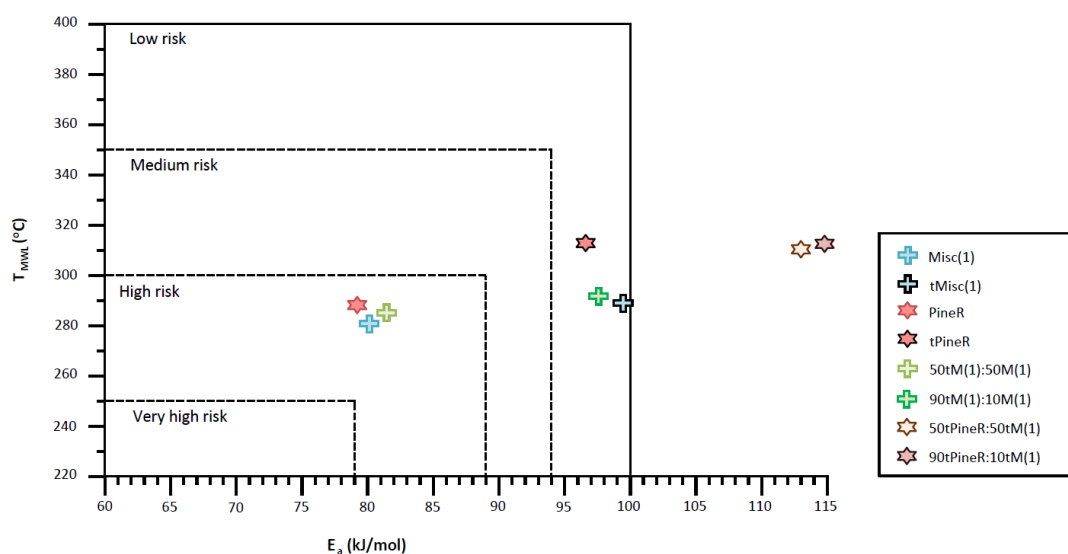


Figure 7. 8 Self-Ignition Risk Ranking of Torrefied, Torrefied-Untreated Blend, Torrefied-Torrefied Blend and Untreated Biomass Samples

7.3 Minimum Ignition Temperature Determination and Ignition Delay Time

Adhering to BS EN 50281-2-1:1999, the minimum dust layer ignition temperature (T_{LIT}) experiment was conducted on all five samples in this torrefaction study to verify if the torrefied samples really show reduced self-ignition risk. The procedures were as described in **Chapter 3** where all treated and untreated biomass were milled and sieved to $<180 \mu\text{m}$. Due to material limitation, dust samples of $<180 \mu\text{m}$ (see **Figure 7. 9**) were experimented in Ring A only (5 mm dust layer).

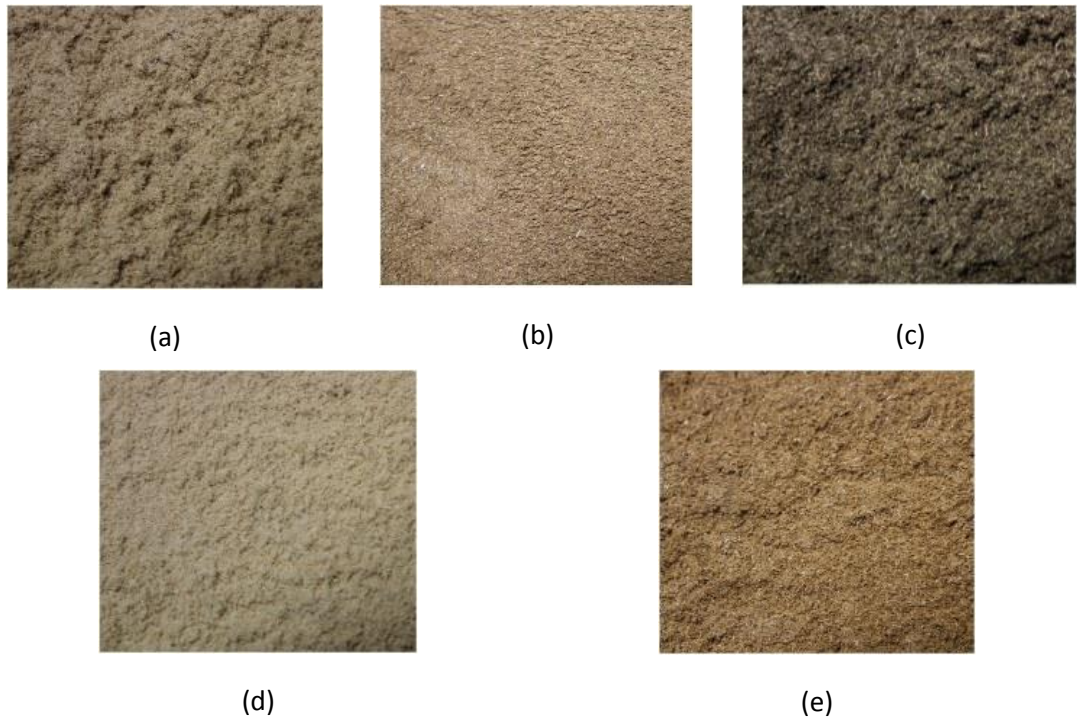


Figure 7.9 Samples <math><180\mu\text{m}</math> for Dust Layer Experiment (a) Misc(1) (b) tMisc(1) (c) 50tM(1):50M(1) (d) PineR (e) tPineR

Similar to experiments on other biomass samples, dust was poured into Ring A located at the centre of the hot plate with pre-defined temperature and timer was started once the dust was levelled properly within the ring. Whether or not ignition occurred was observed – if ignition occurred within 30 minutes, the time taken was recorded as the ignition delay time.

The results of this minimum dust layer ignition temperature (T_{LIT}) determination and the corresponding ignition delay times are shown in **Table 7.1** and an example of biomass igniting on hotplate is shown in **Figure 7.10**. As shown in **Table 7.4**, tMisc(1) had ignited at a lower temperature (at 280°C , i.e. 30°C lower) than the untreated Misc(1) that had ignited only at 310°C . The 50tM(1):50M(1) had ignited at 290°C , somewhat closer to that of tMisc(1).

Table 7. 4 Minimum Dust Layer Ignition Temperature (T_{LIT}), Ignition Delay Time and Density in Ring A of Torrefied Biomass, Untreated Biomass and Torrefied-Untreated Biomass Blend

Sample Name	Minimum Layer Ignition Temperature, T_{LIT} ($^{\circ}C$)	Ignition Delay Time (min)	Material Density in Ring A (kg/m^3)
Misc(1)	310	4.10	207.26
PineR	350	7.40	213.36
tMisc(1)	280	8.05	425.39
tPineR	350	4.12	190.83
50tM(1):50M(1)	290	7.42	325.47

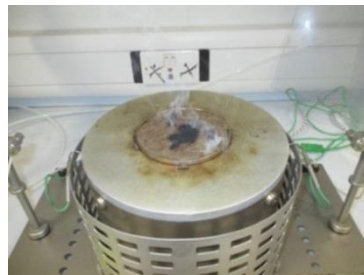
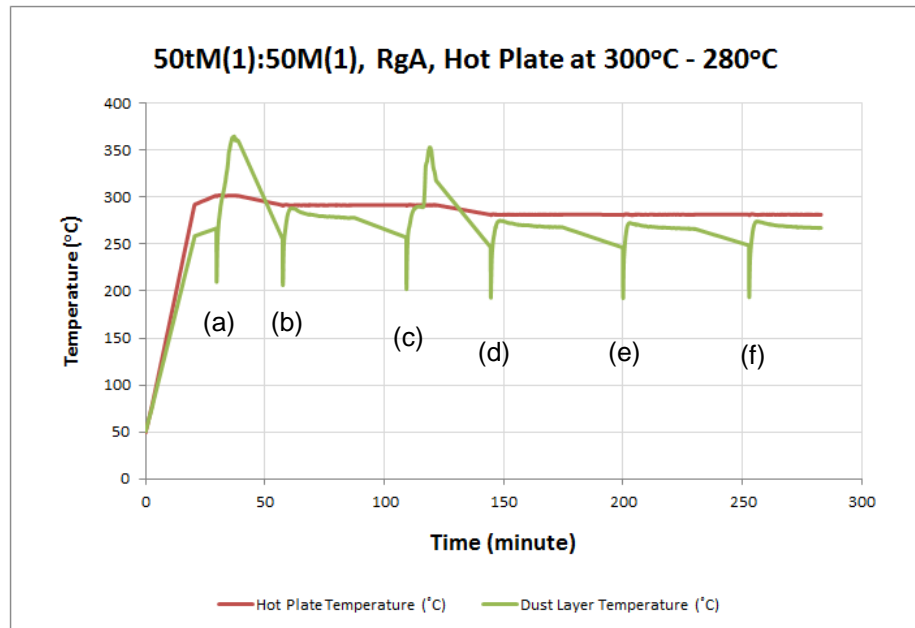


Figure 7. 10 50tM(1):50M(1) in Ring A Igniting on 290 $^{\circ}C$ Hotplate

As shown in **Figure 7. 11** (the temperature-time results for 50tM(1):50M(1) dust), the first experiment at a hot plate of 300 $^{\circ}C$ ignited, but the dust failed to ignite for the first trial when the hot plate was at 290 $^{\circ}C$ but ignited at the second trial. This was followed by three non-ignition when hot plate temperature was fixed at 280 $^{\circ}C$. As for tPineR, its dust layer ignited at the same temperature i.e. 350 $^{\circ}C$ as that of the untreated counterpart but with a shorter ignition delay time, 4.12 minutes for tPineR and 7.40 minutes for PineR.



- (a) 50tM(1):50M(1) Dust Sample 1 – Hot plate temperature set at 300°C, ignition happened
- (b) 50tM(1):50M(1) Dust Sample 2 – Hot plate temperature set at 290°C, no ignition
- (c) 50tM(1):50M(1) Dust Sample 3 – Hot plate temperature set at 290°C, ignition happened
- (d) 50tM(1):50M(1) Dust Sample 4 – Hot plate temperature set at 280°C, 1st time no ignition
- (e) 50tM(1):50M(1) Dust Sample 5 – Hot plate temperature set at 280°C, 2nd time no ignition
- (f) 50tM(1):50M(1) Dust Sample 6 – Hot plate temperature set at 280°C, 3rd time no ignition

Figure 7. 11 Temperature-Time Plotted by ANKO Software on 50tM(1):50M(1) Blend

The results are intriguing since they contradicted the outcomes from the self-ignition risk-ranking chart derived from TGA. Visual observation of Misc(1) and tMisc(1) dusts (see **Figure 7. 9** (a) & (b)) suggested that sample size was quite different even though the same sieving procedure had been applied. The most straightforward investigation was to check the material density within Ring A. The volume of Ring A was calculated from the cylinder volume formula where Ring A diameter and height were easily determined using Vernier calliper. Masses were estimated by placing Ring A on a tared balance and then filling with dust such that the net weight of sample contained in Ring A was measured (see

Figure 7. 12). The density was then calculated with mass/volume and the values are reported in **Table 7. 4.**



Figure 7. 12 Obtaining Sample Dust Weight using a Balance

It was found that the density of tMisc(1) was >2 times the density of Misc(1). This implied that more tMisc(1) particles were contained within the same volume of Ring A. Consequently, dust particle size investigations were made. The $\leq 180 \mu\text{m}$ dust samples used in the T_{LIT} determination experiment had their particle size analysed using the Malvern Mastersizer 2000E equipment and the result (in volume percentage versus logarithm scale particle size) is shown in **Figure 7. 13.** As seen from the results, the % volume of smaller particles was greater in tMisc(1) compared with untreated Misc(1) – the bell-shaped distribution moved leftwards as the proportion of torrefied miscanthus increased from 0wt%, 50wt% to 100wt% (Misc(1), 50tM(1):50M(1) and tMisc(1)).

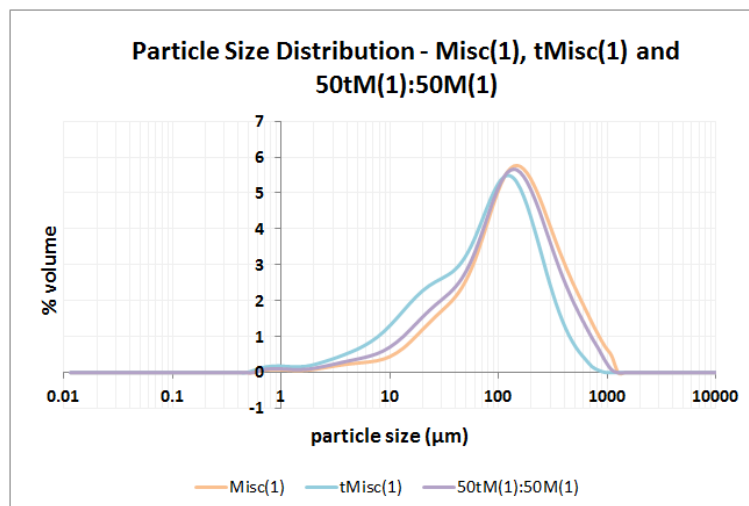


Figure 7. 13 Particles Size Distribution of Misc(1), tMisc(1) and 50tM(1):50M(1) used in T_{LIT} Determination Experiment

Using this light diffraction technique, the light diffraction by actual biomass particles should be measured but this equipment had equate that to the light diffracted by an equivalent sphere. It is well-known that biomass particles are cylindrical and not spherical (Slatter, 2015; Chin, 2007). Although the methods does not measure the true cylindrical particle size, comparison between biomass samples using the same method can provide insight. This particle size measuring method using laser diffraction technology had been adopted by many others in their biomass combustion studies, including a study about effects of inerts on ignition sensitivity of dust (Janès and Carson, 2013b), Medina (2014) in her study on explosion safety of biomass and torrefied biomass powders and Slatter (2015) in his study on explosibility of coarse biomass powders.

The consequence of changing particle size distribution in the sieved samples is a decrease in voids in the dust layer and an increase in density. During the trial for tMisc(1) there was more mass contained in Ring A. As a result there is more insulation within the dust layer and heat remained trapped and further accelerated the exothermic reaction that caused tMisc(1) to ignite at lower temperature. As determined previously (in **Section 7.2**), the E_a had increased due to the lower volatile contents of torrefied biomass. However, particle size can play a role in the overall reactivity of dusts too, and because faster combustion rate was found in dispersed dust clouds when particle size was smaller (Medina, 2014). Hehar (2013) in his study on physiochemical and ignition properties of dust from Loblolly wood found that the fine dust fraction showed lower hot surface ignition temperature than other size fractions. Hwang and Litton (1988) in study on combustible dust layers on a hot surface where a variety of dusts (included coal, lycopodium spores, corn starch and grain) were studied, and demonstrated that hot surface ignition temperature increased with increasing particle size.

From the Van Krevelen diagram (see **Section 7.1.2**), torrefied biomass had become more coal-like, therefore it was possible that torrefied biomass dust layer ignited at a temperature closer to that of coal dust layer, which was lower than its untreated counterpart. This finding is consistent with results from a study concerning ignition of dust clouds and dust deposits by friction sparks and hotspots by Rogers et al. (2006). Here it was found that a coal dust layer of 5 mm thickness ignited at 225°C, but sawdust of the same thickness ignited at 315°C. Furthermore, the studies of Pastier et al. (2013) also concluded that particle size hence density affected ignition temperatures of thin layers, as in the case here. Torrefaction makes biomass more brittle and made handling harder because of the formation of more dust that could be ignited more easily than coal. This might imply an increase in the fire and explosion risk of using torrefied biomass in conveying pipes or within the mill.

Considering PineR and tPineR that ignited at the same temperature, the densities of both were quite close, with tPineR ~0.9 times the density of PineR. Since T_{LIT} for both

PineR and tPineR were the same, material density might not have the major effect. tPineR was a bit drier than PineR (moisture content from proximate analysis showed ~1.3wt% and ~1.8wt% for tPineR and PineR respectively) and it was believed that the layer density effect was compensated by the dryness effect of tPineR therefore both PineR and tPineR showed the same T_{LIT} . Being dryer, without the need to evaporate moisture caused tPineR to ignite with a shorter delay time.

Looking at the TGA weight loss curves for untreated, torrefied and blend of both materials, it is obvious that the weight loss of torrefied biomass has become slower (curve shifted rightward, as shown in **Figure 7. 14**). The blend of untreated and torrefied biomass lay in between curves of the two. These TGA results showed torrefied material has become less reactive and this contradicts the finding from dust layer test which the torrefied materials had actually ignited at lower temperature than the untreated counterpart. Besides noting the change in particle size and thus density as discussed earlier, the kinetics data in **Appendix A** provide some insights too. Although the activation energy has increased upon torrefaction, the pre-exponential factor rises too. With the reduced particle size and increase reaction surface area of torrefied material, an increase in reaction frequency justifies the lower T_{LIT} in dust layer test.

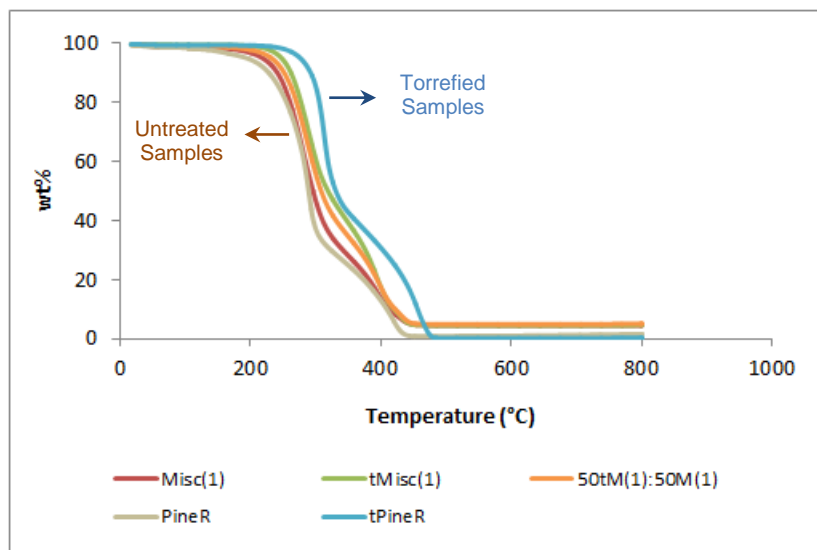


Figure 7. 14 TGA Slow Combustion Weight Loss Curves Comparison of Five Samples – Untreated, Torrefied and Untreated-Torrefied Blend

7.4 Particle Surface Area Determination and Morphology Analysis

Besides determining the dust density contained in Ring A and particle size distribution, particle surface area of all samples was determined using the Brunauer-Emmett-Teller (BET) method and particle morphology was inspected qualitatively from Scanning Electron Microscopy (SEM) images to justify further the T_{LIT} obtained. The BET analysis results are tabulated in **Table 7. 5** as follows.

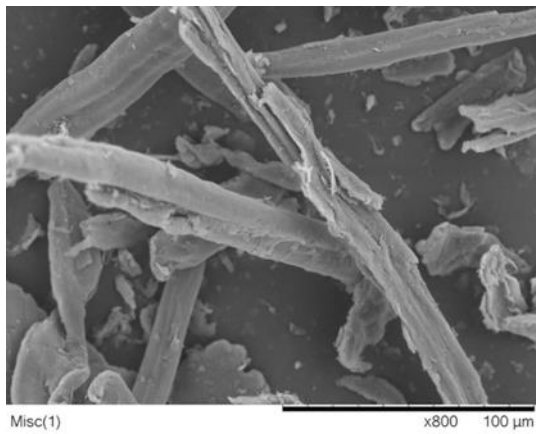
Table 7. 5 BET Surface Area Analysis of Five Samples

Sample Name	BET Surface Area (m ² /g)	R ² of BET Plot
Misc(1)	0.47 ± 0.03	0.990
PineR	1.42 ± 0.04	0.991
tMisc(1)	1.45 ± 0.03	0.993
tPineR	1.11 ± 0.04	0.994
50tM(1):50M(1)	1.16 ± 0.04	0.988

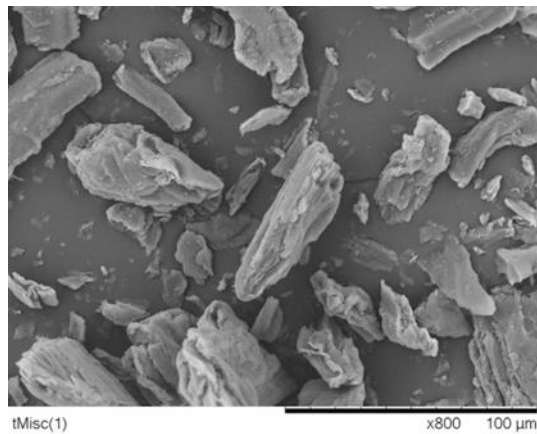
As seen from the BET surface area results, there were ~1.45 m² in every gram of tMisc(1) dust but only ~0.47 m² in the same weight of Misc(1) dust, i.e. around 0.3 times the surface area of the torrefied counterpart. Although both surface areas are low, torrefied miscanthus had much more surface area than the untreated counterpart, and so, there were more sites readily available for combustion reaction. This can also contribute to lower T_{LIT} values. For the blend of 50tM(1):50M(1), the surface area was somewhere between that of tMisc(1) and Misc(1), and the T_{LIT} was about midway of tMisc(1) and Misc(1). Pine showed an opposite trend when compared with miscanthus – the surface area of the torrefied pine is slightly less than that of PineR (1.11 m²/g vs ~1.40 m²/g). Medina (2014) had similar findings in her study on explosion safety of biomass and torrefied biomass powders: Her two different sets of torrefied pine showed 1.09 m²/g for the torrefied and 1.108 m²/g for the untreated counterpart; and the other set, 1.47 m²/g for the torrefied and 1.71 m²/g for the untreated pine.

The particle surface morphology of untreated biomass particles were compare with that of the torrefied ones via SEM imaging. The SEM micrographs for Misc(1), tMisc(1) and 50tM(1):50M(1) are shown in **Figure 7. 15(a),(b) & (c)** respectively. At the same magnification of 800x, comparing Misc(1) and tMisc(1), it was obvious that Misc(1) had longer and cylindrical fibrous structure whereas after torrefaction, tMisc(1) showed

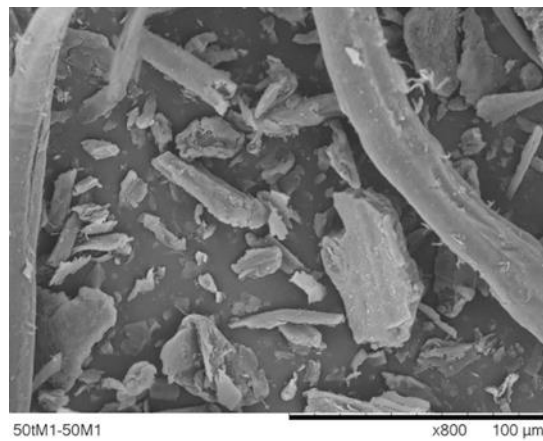
smaller and more spherical particles. 50tM(1):50M(1) was a mixture of both types of particles. Since miscanthus loses its fibrous structure upon torrefaction, tMisc(1), with improved grindability, formed finer dust easily and this corroborated well with the particle size distribution reported in **Section 7.3**. The respective SEM images for PineR and rPineR are shown in **Figure 7. 15(d) & (e)**. Apart from tPineR showing smoother surfaces than the untreated counterpart, no major changes were detected from both the SEM micrographs. These findings agree with the similar BET surface area values of untreated PineR and torrefied tPineR.



(a)



(b)



(c)

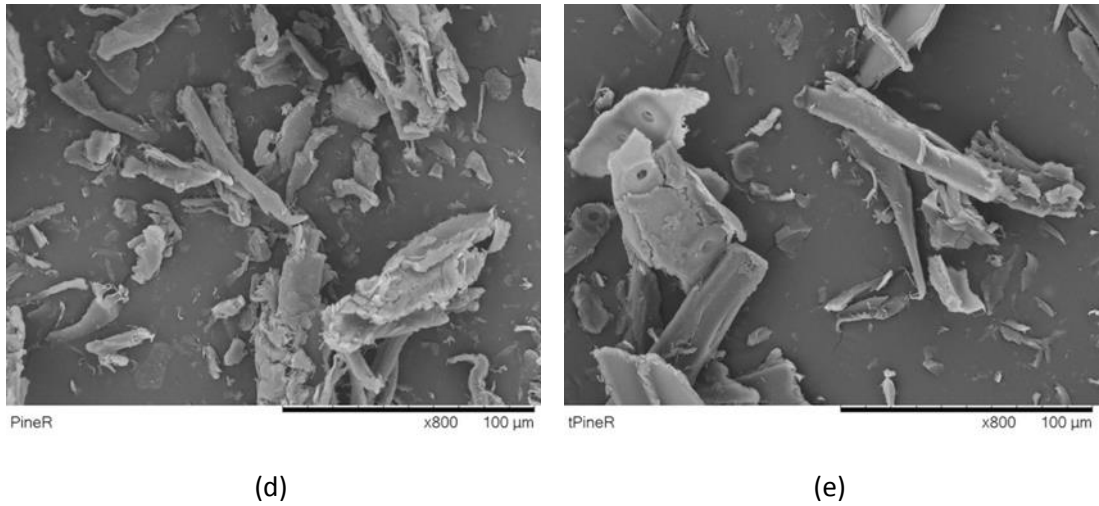


Figure 7. 15 SEM Micrograph of (a) Misc(1) (b) tMisc(1) (c) 50tM(1):50M(1) (d) PineR (e) tPineR at 800x Magnification

7.5 Industrial Significance

The maximum surface temperature allowable (MPST) on machineries when these five samples are deposited on them were determined using three methods described in **Section 2.3** and results are plotted in **Figure 7. 16**. When Guideline1 was followed, the estimated MPST for samples contained in Ring A (5 mm) was calculated from the results obtained from dust layer experiments whereas Ring B (12.5 mm thick) results were estimated.

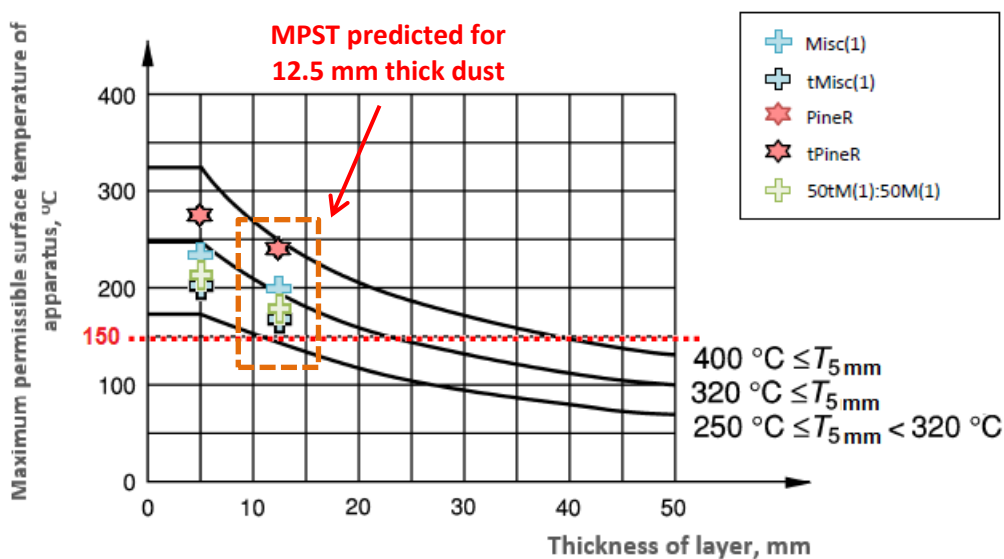


Figure 7. 16 MPST Estimation with Three Different Methods – Guideline 1 (Points), Guideline 2 (Curves, T_{LIT} from Pre-Refinement) and Power Station Practice (Constant at 150°C) on Torrefied, Torrefied-Untreated Blend and Untreated Biomass Samples

Miscanthus, torrefied miscanthus and the blend, all have T_{LIT} for a 5 mm dust layer in the range $250\text{ °C} \leq T_{5\text{mm}} < 320\text{ °C}$ and so extrapolation to thicker dust layers is given from the bottom curve in **Figure 7. 16** when Guideline 2 is adopted. The Dangerous Substances and Explosive Atmospheres Regulations 2002 (DSEAR) limit for safe surface temperature is 220°C, is considered a bit too lenient for Misc(1), tMisc(1) or 50tM(1):50M(1) when compared with Guideline2 that allows only ~175°C for these materials. PineR and tPineR have $T_{5\text{mm}} \geq 320\text{ °C}$ and so extrapolation to thicker dust layers makes use of the middle curve and results in safe layer thickness of ~10 mm if the DSEAR limit of 220°C is followed.

As seen in **Section 7.4**, we have two opposing effects for ignition risk: Torrefaction makes the decomposition kinetics slower, but decreased particle size counters this such that dust layer densities change. This together with possible changes in thermal conductivity and heat capacity affects the heat dissipation in the dust layer and causes the MPST to decrease.

7.6 Concluding Remarks and Suggestions for Future Work

A torrefaction condition of 270°C for 30 minutes has been applied on herbaceous miscanthus and woody pine. It was found that the self-ignition risk of torrefied biomass dust relied on many factors. Even though the volatile matter component is reduced via torrefaction, this did not actually make torrefied biomass a safer solid fuel. The improved grindability of torrefied biomass causes the production of torrefied fines which impose

extra hazard in a power station, since this drier dust catches fire easily and at temperatures lower than before under certain circumstances. It is important to note that dust layer ignitions usually happens at temperatures lower than dust cloud ignition and a smouldering torrefied dust layer serves as an ignition source of the corresponding dust cloud (Rottner, 2006) and can eventually leads to catastrophic explosion that causes assets and lives.

Thus, when handling torrefied biomass, extra precautions, stricter housekeeping guidelines than before are needed, both for milling plants and power stations. Material classification for ocean vessels transportation, that considers self-ignition risk from various torrefied materials need to be considered by the International Maritime Organization (IMO) as at present, only torrefied wood (IMO, 2013) has been categorised in Group B (cargo with chemical hazards which could give rise to a dangerous situation on a ship) under its Solid Bulk Cargoes (IMSBC) Code.

Further studies need to consider the influence of improved feedstock grindability, since increased density due to particle size reduction are among the factors needed in characterising self-ignition risk of torrefied biomass. A method that considers three variables that determine the risk (in terms of T_{LIT} or T_{max}) of whether self-ignition would happen on torrefied dust layers could be plotted. The three variables proposed are:

- i) T_{LIT} , torrefied dust layer minimum ignition temperature or T_{MWL} , maximum weight loss temperature from TGA
- ii) K , Arrhenius equation rate constant or E_a , reaction activation energy in slow combustion reaction
- iii) Material particle size or particle surface area or density

There are some suggestions for further study to enhance the understanding of self-heating and self-ignition risk from torrefied biomass dust. To make the study more thorough, more biomass species could be used under a wider variety of torrefaction conditions. Vegetation based industrial waste, like potato peels could be a potential candidate for torrefaction studies, just like tomato peel torrefaction study carried out by Toscano et al. (2015). Besides torrefying at atmospheric pressure, effects of torrefaction under pressure is worth investigating, like the work by (Agar et al., 2016; Wannapeera and Worasuwanarak, 2012) is worth investigating. Compared to torrefying under atmospheric pressure, torrefaction at elevated pressure was found to result in higher energy yield with similar mass yield within a shorter residence time (Agar et al., 2016) but there is not much study on the risks of torrefied dust deposition on heated surfaces. Besides health risk caused by exposure to excessive dust; fire and explosion risks initiated by self-heated

torrefied biomass dust depositions on hot surfaces like overheated mechanical components (bearings, gearboxes) and overheated motors, sparks from static discharge that happened during pneumatic conveying/transportation of torrefied biomass could cause massive explosions apart from fire outbreaks that may reignite after extinguished (Hoeft, 2013).

Chapter 8

Comparisons of Emissions from Pre-Igniting and Igniting Biomass Dust Layers

In the current smoke/emission capture experiment, two single-material biomass samples and their blends in two different ratios were studied. The two biomass samples were Pine and Miscanthus(2) whereas the blends were PM(2)9010 and PM(2)5050, which the first blend consisted of 90% Pine and 10% Miscanthus(2) and the second blend had 50% pine and 50% Miscanthus(2) by weight. Pine and Miscanthus(2) were chosen because they are from two major vegetation groups – woody and herbaceous groups respectively. Furthermore, as found from previous experiments, the two showed the greatest difference in their respective T_{LIT} .

In this study, only thin layers of dust contained in Ring A (5 mm depth) deposited on hot surface were studied. $T_{LIT,A}$ of pine alone was 310°C and 350°C for Miscanthus(2) whereas it was 320°C and 340°C for PM(2)9010 and PM(2)5050 respectively. **Table 8. 1** shows the temperatures that this experiment was run on the four samples. For the experiment duration, adhering to BS EN 50281-2-1, when a dust sample did not ignite, the sampling time should be at least 30 minutes. In this emission capture experiment, the sampling time was fixed at 30 minutes for both the critically igniting (at T_{LIT}) and pre-igniting (at $T_{LIT} - 10^{\circ}C$) samples such that the emissions in either scenario were captured over the same length of time. The universal flowmeter that had been calibrated with some assumptions described in **Section 3.3** was used to control the emission flow rate.

Table 8. 1 Biomass Samples and Their Respective Temperatures for Emission Capture Experiment

Biomass Sample	Temperature (°C)	
	Critical Ignition (T_{LIT})	Pre-Ignition ($T_{LIT} - 10^{\circ}C$)
Pine	310	300
Miscanthus (2)	350	340
PM(2)9010	320	310
PM(2)5050	340	330

The top of metal Ring A to the edge of inverted funnel had their distance fixed at 1 cm for all experiments. The emission flow capture rate was fixed at 13.05 ml/s for all runs. In a study of Oros et al. (2006) about organic aerosols from biomass burning, they sampled the emissions for a duration of 5-7 minutes and at suction flow rate of 1.13 m³/min. Among all flowrate determined during calibration in this experiment, 13.05 ml/s was selected following the study of Tyler and Henderson (1987), which had discovered that though dust layer ignition could be affected considerably by the air flow patterns (from uncontrolled flow i.e. natural convection to controlled flow i.e. forced convection) over the layer, when the air flow was fixed below 35 dm³/min (equivalent to ~583 ml/s), the flow was not forceful enough to disturb the layer of ≤ 20 mm depth. Thus, capturing at 13.05 ml/s of emission over a 5 mm thick (in Ring A) biomass dust layer used in this study would not expect major gas flow disruption that would significantly alter the results

All emissions collected along the emission sampling line had their chemical components analysed with Perkin Elmer Clarus 560 GC-MS equipment. Perkin auto sampler vials preparation have been detailed in **Chapter 3** and blank samples were included in every GC-MS batch as means of control. The Total Ion Chromatogram (TIC) showed the reagent grade DCM (solvent for all GC-MS injections and control sample for Sampler 1 – Inverted Funnel) contained only siloxanes (Cyclohexasiloxane, Cyclopentasiloxane, Hexasiloxane were some of the examples), which was a good sign indicating only degradation from the GC column and not contamination in the DCM used. However, besides siloxane peaks, there were four other major peaks (indicating four elements – Phenol, 2,4-bis(1,1-dimethylethyl)-, 1-Octadecene, 1-Hexadecene and Hexadecane) detected in the TIC of blank filter paper sample (control sample for Sampler 2 – Filter Paper). The TIC for blank ORBO tube (control sample for Sampler 3 – ORBO tube) did not show any significant peaks apart from siloxanes disintegrated from GC column. Since the DCM was confirmed earlier that it was emission-free, thus the four corresponding elements from blank filter paper were disregarded as elements originated from biomass emissions. Column disintegration elements identified on all TICs of blank and samples from each sampler were not considered either.

8.1 Emissions from Sampler 1 – Inverted Funnel

The inverted borosilicate glass funnel was the first component to capture biomass emission. Some of the vapour phase emission condensed upon contact with cooler funnel wall and deposited as a brownish/yellowish layer (colour depends on components present in the emission but will not be discussed here) on the glass wall. This is the oil fraction of the condensed fumes (Jenkins et al., 1998b) that occurs in biomass combustion/smouldering and is referred to as bio-oil hereafter.

GC-MS was performed on the DCM solutions of the yellowish/brownish oil deposits as described in **Section 3.3**. Being volatile, colourless with a mildly sweet scent, immiscible with water but capable of dissolving a wide range of organic compounds (James, 2014) has made DCM a common solvent used in many laboratories. Medium polar DCM solvent was selected here because biomass emission is organic in nature.

The TICs of emissions from some biomass samples pyrolysing/igniting at two different temperatures are shown in **Figure 8.1(a)&(b)** and **Figure 8.2(a)&(b)** with peak of significant emission components labelled. The peaks with chemical structure by the side showed the same elements found common to all the eight samples experimented here. It is important to note that all siloxanes identified were not regarded as biomass emission.

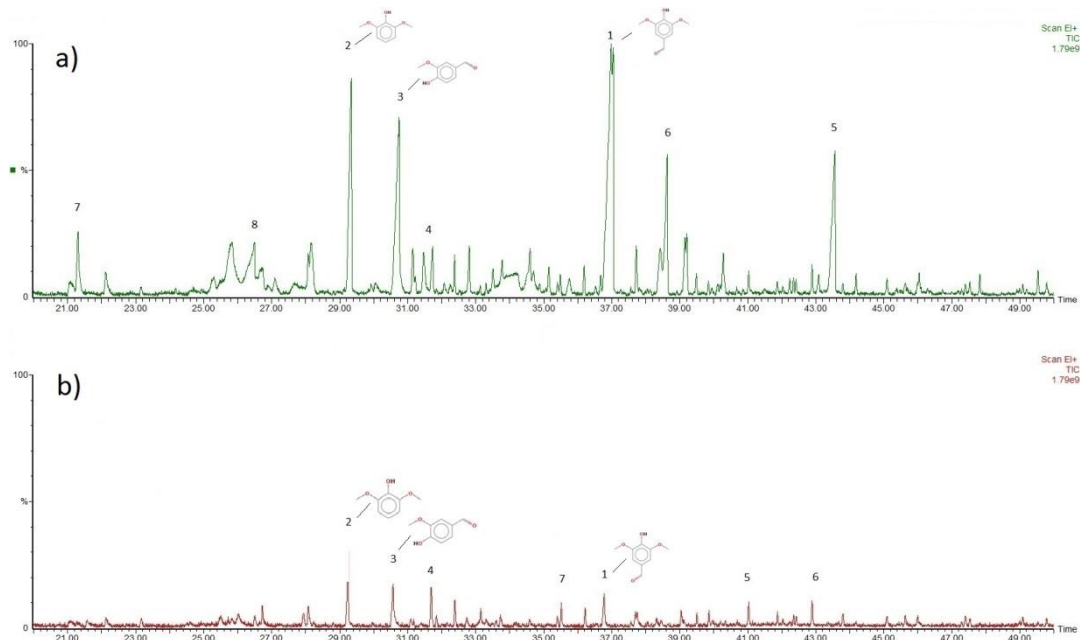


Figure 8.1 Sampler 1 – TIC of Woody Pine Emissions

(a) Before Igniting (at 300°C); Elements Identified **a1)** Benzaldehyde, 4-hydroxy-3,5-dimethoxy- **a2)** Phenol, 2,6-dimethoxy- **a3)** Vanillin **a4)** Benzoic acid, 4-hydroxy-3-methoxy- **a5)** 3,5-Dimethoxy-4-hydroxycinnamaldehyde **a6)** 2-Propenal, 3-(4-hydroxy-3-methoxyphenyl)- **a7)** Phenol, 2-methoxy- **a8)** 2-Furancarboxaldehyde, 5-(hydroxymethyl)-

(b) Critically Igniting (at 310°C); Elements Identified **b1)** Benzaldehyde, 4-hydroxy-3,5-dimethoxy- **b2)** Phenol, 2,6-dimethoxy- **b3)** Vanillin **b4)** Benzoic acid, 4-hydroxy-3-methoxy- **b5)** Phthalic acid, isobutyl 2-pentyl ester **b6)** 1,2-Benzenedicarboxylic acid, butyl 2-methylpropyl ester **b7)** Dodecane, 2,7,10-trimethyl-

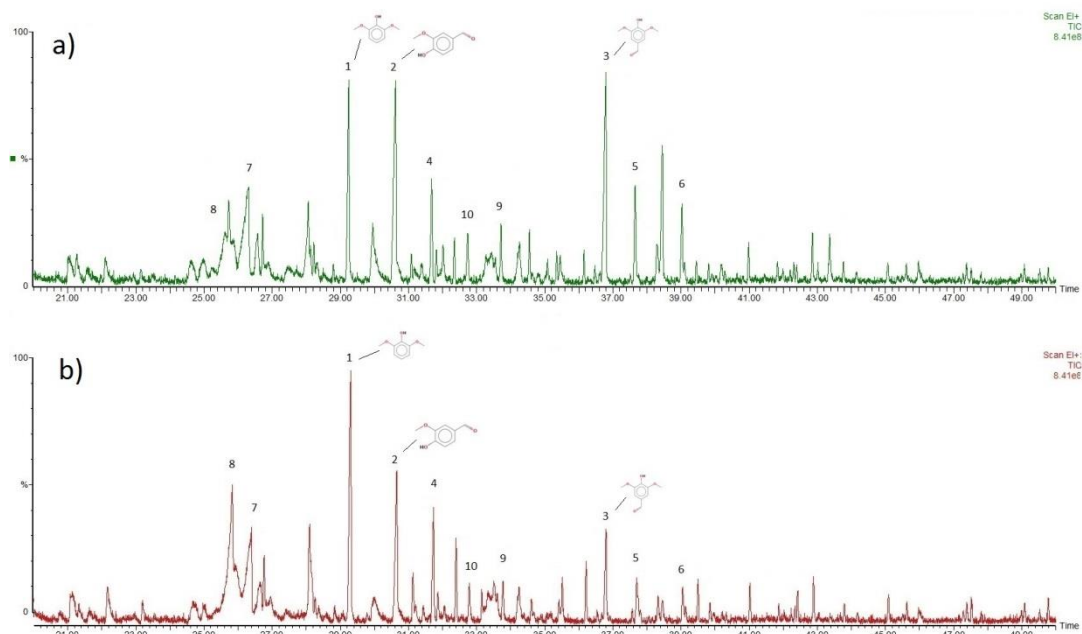


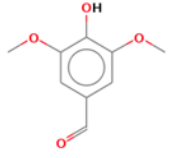
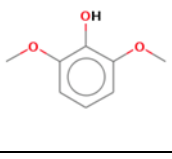
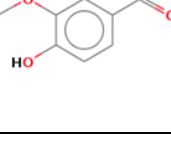
Figure 8.2 Sampler 1 – TIC of Blend PM(2)5050 Emissions

(a) Before Igniting (at 330°C); Elements Identified **a1)** Phenol, 2,6-dimethoxy-
a2) Vanillin **a3)** Benzaldehyde, 4-hydroxy-3,5-dimethoxy- **a4)** Benzoic acid, 4-hydroxy-3-
methoxy- **a5)** Phenol, 2,6-dimethoxy-4-(2-propenyl)- **a6)** Desaspidinol **a7)** 2-
Furancarboxaldehyde, 5-(hydroxymethyl)- **a8)** 1,4:3,6-Dianhydro-à-d-glucopyranose
a9) 2-Propanone, 1-(4-hydroxy-3-methoxyphenyl)- **a10)** Ethanone, 1-(3-hydroxy-4-
methoxyphenyl)-

(b) Critically Igniting (at 340°C); Elements Identified **b1)** Phenol, 2,6-dimethoxy-
b2) Vanillin **b3)** Benzaldehyde, 4-hydroxy-3,5-dimethoxy- **b4)** Benzoic acid, 4-hydroxy-3-
methoxy- **b5)** Phenol, 2,6-dimethoxy-4-(2-propenyl)- **b6)** Desaspidinol **b7)** 2-
Furancarboxaldehyde, 5-(hydroxymethyl)- **b8)** 1,4:3,6-Dianhydro-à-d-glucopyranose
b9) 2-Propanone, 1-(4-hydroxy-3-methoxyphenyl)- **b10)** Ethanone, 1-(3-hydroxy-4-
methoxyphenyl)-

Comparing TICs from all four material pairs, generally the emission intensities collected at the funnel were slightly less when each sample was critically igniting. This was particularly obvious for woody Pine (see **Figure 8.1**) but not that significant for herbaceous Miscanthus(2). As seen in **Figure 8.2**, the PM(2)5050 shows only small differences between the pre-igniting and critically igniting TICs. Also, more emission components were rinsed out from Sampler 1 of energy crop Miscanthus(2) than of woody pine and thus, the blends with Miscanthus(2) added to pine showed more TIC peaks. The three similar components for all eight samples were listed in **Table 8. 2** with their chemical structures and key markers shown.

Table 8. 2 Funnel – Similar Emission Components identified for all Eight Samples

No.	Element /Chemical Formula	Chemical Structure	Type of Key Marker
1	Benzaldehyde, 4-hydroxy-3,5-dimethoxy- (C ₉ H ₁₀ O ₄)		Syringol lignin (Nowakowski, 2008)
2	Phenol, 2,6-dimethoxy- (C ₈ H ₁₀ O ₃)		Syringol lignin (Nowakowski, 2008)
3	Vanillin (C ₈ H ₈ O ₃)		Guaiacol lignin (Nowakowski, 2008)

In biomass burning, the number of organic compounds that could be identified are generally large. This is because biopolymers like cellulose, hemicellulose and lignin are partially degraded, and the partly broken down products vaporise into smoke (Ikan, 2008). GC-MS TIC is a popular technique to trace the total aerosol extracts from biomass burning and vanillin, syringaldehyde are examples of major molecule tracers identified in biomass burning smoke particles. Consistent with Ikan (2008) that there were numerous organic compounds emitted when burning biomass, therefore only some elements were discussed in length in the current study.

Benzaldehyde,4-hydroxy-3,4-dimethoxy-, also known as syringaldehyde (The National Institute of Standards and Technology, 2016b), is a common element found in biomass burning emissions. In a study by Meuzelaar et al. (2016) about identifying local source contributions of organic particulate matter components, employing the GC-MS technique, syringaldehyde had been identified as a significant element contributed by combustion of biomass from various sites selected in the United States. Since biomass smoke aerosols are efficient cloud condensation nuclei (CCN), there was a study on organic aerosols emitted from five biomass (woody, herbaceous vegetation and animal waste) indigenous to South Asia, with the purpose to understand the impact on air quality and climate change (Sheesley et al., 2003). A detailed organic characterization of the combustion smoke from all samples conducted by GC-MS method revealed that syringaldehyde, Phenol, 2,6-dimethoxy- (syringol), vanillin (4-hydroxy-3-methoxy benzaldehyde) were found.

Knowing wood smoke emissions can cause many long and short term negative impacts on human health (Bari et al., 2011), there was a study on wood smoke pollution in

residential areas of southern Germany. They had applied GC-MS technique to analyse emission samples collected on glass fibre filters and discovered that syringaldehyde element was more dominant in hardwood burning emissions than softwood. Pine used in this study (and widely used as biofuel in power stations) could be a better option than hardwood eucalyptus from this syringaldehyde emission view point.

In a study regarding secondary organic aerosol formation from biomass burning, Yee et al. (2013) focused on investigating the possibility to use syringol as aerosol marker for wood combustion after discovering syringol a significant emission element in wood combustion. Schauer et al. (2001) had tried to determine the organic compound emission profiles from combustion of three wood species; pine, oak and eucalyptus. From their measurement on the gas-phase and particle-phase organic compound emissions, syringaldehyde, syringol and vanillin traces were found.

Li et al. (2014) had concluded that vanillin is an important emission in biomass burning in their study about methoxy phenols from biomass burning. They stressed that biomass burning besides being an important source of primary organic aerosol, it is also a precursor of secondary organic aerosol due to the abundant organic compounds with a wide range of volatilities emitted.

Oros and Simoneit (2001) in their study on molecular biomarker components in smoke from burning of six tree species had identified vanillin and 2,6-Dimethoxyphenol as major tracers, originated from lignin pyrolysis. Oros et al. (2006) in another study on smoke from burning various grass species collected from different climate regions had detected with GC-MS TIC method, syringaldehyde, syringol and vanillin as major biomarker tracers originated from lignin pyrolysis products.

Disregarding peak areas contributed by non-biomass emissions, i.e. GC column disintegration, the peak area percentages of emission TICs were re-calculated and the results are displayed in **Figure 8. 3**. Of the three similar components identified in **Table 8. 2** for all the four biomass materials tested, a lot more Benzaldehyde,4-hydroxy-3,5-dimethoxy- (indicated by blue bar) was emitted during pre-ignition stage than during the critically-ignition stage. This is particularly obvious for woody pine in which at pre-igniting stage of 300°C showed peak percentage of ~3.5 times higher than when it has ignited. However, no obvious trends were observed for Phenol, 2,6-dimethoxy- and Vanillin emissions during pre-igniting and critically-igniting of all biomass samples.

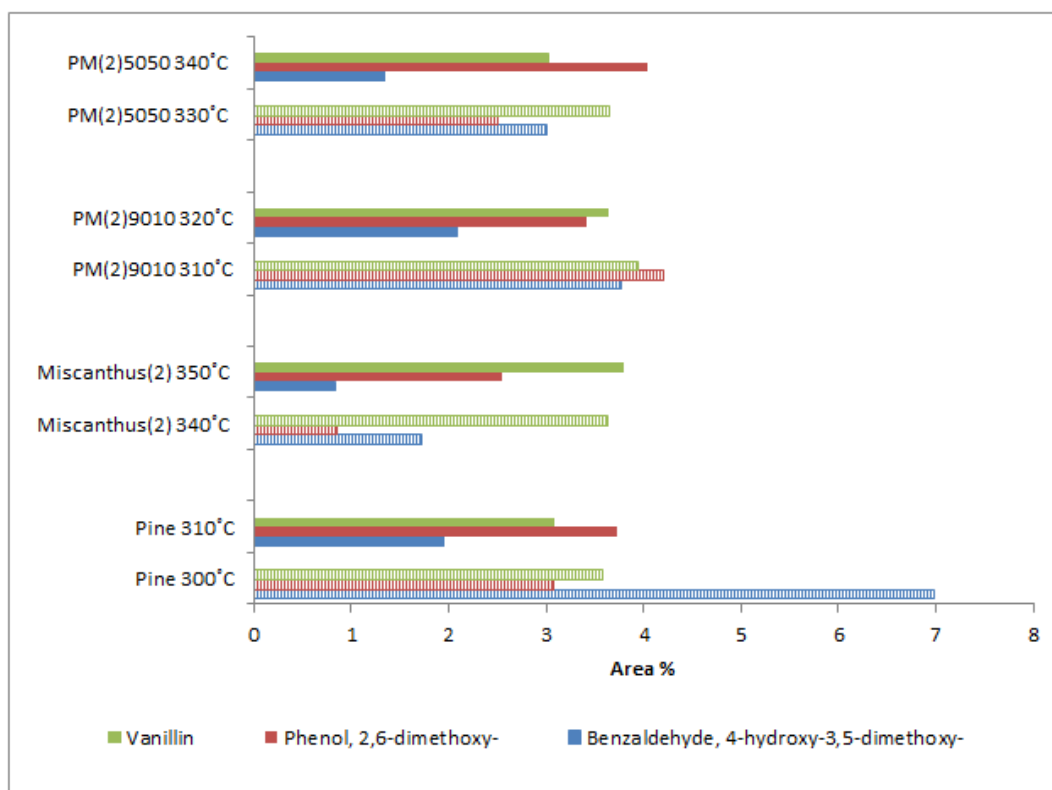


Figure 8. 3 Sampler 1 – Peak Area Percentages of Similar Components at Pre-ignition and Critical Ignition Stages

8.2 Emissions from Sampler 2 – Filter Paper

Typical chromatograms of emissions collected from pyrolysing/critically igniting biomass samples are shown in **Figure 8. 4(a)&(b)** and **Figure 8. 5(a)&(b)**, with peaks of significant emission elements numbered. Components found common to all experimented samples had their chemical structures illustrated next to respective peak numbers. All siloxanes and the four non-emission related components originated from blank filter paper were excluded in the peak numbers.

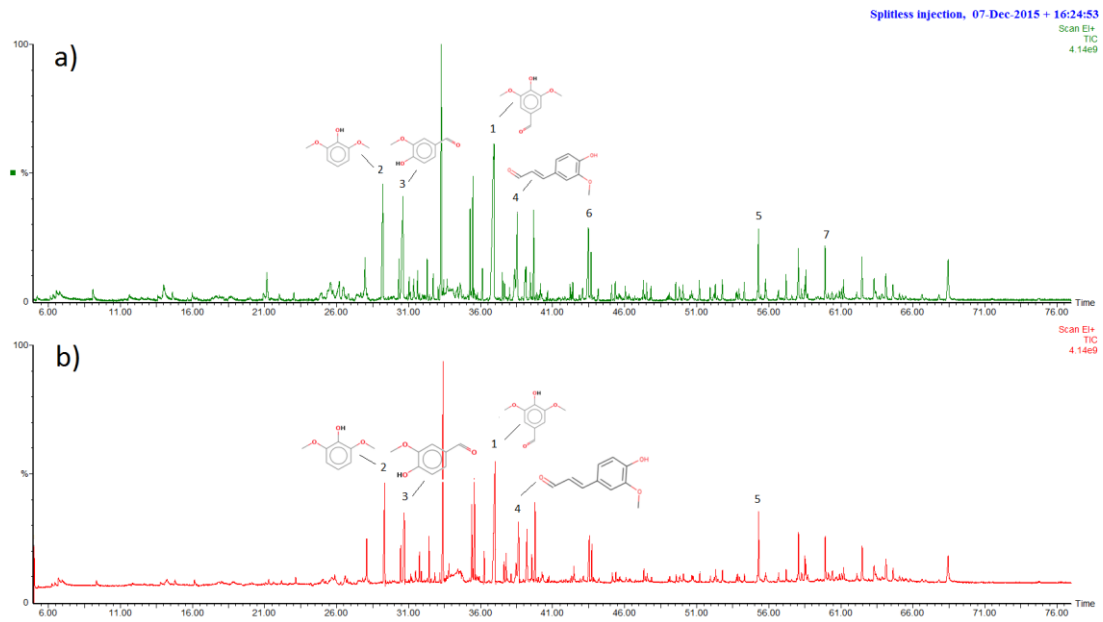


Figure 8. 4 Sampler 2 – TIC of Woody Pine Emissions

(a) Before Igniting (at 300°C); Elements Identified **a1)** Benzaldehyde, 4-hydroxy-3,5-dimethoxy- **a2)** Phenol, 2,6-dimethoxy- **a3)** Vanillin **a4)** 2-Propenal, 3-(4-hydroxy-3-methoxyphenyl)- **a5)** Eicosane **a6)** Asarone **a7)** Hexadecanal

(b) Critically Igniting (at 310°C); Elements Identified **b1)** Benzaldehyde, 4-hydroxy-3,5-dimethoxy- **b2)** Phenol, 2,6-dimethoxy- **b3)** Vanillin **b4)** 2-Propenal, 3-(4-hydroxy-3-methoxyphenyl)- **b5)** Eicosane

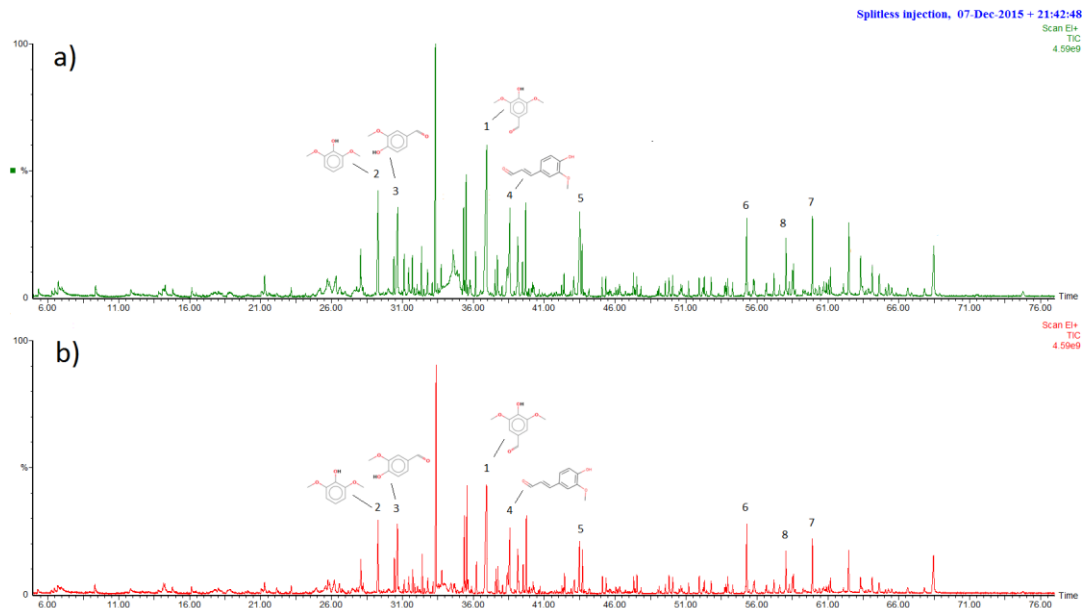


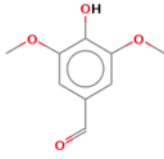
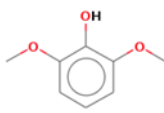
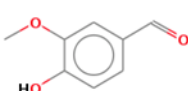
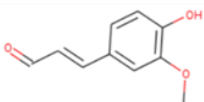
Figure 8.5 Sampler 2 – TIC of Blend PM(2)9010 Emissions

(a) Before Igniting (310°C); Elements Identified **a1)** Benzaldehyde, 4-hydroxy-3,5-dimethoxy- **a2)** Phenol, 2,6-dimethoxy- **a3)** Vanillin **a4)** 2-Propenal, 3-(4-hydroxy-3-methoxyphenyl)- **a5)** Asarone **a6)** Eicosane **a7)** Hexadecanal **a8)** Tetracosane
(b) Critically Igniting (320°C); Elements Identified **b1)** Benzaldehyde, 4-hydroxy-3,5-dimethoxy- **b2)** Phenol, 2,6-dimethoxy- **b3)** Vanillin **b4)** 2-Propenal, 3-(4-hydroxy-3-methoxyphenyl)- **b5)** Asarone **b6)** Eicosane **b7)** Hexadecanal **b8)** Tetracosane

When the paired TICs from four materials were compared, the peak intensities showed the critically igniting ones were slightly less than the pyrolysing ones, though the difference was not too significant. The emission elements found from PM(2)9010 pyrolysing or critically igniting did not differ much from those found from 100% Pine, implying a 10% composition change from Pine to Miscanthus(2) did not alter the emissions with great impact.

There were four components found in common for all eight samples, as listed in **Table 8.3** with their chemical structures and key markers shown. Interestingly, three out of the four similar components found from emissions captured by Sampler 2 were exactly the same as those similar ones obtained from Sampler 1. They were Benzaldehyde, 4-hydroxy-3,5-dimethoxy-, Phenol, 2,6-dimethoxy- and Vanillin. The common component captured by Sampler 2 but not Sampler 1 was 2-Propenal, 3-(4-hydroxy-3-methoxyphenyl)-

Table 8. 3 Filter Paper – Similar Emission Components identified for all Eight Samples

No.	Element /Chemical Formula	Chemical Structure	Type of Key Marker
1	Benzaldehyde, 4-hydroxy-3,5-dimethoxy- (C ₉ H ₁₀ O ₄)		Syringol lignin (Nowakowski, 2008)
2	Phenol, 2,6-dimethoxy- (C ₈ H ₁₀ O ₃)		Syringol lignin (Nowakowski, 2008)
3	Vanillin (C ₈ H ₈ O ₃)		Guaiacol lignin (Nowakowski, 2008)
4	2-Propenal, 3-(4-hydroxy-3-methoxyphenyl)- (C ₁₀ H ₁₀ O ₃)		Lignin (Fine et al., 2002)

Coniferyl aldehyde (The National Institute of Standards and Technology, 2016a) is another more commonly known name for 2-Propenal,3-(4-hydroxy-3-methoxyphenyl). The bio-oil GC-MS results from a pyrolysis study by Aziz et al. (2013) showed that Coniferyl aldehyde was one of the many aldehydes found from their wood chips samples. In two other studies investigating the possibility of upgrading bio-oil to industrial grade transportation biofuel, GC-MS results in both studies revealed that 2-Propenal,3-(4-hydroxy-3-methoxyphenyl) present in pyrolysis oil samples originated from Eucalyptus in the first study (Merckel, 2015) and Douglas-Fir from the second (McDonald et al., 2014).

Similar to the method applied on TICs from emissions captured by Sampler 1, omitting peak areas contributed by non-biomass emissions, i.e. GC column disintegration, the peak area percentages of emission TICs were re-calculated and the results are displayed in **Figure 8. 6**. For all similar components identified in **Table 8. 3** for pre-ignition and critical-ignition of four biomass materials, there was no common trend observed for all the similar components. Except for Miscanthus(2), Pine and the other two biomass blends all showed reduction of Benzaldehyde,4-hydroxy-3,5-dimethoxy- (indicated by blue bar) emission when critically-ignited as compared with pre-igniting. The other three similar components, Phenol, 2,6-dimethoxy-, Vanillin and 2-Propenal, 3-(4-hydroxy-3-methoxyphenyl)-, however, showed inconsistent trend of increase or decrease when pre-igniting emissions was compared to critically-igniting emissions.

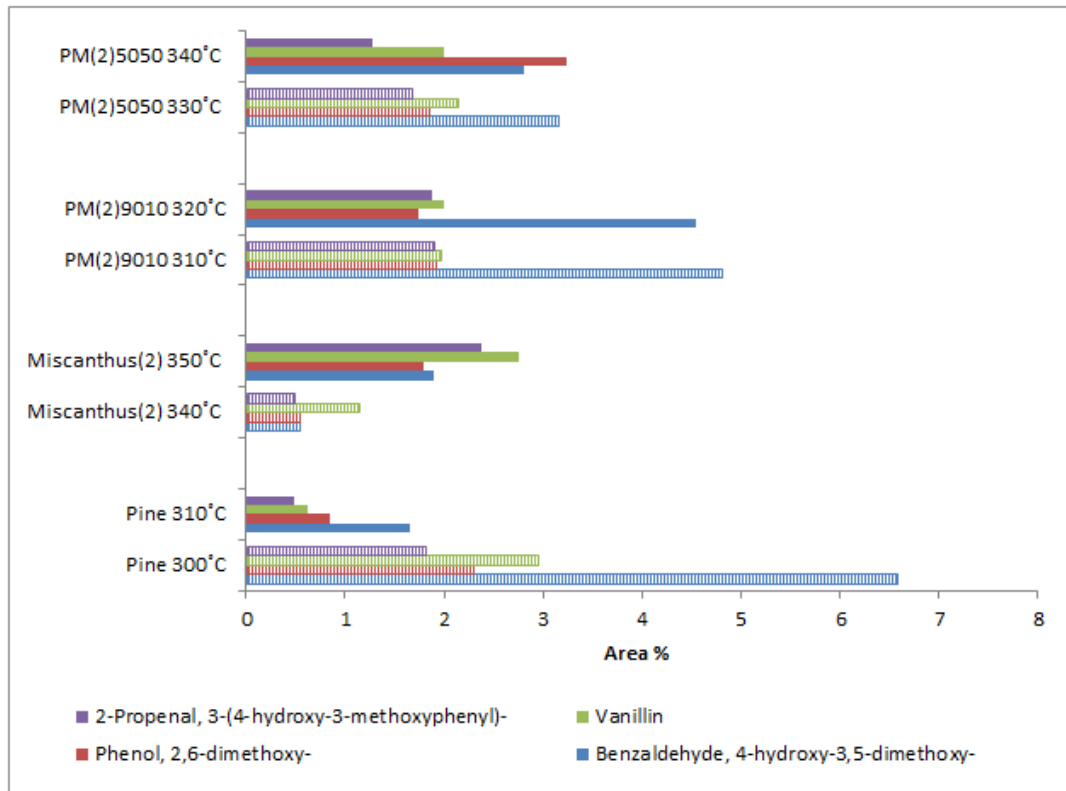


Figure 8. 6 Sampler 2 – Peak Area Percentages of Similar Components at Pre-ignition and Critical Ignition Stages

8.3 Emissions from Sampler 3 – ORBO™ 43

Emission TICs from some of the pyrolysing/critically igniting biomass are shown in **Figure 8. 7(a)&(b)** and **Figure 8. 8(a)&(b)**. As in Samplers 1 & 2, peaks of significant emissions were numbered in their respective TICs.

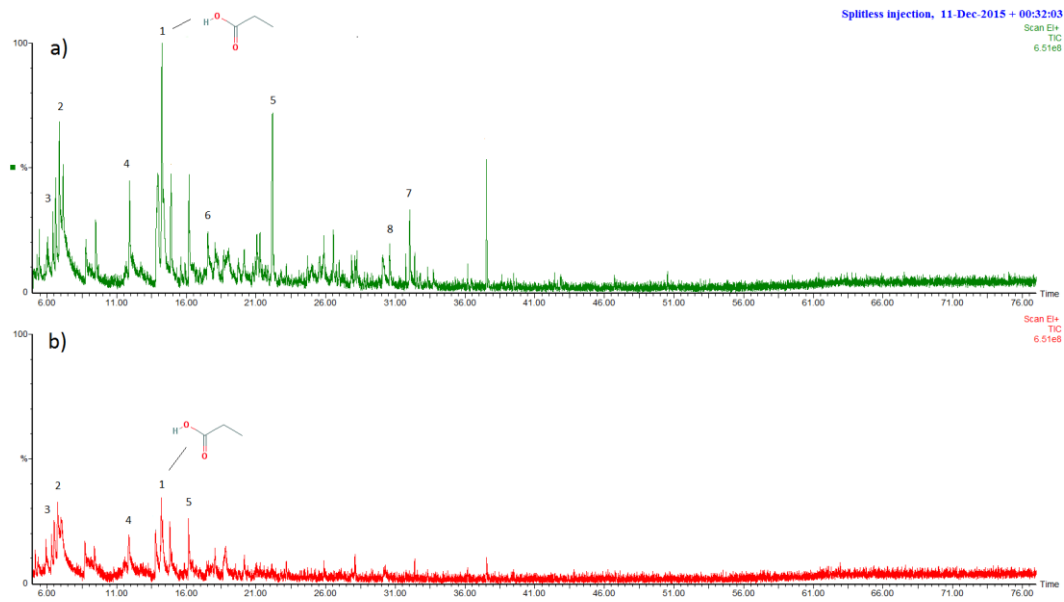


Figure 8. 7 Sampler 3 – TIC of Herbaceous Miscanthus(2) Emissions

(a) Before Igniting (at 340°C); Elements Identified **a1)** Propanoic acid **a2)** 3-Hexanol
a3) 3-Hexanone **a4)** 2,4-Hexanedione **a5)** Levoglucosenone **a6)** Phenol
a7) Phenol, 2-methoxy-4-propyl- **a8)** Phenol, 2-propyl-

(b) Critically Igniting (at 350°C); Elements Identified **b1)** Propanoic acid **b2)** 3-Hexanol
b3) 3-Hexanone **b4)** 2,4-Hexanedione **b5)** 3-Hexanone, 4-methyl-

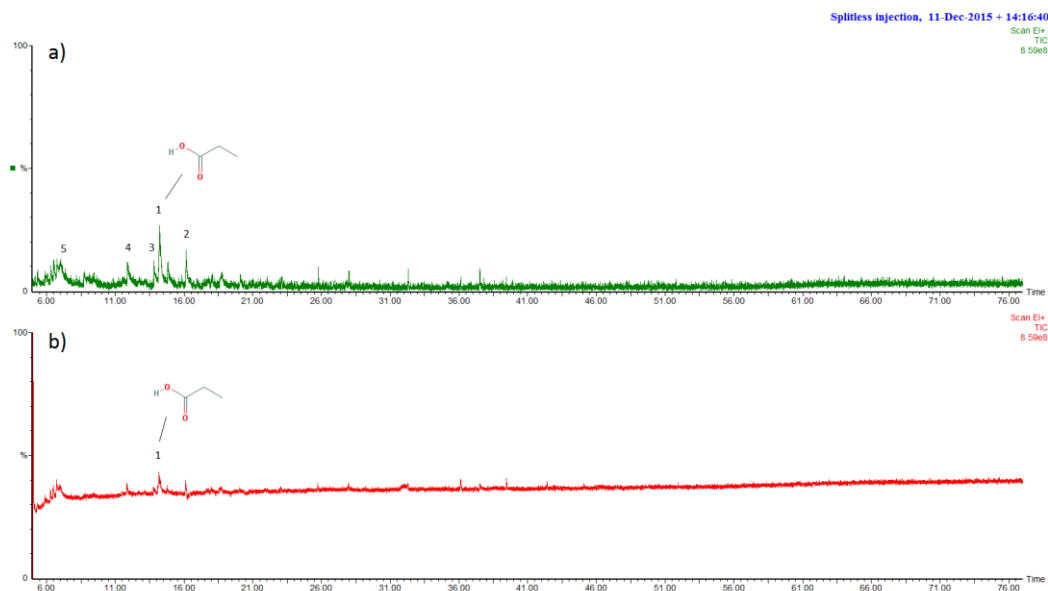


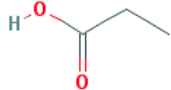
Figure 8. 8 Sampler 3 – TIC of Blend PM(2)9010 Emissions

(a) Before Igniting (at 310°C); Elements Identified **a1)** Propanoic acid **a2)** 3-Hexanone,
 4-methyl- **a3)** 3-Hexanol **a4)** 2,4-Hexanedione **a5)** Furfural

(b) Critically Igniting (at 320°C); Elements Identified **b1)** Propanoic acid

There was only one chemical element found common to all the eight experimented samples (see **Table 8. 4**, for chemical structure and key marker), which was propanoic acid ($C_3H_6O_2$). It was also known as propionic acid in some literatures. Like before, the chemical structure of this element was shown next to the relevant TIC peak and all siloxanes from column disintegration had been disregarded as elements related to biomass emission when TIC peaks were looked into. Except for Miscanthus(2) (see **Figure 8. 7**), all the chromatograms were rather flat, showing less peaks, suggesting relatively little components were captured by ORBO tubes. For PM(2)5050 with half its ingredients made up of Miscanthus(2), the peak intensities were about similar to those of PM(2)9010 (see **Figure 8. 8**). Most of the peak intensities of critically igniting biomass were lower than when they were pyrolysing. Also, it had been observed from ORBO TICs that most peaks inclined towards short retention time, indicating components captured by ORBO tube were low in molecular weight. Comparing pyrolysing and critically igniting emissions intensities from the same material, the difference between each pair were not too significant.

Table 8. 4 ORBO Tube – Similar Emission Component Identified for all Eight Samples

No.	Element /Chemical Formula	Chemical Structure	Type of Key Marker
1	Propanoic acid ($C_3H_6O_2$)		Hemicellulose (Yokelson et al., 2009; Liu et al., 2014)

Propanoic acid, a volatile fatty acid (VFA), is a naturally occurring carboxylic acid. From the work of Yokelson et al. (2009) regarding emissions from biomass burning in the Yucatan that focused on crop residue fires and deforestation in relation to forest fire, ~49 gases had been measured. Besides gases like hydrogen cyanide (HCN) and acetonitrile, other acidic species like peroxyacetic acid, propanoic acid, methane sulfonic acid, and sulfuric acid were found. It was also concluded that crop residue fires emitted more organic acids than deforestation fires. Nowakowski et al. (2008) in the study on phosphorous catalysis in pyrolysis behaviour of biomass had found propanoic acid as one of the main xylan (a type of hemicellulose) decomposition products at 600°C.

Similar to the method applied on TICs from emissions captured by Samplers 1 and 2 in which peak areas contributed by non-biomass emissions, i.e. GC column disintegration, were neglected, the peak area percentages of emission TICs were re-calculated and the results are displayed in **Figure 8. 9**. As displayed in **Table 8. 4**, only one

similar component was identified for all the four pre-igniting & critical-igniting biomass pairs. All samples showed very little propanoic acid emission (<2 peak area%) at both pre-igniting and critically igniting stages. Except for Pine, all other three biomass pairs showed slightly higher propanoic acid peak area% at pre-ignition as compared with that when critically-ignited.

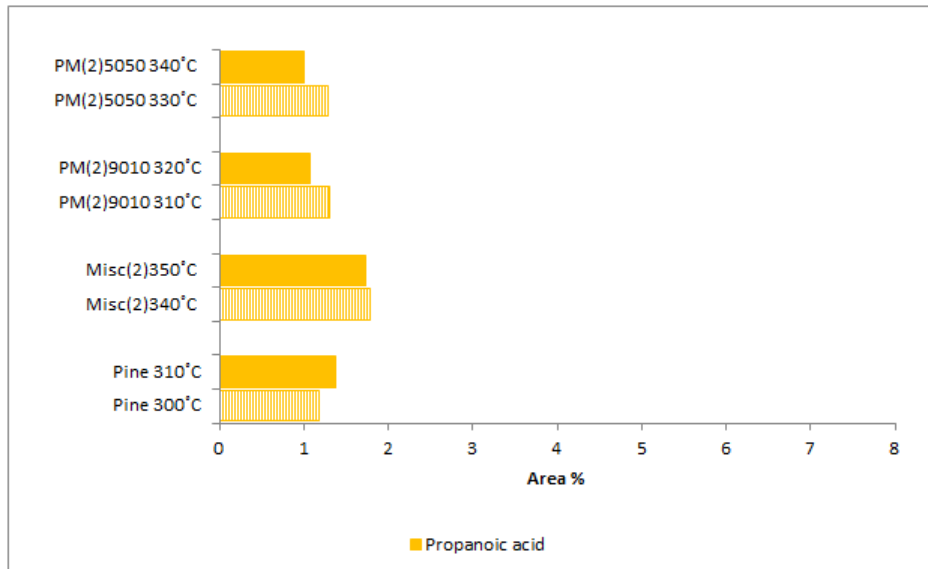


Figure 8. 9 Sampler 3 – Peak Area Percentages of Similar Component at Pre-ignition and Critical Ignition Stages

All in all, emissions from biomass burning have negative effects on both the environment and to human health. Upon knowing the pollution potential, one should avoid combusting biomass unnecessarily and as far as possible, avoid the possibility for biomass to catch fire since smouldering biomass could be more harmful to both environment and human health in the long run.

8.4 Elemental Carbon and Organic Carbon from Biomass Emissions

The EC/OC ratio was simply assumed to be the ratio of Fixed Carbon (FC) to Volatile Matter (VM), following the method adopted by Mitchell et al. (2016). **Figure 8. 10** shows the VM and FC content in the PM retained by filter papers for the eight biomass samples investigated here. All the eight samples showed slightly greater VM and FC contents at the higher critically igniting temperature. It is believed that at temperature 10°C higher i.e. the critically igniting temperature for each biomass, more organic carbon and elemental

carbon managed to be released since the reaction rate had sped up at this higher temperature.

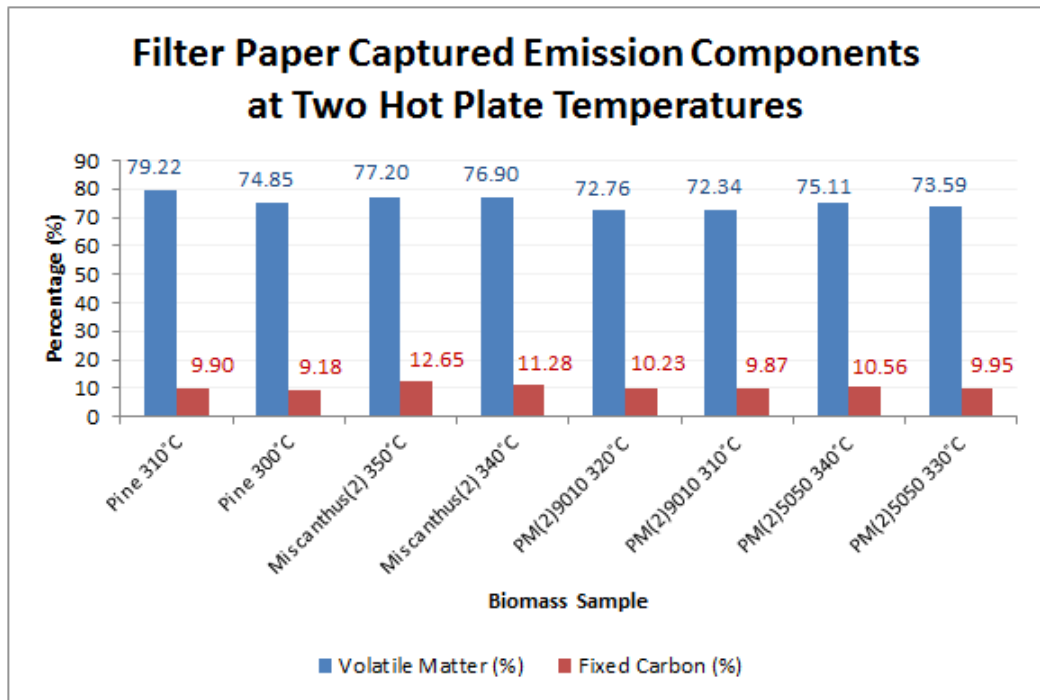


Figure 8. 10 VM and FC of PM Retained by Filter Paper

The EC/OC ratios for the 8 biomass samples are shown in **Figure 8. 11**. It was found that the ratio was higher at critically igniting temperature than the 10°C lower pre-igniting temperature, $\left(\frac{EC}{OC}\right)_{\text{igniting}} > \left(\frac{EC}{OC}\right)_{\text{pre-igniting}}$, for pure woody or herbaceous biomass and their blends at different weight ratios. The difference for all four materials was not too big with miscanthus showing a slightly bigger difference. This simply implied that at the higher critically igniting temperature, more carbonaceous emissions failed to condense at the cooler glass funnel but retained by the filter paper as the emissions travel further.

At higher temperature, emission components are more energetic thus can travel further before retained by a physical barrier i.e. the filter paper. Also, it may indicate that there is more PAH growth to soot as it approaches the higher critically-igniting temperature. With this, even higher EC could be expected on the filter paper analysis if the biomass sample is tested at a temperature much higher than the critically-igniting temperature.

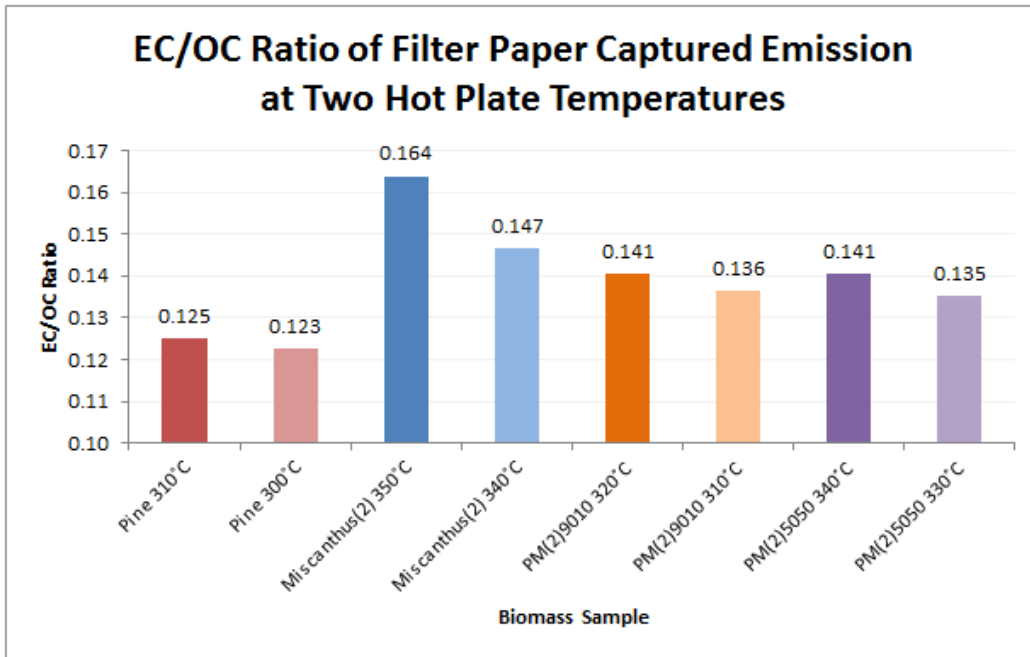


Figure 8. 11 EC/OC Ratio of Filter Paper Captured PM from Biomass Samples at Critically Igniting and Pre-Igniting Temperatures

8.5 Predicted Volatile Species and Intensities Modelled by FG-BioMass

Referring to the work of McNamee et al. (2016), the composition and yields of volatile stream species were modelled with FG-BioMass. Here, there were thirteen major volatile species identified, since methane, hydrogen cyanide and isocyanic acid were determined in addition to those determined by McNamee et al. (2016) and the results for four pre-igniting biomass and four critically-igniting biomass are shown in **Figure 8. 12** and **Figure 8. 13** respectively.

In both pre-igniting and critically igniting scenarios, acetaldehyde topped the yields for herbaceous Miscanthus(2) and PM(2)5050, followed by water, carbon dioxide then acetic acid. As explained in a study of Prins et al., the water, carbon dioxide and acetic acid yields were contributed by decomposition of the hemicellulose fraction (Prins et al., 2006). This was consistent with the hot plate temperature range used in this study (300°C to 350°C) and was within the temperature range which hemicellulose decomposition was dominant (Mathew and Zakaria, 2015).

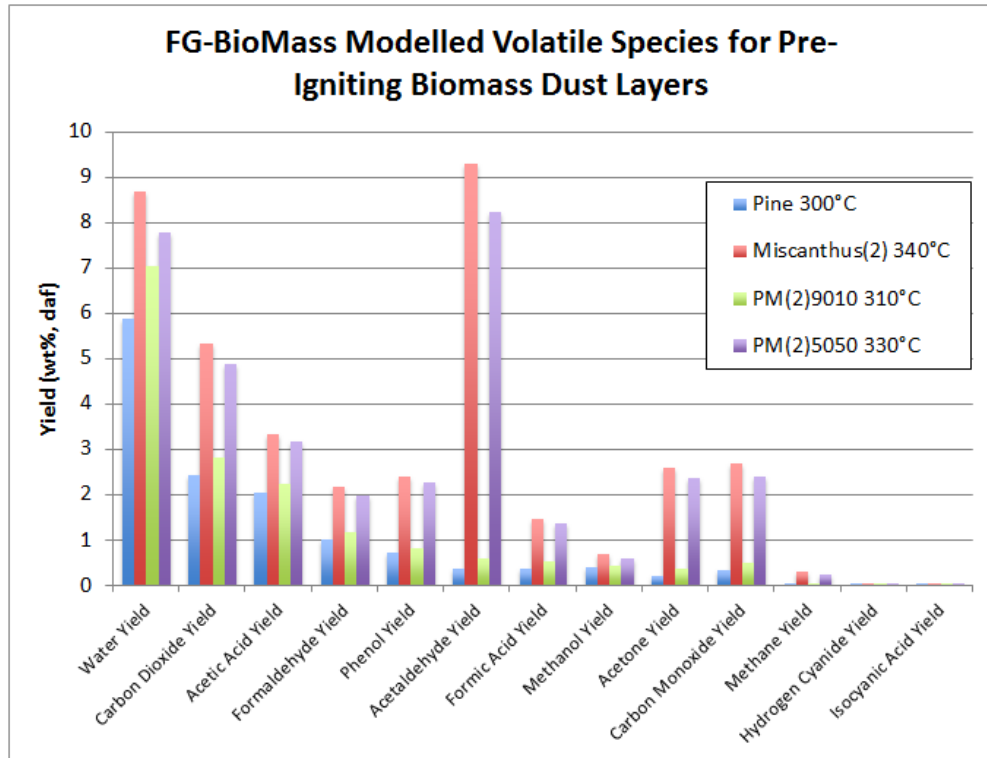


Figure 8.12 Yields (dry-ash-free basis) of Volatile Species from Eight Pre-Igniting Biomass as modelled by FG-BioMass

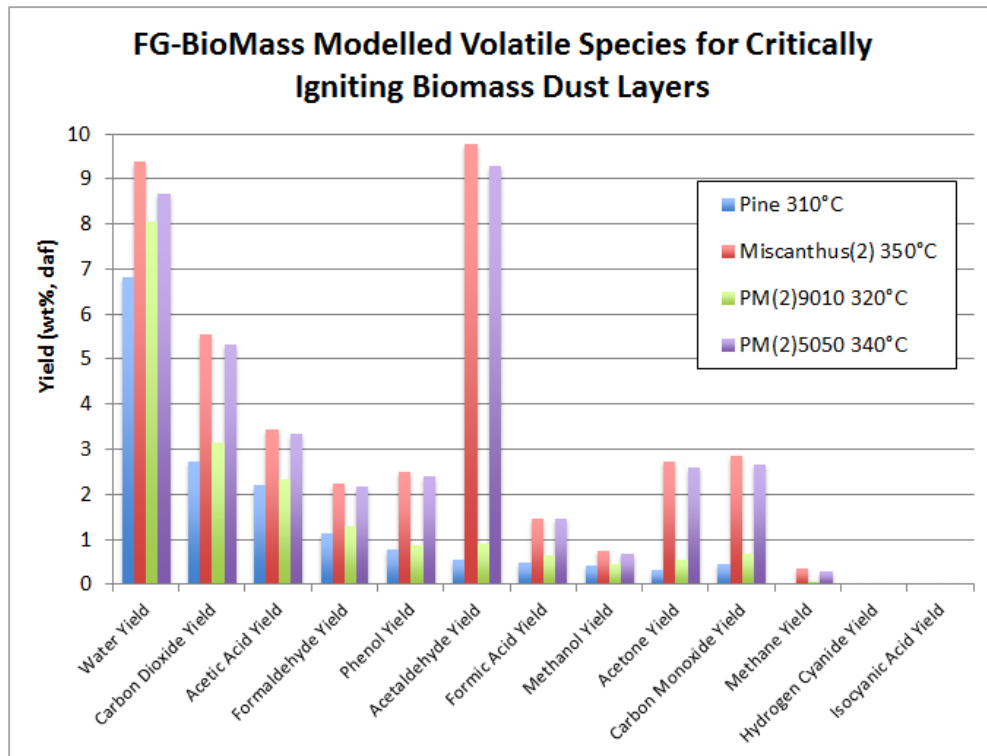


Figure 8.13 Yields (dry-ash-free basis) of Volatile Species from Eight Critically Igniting Biomass as modelled by FG-BioMass

In the present study, the same approach as applied by Jones et al. had been adopted whereby the LFLs from all the eight sample were calculated (Jones et al., 2015). From the risk of ignition of volatiles aspect, reactivity of each sample was ranked, the smaller the LFL value, the easier for the volatiles to ignite. **Table 8. 5** and **Table 8. 6** show the two LFL values for each of the four pre-igniting and four critically igniting biomass dust layers. it was estimated that PM(2)9010 that consisted mostly of pine was more reactive than PM(2)5050 and this was evident by herbaceous miscanthus having LFL value that was far smaller than woody pine.

Table 8. 5 LFL for Gases and Light Volatiles Estimated for Eight Pre-Igniting Biomass Samples

Sample	Pine, 300°C	Miscanthus(2), 340°C	PM(2)9010, 310°C	PM(2)5050, 300°C
LFL ^a (%) in air	22.30	9.67	21.71	9.64
LFL ^b (%) in air	7.79	5.73	7.66	5.73

^a Include dilution effect of reaction water vapour but exclude 'tar'

^b Exclude dilution effect of reaction water vapour and 'tar'

Table 8. 6 LFL for Gases and Light Volatiles Estimated for Eight Critically-Igniting Biomass Samples

Sample	Pine, 310°C	Miscanthus(2), 350°C	PM(2)9010, 320°C	PM(2)5050, 340°C
LFL ^a (%) in air	21.83	9.76	20.91	9.67
LFL ^b (%) in air	7.68	5.72	7.51	5.73

^a Include dilution effect of reaction water vapour but exclude 'tar'

^b Exclude dilution effect of reaction water vapour and 'tar'

8.6 Concluding Remarks and Suggestions for Future Work

When the hot plate is close to (but below) the critically igniting temperature, volatile emissions is clearly visible. In this study the emissions were sampled and analysed via the GC-MS-TIC method. Sampling in a three-stage procedure showed heavier volatiles were captured by the first two samplers whereas the lighter ones were trapped by the final sampler. Decompositions of different biomass components were detected in different emission sampler, just before and at ignition. Components that were mainly detected originated from lignin decomposition, though a small amount originated from hemicellulose had been detected too. This is consistent with the fact that lignin decomposes over a wide range of temperature, starting from 150°C whereas hemicellulose decomposed at slightly higher temperature range of 220 to 315°C (Yang et al., 2007). Towards the end of the sampling train, traces of propanoic acid cleaved from hemicellulose was detected.

Unfortunately, results obtained from this experiment did not provide firm conclusion as to which emission component has potential to be a biomass self-ignition indicator. This is probably due to the tiny amount of biomass used in this experiment that failed to provide statistically large enough emissions amount to be quantified accurately, thus more work in this area is needed. Perhaps, predicting biomass self-ignition from volatile organic compounds (VOC) emission from little sample amount is not a practical approach. However, if the samples are limited, the first sampler (i.e. the inverted funnel) could provide some insights to distinguish pre-igniting and critically-igniting biomass dust since the results of all samples consistently showed higher Benzaldehyde, 4-hydroxy-3,5-dimethoxy- at pre-igniting stage.

The LFL values were calculated from volatile species and intensities predicted by FG-BioMass model. Comparing the LFL of each biomass sample, the values were much smaller when dilution effect from water vapour and tar were neglected than when the water vapour effect was included. In general, PM(2)9010 prediction was close to that of 100% pine whereas PM(2)5050 were close to that of Miscanthus(2). Generally, the LFLs 10°C before critical ignition did not differ much from critically ignited ones, implying that there was high risk from smouldering at a high temperature as it could turn into flaming combustion easily.

The results could be further strengthened with emission factors calculation. By doing that, one could track from which sampler that most emissions had been captured along the emission sampling line. In the future, a front and back-up filter sampling approach (Yee et al., 2013) may be adopted like suggested by Yee et al.. With this setup, back-up filter would play its role in aerosols collection when the front filter was broken through or when evaporation of semivolatiles collected from front filter happened.

There are a few parameters that could be varied here for a comprehensive and detailed study. Firstly, the screw valve opening can be altered to check if varying emission flowrate will yield results that are significantly varied from the current flowrate set. Secondly, biomass dust contained in different rings could be used – either taller ring height (increased dust thickness but with fixed diameter) or bigger diameter ring (increased dust spread area but with fixed thickness); or even varying both the height and diameter parameters. Thirdly, the polytetrafluoroethylene (PTFE) tubing lengths could be varied and with the emission factor calculation, the effect of connecting tube lengths could be known.

Some parameters in the analysis procedure can be varied too. For the GC-MS procedures adopted by all the three emission samplers, the flowrate of carrier gas helium or oven temperature of the GC may be changed and whether or not the results would be affected is worth checking. Also, the emissions could also be dissolved in other solvents apart from medium polar DCM, for instance toluene to see what would be the elements extracted by another solvent.

Chapter 9

Hot Surface Ignition Test – Reaction Kinetics Estimation and Ignition Delay Time Prediction

Following the temperature measurements reported in **Chapter 3**, the average ambient temperature T_a 20°C. The dust layer top surface temperature, T_s , was measured with an infrared thermometer at the centre of the circular top surface area. This was consistent with the T_s measurement location in other studies (El-Sayed and Mostafa, 2016; Wu et al., 2014; Park et al., 2009), where the thermocouple for T_s measurement had its measuring junction located at the centre. For igniting cases, T_s was measured immediately once a glow indicating commencement of ignition was noticed. The thermal conductivities that were determined from the thermal conductivity-density correlation showed 0.06 W/m·K; 0.04 W/m·K and 0.06 W/m·K for Miscanthus(1) and Miscanthus(2); Wheat Straw and Pine and biomass blends, respectively. It had been noticed from the hot plate experiments that the dust layer ignition temperatures did not make significant difference when the 10°C interval was adopted and therefore, the results from the 5°C interval i.e. after the refinement step were referred to. Furthermore, a 5°C interval was applied by Park et al. (2009) and El-Sayed and Mostafa (2016) in respective thermal and kinetic parameters estimation study.

9.1 Reaction Kinetics Estimation

The iterative method for activation energy estimation as described in **Chapter 3** was termed 'detailed method' henceforth. For the same Miscanthus(1) example used in **Chapter 3**, the plot using **Equation 2.13** i.e. $\ln\left(\frac{\delta_c T_p^2}{r^2}\right) = -\frac{E}{RT_p} + \ln\left(\frac{E}{R} \frac{\rho Q A}{\lambda}\right)$ at final iteration is shown in **Figure 9. 1**. For Miscanthus(1) dust that ignited at 305°C (~578K) in Ring A which the r value was 0.0025 m, with Bi that was calculated to be ~0.93 and θ_a at final iteration was found at ~13.8; these Bi and θ_a values had resulted in δ_c of ~12.26 when **Equation 2.6** was applied. With these numbers, one data point for Miscanthus(1) dust was calculated. The similar was conducted for Ring B with r at 0.00625 m in which Miscanthus(1) ignited at 275°C (~548K) and the second data point was obtained. In summary, the two data points from different dust thicknesses contained in Ring A and Ring B obtained for graph plotting were:

$$\left(\left(1/T_p \right), \ln \left(\frac{\delta_c T_p^2}{r^2} \right) \right)_{\text{Ring A}} = (0.00173, 27.209)$$

and

$$\left(\left(1/T_p \right), \ln \left(\frac{\delta_c T_p^2}{r^2} \right) \right)_{\text{Ring B}} = (0.00182, 25.675)$$

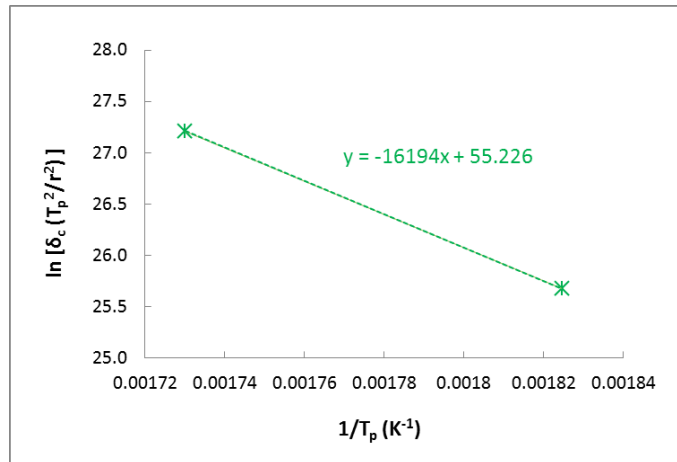


Figure 9. 1 Reaction Activation Energy Estimation –Plot from Final Iteration for Miscanthus(1) Dust Layers, Detailed Method

The linear equation was found to be $\ln \left(\delta_c \frac{T_p^2}{r^2} \right) = -\frac{16194}{T_p} + 55.226$, in which the activation energy E was obtained from slope $\frac{E}{R}$ that read 16194 and pre-exponential factor A was obtained from the y-intercept, $\ln \left(\frac{E}{R} \frac{\rho Q A}{\lambda} \right)$, that showed a value of 55.226. The density, ρ , when Miscanthus(1) was filled in Ring A had been determined to be ~ 201.4 kg/m³ (228.6 kg/m³ in Ring B); thermal conductivity, λ , 0.06 W/m·K and Q of 18.22 kJ/g, in which higher heating value of Miscanthus(1) was taken as Q , following a study of Wu et al. (2014). With these values, the pre-exponential factor A was calculated to be $9.738 \times 10^8 \text{ s}^{-1}$ and $8.581 \times 10^8 \text{ s}^{-1}$ when contained in Ring A and B respectively.

The heat transfer dimensionless number determination approach as described in **Chapter 3**, coupled with the activation energy estimation steps described here in this chapter, the reaction activation energy (E) of ten biomass samples igniting on the hot plate and their corresponding reaction pre-exponential factor (A) was tabulated in **Table 9. 1**, with the heat transfer dimensionless number, Bi , and critical heat generation rate term, δ_c , included as well.

Table 9. 1 Reaction Activation Energy (E) and Pre-Exponential Factor (A) Estimated with Some Dimensionless Parameters Involved

Sample	$2r$ (mm)	Bi	δ_c	E (kJ/mol)	A (s^{-1})
Miscanthus(1)	5	0.93	12.26	134.64	9.738×10^8
	12.5	2.01	18.39	134.64	8.581×10^8
Miscanthus(2)	5	1.05	8.52	105.58	7.584×10^5
	12.5	2.16	12.33	105.58	6.963×10^5
Pine	5	0.81	10.82	132.92	5.288×10^8
	12.5	1.75	16.98	132.92	4.657×10^8
Wheat Straw	5	1.42	14.17	126.65	1.564×10^8
	12.5	3.01	18.89	126.65	1.454×10^8
PM(1)9010	5	0.93	16.86	160.24	2.243×10^{11}
	12.5	2.04	25.50	160.24	1.981×10^{11}
PM(1)5050	5	0.93	16.86	160.24	2.284×10^{11}
	12.5	2.04	25.50	160.24	2.187×10^8
PM(2)9010	5	0.96	13.38	139.69	1.920×10^9
	12.5	2.07	19.99	139.69	1.691×10^9
PM(2)5050	5	1.02	9.62	114.07	4.860×10^6
	12.5	2.13	14.07	114.07	4.318×10^6
PWS9010	5	0.93	16.86	160.24	2.444×10^{11}
	12.5	2.04	25.50	160.24	2.123×10^{11}
PWS5050	5	0.95	12.82	137.16	1.524×10^9
	12.5	2.04	19.18	137.16	1.323×10^9

All the E values found for the ten materials were consistent with the findings by Bowes (1981) in the study of developing a general approach to predicting and controlling potential runaway reaction, which stated that many systems typically showed $\frac{E}{R}$ value in the order of $\geq 10^4$ K.

Looking at the pre-exponential factor, A , of all the ten biomass samples evaluated, a common trend that showed a slightly higher A for the same material when contained in

Ring A than in Ring B was observed. A higher A value implies higher molecules collision frequency in a chemical reaction. The ignition happened in Ring A at a higher temperature than in Ring B for the same material, thus it was expected that the molecules moved more rapidly at the higher temperature when filled in Ring A and resulting a higher pre-exponential factor.

For the four single-material samples, Miscanthus(2) was found to have an activation energy a bit lower than the other three that showed comparable values to each other. In addition, Miscanthus(2) had a pre-exponential factor with an order of magnitude of only 10^5 , less than the other three samples that consistently showed 10^8 order of magnitude. Looking again at the T_{LIT} results, Miscanthus(2) was the only material that showed results quite different from those of the other three, in which Miscanthus(2) manage to sustain a higher temperature before igniting. Judging from the smaller pre-exponential factor, the reaction within Miscanthus(2) was less vigorous than the other three materials.

Consistent results were observed for the six biomass binary blends. The two blends with Miscanthus(2) in the composition showed lower activation energy value than other blends and lower pre-exponential factor as well. The effect on both E and A values was obvious when PM(2)9010 and PM(2)5050 were compared. The E and A values of PM(2)5050 were less than those of PM(2)9010, the lowering of E and A became obvious with more Miscanthus(2) present in the blend.

The activation energy estimated with **Equation 2.13** that had considered the effects of δ_c (the detailed method) was compared with corresponding value obtained from crude estimation via a simple correlation relating $\ln(T_h^2/d^2)$ with $1/T_h$ in which the slope of this plot was assumed to be $\frac{E}{R}$, having T_h as the hot plate temperature and d the dust layer thickness (Babrauskas, 2003a). The crude estimation method had been applied on all the ten samples used and the results for Miscanthus(1) is illustrated in **Figure 9.2**. In this example of Miscanthus(1), the gradient $\frac{E}{R}$ with value of 17867 had led to reaction activation energy of 148.77 kJ/mol, ~ 14 kJ/mol higher than predicted by the detailed method.

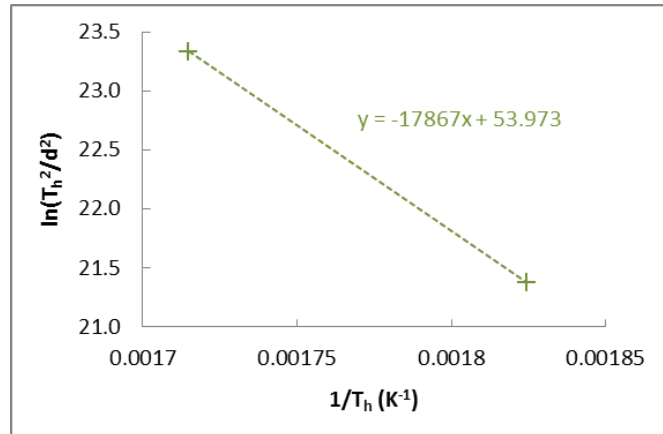


Figure 9. 2 Reaction Activation Energy Estimation –Plot for Miscanthus(1) Dust Layers, Crude Estimation Method

With the detailed method, the E range obtained for the four single-material biomass samples was ~ 106 to ~ 135 kJ/mol (see **Table 9. 1**), a ~ 29 kJ/mol difference between the highest and lowest of E . When the crude E estimation method was applied, the E values for the four materials ranged between ~ 130 to ~ 173 kJ/mol and a ~ 43 kJ/mol difference between the highest and lowest E . As for the six binary blends, the E range was ~ 114 kJ/mol to ~ 160 kJ/mol (see **Table 9. 1**) with ~ 46 kJ/mol difference between the highest and lowest E values when the detailed method was adopted. However, when crude estimation method was carried out, the E range became ~ 141 to 205 kJ/mol, giving a ~ 63 kJ/mol difference between the range limits. The difference between the reaction activation energy, E , and the Arrhenius pre-exponential factor, A (represented by $\ln A$), estimated by the two methods is summarised in **Figure 9. 3**. Both the x-axis range (activation energy E) and y-axis range ($\ln A$) show greater differences when the crude estimation method was used.

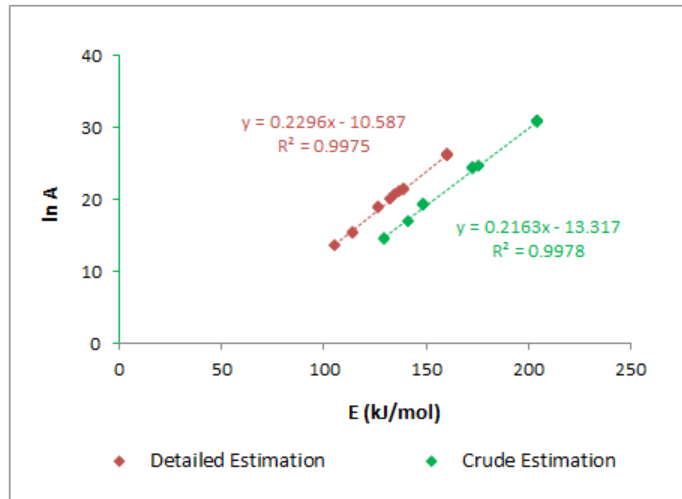


Figure 9. 3 Reaction Activation Energy E and $\ln(\text{pre-exponential factor})$ Comparison between Two Estimation Methods

This deviation between the two methods was consistent with described by Babrauskas (2003a) in which an actual E value of 100 kJ/mol was estimated as 140 kJ/mol by the crude estimation method. The deviation was mainly because the δ_c value was never constant (Babrauskas, 2003a) for hot surface ignition cases, unlike those that involved infinite Biot number e.g. when the system is subjected to fan blowing, where δ_c of the system was simplify to a constant that depends only on its geometrical shape.

From the detailed and crude methods of E estimation applied in this study, it was found that the δ_c term did give a significant impact on activation energy estimation. It was noticed that the E range estimated for the four single-material biomass showed lower than those that estimated for the six binary blends when crude estimation method was used, which was consistent with the trend estimated using the detailed method. Though different numerical values were obtained with the two methods, the crude estimation method nevertheless provides a clue on E when biomass materials were blended without needing to go through the time consuming iterative process.

9.2 Ignition Delay Time Prediction

The biomass dust layer ignition delay time (t_{ig}) relation with layer ignition temperature (T_{LIT}) has been determined as a second order polynomial, whereas a linear, first order function has been determined with layer thickness (*dust thickness*). As seen in **Figure 9. 4** and **Figure 9. 5**, as the hot plate temperature increased, the ignition delay time of the dust layer of a known thickness decreased in a non-linear fashion for both single-material biomass dust and binary biomass dust blends with correlations

$t_{ig} = 0.003 T_{LIT}^2 - 2.0806 T_{LIT} + 362.68$ and $t_{ig} = 0.0046 T_{LIT}^2 - 3.1241 T_{LIT} + 531.38$ respectively where t_{ig} represents the ignition delay time expressed in minutes and T_{LIT} represented the layer ignition temperature in °C. It was noticed that the ignition delay time was less scattered when two biomass materials were blended. It is believed that blending had somehow homogenised the biomass behaviour towards the more dominant behaviour between the two parents. The impact of dust layer thickness (in mm) of each biomass sample to respective ignition delay time (in minutes) showed linear a relationship, regardless single-material or blended material, as shown in **Figure 9. 6** and **Figure 9. 7**. The relation between the ignition delay time and dust layer thickness was found to be $t_{ig} = 1.6637 \text{ dust thickness} - 1.7958$ for the single-material sample and $t_{ig} = 1.3456 \text{ dust thickness} + 0.8872$ for the binary blends used in this study.

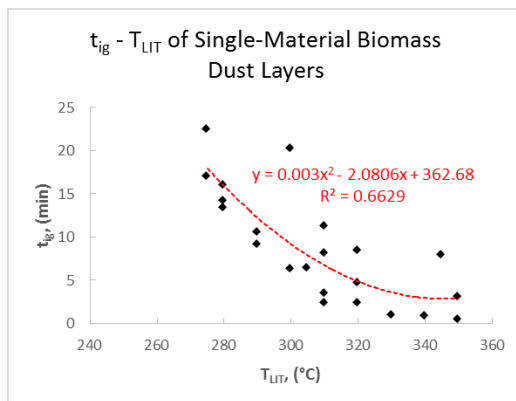


Figure 9. 4 Second Order Relation of Layer Ignition Delay Time with Layer Ignition Temperature for Four Single-Material Biomass

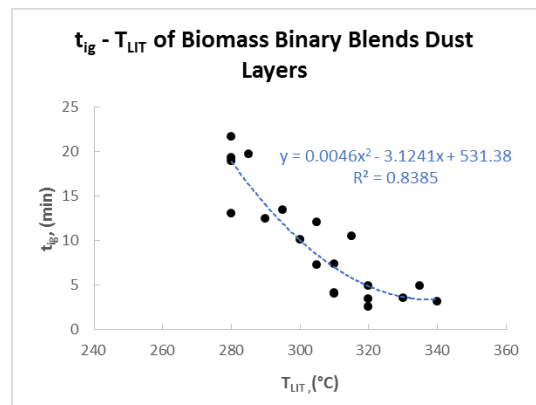


Figure 9. 5 Second Order Relation of Layer Ignition Delay Time with Layer Ignition Temperature for Six Biomass Binary Blends

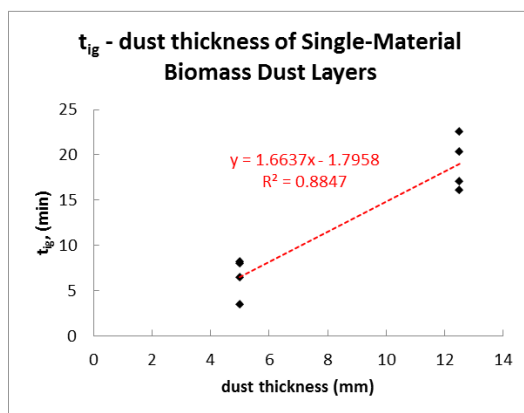


Figure 9. 6 Linear Relation of Layer Ignition Delay Time with Dust Layer Thickness for Four Single-Material Biomass

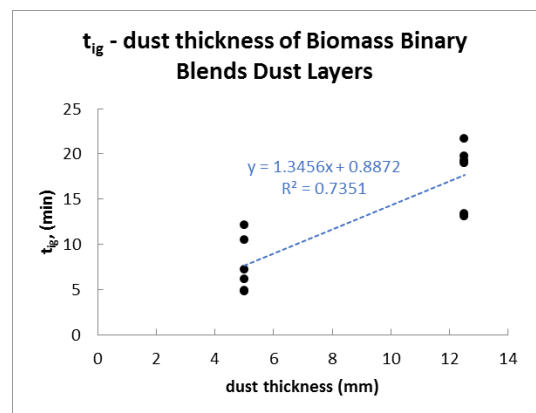


Figure 9. 7 Linear Relation of Layer Ignition Delay Time with Dust Layer Thickness for Six Biomass Binary Blends

Adopting the SI base unit for time and temperature, i.e. second and Kelvin, the relationship between ignition delay time and layer ignition temperature are shown in **Figure 9. 8 & Figure 9. 9** and **Figure 9. 10 & Figure 9. 11** for four single-material biomass dust layer and six biomass binary blends respectively. The correlations in the figures implied the following for,

a) single-material biomass dust layer:

$$t_{ig} = e^{-0.0339 T_{LIT} + 25.607} \dots\dots \text{Equation 9.1}$$

$$\ln(t_{ig}) = \frac{11564}{T_{LIT}} - 14.047 \dots\dots \text{Equation 9.2}$$

and

b) binary biomass blends:

$$t_{ig} = e^{-0.0325 T_{LIT} + 24.959} \dots\dots \text{Equation 9.3}$$

$$\ln(t_{ig}) = \frac{10924}{T_{LIT}} - 12.739 \dots\dots \text{Equation 9.4}$$

Dust from binary blends showed less variation among themselves when compared to the dust from single-material parent materials. If the equations were used to predict the ignition delay time for other biomass with similar characteristics for ignition temperatures ranged from 200°C to 400°C, the results shown in **Table 9. 2** would be expected.

Table 9. 2 Ignition Delay Time Prediction with Four Correlations for Dust Layers Igniting on Low Temperature Hotplate

Equation for t_{ig} (minute) prediction	Hot Plate temperature (°C)				
	200	250	300	350	400
Equation 9.1	239.36	43.95	8.07	1.48	0.27
Equation 9.2	548.32	52.967	7.69	1.52	0.38
Equation 9.3	242.78	47.81	9.41	1.85	0.37
Equation 9.4	524.16	57.62	9.31	2.02	0.55

The greatest prediction difference with the four correlations was notice at 200°C, the lowest in the prediction range. As the hot plate temperature approached the higher of range at 400°C, the ignition delay time for all was <1 min. All in all, these equations converged to one main point – the higher the hot plate temperature, the shorter the ignition delay time.

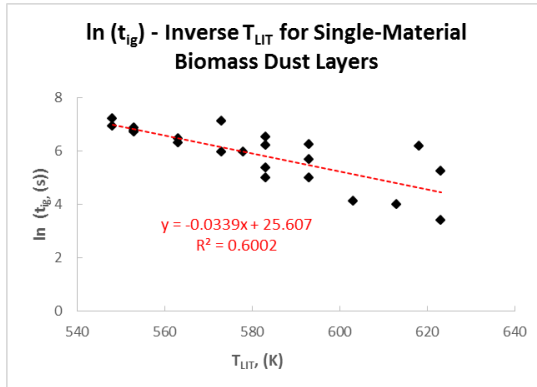


Figure 9. 8 Logarithm Ignition Delay Time in Seconds versus Layer Ignition Temperature in Kelvin for Four Single-Material Biomass

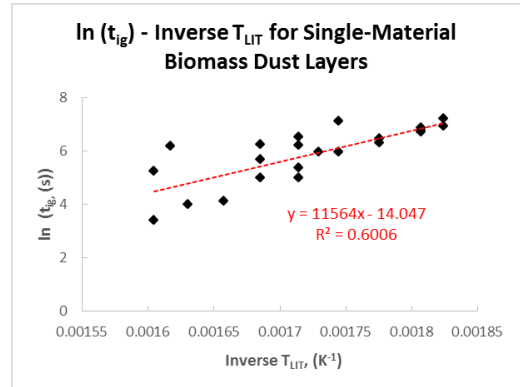


Figure 9. 9 Logarithm Ignition Delay Time in Seconds versus Inverse Layer Ignition Temperature in Kelvin for Four Single-Material Biomass

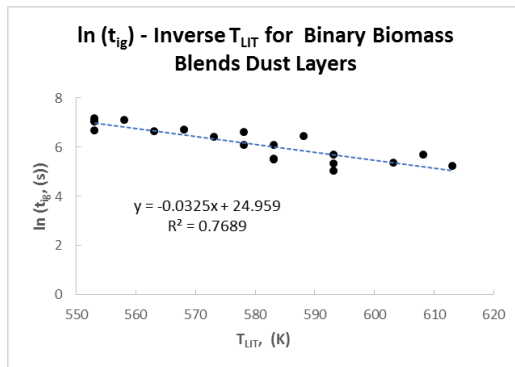


Figure 9. 10 Logarithm Ignition Delay Time in Seconds versus Layer Ignition Temperature in Kelvin for Six Biomass Binary Blends

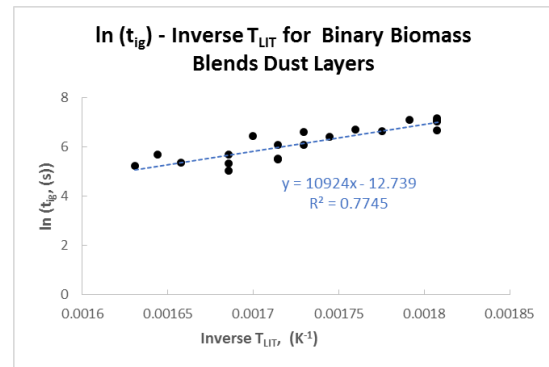


Figure 9. 11 Logarithm Ignition Delay Time in Seconds versus Inverse Layer Ignition Temperature in Kelvin for Six Biomass Binary Blends

9.3 Concluding Remarks and Suggestions for Future Work

From the hot surface ignition experiments, reaction kinetics that included the activation energy, E , and the corresponding Arrhenius pre-exponential factor, A , have been estimated for four single-material biomass and six binary biomass blends. The estimation process involved several dimensionless coefficients and some inputs from experiments. Dimensionless terms and iterations in numerical methods were applied when an analytical solution was impossible and numerical method provides a promising way forward.

For the four single-material samples and six of their binary blends used in this work, the kinetics estimation showed lower range of E and A values for the four single-material biomass as compared with those of the six binary biomass blends. The blends though, have relatively higher E than their parent materials (which implied a tougher energy barrier to reach ignition), and the Arrhenius pre-exponential factor that were higher too, i.e. a compensation effect is displayed which leads to comparable T_{LIT} in the dust layer experiments.

The detailed method involving iterations used in activation energy estimation highlighted the importance of including the varying critical dimensionless heat generation term, δ_c , in the correlation. Nevertheless, the crude estimation for activation energy did provide a rough but quick idea on reaction activation energy when something else was blended into an existing sample.

Ignition delay time prediction for both categories of single-material biomass dust layers and biomass binary blends on the other hand, showed that two major conclusions – regardless the dust composition, increased dust layer thickness pro-long the time-to-ignition and shorter delay time was expected at higher the hot plate temperatures.

There are some recommendation to improve the accuracy of this estimation method.

Since this study had used an infrared thermometer to measure the biomass layer top surface temperature, T_s , it is worth checking the T_s accuracy and consistency by other means, e.g. with another type-K thermocouple. The dust layer test rig could be modified to include another thermocouple placed close to the top surface of the sample dust layer.

The correlations obtained in this study (for both the kinetics estimation and ignition delay time prediction) were based on only two dust layer thicknesses. To improve the accuracy, another dust sample ring with the same diameter as Ring A and Ring B but taller could be fabricated such that the correlations determined from at least three data points could provide a higher accuracy.

Chapter 10

Storage – Hot Storage Basket Experiment

As mentioned in **Chapter 5**, to ease biomass fuel transportation, solid fuel had been condensed into the briquettes or pellets form. From the fuel source to pre-usage storage in a power station, along the long distance transportation e.g. from North America to the U.K., some briquettes or pellets disintegrate into biomass dust. Therefore, it is of interest to compare the self-ignition temperature or critical ignition temperature of the pellet and that of the disintegrated dust.

Henriksen et al. (2008) in their study regarding fundamental understanding of pelletisation had mentioned that increasing bioenergy usage served to meet two important purposes – lowering the CO₂ emissions and reducing the dependency on fossil fuels. Utilising biomass fuel in the form of pellets i.e. bio-pellets has been recognised as an effective way in bridging the energy gap in transition from dependence on fossil fuel to renewable bioenergy. Bio-pellets as compared with loose, unprocessed biomass exhibit several advantages; besides having higher energy density, ease in handling and storage due to the more uniform size is another added benefit. However, pellets storage is not without risk. Owing to the biological nature of biomass, these organic materials experience respiration that is exothermic at all times, releasing heat to the surroundings. Part of the released heat accumulates within the storage pile, resulting in heap temperature rise and the risk of fire. Storing large quantity of biomass in massive heaps or piles are considered a fire hazard that risks life and property should a fire happen.

White wood pellets (WWP) were selected for this storage self-ignition study since it is a common biomass solid fuel used in power stations whose storage is crucial to ensure a continuous power generation process. WWP or any other biomass fuel are stored in large quantity for sufficient fuel supply but any temperature rise, if left unchecked, could cause the biomass heap to self-ignite.

As mentioned in **Chapter 2**, there are two major kinds of analysis that could be carried out concerning material self-heating leading to self-ignition: adiabatic and isothermal methods. This study focused on the isothermal method, in which the procedures outlined in BS 15188 Determination of spontaneous ignition behaviour of dust accumulations (British Standard, 2008) were followed closely (see **Chapter 3** for details in setting up). In this comparison of criticality between pelleted and pulverised biomass of the same species, i.e. WWP, each of the samples and their respective appearance description is summarised in **Table 10. 1**.

Table 10. 1 WWP Samples Used in Hot Storage Basket Test

Sample Name	Description (wt%, particle size)
WWP-Pellets	100% North American white wood pellets >2.8 mm
WWP<180µm	100% North American white wood pellets >2.8 mm, milled and sieved down to <180 µm

Since the sample particle size used in this study differed from the recommendation in BS 15188 which specified the particles to pass through a sieve of 250 µm mesh aperture, the size distribution of WWP-Pellets and WWP<180µm was determined. The as received (a.r.) WWP consisted of 8mm diameter pellets with various lengths that were <20 mm. Most of these pellets were ~10 mm length, only a small fraction fell in either of these two extremes – very long (~20mm) and very short (~5 mm). The size distributions are shown in **Table 10. 2** and **Figure 10. 1** for the milled, as received pelleted WWP and pulverised WWP respectively. The size distribution of milled a.r. WWP was obtained from progressive sieving method whereas the pulverised one (<180 µm) was conducted in Malvern Mastersizer 2000, adopting the same laser diffraction method as described in **Chapter 3** where sphere was the assumed shape of the particles. From the size distribution, milled a.r. WWP mostly consisted of particles in the range 500 to 1000 µm whereas most of WWP<180µm were made up of ~160 µm particles as estimated by the Malvern Mastersizer.

Table 10. 2 Particle Size Distribution of Milled a.r. WWP Samples (Dooley, 2016)

Size Fraction, µm	Compositions wt%
< 250	11.78
250 -1000	51.67
1000 – 2000	34.67
> 2000	1.67
Loss	0.21
TOTAL	100

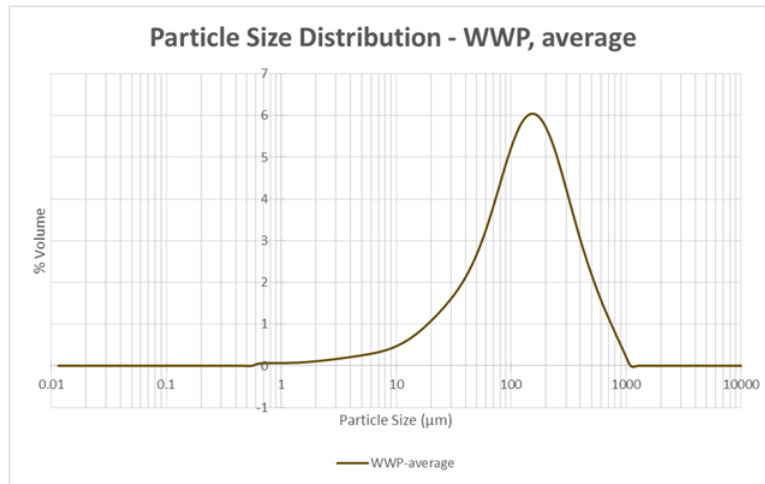


Figure 10. 1 Particle Size Distribution of WWP<180μm

10.1 Fuel Characterisation and Self-Ignition Risk Ranking of White Wood Pellets (WWP)

Like all other biomass samples, material characterisation via proximate and ultimate analyses were performed and the higher heating value was calculated using correlation from Friedl et al. (2005). The results of WWP characterisation are shown in **Table 10. 3**, **Table 10. 4** and **Table 10. 5** for proximate, ultimate and calorific value estimation respectively where all these results were mean values of tests done in duplicates or triplicates. The details of the experiments had been described in length in **Chapter 3**.

Table 10. 3 Proximate Analysis of WWP Sample

Biomass Sample	Moisture (wt%)	Volatile Matter (wt%)	Fixed Carbon (wt%)	Ash (wt%)
White Wood Pellets^a	4.9 ± 0.5	82.6 ± 0.3	11.2 ± 0.2	1.29 ± 0.01
White Wood Pellets^c	-	88.0 ± 0.3	12.0 ± 0.2	-

^a as received (ar) ^c dry-ash-free basis (daf)

Table 10. 4 Ultimate Analysis of WWP Sample

Biomass Sample	C (wt%)	H (wt%)	N (wt%)	S (wt%)	O (wt%)
White Wood Pellets^a	48.7 ± 0.9	6.3 ± 0.2	0.24 ± 0.04	0.01 ± 0.03	44.8 ± 0.9
White Wood Pellets^c	51.9 ± 0.9	6.7 ± 0.2	0.26 ± 0.04	0.01 ± 0.03	41.2 ± 0.9

^a as received (ar) ^c dry-ash-free basis (daf)

Table 10. 5 Higher Heating Value (HHV) Estimation of WWP Sample

Biomass Sample	HHV (MJ/kg)
White Wood Pellets^b	20.62

^b dry basis (db)

As compared with the results of other biomass samples before washing or torrefaction pre-treatments (see **Chapter 4**), the WWP results of proximate, ultimate analyses did not vary much. The correlation estimate calorific value on dry basis was a typical value of biomass too.

The self-ignition risk ranking of WWP was carried out following the same method applied on other biomass samples (details in **Chapter 3**), in which the T_{MWL} was obtained from the peak of TGA derivative weight loss curve (see **Figure 10. 2**) and E_a for volatiles combustion (see **Figure 10. 3**) was calculated using the first order reaction rate constant method (Ramírez et al., 2010; Saddawi et al., 2010), assuming the Arrhenius function holds.

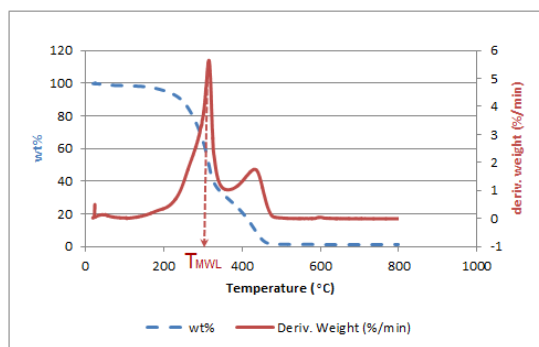


Figure 10. 2 T_{MWL} Determination for WWP

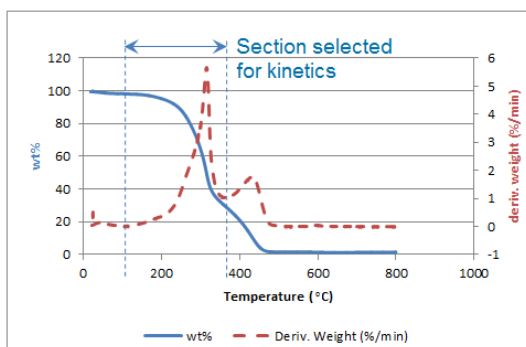


Figure 10. 3 Section Selected for WWP E_a Calculation

The graphical self-ignition risk ranking method showed that WWP was slightly safer than other single-material biomass samples studied here, namely Miscanthus(1), Pine, Miscanthus(2) and Wheat Straw since it fell into the ‘medium risk’ territory. It should be noted that its location on the risk ranking chart was quite close to the boundary of the ‘high risk’ category. **Figure 10. 4** shows the WWP self-ignition risk evaluated using the method modified by Jones et al. (2015) on the pictorial representation developed by Ramírez et al. (2010), alongside with other biomass materials for comparison. Evaluating WWP powder with either binder, the self-ignition risk evaluated using this method was on par with four other biomass samples with binder, i.e. Misc(2)Lg980, Misc(2)CF980, PineLg980 and PineCF980 that had been discussed in length in **Chapter 5**. Among these four materials with binder, the risk of WWP with either binder was quite close to that of PineLg980 and PineCF980, probably because WWPLg980 or WWPCF980 was a woody-based biomass of a similar kind as woody-based PineLg980 and PineCF980 (see **Figure 10. 4**). Adding Ligno-Bond-DD or cornflour binder to WWP had neither increased or decreased the self-ignition risk, as seen in **Figure 10. 4** since the self-ignition propensity remained in the same ‘medium risk’ category.

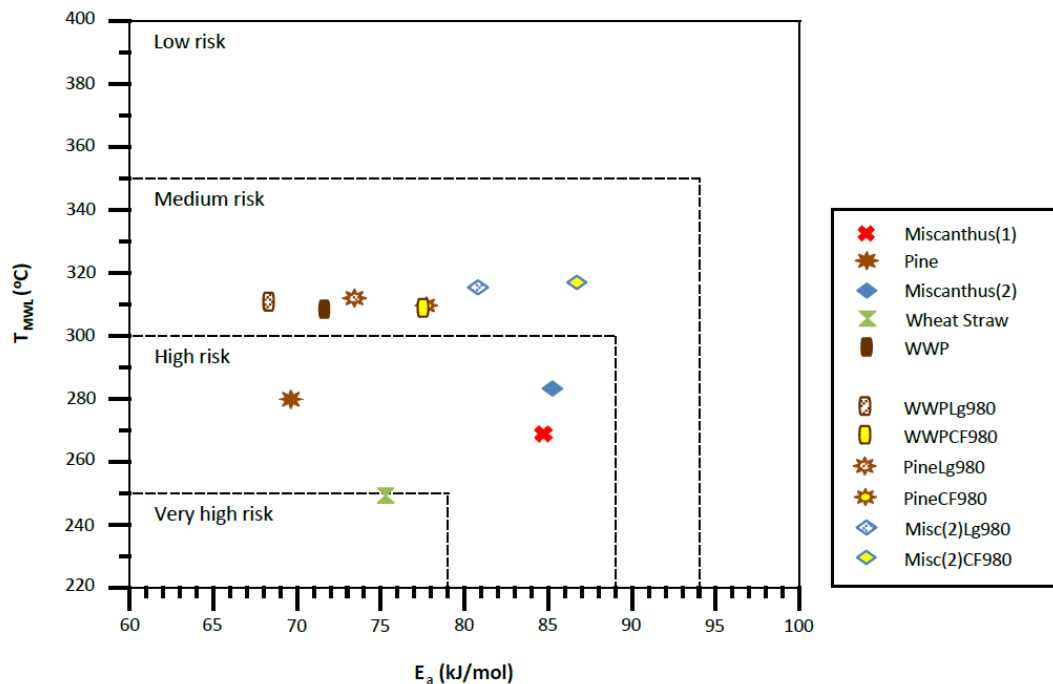


Figure 10. 4 Self-Ignition Propensity Risk Ranking of WWP and other Single-Material Biomass

10.2 Scaling Up Method – Critical Ignition Temperature and Ignition Delay Time Comparisons between Biomass Samples in Different Forms

As described in **Chapter 3**, the temperature-time profile of each HSBT experiment had been recorded, later plotted and analysed according to methods in BS 15188 (British Standard, 2008). A typical temperature-time plot of a WWP experiment is shown in **Figure 10. 5**, in which WWP<180 μ m contained in Basket S had ignited when the hot storage temperature was set at 210°C.

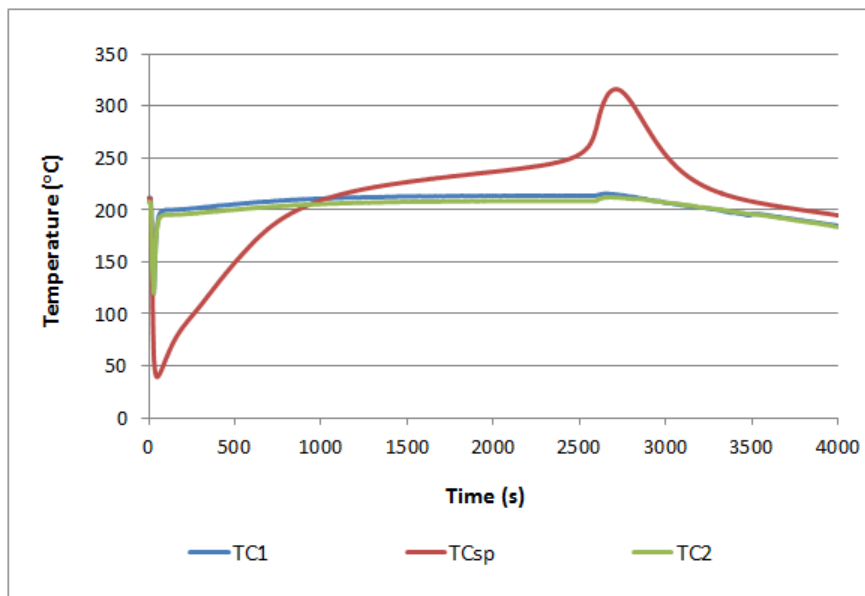


Figure 10. 5 HSBT Temperature-Time Profile of WWP<180 μ m in Basket S at 210°C Hot Storage Temperature

From the figure, the early drop in the three temperatures (TC1 and TC2 dropped to ~120°C whereas TCsp to ~45°C) within the first <60 seconds indicated the time when the oven inner chamber was opened and the prepared Basket S with WWP<180 μ m filled to the brim was transferred onto the metal structure and the TCsp was inserted into the basket centre. The sudden temperature decrease was due to an abrupt colder temperature surge from the atmosphere to the much hotter oven inner chamber temperature. The hot storage temperature as indicated by TC1 and TC2 eventually increased back to the desired value and both TC1 and TC2 temperatures did not vary too much from the set point of 210°C.

The sample temperature (as sensed by TCsp) and indicated by the red line increases slowly from ~45 to <250°C from ~60 to ~2500s. At ~1000s, TCsp surpassed that of TC1 and TC2 and kept rising, and when the time reached ~2500s, the temperature increase

was accelerated, reaching >300°C in less than 300s. Since the temperature rose >65°C relative to the hot storage temperature, ignition was considered to have occurred and LabView programme was coded to trigger nitrogen valve to open and the inert gas began to cool the ignited sample. It is crucial to cool the ignited sample as a safety measure because the temperature increased exponentially once ignited and following a study by Beever (1986), a temperature as high as 1230°C was detected when woodflour was subjected to a similar hot storage test. Thus, the danger of biomass storage could not be neglected – once the critical self ignition temperature (T_{SI}) was reached, the temperature rise that followed was rapid, possible to cause a fire outbreak, posing danger that threatens human lives and resulting in properties loss.

For the cases when ignition did not occur, the TCsp did increase from ambient temperature: In cases when the hot storage temperature was way below the T_{SI} of the sample, TCsp reached just the hot storage temperature (TC1 and TC2), or was slightly below TC1 and TC2. In cases close to the T_{SI} , TCsp increased above TC1 and TC2 but less than 65°C relative to average of TC1 and TC2 and eventually the TCsp remained almost constantly above TC1 and TC2 for an extensive period of time (over night). The temperature-time profile showed a small temperature rise exotherm that eventually flattened out at a constant value.

Since the HSBT results here were intended for extrapolation to much larger industrial fuel storage scale, the two final decisive determination tests for T_{SI} was confined to a small range of 2 K i.e. 2°C, following the recommendation in BS 15188 (British Standard, 2008). Adhering to the method outlined in BS 15188 and technique described by Ramírez et al. (2010) and Saddawi et al. (2013a), the final T_{SI} of a sample was determined from the arithmetic mean of two temperatures, mathematically represented by this equation:

$$T_{SI} = \frac{T_B + T_C}{2}$$

where T_B here is analogous to ϑ_B , T_C to ϑ_C used in BS 15188, signifying hot storage temperatures just slightly below T_{SI} (or subcritical temperature) and just above T_{SI} (or supercritical temperature) respectively. Temperatures T_B and T_C are illustrated in **Figure 10. 6**. A similar way of determining T_{SI} had been used by Leuschke (1981) in which T_{SI} was defined as situated between the highest measured non-ignition temperature (T_{NI} , analogous to T_B or ϑ_B) and lowest measured ignition temperature (T_I , analogous to T_C or ϑ_C). All these temperatures were experimentally determined from heated oven experiment on respective dust samples.

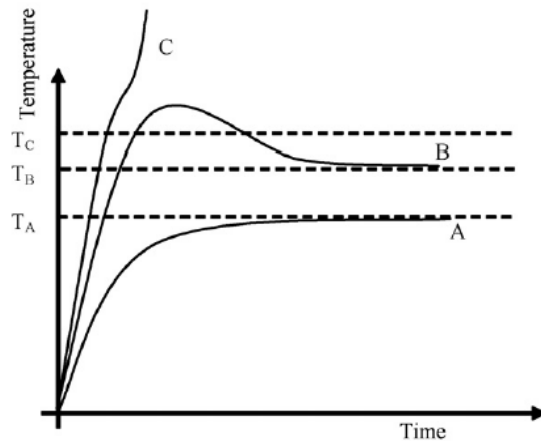


Figure 10. 6 T_{SI} Definition Used by Ramírez et al. and Saddawi el al. [Source: Ramírez et al. (2010)]

Besides this T_{SI} parameter, ignition delay time, t_i is another parameter and both results were plotted as described in BS 15188, in two separate plots: Namely, a pseudo-Arrhenius plot of self-ignition temperatures and the dependence of combustion induction times (t_i) on the volume/surface ratios of dust heaps. Both graphs had a common y-axis of $\log(V/A)$, in which V/A is known as the characteristic dimension in this study. As mentioned in **Chapter 2**, this y-axis was plotted against inverse of T_{SI} in Kelvin scale and logarithm of ignition delay time t_i in hours to illustrate two respective self-ignition characteristics in relation with storage volume.

The results obtained from HSBTs conducted on both WWP samples were plotted onto these graphs that had provided useful insights of about self-ignition characteristics. When superimposed onto the graphs readily available in BS 15188, the data points obtained from Basket S, Basket M and Basket L are as shown in **Figure 10. 7** and **Figure 10. 8** for T_{SI} parameter and t_i parameter respectively. For **Figure 10. 7**, the Y1 axis represents $\lg\left(\frac{V/1\text{ m}^3}{A/1\text{ m}^2}\right)$ and Y2 indicates volume V when the cylinder diameter d equals to its height h and X axis was the reciprocal of self-ignition temperature in Kelvin scale, $\frac{1}{T_{SI}/1\text{ K}}$. For **Figure 10. 8**, Y1 and Y2 indicates the same as those in **Figure 10. 7** but with its X axis representing $\lg(t_i/1\text{ h})$ with time in unit of hour. The lines existing on BS graphs simply indicate that as storage volume increases, the T_{SI} decreases and t_i lengthens.

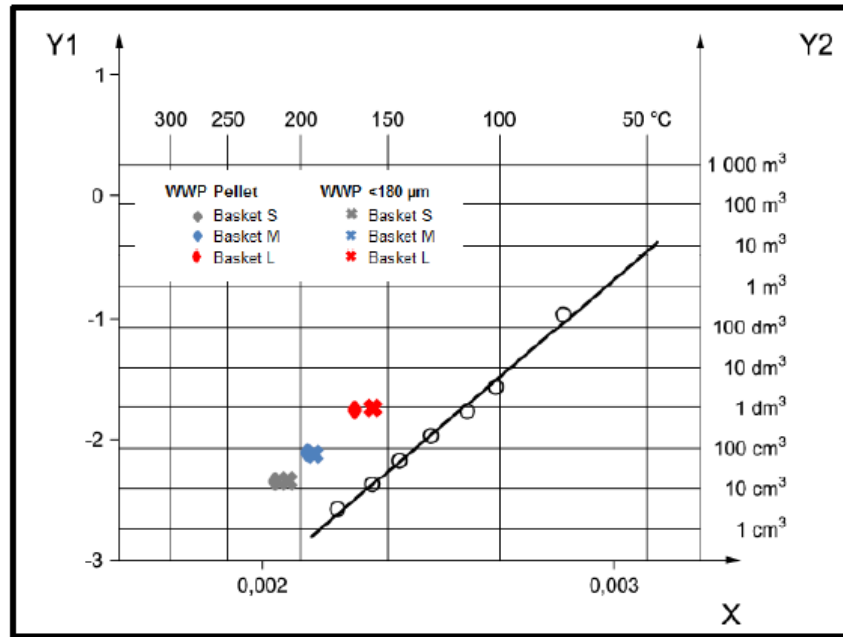


Figure 10. 7 Superimposing HSBT Results from Baskets S, M, L onto BS 15188 T_{SI} Graph (Pseudo-Arrhenius Plot of Self-Ignition Temperatures) [Edited from: British Standard (2008)]

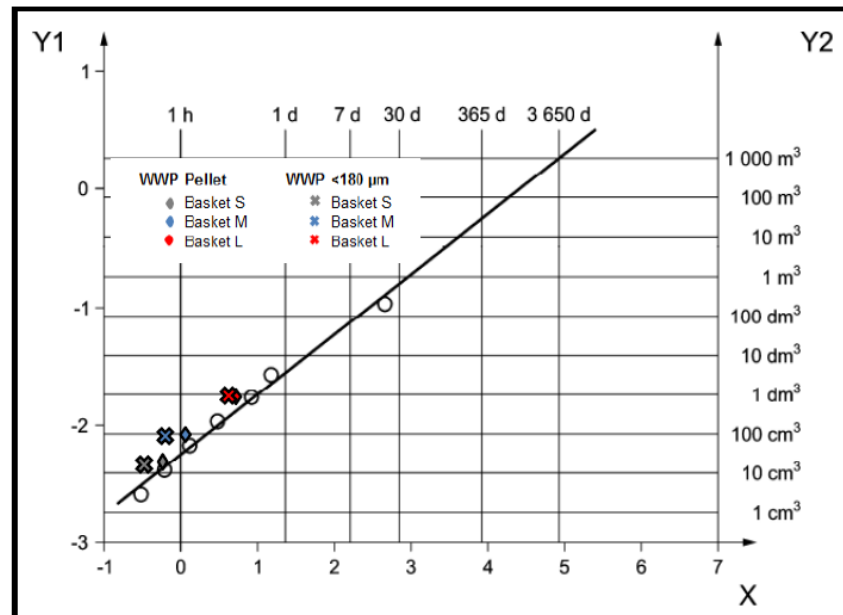


Figure 10. 8 Superimposing HSBT Results from Baskets S, M, L onto BS 15188 t_i Graph (Dependence of Combustion Induction Times (t_i) on the Volume/Surface Ratios of Dust Heaps) [Edited from: British Standard (2008)]

The T_{SI} and t_i plots, alongside with the estimated linear equations and regression coefficients of both WWP-Pellet and WWP<180µm are shown in **Figure 10. 9** and **Figure 10. 14** respectively.

With the linear equation estimated for T_{SI} via empirical method, the critical temperature for a larger storage volume could be predicted by extrapolating the best fit line to other bigger volumes. For instance, a 1m^3 pile of WWP-Pellets was predicted to self-ignite at $\sim 110^\circ\text{C}$ whereas WWP $<180\mu\text{m}$ at $\sim 100^\circ\text{C}$.

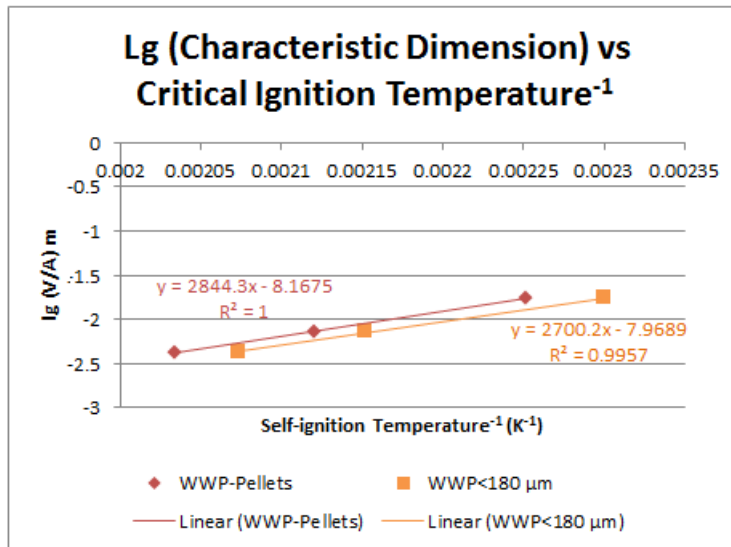


Figure 10. 9 Comparison of T_{SI} of WWP-Pellet and WWP $<180\mu\text{m}$ via Pseudo- Arrhenius-type self-ignition diagram, [$\lg(V/A)$ vs. $1/T$]

The T_{SI} results from all the three baskets representing three different volumes each of WWP-Pellets and WWP $<180\mu\text{m}$ sample showed the same trend – as the volume increased, the T_{SI} decreased, signifying the critical ignition temperature decreases with pile size. This is due to the insulating effect of larger piles. As the storage volume gets larger, more heat is trapped within the pile and exothermic reactions accelerate as temperature increases. Therefore, with the accelerated exothermic reactions, the whole biomass pile ignites at a lower temperature as compared with that of an analogous smaller volume i.e. smaller biomass pile. This T_{SI} -storage volume trend from this study was similar to the findings of Saddawi et al. (2013a) in a study on self-ignition characteristics of various raw and processed biomass fuels and Ferrero et al. (2009) that conducted studies on predicting heating-up of wood piles. Both had concluded that the larger the sample, the lower the ignition temperature.

Comparing WWP-Pellets and WWP $<180\mu\text{m}$ samples of the same volume i.e. same basket size, WWP-Pellets always ignited at higher temperature than WWP $<180\mu\text{m}$. For the pulverised material, there is more surface area per volume for reaction and thus there is more area exposed for heat absorption that accelerates the exothermic reaction that triggers the ignition process. In addition, heat dissipation is poorer in a packed bed of

pulverised material, compared to a bed of pellets. This observation was similar to findings from Saddawi et al. (2013a) when T_{SI} of various raw and processed fuel were compared (see **Figure 10. 10**) and Ferrero et al. (2009) in their study about the self-ignition characteristics of pine chips and pine sawdust. The pine chips with average particle size of 10 mm had shown T_{SI} that was greater than T_{SI} of pine sawdust with average particle size of just 0.25 mm (see **Figure 10. 11**).

Compatible findings had been observed in the work of Everard et al. (2014) regarding storage of Miscanthus chip piles. It was found that ground Miscanthus had lower self-ignition temperatures than chipped Miscanthus from the hot storage test (that followed guidelines in EN 15188) using cubic mesh wire basket. However, as shown in **Figure 10. 12**, it was noticed that as the storage pile size enlarged, T_{SI} of both Miscanthus chips or powder converged to a same temperature, but this had not been observed in this study with WWP samples. From the estimated linear equations in this study, the intersection point i.e. same value of T_{SI} happened at extremely small volume which implied very small storage size, although the regression are close to parallel.

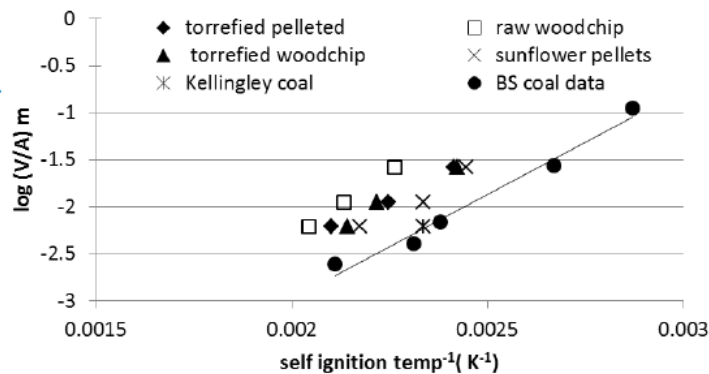


Figure 10. 10 Self-Ignition Temperature of Various Raw and Processed Biomass Samples as a Function of Storage Size [Source: Saddawi et al. (2013a)]

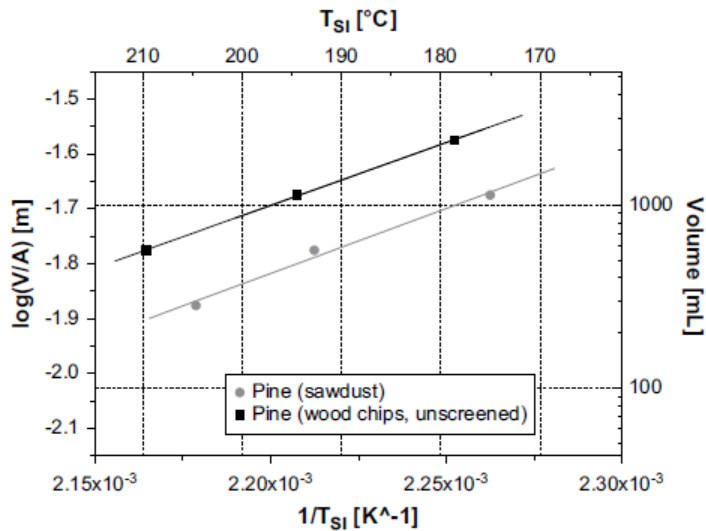


Figure 10. 11 Self-Ignition Temperature of Pine Wood as a Function of Storage Size – Chips and Sawdust Comparison [Source: Ferrero et al. (2009)]

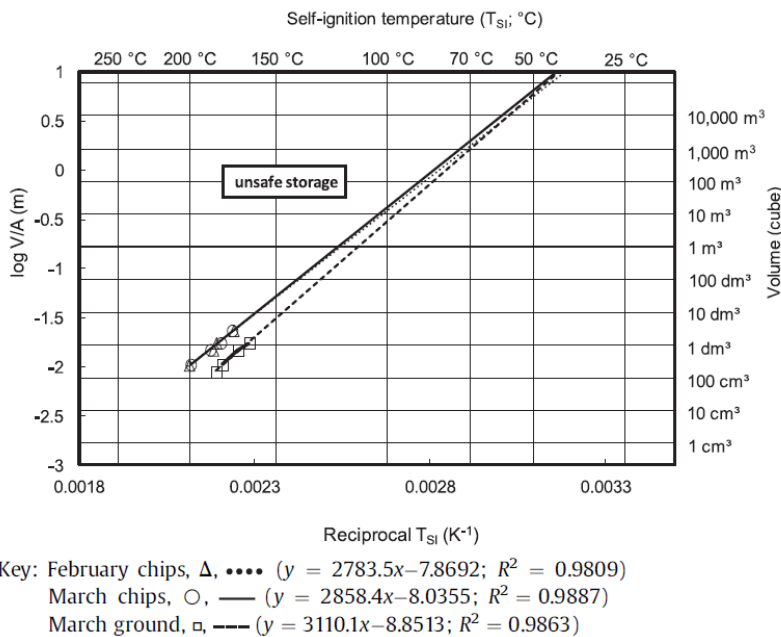


Figure 10. 12 Hot Storage Basket Experiment – T_{SI} Results of Miscanthus at Different Harvest Period [Edited from: Everard et al. (2014)]

Janes et al. (2008) developed correlations between the results from hot surface dust layer test and the hot storage test had conducted HSBT on fourteen samples using four cubic baskets of 8, 125, 343 and 1000 cm³. All the samples, namely purified station mud dust, three wheat dust samples, potatoes powder, crushed waste dust, zinc powder, cacao powder, wood and flax dust, activated carbon dust, white wood dust, wood with

asphalt dust, persulphate powder and coal dust, showed a similar trend – as the test volume increased, the T_{SI} decreased.

In a study about critical ambient temperature (CAT) that caused wood pellets to ignite, Pauner and Bygbjerg (2006) had compared CATs of 6 mm-long wood pellets and that of the same species but of 8 mm length. Results showed that the 8 mm wood pellets exhibited higher CAT value than the 6 mm counterpart when held in mesh wire baskets having the same volume. The comparisons of the 6 mm and 8 mm wood pellets at the same cubic volume (50 implied 50 mm length of a cube side) is displayed in **Figure 10. 13**, in which < 5 K difference was discovered between the two wood pellets samples with 2 mm difference in length. Results are analogous to the observations in the current work, i.e. the sample with larger dimension shows critical ignition temperature that was higher.

CAT of 6 mm wood pellets

Cube	Found CAT [K]
50	464.8 ± 0.6
100	439.6 ± 0.6
150	427.7 ± 0.5
200	414.4 ± 0.5
300	402.0 ± 0.9

CAT of 8 mm wood pellets

Cube	Found CAT [K]
50	467.5 ± 0.5
100	440.7 ± 0.5
150	430.6 ± 0.5
200	418.5 ± 0.5

* NOTE: 50 implies 50 mm cube side and the rest follow suit

Figure 10. 13 Critical Ambient Temperature that Ignited 6 mm- and 8 mm-Wood Pellets
[Edited from: Pauner and Bygbjerg (2006)]

In the event when ignition was achieved, the sample-filled basket from the hot oven inner chamber was removed for visual observation. After obtaining T_{SI} and t_i results of some samples, repeated trials were conducted on these selected samples. Then nitrogen purge for sample cooling was disabled from the LabView programme and the hot sample in the experiment was removed from the oven inner chamber once its TCsp exceeded 65°C of a particular hot storage temperature. At the instant the hot sample basket was taken out to atmospheric condition, lots of smoke was observed with some glowing red spots which later burst into small flames. This hot basket with flaming samples was then quickly quenched in a pool of water on standby next to the rig to prevent fire issues in the lab. From here, it could be concluded that air flow disturbances (by moving hot sample from the controlled environment in an oven inner chamber to an exposed atmosphere) on a critically hot sample had caused the sample to catch fire. Applying this observation to an actual huge fuel storage pile in a power station, if a critically high temperature had developed in the storage pile but was unnoticed, even the slightest disturbance (e.g. wind) to that pile would cause a fire outbreak. Furthermore, biomass is

an easily ignited combustible organic material and disastrous tragedy could happen in the plant once a spark started anywhere on the pile.

The other important parameter that describes the self-ignition characteristics is the ignition delay time or also known as induction time, t_i . This was determined from the temperature-time profile of each experiment. As defined in **Chapter 2**, t_i was obtained from the time when TCsp equalled to average of TC1 and TC2, to the point when TCsp exceeded the hot storage temperature by 65°C (the ignition criterion defined in this study).

For this ignition delay time or induction time (t_i) parameter, following the method in BS 15188 (British Standard, 2008), graph of logarithms volume/surface ratios [$\lg(V/A)$] versus the logarithms of respective ignition delay time in hours ($\lg t_i$) obtained from three different baskets was plotted. The relation between the characteristic dimension with the ignition delay time of WWP samples used in this study was estimated with two linear equations, as indicated in **Figure 10. 14**.

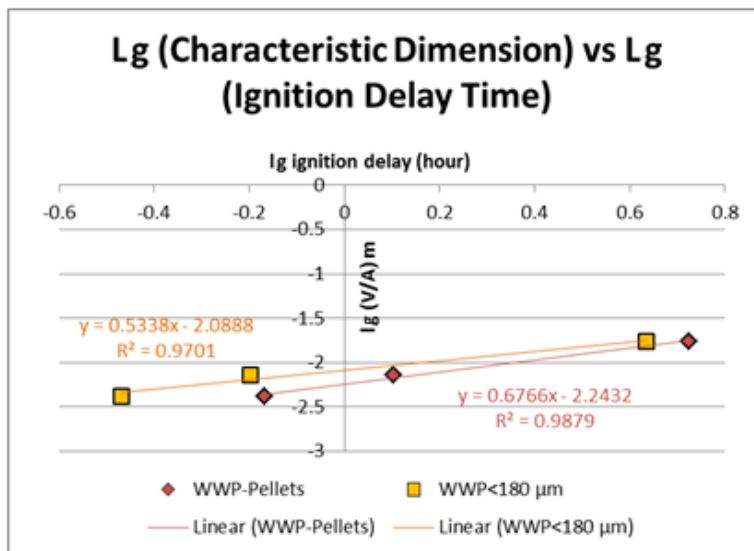


Figure 10. 14 Comparison of t_i for WWP-Pellet and WWP<180μm at the different characteristic dimensions tested, [$\lg(V/A)$ vs. $\lg t_i$]

From **Figure 10. 14**, the t_i of Basket S was always shorter than that of Basket M and Basket L always showed the longest t_i among the three basket sizes. This trend applied to for both WWP-Pellets and WWP<180μm samples. Comparing the small and larger baskets, since there was less mass contained in Basket S, heat transfer occurred much quicker than in the larger mass e.g. Basket M or Basket L at the critical igniting temperature of each and therefore the t_i was longer for the latter. Similar results leading to the conclusion that the larger the sample, the longer the induction time had been reported by Saddawi et al. (2013a) and Ferrero et al. (2009) in respective studies about

self-ignition characteristics of various fuels. Results from both work are shown in **Figure 10. 15** and **Figure 10. 16**.

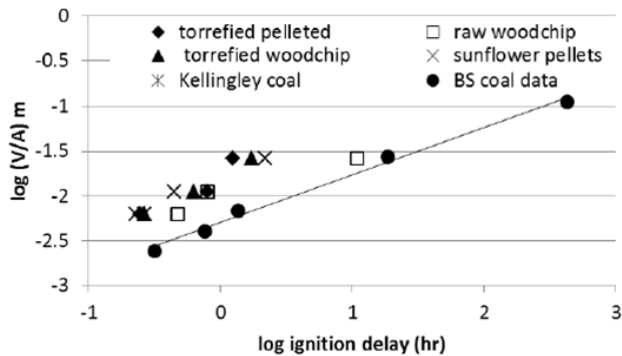


Figure 10. 15 t_i of Various Raw and Processed Biomass Samples as Predicted with BS 15188 Method [Source: Saddawi et al. (2013a)]

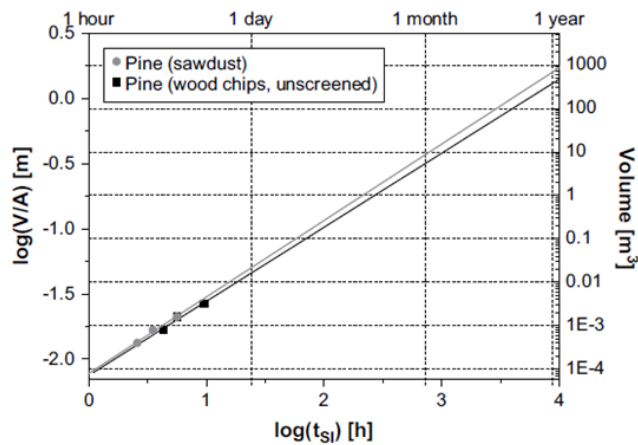


Figure 10. 16 t_i of Pine Samples as Predicted with BS 15188 Method [Source: Ferrero et al. (2009)]

When comparing samples of the same volume (i.e. same basket size), the WWP-Pellets always resulted in a longer ignition delay time than that of WWP<180 μ m. This finding was comparable to those of Ferrero et al. (2009), who reported a longer t_i for pine chips than for pine sawdust.

The result from this study showed the t_i from both WWP samples got closer as storage volume became bigger and the results would cross over upon reaching a certain larger volume than experimented. A simple calculation by equating the two linear equations ($y=0.6766x - 2.2432$ of WWP-Pellets and $y=0.5338x - 2.0888$ of WWP<180 μ m) found the intersection happened when t_i was ~ 1.08 h. This corresponded to a volume of ~ 4952 cm³, which was ~ 6 times the volume of Basket L. The predictions from experiments

with the current rig setup in the this study showed that ignition delay time were the same for WWP in either pelleted or pulverised form at this volume. However, as the volume increased even further, the trend of ignition delay time would be reversed – longer for the pulverised WWP.

It should be noted that there is definitely room for improvement in predicting the result for t_i . The reason for this is unclear. However, it could be related to the air flow in the oven – no flow rate is specified in the standard which makes comparisons between laboratories difficult.

Looking at the regression coefficients of best fit line predicted for t_i results, they were much poorer (0.9879 and 0.9701 for WWP-Pellets and WWP<180 μ m respectively) as compared with those of T_{SI} (1 and 0.9957 for WWP-Pellets and WWP<180 μ m respectively). Furthermore, the high level of uncertainty in t_i prediction was observed in the results of Saddawi et al. and Ferrero et al. too. It could be seen from **Figure 10. 15** that t_i prediction was not as well defined as T_{SI} prediction in **Figure 10. 10**. As for the study of Ferrero et al. (2009), the t_i result of pine samples (chips and sawdust) was quite close to each other, as seen in **Figure 10. 16**. In another study by García-Torrent et al. (2012), hot storage test had been carried out on various fuel samples, namely animal waste, lycopodium, dry sludge, bituminous coal and wheat flour with small sample baskets and t_i estimation for very large volumes was performed via extrapolation . It was concluded that the ignition delay time t_i did increase as the storage volume increased, as shown in **Figure 10. 17**. An exact quantitative prediction of ignition delay time t_i was rather challenging since ignition of fuel seem to exhibit a probabilistic nature (Shiyani, 2011), but a general conclusion that ignition delay time did lengthen as fuel storage volume increased could be reasonably drawn, and in most cases it increases with particle size also, although it may converge for high volumes.

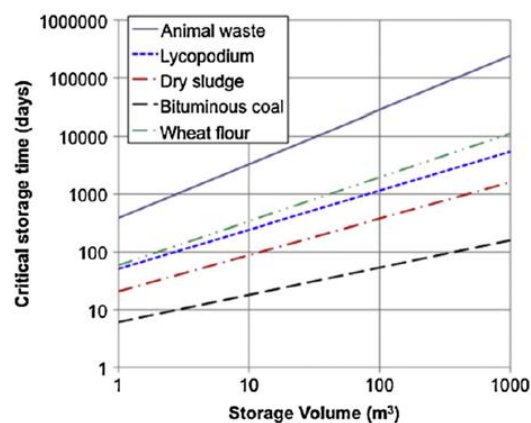


Figure 10. 17 t_i of Various Fuel at Different Storage Volume [Source: García-Torrent et al. (2012)]

Assuming the T_{SI} and t_i linear equations predicted for both WWP-Pellets and WWP<180 μm samples from HSBTs of Basket S, Basket M and Basket L in this study were valid for extrapolation, scaling up to massive industrial storage size had been attempted. Since cylindrical baskets used here had diameter to height ratio of one adhering to the BS 15188 guideline (British Standard, 2008), volume (V) of each cylinder was $V = 2\pi r^3$ and the surface area (A) subjected to hot storage temperature was simplified to be $A = 6\pi r^2$, where r was the radius of cylindrical basket. Prediction of T_{SI} and t_i for both WWP-Pellets and WWP<180 μm samples followed the linear equations summarised in **Table 10. 6**, and are the same equations shown in **Figure 10. 9** and **Figure 10. 14**.

Table 10. 6 Scaling Up Method Predicted Linear Equations for T_{SI} and t_i Extrapolation to Larger Storage Volumes with Regression Coefficient, R^2 and Uncertainty /Error Associated

Sample Name	Predicted T_{SI} Equation (Scale Up Method), R^2	Uncertainty / Error of T_{SI} (%)	Predicted t_i Equation (Scale Up Method), R^2	Uncertainty / Error of t_i (%)
WWP-Pellets	$y = 2844.3x - 8.1675,$ $R^2 = 1$	0.84	$y = 0.6766x - 2.2432,$ $R^2 = 0.9879$	111.74
WWP<180 μm	$y = 2700.2x - 7.9689,$ $R^2 = 0.9957$	8.13	$y = 0.5338x - 2.0888,$ $R^2 = 0.9701$	119.36
NOTE:	y is $lg\left(\frac{V/1\text{ m}^3}{A/1\text{ m}^2}\right)$ x is $\frac{1}{T_{SI}/1\text{ K}}$		y is $lg\left(\frac{V/1\text{ m}^3}{A/1\text{ m}^2}\right)$ x is $lg(t_i/1\text{ h})$	

Besides the three data points corresponded to $\sim 11\text{ m}^3$, $\sim 67\text{ m}^3$ and $\sim 864\text{ m}^3$ storage volume of Basket S, Basket M and Basket L, the linear equations in **Table 10. 6** were applied for T_{SI} and t_i estimations for larger volumes of 1 m^3 to as large as $500,000\text{ m}^3$. The results of these large volumes extrapolation are illustrated in **Figure 10. 18** and **Figure 10. 19** for T_{SI} and t_i respectively. The uncertainty involved in extrapolations of both parameter are indicated on the figures and it is obvious that massive error is associated with the ignition delay time prediction as compared with critical ignition temperature.

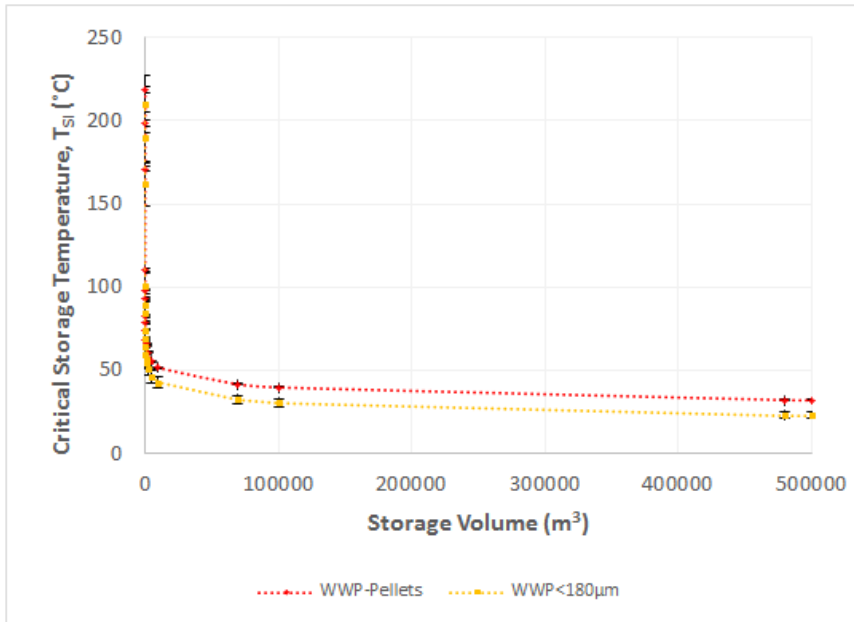


Figure 10. 18 T_{SI} Estimations to 500,000 m³ via Extrapolation, with error margin included

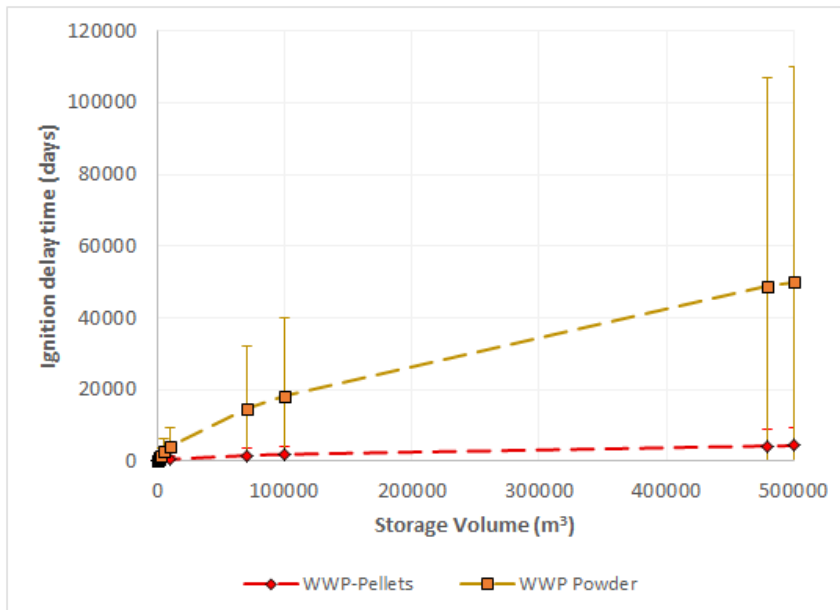


Figure 10. 19 t_i Estimations to 500,000 m³ via Extrapolation, with error margin included

For the T_{SI} estimation of WWP-Pellets sample, the estimated value was seen dropping rapidly from >200°C resulted from Basket S with volume of ~ 11cm³ to around >40°C at storage volume of ~50,000 m³, after which the critical temperature reduction was very slow and upon reaching massive volume of 500,000 m³, T_{SI} was estimated to be around room temperature of ~32°C. As for WWP<180µm, at Basket S volume, T_{SI} slightly

lower than that of WWP-Pellets had been determined from HSBT and upon extrapolation, the same swiftly decreasing trend was observed, but to $>30^{\circ}\text{C}$ at storage volume of $\sim 50,000\text{ m}^3$, after which the critical temperature reduction dwindled and upon reaching extremely large volume of $500,000\text{ m}^3$, T_{SI} was estimated to be $\sim 22^{\circ}\text{C}$, around 10°C less than WWP-Pellets estimation at the same volume.

For the t_i determination from HSBT, Baskets S, M and L results showed the ignition delay time of WWP-Pellets was longer than that of WWP $<180\mu\text{m}$ until about 6 times the volume of Basket L i.e. $\sim 4952\text{ cm}^3$ (when t_i was $\sim 1.08\text{ h}$), whereby the reverse trend was observed where WWP $<180\mu\text{m}$ revealed longer delay time than WWP-Pellets. From then on, as seen in **Figure 10. 19**, the delay time for the pulverised WWP increased tremendously, indicating a safe storage situation. Like mentioned before, estimation of ignition delay time showed high level of uncertainty with regression coefficient weaker than that of critical ignition temperature. Thus **Figure 10. 19** (with error/uncertainty indicated) and **Figure 10. 22** (without error/uncertainty indicated) have high uncertainties especially for the $< 180\ \mu\text{m}$ sample, and the extrapolation to large storage volume is not sensible. Investigation that compared ignition delay time from three different experimental methods, i.e. hot storage basket test, dust layer ignition test and single particle combustion test (Saddawi et al., 2013b) showed scattered results from hot storage basket experiment, circled in red in **Figure 10. 20**. This simply indicates that higher uncertainty level occurs in ignition delay time determination from basket test as compared with the other two methods.

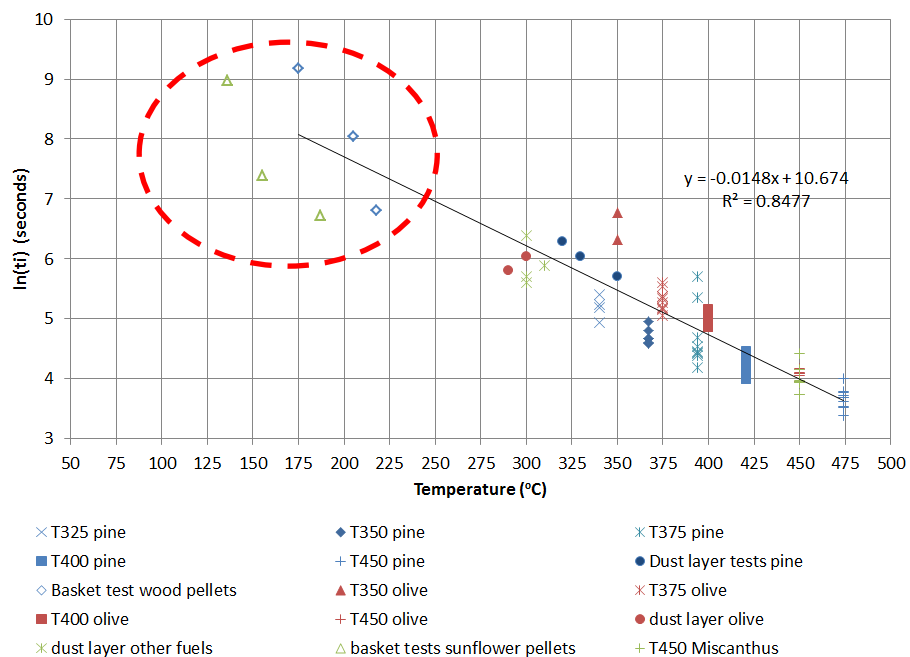


Figure 10. 20 Ignition Delay Time (t_i) from Three Different Methods [Edited from: Saddawi et al. (2013b)]

If the original BS 15188 graphs (British Standard, 2008) were scrutinised carefully, the points plotted based on actual data ranged $<1 \text{ m}^3$, thus volumes larger than this often involve high degree of uncertainty. Zooming into a smaller volume range from $\sim 11 \text{ cm}^3$ (volume of Basket S) to $1,000 \text{ m}^3$ (maximum volume depicted in BS 15188 graphs), the extrapolated estimates are shown in **Figure 10. 21** and **Figure 10. 22** for T_{SI} and t_i respectively. Within this narrower volume range, the T_{SI} extrapolation results showed critical ignition temperature was sensitive to volume change in range of $<200 \text{ m}^3$ whereas the t_i extrapolation still has a high level of uncertainty and a result for the $<180 \mu\text{m}$ that is not sensible.

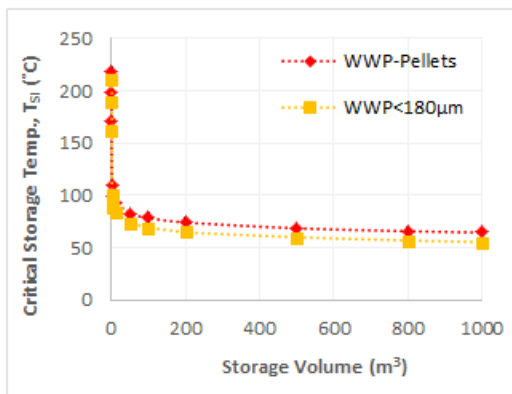


Figure 10. 21 T_{SI} Estimations to $1,000 \text{ m}^3$ via Extrapolation (Uncertainty Margins Not Shown)

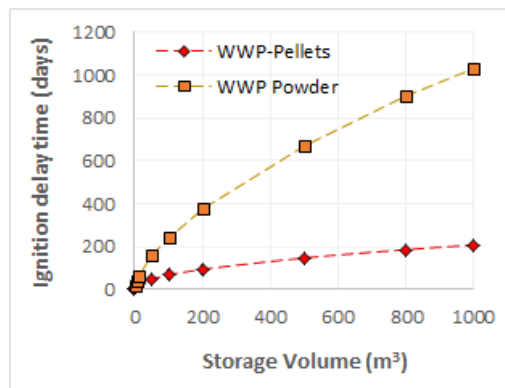


Figure 10. 22 t_i Estimations to $1,000 \text{ m}^3$ via Extrapolation (Uncertainty Margins Not Shown)

10.3 F-K Method – Self-Ignition Characteristics Comparison between Biomass Samples in Different Forms and Using Different Methods

Besides the Scaling Up method demonstrated in **Section 10.2**, the self-ignition characteristics of a sample can also be estimated using the well-known thermal explosion theory that had been worked out by Frank-Kamenetskii (British Standard, 2008). This theory developed a correlation between the characteristic length of sample, r (signifying storage volume) and its corresponding critical ignition temperature, T_{SI} . When term $\ln\left(\delta_{cr} \frac{T_{SI}^2}{r^2}\right)$ was plotted against $\left(\frac{1}{T_{SI}}\right)$, with $\frac{E}{R}$ representing the slope and $\ln\left(\frac{\rho QEA}{\lambda R}\right)$ the y-intercept; easier interpretation was made possible from the complex F-K correlation, whereby the complex correlation was now represented in a simpler linear fashion, as follows:

$$\ln\left(\delta_{cr} \frac{T_{SI}^2}{r^2}\right) = -\frac{E}{R} \left(\frac{1}{T_{SI}}\right) + \ln\left(\frac{\rho QEA}{\lambda R}\right) \dots \dots \text{Equation 10.1}$$

where

- δ_{cr} is critical Frank-Kamenetzki parameter
- T_{SI} is ambient temperature
- r is radius or characteristic length of sample
- E is apparent activation energy
- R is universal gas constant
- ρ is bulk density
- Q is gross calorific value
- A is pre-exponential factor of Arrhenius equation
- λ is heat conductivity (thermal conductivity)

and the δ_{cr} is 2.76 (British Standard, 2008) for the HSBT basket geometry used here.

For each WWP sample, three T_{SI} values had been obtained from the HSBT experiments. The density of WWP-Pellets for all the three samples were made as close as possible to each other, reading a value $\sim 613 \text{ kg/m}^3$ for Baskets S, M and L sample. From the thermal conductivity comparative study of various solid biomass fuel from Mason et al. (2016), it was noted that density, ρ , affected the thermal conductivity, λ ; the denser the material the higher the λ . Applying a generalised correlation developed through that study, $\lambda = 0.00013\rho + 0.037$, density values of ~ 613 and $\sim 397 \text{ kg/m}^3$ for WWP-Pellets and WWP<180 μm respectively had resulted λ values of ~ 0.11 and $0.09 \text{ W/m}\cdot\text{K}$ for each of the WWP sample. With all known values substituted into **Equation 10.1**, three data points resulted from each of WWP-Pellets and WWP<180 μm basket tests could be plotted onto the $\ln\left(\delta_{cr} \frac{T_{SI}^2}{r^2}\right)$ vs $\left(\frac{1}{T_{SI}}\right)$ graph, as shown in **Figure 10. 23**. Apparent activation energy, E , and pre-exponential factor, A , could respectively be determined from the gradient and y-intercept for each sample type. The E and A were found to be $\sim 118 \text{ kJ/mol}$ and $9.39 \times 10^6 \text{ s}^{-1}$ for WWP-Pellets and $\sim 112 \text{ kJ/mol}$ and $4.41 \times 10^6 \text{ s}^{-1}$ for WWP<180 μm . As shown in **Figure 10. 23**, the gradient of both WWP sample lines were quite similar and therefore the resulted apparent activation energy of each was quite similar to each other.

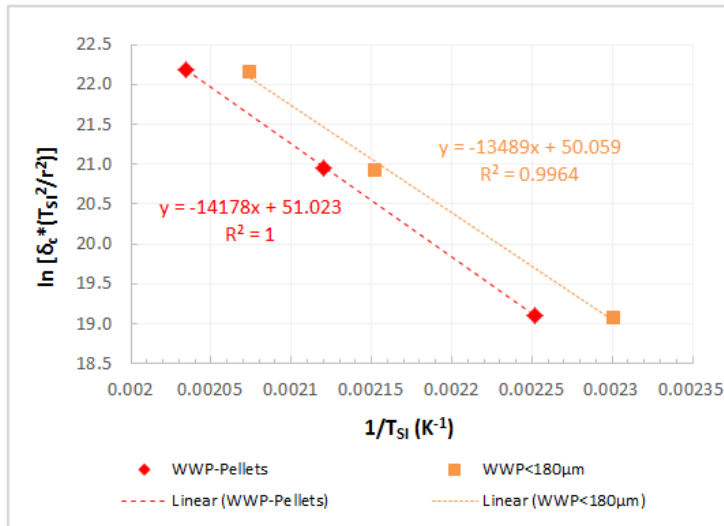


Figure 10.23 F-K Method – Correlation between Characteristic Length of WWP Samples and Self-Ignition Temperature

As described in **Section 10.2**, estimations of T_{SI} corresponding to storage volumes ranging from 1 m³ to 500,000 m³ had been performed via the Scaling Up method and the graph plotted (see **Figure 10.18**). Subjected to the same critical ignition or self-ignition temperature T_{SI} , it is of interest to compare the safe storage volume when these two methods, i.e. scaling up method and F-K method are used. For some T_{SI} values, the comparison of safe storage volume obtained from both methods is shown in **Table 10.7**.

Table 10.7 Comparison between Scaling Up Method and F-K Method

Self-Ignition Temperature (°C)	Safe Storage Volume (m ³)			
	WWP-Pellets		WWP<180μm	
	Scaling-Up Method	F-K Method	Scaling-Up Method	F-K Method
40	94,546.74	151,703.37	15,522.37	23,750.22
60	2,186.91	3,097.60	434.53	591.21
80	77.50	99.29	18.24	22.59
100	3.93	4.64	1.08	1.24
120	0.27	0.30	0.085	0.092

At T_{SI} of 100°C for example, the scaling up method predicted a storage volume of $\sim 3.93\text{m}^3$ but 0.71 m^3 higher (i.e. 4.64 m^3) was predicted by the F-K method. As for the other sample i.e. WWP<180 μm , T_{SI} of 100°C predicted 1.08 m^3 and 1.24 m^3 storage by Scaling Up and F-K Method respectively. It is obvious from **Table 10. 7** that storage volume prediction from both methods do not vary much at relatively higher T_{SI} . As expected, decreased T_{SI} allows a greater storage volume, since the insulating effect of larger storage pile traps heat within the pile and accelerates the exothermic reactions which eventually causes an ignition at lower temperatures.

For both WWP-Pellets and WWP<180 μm samples, it was noticed that for the same T_{SI} , the storage volume predicted by Scaling Up method was always less than that predicted by F-K method, but predictions from both methods were at the same order of magnitude. For instance, at T_{SI} of 80°C, for WWP-Pellets, the Scaling Up method estimated the storage size to be 77.50 m^3 but 99.79 m^3 was predicted by F-K method. Similar trend was observed for WWP<180 μm sample in which 18.24 m^3 from Scaling Up method and 22.59 m^3 from F-K method; Scaling Up method estimates lower than estimated with F-K method but both predictions are at the same order of magnitude. The volume difference estimated by both methods enlarged as the T_{SI} becomes smaller – at T_{SI} of 40°C, Scaling Up method predicted storage volume of $\sim 94,547\text{ m}^3$ but F-K method predicted $\sim 151,704\text{ m}^3$ for WWP-Pellets; $\sim 15,522\text{ m}^3$ by Scaling Up method and $\sim 23,750\text{ m}^3$ by F-K method.

Referring to **Table 10. 7**, at relatively higher T_{SI} of 120°C, the F-K method had predicted ~ 1.1 times the volume estimated by Scaling Up method but it became ~ 1.6 times at the lower T_{SI} of 40°C. As discussed in **Section 10.2**, predictions for very large volume that were based on small lab-scale results involve high level of uncertainty and it seems that the higher the storage volume, the higher the uncertainty since greater variation is observed between the two prediction methods.

Regardless which estimated method was applied, the T_{SI} of biomass sample definitely reduced as the storage volume increased. This finding that the self-ignition temperature decreased as the storage size increased had long been recognised. Referring to a work that assessed the dangers in handling large quantity of a products by Bartknecht back in the 1980s (Brauer et al., 2012) a general conclusion was that auto-ignition temperature decreased with increasing basket volume in a non-linear fashion. The results of three materials i.e. methylcellulose, cork dust and lycopodium from that study are displayed in **Figure 10. 24**, in which the auto-ignition temperature (analogous to critical self-ignition temperature here) relation with the volume of dust were plotted. The samples studied here were found to have reactivity on par with cork meal and methylcellulose since the autoignition temperature for a similar volume laid around the same area. Lycopodium seemed to be more reactive than the current WWP samples since much lower autoignition temperatures at volumes similar to those experimented in this study were observed.

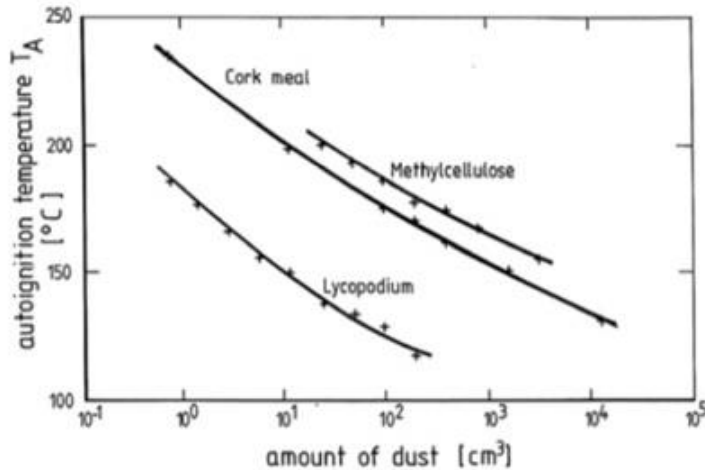


Figure 10.24 Autoignition Temperature – Sample Volume Relationship for Three Samples [Source: Brauer et al. (2012)]

10.4 Concluding Remarks and Suggestions for Future Work

This self-ignition study involved evaluating two parameters, the critical self-ignition temperature, T_{SI} and ignition induction or delay time, t_i for two identical samples appearing in two different particle sizes i.e. pelleted and pulverised. Some general conclusion were made: Regardless of the form in which the biomass appear, T_{SI} decreased as storage volume increased whereas t_i became longer as the storage size increased. Particle size of the sample does matter, in which the finer the particles, the lower the T_{SI} would be and the shorter the delay time required to initiate ignition.

As a result of all the HSBTs conducted based on three sample volumes fixed here, the T_{SI} and t_i comparisons between WWP-Pellets and WWP<180 μm were obtained and linear equations had been estimated for the purpose of interpolation or extrapolation of other sample sizes. The T_{SI} and t_i of the milled a.r. WWP could be estimated from these results based on the size distribution analysis seen in **Table 10.2**. Since a large portion (~52 wt%) (Dooley, 2016) of the milled a.r. WWP ranged within 250 to 1000 μm (a size bigger than WWP<180 μm but much smaller than WWP-Pellets), it was predicted that the T_{SI} and t_i values would lay between the values of WWP<180 μm and WWP-Pellets, with values nearer to those of WWP<180 μm . This was because the milled a.r. were in powdered form and having particle size closer to that of WWP<180 μm .

Two methods recommended in BS 15188 had been used – the Scaling Up Method and the F-K Method. Both method showed increasing level of uncertainty as storage volume increased and the discrepancies between the two methods enlarged as the storage volume became bigger. Regarding the high level of uncertainty in the HSBTs conducted, it

could be overcome by using an additional storage volume i.e. fabricating another sample basket. Since Basket L in this study was $\sim 864 \text{ cm}^3$, there are two options on the new basket size. If higher accuracy was intended within a volume range up to $\sim 1 \text{ m}^3$, a new basket of $< 1 \text{ m}^3$ could be fabricated. On the other hand, if the intention was to extrapolate to storage volume of industrial size, much bigger basket volume would be good. In any event, the oven properties and experiment duration could be other important considerations before deciding which new basket size to use. In particular air flow could be an important (and overlooked) parameter.

There are a few quick recommendations to improve the current experiment. For the pulverised material, the effects of different powder size of the same material on T_{SI} and t_i could be evaluated. Since dust size of $250 \mu\text{m}$ was recommended in BS 15188 (British Standard, 2008) and $< 180 \mu\text{m}$ had been used in this study, other sizes that are extremely fine e.g. $< 63 \mu\text{m}$ or much coarser dust e.g. $< 500 \mu\text{m}$ could be utilised. The sensitivity of material self-ignition characteristics based on particle size, as characterised by T_{SI} and t_i , could then be noticed. As for the pelleted biomass, much shorter or longer pellets with the lengths (since pellet diameter is constant) segregated upon receiving these pellets could have their size i.e. pellet length influence on self-ignition characteristics investigated.

The presence of extremely fine particles generates an explosion risk besides risk of self-heating that leads to self-ignition. As mentioned by Medina (2014) in the work that concerned explosion safety of biomass powders, following the definition in BS 14034 (British Standard, 2004), dust are particles $< 500 \mu\text{m}$ and fine powder of $< 60 \mu\text{m}$ had been used to examine the worst case scenario for material explosions as mentioned in ISO-6184/1 (ISO, 1985). Besides exploring the sensitivity of material self-ignition characteristics (characterised by T_{SI} and t_i) based on fineness of particles, it is of interest to examine the relation of self-ignition risk to the explosion risk of biomass powder since accidents that involved biomass ignition often coupled with and explosions.

This HSBT study on WWP could be conducted on more materials under the same condition and may also be extended to conditions under different atmospheric pressure e.g. inerting. Since Seitz et al. (2016) had proven that higher T_{SI} was achieved when lower than atmospheric pressure was applied in the HSBT, it would be worth checking with a few below atmospheric pressure settings the effects pressure on the T_{SI} and t_i of various biomass fuels commonly used in power stations. Alternatively, using different partial pressures of O_2 would yield insight into the benefits of inerting in large-scale storage.

The sensitivity of T_{SI} and t_i towards the pressure or partial pressure change could be monitored. This would be indeed useful for fuel storage in a power station because a higher T_{SI} and longer t_i implied safer storing condition when fire risk is concerned and more biomass stock could be stored without worrying fuel shortage problem.

As mentioned earlier in **Chapter 2**, besides this isoperibol (close to isothermal) way of detecting and therefore preventing self-ignition of various materials via the hot storage basket test, another method that applied the adiabatic concept could be considered. As explained by Pauner and Bygbjerg (2007), material spontaneous ignition in storage or along the production line could be initiated by physical, chemical or biological activities within an organic material that were exothermic in nature. The adiabatic method was particularly useful in detecting early signs of self-heating since it was capable of detecting faint heat generation in a material. Spontaneous Ignition Tester (SIT) and Accelerating Rate Calorimeter (ARC) are some examples of adiabatic calorimeters useful for preventing self-ignition fire outbreak since an early stage.

It will be good to obtain the T_{LIT} via dust layer ignition test on WWP<180 μ m sample. The ignition temperatures from WWP<180 μ m dust layer test can then be coupled with the T_{SI} from the three sample volumes experimented in HSBT and have a correlation between sample ignition temperature and sample volume (least from dust layer test and increase gradually in HSBT) developed. Since both tests are conducted in different environments, the important bridge that links both results is the Biot number. The approach used by Janes et al. (2008) in correlating results from both test could be referred to.

it is recommended to delve into the details of self-heating and therefore self-ignition characteristic of torrefied material, as torrefaction is gaining popularity nowadays. From the T_{SI} and t_i results of various biomass materials studied by Saddawi et al. (2013a), an interesting observation was seen when comparing T_{SI} of raw woodchip (represented by open square icon in **Figure 10. 10**) and torrefied wood chips (represented by black triangular icon in **Figure 10. 10**) – torrefied wood chips ignited at a lower temperature when contained in basket of the same size. The ignition delay time, t_i , showed a shorter duration for torrefied woodchip (represented by black triangular icon in **Figure 10. 15**) than that of the raw woodchip (represented by open square icon in **Figure 10. 15**). Apart from storage results comparison from Saddawi et al. (2013a), the dust layer ignition results reported in **Chapter 7** revealed that the torrefied material had a lower T_{LIT} or shorter ignition delay time when the T_{LITs} of untreated and torrefied samples were the same. These results, from both the storing and handling perspectives had showed that torrefied material exhibits a higher fire risk, more prone to self-ignition than its untreated counterpart when stored or handled. This may be related to the higher density of torrefied biomass dust.

It may be of interest to check if moisture content in samples affect the T_{SI} and t_i results in HSBT experiments. Without conditioning to constant weight at 50°C before any hot storage test, samples with known moisture content could be taken to the HSBT oven right away. Practically, a power station had very little control regarding the moisture

content of solid fuels it received, but knowing the correlation between sample moisture and its corresponding T_{SI} might help in designing a more appropriate storage environment.

The HSBT experiments can be extended to materials with binder additives. As seen in **Chapter 5**, with just 2 wt% of binder (Ligno-Bond DD powder or commercial corn flour), an inerting effect seemed to be present. The maximum dust layer ignition temperature (T_{LIT}) or the ignition delay time differed from that of the pure biomass dust that was without any additives. From a study by Binkau et al. (2015) about the influence of inert materials on self-ignition of flammable dust, non-combustible additives like calcium oxalate (CaOx), ammonium sulphate (AS) or ammonium phosphate (AP) were added to lignite coal, bituminous coal or activated carbon dust and DIN EN 15188 hot storage test was performed. A difference as high as $\sim 60^{\circ}\text{C}$ had been detected in the T_{SI} results with the presence of additives. Therefore, it is of interest to investigate how much changes would there be should 2 wt% of either binder discussed in **Chapter 5** was included in the dust heaps for HSBT here.

Chapter 11

Overall Findings, Conclusions and Recommendations for Future Work

Some major findings leading to conclusions that answered the objectives of this work were achieved upon completion of this research. These findings lead to recommendations to further strengthen the understanding of biomass burning at low temperatures and making the results more applicable in an industrial context.

11.1 Overall Findings and Conclusions

Following the self-ignition propensity risk ranking method proposed by Ramírez et al. (2010) and modified by Jones et al. (2015), the risk of all the biomass samples examined in this work was summarised in **Figure 11. 1**.

All untreated biomass samples, regardless of whether made up of woody or herbaceous compositions, displayed self-ignition risk. Most are at high risk with wheat straw possesses the highest risk than all others. Blends of woody and herbaceous materials did not make the material any safer – the ignition risk is on par with the riskier of the biomass parents. Adding binder slightly decreased the ignition risk but they are still very close to the riskier border. Therefore, material self-ignition propensity is not a significant parameter in binder selection. Other parameters from the economics or environment aspect could be more important. Water washing pre-treatment showed a small improvement to the parent materials when self-ignition risk was concerned, as seen the **Figure 11. 1** that shows their risk improved from high risk to the boarder very close to medium risk. The few samples that showed lower risk are the torrefied ones or having torrefied material in their compositions.

The dust layer test did show a slightly higher minimum dust layer ignition temperature (T_{LIT}) for some biomass blends and biomass with binders but the improvement was rather small. The same level of improvement was observed with binders inclusion, and if biomass had been washed. Dust layer tests on these materials showed findings consistent with results of the self-ignition but improvements were minor especially when the dust deposits were thick. However, the dust layer test on torrefied materials showed a trend opposed that found from self-ignition risk ranking method. This is because **Figure 11. 1** does not consider density. As discussed in **Chapter 7**, ranking self-ignition risk this way is insufficient to capture the actual fire risk of torrefied material because of the finer particles and higher density of torrefied dust layer used.

All in all, biomass are prone to self-ignition and therefore the ignition risk that potentially leads to primary and secondary explosions is not to be neglected in power

followed. Nevertheless, power stations do have housekeeping procedures that prevent dust accumulations that are too thick and compromise the plant safety.

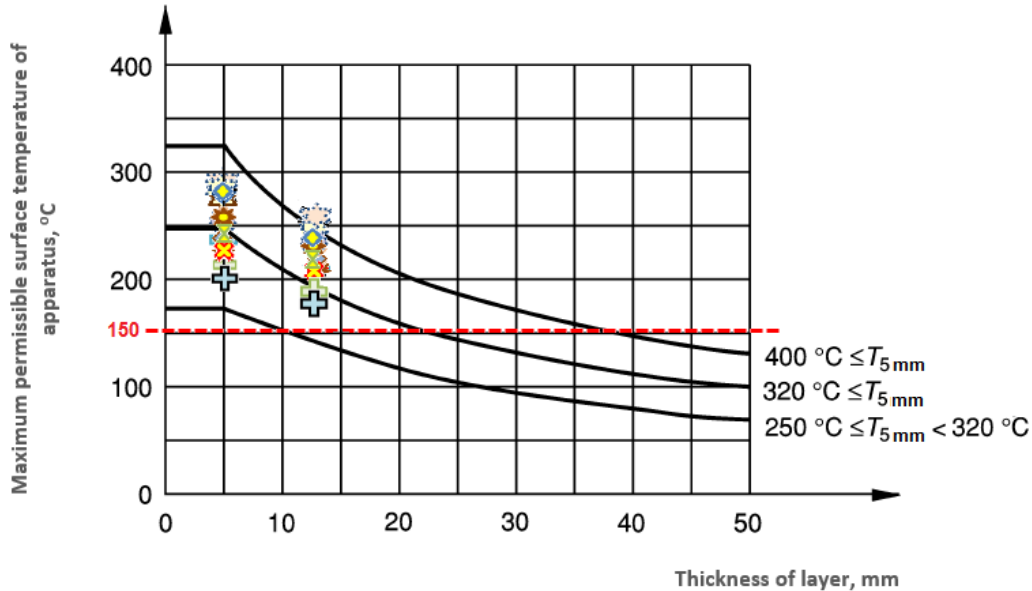


Figure 11. 2 Industrial Application: Maximum Permissible Surface Temperature Estimations with Three Methods – Guideline 1 (Points), Guideline 2 (Curves, T_{LIT} from Pre-Refinement) and Power Station Practice (Constant at 150°C)

Emissions that consisted of particulate matters (PM) and polycyclic aromatic hydrocarbon (PAH) as captured by three samplers – inverted funnel, filter paper and ORBO™ tube showed pyrolysing/smouldering dust released more volatile species and with greater intensities than the critically ignited counterpart. This simply implied that the emissions from smouldering biomass before it catches fire should not be neglected; besides polluting the environment, fire risk exist as these volatiles would burst into flame as soon as the required conditions are met.

The hot storage basket test suggested that the fines from disintegrated pellets are more likely to catch fire when subjected to the same storage condition. Coupled with a shorter ignition delay time from the fines, the dust from disintegrated fuel pellets would probably initiate self-ignition when the pelleted fuels are stored with presence of its fines. Using binder to hold the pellets in shape probably is one of the ways to reduce biomass pellets generating fines.

Activation energies have been determined for white wood pellets and fines and extrapolation to large volumes suggest critical ignition temperatures can be easily reached during storage. There is a great deal of uncertainty in predicting ignition delay times from laboratory measurements and this is an area where an improvement is required.

11.2 Recommendations for Future Work

Apart from the suggestions to improve the respective experimental methods recommended at the end of each chapter, an overall recommendation that considered everything all together can be drawn.

From all investigations carried out, the results showed that probably combining the two pre-treatment methods investigated (washing and torrefying) with binder adding would yield a relatively safer biomass fuel with desirable transportation properties.

This study had found that washing pre-treatment elevated the minimum dust layer ignition temperature (T_{LIT}) of a biomass through removal of catalytic ignition minerals but torrefying gave the opposite effect mainly due to particle dryness, particle size reduction and overall particle surface area increment. Samples with Ligno-Bond-DD powder binder showed a slight inerting effect on biomass low temperature ignition, complimenting the washing effect. Thus, it would be really interesting to find out the final effect on T_{LIT} from the combination of both pre-treatments, to check which pre-treatment is actually dominating the overall characteristics of a solid biomass fuel when pre-treatments are combined. Though binder complimented the washing effect by increasing the T_{LIT} , it should be noted that the sulfur content had increased as well. If sulfur dioxide (SO_2) emission is of concern, the SO_2 contribution from this small amount of binder probably could be remedied by a simple technology – fixing a flue-gas desulfurisation (FGD) system before releasing the flue gas to atmosphere.

The dust layer ignition test that used a hot plate could be modified by introducing removable hot spots of fixed temperature into dust accumulation instead of having fixed temperature hot plate, e.g. dropping metal ball heated to a fixed temperature into the dust layer. The temperature that causes dust ignition this way could then be compared to the T_{LIT} obtained with hot plate at a fixed temperature. By doing this, the ignition risk from both methods could be compared and precautions could be taken to prevent the riskier one. The experimental setup used by Rogers et al. (2006) in a study on dust clouds and dust deposits ignited by friction sparks and hotspots and that adopted by Fernandez-Anez et al. (2015) in an investigation of waste/biomass mixtures dust layer ignition can be referred to.

The same materials with compatible particle sizes could be experimented in both dust layer test and hot storage basket test and have their results compared. It is known that the critical temperature determined by the hot storage basket test is lower than that determined in the dust layer test using a hot plate (Joshi, 2012) due to uniform heating in the oven as compared with asymmetrical heating from the hot plate. A correlation could be developed between the two tests and this would ease the determination of the critical temperature for storage from the relatively quicker dust layer test using a hot plate.

There is a need for a more robust laboratory method for determining ignition delay time during storage, that would enable extrapolation to higher volume with higher accuracy. The introduction of calibration standards might be one such approach.

List of References

- Abdullah, N. and Gerhauser, H. 2008. Bio-oil derived from empty fruit bunches. *Fuel*. **87**(12), pp.2606-2613.
- Abdullah, N. and Sulaiman, F. 2013. The Properties of the Washed Empty Fruit Bunches of Oil Palm. *Journal of Physical Science*. **24**(2), pp.117-137.
- Agar, D. et al. 2016. Influence of Elevated Pressure on the Torrefaction of Wood. *Energy & Fuels*. **30**(3), pp.2127-2136.
- Agilent Technologies Inc. 2015. *Flame Atomic Absorption Spectrometry - Analytical Methods* [Online]. Available from: <https://www.agilent.com/cs/library/usermanuals/Public/0009.pdf>.
- Akinrinola, F.S. 2014. *Torrefaction and Combustion Properties of some Nigerian Biomass*. Ph.D thesis, University of Leeds.
- Allison, G.G. et al. 2011. Genotypic variation in cell wall composition in a diverse set of 244 accessions of Miscanthus. *Biomass and Bioenergy*. **35**(11), pp.4740-4747.
- Allison, G.G. et al. 2012. Effect of nitrogen fertiliser application on cell wall composition in switchgrass and reed canary grass. *Biomass & Bioenergy*. **40**, pp.19-26.
- Amyotte, P. 2013. *An Introduction to Dust Explosions, Understanding the Myths and Realities of Dust Explosions for a Safer Workplace, Chapter 1: Introduction: Dust Explosions- Myth or Reality?* 1st Edition ed. IChE Imprint Butterworth-Heinemann.
- Anez, N.F. et al. 2015. Detection of incipient self-ignition process in solid fuels through gas emissions methodology. *Journal of Loss Prevention in the Process Industries*. **36**, pp.345-353.
- Anthony, E. and Field, P. 1975. *An Apparatus and Method for Determining the Self-Ignition Temperature of Dust Layers*. . Department of the Environment and Fire Offices' Committee Joint Fire Research Organisation: Fire Research Station, Borehamwood, UK, .
- Arthur Nelsen. 2016. *UK ratifies Paris climate agreement*. [Online]. Available from: <https://www.theguardian.com/environment/2016/nov/17/uk-boris-johnson-ratifies-paris-climate-agreement>.
- ASTM. 2015. *ASTM E2021-15 Standard Test Method for Hot-Surface Ignition Temperature of Dust Layers*. Pennsylvania United States: American Society for Testing and Materials (ASTM) International, West Conshohocken.
- Atiku, F.A. 2015. *Combustion of Bio-oil and Heavy Fuel Oil*. Ph.D thesis, University of Leeds.
- Atiku, F.A. et al. 2016. The Impact of Fuel Properties on the Composition of Soot Produced by the Combustion of Residential Solid Fuels in a Domestic Stove. *Fuel Processing Technology*. **151**, pp.117-125.
- Atkinson, I. 2016. *Rail Loading of Wood Pellets at UK Ports*. [Online]. Available from: <https://thespencergroup.co.uk/our-work/renewables/rail-loading-of-wood-pellets-at-uk-ports>.
- Aziz, S.M.A. et al. 2013. Bio-oils from microwave pyrolysis of agricultural wastes. *Fuel Processing Technology*. **106**, pp.744-750.
- Babrauskas, V. 2003a. *Ignition Handbook*. Issaquah WA, USA: Fire science Publishers, Co-published by the Society of Fire Protection Engineers.

- Babrauskas, V. 2003b. 'Pyrophoric Carbon' and Long-Term, Low-Temperature Ignition of Wood. *Ignition Handbook*. [Online]. Washington: Fire Science Publishers. [Accessed 19 March 2014]. Available from: http://www.doctorfire.com/low_temp_wood1.pdf.
- Babrauskas, V. et al. 2009. *Fires in Silos, Hazards, Prevention and Fire-Fighting*. Germany: Wiley-VCH.
- Bari, M.A. et al. 2011. Air Pollution in Residential Areas from Wood-fired Heating. *Aerosol and Air Quality Research*. **11**(6), pp.749-757.
- Barlin et al. 2016. Thermal Evolution Profile Analysis for Pyrolysis of Coal-Acacia Mangium Wood Blends. *International Journal of Technology*. **7**(5), pp.881-888.
- Barton, J. 2001. *Dust explosion prevention and protection-A Practical Guide*. Gulf Publishing Company: Institute of Chemical Engineers.
- Basu, P. 2013. *Biomass Gasification, Pyrolysis and Torrefaction - Practical Design and Theory*. [Online]. 2nd Edition ed. United States of America: Academic Press, Elsevier Inc. Available from: <http://store.elsevier.com/Biomass-Gasification-Pyrolysis-and-Torrefaction/Prabir-Basu/isbn-9780123965431/>.
- BBC Ltd. 2014. *Geography Energy*. [Online]. [Accessed 4 April 2014]. Available from: http://www.bbc.co.uk/schools/gcsebitesize/geography/energy_resources/energy_rev1.shtml.
- BBRG Biomass Pelletization Workshop. 2013. *Self-Heating of Stored Biomass and Pellets*. [Online]. [Accessed 8 January 2014]. Available from: <http://biomass.ubc.ca/wp-content/uploads/2013/12/Self-heating-of-stored-biomass-and-pellets.pdf>
- Beever, P.F. 1986. *Initiation and Propagation of Smouldering Reactions*. United Kingdom: University of Leeds.
- Beever, P.F. and Thorne, P.F. 1981. Isothermal Methods for Assessing Combustible Powders - Theoretical and Experimental Approach. *I. Chem. E Symposium Series No. 68*.
- Bergman, P.C.A. et al. 2005. *Torrefaction for biomass co-firing in existing coal fired power station "BIOCOAL", ECN-C-05-013*, . Energy Research Centre of Netherlands (ECN).
- Bernard, B.B. et al. 2016. *Determination of Total Carbon, Total Organic Carbon and Inorganic Carbon in Sediments* [Online]. Available from: http://www.tdi-bi.com/analytical_services/environmental/NOAA_methods/TOC.pdf.
- Biller, P. and Ross, A.B. 2014. Pyrolysis GC-MS as a novel analysis technique to determine the biochemical composition of microalgae. *Algal Research-Biomass Biofuels and Bioproducts*. **6**, pp.91-97.
- Binkau, B. et al. 2015. Influence of inert materials on the self-ignition of flammable dusts. *Journal of Loss Prevention in the Process Industries*. **36**, pp.337-344.
- bioenarea. 2016. *The Bioenergy System Planners Handbook - BISIPLAN, Descriptions of the biomass fuel composition*. [Online]. [Accessed 1 February 2014]. Available from: http://bisiplan.bioenarea.eu/fuel_appendix.html.
- BioEnergyConsult. 2016. *Summary of Biomass Combustion Technologies*. [Online]. Available from: <http://www.bioenergyconsult.com/biomass-combustion-systems/>.
- Biomass Energy Centre. 2011. *What is BIOMASS?* . [Online]. [Accessed 1 January 2017]. Available from: <https://www.forestry.gov.uk/fr/beeh-9uhlqv>.
- Biomass Power Association. 2011. *Biopower - It's Not Just Carbon Neutral*. [Online]. [Accessed 1 January 2017]. Available from: http://www.usabiomass.org/docs/Biopower_is_Carbon_Neutral_Fact_Sheet2.pdf.
- Blanchard, E. 2007. Simulation of self-heating in wood pellet storage using input data from small-scale experiments. *SP Technical Note 2007:23*. [Online]. [Accessed 10 March 2014]. Available from: <http://www.v2.sp.se/publ/ViewDocument.aspx?RapportId=8390>.
- Blasi, C.D. et al. 2000. Degradation characteristics of straw and washed straw. *Thermochimica Acta*. **364**(1-2), pp.133-142.

- Bombay, C.E.I. 2016. *Gas Chromatography Mass Spectrometer*. [Online]. Available from: <http://www.che.iitb.ac.in/online/labfacility/gas-chromatography-mass-spectrometer>.
- Borregaard. 2016. *LIGNOBOND DD*. [Online]. Available from: <http://www.lignotechfeed.com/Pelleting-Aids/LignoBond-DD>
- Bowes, P.C. 1981. A General Approach to the Prediction and Control of Potential Runaway Reaction. *I. Chem. E Symposium Series*. **No. 68**.
- Bowes, P.C. and Establishment, B.R. 1984. *Self-heating: evaluating and controlling the hazards*. Dept. of the Environment, Building Research Establishment.
- Bowes, P.C. and Townshend, S.E. 1962. Ignition of Combustible Dusts on Hot Surfaces. *British Journal of Applied Physics*. **13**(3), pp.105-&.
- Brauer, H. et al. 2012. *Dust Explosions: Course, Prevention, Protection*. Springer Berlin Heidelberg.
- BRE. 2016. *Dust Explosion Testing Explained*. [Online]. [Accessed 1 January 2016]. Available from: http://www.bre.co.uk/filelibrary/pdf/cap/dust/dusttesting_explained_1_pdf.pdf.
- Bridgeman, T.G. et al. 2008. Torrefaction of reed canary grass, wheat straw and willow to enhance solid fuel qualities and combustion properties. *Fuel*. **87**(6), pp.844-856.
- Bridgeman, T.G. et al. 2010. An investigation of the grindability of two torrefied energy crops. *Fuel*. **89**(12), pp.3911-3918.
- British Standard. 1999a. 1999a. *BS EN 50281-1-2:1999: Electrical apparatus for use in the presence of combustible dust — Part 1-2: Electrical apparatus protected by enclosures — Selection, installation and maintenance*. London: BSI.
- British Standard. 1999b. 1999b. *BS EN 50281-2-1:1999: Electrical Apparatus for Use in the Presence of Combustible Dust – Part 2-1: Test Methods – Methods of Determining Minimum Ignition Temperature*. London: BSI.
- British Standard. 2004. 2004. *BS EN 14034-1: Determination of explosion characteristics of dust clouds Part 1: Determination of maximum pressure Pmax of dust clouds*. London: BSI Group.
- British Standard. 2008. 2008. *BS EN 15188:2007: Determination of Spontaneous Ignition Behaviour of Dust Accumulations*. London: BSI Group Headquarters.
- British Standard. 2009a. 2009a. *BS EN 14774-3:2009 Solid biofuels-Determination of moisture content-Oven dry method Part 3: Moisture in general analysis sample*. . London: BSI.
- British Standard. 2009b. 2009b. *BS EN 14775:2009 Solid biofuels-Determination of ash content*. London: BSI.
- British Standard. 2009c. 2009c. *BS EN 15148:2009 Solid biofuel-Determination of the content of volatile matter*. London: BSI.
- British Standard. 2009. 2009 *BS EN 14918: 2009: Solid biofuels -Determination of calorific value*. London: BSI.
- British Standard. 2011. 2011. *BS EN 15104:2011 Solid biofuels — Determination of total content of carbon, hydrogen and nitrogen — Instrumental methods*. London: BSI Group Headquarters.
- British Standard. 2015. 2015. *BS EN 60079-10-2-2015: Explosive atmospheres Part 10-2: Classification of areas - Explosive dust atmospheres*. London: BSI
- CCPS-AIChE. 2005. *Guidelines for Safe Handling of Powders and Bulk Solids*. CENTER FOR CHEMICAL PROCESS SAFETY - industry technology alliance of the American Institute of Chemical Engineers (AIChE): American Institute of Chemical Engineers.
- CDS. 2011. *The CDS 5000 Series Pyroprobes*. [Online]. Available from: http://www.ingenieria-analitica.com/downloads/dl/file/id/664/product/18/5000_series_product_family_pyroprobe_brochure.pdf.

- Cengel, Y.A. and Boles, M.A. 2008. *Thermodynamics: An Engineering Approach*. McGrawHill
- Center for Public Environmental Oversight, C. 2016. *Gas Chromatography/Mass Spectrometry (GC/MS)*. [Online]. Available from: <http://www.cpeo.org/techtree/ttdescript/msgc.htm>.
- ChemicalRegister. 2016. *Lignosulfonates* [Online]. Available from: <http://www.chemicalregister.com/lignosulfonates/suppliers/pid7917.htm>.
- Chilworth Technology Inc. 2012. *Transportation Testing*. [Online]. [Accessed 10 March 2014]. Available from: <http://www.chilworth.com/laboratory-testing/transportation-testing>.
- Chilworth Technology Ltd. 2013. *A strategic guide to characterisation & understanding- Handling Dusts & Powders Safely*.
- Chin, Y.S. 2007. *Study of Biomass Burning with Coal in a Furnace*. MSc thesis, Cranfield University.
- Chin, Y.S. and Aris, M.S. 2012. An Experimental Investigation on the Handling and Storage Properties of Biomass Fuel Briquettes Made from Oil Palm Mill Residues. *Journal of Applied Sciences*. **Asian Network of Scientific Information**
- Chin, Y.S. and Aris, M.S. 2013 A Study of Biomass Fuel Briquettes from Oil Palm Mill Residues. *Asian Journal of Scientific Research* **6**(3), pp.537-545.
- Chin, Y.S. et al. 2013. Experimental Investigations on the Characteristics of Biomass and Coal-Biomass Fuel Briquettes. *Advanced Materials Research*. **683**, pp.246-249.
- CHROMacademy, e.-l.f.a.c.c. 2016. *The CHROMacademy Essential Guide: Understanding GC-MS Analysis Part 1*. [Online]. Available from: http://www.chromacademy.com/Essential_Guide_Webcast/Understanding_GC-MS_Analysis_Part_1/Understanding_GC-MS_Analysis_Part_1.pdf.
- Chronicle Live Publication. 2013. *Firefighters Battle Biomass Blaze at Port of Tyne*. [Online]. [Accessed 1 January 2017]. Available from: <http://www.chroniclelive.co.uk/news/firefighters-battle-biomass-blaze-port-6177485>.
- Ciolkosz, D. 2010. Renewable and Alternative Energy Fact Sheet. [Online]. Available from: <http://www.energy.psu.edu/sites/default/files/files/CoFiringBiomass.pdf>.
- Committee on Climate Change. 2016. *UK climate action following the Paris Agreement*. London.
- Dahlquist, E. 2013. *Technologies for Converting Biomass to Useful Energy: Combustion, Gasification, Pyrolysis, Torrefaction and Fermentation*
Taylor & Francis Group CRC Press
- Das, P. et al. 2004. Influence of pretreatment for deashing of sugarcane bagasse on pyrolysis products. *Biomass & Bioenergy*. **27**(5), pp.445-457.
- Davidsson, K.O. et al. 2002. The effects of fuel washing techniques on alkali release from biomass. *Fuel*. **81**(2), pp.137-142.
- DEFRA. 2016. *Emissions of Air Pollutants in the UK 1970 to 2015*. Department of Environment, Food and Rural Affairs: London.
- DeHann, J.D. 1996. Spontaneous Ignition, Part II: Investigation. *Fire and Arson Investigator*. **46**(4), pp.8-11.
- Demirbas, A. 1999. Physical properties of briquettes from waste paper and wheat straw mixtures. *Energy Conversion and Management*. **40**(4), pp.437-445.
- Demirbas, A. 2004. Combustion characteristics of different biomass fuels. *Progress in Energy and Combustion Science*. **30**(2), pp.219-230.
- Deng, L. et al. 2013. Effect of Water Washing on Fuel Properties, Pyrolysis and combustion Characteristics, and Ash Fusibility of Biomass. *Fuel Processing Technology*. **106**, pp. 712-720.
- Department of Energy & Climate Change. 2016. *2014 UK Greenhouse Gas Emissions*.

- DeVallance, D. 2013. *Pellet feedstock characteristics and pellet quality*. [Online]. Available from: http://bioenergy.psu.edu/shortcourses/2013PelletsnPower/03_Properties_DeVallance2013.pdf.
- DIN. 1996. 1996. *DIN ISO 4225:1996-08: Air quality-General aspects-Vocabulary*. Germany: Deutsches Institut für Normung (German Institute for Standardization) International Standardization Organisation.
- Dodd, K.J. and Lowe, J. 2002. *A PRACTICAL APPROACH TO FIRE AND EXPLOSION SAFETY RISK ASSESSMENT AND COMPLIANCE WITH THE DANGEROUS SUBSTANCES AND EXPLOSIVE ATMOSPHERES REGULATIONS (DSEAR)*
- Dooley, B. 2013. *Large scale storage and handling of biomass and the potential fire risks – Dust Layer Ignition and Spontaneous Combustion*. Master thesis, University of Leeds.
- Dooley, B. 2016. *PACT Milled WWP Particle Size Distribution*. Unpublished.
- Doosan. 2014. *Biomass: Coal-to-biomass conversions for efficient thermal power*. Doosan House: Doosan Babcock.
- Drax. 2012. *Biomass: the fourth energy source*. [Online]. [Accessed 1-08-2006]. Available from: <http://www.drax.com/media/41932/biomass-the-fourth-energy-source-final.pdf>.
- Drysdale, D. 2011. *An Introduction to Fire Dynamics*. United Kingdom: John Wiley & Sons, Ltd., Publication.
- Dyduch, Z. and Majcher, B. 2006. Ignition of a dust layer by a constant heat flux-heat transport in the layer. *Journal of Loss Prevention in the Process Industries*. **19**(2-3), pp.233-237.
- Earth Institute. 2011. *Ion Chromatograph to detect major anions in precipitation (snow), groundwaters and drinking waters from New York*. [Online]. [Accessed 1 August 2016]. Available from: <http://www.ldeo.columbia.edu/~martins/eda.html>.
- Ehimen, E.A. 2016. 14 - Algae biomass supply chains. *Biomass Supply Chains for Bioenergy and Biorefining*. Woodhead Publishing, pp.319-332.
- El-Sayed, S.A. and Abdel-Latif, A.M. 2000. Smoldering combustion of dust layer on hot surface. *Journal of Loss Prevention in the Process Industries*. **13**(6), pp.509-517.
- El-Sayed, S.A. and Khass, T.M. 2013. Smoldering combustion of rice husk dusts on a hot surface. *Combustion Explosion and Shock Waves*. **49**(2), pp.159-166.
- El-Sayed, S.A. and Mostafa, M.E. 2016. Estimation of Thermal and Kinetic Parameters of Sugarcane Bagasse and Cotton Stalks Dust Layers from Hot Surface Ignition Tests. *Combustion Science and Technology*. **188**(10), pp.1655-1673.
- Elmer, P. 2016. *Clarus 600/560 D: Gas Chromatograph/Mass Spectrometer (GC/MS), Tutorial*. [Online]. [Accessed 1 July 2016]. Available from: http://www.perkinelmer.com.cn/CMSResources/Images/46-74535GDE_Clarus600560DGCMSTutorial.pdf.
- Energy Research Institute. 2016. *Ion Chromatography (IC Dionex)*. [Online]. [Accessed 1st August 2016]. Available from: <http://fengsrv1c.leeds.ac.uk/eri/facilities/IonChromatography.shtml>.
- Energy UK. 2016. *Energy in the UK 2016 - Delivering jobs, growth and choice through sustainable investment in 2015*. London: Energy UK Charles House.
- Engel, L. et al. 2016a. Determination of the smoldering temperature on the basis of adiabatic tests. *Chemical Engineering Transactions*. **48**, pp.127-132
- Engel, L. et al. 2016b. Determination of the Smoldering Temperature on the Basis of Adiabatic Tests. *15th International Symposium on Loss Prevention and Safety Promotion (Loss 2016)*. **48**, pp.127-132.
- Engineer, P.S. 2015. *Binder Practice*, 1 February 2015.
- Engineer, P.S. 2016. *MPST Practice*, November 2016.

- Everard, C.D. et al. 2014. Heating processes during storage of Miscanthus chip piles and numerical simulations to predict self-ignition. *Journal of Loss Prevention in the Process Industries*. **30**, pp.188-196.
- Exponent Engineering and Scientific Consulting Inc. 2010. *Combustible-Dust Testing Laboratory*. [Online]. [Accessed 10 March 2014]. Available from: http://www.exponent.com/combustible_dust_testing_laboratory_2/.
- Fahmi, R. et al. 2008. The effect of lignin and inorganic species in biomass on pyrolysis oil yields, quality and stability. *Fuel*. **87**(7), pp.1230-1240.
- Fahmi, R. et al. 2007. The effect of alkali metals on combustion and pyrolysis of Lolium and Festuca grasses, switchgrass and willow. *Fuel*. **86**(10-11), pp.1560-1569.
- Fei, F. and Liang, D. 2011. Research Progress and Comparison of Methods for Testing Self Ignition Materials. *Procedia Engineering*. **11**, pp.91- 99.
- Fernandez-Anez, N. et al. 2015. Ignition of waste/biomass mixtures deposited as dust layers. In: *25th International Colloquium on the Dynamics of Explosions and Reactive Systems, 2-7 Aug 2015, Leeds UK*.
- Ferrero, F. et al. 2009. A mathematical model to predict the heating-up of large-scale wood piles. *Journal of Loss Prevention in the Process Industries*. **22**(4), pp.439-448.
- Ferro, D.T. et al. 2004. Torrefaction of agricultural and forest residues. In: *Cubasolar 2004 April 12-16, 2004, Guantánamo, Cuba*.
- Fine, P.M. et al. 2002. Organic compounds in biomass smoke from residential wood combustion: Emissions characterization at a continental scale. *Journal of Geophysical Research: Atmospheres*. **107**(D21), pp.11-1-11-9.
- Fire Safety Advice Centre. 2016. *Information about the Fire Triangle/Tetrahedron and Combustion*. [Online]. [Accessed 1 July 2016]. Available from: <https://www.firesafe.org.uk/information-about-the-fire-triangle-tetrahedron-and-combustion/>.
- Fisher, E.M. et al. 2011. Combustion characteristics of chars from raw and torrefied willow In: *7th US National Technical Meeting of the Combustion Institute, March 20-23, 2011 Georgia Institute of Technology, Atlanta*.
- Fitzpatrick, E.M. et al. 2009. The mechanism of the formation of soot and other pollutants during the co-firing of coal and pine wood in a fixed bed combustor. *Fuel*. **88**(12), pp.2409-2417.
- Friedl, A. et al. 2005. Prediction of heating values of biomass fuel from elemental composition. *Analytica Chimica Acta 2005*. **544**(1-2), pp.191-198.
- García-Torrent, J. et al. 2012. Determination of the risk of self-ignition of coals and biomass materials. *Journal of Hazardous Materials*. **213-214**, pp.230-235.
- Gårdbro, G. 2014. *Techno-economic modeling of the supply chain for torrefied biomass*. Masters thesis, Umeå University, Sweden
- GeeJay. 2016. *What is silica gel ?* [Online]. [Accessed 1 January 2016]. Available from: <http://www.geejaychemicals.co.uk/silicagel.htm>.
- Gil, M.V. et al. 2010. Thermal behaviour and kinetics of coal/biomass blends during co-combustion. *Bioresource Technology*. **101**(14), pp.5601-5608.
- Gucho, E.M. et al. 2015. Experimental Study on Dry Torrefaction of Beech Wood and Miscanthus. *Energies*. **8**(5), pp.3903-3923.
- Gudka, B. et al. 2012. Fuel characteristics of wheat-based Dried Distillers Grains and Solubles (DDGS) for thermal conversion in power plants. *Fuel Processing Technology*. **94**(1), pp.123-130.
- Gudka, B. et al. 2016. A review of the mitigation of deposition and emission problems during biomass combustion through washing pre-treatment. *Journal of the Energy Institute*. **89**(2), pp.159-171.
- Guillermo Rein. 2012. Biomass self-heating fire in Tilbury Power Plant? [Online]. Available from: http://guillermo-rein.blogspot.co.uk/2012_03_01_archive.html.

- Hagen, B.C. 2013. *Onset of smoldering and transition to flaming fire*. Philosophiae Doctor (PhD) thesis, University of Bergen.
- HARIBO Scientific. 2016. *Sample Digestion*. [Online]. [Accessed 1 August 2016]. Available from: <http://www.horiba.com/uk/scientific/products/sample-preparation/sample-digestion/>.
- Hayhurst, A.N. 2013. The kinetics of the pyrolysis or devolatilisation of sewage sludge and other solid fuels. *Combustion and Flame*. **160**(1), pp.138-144.
- Ház, A. et al. 2013. Determination of Temperature Regions in Thermal Degradation of Lignin In: *4th International Conference Renewable Energy Sources 2013, May 21-23, 2013 Tatranské Matliare, High Tatras, Slovak Republic*.
- Hehar, G.S. 2013. *Physicochemical and Ignition Properties of Dust from Loblolly Pine Wood*. MSc thesis, Auburn University.
- Henderson, D.K. and Tyler, B.J. 1988. Dual Ignition Temperatures for Dust Layers. *Journal of Hazardous Materials*. **19**(2), pp.155-159.
- Henriksen, U.B. et al. 2008. *Fundamental Understanding of Pelletization- EFP-2005 project (33031-037) Summary report*. Denmark.
- Hensel, W. et al. 1994. Critical Parameters for the Ignition of Dust Layers at Constant Heat-Flux Boundary-Conditions. *Process Safety Progress*. **13**(4), pp.210-213.
- Hoefl, M. 2013. *Deliverable No. 8.2 - Requirements for a MSDS for torrefied material*. Production of Solid Sustainable Energy Carriers from Biomass by Means of Torrefaction (SECTOR).
- Hogland, W. and Marques, M. 2003. Physical, biological and chemical processes during storage and spontaneous combustion of waste fuel. *Resources Conservation and Recycling*. **40**(1), pp.53-69.
- Holm-Nielsen, J.B. 2016. 1-Introduction to biomass supply chains. *Biomass Supply Chains for Bioenergy and Biorefining*. Woodhead Publishing, pp.3-13.
- Hornung, A. 2014. *Transformation of Biomass: Theory to Practice*. United Kingdom: John Wiley & Sons, Ltd.
- Huang, X. and Rein, G. 2016. Thermochemical conversion of biomass in smouldering combustion across scales: The roles of heterogeneous kinetics, oxygen and transport phenomena. *Bioresource Technology*. **207**, pp.409-421.
- Hübschmann, H.-J. 2015. *Handbook of GC-MS: Fundamentals and Applications*. Third Edition ed. Wiley-VCH.
- Hwang, C.C. and Litton, C.D. 1988. Ignition of Combustible Dust layers on a Hot Surface. *FIRE SAFETY SCIENCE-PROCEEDINGS OF THE THIRD INTERNATIONAL SYMPOSIUM*. pp.187-196.
- Ibrahim, R.H.H. 2013. *Fundamentals of Torrefaction of Biomass and Its Environmental Impacts*. Ph.D thesis, University of Leeds.
- Ibrahim, R.H.H. et al. 2013. Physicochemical characterisation of torrefied biomass. *Journal of Analytical and Applied Pyrolysis*. **103**, pp.21-30.
- IEA Bioenergy. 2013. Health and Safety Aspects of Solid Biomass Storage, Transportation and Feeding. [Online]. [Accessed 20 November 2013]. Available from: <http://www.ieabioenergy.com/wp-content/uploads/2013/10/Health-and-Safety-Aspects-of-Solid-Biomass-Storage-Transportation-and-Feeding.pdf>
- IEC. 1994. 1994. *IEC 61241-2-1 Electrical apparatus for use in the presence of combustible dust - Part 2: Test methods - Section 1: Methods for determining the minimum ignition temperatures of dust*. Geneva Switzerland: International Electrotechnical Commission
- Ikan, R. 2008. *Selected Topics in the Chemistry of Natural Products*. Singapore: World Scientific Publishing Co. Pte. Ltd.
- Ilona, Š. 2015. Risk of biomass dust layer in industrial processes. *Research Journal of Recent Sciences*. **4**(1), pp.94-98.

- Amendments to the International Maritime Solid Bulk Cargoes (IMSBC) Code*. 2013. [Database]. International Maritime Organization.
- Incropera, F.P. and DeWitt, D.P. 2002 *Introduction to Heat Transfer*. Fourth Ed. ed. John Wiley & Sons, Inc, .
- Industry, P.A.-A.f.t.P. 2016. *Introduction to BET (Brunauer, Emmett and Teller)* [Online]. [Accessed 1 August 2016]. Available from: <http://particle.dk/methods-analytical-laboratory/surface-area-bet-2/>.
- ISO. 1985. 1985. *ISO-6184/1 Explosion Protection Systems- Part 1: Determination of Explosion Indices of Combustible Dusts in Air*. . Geneva: International Organization of Standardization,.
- ISO/IEC, B.E. 2016. 2016. *BS EN ISO/IEC 80079-20-2:2016 Explosive atmospheres - Part 20-2: Material characteristics - Combustible dusts test methods*. London: BSI.
- James, E. 2014. *Dichloromethane*. [Online]. Available from: <http://www.rsc.org/chemistryworld/2014/04/dichloromethane-dcm-methylene-chloride-solvent-decaffeinated-podcast>.
- Janes, A. et al. 2008. Correlation between self-ignition of a dust layer on a hot surface and in baskets in an oven. *J Hazard Mater*. **159**(2-3), pp.528-35.
- Janès, A.s. and Carson, D. 2013a. Effect of Inerts on Ignition Sensitivity of Dusts. *Chemical Engineering Transactions* **31**.
- Janès, A.s. and Carson, D. 2013b. Effect of Inerts on Ignition Sensitivity of Dusts. *Chemical Engineering Transactions*. **31**.
- Jaskółowski, W. et al. 2014. Effects of particle size on minimum ignition temperature of dust layers and dust clouds of selected wood dusts, . *Annals of Warsaw University of Life Sciences. SGGW Forestry and Wood Technology* (No 86), pp.138-143
- Jenkins, B.M. et al. 1996. On the properties of washed straw. *Biomass & Bioenergy*. **10**(4), pp.177-200.
- Jenkins, B.M. et al. 1998a. Combustion properties of biomass. *Fuel Processing Technology*. **54**(1-3), pp.17-46.
- Jenkins, B.M. et al. 1998b. Combustion properties of biomass. *Fuel Processing Technology*. **54**(1-3), pp.17-46.
- Jespen, T. 2016. *ATEX—Explosive Atmospheres: Risk Assessment, Control and Compliance*. [Online]. Switzerland: Springer International Publishing Switzerland 2016.
- Jones, J.M. et al. 2015. Low temperature ignition of biomass. *Fuel Processing Technology*. **134**, pp.372-377.
- Jong, W.d. and Ommen, J.R.v. 2015. *Biomass as a Sustainable Energy Source for the Future: Fundamentals of Conversion Processes*. New Jersey: American Institute of Chemical Engineers, Inc, Jon Wiley & Sons, Inc.
- Joshi, K.A. 2012. *Factors Governing Spontaneous Ignition of Combustible Dusts*. thesis, Worcester Polytechnic Institute.
- Kasalová, I. and Balog, K. 2011. Minimum Ignition Temperatures of Food Dust Clouds Determined by Planned Experiment
Annals of Faculty Engineering Hunedoara - International Journal of Engineering. **Tom IX**(Fascicule 1), pp.97-102
- Kasparbauer, R.D. 2009. *The effects of biomass pretreatments on the products of fast pyrolysis, 2009, MSc Thesis*. Master of Science thesis, Iowa State University.
- Kenkel, J. 2014. *Analytical Chemistry for Technicians*. Fourth Edition ed. CRC Press, Taylor & Francis LLC.
- Kuokkanen, M. et al. 2011. Additives in Wood Pellet Production - a Pilot-Scale Study of Binding Agent Usage. *Bioresources*. **6**(4), pp.4331-4355.
- Lasode, O.A. et al. 2014. Torrefaction of some Nigerian lignocellulosic resources and decomposition kinetics. *Journal of Analytical and Applied Pyrolysis*. **109**, pp.47-55.

- Leuschke, G. 1981. Experimental Investigations on Self-Ignition of Dust Deposits in Hot Environments. *J. Chem. E. Symposium Series* **no.68**.
- Li, J. et al. 2016. Studies of Ignition Behavior of Biomass Particles in a Down-Fire Reactor for Improving Co-firing Performance. *Energy & Fuels*. **30**(7), pp.5870-5877.
- Li, X.R. et al. 2006. Evaluation of danger from fermentation-induced spontaneous ignition of wood chips. *J Hazard Mater*. **135**(1-3), pp.15-20.
- Li, X.R. et al. 2008. Thermal behavior of sewage sludge derived fuels. *Thermal Science*. **12**(2), pp.137-148.
- Li, Y.J. et al. 2014. Aqueous-phase photochemical oxidation and direct photolysis of vanillin – a model compound of methoxy phenols from biomass burning. *Atmospheric Chemistry and Physics*. **14**(6), pp.2871-2885.
- Liaw, S.B. and Wu, H.W. 2013. Leaching Characteristics of Organic and Inorganic Matter from Biomass by Water: Differences between Batch and Semi-continuous Operations. *Industrial & Engineering Chemistry Research*. **52**(11), pp.4280-4289.
- Lignotech. 2002. *MSDS-Ligno-Bond DD Powder*. [Online]. Available from: <http://www.stobec.com/documents/msds/8128.pdf>.
- Liu, C.J. et al. 2014. Catalytic fast pyrolysis of lignocellulosic biomass. *Chemical Society Reviews*. **43**(22), pp.7594-7623.
- Livingston, W.R. et al. 2016. *IEA-The status of large scale biomass firing-The milling and combustion of biomass materials in large pulverised coal boilers*.
- Luke Walsh. 2016. *Explosion at DONG's biomass plant* [Online]. Available from: <http://www.endswasteandbioenergy.com/article/1412737/explosion-dongs-biomass-plant>.
- Maciejewska, A. et al. 2000. *CO-FIRING OF BIOMASS WITH COAL: CONSTRAINTS AND ROLE OF BIOMASS PRE-TREATMENT*. Netherlands: European Commission Directorate-General Joint Research Centre (DG JRC).
- Maloney, J.O. 2007. *Perry's Chemical Engineers' Handbook*. The McGraw-Hill Companies, Inc.,.
- Martin, A.J.P. and Synge, R.L.M. 1941. A new form of chromatogram employing two liquid phases. *Biochemical Journal*. **35**(12), pp.1358-1368.
- Martinka, J. et al. 2012. Influence of the Flow Rate of Oxidising Atmosphere on the Flame Spread Rate on the Surface of Organic Settled Dust. *Research Papers-Faculty of Materials Science and Technology in Trnava Slovak University of Technology in Bratislava*. [Online]. **No. 32**(1 January 2016). Available from: <http://citeweb.info/20131850557>.
- Martínez, I. 1995-2017. *COMBUSTION CHARACTERISTICS*. Ciudad Universitaria.
- Mason, P.E. et al. 2016. Comparative Study of the Thermal Conductivity of Solid Biomass Fuels. *Energy Fuels*. **30**(3), pp.2158-2163.
- Mathew, S. and Zakaria, Z.A. 2015. Pyroligneous acid-the smoky acidic liquid from plant biomass. *Appl Microbiol Biotechnol*. **99**(2), pp.611-22.
- McDonald, A. et al. 2014. *Pyrolysis Bio-Oil Upgrading to Renewable Fuels-Final Report* University Transportation Centers Program.
- McMaster, M.C. 2008. *GC/MS A Practical User's Guide*. 2nd ed. ed. Wiley Interscience, A John Wiley & Sons, Inc., Publication.
- McNamee, P. et al. 2016. An assessment of the torrefaction of North American pine and life cycle greenhouse gas emissions. *Energy Conversion and Management*. **113**, pp.177-188.
- McNamee, P. et al. 2015. The combustion characteristics of high-heating-rate chars from untreated and torrefied biomass fuels. *Biomass & Bioenergy*. **82**, pp.63-72.
- Medina, C.H. 2014. *Explosion safety of biomass and torrefied biomass powders*. thesis, University of Leeds.
- Merckel, R.D. 2015. *Fast and microwave-induced pyrolysis bio-oil from Eucalyptus grandis: Possibilities of upgrading*. Master in Engineering thesis, University of Pretoria.

- Meuzelaar, H.L.C. et al. 2016. *Receptor Modeling of Organic Particulate Matter Components*. University of Utah, Sierra Research, U.S. Army Corps of Engineers, Instituto Tecnológico Y De Estudios.
- Mills, J.E. 1908. *Binders for Coal Briquets*. Washington Government Printing Office.
- Miron, Y. and Lazzara, C.P. 1988. Hot-Surface Ignition Temperatures of Dust Layers. *Fire and Materials*. **12**(3), pp.115-126.
- Mitchell, E.J.S. et al. 2016. The impact of fuel properties on the emissions from the combustion of biomass and other solid fuels in a fixed bed domestic stove. *Fuel Processing Technology*. **142**, pp.115-123.
- Mohammed, I.Y. et al. 2016. Effects of Pretreatments of Napier Grass with Deionized Water, Sulfuric Acid and Sodium Hydroxide on Pyrolysis Oil Characteristics. *Waste and Biomass Valorization*.
- Mortari, D.A. et al. 2010. Study of Thermal Decomposition and Ignition Temperature of Bagasse, Coal and Their Blends. *Engenharia Térmica (Thermal Engineering)*. **9**, pp.81-88.
- National Aeronautics and Space Administration. 2014. *Global Climate Change, Vital Signs of the Planet*. [Online]. [Accessed 1 January 2017]. Available from: <http://climate.nasa.gov/scientific-consensus>
- National Fire Protection Association. 2006. *Standard for the Prevention of Fire and Dust Explosions from the Manufacturing, Processing, and Handling of Combustible Particulate Solids*. Quincy, Massachusetts: United States trade association.
- New Zealand Ministry of Transport. 2008. *Transporting Dangerous Goods Safely, An industry guide*. [Online]. [Accessed 10 March 2014]. Available from: <http://www.maritimenz.govt.nz/Publications-and-forms/Commercial-operations/Shipping-safety/Transporting-Dangerous-Goods-Safely.pdf>.
- NFPA. 2013. *NFPA 499, Recommended Practice for the Classification of Combustible Dusts and of Hazardous (Classified) Locations for Electrical Installations in Chemical Process Areas*. United States: National Fire Protection Association.
- Nhuchhen, D. et al. 2014. A Comprehensive Review on Biomass Torrefaction. *International Journal of Renewable Energy & Biofuels*. **24**, pp.1-56.
- Nichols, S. 2013. *Hot Surface Ignition*. [Online]. [Accessed 1 January 2016]. Available from: http://www.ase.uc.edu/~pdisimil/classnotes/Aviation%20Fire%20Dynamics/Reserach%20Papers/HSI_Nichols_12Apr2013.pptx.
- nordtest method. 1992. *Solid Materials: Spontaneous Ignition Temperature by Continuous Heating*. [Online]. Available from: <http://www.nordtest.info/index.php/methods/item/solid-materials-spontaneous-ignition-temperature-by-continuous-heating-nt-fire-045.html>.
- Nowakowski, D.J. 2008. *Influence of Potassium and Phosphorus on the Thermochemical Conversion of the Cell Wall Components of Biomass*. Ph.D thesis, University of Leeds.
- Nowakowski, D.J. and Jones, J.M. 2008. Uncatalysed and potassium-catalysed pyrolysis of the cell-wall constituents of biomass and their model compounds. *Journal of Analytical and Applied Pyrolysis*. **83**(1), pp.12-25.
- Nowakowski, D.J. et al. 2007. Potassium catalysis in the pyrolysis behaviour of short rotation willow coppice. *Fuel*. **86**(15), pp.2389-2402.
- Nowakowski, D.J. et al. 2008. Phosphorus catalysis in the pyrolysis behaviour of biomass. *Journal of Analytical and Applied Pyrolysis*. **83**(2), pp.197-204.
- Office for National Statistics. 2016. *UK Perspectives 2016: Energy and emissions in the UK*. [Online]. [Accessed 1 January 2017]. Available from: <http://visual.ons.gov.uk/uk-perspectives-2016-energy-and-emissions-in-the-uk/>.

- OMEGA. 2016. *Thermocouples-Using Thermocouples in Temperature Measurement*. [Online]. [Accessed 1 January 2015]. Available from: <http://www.omega.com/prodinfo/thermocouples.html>.
- Oros, D.R. et al. 2006. Identification and emission factors of molecular tracers in organic aerosols from biomass burning: Part 3. Grasses. *Applied Geochemistry*. **21**(6), pp.919-940.
- Oros, D.R. and Simoneit, B.R.T. 2001. Identification and emission factors of molecular tracers in organic aerosols from biomass burning Part 2. Deciduous trees. *Applied Geochemistry*. **16**(13), pp.1545-1565.
- Owski, W.J. et al. 2010. Study on the influence of thickness of dust layer to ignition temperature in selected types of exotic woods. *Annals of Warsaw University of Life Science - SGGW Forestry and Wood Technology* **No 71**, pp.300-303.
- Palmer, K.N. and Tonkin, P.S. 1957. The Ignition of Dust Layers on a Hot Surface. *Combustion and Flame*. **1**(1), pp.14-18.
- Park, H. 2006. *Hot Surface Ignition Temperature of Dust Layers with and without Combustible Additives*. MSc thesis, Worcester Polytechnic Institute.
- Park, H. et al. 2009. A means to estimate thermal and kinetic parameters of coal dust layer from hot surface ignition tests. *J Hazard Mater*. **168**(1), pp.145-55.
- Parr ®. 2007. *Introduction to Bomb Calorimetry*. [Online]. Available from: <http://www.scimed.co.uk/wp-content/uploads/2013/03/Introduction-to-bomb-calorimetry.pdf>.
- Partnership for Policy Integrity, P. 2011. Air pollution from biomass energy
- Pastier, M. et al. 2013. Minimum Ignition Temperature of Wood Dust Layers. *RESEARCH PAPERS FACULTY OF MATERIALS SCIENCE AND TECHNOLOGY IN TRNAVA*. [Online]. **Special Number**. [Accessed 15 August 2014]. Available from: http://www.mtf.stuba.sk/docs/doc/casopis_Vedecke_prace/32SN/021_Pastier.pdf
- Paul Newton. 2012. *Tilbury biomass plant returns to service after fire*. [Online]. Available from: <http://utilityweek.co.uk/news/Tilbury-biomass-plant-returns-to-service-after-fire/830812#.WMQXx8dw81g>.
- Pauner, M.A. and Bygbjerg, H. 2006. *Spontaneous ignition in storage and production lines-Part 6: Comparison of 6 mm and 8 mm wood pellets*. Denmark: Danish Institute of Fire and Security Technology.
- Pauner, M.A. and Bygbjerg, H. 2007. Spontaneous ignition in storage and production lines: Investigation on wood pellets and protein powders. *Fire and Materials*. **31**(8), pp.477-494.
- Pauner, M.A. et al. 2004. *Spontaneous ignition in storage and production lines, Part 1: Investigation of protein powders*. Denmark: Danish Institute of Fire and Security Technology.
- PBL Netherlands Environmental Assessment Agency. 2016. *Trends in Global CO2 emissions: 2016 report*. PBL Publishers: European Commission Joint Research Centre-Institute for Environment and Sustainability.
- Phanphanich, M. and Mani, S. 2011. Impact of torrefaction on the grindability and fuel characteristics of forest biomass. *Bioresour Technol*. **102**(2), pp.1246-53.
- Pimchuai, A. et al. 2010. Torrefaction of Agriculture Residue To Enhance Combustible Properties. *Energy & Fuels*. **24**, pp.4638-4645.
- PlanetPower. 2016. *Biomass Fuel Analysis For Energy Crop (Closed-Loop) and Wood Derived Fuel/Yardwaste (Open-Loop)*. [Online]. Available from: <http://www.treepower.org/fuels/analysis.html>.
- Polka, M. et al. 2012. Experimental analysis of minimal ignition temperatures of a dust layer and clouds on a heated surface of selected flammable dusts. *2012 International Symposium on Safety Science and Technology*. **45**, pp.414-423.

- Postmedia Network Inc. 2012. *Fatal Sawdust Blast in B.C. comes after five explosions at similar plants since 2009*. [Online]. [Accessed 8 January 2014]. Available from: <http://news.nationalpost.com/2012/04/28/fatal-sawdust-blast-in-b-c-comes-after-five-explions-at-similar-plants-since-2009/>.
- Prins, M.J. et al. 2006. Torrefaction of wood - Part 2. Analysis of products. *Journal of Analytical and Applied Pyrolysis*. **77**(1), pp.35-40.
- PubChem. 2016. *Cornstarch*. [Online]. Available from: <https://pubchem.ncbi.nlm.nih.gov/compound/24836924#section=Top>.
- Querol, E. et al. 2006. Ignition tests for electrical and mechanical equipment subjected to hot surfaces. *Journal of Loss Prevention in the Process Industries*. **19**(6), pp.639-644.
- Rahman, A.A. et al. 2016. Influence of Washing Medium Pre-treatment on Pyrolysis Yields and Product Characteristics of Palm Kernel Shell. *Journal of Physical Science*. **27**(1), pp.53-75.
- Rajaseenivasan, T. et al. 2016. An investigation on the performance of sawdust briquette blending with neem powder. *Alexandria Engineering Journal*. **55**(3), pp.2833-2838.
- Ramírez, A. et al. 2010. Experimental Determination of Self-Heating and Self-Ignition Risks Associated with the Dusts of Agricultural Materials Commonly Stored in Silos. *Journal of Hazardous Materials*. **175**, pp.920-927.
- Raveendran, K. et al. 1995. Influence of Mineral Matter on Biomass Pyrolysis Characteristics. *Fuel*. **74**(12), pp.1812-1822.
- Reddy, P.D. et al. 1998. Effect of inerts on layer ignition temperatures of coal dust. *Combustion and Flame*. **114**(1-2), pp.41-53.
- Reed, T.B. 1981. *Principles and Technology of Biomass Gasification*. [Online]. Park Ridge, New Jersey: Noyes Data Corporation. [Accessed 1 January 2015]. Available from: http://link.springer.com/chapter/10.1007%2F978-1-4613-9951-3_3.
- Rein, G. 2016. Smoldering Combustion. *SFPE Handbook of Fire Protection Engineering* 5th ed. Springer, pp.581-603.
- Retsch. 2010. *Operating Instructions Ball Mills Type PM100 / PM200 / PM100cm*. [Online]. Available from: http://www.retsch.com/dltmp/www/53e4b55a-36f8-4c5a-9812-636500000000-c58b206a07da/manual_pm100_pm200_pm100cm_en.pdf.
- Rogala, I. 2015 Hazardous Area Classification - dust atmospheres new plant design and operation and re-evaluate changes to existing plant. In: *IECEx International Conference on Equipment and Services in Explosive Atmospheres, 22-23 April 2015, Gdańsk, Poland*.
- Rogers, R.L. et al. 2006. Ignition of Dust Clouds and Dusy Deposits by Friction Sparks and Hotspots. *iCheme. Symposium Series No.151*.
- Rottner, B.L. 2006. *Combustible Dusts*. [Online]. [Accessed 1 Aug 2016]. Available from: <https://www.aiha.org/aihce06/handouts/cr314rottner.pdf>.
- Runge, T. et al. 2013. Improving biomass combustion quality using a liquid hot water treatment. *Biofuels*. **4**(1), pp.73-83.
- Saddawi, A. et al. 2013a. Assessment of the Self-Ignition Characteristics of Raw and Processed Biomass Fuels. In: *European Combustion Meeting 2013,, 26-28 June 2013, Lund, Sweden*.
- Saddawi, A. et al. 2012. Commodity Fuels from Biomass through Pretreatment and Torrefaction: Effects of Mineral Content on Torrefied Fuel Characteristics and Quality. *Energy & Fuels* **26**, pp.6466-6474.
- Saddawi, A. et al. 2010. Kinetics of the Thermal Decomposition of Biomass. *Energy & Fuels*. **24**, pp.1274-1282.
- Saddawi, A. et al. 2013b. *Low Temperature Ignition of Biomass*. BF2RA-University of Leeds Grant#10.

- San Diego Miramar College. 2016. *Principle of Atomic Absorption /Emission Spectroscopy*. [Online]. [Accessed 1 August 2016]. Available from: http://faculty.sdmiramar.edu/fgarces/labmatters/instruments/aa/AAS_Theory/AASTheory.htm.
- Schauer, J.J. et al. 2001. Measurement of Emissions from Air Pollution Sources. 3. C1-C29 Organic Compounds from Fireplace Combustion of Wood. *Environ. Sci. Technol.* (35), pp.1716-1728.
- Seitz, S. et al. 2016. Determination of the Self-ignition Behaviour of Bulk Materials from Heat Storage Tests below Atmospheric Pressure. *15th International Symposium on Loss Prevention and Safety Promotion (Loss 2016)*. **48**, pp.583-588.
- Sheesley, R.J. et al. 2003. Characterization of organic aerosols emitted from the combustion of biomass indigenous to South Asia. *Journal of Geophysical Research-Atmospheres*. **108**(D9).
- SHIMADZU. 2008. *Accessories and Supplies for Shimadzu Gas Chromatographs*. [Online]. [Accessed 1 January 2015]. Available from: http://www.chemshow.cn/UploadFile/datum/1003/shjohntec_2008218115733800771.pdf.
- Shimadzu, E.i.S. 2016. *Total Ion Chromatogram (TIC)*. [Online]. Available from: http://www.shimadzu.com/an/total_ion.html.
- Shirtliffe, C.J. and Orr, H.W. 1967. Comparison of Modes of Operation for Guarded Hot Plate Apparatus with Emphasis on Transient Characteristics, Thermal conductivity : Proceedings of the Seventh Conference. In: *Seventh Conference of the National Bureau of Standards, November 13-16, 1967, Gaithersburg Maryland*. The National Bureau of Standards, pp.229-240.
- Shiyani, D. 2011. *Hot Surface Ignition of Combustible Fuels*. [Online]. [Accessed 1 Jan 2016]. Available from: [http://www.ase.uc.edu/~pdisimil/classnotes/Aviation%20Fire%20Dynamics/Research%20Papers/Hot%20Surface%20Ignition%20of%20Combustible%20Fuels\(Dhaval%20Shiyani\).pptx](http://www.ase.uc.edu/~pdisimil/classnotes/Aviation%20Fire%20Dynamics/Research%20Papers/Hot%20Surface%20Ignition%20of%20Combustible%20Fuels(Dhaval%20Shiyani).pptx).
- Slatter, D.J.F. 2015. *Explosibility of Coarse Biomass Powders*. thesis, University of Leeds.
- Society of Fire Protection Engineers. 2002. *SFPE Handbook of Fire Protection*. Third Edition ed. Massachusetts: National Fire Protection Association Inc.
- SP Swedish National Testing and Research Institute. 2003. Spontaneous Ignition of Biofuels – A Literature Survey of Theoretical and Experimental Methods. [Online]. [Accessed 1 January 2017]. Available from: <https://rib.msb.se/Filer/pdf%5C26254.pdf>.
- SPECAC. 2013. *Easy to use, rugged and durable hydraulic presses suitable for a wide range of applications*. [Online]. [Accessed 1 January 2015]. Available from: <http://www.specac.com/userfiles/file/MD20ManualPress.pdf>.
- SPEX. 2010. *6770 FREEZER/MILL OPERATION MANUAL*. [Online]. [Accessed 1 January 2016]. Available from: <http://www.spexsampleprep.com/knowledge-base/resources/manuals/6770%20FreezerMill%20Manual%20-%20100118.pdf>.
- Springer Science+Business Media B.V. 1997. *Developments in Thermochemical Biomass Conversion*. [Online]. Netherlands: Springer Netherlands.
- Sweis, F.K. 1998. The effect of admixed material on the ignition temperature of dust layers in hot environments1. *Journal of Hazardous Materials*. **63**(1), pp.25-35.
- Tamburello, S.M. 2011. *On Determining Spontaneous Ignition in Porous Materials*. MSc thesis, University of Maryland.
- Tan, H. and Wang, S.-r. 2009. Experimental study of the effect of acid-washing pretreatment on biomass pyrolysis. *Journal of Fuel Chemistry and Technology*. **37**(6), pp.668-672.
- Tarasov, D. et al. 2013. Effect of Additives on Wood Pellet Physical and Thermal Characteristics: A Review. *ISRN Forestry*. **2013**, pp.1-6.

- Teixeira, J. et al. 2013. Hydroxycinnamic acid antioxidants: an electrochemical overview. *Biomed Res Int.* **2013**, p251754.
- The Carbolea Research Group. 2014. Storage of Biomass. [Online]. [Accessed 8 January 2014]. Available from: <http://www.carbolea.ul.ie/storage.php>
- The Green Age Ltd. 2014. *Summary of Key Facts – Tilbury Biomass Power Plant*. [Online]. [Accessed 1 January 2017]. Available from: <http://www.thegreenage.co.uk/cos/tilbury-biomass-plant/>
- The National Institute of Standards and Technology, N. 2016a. *Coniferyl aldehyde*. [Online]. Available from: <http://webbook.nist.gov/cgi/cbook.cgi?ID=458-36-6>.
- The National Institute of Standards and Technology, N. 2016b. *Benzaldehyde, 4-hydroxy-3,5-dimethoxy-*. [Online]. Available from: <http://webbook.nist.gov/cgi/cbook.cgi?ID=134-96-3>.
- ThermoFisherScientific. 2016. *ASE 350 Accelerated Solvent Extractor*. [Online]. Available from: <http://www.dionex.com/en-us/products/sample-preparation/ase/instruments/ase-350/lp-72866.html>.
- ThermoScientific. 2016. *Use of Accelerated Solvent Extraction for Cleaning and Elution of XAD Resin*. [Online]. Available from: http://www.dionex.com/en-us/webdocs/114347-AN347-ASE-Cleaning-Elution-XAD-Resin-AN70641_E.pdf.
- Thomas, P.H. and Bowes, P.C. 1961. Thermal Ignition in a Slab with One Face at a Constant High Temperature. *Trans. Faraday Soc.* **1961**(57), pp.2007-2017.
- Toscano, G. et al. 2015. Torrefaction of tomato industry residues. *Fuel.* **143**, pp.89-97.
- Trajan Scientific Australia. 2015. *Splitless Injection*. [Online]. Available from: <http://www.sge.com/support/training/injection/injectionsplit-and-splitless-injection/splitless-injection>.
- Trunschke, A. 2007. Surface Area and Pore Size Determination. [Online]. Available from: http://www.fhi-berlin.mpg.de/acnew/departement/pages/teaching/pages/teaching_wintersemester_2007_2008/trunschke_surface_area_pores_191007.pdf.
- Tumuluru, J. 2016. Effect of Deep Drying and Torrefaction Temperature on Proximate, Ultimate Composition, and Heating Value of 2-mm Lodgepole Pine (*Pinus contorta*) Grind. *Bioengineering.* **3**(2), p16.
- Tumuluru, J.S. et al. 2012. Formulation, Pretreatment, and Densification Options to Improve Biomass Specifications for Co-Firing High Percentages with Coal. *Industrial Biotechnology.* **8**, pp.113-132.
- Tumuluru, J.S. et al. 2011a. A review on biomass torrefaction process and product properties for energy applications. *Industrial Biotechnology* **7**, pp.384-401.
- Tumuluru, J.S. et al. 2011b. *A Review on Biomass Classification and Composition, Co-Firing Issues and Pretreatment Methods*
- Tyler, B.J. and Henderson, D.K. 1987. Spontaneous Ignitions in Dust Layers: Comparison of Experimental and Calculated Values. *ICHEME Symposium series no. 102*. pp.45-59.
- U.S. Energy Information Administration. 2016 *International Energy Outlook 2016 with Projections to 2040*. Washington, DC 20585: U.S. Department of Energy
- Ugwu, K. 2013. Evaluation of Binders in the Production of Briquettes from Empty Fruit Bunches of *Elais Guinensis*. *International Journal of Renewable and Sustainable Energy.* **2**(4), p176.
- United Nations. 2009. Recommendations on the Transports of Dangerous Goods, Manual of Tests and Criteria. [Online]. [Accessed 10 March 2014]. Available from: <http://www.unece.org/trans/danger/publi/manual/Rev5/English/ST-SG-AC10-11-Rev5-EN.pdf>.
- van der Stelt, M.J.C. et al. 2011. Biomass upgrading by torrefaction for the production of biofuels: A review. *Biomass and Bioenergy.* **35**(9), pp.3748-3762.

- Veznikova, H. et al. 2014. Safe storage of selected fuels with regard to their tendency to spontaneous combustion. *Journal of Loss Prevention in the Process Industries*. **29**, pp.295-299.
- Wang, T. et al. 2014. Catalytic Dehydration of C6 Carbohydrates for the Production of Hydroxymethylfurfural (HMF) as a Versatile Platform Chemical. *Green Chem.* **16**, pp.548-572.
- Wannapeera, J. and Worasuwanarak, N. 2012. Upgrading of woody biomass by torrefaction under pressure. *Journal of Analytical and Applied Pyrolysis*. **96**, pp.173-180.
- Wikipedia. 2016. *Lignosulfonates*. [Online]. [Accessed 1 January 2015]. Available from: <https://en.wikipedia.org/wiki/Lignosulfonates>.
- Wilén, C. et al. 2013. *Wood torrefaction –pilot tests and utilisation prospects*. Vtt Technical Research Centre of Finland: Energy Research Centre of the Netherlands.
- WMBF News. 2012. *Units fight another blaze at NC wood pellet plant*. [Online]. Available from: <http://www.wmbfnews.com/story/17110667/units-fight-blaze-at-nc-kitty-litter-plant>.
- Wu, D. et al. 2014. Experimental Analysis of Minimum Ignition Temperature of Coal Dust Layers in Oxy-fuel Combustion Atmospheres. *Procedia Engineering*. **84**, pp.330-339.
- Yaman, S. et al. 2000. Production of fuel briquettes from olive refuse and paper mill waste. *Fuel Processing Technology*. **68**(1), pp.23-31.
- Yang, H.P. et al. 2007. Characteristics of hemicellulose, cellulose and lignin pyrolysis. *Fuel*. **86**(12-13), pp.1781-1788.
- Yee, L.D. et al. 2013. Secondary organic aerosol formation from biomass burning intermediates: phenol and methoxyphenols. *Atmospheric Chemistry and Physics*. **13**(16), pp.8019-8043.
- Yohe, G.R. 1964. *Binding Materials Used in Making Pellets and Briquets*. Urbana: Library of the Illinois State Geological Survey.
- Yokelson, R.J. et al. 2009. Emissions from biomass burning in the Yucatan. *Atmospheric Chemistry and Physics*. **9**(15), pp.5785-5812.
- Yokelson, R.J. et al. 1997. Emissions from smoldering combustion of biomass measured by open-path Fourier transform infrared spectroscopy. *Journal of Geophysical Research-Atmospheres*. **102**(D15), pp.18865-18877.

Appendix A Kinetic Parameters of Samples Evaluated

The kinetic parameters for 36 biomass samples are summarised in **Table A.1**:

Table A.1 Biomass Slow Combustion Activation Energy, E_a , and $\ln A$

Sample	E_a (kJ/mol)	$\ln A$ (s ⁻¹)
Miscanthus(1)	84.87	13.17
Pine	69.62	9.18
Miscanthus(2)	85.40	12.89
Wheat Straw	75.40	11.04
PM(1)9010	74.03	10.31
PM(1)5050	81.03	12.18
PM(2)9010	60.07	6.97
PM(2)5050	78.64	11.32
PWS9010	85.96	13.10
PWS5050	84.75	13.06
Misc(1)Lg980	83.49	11.76
Misc(1)CF980	87.80	12.731
PineLg980	73.54	9.21
PineCF980	76.75	9.92
Misc(2)Lg980	81.15	10.59
Misc(2)CF980	86.60	11.98
WSLg980	66.35	7.84
WSCF980	67.35	8.02
Misc(1)	80.63	12.28

Sample	E_a (kJ/mol)	$\ln A$ (s⁻¹)
wMisc(1)	83.56	12.47
PineC	80.59	11.28
wPineC	81.94	11.45
90PineC-10Misc(1)	82.91	11.89
90wPineC-10wMisc(1)	85.21	12.33
50PineC-50Misc(1)	85.61	12.84
50wPineC-50wMisc(1)	86.45	12.88
PineR	80.59	11.28
tMisc(1)	99.25	14.97
tPineR	95.73	12.11
50tM(1):50M(1)	80.85	11.18
90tM(1):10M(1)	97.21	14.52
50tPineR:50tM(1)	112.46	17.51
90tPineR:10tM(1)	112.16	16.87
WWP	73.50	8.98
WWPLg980	69.81	8.14
WWPCF980	76.01	9.57

Appendix B

Input and Property Values Used in Computation of Reaction Kinetics

Some important input and property values used in estimating the reaction kinetics for each biomass sample are summarised in **Table B.1**:

Table B.1 Important Input and Property Values for Reaction Kinetics Estimation of Ten Biomass Dust Samples

Sample	Hot Plate Temperature, T_p (K)	Dust Layer Thickness, $2r$ (m)	Biomass Thermal Conductivity, λ ($W/m \cdot K$)	Inverse Film Temperature, β (K^{-1})	Air Kinematic Viscosity, ν (m^2/s)	Air Thermal Diffusivity, α (m^2/s)	Air Thermal Conductivity, λ_a ($W/m \cdot K$)	Total Effective Heat Transfer Coefficient, h_t ($W/m^2 \cdot K$)
Miscanthus(1)	578.15	0.005	0.06	2.528×10^{-3}	2.592×10^{-5}	3.754×10^{-5}	3.346×10^{-2}	22.38
	548.15	0.0125	0.06	2.699×10^{-3}	2.317×10^{-5}	3.334×10^{-5}	3.156×10^{-2}	19.27
Miscanthus(2)	618.15	0.005	0.06	2.407×10^{-3}	2.826×10^{-5}	4.106×10^{-5}	3.489×10^{-2}	25.09
	573.15	0.0125	0.06	2.611×10^{-3}	2.454×10^{-5}	3.544×10^{-5}	3.251×10^{-2}	20.78
Pine	583.15	0.005	0.07	2.513×10^{-3}	2.641×10^{-5}	3.830×10^{-5}	3.380×10^{-2}	22.71
	553.15	0.0125	0.07	2.681×10^{-3}	2.367×10^{-5}	3.410×10^{-5}	3.190×10^{-2}	19.56
Wheat Straw	583.15	0.005	0.04	2.513×10^{-3}	2.619×10^{-5}	3.796×10^{-5}	3.365×10^{-2}	22.71
	548.15	0.0125	0.04	2.699×10^{-3}	2.317×10^{-5}	3.334×10^{-5}	3.156×10^{-2}	19.27
PM(1)9010	578.15	0.005	0.06	2.528×10^{-3}	2.592×10^{-5}	3.754×10^{-5}	3.346×10^{-2}	22.38
	553.15	0.0125	0.06	2.681×10^{-3}	2.345×10^{-5}	3.376×10^{-5}	3.175×10^{-2}	19.56

Sample	Hot Plate Temperature, T_p (K)	Dust Layer Thickness, $2r$ (m)	Biomass Thermal Conductivity, λ (W/m · K)	Inverse Film Temperature, β (K ⁻¹)	Air Kinematic Viscosity, ν (m ² /s)	Air Thermal Diffusivity, α (m ² /s)	Air Thermal Conductivity, λ_a (W/m · K)	Total Effective Heat Transfer Coefficient, h_t (W/m ² · K)
PM(1)5050	578.15	0.005	0.06	2.528 x 10 ⁻³	2.592 x 10 ⁻⁵	3.754 x 10 ⁻⁵	3.346 x 10 ⁻²	22.38
	553.15	0.0125	0.06	2.681 x 10 ⁻³	2.367 x 10 ⁻⁵	3.410 x 10 ⁻⁵	3.190 x 10 ⁻²	19.56
PM(2)9010	588.15	0.005	0.06	2.497 x 10 ⁻³	2.647 x 10 ⁻⁵	3.839 x 10 ⁻⁵	3.384 x 10 ⁻²	23.04
	558.15	0.0125	0.06	2.663 x 10 ⁻³	2.367 x 10 ⁻⁵	3.410 x 10 ⁻⁵	3.190 x 10 ⁻²	19.86
PM(2)5050	608.15	0.005	0.06	2.436 x 10 ⁻³	2.767 x 10 ⁻⁵	4.017 x 10 ⁻⁵	3.454 x 10 ⁻²	24.39
	568.15	0.0125	0.06	2.628 x 10 ⁻³	2.427 x 10 ⁻⁵	3.502 x 10 ⁻⁵	3.232 x 10 ⁻²	20.47
PWS9010	578.15	0.005	0.06	2.528 x 10 ⁻³	2.592 x 10 ⁻⁵	3.754 x 10 ⁻⁵	3.346 x 10 ⁻²	22.38
	553.15	0.0125	0.06	2.681 x 10 ⁻³	2.345 x 10 ⁻⁵	3.376 x 10 ⁻⁵	3.175 x 10 ⁻²	19.56
PWS5050	583.15	0.005	0.06	2.513 x 10 ⁻³	2.619 x 10 ⁻⁵	3.796 x 10 ⁻⁵	3.365 x 10 ⁻²	22.71
	553.15	0.0125	0.06	2.681 x 10 ⁻³	2.345 x 10 ⁻⁵	3.376 x 10 ⁻⁵	3.175 x 10 ⁻²	19.56

